

Evaluation of Ventilation-Controlled Fires in L-Shaped Training Props

Joseph Willi
Keith Stakes
John Regan
Robin Zevotek

UL Firefighter Safety Research Institute
Columbia, MD 21045



Evaluation of Ventilation-Controlled Fires in L-Shaped Training Props

Joseph Willi
Keith Stakes
John Regan
Robin Zevotek

UL Firefighter Safety Research Institute
Columbia, MD 21045

October 16, 2018



UL Firefighter Safety Research Institute
Stephen Kerber, Director

In no event shall UL be responsible to anyone for whatever use or non-use is made of the information contained in this Report and in no event shall UL, its employees, or its agents incur any obligation or liability for damages including, but not limited to, consequential damage arising out of or in connection with the use or inability to use the information contained in this report. Information conveyed by this report applies only to the specimens actually involved in these tests. UL has not established a factory Follow-Up Service Program to determine the conformance of subsequently produced material, nor has any provision been made to apply any registered mark of UL to such material. The issuance of this report in no way implies Listing, Classification, or Recognition by UL and does not authorize the use of UL Listing, Classification or Recognition Marks or other reference to UL on or in connection with the product or system.

Contents

List of Figures	iii
List of Tables	vi
List of Abbreviations	viii
1 Introduction	1
1.1 Motivation	1
1.2 Objectives	3
1.3 Limitations	3
2 Literature Review	5
2.1 Line of Duty Deaths & Injuries	6
2.2 Fire Service Publications	7
2.3 Previous Research	9
3 Experimental Configuration	11
3.1 Training Props	11
3.1.1 Gypsum Prop	12
3.1.2 Metal & Insulated Metal Props	13
3.2 Fuel Loads	18
3.2.1 Pallets	18
3.2.2 Pallets & OSB	19
3.2.3 Furniture	20
3.3 Instrumentation	23
3.3.1 Measurement Locations	23
3.3.2 Measurement Uncertainty	26
4 Experimental Procedure	28
4.1 Burn In Experiments	30
4.2 Prop & Fuel Comparison Experiments	31
4.3 Ventilation Effects Experiments	32
4.4 Suppression Effects Experiments	33
5 Results & Discussion	35
5.1 Methodology	35
5.1.1 Growth Times & Rates	35

5.1.2	Critical Values & Exposure Limits	36
5.1.3	Evaluation of Agreeableness Between Data Sets	37
5.2	Repeatability of Wall Configurations & Fuel Loads	41
5.3	Comparison of Burn In Tests to Later Replicates	49
5.4	Comparison of Wall Configurations	54
5.5	Comparison of Fuel Loads	58
5.6	Ventilation Effects	63
5.6.1	Vent Door vs. Vent Window	63
5.6.2	Open Door, No Action vs. Open Door, Vent Window	74
5.7	Suppression Effects	80
6	Considerations	85
6.1	Training Considerations	85
6.1.1	Specific Aspects of Ventilation-Controlled Fires can be Generated in Metal Props	85
6.1.2	NFPA 1403-Compliant Fuels can Produce Ventilation-Limited Conditions in Metal Props	88
6.1.3	NFPA 1403-Compliant Fuels can be used to Demonstrate Flow Path & Neutral Plane Development in L-Shaped Props	91
6.1.4	NFPA 1403-Compliant Fuels can Produce Conditions with the Potential to Cause Thermal Injury to Firefighters in Full PPE	94
6.1.5	NFPA 1403-Compliant Fuels can Create Repeatable Fire Behavior	97
6.1.6	Thermal Exposures Experienced During Interior Suppression may Differ Between the Gypsum Prop & Metal Props	99
6.2	Prop Durability & Performance Considerations	100
6.2.1	Awareness of Prop Degradation is Important	100
6.2.2	Insulating the Metal Prop did not Noticeably Change the Overall Thermal Environment	106
6.2.3	Insulating the Metal Prop Increased the Cooling Time of the Prop	108
7	Summary	110
	References	113
A	Example of Sample Set Comparison & Bias/ICC Calculation	117
B	Bias & ICC Tables	121
B.1	Fuel Load Comparisons	121
C	Experimental Data	123
C.1	Burn In Experiments	124
C.2	Prop & Fuel Comparison Experiments	148
C.3	Ventilation Effects Experiments	238
C.4	Suppression Effects Experiments	328

List of Figures

3.1	Gypsum Prop Exterior & Interior	12
3.2	Gypsum Prop Floor Plan	13
3.3	Isometric View of Gypsum Prop CAD Model	13
3.4	Metal Prop Exterior	14
3.5	Metal Prop & Insulated Metal Prop Interior Wall Linings	15
3.6	Metal Prop Floor Plan	16
3.7	Insulated Metal Prop Floor Plan	17
3.8	Isometric View of Metal Prop CAD Model	17
3.9	Pallets Fuel Load	18
3.10	Pallets Fuel Load Location	19
3.11	Pallets & OSB Fuel Load	20
3.12	Furniture Fuel Load	21
3.13	Furniture Fuel Load Location	22
3.14	Floor Plan of Instrumentation Locations	23
3.15	Firefighter Helmet with Heat Flux Gauges	25
4.1	Exterior Fire Spread Observed During Burn In Tests	30
4.2	Vent Door Layout	31
4.3	Vent Window Layout	32
4.4	Open Door, No Action & Open Door, Vent Window Layouts	33
4.5	Suppression Effects Layout	34
5.1	Plots of Fire Room Ceiling Temperature Data with Highlighted Growth & Re-growth Times	36
5.2	Locations of Thermocouple Arrays used in Agreeableness Evaluation	38
5.3	Plotted Data Samples used for Comparison Example	38
5.4	Scatter Plot of Measurement Pairs Formed by Example Data Sets from Test 12 & Test 13	39
5.5	Plot of Fire Room Ceiling Temperature Data with Highlighted Initial Growth & Post-Vent Sample Ranges	43
5.6	End Hall & Start Hall Measurement Locations	46
5.7	Images of Fire Growth After Ignition of Furniture & Pallets Fuel Loads	48
5.8	Burning Paint on the Exterior of the Metal Prop During the Burn In Test	52
5.9	Images of the Metal Prop from Before & After Burn In Test	52
5.10	Images of the Insulated Metal Prop from Before & After Burn In Test	53
5.11	End Hall & Start Hall Temperatures at Facepiece Level During Fuel Load Comparison Tests in Metal Prop	61

5.12	End Hall Heat Flux During Post-Vent Period of Fuel Load Comparison Tests in Metal Prop	62
5.13	Post-Vent Fire Room Temperatures for Vent Door & Vent Window Furniture Tests in Gypsum Prop	67
5.14	Post-Vent Fire Room Temperatures for Vent Door & Vent Window Pallets & OSB Tests in Gypsum Prop	68
5.15	Post-Vent O ₂ Concentrations 4.0 in. (10.2 cm) Above the Floor in Fire Room for Vent Door & Vent Window Tests in Insulated Metal Prop	70
5.16	Furniture Fuel Load after Suppression in Vent Door & Vent Window Tests	71
5.17	End Hall & Start Hall Firefighter Level Temperatures During Vent Door & Vent Window Experiments in Insulated Metal Prop	72
5.18	End Hall Heat Flux During Post-Vent Period of Fuel Load Comparison Tests in Metal Prop	73
5.19	O ₂ Concentrations During Open Door Tests with Furniture Fuel Load	77
5.20	Neutral Plane at Doorway for Each Fuel Load	78
5.21	Comparison of Flow Path Change During Furniture and Pallets & OSB Tests	79
5.22	Plot of Incident Heat Flux to Firefighter Around Time of Suppression During Suppression Effects Tests	81
5.23	Temperatures 4.0 ft (1.2 m) Below Ceiling at End Hall & Start Hall Locations During Suppression Effects Tests	82
5.24	Start Hall Heat Flux from Open Door, No Action Test with Pallets & OSB Plotted with Incident Heat Flux to Firefighter Around Time of Suppression During Suppression Effects Tests	83
6.1	Fire Room Temperatures during the Vent Door Gypsum & Metal Prop Furniture Tests	86
6.2	Location of End Hall & Start Hall Heat Flux Measurement Locations	87
6.3	Hallway Heat Flux After Ventilation During Gypsum Prop & Metal Prop Furniture Tests	88
6.4	Idealized Ventilation-Controlled Fire Curve Compared to Fire Room Temperature Plot	89
6.5	Fire Room Temperatures from Vent Door Tests with Pallets and Pallets & OSB in Metal Prop	90
6.6	Comparison of Smoke Color & Neutral Plane at Doorway for Different Fuel Loads	92
6.7	Comparison of Flow Path Change During Furniture and Pallets & OSB Tests	93
6.8	Hallway Heat Flux & Temperature Plots from Vent Door Tests in Metal Prop with Wood-Based Fuel Loads	95
6.9	Location of Thermocouple Array & Heat Flux Gauge Pairs in Hallway	96
6.10	Plots of Fire Room Ceiling Temperature During Replicate Tests with Pallets and Pallets & OSB Fuel Loads	98
6.11	Plot of Incident Heat Flux to Firefighter During Interior Suppression Tests	99
6.12	Gypsum Prop Damage after a Single Fire with the Pallets Fuel Load	101
6.13	Exterior Fire During Burn In Test	102
6.14	TIC Video Frame of Metal Prop Exterior during Burn In Test & Image of Damaged Exterior Afterwards	102

6.15 Images of the Insulated Metal Prop from Before & After Burn In Test 103

6.16 Fire Room Temperatures During Initial Growth Period of the Burn In & Later
Replicate Tests with Pallets in Metal Prop 104

6.17 Bar Graph of Prop Leakage Measured Before & After Burn In Tests 105

6.18 Temperatures 3 ft Below the Ceiling & Heat Flux 3 ft Above the Floor at the Start
of the Hall During Comparable Fires in the Metal & Insulated Metal Prop 107

List of Tables

3.1	Average Weight of Each Item from the Furniture Fuel Load Configurations	20
4.1	Summary of Experiments	29
4.2	Event Times for Vent Door Test Procedure	31
4.3	Event Times for Vent Window Test Procedure	32
4.4	Event Times for Open Door, No Action & Open Door, Vent Window Test Procedures	33
4.5	Event Times for Suppression Effects Test Procedure	34
5.1	Exposure Limits of Firefighter PPE	37
5.2	Defined Levels of Agreeableness	41
5.3	Overall Bias & ICC Values from Sample Comparisons Between Repeatability Tests	44
5.4	Peak Temperature & Heat Flux Measured at Firefighter Level in Hallway During Repeatability Tests	45
5.5	Growth Times & Rates from Repeatability Tests	47
5.6	Overall Bias & ICC Values from Burn In vs. Later Replicate Sample Comparisons	49
5.7	Peak Temperature & Heat Flux Measured at Firefighter Level During Initial Growth Period of Burn In & Later Replicate Tests	50
5.8	Prop Leakage Values Measured Before & After Burn In Tests	51
5.9	Overall Bias & ICC Values from Post-Vent Comparisons Between Prop Constructions for each Fuel Load	55
5.10	Thermal Conductivity of Common Materials at 20 °C	56
5.11	Average Cooling Rate Across Upper Thermocouples in Fire Room & End Hall Arrays During Final 90 seconds of Tests with Wood-Based Fuels in Metal & Insulated Metal Props	57
5.12	Peak Temperature & Heat Flux Measured at Firefighter Level in Hallway During Wall Configuration Comparison Tests	57
5.13	Overall Bias & ICC Values for Comparisons of Post-Vent Data from each Thermocouple Array Between Fuel Loads in the Metal Prop	60
5.14	Overall Bias & ICC Values for Vent Door vs. Vent Window Comparisons of Post-Vent Data from each Interior Thermocouple Array in the Gypsum Prop	64
5.15	Overall Bias & ICC Values for Vent Door vs. Vent Window Comparisons of Post-Vent Data from each Interior Thermocouple Array in the Metal Prop	64
5.16	Overall Bias & ICC Values for Vent Door vs. Vent Window Comparisons of Post-Vent Data from each Interior Thermocouple Array in the Insulated Metal Prop . . .	65
5.17	Overall Bias & ICC Values from Open Door, No Action vs. Open Door, Vent Window Comparisons of Post-Growth Data from each Interior Thermocouple Array	75

6.1 Average Rate of Temperature Decline Across Upper Thermocouples in Fire Room & End Hall Arrays During Final 90 seconds of Wood-Based Fuel Load Tests in Metal & Insulated Metal Props 108

List of Abbreviations

BDP	Bi-directional probe
CAD	Computer-aided design
HRR	Heat release rate
IC	Incident command
ICC	Intraclass correlation coefficient
IDLH	Immediately dangerous to life and health
LODD	Line of duty death
NIOSH	National Institute of Occupational Safety and Health
NIST	National Institute of Standards and Technology
NFPA	National Fire Protection Association
OSB	Oriented strand board
O ₂	Oxygen
PPE	Personal protective equipment
RIT	Rapid intervention team
UL FSRI	UL Firefighter Safety Research Institute

Acknowledgments

This work was funded through a grant from the Department of Homeland Security Federal Emergency Management Agency's Assistance to Firefighters Grant Program under the Fire Prevention and Safety Grants: Research and Development. This critical fire service research project would not be possible without this funding and support.



The authors wish to thank the members of the project's fire service technical panel, listed in the table on the following page, for providing support during the development and planning phase of this project and for contributing valuable feedback regarding the project results and conclusions. The enthusiasm of panel members to share their diverse range of knowledge and experience was integral to this project's success and relevance to the fire service.

Thanks to the following individuals from the UL FSRI team for their assistance during all portions of the project: Michael Alt, Joshua Crandall, Sarah Huffman, Steve Kerber, Dan Madrzykowski, and Craig Weinschenk.

The authors thank Roy McLane of Thermal Fabrication and Brad Morrissey of Eastern Kentucky University for their tireless support in conducting the experiments.

Finally, under the direction of Kerby Kerber, the Delaware County (PA) Emergency Services Training Center provided the much needed logistical support for these experiments.

Fire Service Technical Panel

Name	Affiliation
Derek Alkonis	Los Angeles County Fire Department
Brian Arnold	Oklahoma City Fire Department
Charles Bailey	Montgomery County (MD) Fire & Rescue Services
John Ceriello	Fire Department of the City of New York
Sean DeCrane	Cleveland Fire Department (Ret.)
James Dominik	Northeastern Illinois Public Safety Training Academy
Michael Cox	Maryland Fire and Rescue Institute
Kenny Fent	National Institute for Occupational Safety and Health
Michael Gagliano	Seattle Fire Department (Ret.)
Sean Gray	Cobb County Fire Department
Bobby Halton	Fire Engineering Magazine
Todd Harms	Sacramento Fire Department
Ed Hartin	Central Whidbey Island Fire & Rescue
George Healy	Fire Department of the City of New York
Gavin Horn	University of Illinois Fire Service Institute
David Rhodes	Atlanta Fire Department
John Cunningham	Alabama Fire College; North American Fire Training Directors
Ken Richards	Old Mystic Fire Department; NFPA 1403
Erich Roden	Milwaukee Fire Department; Fire Rescue Magazine
Tim Sendelbach	Firehouse Magazine
Dan Shaw	Fairfax County Fire Rescue; NFPA 1403
Denise Smith	Skidmore College
Jens Stiegel	Frankfurt am Main Fire & Rescue Services
Stefan Svensson	Lund University, Department of Fire Safety Engineering
Adam Thiel	Philadelphia Fire Department
Peter Van Dorpe	Algonquin-Lake in the Hills Fire Department
Devon Wells	International Society of Fire Service Instructors

Abstract

Investigations of recent firefighter line of duty deaths caused by rapid fire progression have highlighted a deficiency in firefighters' understanding of how certain tactics affect the fire dynamics of ventilation-controlled fires. Many fires are in a ventilation-limited, decay state by the time firefighters arrive at the scene, meaning that introducing additional ventilation to the environment has the potential to cause rapid and intense fire growth. To more effectively teach firefighters about the potential effects of ventilation on a compartment fire, ventilation-controlled fires should be generated during training. Safely creating such fires while maintaining compliance with *NFPA 1403: Standard on Live-Fire Training Evolutions* allows instructors to educate students on this important principle of fire dynamics in the training environment.

Structures utilized for live-fire training have evolved from typical concrete burn buildings to now include smaller purpose-built props, like those constructed from steel shipping containers or wood and gypsum board. Such props have been embraced by organizations due to their cost-effectiveness and potential to improve fire behavior training. Obtaining a thorough understanding of the capabilities and limitations of such props is critical for instructors to convey accurate messages during training and properly prepare firefighters for scenarios they'll encounter in the field.

Experiments were conducted to quantify the fire environment in L-shaped props with different wall constructions. One prop had an interior wall lining of gypsum board over wood studs and fiberglass insulation. The two other props were constructed from metal shipping containers with corrugated steel walls; one had ceilings and walls comprised solely of the corrugated steel, while the other had ceilings and walls comprised of rolled steel sheeting over mineral wool insulation with the corrugated steel wall as its backing. Three fuel packages were compared between the props: one contained furnishings mainly composed of synthetic materials and foam plastics; another contained wooden pallets and straw; and the third contained wooden pallets, straw, and oriented strand board (OSB).

A stochastic approach was used to compare data between replicate tests and quantify the repeatability of the different props and fuel packages, all of which were deemed sufficiently repeatable. Comparisons of data between the three props revealed that thermal conditions between experiments in the two metal props were indistinguishable, suggesting that the additional layer of insulation did not significantly alter the fire environment. Additionally, thermal conditions in the gypsum-lined prop were more severe than those in the metal props. The effects of ventilation changes on fire conditions were also analyzed across various prop and fuel load combinations. Lastly, the response of the thermal environment in each prop during interior suppression was evaluated, and the results implied that the thermal exposure to the firefighter was more severe in the metal props than the gypsum prop for a brief period following the start of suppression.

1 Introduction

1.1 Motivation

Several firefighter line of duty deaths (LODDs) and injuries have occurred in recent years on the fireground as a result of rapid fire progression [1–4]. Among the contributing factors listed in the investigative reports of these incidents was a lack of understanding of fire behavior [1–3]. Recent studies on firefighter safety have identified that the shift from natural fibers and wood to synthetics and foam plastics in the contents of modern structures has resulted in fires with higher heat release rates (HRRs) [5, 6]. This shift has created a more unforgiving fireground where poorly timed actions, such as uncoordinated ventilation, can cause a rapid deterioration of thermal conditions. Among other items, the necessity for firefighters to understand the fire dynamics encountered on the fireground has been identified as essential for effective firefighting and increased safety.

Previous research has illustrated the importance of understanding how fires respond to ventilation [5–8]. Many fires are in a ventilation-limited, decay state by the time firefighters arrive at the scene, meaning that introducing additional ventilation to the environment has the potential to cause rapid and intense fire growth. To more effectively teach firefighters about the potential effects of ventilation on a compartment fire, ventilation-limited fires should be utilized during training. The ability to reproduce aspects of the ventilation-controlled fire environment during training provides instructors with a tool to effectively demonstrate principles of fire dynamics that are applicable to present-day residential structure fires.

As fire service training has evolved, several props have been developed in an attempt to better demonstrate fire behavior principles. The use of firefighter concrete burn buildings has been supplemented with purpose-built training props, like those constructed from steel shipping containers [9, 10], due to their cost-effectiveness and potential to improve fire behavior training. Some departments cannot afford concrete training buildings but may be able to purchase smaller props made of metal or wood and gypsum board. Props that began as single or double cell containers have become multi-story structures with many compartments meant to be used in place of concrete training buildings [11]. Companies have started selling structures fabricated from steel containers specifically for live-fire training (e.g., Fire Training Structures LLC in the United States, BigSteel-Box Structures in Canada, Port Shipping Containers in Australia). It's critical that such props are understood, characterized, and correctly implemented into live-fire training. These props have the potential to improve the understanding of fire dynamics and increase the fidelity of training fires. They also have the flexibility to be used for demonstrations in addition to hands-on training, which allows for important fire behavior principles, such as those related to ventilation-controlled fires, to be shown in a cost-effective manner without exposing students to a severe thermal environment. However, like many training tools, these props have the potential to be used incorrectly, resulting in exposing students to hazardous conditions and/or improper context of lessons during exercises. Understanding the limitations of such tools and their practical impact on training is essential to

ensuring that the most accurate messages are transmitted to students.

The National Fire Protection Association (NFPA) developed *NFPA 1403: Standard on Live-Fire Training Evolutions* to outline methods and procedures that should be implemented to conduct live-fire training in a safe manner [12]. The standard requires that only wood-based fuels be used during training fires because they can create predictable fires and are easy to procure. Thus, wooden pallets and straw are commonly used as fuel for training fires. However, some academies and training groups have recognized that the conditions produced by wood-based training fuel packages are not representative of those encountered in residential fires, where the main fuel load consists of synthetics and foam plastics. In an effort to better replicate conditions experienced on the fireground, these organizations have begun to incorporate different fuels into live-fire training evolutions, including types of engineered lumber (e.g., oriented strand board (OSB), particleboard, etc.). The addition of such products to a traditional pallets and straw fuel load can increase the severity of the thermal conditions produced during training fires while still remaining compliant with *NFPA 1403*.

The introduction of these new fuels into the training environment raises the issue of balancing the fidelity of training fires with the safety of those participating in such burns. Many instructors assume that producing a training fire with high fidelity involves replicating the severity of thermal conditions that students are likely to encounter on the fireground. As the training fuel package is modified to produce conditions consistent with a furnished room, the thermal environment becomes more hazardous. It is important that the thermal hazard of the training environment is considered, as several firefighter LODDs have resulted from excessive thermal exposure during training evolutions [13–15]. Rather than mirroring the conditions experienced in a residential home with fuels composed of synthetic materials and foam plastics, the goal should be to simulate the response of the fire to firefighter tactics. This will minimize the potential of forming bad habits as a result of low-fidelity live-fire training while still preserving a reasonable margin of safety. The location and size of fire(s) during a training evolution should be based on the learning objectives of the specific exercise.

Experiments for this project were conducted in three types of L-shaped props that simulated a hallway connected to a room. Props with similar layouts are utilized at numerous training academies across the United States and around the world (e.g., Los Angeles County, Illinois Fire Service Institute, PIVO in Belgium). Such layouts provide students with the ability to practice advancing a hoseline down a hallway while flowing water and instructors with a tool to demonstrate flow path formation between the fire room and the doorway at the hall entrance.

The differentiating factor between the three props considered for this project was the construction of the ceilings and walls. One layout consisted of gypsum board on top of wood studs and fiberglass insulation to resemble modern residential construction. Two additional props were constructed from shipping containers made of corrugated steel; one had ceilings and walls composed solely of the corrugated steel, while the other had ceilings and walls composed of rolled steel sheeting over mineral wool insulation with the corrugated steel as its backing.

1.2 Objectives

The project described in this report is concerned with measuring, analyzing, and understanding the capabilities and limitations of conducting live-fire training in L-shaped props so that accurate messages can be conveyed by instructors who use such props. Specifically, the objectives of this study are to:

- Assess the repeatability of thermal environments created by ventilation-controlled fires in each type of L-shaped prop
- Compare the conditions produced by ventilation-controlled fires from various fuel packages between the different prop constructions
- Study the effects of ventilation changes on the fire environment in L-shaped training props
- Evaluate the response of thermal conditions during interior suppression in each type of prop

1.3 Limitations

There are a variety of limitations regarding the conclusions derived from the analysis of experimental data described in this report. A number of these limitations rise from keeping certain aspects constant across experiments so that differences between other parameters could be properly quantified. For example, the three props used for the experiments contained the same L-shaped layout comprised of a hallway connected to a room, and only three fuel loads were utilized during the experiments. The amount of fuel in each package, its positioning inside the fire room, and the ignition location were designed to be as consistent as possible between tests. Lastly, the experiments conducted for this project followed a limited set of procedures over similar durations of time.

Training props, especially those constructed from metal shipping containers, exist in many different shapes and sizes. Additionally, parameters such as the fuel load size and the duration of a scenario are likely to vary during training depending on available resources and the purpose of the exercise. While the experimental results from this project provide insight into the topics covered by the objectives listed in the previous section, the findings are by no means universal to any fire training exercise in L-shaped props. It's possible that components of a training evolution in a metal container prop could differ from those considered in this report to an extent that produces an outcome that deviates from some result described in this report.

Another limitation of the details provided in this report originates from the analysis being focused primarily on quantitative aspects of the fire environment measured during experiments. Thus, the findings in this report do not fully encompass how “real” the fire conditions looked and felt compared to those encountered by firefighters on the fireground, a metric sometimes referred to as “physical fidelity” [16]. How a fire environment “feels” to a firefighter compared to thermal measurements collected from the environment is a topic that requires further research.

Finally, the results from the experiments performed to study the effects of interior suppression between the different props apply exclusively to the specific setup that was tested. That is, the conclusions should not be generalized to encompass all training scenarios with suppression inside any given training prop constructed from metal shipping containers. Further investigation is needed to evaluate different suppression techniques in training props of varying shapes and sizes before the possibility of such generic claims can even be considered.

2 Literature Review

NFPA 1403: Standard on Live-Fire Training Evolutions outlines the requirements for live-fire evolutions in acquired and fixed facility training structures [12]. The document discusses the responsibilities of the instructors, safety officers, and participants, and provides guidelines for the types of fuels that can be included in the fuel package. The standard defines acceptable fuels as “pine excelsior, wooden pallets, straw, hay, and other wood-based products” [12]. The standard specifically forbids treated wood products, rubber, plastic, polyurethane foam, upholstered furniture, and chemically treated straw as fuels. *NFPA 1403* additionally makes several specific recommendations for acquired structure training burns. The standard recommends against the use of low-density particleboard and unidentified materials found within the structure. Furthermore, the document mandates that combustible materials not included in the fuel load should be moved to an area of the structure remote from the fire room.

Despite the procedures and precautions contained in *NFPA 1403*, there have been several instances where firefighters have been killed or injured during live-fire evolutions. The National Institute of Occupational Safety and Health (NIOSH) investigated several of these incidents, which are described below. These incidents have resulted in a series of revisions to the document since its initial release in 1986. The 2018 Edition of *NFPA 1403* lists a series of prerequisites that students must have prior to participating in live-fire training. Among these prerequisites are training on the proper use of personal protective equipment (PPE), ventilation, and fire behavior. Specifically, students should have a proper understanding of fire dynamics, including heat transfer, basic chemistry, and compartment fire behavior; the components, capabilities, and limitations of their PPE; and nozzle techniques and door control.

Additionally, *NFPA 1403* provides guidelines for selecting an appropriate fuel load and cautions that an excessive fuel load can result in a ventilation-controlled fire. Such fires present a hazard because additional ventilation results in fire growth or flashover. It is important that firefighters understand the concept of ventilation-controlled fires, however, because such conditions are usually present in residential structure fires. Thus, the most recent version of *NFPA 1403* includes a methodology for conducting controlled ventilation-limited fires. These scenarios are intended to teach ventilation-controlled fire behavior and the impact of ventilation (e.g., door control) rather than firefighting skills, such as line advancement or search and rescue. *NFPA 1403* stipulates that students and instructors should be positioned in a “safe observation space” — a space outside the fire room at the same level or below the fire room that is removed from the exhaust portion of the flow path. The observation space must have a charged hoseline capable of suppressing the fire and an unimpeded path of egress. When performed safely and correctly, a demonstration of a ventilation-controlled fire can be a useful tool for teaching fire dynamics, a job performance requirement identified in *NFPA 1001: Standard for Fire Fighter Professional Qualifications* [17].

2.1 Line of Duty Deaths & Injuries

NIOSH led an investigation of a 2005 incident in Pennsylvania that resulted in the death of a 47-year-old fire instructor and attracted further studies into the hazards of the training fire environment. The instructor experienced a catastrophic failure of his facepiece lens during a live-fire “train the trainer” course and died of his injuries two days after the event. The burn building was a two-and-a-half story concrete block structure. Investigators attributed the facepiece failure to the high thermal conditions that were present in the basement during the evolution. The investigation emphasized the importance of using the minimum amount of fuel necessary to meet the live-fire training objective and maintain firefighter safety. Additionally, this incident demonstrated the dangers of repeated evolutions without allowing sufficient time between evolutions for the burn building and the instructor’s PPE to cool down [14].

In a 2007 incident, a probationary firefighter was killed during a training evolution in a vacant end-of-the-row townhouse in Maryland. The scenario used approximately 12 wooden pallets, 11 bales of excelsior, and miscellaneous trash from the structure (tires, mattresses, foam rubber chair, tree branches, etc.) as fuel and featured fire sets on all three floors of the townhouse. The victim was on the nozzle of the first hoseline and was instructed to bypass the fires on the first and second floors and make an attack on the third floor fire. When the attack team reached the high heat conditions, two of the participants exited the structure through a window. The victim reached the window, but was unable to get the lower half of her body through the window. While the instructor was trying to remove her from the fire room through the window, her mask became dislodged. She was finally removed when another instructor came up the stairs and helped her legs through the window. The victim succumbed to thermal injuries and asphyxia. NIOSH attributed the outcome of the incident to several factors, including a lack of equipment, a lack of physical fitness performance requirements, and a failure to follow the requirements of *NFPA 1403* [13].

Two career firefighters were killed during a training fire in an acquired structure in Florida. The structure was a one story, single-family house with three bedrooms, two bathrooms, and a kitchen. The fire was ignited in one of the bedrooms and had a fuel load of wooden pallets, straw, and a urethane foam mattress. Before ignition, other materials in the room, such as urethane foam carpet padding, hollow core wood doors, and carpeting were not removed, and thus contributed to the fuel load. The victims entered the structure and performed a primary search of the building. Shortly after, the primary attack crew followed the search and rescue crew into the structure with a charged hoseline. After searching the living room, the two victims made their way to the fire room as smoke conditions intensified. Approximately three and a half minutes after the search team had entered the structure, the exterior ventilation firefighter was ordered to break out the window of the fire room. This caused the fire in the room to rapidly transition to flashover. The interior attack company, positioned outside the fire room doorway, began to apply water in short-flow increments into the room. After the victims failed to acknowledge repeated attempts by the Incident Commander (IC) to contact them, the IC activated the rapid intervention team (RIT), who found the victims in the fire room. The investigation identified the fuel load contents and uncoordinated ventilation as contributing factors, noting that the use of fuel with unknown burning characteristics can lead to unexpected fire development and rapid fire progression [18].

In another LODD incident, a New York volunteer firefighter was killed during a simulated “may-day” scenario, where he and another firefighter were acting as the simulated victims. The victim had very little training prior to the incident and had never previously worn a self-contained breathing apparatus (SCBA) under live-fire conditions. The training was conducted in a vacant two story duplex. The scenario called for two firefighters trapped in an upstairs bedroom in one half of the duplex and involved the engine and rescue company making entry through the other half of the duplex, breaching a wall, and rescuing the downed firefighters. The intended fuel source was a burn barrel in one of the bedrooms, but an assistant chief ignited the foam mattress of a sleeper chair after the ignition firefighter experienced difficulty with igniting the barrel. The ignition of the mattress led to rapid fire growth and caused conditions throughout the duplex to deteriorate. The ignition firefighter attempted to help the two trapped firefighters but in the process of doing so, lost his gloves, received burns to his hands, and was forced to exit out a second story window. When the engine and rescue companies arrived on scene, they both acted as RIT teams and removed the trapped firefighters from the structure. The victim was transported to a local hospital where he was pronounced dead. The other firefighter who was removed from the structure and the ignition firefighter who jumped from the second floor were flown to a regional burn center. The post-incident investigation highlighted the importance of not using live victims during live-fire training and ensuring that the fuels used in training burns are in accordance with *NFPA 1403* [15].

2.2 Fire Service Publications

Incidents such as those described above highlight the debate within the fire service about balancing safety requirements, such as those recommended in *NFPA 1403*, with realistic fire training that prepares recruits for the modern fireground. Many articles published in fire service trade magazines have focused on various aspects of live-fire training, namely, the usefulness of conducting training that adheres to the guidelines of *NFPA 1403*; methods and techniques to implement during exercises to increase the effectiveness of the training; and limitations of *NFPA 1403*-compliant training to replicate conditions experienced on the fireground.

One such article, written by Greg Fisher, highlights the importance of following *NFPA 1403* during live-fire training [19]. Fisher cautions against including loose trim, furnishings, and debris in the fuel package as was done in acquired structure burns for many years. The inclusion of such materials whose composition may be unknown, can lead to unpredictable fire behavior. In addition to removing loose materials from the acquired structure, Fisher stresses discretion when determining the size of the fire set. He points out that fuel sets larger than what students are comfortable with may cause students to panic, invalidating the training. When constructing a fuel package with pallets, Fisher highlights geometry as an important factor. He states that the pallets and straw should be arranged in a corner as close to the ceiling as possible. Such an arrangement allows for the fire to rapidly reach a fully-developed stage and mimic the behavior of a room-and-contents fire. Fisher adds that it is important to watch for window and ceiling failure during the training evolution, as these events could cause unwanted changes in fire behavior. Lastly, he stresses that students’ safety and comfort level should be prime considerations in the orchestration of acquired structure training burns [19].

In an article published by *Fire Engineering*, Kriss Garcia and Reinhard Kauffmann [20] present some of the challenges associated with conducting acquired structure training. The authors describe an instance in which many hours of work were performed to prepare a building for a live burn, only to find that the previous owner of the house had plastered over layers of medium-density particleboard, concealing the engineered wood board and leading to unexpected fire growth. The article presents instructions for a training structure prop, comprised of dimensional lumber and gypsum board walls. The authors maintain that this “build and burn” prop provides students with a safer and more realistic fire training experience by combining the realistic building materials and geometry of acquired structures with the predictability and more controlled environment of fixed-facility burn structures. The authors describe the standard fuel package that they use as consisting of five pallets. The first two pallets are leaned against each other diagonally, the second two are oriented vertically next to the first two, and the fifth pallet is laid across the top of the bottom four. The authors recommend that this fuel package should be placed in the center of the fire room, where they claim it will generate enough energy to bring the room to flashover and realistic amounts of combustion products [20].

In January 2012, four firefighters were injured during a training evolution that utilized a gypsum training prop similar to that described above. The incident resulted in the dismissal of several chief officers. The 1500 ft² (140 m²) prop was being used to conduct a demonstration of positive pressure fire attack. Several fuel packages were placed throughout the structure. During the first evolution, the fire grew and developed until window coverings of the fire room were removed, and a positive pressure ventilation fan was turned on to expedite the ventilation process. Seconds later, rapidly devolving conditions on the interior forced four students and an instructor to evacuate through windows on opposite ends of the prop, and subsequent training evolutions were canceled [21].

Forest Reeder presents the debate within the fire service about balancing the need for realistic training with safety requirements in his article [22]. Reeder highlights some of the complaints that are frequently voiced against the standard. Some instructors are frustrated that *NFPA 1403* prohibits what they consider to be more realistic training evolutions: ones with more smoke and higher heat conditions. These instructors feel that the standard is too restrictive and that the safety requirements invalidate the training experience. These instructors argue that Class A and gas-fired training fires do not create realistic smoke or heat conditions, leaving recruits unprepared for the high heat conditions frequently encountered on the modern fire ground. Reeder emphasizes that the safety requirements seen by some as overbearing or restrictive are necessary to prevent tragic accidents in live-fire evolutions. Furthermore, building the fire sets so that heat and smoke conditions are unbearably high may instill the idea that such high heat conditions are acceptable, leaving recruits vulnerable to rapid fire events on the fireground. Reeder maintains that control and pre-planning are important facets of a successful live-fire training evolution [22].

In a 2018 *FireRescue Magazine* article by David Rhodes, the limitations and value of training in different types of live-fire training buildings are discussed [23]. Rhodes states that the environment created by a fire with a standard wood pallets and straw fuel load in a Class A building is more realistic in creating heat and flow paths compared to Class B burn buildings, which use gas-fed props and artificial smoke to simulate fireground conditions. Yet, they are still limited in their ability to replicate typical fireground conditions in that the fire itself doesn't spread, gases rarely

burn, and the amount of water flow needed to improve conditions is very minimal. Adding OSB to the fuel load and using low flow nozzles are techniques that can reduce the significance of these limitations. Rhodes declares, “In both Class A and Class B buildings, one of the most unrealistic tactics practiced is that of ventilation.” He explains that in the majority of these buildings, ventilation is always effective at clearing conditions and reducing heat without causing an increase in fire intensity, which is not the response of the ventilation-limited fires often encountered on the job. He expresses concern that failing to properly emphasize the limitations of *NFPA 1403*-compliant training fires in replicating modern fire behavior could lead to forming habits that are ineffective, and sometimes counterproductive, when implemented on the fireground [23].

In 2010, the Irish National Directorate for Fire and Emergency Management published a document with guidelines to assist firefighters in the preparation and execution of compartment fire behavior training [24]. The manual focuses on training conducted in steel containers. It endorses the use of OSB as fuel, recommending that test or control burns are performed beforehand by instructors to determine the amount of OSB needed to produce desired conditions and that chains be used to restrain the boards. The document describes a number of potential training exercises and fire demonstrations that could be conducted in props constructed from 8.2 ft (2.5 m) wide by 8.2 ft (2.5 m) high single steel containers varying in length from 21.3 ft (6.5 m) to 42.7 ft (13.0 m).

2.3 Previous Research

One common factor among the LODD incidents described in previous paragraphs is the improper use of fuels and/or fuel loads. In several of the acquired structure burns, the addition of debris found around the house had the effect of increasing the fire size beyond what was manageable or expected. To better understand the training fuels utilized by firefighters, a series of research studies have aimed to quantify parts of the training fire environment.

Madrzykowski [25] investigated a pair of training fires in which firefighters had been killed. The first investigated incident was the previously mentioned LODD in Florida, where two firefighters died while conducting a search when the fire room transitioned to flashover [18]. The National Institute of Standards and Technology (NIST) recreated the fire room and two adjacent spaces and evaluated the thermal conditions produced by five different combinations of fuel load and ventilation conditions. Flashover conditions were generated in all five scenarios. Furthermore, during every experiment, temperatures measured 1.0 ft (0.3 m) above the floor of the fire room exceeded 500 °F (260 °C), and heat fluxes measured 3.3 ft (1.0 m) above the floor exceeded 20 kW/m², indicating conditions in the fire room were untenable for a firefighter in full PPE. An additional experiment examined the peak HRR of the pallets and straw and found it to be 2.8 MW [25]. The author compared this HRR to the theoretical HRR required for flashover in the room and discovered that the measured peak HRR exceeded the theoretical HRR required for flashover.

The second incident investigated by Madrzykowski was the previously mentioned LODD that occurred in Pennsylvania during a “train the trainer” class conducted in a concrete live-fire training building. After the last burn of the day, an instructor was found lying face-down on the floor in the

basement with damage to his facepiece. He later succumbed to his injuries. NIST instrumented the burn building in which the incident occurred and attempted to recreate the thermal conditions that were present at the time of the instructor's death. They first used a fuel load of pallets and excelsior to "pre-heat" the training structure. Then, additional pallets and straw were added. When the fires peaked, the fuel was suppressed with a hose stream, and the compartment was hydraulically ventilated. Once the compartment was cleared, additional pallets were added to the embers, and the process was repeated. The ambient heat flux at 4.9 ft (1.5 m) from the ceiling before the last evolution was 6 kW/m^2 , and the ambient temperature measured 5.0 ft (1.5 m) below the ceiling in the burn structure was $302 \text{ }^\circ\text{F}$ ($150 \text{ }^\circ\text{C}$). The instructor was in the process of adding two additional pallets to the fire burning in the basement fire room when he was overcome by hot gases from the existing fire, which resulted in the catastrophic failure of his SCBA facepiece. Based on the charring of some neoprene components of the facepiece, it was determined that the facepiece was exposed to temperatures of at least $647 \text{ }^\circ\text{F}$ ($342 \text{ }^\circ\text{C}$), which is well above the glass transition temperature and melting temperature of the high-temperature polycarbonate facepiece [14]. The recreation of the fire conditions in the training building showed peak temperatures in excess of $932 \text{ }^\circ\text{F}$ ($500 \text{ }^\circ\text{C}$) and peak heat flux values in excess of 20 kW/m^2 at 5.0 ft (1.5 m) above the floor [25]. Laboratory experiments indicated that a fuel load consisting of six pallets and straw had a peak HRR of 4.5 MW.

In both fatal training fire incidents, the thermal conditions produced by the fuel loads exceeded the protective capabilities of firefighter PPE. This highlights the necessity of using discretion when determining the fuel load to use for training fires.

Anna Back from Lund University studied the effects of insulation on compartment fires in metal containers [26]. Four experiments were performed with heptane pool fires and wood crib fires in insulated and non-insulated containers. It was found that the fires in the insulated container reached a higher HRR than in the non-insulated container. Also, it was discovered that the peak gas temperatures were significantly greater during fires in the insulated container than in the non-insulated container. It was reported that the average maximum gas temperature was 26 % greater during the heptane pool fires and 18 % greater during the wood crib fires in the insulated container than in the non-insulated container [26].

3 Experimental Configuration

This chapter describes various aspects of the 37 experiments conducted to quantify the fire environment in L-shaped training props. The first section presents details of the training props, including construction features, dimensioned floor plans, and a thorough description of the wall constructions. The next section is focused on the different fuel loads utilized throughout this series of experiments and contains information regarding the background, weight, and configuration of each fuel package. The final section of this chapter includes descriptions of the instrumentation used to measure gas temperature, total heat flux, pressure, gas velocity, and oxygen concentration; the device locations within the training props; and the total expanded uncertainties associated with the different measurement types.

3.1 Training Props

Experiments were performed in three training props constructed at the Delaware County Emergency Services Training Center in Sharon Hill, Pennsylvania. The walls of the “Gypsum Prop” were composed of R-13 insulation covered by 0.5 in. (13 mm) thick lightweight gypsum board on the interior side and by 0.5 in. (13 mm) thick plywood on the exterior side. The “Metal Prop” walls were comprised of a single layer of 0.25 in. (6 mm) thick corrugated steel. Lastly, the walls of the “Insulated Metal Prop” consisted of high-temperature, foil-backed mineral wool insulation between 0.25 in. (6 mm) thick corrugated steel (exterior side) and 0.125 in. (3 mm) thick rolled steel sheets (interior side).

Each prop contained an L-shaped layout formed by a room with an adjoining hallway. Similar configurations are commonly used by training academies when incorporating metal container props into live-fire training. The simple layout can be directly related to residential dwellings. The long hallway attached to a room via a perpendicular doorway allows firefighters to practice “making an approach” to the fire room. Firefighters are able to experience how flowing water during the approach can cool the atmosphere while also recognizing that the water does not reach the fire room until the stream is directed through the open doorway at the end of the hall.

The upcoming subsections contain specific information about the training props, including details of the construction and figures of dimensioned floor plans. Some aspects were identical across all three props. The fire room of each prop contained a 4.0 ft (1.2 m) by 5.0 ft (1.5 m) window opening with a sill height of 3.0 ft (0.9 m) above the floor and a 2.5 ft (0.8 m) by 6.7 ft (2.0 m) open doorway connecting the room to the hallway. A 2.5 ft (0.8 m) by 6.7 ft (2.0 m) door that opened to the exterior was located at the opposite end of the hall. This door along with a pair of shutters over the fire room window opening were controlled by latching mechanisms and were used to change the ventilation configuration during experiments. The total interior volume varied by less than 2 % between the props, which were each designed to have a total volume of 1440 ft³ (40.8 m³).

3.1.1 Gypsum Prop

The Gypsum Prop was constructed to replicate a typical hallway and room of a single-family dwelling that utilizes modern construction practices. The size and layout of the Gypsum Prop were selected to resemble the metal container props, which were constrained by the fixed sizes of steel shipping containers. Additionally, the hallway size was similar to that of the ranch structure used for full-scale fire experiments during a previous research project that focused on studying fire attack with interior and exterior streams [27]. Figure 3.1 contains pictures of the exterior and interior of the Gypsum Prop.



Figure 3.1: Images of the Gypsum Prop exterior (left) and interior (right). The exterior view is from the AB corner of the Gypsum Prop, and the interior view is looking down the hallway towards the fire room.

The walls of the Gypsum Prop were composed of nominally 2.0 in. (5.1 cm) by 4.0 in. (10.2 cm) wooden studs, actual dimensions 1.5 in. (3.8 cm) by 3.5 in. (8.9 cm), with 16.0 in. (40.6 cm) on-center spacing. Fiberglass insulation (R-13 value) was placed in the spaces between studs, as is typical in residential structures. The insulation, commonly referred to as “batt” insulation, contained a paper face and was pre-cut into sections that filled the entire volume between studs. The exterior sides of the walls were lined with a layer of 0.5 in. (13 mm) thick plywood covered by plastic home wrap to provide weather-proofing. The interior side was lined with a layer of 0.5 in. (13 mm) thick lightweight gypsum board. Normal weight drywall compound, screws, and joint tape were utilized during the installation. The floor of the structure was comprised of nominally 2.0 in. (5.1 cm) by 6.0 in. (15.2 cm) boards, actual dimensions 1.5 in. (3.8 cm) by 5.5 (14.0 cm), arranged on edge with 16.0 in. (40.6 cm) on-center spacing. A base layer of 0.75 in. (19 mm) thick plywood formed the subfloor and was covered by a top layer of 0.5 in. (13 mm) thick cement board. The hallway door was a hollow core interior door, commonly used for interior doors of residential structures, and the window contained two plywood panels covered by Kaowool insulation that

allowed for manipulation (opening and closing) during experiments. The ceiling height throughout the prop was 8.0 ft (2.4 m). Lastly, the Gypsum Prop included an “instrumentation room” that was used to store and protect instrumentation during testing. Note, the room did not affect the layout or dimensions of the test area (hallway and attached room) with regards to the comparison between the Gypsum Prop and the two metal container props. A dimensioned floor plan of the Gypsum Prop is presented in Figure 3.2, and isometric views of a computer-aided design (CAD) model of the Gypsum Prop are shown in Figure 3.3.

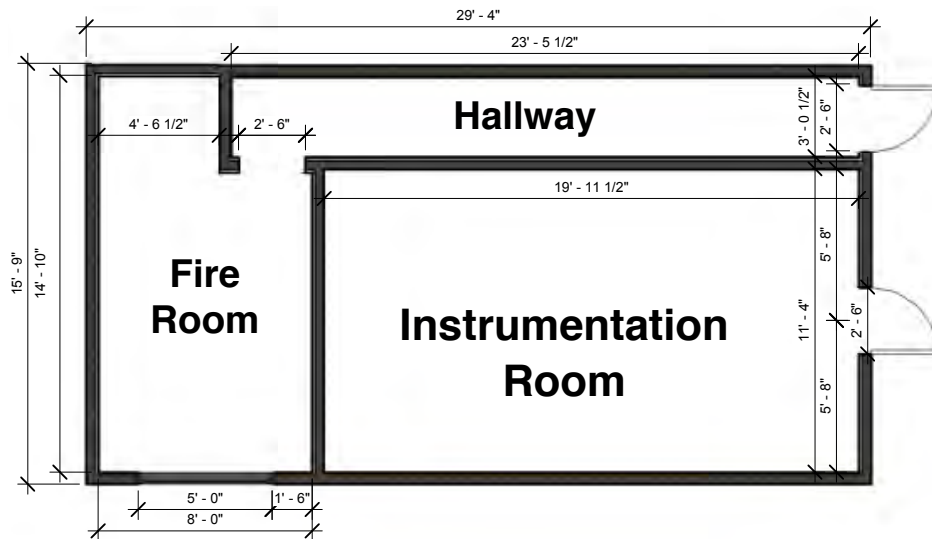


Figure 3.2: Dimensioned floor plan of the Gypsum Prop.

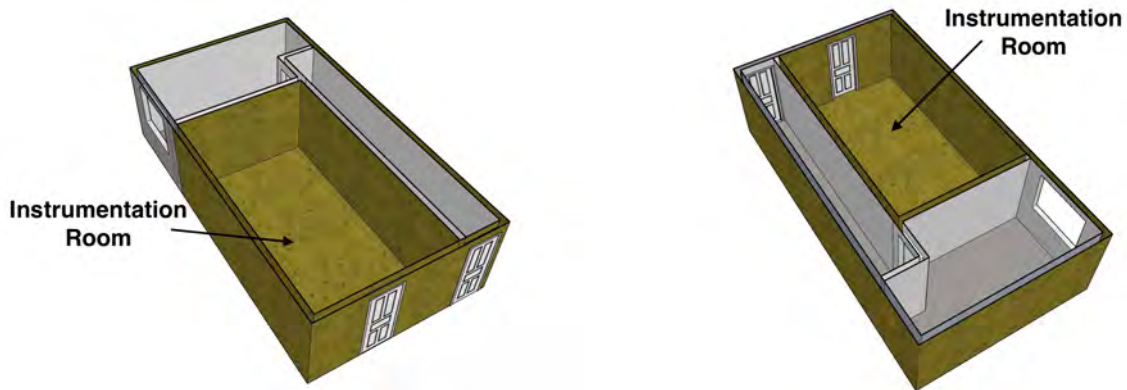


Figure 3.3: Isometric views of the Gypsum Prop CAD Model. The left view is from the AB corner, and the right view is from the CD corner.

3.1.2 Metal & Insulated Metal Props

The Metal Prop and Insulated Metal Prop were of similar design and construction. Each prop was in the shape of a “T” and contained a dividing wall down the middle, separating the prop into two

L-shaped sides that were mirror images of one another. Dividing the T-shape into two L-shaped props with identical dimensions provided the ability to conduct two experiments with the same wall configuration in rapid succession. The layout was formed by two steel shipping containers — a 30.0 ft (9.1 m) long by 8.0 ft (2.4 m) wide shipping container formed the two burn rooms, or the top part of the “T”, and a 20.0 ft (6.1 m) long by 8.0 ft (2.4 m) wide container formed both hallways, or the bottom portion of the “T”. Exterior views of the Insulated Metal Prop are shown in Figure 3.4.



Figure 3.4: Exterior views of the Insulated Metal Prop. The top image is of the front, and the bottom images are of the left and right sides.

The walls of the Metal Prop consisted of 0.25 in. (6 mm) thick corrugated steel. The window in the fire room and door at the start of the hallway were composed of steel and contained latching mechanisms that allowed for the manipulation of the vent during experiments. Like the Gypsum Prop, a layer of 0.5 in. (13 mm) thick cement board was installed on top of the subfloor in the Metal Prop. The ceiling height throughout the Metal Prop was 7.75 ft (2.4 m). Although the ceiling was lower in the metal props than in the Gypsum Prop, the hallways in the metal props were slightly wider than in the Gypsum Prop, resulting in a variation of less than 2 % between total volumes of the props as previously mentioned.

The Insulated Metal Prop consisted of 0.25 in. (6 mm) thick steel corrugated steel lining the

exterior side of the walls. Square steel tubing was used as framing along the interior walls, and high-temperature, foil-backed mineral wool insulation filled the void spaces between the tubing. Flat steel sheeting of 0.125 in. (3 mm) thickness covered the steel framing and insulation. The window in the fire room and steel door at the start of the hallway were identical to that of the Metal Prop. A layer of 0.5 in. (13 mm) thick cement board was installed over the subfloor as in the other two props.

The interior wall linings of the Metal Prop and Insulated Metal Prop are pictured in Figure 3.5. Dimensioned floor plans of the Metal Prop and Insulated Metal Prop are presented in Figures 3.6 and 3.7, respectively. Additionally, isometric views of a CAD model of the Metal Prop are shown in Figure 3.8. Note that because the interior wall lining was the only differentiating factor between the Metal Prop and Insulated Metal Prop, the exterior views of their CAD models are identical.



Figure 3.5: Images of interior wall linings of the Metal Prop (left) and Insulated Metal Prop (right). Both views are looking down the hallway towards the fire room.

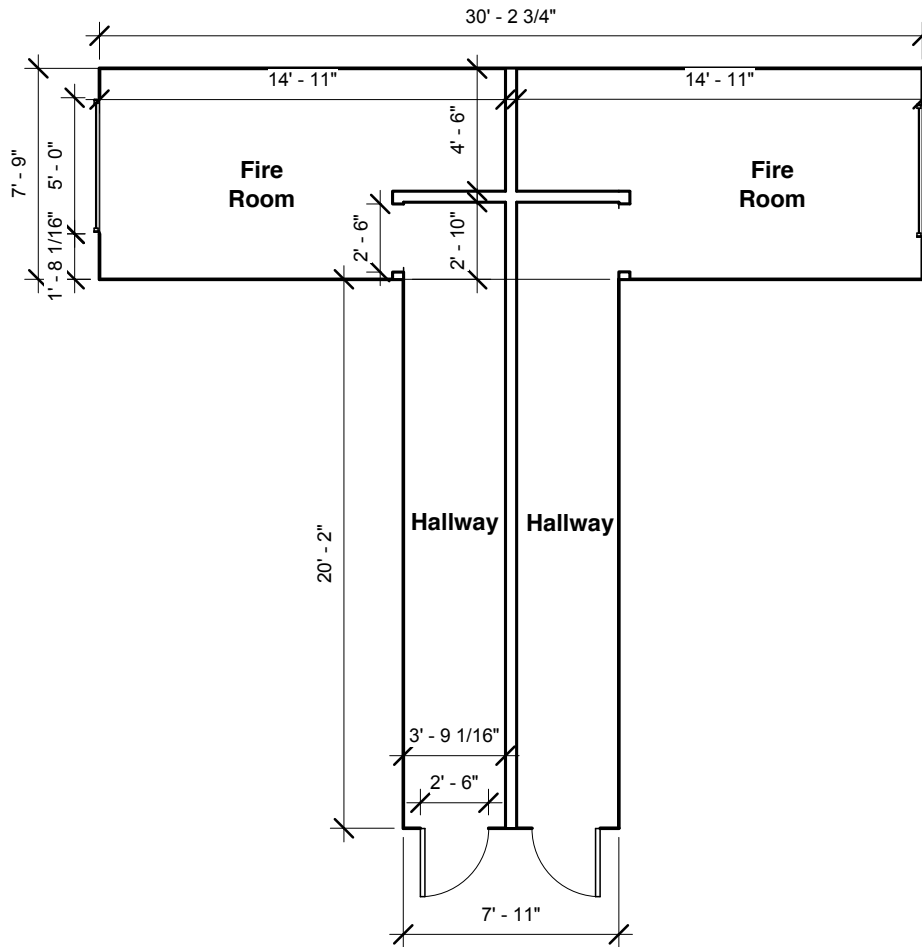


Figure 3.6: Dimensioned floor plan of the Metal Prop.

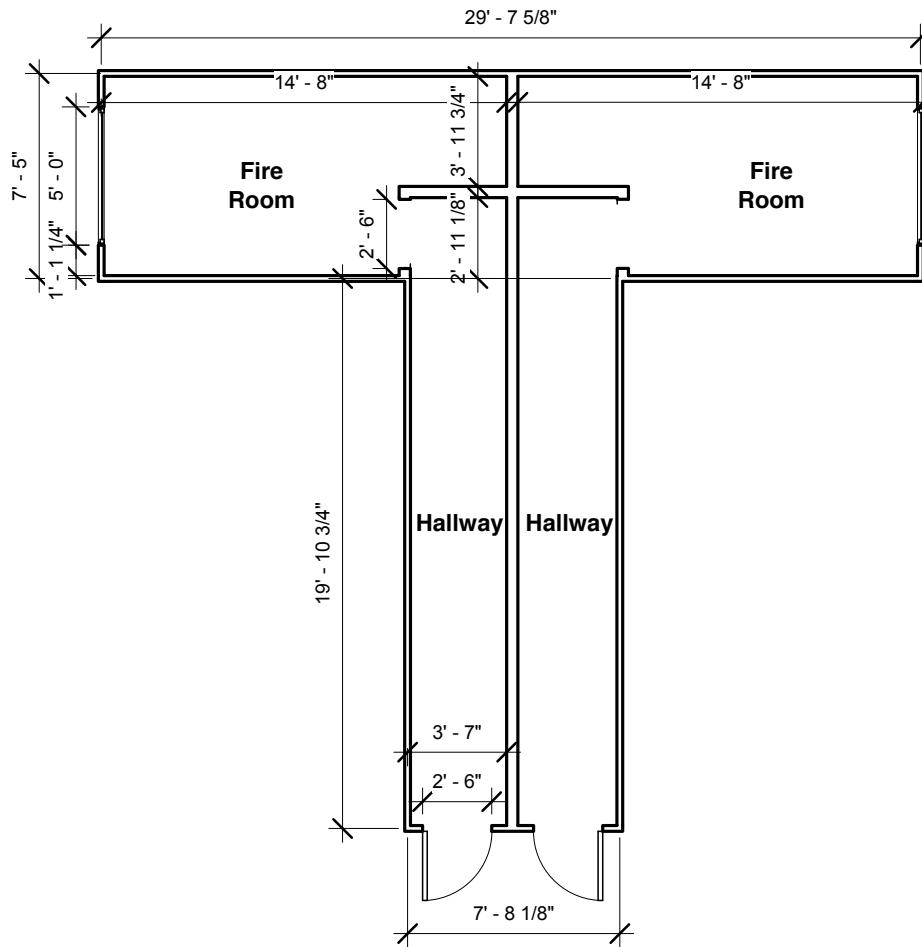


Figure 3.7: Dimensioned floor plan of the Insulated Metal Prop.

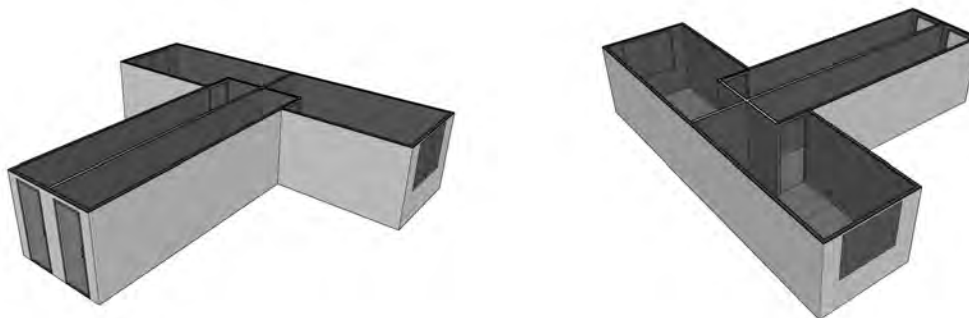


Figure 3.8: Isometric views of the Metal Prop CAD Model. The left view is from the AD corner, and the right view is from the BC corner. These views also resemble those of the Insulated Metal Prop CAD model because the differentiating factor between the two props was the interior wall lining.

3.2 Fuel Loads

Three different fuel loads were used throughout the experiments: one consisting of three wooden pallets and a bale of straw; one composed of three wooden pallets, a bale of straw, and three sheets of OSB; and one containing modern furnishings, specifically a couch, a coffee table, and an end table on top of carpet and padding over a layer of OSB.

3.2.1 Pallets

Pallets and straw is a common fuel package that's compliant with *NFPA 1403* and utilized throughout the fire service during live-fire training. This configuration, referred to as the “pallets” fuel load in this document, is shown in Figure 3.9. Three pallets were positioned in a triangular configuration with one pallet laying flat and the two remaining pallets standing on end leaning against each other. A bale of straw was scattered in the open spaces between the pallet slats, as well as the cavity between the two standing pallets. The average weight of each pallet was $41.7 \text{ lbs} \pm 5.1 \text{ lbs}$ ($18.9 \text{ kg} \pm 2.3 \text{ kg}$), and the average weight of each straw bale was $32.2 \text{ lbs} \pm 7.9 \text{ lbs}$ ($14.6 \text{ kg} \pm 3.6 \text{ kg}$). A 4.0 ft (1.2 m) by 4.0 ft (1.2 m) steel platform was used to elevate the fuel load 1.0 ft (0.3 m) above the floor. The location of the platform within the fire room can be seen in Figure 3.10. Remote ignition of this fuel load occurred via an electronic matchbook located within the straw in the center of the pallet formation.

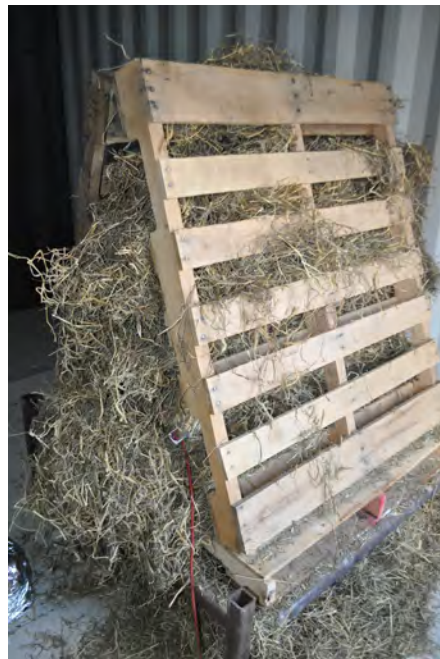


Figure 3.9: Image of the pallets fuel load.

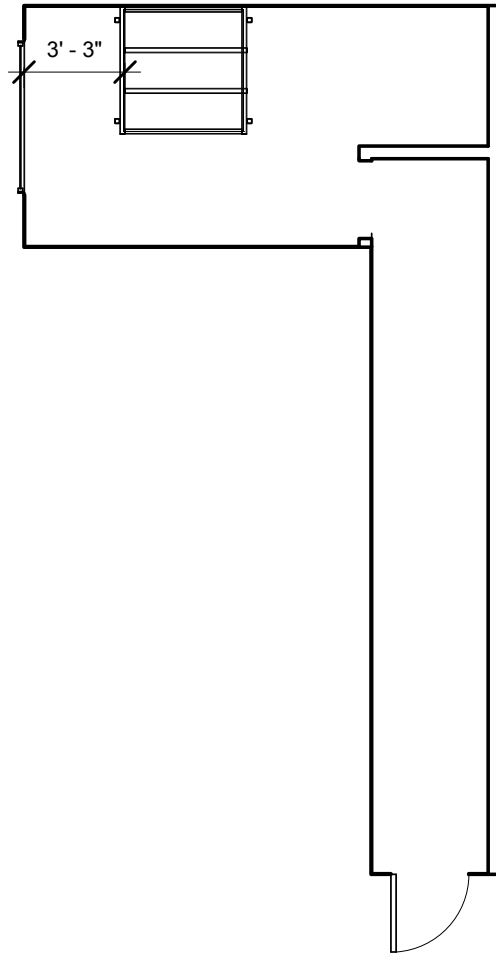


Figure 3.10: Floor plan showing dimensioned location of the steel platform used to support the pallets fuel load within the fire room.

3.2.2 Pallets & OSB

Some fire training academies incorporate the use of OSB in addition to pallets and straw with the expectation that adding OSB in varying configurations creates a more realistic experience for students. The variation studied for this project, referred to as the “pallets and OSB” fuel package throughout this report, contained three pallets and one bale of straw configured on a steel platform like the pallets fuel load. Three 0.625 in. (16 mm) thick sheets of OSB were positioned around the pallets and straw setup as shown in Figure 3.11. Two of the sheets, each measuring 7.5 ft (2.3 m) by 4.0 ft (1.2 m) with an average weight of 36.2 lbs \pm 5.3 lbs (16.4 kg \pm 2.4 kg), were centered behind the steel platform and held against the wall by steel chains. The third sheet, measuring 8.0 ft (2.4 m) by 4.0 ft (1.2 m) with an average weight of 37.0 lbs \pm 4.6 lbs (16.8 kg \pm 2.1 kg), was centered above the pallets and straw fuel load and supported by steel chains. The location of the steel platform in the fire room was the same as in the pallets fuel load configuration, shown in Figure 3.10. Remote ignition for this fuel load occurred via an electronic matchbook located within the straw in the center of the pallet formation.



Figure 3.11: Image of the pallets & OSB fuel load.

3.2.3 Furniture

To provide a real-world comparison to the wood-based fuel packages, a fuel load with residential furnishings was also utilized during experiments. This fuel package, referred to as the “furniture” fuel load, is pictured in Figure 3.12. It contained six components: a couch with polyurethane cushions, coffee table, end table, and polyolefin carpet on top of a layer of polyurethane padding and OSB. The average weight of each item is listed in Table 3.1, and their locations within the fire room are shown in Figure 3.13. Remote ignition for this fuel load occurred via an electronic matchbook resting on the couch corner closest to the fire room window.

Table 3.1: Average Weight of Each Item from the Furniture Fuel Load Configurations

Item	Average Weight [lbs (kg)]
Couch	104 lbs \pm 5.7 lbs (47.4 kg \pm 2.6 kg)
Coffee table	45.0 lbs \pm 0.4 lbs (20.4 kg \pm 0.2 kg)
End table	34.4 lbs \pm 0.2 lbs (15.6 kg \pm 0.1 kg)
Carpet	28.0 lbs \pm 0.9 lbs (12.7 kg \pm 0.4 kg)
Padding	13.0 lbs \pm 0.2 lbs (5.9 kg \pm 0.1 kg)
OSB floor	156 lbs \pm 7.0 lbs (70.8 kg \pm 3.2 kg)



Figure 3.12: Furniture fuel load consisting of a couch, coffee table, end table, and carpet on top of padding and OSB.

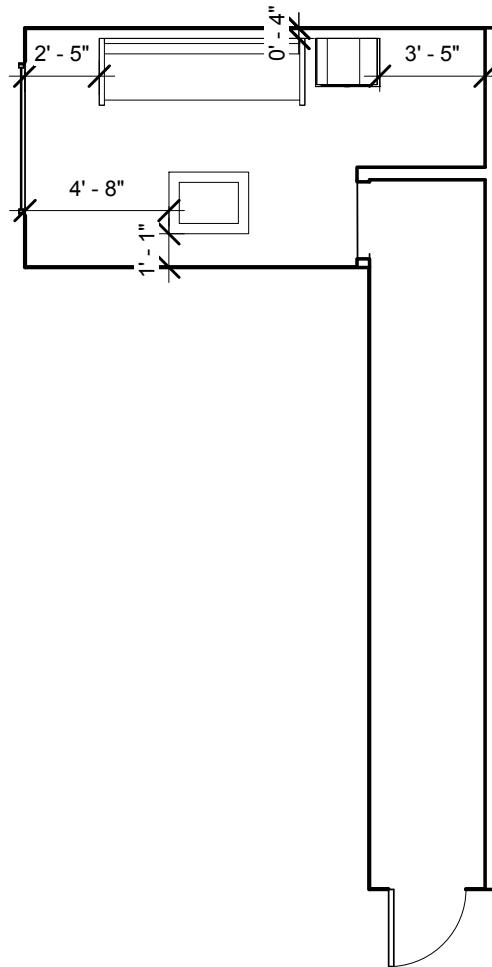


Figure 3.13: Floor plan showing dimensioned locations of the various items from the furniture fuel package within the fire room.

3.3 Instrumentation

Various types of measurement devices were installed throughout the training props to determine gas temperature, total heat flux, pressure, gas velocity, and oxygen concentration during experiments. This section provides specific details about the instrumentation, specifically the measurement locations within the props and the uncertainty associated with the different measurements.

3.3.1 Measurement Locations

Each prop contained one vertical array of eight thermocouples paired with a heat flux gauge, two vertical arrays of seven thermocouples each paired with a heat flux gauge, two vertically-aligned pairs of pressure probes, two vertically-aligned pairs of gas sampling probes, and two vertically-aligned pairs of pressure probes.

A floor plan of the instrumentation locations throughout the prop is presented in Figure 3.14. Overall, the measurement device locations were similar between the three props. Note, some measurement locations varied slightly during certain tests; these specific instances are described below.

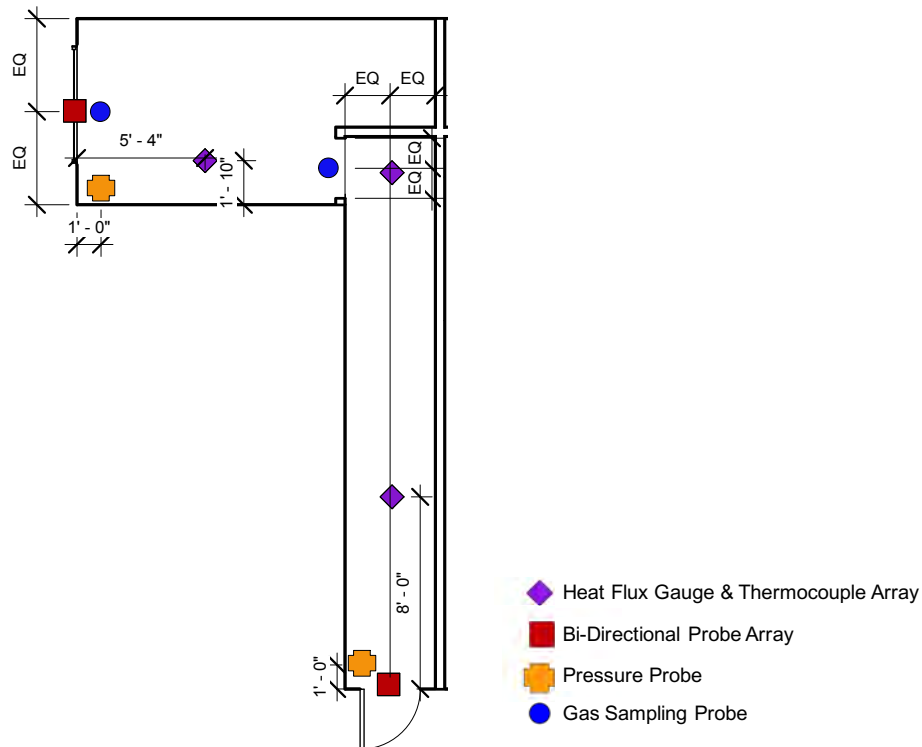


Figure 3.14: Floor plan showing the standard locations of the instrumentation devices used to collect data from the fire environment during experiments.

Thermocouple Arrays Chromel-alumel, or type K, thermocouple wire was used to create vertical arrays of bare-bead thermocouples with nominal diameters of 0.02 in. (0.5 mm). The thermocouples were spaced at 1.0 ft (0.3 m) increments from the ceiling to the floor at the locations marked by purple diamonds in Figure 3.14. In the fire room, a vertical array consisting of eight thermocouples provided measurements at 1.0 in. (25 mm), 1.0 ft (0.3 m), 2.0 ft (0.6 m), 3.0 ft (0.9 m), 4.0 ft (1.2 m), 5.0 ft (1.5 m), 6.0 ft (1.8 m), and 7.0 ft (2.1 m) below the ceiling. In the hallway, two vertical arrays consisting of seven thermocouples provided measurements at 1.0 ft (0.3 m), 2.0 ft (0.6 m), 3.0 ft (0.9 m), 4.0 ft (1.2 m), 5.0 ft (1.5 m), 6.0 ft (1.8 m), and 7.0 ft (2.1 m) below the ceiling. The vertical spacing of the thermocouples were consistent across the training props.

Heat Flux Gauges Total heat flux (convective and radiative) was measured by nominal 1.0 in. (25 mm) diameter, water-cooled, Schmidt-Boelter heat flux gauges located at the positions marked by purple diamonds in Figure 3.14. The gauge in the fire room was located 8.0 in. (20.3 cm) above the floor and faced upwards at the ceiling to measure the total heat flux from the hot gas layer in the vertical direction. Additionally, the two hallway gauges were positioned to measure the total heat flux from the fire room in the horizontal direction 3.0 ft (0.9 m) above the floor.

Pressure Probes Setra Model 264 differential pressure transducers (measurement range of 0–0.5" W.C.) connected to the copper sampling probes via polyvinyl tubing were used to acquire pressure data during experiments. Pressure sensors were installed in the fire room and in the hallway at the positions marked by the orange symbol in Figure 3.14. At each location, pressure probes were located 1.0 ft (0.3 m) and 7.0 ft (2.1 m) above the floor.

Bi-Directional Probes Bi-directional probes (BDPs) paired with single type K, inconel-sheathed thermocouples having nominal diameters of 0.63 in. (16 mm) were used to measure gas velocity. Each stainless steel probe was connected to a Setra Model 264 differential pressure transducer (measurement range of 0–0.1" W.C.) that was similar to those described in the previous paragraph. Five BDPs were centered laterally in the fire room window and hallway door openings, as denoted by the red squares in Figure 3.14. The probes at the window were vertically-spaced at increments of 8.0 in. (20.3 cm) above the sill, which was located 3.0 ft (0.9 m) above the floor of the fire room. The five BDPs at the hallway door opening were vertically-spaced at increments of 13.5 in. (34.3 cm) above the floor.

Gas Sampling Probes Gas samples were collected through stainless steel tubes at heights of 4.0 in. (10.2 cm) and 4.0 ft (1.2 m) above the floor at the locations marked by blue circles in Figure 3.14. A nominal 0.75 CFM pump (Cole Palmer Model L-79200-30) was used to pull gas samples from each measurement location through a steel tube, a coarse paper filter (Solberg Model 8242), and a condensing trap (Clean Air 0517SS) to remove moisture from the sample. The samples were then transported through a drying tube (Perma Pure Model FF-250-SG-2.5G) and a fine filter (FF-250-E-2.5G) before reaching the Siemens OxyMat6 Gas Analyzers.

Measurement Location Variances There were instances during some experiments in which the positions of certain instrumentation devices varied slightly from the typical locations described in the above paragraphs.

The location of the paired heat flux gauge and thermocouple array in the fire room during experiments with the furniture fuel package varied slightly from that shown in Figure 3.14. Due to the coffee table and couch components of the furniture fuel load, the heat flux gauge and thermocouple array were moved to a position located 5.8 ft (1.8 m) from the wall with the window and 3.5 ft (1.1 m) from the front wall of the fire room, a position that approximately centered the instrumentation pair between the coffee table and couch.

Aspects of the typical instrumentation layout pictured in Figure 3.14 were modified to reduce potential obstructions and create more space for the firefighters to advance down the hall during experiments that involved interior suppression. First, the two thermocouple arrays in the hall were moved from being centered between the walls to being mounted against the longer wall. Also, the five BDPs in the door opening were moved approximately 8 in. (20 cm) away from the center of the opening. Lastly, the two heat flux gauges in the hallway were removed entirely and replaced by Schmidt-Boelter heat flux gauges mounted on the helmet of the firefighter at the nozzle. To measure the incident heat flux from conditions in front of and above the firefighter, one gauge was positioned to “look” horizontally in front of the firefighter, and the other was positioned to “look” vertically above the firefighter. The sensors, labeled “HF1” and “HF2”, respectively, are pictured in Figure 3.15. Data from the two gauges were recorded by a microcontroller (Arduino Yun) that was also mounted to the helmet.



Figure 3.15: Image of the helmet worn by the firefighter at the nozzle during experiments involving interior suppression. Two heat flux gauges mounted on the helmet, labeled “HF1” and “HF2” measured the incident heat flux exposure to the firefighter in the horizontal and vertical directions, respectively.

3.3.2 Measurement Uncertainty

There are different components of uncertainty in the measured values reported in this document, specifically gas temperature, total heat flux, pressure, gas velocity, oxygen concentration, length, mass, structure leakage, and water flow rate. Uncertainties are grouped into two categories according to the method used to estimate them. Type A uncertainties are those evaluated by statistical methods, and Type B are those evaluated by other means [28]. Type B analysis of systematic uncertainties involves estimating the upper (+ a) and lower (− a) limits for the quantity in question such that the probability that the value would be in the interval ($\pm a$) is essentially 100 %. After estimating uncertainties by either Type A or B analysis, the uncertainties can be combined in quadrature to yield the combined standard uncertainty. Multiplying this combined standard uncertainty by a coverage factor of two results in an expanded uncertainty with a 95 % confidence interval (2σ). For some components, such as the zero and calibration elements, uncertainties were derived from referenced instrument specifications. For other components, referenced research results and past experience with the instruments provided input for the uncertainty determination.

Gas Temperature According to Omega Engineering, the manufacturer of the thermocouple wire utilized during the experiments, the standard uncertainty associated with the wire itself is ± 2.2 °C at 277 °C and ± 9.5 °C at 871 °C [29]. Additionally, radiative effects to the thermocouple should be considered. Several studies have attempted to quantify these effects on thermocouple measurement uncertainty in compartment fires [30, 31]. These studies indicated that when the thermocouple is located in the upper gas layer, the actual temperature of the surrounding gas is typically higher than the measured temperature, although this difference is not as pronounced as when the thermocouple is in the lower layer. When the thermocouple is in the lower layer, particularly during a fully involved compartment fire, the percent error in measured temperature can be much larger. Because of these radiative contributions, the expanded total uncertainty is estimated as ± 15 %.

Heat Flux The manufacturer of the heat flux gauges, Medtherm Corporation, reports a ± 3 % calibration expanded uncertainty for the devices [32]. Results from an international study on total heat flux gauge calibration and response demonstrated that the total expanded uncertainty of a Schmidt-Boelter gauge is typically ± 8 % [33].

Pressure Differential pressure reading uncertainty components were derived from pressure transducer instrument specifications and previous experience with the transducers. Each transducer was factory calibrated by the manufacturer to verify that the zero and span resulted in an accuracy of ± 1 % [34]. The total expanded uncertainty associated with the pressure data from these experiments is estimated to be ± 10 %.

Gas Velocity A gas velocity measurement study that focused on flow through doorways during pre-flashover compartment fires yielded total expanded uncertainties ranging from ± 14 %

to $\pm 22\%$ for measurements from BDPs similar to those used throughout the experiments described in this report [35]. The total expanded uncertainty for gas velocity measured during these experiments is estimated to be $\pm 18\%$.

Oxygen Concentration The oxygen concentration measurement range of Each Siemens Oxy-Mat6 Gas Analyzer was 0–25 %. The gas sampling instruments used throughout the experiments described in this report have demonstrated a relative expanded uncertainty of $\pm 1\%$ when compared to span gas volume fractions [36]. According to a study by Lock et al. [37], the non-uniformities and movement of combustion gases in addition to the limited amount of sampling points considered in each experiment result in an estimated expanded uncertainty of $\pm 12\%$.

Length Length measurements, such as the room dimensions and instrumentation locations, were made with either a hand held laser measurement device with an accuracy of ± 0.25 in. (± 6.0 mm) over a range of 2 ft (0.6 m) to 50 ft (15.2 m) [38] or a ± 0.02 in. (± 0.51 mm) resolution steel measuring tape manufactured in compliance with NIST Manual 44 [39], which specifies a tolerance of ± 0.06 in. (± 1.5 mm) for 30 ft (9.1 m) tapes and ± 0.25 in. (± 6.4 mm) for 100 ft (30.5 m) tapes. These uncertainties are all well within the precision of the reported dimensions, which are typically rounded to the nearest inch. Some issues, such as levelness of the device and “soft” edges on upholstered furniture, result in an estimated expanded uncertainty of $\pm 1.0\%$ for reported length measurements.

Mass The load cell used to weigh the fuels prior to the experiments had a measurement range of 0 lb (0 kg) to 441 lb (200 kg) with a resolution of 0.11 lb (0.05 kg) and a calibration uncertainty within 1 % [40]. The total expanded uncertainty for the fuel weights measured by the load cell that are presented in this report is estimated to be less than $\pm 5\%$.

Structure Leakage To characterize ventilation within the structure, an air leakage measurement system was used to measure the amount of leakage associated with the training prop before each test [41]. *ASTM E779-10, Standard Test Method for Determining Air Leakage Rate by Fan Pressurization* was followed to determine the air leakage rate of the prop before each experiment [42]. The measured leakage rates were recorded in units of air changes per hour at 50 Pa (ACPH50). Retrotec, the manufacturer of the leakage measurement system (Model 5101), reports an accuracy of $\pm 5\%$ for the system.

Water Flow Rate Water flow rate was measured with a 1.5 in. (3.8 cm) diameter electromagnetic flow meter from Badger Meter, Inc. (Model M2000). The meter consisted of stainless steel pipe lined with a non-conductive material. Energized coils on the outside of the non-conductive material imposed a magnetic field across the pipe, and when the conductive fluid (water) flowed across the magnetic field, a voltage proportional to flow velocity was produced. The manufacturer reports a $\pm 0.25\%$ calibration uncertainty for the flow rate measurement [43].

4 Experimental Procedure

The experiments detailed throughout this report can be divided into five categories:

1. *Burn In*: Initial experiments conducted in each side of the Metal Prop and Insulated Metal Prop
2. *Prop & Fuel Comparison*: Experiments designed to study the differences between wall configurations and fuel loads
3. *Prop & Fuel Repeatability*: Replicates of prop and fuel comparison experiments performed to evaluate the repeatability of wall configurations and fuel loads
4. *Ventilation Effects*: Experiments focused on examining the impact of changing ventilation to the fire room
5. *Suppression Effects*: Experiments to determine changes in the thermal conditions that occurred as a result of interior suppression by a firefighter in each type of prop

The 37 experiments were conducted following four types of procedures. In general, the phrase “vent door” or “vent window” in the test procedure name means either the door or window, respectively, was opened at some time after ignition, and the phrase “open door” in the procedure name means the hallway door was open for the entire duration of the test.

The following sections include thorough descriptions of each test category and their procedures. Additionally, Table 4.1 is provided on the following page to summarize all experiments in the different test categories.

Table 4.1: Summary of Experiments

Test #	Prop	Fuel Load	Procedure	Category
1	Metal	Pallets	Vent Door	Burn In
2	Metal	Pallets & OSB	Vent Door	Burn In
3	Insulated Metal	Pallets	Vent Door	Burn In
4	Insulated Metal	Pallets & OSB	Vent Door	Burn In
5	Gypsum	Furniture	Vent Door	Prop & Fuel Comparison
6	Gypsum	Furniture	Vent Door	Prop & Fuel Repeatability
7	Gypsum	Furniture	Vent Door	Prop & Fuel Repeatability
8	Gypsum	Pallets	Vent Door	Prop & Fuel Comparison
9	Gypsum	Pallets & OSB	Vent Door	Prop & Fuel Comparison
10	Metal	Furniture	Vent Door	Prop & Fuel Comparison
11	Metal	Pallets	Vent Door	Prop & Fuel Comparison
12	Metal	Pallets	Vent Door	Prop & Fuel Repeatability
13	Metal	Pallets	Vent Door	Prop & Fuel Repeatability
14	Metal	Pallets & OSB	Vent Door	Prop & Fuel Comparison
15	Insulated Metal	Furniture	Vent Door	Prop & Fuel Comparison
16	Insulated Metal	Pallets	Vent Door	Prop & Fuel Comparison
17	Insulated Metal	Pallets & OSB	Vent Door	Prop & Fuel Comparison
18	Insulated Metal	Pallets & OSB	Vent Door	Prop & Fuel Repeatability
19	Insulated Metal	Pallets & OSB	Vent Door	Prop & Fuel Repeatability
20	Gypsum	Furniture	Vent Window	Ventilation Effects
21	Gypsum	Pallets	Vent Window	Ventilation Effects
22	Gypsum	Pallets & OSB	Vent Window	Ventilation Effects
23	Metal	Furniture	Vent Window	Ventilation Effects
24	Metal	Pallets	Vent Window	Ventilation Effects
25	Metal	Pallets & OSB	Vent Window	Ventilation Effects
26	Insulated Metal	Furniture	Vent Window	Ventilation Effects
27	Insulated Metal	Pallets	Vent Window	Ventilation Effects
28	Insulated Metal	Pallets & OSB	Vent Window	Ventilation Effects
29	Metal	Pallets	Open Door, No Action	Ventilation Effects
30	Metal	Pallets	Open Door, Vent Window	Ventilation Effects
31	Metal	Furniture	Open Door, No Action	Ventilation Effects
32	Metal	Furniture	Open Door, Vent Window	Ventilation Effects
33	Metal	Pallets & OSB	Open Door, No Action	Ventilation Effects
34	Metal	Pallets & OSB	Open Door, Vent Window	Ventilation Effects
35	Gypsum	Pallets & OSB	Open Door, No Action	Suppression Effects
36	Metal	Pallets & OSB	Open Door, No Action	Suppression Effects
37	Insulated Metal	Pallets & OSB	Open Door, No Action	Suppression Effects

4.1 Burn In Experiments

The “Burn In” test category is composed of the first experiment conducted in each side of both metal props. These four initial tests were categorized as Burn In experiments after discovering that some visual observations from the first test in each side of the metal containers were unique and did not occur during later experiments. For example, the flame spread along the exterior surface of the prop pictured in Figure 4.1 only occurred during the first experiment in each side of the Metal Prop. Data from the Burn In experiments were compared to data from later replicate tests to determine if the visual differences translated to quantifiable differences in fire dynamics.



Figure 4.1: Example of fire spread to the exterior surface of the Metal Prop during the initial experiment. This phenomenon was caused by the exterior paint reaching its autoignition temperature and igniting.

The Burn In tests executed in the right side of each metal container used the pallets fuel load, while those conducted in the left side of the containers used the pallets and OSB fuel load. The four experiments followed an identical procedure, referred to as the “vent door” procedure, outlined in Table 4.2 and Figure 4.2. The window and door of the prop were closed at the start of the test. The fuel load was ignited, and the hall door was opened six minutes later. Twelve minutes after the hall door was opened, the experiment was completed, the fire room window was opened, and water was applied to any remaining fuel to suppress the fire.

Table 4.2: Event Times for Vent Door Test Procedure

Event	Time (mm:ss)
Ignition (hall door & window closed)	0:00
Hall door opened	6:00
Window opened & fire suppressed	18:00

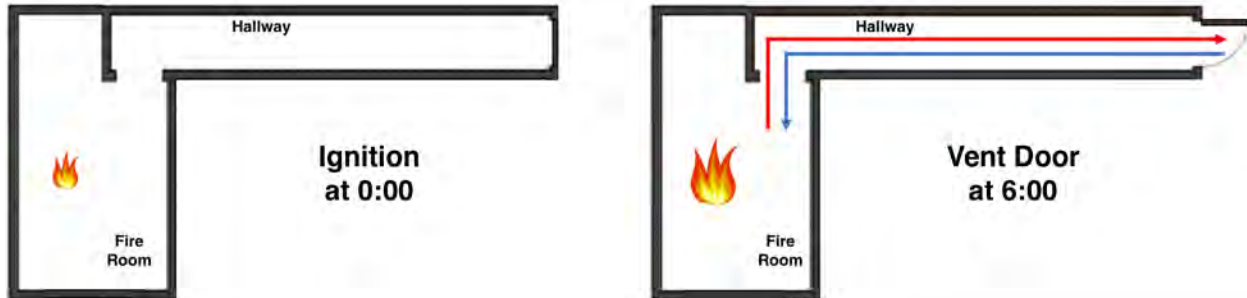


Figure 4.2: Floor plans highlighting the flow path created during tests that followed the vent door procedure. The red arrow shows the direction in which the hot exhaust gases flowed, and the blue arrow shows the direction in which the cool inlet air flowed to the fire for combustion.

4.2 Prop & Fuel Comparison Experiments

Fifteen experiments were designed to assess the repeatability of and differences between the three wall constructions and three fuel packages. Five tests were conducted in each of the three props following the vent door procedure outlined in Table 4.2. The five experiments were composed of one experiment using each type of fuel load and two additional replicate tests with the same fuel load to quantify the repeatability associated with each fuel and wall configuration.

The vent door procedure followed by the fifteen experiments started with both the hall door and fire room window closed when the fuel load was ignited at the start the experiment. Then, six minutes after ignition, the hall door was opened.¹ Twelve minutes later, the window was opened and fire suppressed, marking the end of the test.²

Two experiments in each set of five were replicates of a vent door test. Results from the two replicates and the original experiment that they replicated were compared amongst each other to quantify the repeatability associated with each wall construction and fuel package.

¹When the furniture fuel load was used in either type of metal prop, opening the hall door at six minutes after ignition failed to produce fire regrowth. So, during these experiments (Tests 10 & 15), the door was opened four minutes after ignition to achieve regrowth.

²In Test 5, the fire was suppressed at an earlier time because permanent damage to structural members of the Gypsum Prop due to the intensity of the fire started to become a concern around nine minutes after the hall door was opened.

Relevant comparisons between the fifteen experiments were also made to analyze differences between wall configurations and fuel loads. Additionally, data from the Burn In tests were compared to data from relevant prop and fuel comparison experiments to determine if the unique visual observations from the Burn In experiments translated to quantifiable differences in thermal conditions.

4.3 Ventilation Effects Experiments

To compare how different ventilation configurations affect the fire environment, results from fifteen experiments using three different types of ventilation configurations were analyzed.

Nine of the tests, one for each fuel package and prop combination, followed the “vent window” configuration outlined in Table 4.3 and Figure 4.3. This configuration was similar to the vent door procedure, except the fire room window was opened six minutes after ignition,³ and the hall door remained closed for the entire duration of the experiment.

Table 4.3: Event Times for Vent Window Test Procedure

Event	Time (mm:ss)
Ignition (hall door & window closed)	0:00
Window opened	6:00
Fire suppressed	18:00

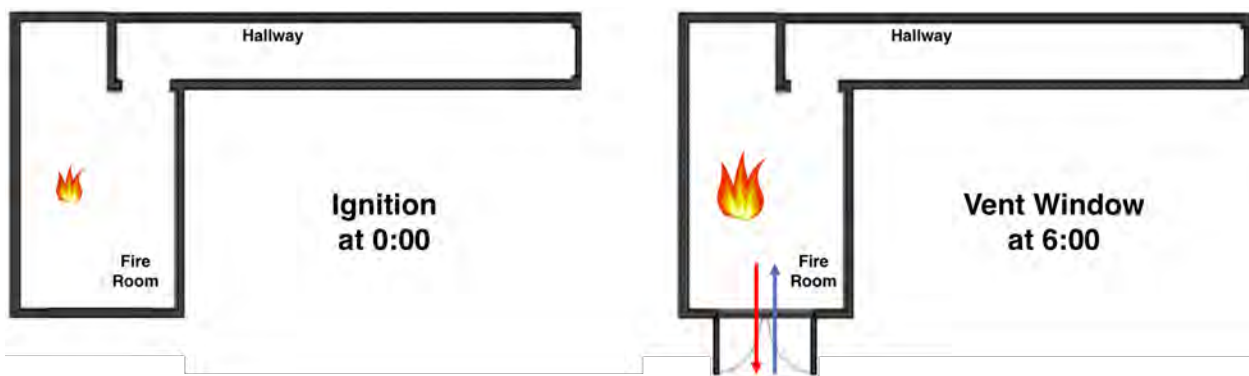


Figure 4.3: Floor plans highlighting the flow path created during tests that followed the vent window procedure. The red arrow shows the direction in which the hot exhaust gases flowed, and the blue arrow shows the direction in which the cool inlet air flowed to the fire for combustion.

³Similar to the vent door procedure, when the furniture fuel load was used in either type of metal prop, the window was opened four minutes after ignition to achieve regrowth. However, even with this earlier vent time, regrowth was not able to be achieved during Test 23 in the Metal Prop.

The six remaining tests were conducted in the Metal Prop and used two different procedures, outlined in Table 4.4 and Figure 4.4, for each fuel package. For both test configurations, referred to as “open door, no action” and “open door, vent window”, the hall door was opened and the fire room window was closed at the start of the experiment when the fuel package was ignited. For the open door, vent window configuration, the fire room window was opened six minutes after ignition. Six minutes after the window was opened, the test was ended and water was applied to any remaining fuel to suppress the fire. Alternatively for the open door, no action procedure, the fire room window was opened and water was applied to any remaining fuel to suppress the fire 12 minutes after ignition.

Table 4.4: Event Times for Open Door, No Action & Open Door, Vent Window Test Procedures

Event	Time (mm:ss)	
	Open Door, No Action	Open Door, Vent Window
Ignition (hall door opened, window closed)	0:00	0:00
Window opened	12:00	6:00
Fire suppressed	12:00	12:00

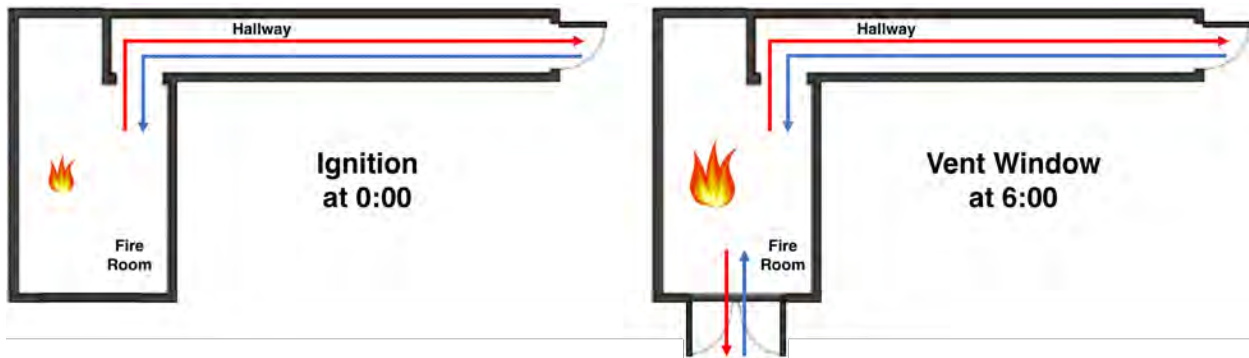


Figure 4.4: Floor plans highlighting the flow path created during tests that followed the open door procedures. The red arrows show the direction in which the hot exhaust gases flowed, and the blue arrows show the direction in which the cool inlet air flowed to the fire for combustion.

4.4 Suppression Effects Experiments

Three experiments were completed to evaluate and compare the effect of suppression on the thermal environment, specifically the immediate thermal exposure encountered by the firefighter at the nozzle, between the three different wall constructions. Each experiment used the pallets and OSB fuel load and followed the procedure outlined in Table 4.5 and Figure 4.5.

The hall door was opened and the fire room window was closed when the fuel load was ignited at the start of each test. Six minutes after ignition, two firefighters advanced a 1.75 in. (44 mm) diameter hoseline through the doorway and down the hall while flowing water from a combination nozzle in a straight stream pattern at 150 gpm and 75 psi at the nozzle. The technique of flowing water while advancing down the hall was implemented to fully utilize the cooling effects of suppression. The stream was applied in a wall-ceiling-wall pattern based on the methodology of a previous research project that examined various aspects of fire attack and suppression [27]. The nozzle firefighter was instructed to stop flowing only after feeling conditions had improved to a tolerable level. After the nozzle was shutdown, the experiment was concluded, and the backup firefighter exited the training prop and opened the fire room window to vent the structure. Note, the window remained closed and the door remained opened throughout the test duration past the point of water flow to maintain a constant ventilation profile so that the changes in conditions during the time of firefighter operation would be independent of changes in ventilation.

Table 4.5: Event Times for Suppression Effects Test Procedure

Event	Time (mm:ss)
Ignition (hall door opened & window closed)	0:00
Firefighters enter hallway & approach fire room while flowing water	6:00

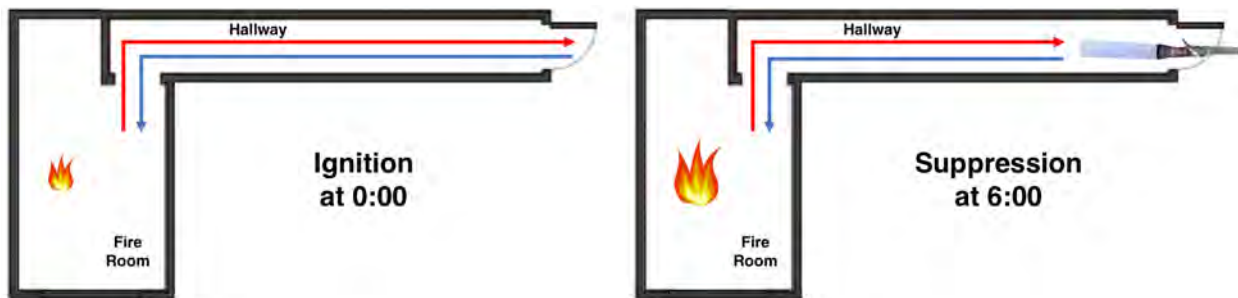


Figure 4.5: Floor plans highlighting the flow path created during suppression effects tests. The red arrows show the direction in which the hot exhaust gases flowed, and the blue arrows show the direction in which the cool inlet air flowed to the fire for combustion.

5 Results & Discussion

The first section of this chapter describes the methods used to analyze and compare data from the 37 experiments listed in Table 4.1. The sections that follow contain results from various analyses and comparisons accompanied by discussions that provide additional insight into the project objectives outlined in Section 1.2.

5.1 Methodology

A variety of techniques were used to analyze experimental data. Fire growth and regrowth start times; fire growth and regrowth rates; critical maximum, minimum, and average values; and results from comparisons between experimental data sets are included and discussed throughout this chapter.

5.1.1 Growth Times & Rates

The start time of fire growth relative to ignition was determined for every experiment. This parameter, referred to as “growth time”, was defined as the time at which the temperature measured by the thermocouple 1.0 in. (25 mm) below the ceiling of the fire room started to increase in response to fire growth following ignition. A temperature increase was determined to be in response to fire growth if the temperature increased with each measurement over a span of five seconds (i.e., five measurements because temperature data were collected at 1 Hz) and if the temperature after the five second increase was measurably larger (greater than 15 %, the estimated measurement uncertainty) than the temperature at the start of the increase.

During some experiments, the fire became ventilation-limited shortly after ignition and decayed towards a new steady state until a vent was opened to supply the fire environment with additional oxygen, causing the fire to regrow and develop. For these tests, a “regrowth time” was computed as the time between the vent being opened and the start of the increase in temperatures 1.0 in. (25 mm) below the fire room ceiling in response to fire regrowth.

Fire growth and regrowth rates were computed alongside the growth and regrowth times. Figure 5.1 contains plots of the temperatures measured 1.0 in. (25 mm) below the fire room ceiling during repeatability tests with the furniture fuel load in the Gypsum Prop. In the figure, vertical lines mark the growth and regrowth times, and shaded areas mark the periods over which the growth and regrowth rates were computed for each experiment. All temperature data plots over periods in which the fire decayed into a ventilation-limited state after initial growth are of similar shape as those appearing in Figure 5.1.

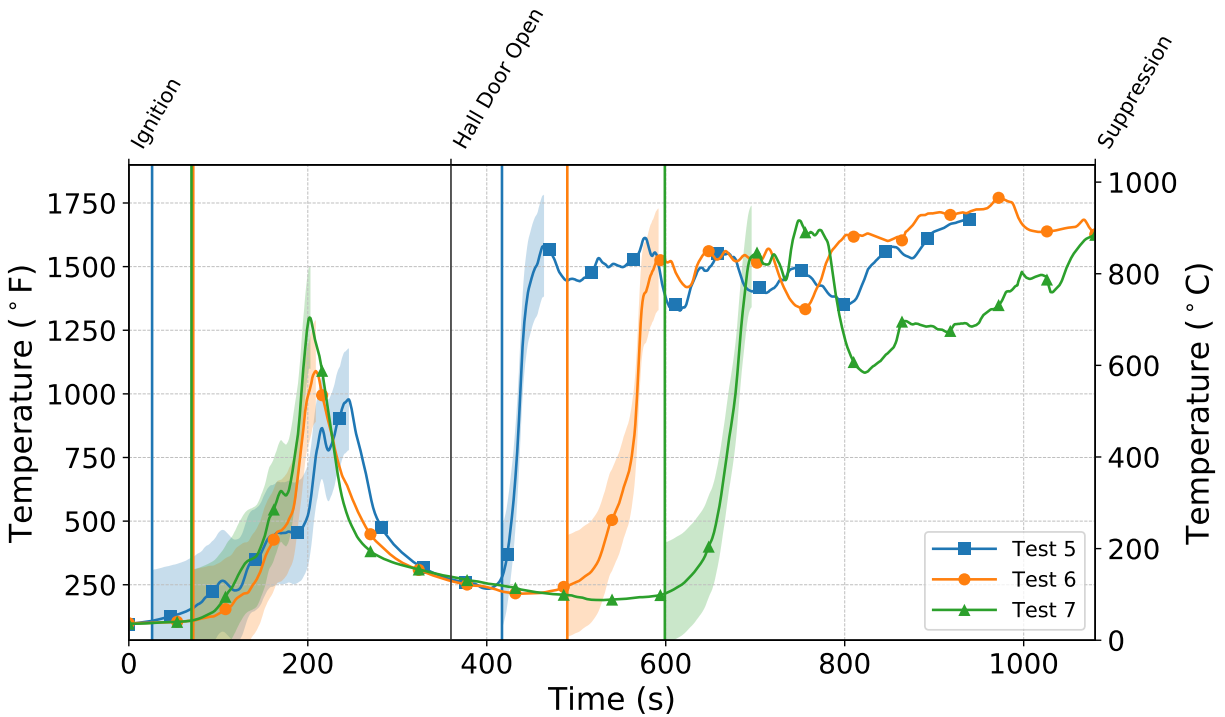


Figure 5.1: Plots of temperature data measured 1.0 in. (25 mm) below the fire room ceiling during the three repeatability tests conducted in the Gypsum Prop with the furniture fuel load. Vertical lines mark the growth and regrowth times for the identically colored plot, and shaded areas represent the duration over which growth and regrowth rates were calculated for the plot of similar color. Note, the fire in Test 5 (blue plot) was suppressed early to prevent the structural members of the prop from being permanently damaged.

5.1.2 Critical Values & Exposure Limits

Maximum, minimum, and average values of various data sets are used to compare and discuss results between experiments in upcoming sections. Differences in these values were considered significant if they were distinguishable from their estimated measurement uncertainty described in Section 3.3. Additionally, plots of temperature, heat flux, gas velocity, and oxygen concentration data were generated and are used to describe certain results. Lastly, heat flux and temperature measurements are compared to the exposure limits of PPE listed in Table 5.1.

The exposure limits in the table were selected based on published research results and NFPA standards. A 2017 NIST grant/contract report by Horn et al. [44] stated that visible thermal damage (cracking, bubbling, grazing) was observed on SCBA facepiece lenses after 90 seconds of radiant exposure to 10 kW/m². Additionally, a 2013 study by NIST [45] discovered that the surface of a facepiece lens under a radiant exposure of 15 kW/m² reached its glass transition temperature of 284 °F (140 °C) after approximately 30 seconds, and one or more holes developed in the lens within 300 seconds of constant radiant exposure. In response to this study, *NFPA 1981: Standard on Open-Circuit SCBA for Emergency Services* [46] was updated to require that positive pressure

Table 5.1: Exposure Limits of Firefighter PPE

Exposure	Duration (s)	Description
10 kW/m ²	90	Visual thermal damage (cracking, bubbling, grazing) to facepiece lens [44]
15 kW/m ²	30	Surface of facepiece lens reaches its glass transition temperature of 284 °F (140 °C) [45]
	300	<i>NFPA 1981</i> requires positive pressure maintained within mask for 24 min after exposure [46]
500 °F (260 °C)	300	<i>NFPA 1971</i> , <i>NFPA 1981</i> require gear to withstand exposure [47]

can be maintained inside an SCBA facepiece for 24 minutes after an exposure to 500 °F (260 °C) for 300 seconds and after an exposure to 15 kW/m² for 300 seconds. Similarly, *NFPA 1971: Standard on Protective Ensembles for Structural Fire Fighting and Proximity Fire Fighting* [47] requires that structural firefighting PPE withstand an exposure to 500 °F (260 °C) for 300 seconds.

5.1.3 Evaluation of Agreeableness Between Data Sets

Basic statistical techniques were used throughout the analysis process to quantify the agreement between data sets from two given tests. These comparable data sets, or sample sets, contained temperature measurements collected at identical locations over similar periods of fire progression. Temperature data were used for the comparisons because temperature was measured at more locations throughout the fire environment than any other data type.

Sample sets used to quantify overall agreeableness of fire conditions between tests were obtained from data collected by thermocouples that were consistently in the upper gas layer during all experiments, regardless of the fuel load or prop. There were 18 thermocouples from five sensor arrays that fulfilled this criteria:

1. Five thermocouples from the BDP array at the fire room window
2. Five thermocouples closest to the ceiling in the fire room array, or the 1TC array
3. Three thermocouples closest to the ceiling in the array at the end of the hallway, or the 2TC array
4. Three thermocouples closest to the ceiling in the array at the start of the hallway, or the 3TC array
5. Two uppermost thermocouples from the BDP array at the hallway door

Figure 5.2 shows the approximate locations of the five thermocouple arrays listed above.

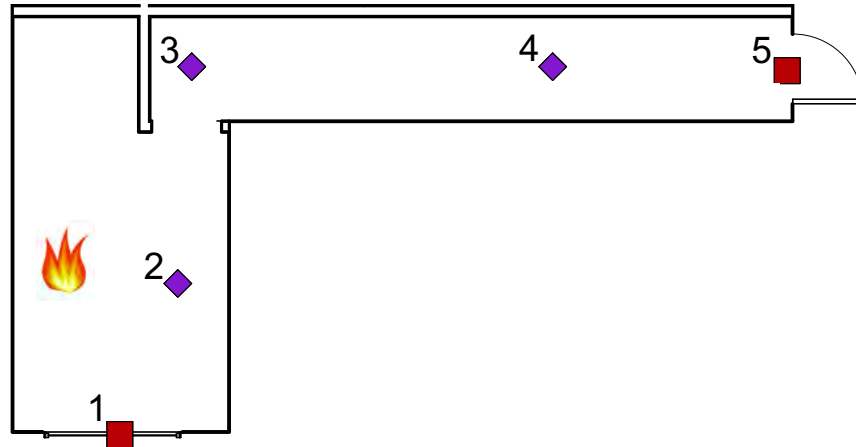


Figure 5.2: Floor plan showing locations of the arrays containing thermocouples considered for the agreeableness evaluation. The numbers correspond to the five thermocouple arrays listed in the beginning of Section 5.1.3.

For each sample set comparison, measurements from the two samples were paired with each other. As an example, consider a comparison between two data sets collected by the thermocouple 2 ft (0.6 m) below the fire room ceiling during the initial growth period of Test 12 and Test 13 plotted in Figure 5.3.

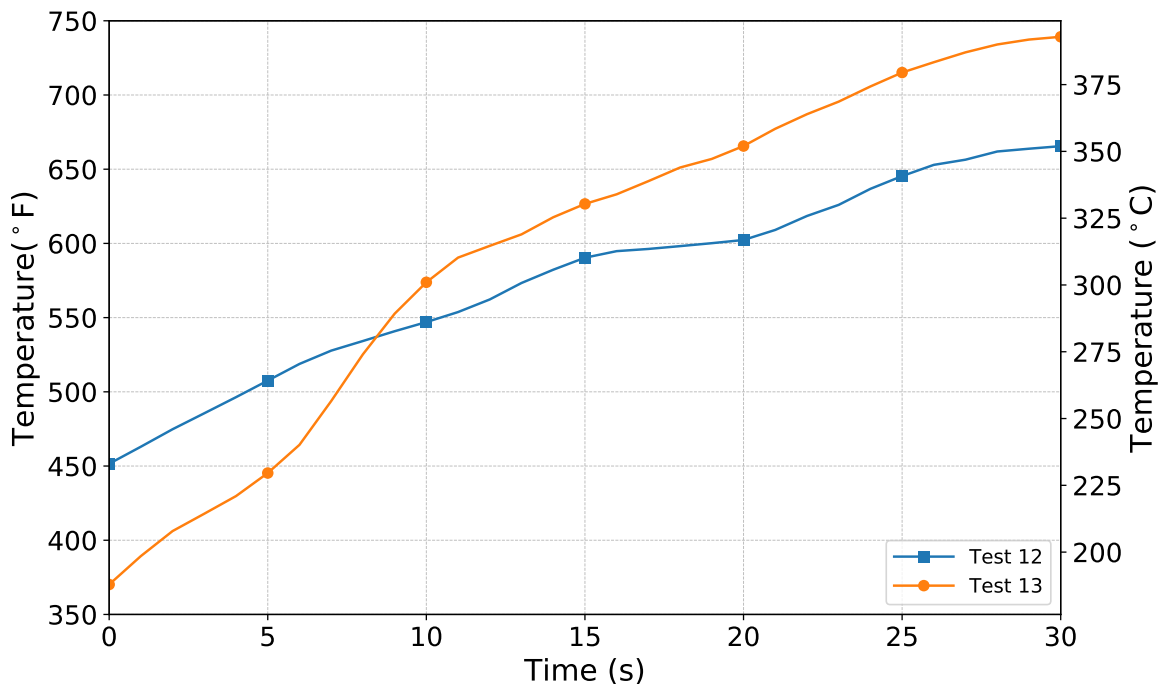


Figure 5.3: Temperature data measured by the thermocouple 2 ft (0.6 m) below the fire room ceiling during the initial growth period of Tests 12 and 13. These data sets are used as an example to outline the method used to quantify overall agreeableness of fire conditions between experiments.

Temperatures in °C, the unit for which the 15 % uncertainty was estimated, at each second from the two experiments were paired with one another. Then, a scatter plot was generated from the paired measurements for each comparison between data sets. For example, Figure 5.4 contains the scatter plot of measurement pairs generated from the data sets plotted in Figure 5.3.

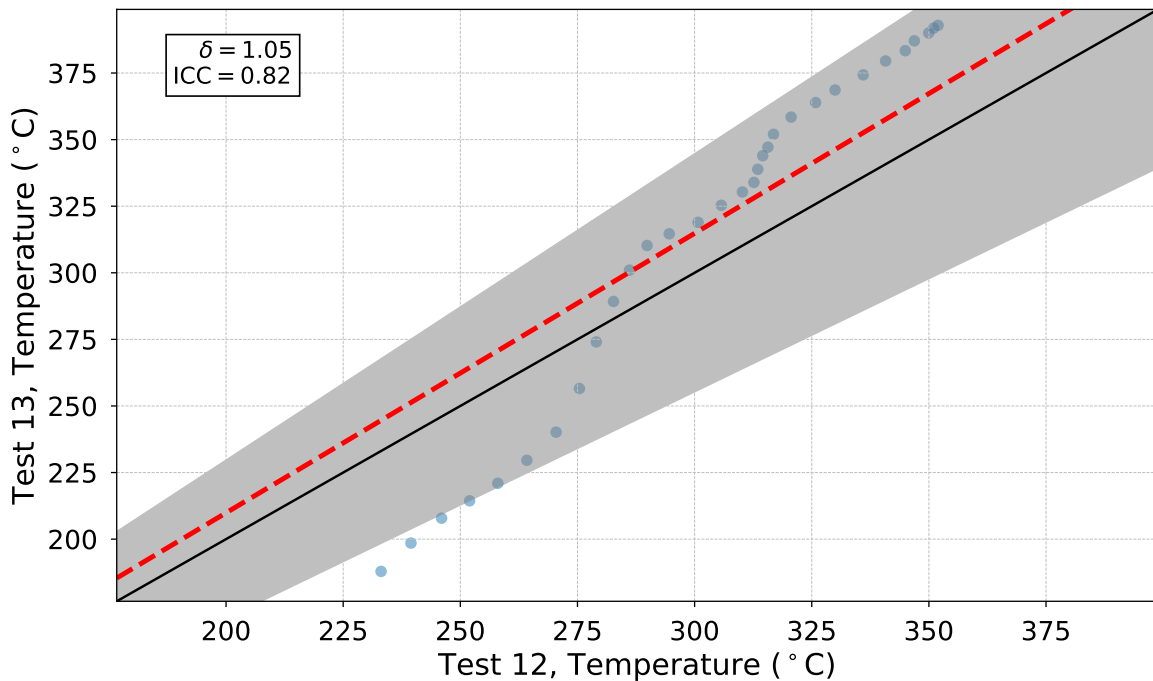


Figure 5.4: Scatter plot of measurement pairs (blue circles) formed by the Test 12 and Test 13 temperature data plotted in Figure 5.3. The black line is the line of perfect agreement, the gray area represents the region on each side of the line within estimated measurement uncertainty, and the red, dashed line corresponds to the linear regression line fitted over the data pairs.

Looking at the chart, the black line represents the line of perfect agreement; if the two samples were identical, all the plotted data pairs (blue circles) would be located on the line. The gray area surrounding the line of perfect agreement represents the area around the line within the range of total measurement uncertainty, $\pm 15\%$ for thermocouple data. Data pairs located in the gray area cannot be distinguished from the measurement uncertainty, and thus, the two values in each of these pairs cannot be considered noticeably different from one another. To determine the extent of the differences between the two sample data sets, a linear regression line forced through (0,0) was fitted over the measurement pairs in each sample comparison. This line is shown as a red, dashed line in Figure 5.4. When the regression line falls outside the gray area, the two sample sets as a whole are considered to be distinguishable, or significantly different, from one another.

Two values were computed across the pairs to evaluate the agreement between the two data sets in a given comparison. First, the intraclass correlation coefficient (ICC) was calculated across measurement pairs. To compute the ICC for a comparison between two data sets forming n pairs of values, the difference between and the sum of the two values in each pair should be determined. For the example comparison between the data plotted in Figure 5.3, lists of the difference between

and sum of the two values in the 31 pairs would resemble L_d and L_a , respectively, defined below. Note, instead of defining all 31 individual pairs within the list, only the pairs obtained at five second intervals from 5 s to 25 s are included.

$$L_a = \{ \dots, 264 + 229, \dots, 286 + 300, \dots, 310 + 330, \dots, 316 + 351, \dots, 340 + 379, \dots \}$$

$$\Rightarrow L_a = \{ \dots, 493, \dots, 586, \dots, 640, \dots, 667, \dots, 719, \dots \}$$

$$L_d = \{ \dots, |264 - 229|, \dots, |286 - 300|, \dots, |310 - 330|, \dots, |316 - 351|, \dots, |340 - 379|, \dots \}$$

$$\Rightarrow L_d = \{ \dots, 35, \dots, 14, \dots, 20, \dots, 35, \dots, 39, \dots \}$$

Then, the ICC can be found using

$$\text{ICC} = \frac{\sigma_a^2 - \sigma_d^2}{\sigma_a^2 + \sigma_d^2 + \frac{2}{n} (n\bar{d}^2 - \sigma_d^2)} \quad (5.1)$$

where σ_a^2 is the variance computed across L_a , σ_d^2 is the variance computed across L_d , and \bar{d} is the mean of the values in L_d [48].

ICC values range from 0 (implying no agreement between measurement pairs) to 1 (implying perfect agreement between measurement pairs). The parameter represents the proportion of the variance between the individual measurement pairs to the total variance across all measurement values; it is the proportion of the total variability in the pairs that is due to differences between the pairs themselves (visually, the difference between the points on the scatter plot) — a type of variability that is independent of the agreeableness of the two sample sets. Thus, the higher the ICC value, the higher the agreement between the two sample sets. An ICC value greater than 0.5 indicates that the majority of the total variance present in the measurements is unrelated to the differences between the two sample sets.

The second value used to assess agreement between compared data sets was the bias factor (δ), which quantified the magnitude of the difference between the linear approximation line and the line of perfect agreement. The bias factor relates a measurement along the x-axis to its corresponding y-axis value on the linear approximation line. Any y value along the linear approximation line can be calculated for a given x measurement as

$$y = \delta x \quad (5.2)$$

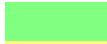


Looking back at Figure 5.4, where Test 12 data and Test 13 data are along the x-axis and y-axis, respectively, a bias factor of 1.05 was computed, meaning that measurements from the Test 13 sample tended to be slightly greater than those from the Test 12 sample. However, because the factor does not exceed 1.15, the difference is within the range of measurement uncertainty, and thus, the two sets are indistinguishable from one another. Alternatively, if δ was less than 1, the experimental data plotted along the x-axis would be larger, on average, than the data plotted along the y-axis.

For all test comparisons presented and discussed throughout this report, the first test mentioned refers to the data along the x-axis, and the second corresponds to the data along the y-axis. For example, consider a comparison labeled “Test 5 vs. Test 7” that has an overall bias value of 0.79. The δ of 0.79 suggests there’s a bias towards the experimental data along the x-axis, which is Test 5 based on the established test order. Furthermore, the bias is considered significant because it’s less than 0.85, the lower limit of δ values that are within the range spanned by the total measurement uncertainty estimated for thermocouples.

To completely quantify agreement between two sample sets for a given comparison, both the bias and the ICC need to be considered. It’s possible for a bias factor computed over a set of measurement pairs to suggest nearly perfect agreement ($\delta \approx 1$) while the ICC value computed over the same group of pairs suggests there is very little relation between the measurement pairs ($ICC \approx 0$). The opposite is also true: the pairs from a given comparison could all be close to the linear approximation line plotted over the scatter of data pairs, producing an ICC value near 1, but the approximation line could be a significant distance away from the line of perfect agreement, resulting in a bias value outside the range spanned by the measurement uncertainty.

Ranges of bias and ICC values based on the total expanded uncertainty of thermocouples ($\pm 15\%$) were established to characterize the level of agreeableness between sets of thermocouple data. Three levels — “highly agreeable”, “agreeable”, and “significantly different” — were defined by the ranges listed in Table 5.2. The colors listed in the table for the three levels were used to shade the cells of tables containing comparison results presented in upcoming sections to denote the level of agreement represented by the tabulated pairs of bias and ICC values.

Table 5.2: Defined Levels of Agreeableness

Level of Agreeableness	Bias Range	ICC Range	Color
Highly Agreeable	0.85–1.15	and 0.75–1.0	
Agreeable	0.85–1.15	and 0.50–0.75	
Significantly Different	< 0.85 or > 1.15	or < 0.50	

To provide further insight into the agreement assessment, a more detailed example outlining each step of the process is presented in Appendix A.

5.2 Repeatability of Wall Configurations & Fuel Loads

As mentioned in Chapter 4, a total of nine experiments — three per prop — were conducted to evaluate the ability of the different props and fuel loads to produce repeatable fire conditions. Each set of three used a different fuel package — the Gypsum Prop set used the furniture fuel load, the Metal Prop set used the pallets fuel load, and the Insulated Metal Prop set used the pallets and OSB fuel load.

All nine tests followed the procedure outlined in Section 4.2, which began with both the door and

window closed at the time of ignition. This starting configuration caused the fire to transition to a ventilation-limited state shortly after initial growth. Six minutes after ignition, the hall door was opened. The new opening allowed enough fresh air into the fire room to cause O₂ concentrations to return to levels suitable for flaming combustion, and the fire regrew and burned until suppression was initiated 12 minutes after the hall door was opened.

Data from experiments with this procedure were divided into two groups: one with data from before ventilation and another with data from after ventilation. Sample data sets were extracted from both groups for each test and compared between replicate experiments to quantify the repeatability of the different prop constructions and fuel loads. The sample sets from before the hall door was opened, referred to as “initial growth” sets, covered a period of time leading up to the fire’s transition to a ventilation-limited state, while those from after the ventilation event, referred to as “post-vent” sets, covered a period of time encompassing the fire’s regrowth and progression into a fully-developed state for the new ventilation configuration.

The temperature data plots formed similar curves during the initial growth period, resembling the shape of those between the “Ignition” and “Hall Door Open” event markers in Figure 5.1. Temperatures throughout the prop increased in response to initial fire growth until the fire transitioned to a ventilation-limited state, at which point they changed trajectory and decreased as the fire decayed. Initial growth sample sets contained data collected over the 30 second period leading up to this change in trajectory.

The start of each post-vent sample was set to be 10 seconds before the regrowth start time, and the end was equal to the second before the end of the experiment when suppression was initiated. Temperature data collected 1.0 in. (25 mm) below the fire room ceiling during the Gypsum Prop repeatability experiments are plotted in Figure 5.5, and colored areas highlight the initial growth and post-vent samples of the similarly colored plot.

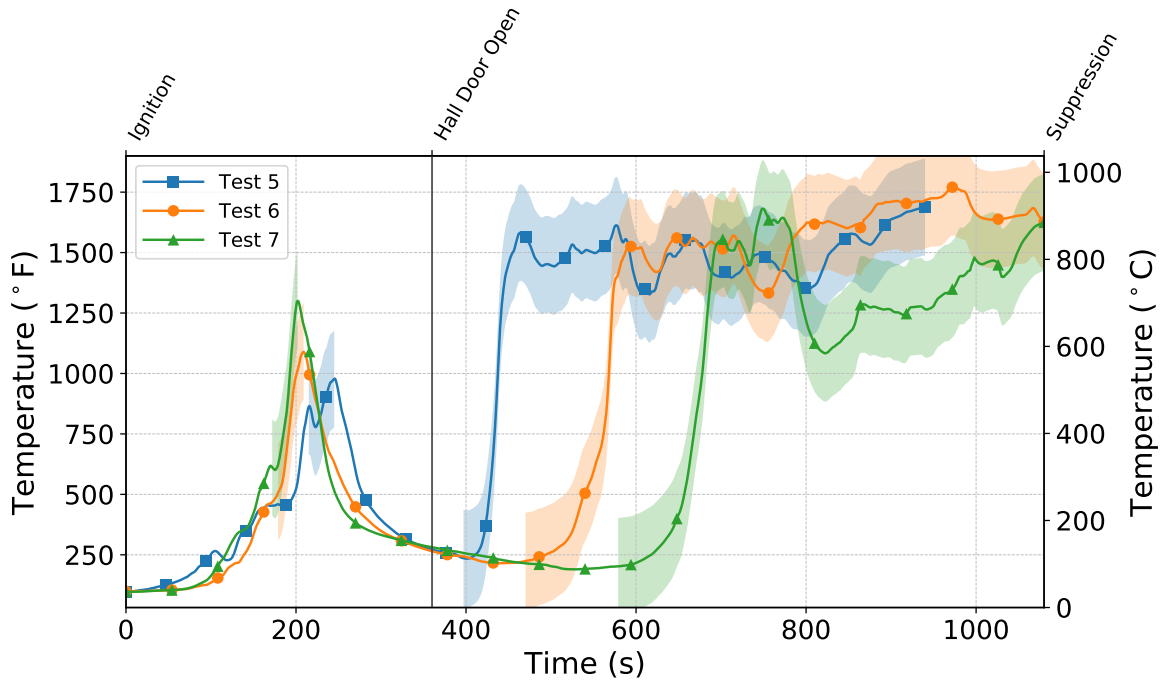


Figure 5.5: Plots of temperature data measured 1.0 in. (25 mm) below the fire room ceiling during the three repeatability tests conducted in the Gypsum Prop with the furniture fuel load. The shaded area represents the span of the data sample sets for the plot of similar color. Note, the fire during Test 5 (blue line) was suppressed at an earlier time to prevent the structural members of the prop from being permanently damaged.

Results from comparisons of initial growth and post-vent thermocouple data between repeatability experiments are presented in Table 5.3. The number of bias values within the range of the thermocouple measurement uncertainty are listed in the table as a fraction of the total number computed for comparisons of data from the specified measurement locations. Also included in the table are the overall bias and ICC values computed across the measurement pairs from all initial growth sample comparisons and all post-vent sample comparisons between repeatability experiments.

Table 5.3: Overall Bias & ICC Values from Sample Comparisons Between Repeatability Tests

Comparison	Initial Growth			Post-Vent		
	Biases in Range	Overall Bias	Overall ICC	Biases in Range	Overall Bias	Overall ICC
<i>Gypsum Prop</i>						
Test 5 vs. Test 6	17/18	0.97	0.85	18/18	0.93	0.80
Test 5 vs. Test 7	13/18	1.11	0.76	16/18	0.88	0.78
Test 6 vs. Test 7	10/18	1.15	0.89	18/18	0.94	0.92
<i>Metal Prop</i>						
Test 11 vs. Test 12	18/18	1.01	0.90	15/18	0.88	0.87
Test 11 vs. Test 13	9/18	1.14	0.89	16/18	0.90	0.76
Test 12 vs. Test 13	10/18	1.10	0.85	17/18	1.03	0.89
<i>Insulated Metal Prop</i>						
Test 17 vs. Test 18	13/18	0.95	0.87	18/18	0.96	0.96
Test 17 vs. Test 19	11/18	0.89	0.90	18/18	0.98	0.93
Test 18 vs. Test 19	8/18	0.90	0.83	15/18	1.02	0.92

Looking at the initial growth sample comparison results in Table 5.3, every overall bias value is within the range bounded by the total measurement uncertainty estimated for thermocouples (1.0 ± 0.15), and the corresponding ICC values are all greater than 0.75. Similarly, every overall bias value from the post-vent sample comparisons in Table 5.3 is within the range of thermocouple measurement uncertainty, and all corresponding ICC values are greater than 0.75.

These results suggest that, as a collective group, the temperatures during the initial growth and post-vent periods were highly agreeable between replicate tests. Thus, repeatable fire conditions were able to be generated in every prop with any of the three fuel loads. The results from these comparisons are used as a benchmark for comparisons between non-replicate experiments included upcoming sections. Values from Table 5.3 can be compared to other bias and ICC results to determine if the differences in fire conditions during two given tests were more drastic than the differences between replicate tests.

Also note from Table 5.3 the difference in the total number of computed biases within the range of measurement uncertainty between the initial growth and post-vent sample comparisons. There tends to be a greater number of bias values within the range for post-vent sample comparisons than for initial growth sample comparisons. The reason for this difference is likely due to the variation in size between the two types of samples. Post-vent data samples covered durations on the order of minutes, whereas the range of initial growth samples was across a span of 30 seconds. As a result, outlier measurement pairs have a greater effect on the overall bias and ICC values of initial growth sample comparisons than on the overall values of post-vent sample comparisons. This result suggests that when comparing the impact of changing a single variable on overall fire conditions (e.g., comparison of fuel loads or comparison of wall constructions), results from post-vent sample comparisons serve as a more robust metric than those from the initial growth sample comparisons. Therefore, some discussions in upcoming sections focus solely on the results of post-vent sample comparisons.

Establishing the repeatability of the fuel loads and wall configurations is significant because it indicates that the experimental results are consistent and applicable across tests with identical setups. Repeatable fires are often desired during live-fire training evolutions so instructors are able to correctly anticipate thermal conditions, which allows them to conduct training in a safer and more effective fashion. The repeatability of training fires also helps ensure that students experience similar thermal environments across replicate exercises.

Table 5.4 contains the peak temperature and peak heat flux measured 3.7 ft (1.1 m) and 3.0 ft (0.9 m) above the floor, respectively, in the hallway during the repeatability experiments in each prop. Measurements from these heights were selected because they are near the level of a crouching or crawling firefighter’s head. The approximate locations of the “end hall” and “start hall” measurements listed in the table are shown in Figure 5.6.

Table 5.4: Peak Temperature & Heat Flux Measured at Firefighter Level in Hallway During Repeatability Tests

	Temperature (°F)		Heat Flux (kW/m²)	
	End Hall	Start Hall	End Hall	Start Hall
<i>Gypsum Prop</i>				
Test 5	895	615	> 20.0*	> 20.0*
Test 6	895	750	> 20.0*	> 20.0*
Test 7	915	815	> 20.0*	> 20.0*
<i>Metal Prop</i>				
Test 11	335	220	10.3	2.7
Test 12	370	195	7.7	2.4
Test 13	290	200	9.8	2.9
<i>Insulated Metal Prop</i>				
Test 17	670	370	> 20.0*	N/A ⁺
Test 18	775	325	> 20.0*	N/A ⁺
Test 19	690	385	> 20.0*	7.8

* Gauge calibrated to measure maximum of 20 kW/m²

+ Gauge malfunctioned during experiment

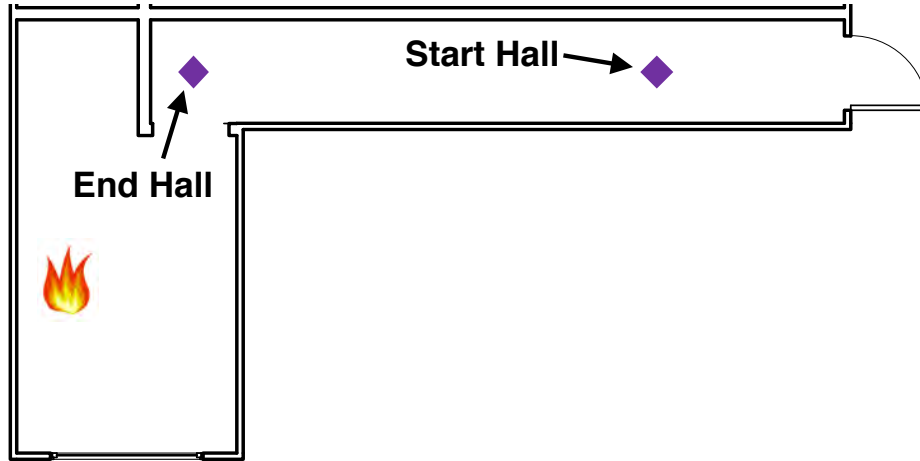


Figure 5.6: Floor plan showing the “end hall” and “start hall” measurement locations. The end hall pair was centered in the fire room doorway and between the hallway walls. Likewise, the start hall pair was centered in the hallway and located approximately 8.0 ft (2.4 m) from the hallway door.

The total heat flux gauges in the hallway were calibrated to measure a maximum heat flux of 20 kW/m^2 . Any measurement recorded by a total heat flux gauge that is greater than the maximum heat flux to which it is calibrated is considered less precise than measurements within the calibration range. Therefore, any tabulated heat flux value that exceeds the maximum heat flux for which the gauge was calibrated is reported only as being greater than the maximum calibration heat flux. Additionally, the start hall heat flux gauge malfunctioned during two of the Insulated Metal Prop repeatability experiments. The tabulated heat flux measurements for these instances are reported as “N/A” and accompanied by a footnote.

Because this section is concerned with assessing the repeatability of the fuel packages and wall configurations, the following discussion regarding Table 5.4 is focused on evaluating if the tabulated values are significantly different between replicate tests. The significance of the peak values with respect to potential hazard for firefighters is explored and discussed in upcoming sections.

The peak values listed in Table 5.4 are consistent with the overall bias and ICC values computed for the sample comparisons between repeatability experiments. The peak temperatures in the hallway were indistinguishable between replicate experiments in each prop. The largest difference in peak temperatures between replicate tests is the difference in peak temperatures at the start hall location between Test 5 and Test 7. These measurements of $615 \text{ }^\circ\text{F}$ ($324 \text{ }^\circ\text{C}$) and $815 \text{ }^\circ\text{F}$ ($435 \text{ }^\circ\text{C}$), respectively, are nearly, although not completely, distinguishable from their measurement uncertainty. Recall that the total measurement uncertainty associated with thermocouples, $\pm 15 \%$, was estimated based on temperatures in $^\circ\text{C}$. The upper bound of $324 \text{ }^\circ\text{C} \pm 15 \%$, $373 \text{ }^\circ\text{C}$, is greater than the lower bound of $435 \text{ }^\circ\text{C} \pm 15 \%$, $370 \text{ }^\circ\text{C}$.

Every peak heat flux measurement listed in the table from the experiments in the Gypsum Prop with the furniture fuel load is greater than the calibration limit of 20 kW/m^2 , so it is not apparent if the differences between values are distinguishable from the estimated measurement uncertainty. The same is also true for the peak heat flux values at the end hall location for tests in the Insulated

Metal Prop with the pallets and OSB fuel package. The heat flux gauge at the start hall location malfunctioned during two of the experiments in the Insulated Metal Prop, so comparisons cannot be made between these values. The peak heat fluxes collected at the end hall and start hall locations during Tests 11 and 13 in the Metal Prop are indistinguishable from their estimated measurement uncertainty of $\pm 8\%$. The peak heat flux measured at the end hall location during Test 12, however, is measurably smaller than those from Tests 11 and 13. Finally, the peak start hall heat flux during Test 12 is indistinguishable from the peak value of Test 11 but is distinguishable from the peak value of Test 13.

Although the thermal conditions produced by each fuel package can be considered repeatable, the time at which fire regrowth begins after ventilation isn't necessarily repeatable. Unlike the temperature measurements, there is no direct measurement uncertainty associated with the start time of growth or regrowth. So, the quantification of variability in these values for each fuel package is focused exclusively on the results from replicate tests. Table 5.5 contains the growth and regrowth times and rates computed for the nine repeatability experiments.

Table 5.5: Growth Times & Rates from Repeatability Tests

Test Name	Initial Growth			Post-Vent Regrowth		
	Time (s)	Rate (°F/s)	Duration (s)	Time (s)	Rate (°F/s)	Duration (s)
<i>Furniture</i>						
Test 5	26	6.3	220	56	33.3	47
Test 6	72	8.6	137	129	15.1	102
Test 7	70	11.3	133	238	16.4	97
<i>Pallets</i>						
Test 11	17	24.8	41	26	79.9	12
Test 12	13	15.1	60	63	17.3	56
Test 13	8	34.9	43	32	42.3	25
<i>Pallets & OSB</i>						
Test 17	9	57.1	27	28	53.1	20
Test 18	13	27.4	58	26	93.2	9
Test 19	9	63.4	22	24	56.3	15

Looking at Table 5.5, all fire growth start times vary by less than 60 seconds between each set of repeatability experiments. Furthermore, the initial growth times are larger for fires with the furniture fuel package, ranging from 26 s to 72 s, than for those with wood-based fuel loads, which range from 8 s to 17 s. Lastly, the growth rates and durations indicate initial fire growth was much slower with the furniture fuel load compared to either wood-based fuel load.

Comparing the regrowth values listed in the table reveals trends similar to those from initial growth comparisons. On average, the fire regrowth rates and durations indicate regrowth was slower with the furniture fuel load than with either wood-based fuel load. The regrowth start times are larger for experiments with the furniture fuel load, ranging from 56 s to 238 s, compared to those with the wood-based training fuels, which range from 24 s to 63 s. The regrowth start times for the

NFPA 1403-compliant fuel loads differ on the order of seconds, while the regrowth start times for the furniture experiments differ on the order of minutes.

The more consistent regrowth times and faster growth rates of fires with the wood-based fuel loads can be at least partially attributed to their geometry and point of ignition. In both fuel packages, the pallets were arranged in a triangular fashion with straw stuffed in the middle opening. The fuel load was ignited near the center of the opening, and the straw's high surface-area-to-mass ratio allowed the fire to quickly propagate from the point of ignition towards the pallets, eventually producing enough heat to ignite the pallets. Alternatively, for the furniture fuel load, the ignition point was at the end corner of the couch. Due to this ignition location and shape of the fuel, flame spread needed to occur laterally to involve additional fuel, causing fire growth to occur at a later time after ignition and, on average, at a slower rate during the furniture tests than the tests with wood-based training fuels. Figure 5.7 contains stills obtained from recorded video of the fire growth after ignition for the furniture and pallets fuel packages in the Gypsum Prop to provide a visual representation of the differences in growth rates and direction of primary flame spread.



Figure 5.7: Still images obtained from recorded video of fire growth after ignition of the furniture fuel load (top images) and pallets fuel load (bottom images) in the Gypsum Prop. The images on the left side are of times shortly after visible flames were seen in the video, and the images on the right are from 30 seconds later for the pallets and one minute later for the furniture.

Certain components of training fuel packages or fuel loads composed of foam plastics and synthetic materials found in present-day residential structures will likely vary more in practice than they did between these experiments. The results discussed in the paragraphs above, such as the fire initially growing at a faster rate with wood-based training fuels, are in no way considered to be generic

findings that apply to all fuel loads regardless of other parameters (e.g., ignition point, geometry, size, etc.).

5.3 Comparison of Burn In Tests to Later Replicates

To determine if the unique visual observations from Burn In tests translated to quantifiable differences in thermal conditions, temperatures from initial growth and post-vent sample sets were compared between each Burn In test and their corresponding replicate. Results from such comparisons are summarized in Table 5.6, which includes the overall bias and ICC values calculated across the measurement pairs from all initial growth sample comparisons and all post-vent sample comparisons between the Burn In and later replicate experiments. The number of bias values within the range of the thermocouple measurement uncertainty are also listed in the table as a fraction of the total number computed for comparisons of data from relevant measurement locations.

Table 5.6: Overall Bias & ICC Values from Burn In vs. Later Replicate Sample Comparisons

Burn In vs. Later Replicate Comparison	Initial Growth			Post-Vent		
	Biases in Range	Overall Bias	Overall ICC	Biases in Range	Overall Bias	Overall ICC
<i>Metal Prop</i>						
Pallets (Left Side)	2/18	1.41	0.59	17/18	0.97	0.95
Pallets & OSB (Right Side)	1/18	1.61	0.59	18/18	1.00	0.94
<i>Insulated Metal Prop</i>						
Pallets (Left Side)	2/18	0.77	0.79	18/18	0.99	0.98
Pallets & OSB (Right Side)	12/18	1.08	0.83	18/18	0.97	0.95

Looking at Table 5.6, the overall bias and ICC values computed for the post-vent sample comparisons ranged from 0.97 to 1.0 and from 0.94 to 0.98, respectively. These ranges are consistent with those from the repeatability test comparisons (Table 5.3) and suggest that the thermal conditions produced after ventilation in every Burn In test were indistinguishable from those in the corresponding replicate test. This is expected because the ventilation profile and fuel loads were identical between experiments during the post-vent period.

The overall bias and ICC values computed for the initial growth sample comparisons, however, suggest the conditions during the initial growth period of the Burn In tests varied significantly from those of the later replicate. The overall bias in both Metal Prop comparisons exceeds the upper limit of the uncertainty range, indicating that the conditions during the initial growth period of the replicate tests were distinctly more severe than those of the Burn In tests. Additionally, the comparison of experiments in the right side of the Insulated Metal Prop suggests the environment of the later replicate test was more severe than the Burn In, but the bias value is less than the upper limit of the estimated measurement uncertainty, so the difference is not considered significant. The comparison between experiments in the left side of the Insulated Metal Prop was the only

comparison that revealed conditions were more intense during the initial growth period of the Burn In test compared to those of the replicate test.

To provide more insight into the differences between the thermal conditions during the initial growth periods of the Burn In and replicate tests, Table 5.4 contains the peak temperature and peak heat flux measured near the level of a crouching or crawling firefighter’s head at the “end hall” and “start hall” locations during the initial growth period of the experiments.

Table 5.7: Peak Temperature & Heat Flux Measured at Firefighter Level During Initial Growth Period of Burn In & Later Replicate Tests

	Temperature (°F)		Heat Flux (kW/m²)	
	End Hall	Start Hall	End Hall	Start Hall
<i>Metal (Left Side)</i>				
Burn In	100	95	1.9	1.5
Later Replicate	140	130	2.6	2.1
<i>Metal (Right Side)</i>				
Burn In	140	145	3.2	2.0
Later Replicate	235	220	8.3	3.8
<i>Insulated Metal (Left Side)</i>				
Burn In	295	225	6.2	3.9
Later Replicate	175	170	3.2	2.5
<i>Insulated Metal (Right Side)</i>				
Burn In	170	175	3.6	4.0
Later Replicate	185	165	4.3	N/A ⁺

⁺ Gauge malfunctioned during experiment

Looking at the table, the peak measurements from the Metal Prop Burn In tests are all significantly lower (i.e., distinguishable from their respective estimated measurement uncertainty) than those from the corresponding replicate tests. All peak temperature and heat flux values from the Burn In experiment in the right side of the Insulated Prop except the start hall temperature were also greater than those from the replicate test. However, they were not distinguishable from their measurement uncertainty. Lastly, the peak values from the Burn In experiments in the left side of the Insulated Metal Prop except the start hall temperature were significantly greater than those from the later replicate experiment. These results are consistent with the bias and ICC comparison results presented in Table 5.6.

Overall, the peak conditions produced during the initial growth period of the Burn In tests were generally less severe than those of the corresponding replicates. This discrepancy between the initial growth conditions is likely due to the fact that the metal props incurred more permanent damage during the initial experiments (Burn In tests) than during later experiments. Significant damage after the first burn was noted by the differences in the prop leakage measurements; values measured before each Burn In test were consistently lower than those measured afterwards, as shown in Table 5.8. In fact, of all leakage values measured before experiments in the metal props, the lowest values correspond to the one obtained before the first experiment (i.e., Burn In test).

This demonstrates the significant impact the initial fire had on the permanent degradation of the metal props.

Table 5.8: Prop Leakage Values Measured Before & After Burn In Tests

Burn In Test	Leakage Before Burn In (ACPH50)	Leakage After Burn In (ACPH50)
Metal Prop (Right Side)	15.2	22.8
Metal Prop (Left Side)	19.6	28.9
Insulated Metal Prop (Right Side)	19.3	26.7
Insulated Metal Prop (Left Side)	23.9	28.5

Consider a fire that becomes ventilation-controlled as it grows in a closed compartment, similar to the initial growth period of the Burn In and replicate experiments. The greater the amount of oxygen provided to the fire before becoming ventilation-limited, the more the fire will grow and develop before decaying. Thus, assuming all other parameters are identical, the greater the leakage of the closed compartment, the more severe the peak thermal conditions generated by the fire before it starts to decay. Each replicate experiment of the Burn In comparisons occurred in a training prop that was more damaged, and thus leakier, than it was at the time of the Burn In test. As a result, more air from the outside environment was provided to the fire during the initial growth period of the replicate experiments.

Permanent damage caused by the Burn In tests was also apparent from visual observations. For example, fire burned on the exterior side of the prop during both Metal Prop Burn In tests due to the exterior side of the wall heating to the autoignition temperature of the paint, causing it to ignite, as seen in the photo presented in Figure 5.8. The deterioration caused by the burning paint is shown by images of the Metal Prop exterior from before and after the test in Figure 5.9.

No exterior fire spread was observed during the Insulated Metal Prop Burn In tests because the layer of insulation prevented the exterior side from reaching the autoignition temperature of the paint. However, significant damage to the prop was still noted after each experiment. A number of the welds that fused the metal sheets overtop the insulation along the interior were broken due to the expansion of the sheets as they absorbed heat produced by the fire. During the Burn In test in the right side of the prop, enough welds along the hinge of the left window shutter broke that the shutter became completely detached from the prop as it was opened at the end of the experiment. Figure 5.10 contains images of the damage caused by the Burn In experiments in the Insulated Metal Prop.



Figure 5.8: Photo of the paint burning on the exterior side of the Metal Prop during the Burn In experiment.



Figure 5.9: Exterior photos of the Metal Prop before (left) and after (right) the Burn In experiment.



Figure 5.10: Images of the Insulated Metal Prop before (left side) and after (right side) the Burn In experiment. The top images are of the exterior side of the fire room window, and the bottom images are looking at welds along the edge of a steel sheet on the interior side near the window. The left window shutter became detached from the prop, and multiple interior welds were broken as a result of the Burn In experiment.

The results from the Burn In tests suggest that at least one fire should be ignited and allowed to burn inside a metal container prop before it's used for live-fire training. This will allow the exterior paint to burn off the prop (if no insulation is present), which will help prevent exterior fire spread during the training fires that follow. It will also allow the prop to sustain significant degradation similar to that observed during the Burn In experiments before being used for training, which will help reduce the variability between the first training evolution and those that follow.

To control prop leakage, modifications that significantly increase leakage, such as cutting holes in the exterior walls, should not be made to the metal props. Furthermore, performing a regular inspection of the prop for potential repairs is recommended. Some components may need to be rewelded or bolted, and any large gaps or openings that exist should be sufficiently covered or plugged. If not properly maintained, a prop could develop enough leakage that fuel packages of a specific type and size may lose the ability to generate ventilation-controlled conditions.

Note, the most fires ignited in one side of either container prop was 16, and minor repairs, like filling gaps with high-temperature, insulating foam sealant and rewelding a detached window shutter, were performed to minimize leakage effects of degradation. It's quite possible that more than 16 training fires could be ignited in a metal container prop throughout a single day of training. Thus, the degradation results described above are limited in their scope, pertaining only to a short period of use. Additionally, the manifestation of prop degradation may vary from that documented here depending on the design of the prop and the duration and severity of fires ignited in the prop. For example, if fires are burned within a metal container prop for shorter periods and/or produce less severe conditions during their development, prop degradation may occur at a slower rate. Additionally, a metal container prop with a more robust design may not show initial signs of degradation to the extent observed after the Burn In experiments, like the window shutter becoming detached from the prop.

5.4 Comparison of Wall Configurations

Sample sets of thermocouple data from the post-vent portion of experiments with each fuel load that followed the vent door procedure were compared between the three props to study the effects of the different wall constructions on fire development. The overall results from the comparisons between wall configurations for each fuel load are listed in Table 5.9, which contains the overall bias and ICC values calculated across the measurement pairs from all post-vent sample comparisons between the listed experiments. The number of bias values within the range of the thermocouple measurement uncertainty are also listed in the table as a fraction of the total number computed for comparisons of post-vent data from the relevant measurement locations.

Table 5.9: Overall Bias & ICC Values from Post-Vent Comparisons Between Prop Constructions for each Fuel Load

Comparison	Post-Vent		
	Biases in Range	Overall Bias	Overall ICC
<i>Gypsum vs. Metal</i>			
Furniture	6/18	0.78	0.56
Pallets	6/18	0.81	0.64
Pallets & OSB	10/18	0.85	0.71
<i>Gypsum vs. Insulated Metal</i>			
Furniture	6/18	0.77	0.54
Pallets	10/18	0.91	0.74
Pallets & OSB	9/18	0.86	0.75
<i>Metal vs. Insulated Metal</i>			
Furniture	10/18	0.98	0.89
Pallets	12/18	1.11	0.90
Pallets & OSB	18/18	1.00	0.93

Table 5.9 reveals that the overall thermal conditions in the Gypsum Prop during the post-vent period were significantly more intense than those in either metal container prop. The results show no indication of highly agreeable conditions between the Gypsum Prop and either metal container prop. Moreover, the comparisons between the Gypsum Prop and metal props within the agreeable range produced bias values near 0.85, the lower bound of the measurement uncertainty range, indicating that while overall conditions were not completely distinguishable, they tended towards more intense conditions during the Gypsum Prop tests. Finally, all comparisons categorized as significantly different contain values in the direction of the Gypsum Prop fire environment being more severe.

The difference in fire environments between the Gypsum Prop and metal props is a result of the variation in wall construction materials. The innermost layer in both metal prop wall configurations was steel, a heat conductor with a thermal conductivity of 40 W/m°C at 300 °C [49], while the innermost layer in the Gypsum Prop was Type X gypsum board, a heat insulator that's been shown to have a thermal conductivity of approximately 0.19 W/m°C at 300 °C [50]. Thus, for similar fire conditions in a compartment with walls constructed from steel and in a compartment with walls composed of gypsum, more heat will be transferred from the environment to the walls in the compartment with steel walls than in the compartment with gypsum walls. To provide more context to the thermal conductivity (k) of the interior lining materials, values of k for common materials at 20 °C are listed in Table 5.10 with the values for steel and gypsum board highlighted.

Table 5.10: Thermal Conductivity of Common Materials at 20 °C [49]

Material	Thermal Conductivity (W/m°C)
Copper	386
Steel	43
Brick	0.69
Water	0.60
Gypsum Board (Type X)	0.26
Air	0.026

The overall bias and ICC values computed for the *Metal vs. Insulated Metal* comparisons reveal that the collective thermal environments produced during the post-vent periods of experiments were highly agreeable between the two metal props for every fuel package. All three bias values are within the range of estimated uncertainty, and all the ICC values are similar to those produced by comparisons of temperature data between replicate experiments. These results indicate that adding a layer of insulation to the metal container did not change the overall fire dynamics during the experiments. It did, however, drastically increase the cooling time of the interior as the fire decayed and after the fire was extinguished. The rate of heat transfer *to* the wall was similar in each case because the innermost layer was steel in both props, while heat transfer *through* the wall was slower in the Insulated Metal Prop due to the additional layer of mineral wool insulation.

The difference in the cooling time is revealed by comparing the rate of temperature decline across similar periods of fire decay during identical tests in the Metal Prop and Insulated Metal Prop. These periods of temperature decrease occurred during experiments with the wood-based training fuel loads; fires from these fuel packages consistently became fuel-limited before the end of the test.

Table 5.11 contains the average temperature decrease measured by the thermocouples 3.0 ft (0.9 m) or closer to the ceiling in the fire room array and end hall array over the final 90 seconds of the wall construction comparison experiment for each wood-based fuel load in the Metal and Insulated Metal Props. Looking at the table, the average cooling rate in the Metal Prop is consistently greater in magnitude compared to that of the Insulated Metal Prop. The rates associated with the Metal Prop range from being almost two times greater in magnitude (fire room, pallets) to being four times greater in magnitude (end hall, pallets and OSB) than the rates associated with the Insulated Metal Prop.

Table 5.11: Average Cooling Rate Across Upper Thermocouples in Fire Room & End Hall Arrays During Final 90 seconds of Tests with Wood-Based Fuels in Metal & Insulated Metal Props

Thermocouple Array	Average Cooling Rate (°F/s)			
	<u>Pallets</u>		<u>Pallets & OSB</u>	
	Metal	Insulated	Metal	Insulated
Fire Room	-1.5 ± 0.2	-0.8 ± 0.1	-1.9 ± 0.3	-0.5 ± 0.2
End Hall	-1.1 ± 0.1	-0.4 ± 0.2	-1.2 ± 0.2	-0.3 ± 0.1

The longer cooling time of the environment inside the Insulated Metal Prop is significant for several reasons. If the interior environment is not given necessary time to cool, excessive heat can be retained within the prop, causing the intensity of the training environment to increase during later evolutions. At least one LODD has been attributed to the failure of PPE after exposure to extreme heat inside a training structure that wasn't allowed sufficient time to cool between training exercises [14]. Prop cooling time can be one of the main factors in determining the number of training exercises able to be conducted within a specific period of time, as the time needed to cool the training structure can dictate the turnaround time between evolutions. These results should be considered by those planning to use metal container props for live-fire training.

To further illustrate the impact of the different thermal environments between the Gypsum Prop and the metal props, Table 5.12 lists the peak temperature and heat flux near the level of a crouching or crawling firefighter's head at the "end hall" and "start hall" locations during the wall construction comparison experiments with each fuel package.

Table 5.12: Peak Temperature & Heat Flux Measured at Firefighter Level in Hallway During Wall Configuration Comparison Tests

	<u>Temperature (°F)</u>		<u>Heat Flux (kW/m²)</u>	
	End Hall	Start Hall	End Hall	Start Hall
<i>Furniture</i>				
Gypsum	895	615	> 20.0*	> 20.0*
Metal	645	350	> 20.0*	5.9
Insulated Metal	775	415	> 20.0*	9.8
<i>Pallets</i>				
Gypsum	805	375	> 20.0*	9.6
Metal	335	220	10.3	2.7
Insulated Metal	390	255	12.1	2.7
<i>Pallets & OSB</i>				
Gypsum	790	515	> 20.0*	13.2
Metal	650	305	> 20.0*	6.3
Insulated Metal	670	370	> 20.0*	N/A ⁺

* Gauge calibrated to measure maximum of 20 kW/m²

+ Gauge malfunctioned during experiment

The peak measurements listed in the table reveal the significance of the elevated conditions produced by each fuel package in the Gypsum Prop. The peak heat flux and temperature measurements from experiments in the Gypsum Prop consistently surpass the PPE exposure limits listed in Table 5.1, while the peak values from similar experiments in the Metal Prop and Insulated Metal Prop are typically below the threshold values, with the major exceptions being the peak end hall temperature and heat flux during experiments with the furniture fuel load and the pallets and OSB fuel load. The peak heat flux values in these instances were greater than 20 kW/m² and the peak temperatures were over 500 °F (260 °C) due to flame impingement on the sensors as fire traveled through the fire room doorway and into the hall. Fire traveled farther down the hall in the Gypsum Prop than in either metal prop. During the experiments in the Gypsum Prop with the furniture and pallets and OSB fuel loads, flames traveled the length of the hall and out the door, whereas no such phenomenon was witnessed during any experiments in the metal props. This was likely caused by the previously discussed differences in interior wall lining materials and is reflected in the peak start hall measurements listed in Table 5.12. For example, the peak start hall temperature and heat flux during furniture experiments exceeded 500 °F (260 °C) and 20 kW/m², respectively, in the Gypsum Prop but remained under 500 °F (260 °C) and 10 kW/m² in both metal props.

5.5 Comparison of Fuel Loads

Results from experiments that followed the vent door configuration were used to compare the thermal environments created by the three fuel packages in each type of prop. The comparison focused on temperature measurements from the post-vent period because the fires reached a fully-developed state for the new ventilation configuration after the door was opened.

To add insight to the discussion of the fuel load comparison results, specific properties of the fuel packages can be used to estimate the theoretical amount of energy released during combustion of each fuel load. If the mass (m_{fuel}) and the effective heat of combustion (ΔH_c) of the material(s) in a fuel package are known, then the theoretical energy release of the fuel load can be computed using Equation 5.3 below.

$$Q = \Delta H_c m_{fuel} \quad (5.3)$$

The synthetic materials of the furniture fuel package have different combustion characteristics compared to the wood-based materials of the *NFPA 1403*-compliant fuel loads. Typically, heat of combustion values for synthetic materials are greater than values for wood-based products. For example, HRR characterization experiments performed for wood-based training fuel packages similar to those used for this project concluded that the effective ΔH_c of the training fuel loads was 13.9 MJ/kg [51]. This value is about 40 % smaller than the ΔH_c of polyurethane, the primary material of the sofa cushions and carpet padding included in the furniture fuel package, which has a heat of combustion of 23.2 MJ/kg [49]. Using these ΔH_c values and the average weights of the fuel loads, Equation 5.3 can be used to estimate the theoretical energy release of each fuel package.

The average weights of each pallet and straw utilized in the wood-based fuel packages were 18.9 kg and 14.6 kg, respectively. Using these average values, the average total mass of the pallets fuel package was 71.3 kg, which, when multiplied by the effective ΔH_c of 13.9 MJ/kg, results in an estimated total energy release of 0.99 GJ. Additionally, the average total weight of the OSB added to the pallets and straw to create the pallets and OSB fuel load was 49.6 kg, which, when added to the total mass of the pallets fuel package and multiplied by the effective ΔH_c of 13.9 MJ/kg, produces an estimated total energy release of 1.7 GJ.

Finally, to simplify the estimate of the total energy release of the furniture fuel package, the items from the fuel load used in the estimation are assumed to be homogenous. The elements primarily composed of synthetic materials — the sofa, carpet, and carpet padding — had an average total mass of 66.0 kg and are treated as being composed solely of polyurethane. The two wood-based items used in the fuel package — the coffee table and end table — had an average total mass of 36.0 kg and are treated as being composed solely of pine wood ($\Delta H_c = 17.9$ MJ/kg [49]). These assumptions combined with the average fuel weights and ΔH_c values result in an estimate of 2.2 GJ for the total energy release of the furniture fuel package.

The theoretical energy release estimations performed above demonstrate that the furniture fuel package contains more potential heat energy than either wood-based fuel load. Of the two wood-based training fuel packages, more potential heat energy is included in the pallets and OSB fuel load than in the pallets fuel load.

Table 5.13 contains the results from the post-vent sample comparisons between tests with different fuel packages for each thermocouple array in the Metal Prop. The bias and ICC values computed across the measurement pairs formed by the post-vent data from the relevant sensors of each thermocouple array are included in the table. Listed alongside each set of bias and ICC values is the number of bias values within the range of the thermocouple measurement uncertainty as a fraction of the total number computed across pairs formed by the relevant sensor data sets from each thermocouple array.

Table 5.13: Overall Bias & ICC Values for Comparisons of Post-Vent Data from each Thermocouple Array Between Fuel Loads in the Metal Prop

Comparison	Biases in Range	Post-Vent	
		Overall Bias	Overall ICC
<i>Furniture vs. Pallets</i>			
Fire Room Window (BDP1)	0/5	0.68	0.28
Fire Room (1TC)	1/5	0.72	0.34
End Hall (2TC)	0/3	0.75	0.36
Start Hall (3TC)	0/3	0.75	0.49
Hall Doorway (BDP2)	0/2	0.80	0.67
<i>Furniture vs. Pallets & OSB</i>			
Fire Room Window (BDP1)	1/5	0.78	0.47
Fire Room (1TC)	5/5	0.91	0.68
End Hall (2TC)	3/3	1.01	0.60
Start Hall (3TC)	3/3	1.05	0.67
Hall Doorway (BDP2)	1/2	1.14	0.69
<i>Pallets vs. Pallets & OSB</i>			
Fire Room Window (BDP1)	3/5	1.11	0.77
Fire Room (1TC)	1/5	1.23	0.44
End Hall (2TC)	0/3	1.34	0.33
Start Hall (3TC)	0/3	1.39	0.36
Hall Doorway (BDP2)	0/2	1.42	0.41

Looking at Table 5.13, nearly all the ICC values indicate there's drastically more variation between temperatures measured during experiments with different fuel loads compared to that of replicate experiments. Additionally, all but one bias value from the *Furniture vs. Pallets* and *Pallets vs. Pallets & OSB* comparisons suggest that the temperatures measured throughout the prop are significantly different between experiments with the different fuel packages. The values computed across the two fuel load comparisons are consistently biased in the direction of the fuel load with the higher total energy content.

Although the ICC values indicate there's more variation between temperatures measured during the *Furniture vs. Pallets & OSB* experiments than between temperatures of replicate tests, the bias values from the comparisons between temperatures measured outside the fire room are indicative of indistinguishable conditions. This means that the addition of OSB to the pallets and straw fuel load resulted in a thermal environment remote from the fire room with upper gas layer temperatures that more closely resembled those produced by the furniture fuel package than those produced by the pallets fuel load.

The trends exhibited by the results displayed in Table 5.13 are consistent across the various props. The comparison results from tests with different fuel packages in the Gypsum Prop and Insulated Metal Prop, which are included in Appendix B, show patterns similar to those discussed above.

The effect of adding OSB to the pallets fuel load is illustrated by the charts in Figures 5.11 and 5.12, which contain temperature data from both hallway array locations and heat flux data from the end hall location, respectively, plotted over the post-vent period for each fuel load comparison test in the Metal Prop. These data were collected at the previously-defined heights that are near the level of a crouching or crawling firefighter’s head; temperature was measured at 3.7 ft (1.1 m) above the floor, and heat flux was measured at 3.0 ft (0.9 m) above the floor. The PPE exposure thresholds introduced in Section 5.1 are marked by red horizontal lines on the charts.

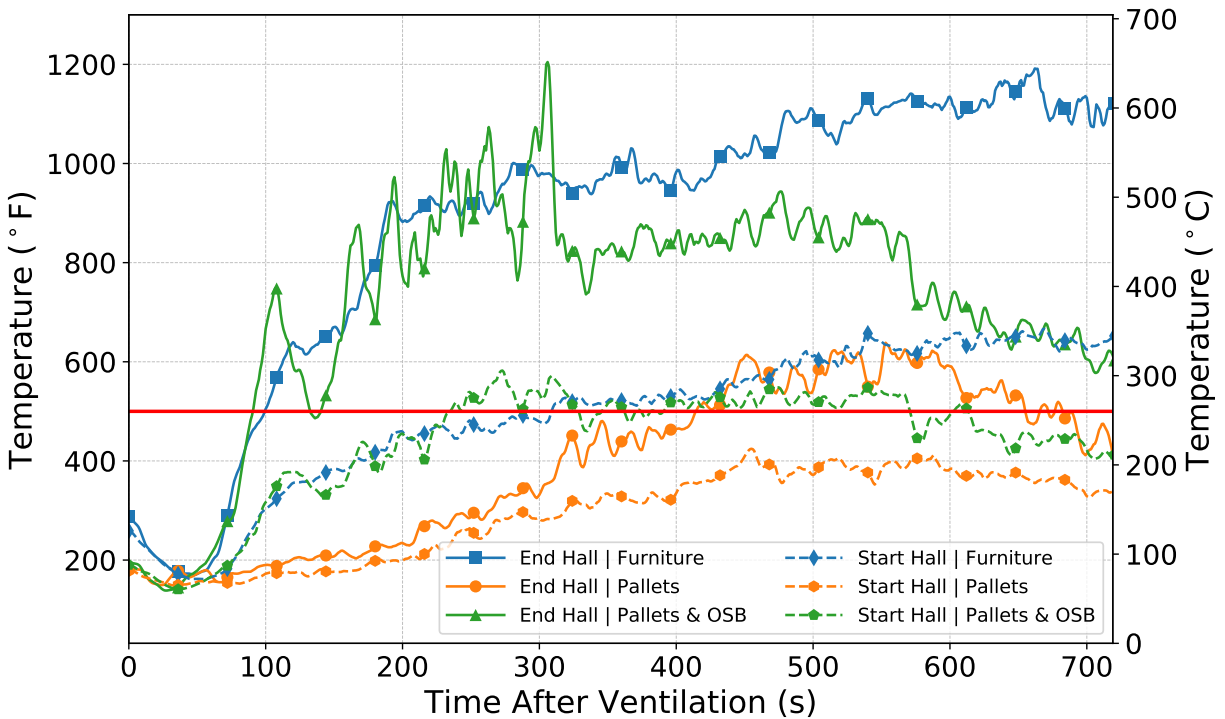


Figure 5.11: Temperatures measured 3.7 ft (1.1 m) above the floor at the end hall (solid lines) and the start hall (dashed lines) locations during the fuel load comparison experiments in the Metal Prop. The red line at 500 °F (260 °C) highlights the firefighter PPE temperature threshold listed in Table 5.1.

Figure 5.11 shows that the temperature measured at the start hall and end hall locations exceeded 500 °F (260 °C) for more than 300 seconds, the exposure to which PPE is tested according to *NFPA 1971* and *NFPA 1981*, during experiments with the furniture and the pallets and OSB fuel packages. During the test with the pallets, the end hall temperature surpassed the exposure limit value but never for more than the duration of 300 seconds associated with the exposure. Additionally, the start hall temperature during the experiment with the pallets fuel load never reached the 500 °F (260 °C) threshold, peaking around 400 °F (204 °C).

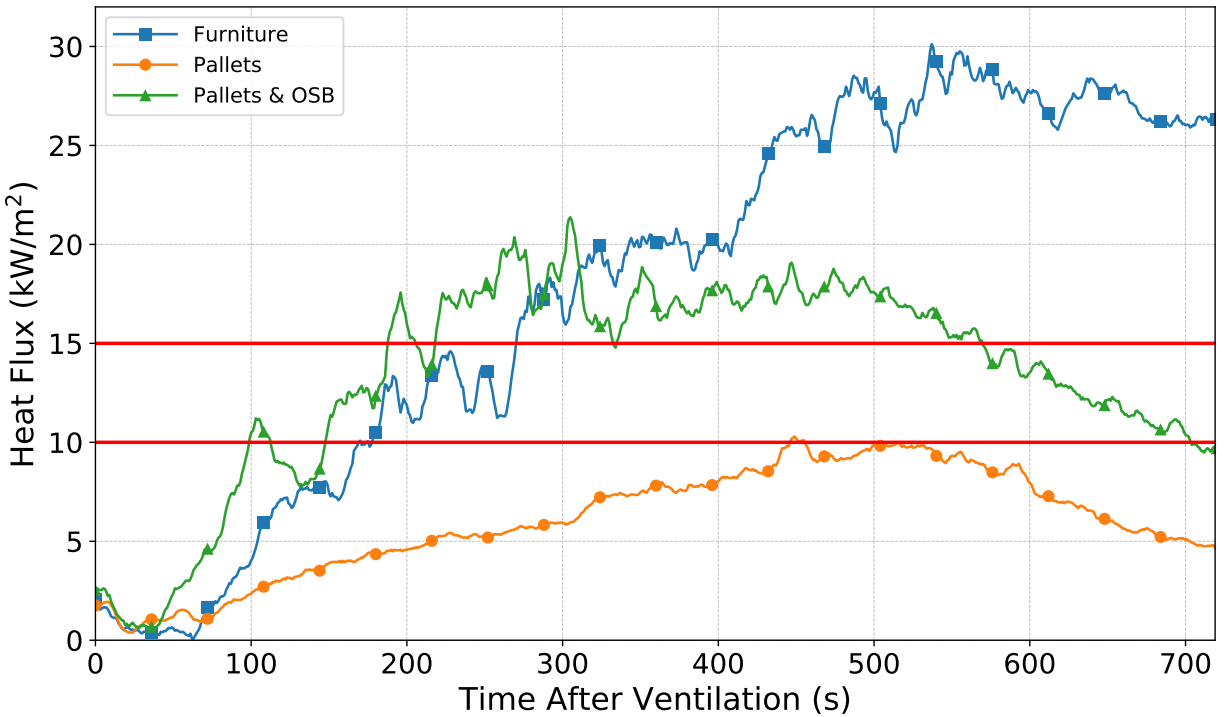


Figure 5.12: Horizontal heat flux measured 3.0 ft (0.9 m) above the floor at the end of the hallway during fuel load comparison experiments in the Metal Prop. The red lines at 10 kW/m² and 15 kW/m² highlight the firefighter PPE exposure thresholds listed in Table 5.1.

Looking at Figure 5.12, the end hall heat flux measured during the experiment with the pallets and OSB fuel load more closely resembled that from the furniture test than that from the pallets test. Approximately 175 s after ventilation, the end hall heat flux from the pallets and OSB test exceeded 15 kW/m² and remained above the limit for about 360 seconds, exceeding the maximum duration of 300 seconds associated with the exposure threshold. Alternatively, during the test with the pallets fuel package, the end hall heat flux peaked around 10 kW/m² and did not exceed the maximum duration of 300 seconds associated with the 10 kW/m² exposure threshold. However, considering the range of the total uncertainty estimated for the heat flux measurements, the heat flux may have surpassed 10 kW/m² for longer than the 30 second limit between 450 s and 550 s after ventilation.

Overall, hazardous conditions existed in different areas of the hallway at heights near the level of a crouching firefighter’s facepiece during fires with wood-based training fuel packages. Furthermore, the conditions produced by the pallets and OSB fuel load were significantly more intense than those produced by the pallets fuel load. In many instances, the intensity of the thermal environment during pallets and OSB tests was closer to that measured during experiments with the furniture fuel package than during experiments with the pallets fuel load. Additionally, although PPE exposure threshold values were exceeded during tests with the pallets fuel load, the duration of the exposure was less than the maximum duration associated with the exposure limit. Whereas during the pallets and OSB test, exposure limits were consistently surpassed for a period of time longer than the

maximum duration. In both scenarios, the potential for firefighters to injure themselves and/or damage their PPE exists. It is also important to keep in mind that firefighters located at higher elevations (e.g., standing) or closer to the fire (e.g., in the fire room) will encounter conditions that pose an even greater hazard than those experienced by crouching firefighters.

5.6 Ventilation Effects

Results from two types of experimental comparisons — vent door vs. vent window and open door, no action vs. open door, vent window — were used to determine the effects of ventilation on the thermal environment within training props. The initial ventilation configurations of the experiments in each comparison were identical and only differed after some intervention was performed that altered the ventilation. Both the fire room window and hallway door were closed at the time of ignition during tests that followed either the “vent door” or “vent window” procedures. Six minutes after ignition, the hallway door was opened during experiments that used the vent door procedure, while the fire room window was opened during experiments that used the vent window procedure. During tests that used either the “open door, no action” or “open door, vent window” procedure, the fire room window was closed and the hallway door was opened at the time of ignition. Six minutes later, the fire room window was opened during experiments that followed the open door, vent window procedure, while no intervention occurred during experiments that followed the open door, no action procedure.

To minimize the effects of the variation in ventilation openings and environmental factors (i.e., wind) on comparison results, the temperatures measured at the ventilation openings (i.e., the window and door) were not considered during the comparisons of temperature data; only sample sets of thermocouple measurements from interior arrays (1TC, 2TC, and 3TC) were used.

5.6.1 Vent Door vs. Vent Window

Data from experiments that followed the vent door procedure were compared to data from experiments that followed the vent window procedure to quantify the effect of vent opening selection on the thermal environment, namely the difference between a door vent and window vent. Results from the vent door vs. vent window comparisons of post-vent data samples from each interior thermocouple array in the Gypsum Prop, Metal Prop, and Insulated Metal Prop for each fuel package are presented in Tables 5.14–5.16, respectively. The bias and ICC values computed across the measurement pairs formed by the post-vent data from the relevant sensors of each thermocouple array are included in the tables. Listed alongside each set of bias and ICC values is the number of bias values within the range of the thermocouple measurement uncertainty as a fraction of the total number of sample sets considered for the given thermocouple array.

No vent door vs. vent window comparison was performed for the furniture fuel load in the Metal Prop because the fire failed to regrow following the window being opened four minutes after igni-

tion. However, as discussed in Section 5.4, overall thermal conditions generated in the Metal Prop and Insulated Metal Prop were indistinguishable from one another. So, the results from the vent door vs. vent window comparison for the furniture experiments in the Insulated Metal Prop should be similar to what would have resulted from the comparison in the Metal Prop had the window vent caused the fire to regrow.

Table 5.14: Overall Bias & ICC Values for Vent Door vs. Vent Window Comparisons of Post-Vent Data from each Interior Thermocouple Array in the Gypsum Prop

Vent Door vs. Vent Window Comparison	Biases in Range	Post-Vent	
		Overall Bias	Overall ICC
<i>Fire Room (1TC)</i>			
Furniture	4/5	0.89	0.57
Pallets	3/5	0.90	0.59
Pallets & OSB	4/5	0.98	0.67
<i>End Hall (2TC)</i>			
Furniture	0/3	0.72	0.46
Pallets	0/3	0.68	0.42
Pallets & OSB	1/3	0.80	0.51
<i>Start Hall (3TC)</i>			
Furniture	0/3	0.50	0.22
Pallets	0/3	0.63	0.33
Pallets & OSB	0/3	0.59	0.21

Table 5.15: Overall Bias & ICC Values for Vent Door vs. Vent Window Comparisons of Post-Vent Data from each Interior Thermocouple Array in the Metal Prop

Vent Door vs. Vent Window Comparison	Biases in Range	Post-Vent	
		Overall Bias	Overall ICC
<i>Fire Room (1TC)</i>			
Pallets	3/5	0.91	0.78
Pallets & OSB	2/5	0.77	0.32
<i>End Hall (2TC)</i>			
Pallets	2/3	0.89	0.71
Pallets & OSB	0/3	0.67	0.21
<i>Start Hall (3TC)</i>			
Pallets	3/3	0.89	0.77
Pallets & OSB	0/3	0.68	0.31

Table 5.16: Overall Bias & ICC Values for Vent Door vs. Vent Window Comparisons of Post-Vent Data from each Interior Thermocouple Array in the Insulated Metal Prop

Vent Door vs. Vent Window Comparison	Biases in Range	Post-Vent	
		Overall Bias	Overall ICC
<i>Fire Room (1TC)</i>			
Furniture	0/5	0.66	0.18
Pallets	1/5	0.77	0.53
Pallets & OSB	4/5	0.95	0.63
<i>End Hall (2TC)</i>			
Furniture	0/3	0.49	0.10
Pallets	1/3	0.73	0.25
Pallets & OSB	0/3	0.77	0.33
<i>Start Hall (3TC)</i>			
Furniture	0/3	0.55	0.17
Pallets	0/3	0.76	0.46
Pallets & OSB	0/3	0.71	0.35

All bias values computed for comparisons between data from interior thermocouple arrays are less than 1.0, suggesting the interior temperatures from the vent door sample sets were, as a whole, greater than those from the vent window samples. Most bias values are less than 0.85, indicating the differences between the respective samples are distinguishable from the thermocouple measurement uncertainty and thus, significant. The ICC values are typically much lower than those computed for comparisons between tests with the same ventilation configuration — implying there was substantially more scatter (i.e., variation) between the values in the paired measurements from the vent door vs. vent window post-vent sample comparisons.

The overall results from the vent door vs. vent window comparisons of fire room temperature data in the Gypsum Prop are within the agreeable range for each fuel load, meaning the upper layer temperatures in the fire room are not distinguishable between tests with the different ventilation configurations. This could be a product of the difference in interior wall lining materials between the Gypsum Prop and metal props because this trend does not exist in either table of comparison results from experiments in the metal props.

From Table 5.15, interior temperatures in the upper layer during the vent door and vent window experiments with the pallets fuel load in the Metal Prop were highly agreeable in the fire room and start of the hall and agreeable at the end of the hall. This suggests that there was no significant difference between the effects of the door vent and window vent on fire development with the pallets fuel load in the Metal Prop. This is likely due to the fuel load having a lower amount of potential heat energy and having most of its contents located in the upper half of the room, which allowed enough oxygen to reach the fuel for efficient combustion through the window opening, despite it being elevated 3.0 ft (0.9 m) above the floor.

Looking at the groups in the vent door vs. vent window comparison results, the fuel load with the highest energy content is almost always associated with the most biased and least correlated comparison (lowest bias and ICC values). For example, the furniture fuel load has the lowest bias and ICC values in nearly every comparison of data from each thermocouple array, with the exception being in the Gypsum Prop results, where the bias and ICC values for the pallets are lower than the furniture values by 0.04 for the 2TC array, and the ICC value for the pallets and OSB is lower than the furniture ICC by 0.01 for the 3TC array. The trend of the most biased and least correlated results corresponding to tests that used the fuel load with the largest amount of potential energy is also present in Table 5.15, which only includes comparison results from experiments with wood-based fuel loads. The bias and ICC values from the post-vent sample comparisons of pallets and OSB tests are consistently lower than those from the corresponding comparisons of tests that used pallets.

In general, combustion during the post-vent period of the vent door experiments was more efficient than that of the vent window experiments. This difference is likely at least partially the reason all bias values in Tables 5.14–5.16 are less than 1.0, which indicates conditions were more severe during the vent door tests than during the vent window tests. The difference in combustion efficiency between the different ventilation openings is highlighted by Figures 5.13 and 5.14, which contain plots of fire room temperature data over the post-vent period of the vent door and vent window tests with the furniture fuel load and pallets and OSB fuel load, respectively, in the Gypsum Prop. The plotted data from the vent door tests are significantly steadier than the data from the corresponding vent window test because combustion of the furniture fuels was much less efficient with the ventilation provided by the window opening.

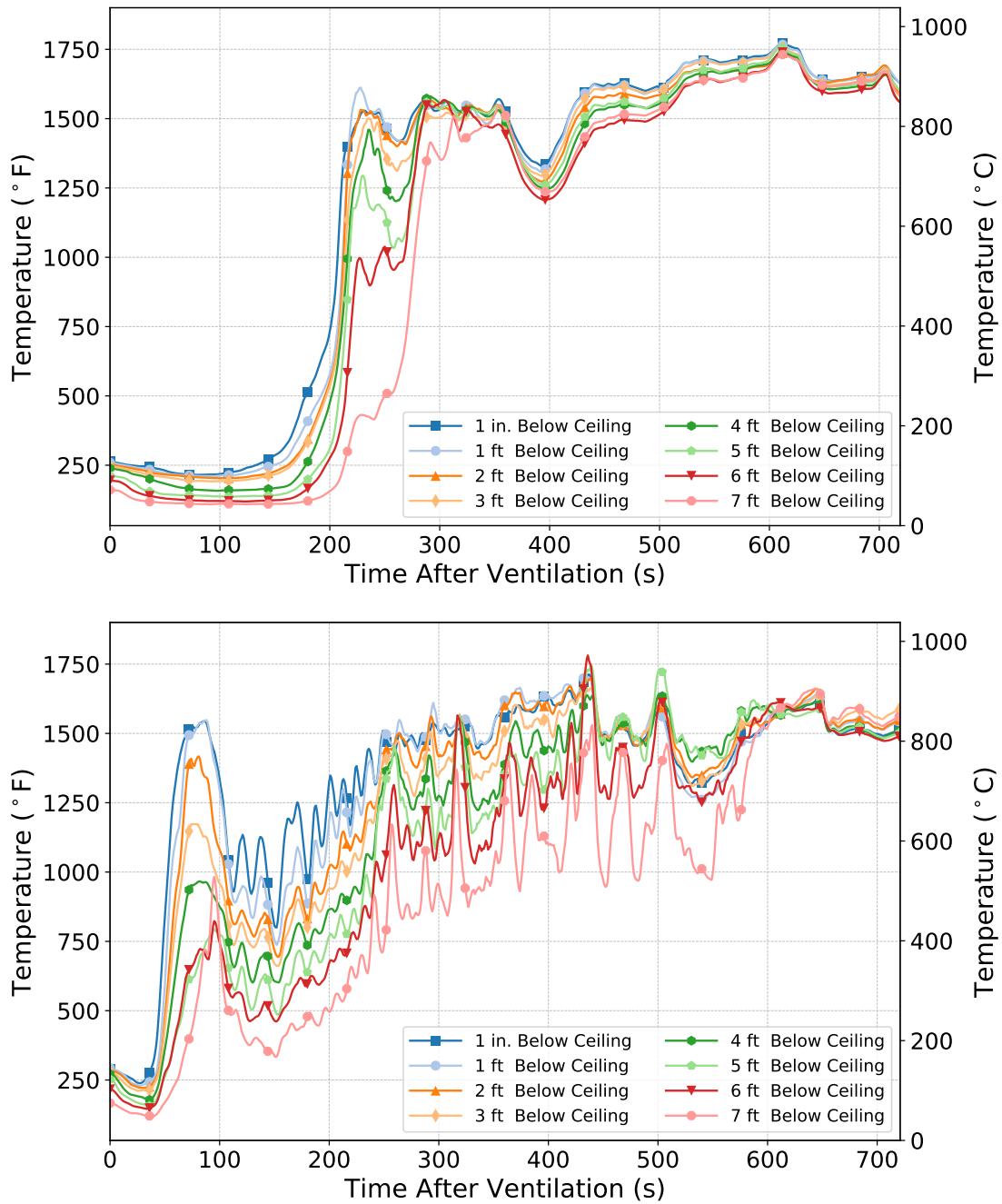


Figure 5.13: Plot of temperatures measured by thermocouples in the fire room array during the post-vent period of the vent door (top) and vent window (bottom) tests with the furniture fuel load in the Gypsum Prop.

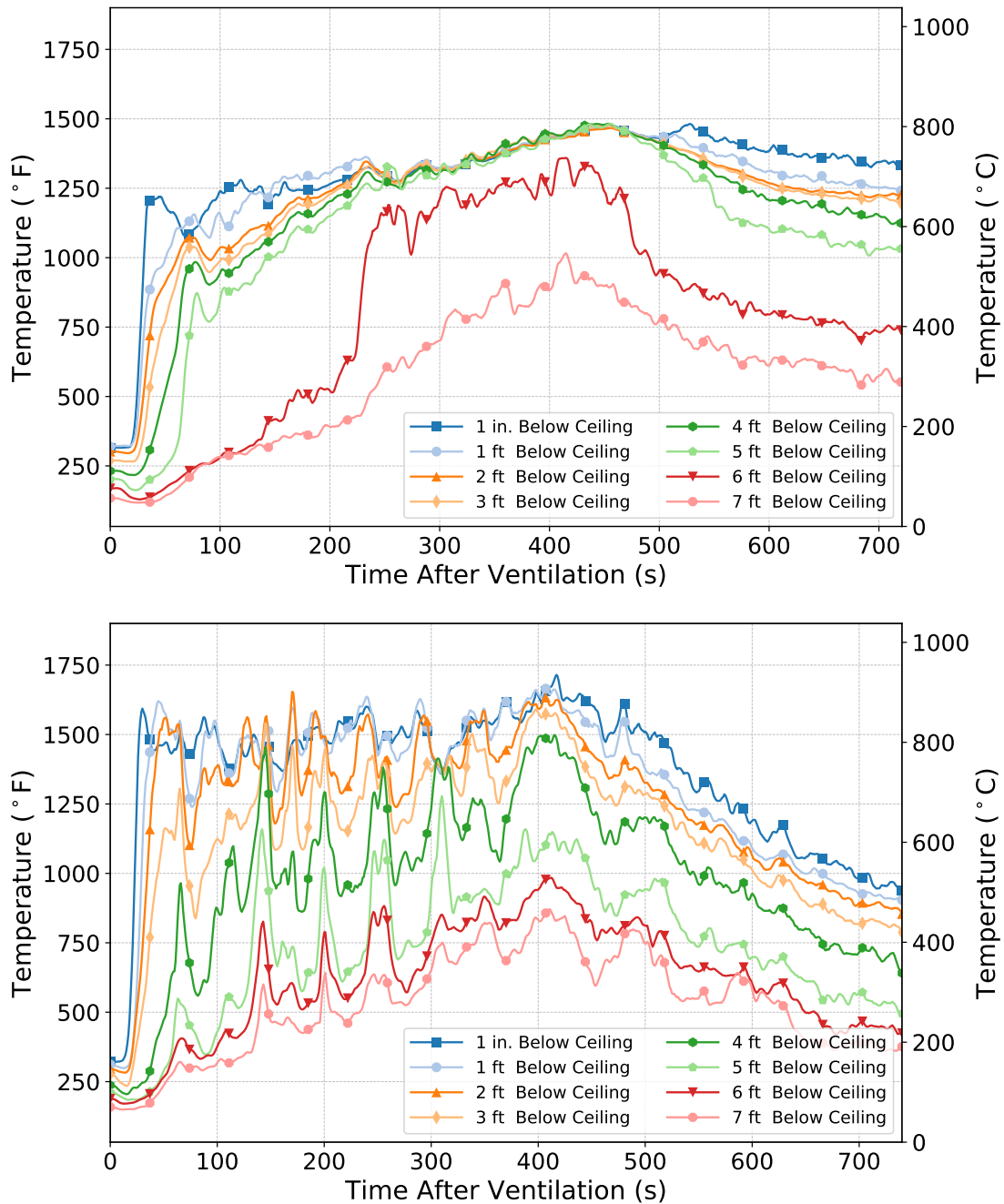


Figure 5.14: Plot of temperatures measured by thermocouples in the fire room array during the post-vent period of the vent door (top) and vent window (bottom) tests with the pallets and OSB fuel load in the Gypsum Prop.

The magnitude of the difference in post-vent thermal conditions between tests with the vent door and vent window configurations was consistently greater for furniture tests than for tests with the wood-based fuels because the furniture fuel package was a much larger fuel source and the majority of its contents was in the lower half of the fire room. The hall door provided a ventilation opening that spanned to the floor level, while the fire room window provided an opening that was elevated above the floor. As a result, air flowed to the fire room through the lower part of the doorway during the post-vent portion of the vent door tests, which allowed O₂ concentrations near the floor in certain areas of the fire room to remain above 16 %, or at levels suitable for flaming combustion [52]. This was especially crucial for the combustion of the furniture fuel package because the majority of the fuel in the configuration was located in the lower half of the room. For the post-vent portion of the vent window tests, however, air flowed to the fire room through the window located 3.0 ft (0.9 m) above the floor, so O₂ concentrations near the floor dropped below the threshold required for flaming combustion. These differences in O₂ concentrations are displayed in Figure 5.15, which includes plots of the O₂ concentrations 4.0 in. (10.2 cm) above the fire room floor near the window and doorway after ventilation during the vent door and vent window tests in the Insulated Metal Prop.

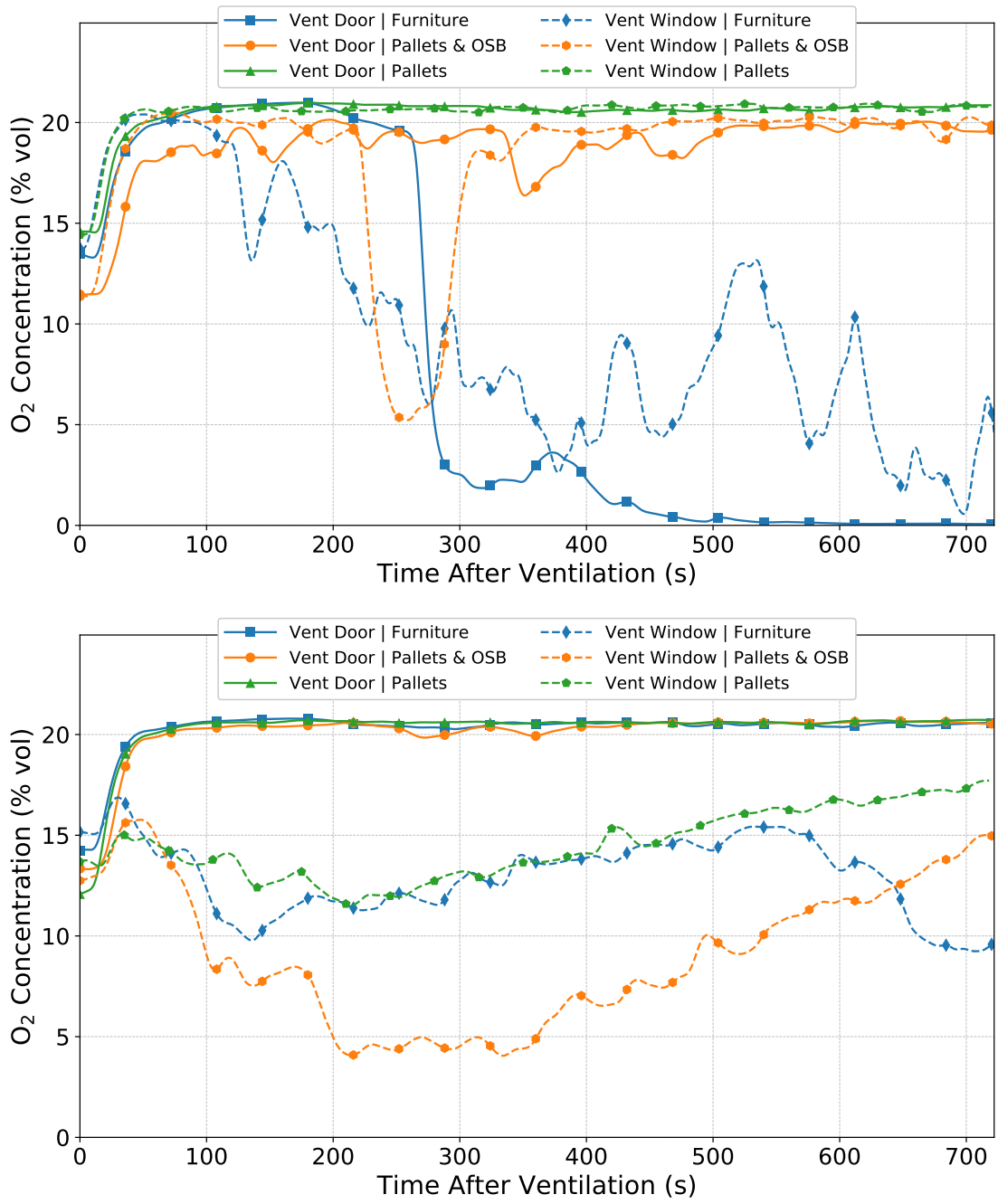


Figure 5.15: O₂ concentrations measured 4.0 in. (10.2 cm) above the floor near the window (top) and doorway (bottom) of the fire room plotted over the duration of the post-vent period of the vent door and vent window tests in the Insulated Metal Prop. Data from vent door tests are plotted as solid lines, and data from vent window tests are plotted as dashed lines.

Due to the lower oxygen concentrations near the floor, more of the furniture fuel package, specifically the parts farthest from the window opening, remained unburned after the vent window experiment than after the vent door experiment. Figure 5.16 shows a side-by-side comparison of the

furniture fuel packages after experiments with the vent door and vent window configurations. The difference between these configurations had less of an impact on the combustion of the wood-based fuel packages because these fuel loads contained a significant amount of fuel at heights around the level of the window opening. Therefore, both ventilation configurations provided enough fresh air to the wood-based fuel packages to sustain flaming combustion over the post-vent portion of the experiment.



Figure 5.16: Images of the furniture fuel package after suppression from the tests with the vent door (left) and vent window (right) configurations. More fuel (end of the couch, carpet and padding near doorway, etc.) remained after the test with the vent window configuration than after the test with the vent door configuration.

To better understand the difference in thermal conditions created by the wood-based training fuel loads in response to a door vent versus a window vent, temperature and heat flux data from the approximate levels of a crouching or crawling firefighter's head during the experiments can be compared to the firefighter PPE limit thresholds listed in Table 5.1. Figures 5.17 and 5.18 contain these temperature and heat flux data, respectively, collected during the vent door and vent window experiments in the Insulated Metal Prop.

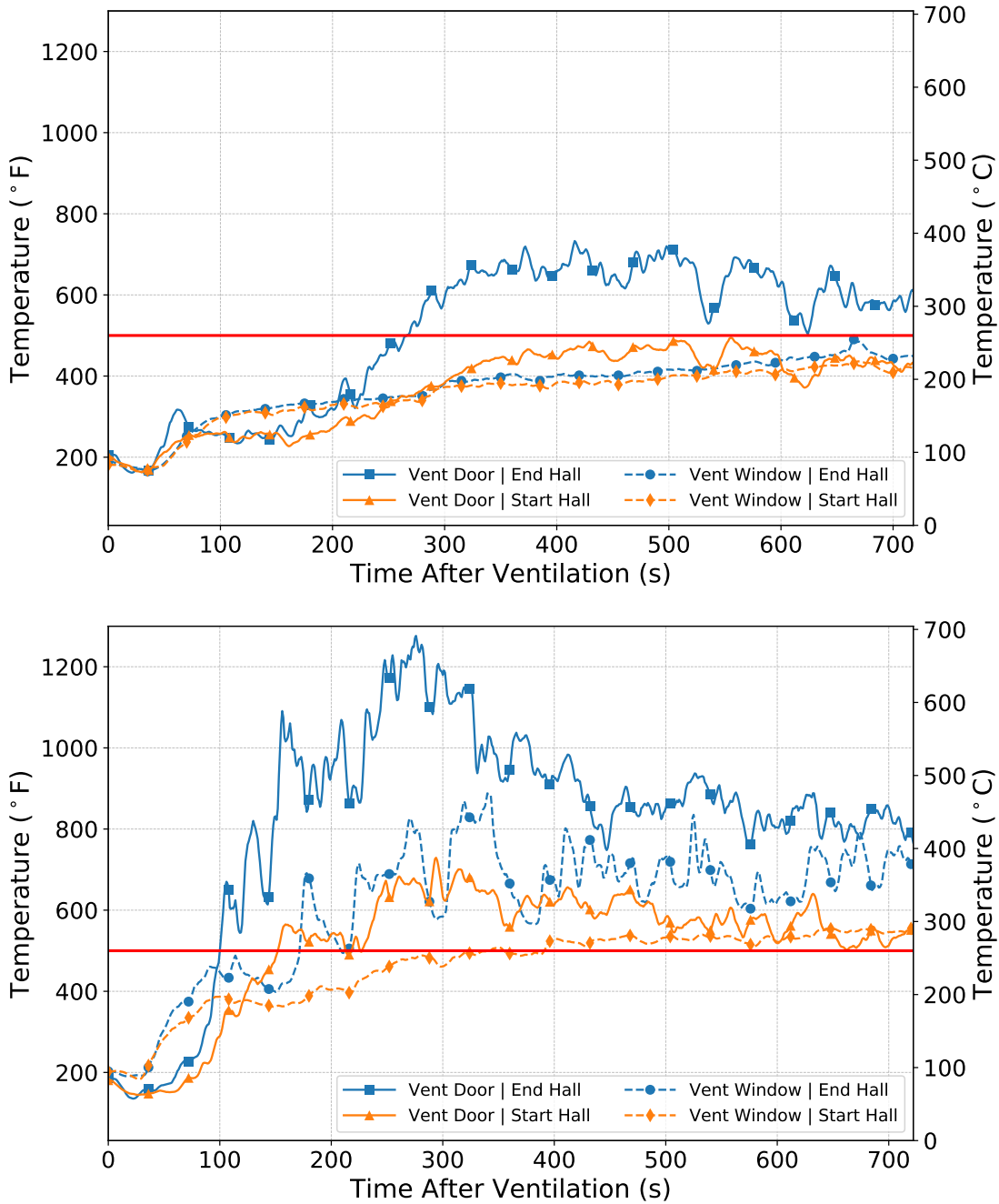


Figure 5.17: Temperatures measured 3.7 ft (1.1 m) above the floor at the end hall (blue lines) and start hall (orange lines) locations after ventilation during the vent door (solid lines) and vent window (dashed lines) experiments in the Insulated Metal Prop. The top graph is from experiments with the pallets fuel load, and the bottom graph is from experiments with the pallets and OSB fuel load. The red line at 500 °F (260 °C) highlights the firefighter PPE temperature threshold listed in Table 5.1.

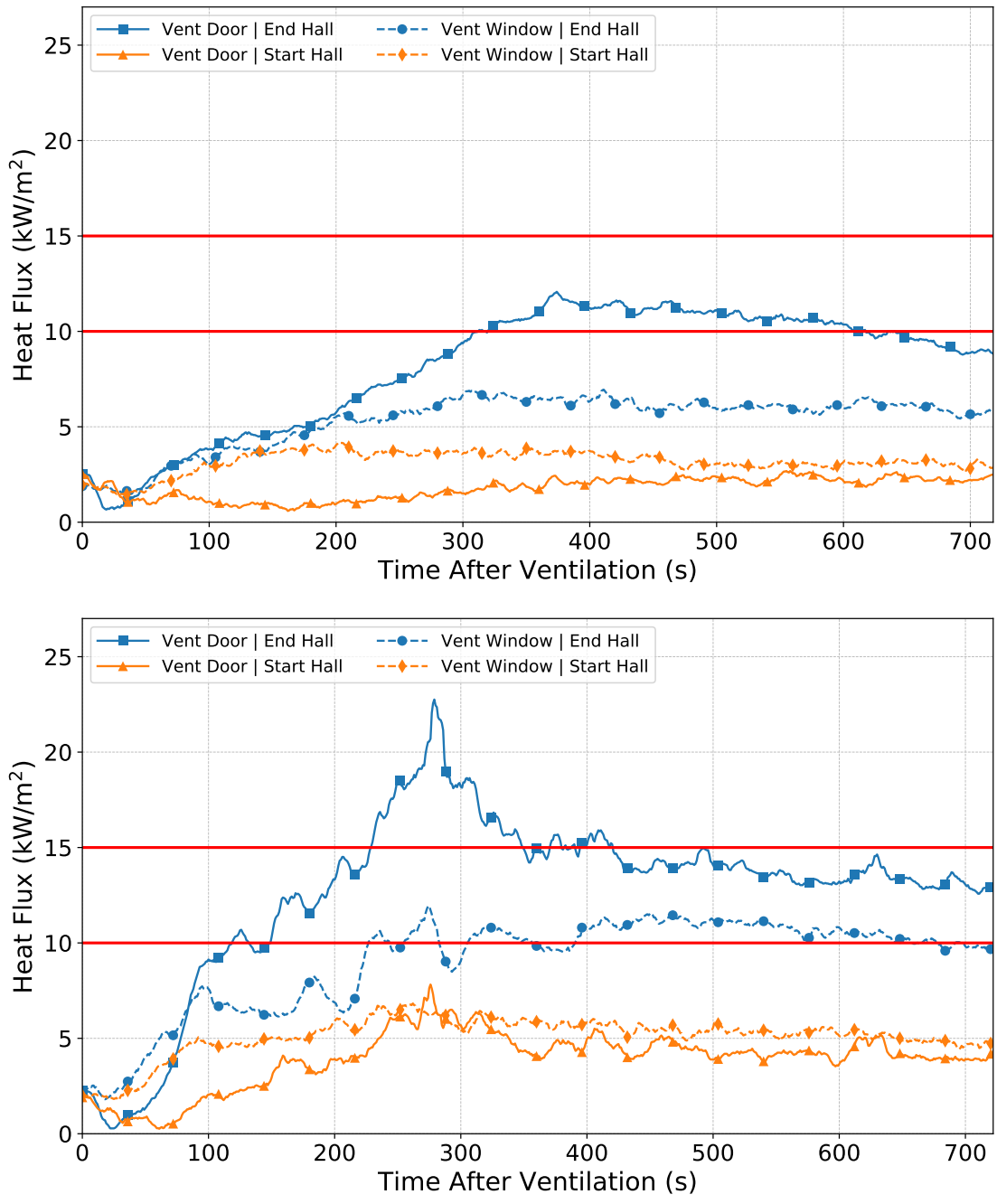


Figure 5.18: Heat flux in the horizontal direction measured at 3.0 ft (0.9 m) above the floor at the end hall (blue lines) and start hall (orange lines) after ventilation during the vent door (solid lines) and vent window (dashed lines) experiments in the Insulated Metal Prop. The top graph is from experiments with the pallets fuel load, and the bottom graph is from experiments with the pallets and OSB fuel load. The red lines at 10 kW/m² and 15 kW/m² highlight the firefighter PPE heat flux exposure thresholds listed in Table 5.1.

A few things can be noted from the plots displayed in the two figures. First, the temperatures and heat fluxes measured at the start hall location were not significantly different between the vent door and vent window cases with either fuel load. The disparity in thermal conditions between the vent door and vent window experiments is much clearer in the plots of data collected at the end of the hall. These plots also show that if located too close to the fire room, a firefighter could encounter thermal exposures that exceed the limits of their PPE; the end hall temperatures and heat fluxes measured during experiments with the pallets and OSB fuel load exceeded threshold limits for periods longer than their maximum durations in nearly every case. During experiments with the pallets fuel load, the temperature threshold of 500 °F (260 °C) was surpassed for longer than 300 seconds during the vent door case. The end hall heat flux during the same experiment exceeded the 10 kW/m² limit for nearly 300 seconds over the span from around 315 s to 615 s. The data plots show that both wood-based fuel packages have the potential to create thermal conditions that could cause damage to firefighter PPE, specifically to an SCBA facepiece.

Caution should be used when designing any training scenario. The comparisons between vent door and vent window experiments show that even with the pallets fuel package, firefighters at the end of the hallway can be exposed to conditions that have the potential to damage their PPE. The hazard significantly increases when OSB is added to the fuel load. Finding proper locations for students during exercises depends on a number of factors, such as the experience level of the students and the purpose and duration of the training exercise. Instructors can use trial and error to find the configuration that works best for a specific exercise, erring on the side of caution and following the guidelines included in *NFPA 1403*. The results presented above show that it's possible for students to experience the difference between a door vent and window vent during a fire from a basic pallets and straw fuel load.

5.6.2 Open Door, No Action vs. Open Door, Vent Window

Data were compared between three pairs of experiments to analyze the extent to which additional ventilation via the window affects the behavior of a fire in an environment already containing sufficient ventilation to promote fire growth to a steady state. All six experiments were conducted in the Metal Prop with the hall door open for the entire test duration to provide ventilation to the fire. The experimental results were used to compare a scenario in which the fire room window remained closed until the end of the test at 12 minutes after ignition (referred to as “open door, no action”) to a scenario in which the fire room window was opened at six minutes after ignition (referred to as “open door, vent window”) for each fuel load type. The comparison results are concerned with temperature data from the “post-growth” portion of the tests, or the period from six minutes after ignition to the end of the test at 12 minutes after ignition. Data comparisons between experiments were focused on the post-growth period because it was over this time that the ventilation configurations varied.

The results from the post-growth data comparisons between the open door, no action and open door, vent window experiments for each fuel package are presented in Table 5.17. The bias and ICC values computed across the measurement pairs formed by the post-growth data from the relevant

sensors of each thermocouple array are included in the table. Listed alongside each set of bias and ICC values is the number of bias values within the range of the thermocouple measurement uncertainty as a fraction of the total number of sample sets considered for the given thermocouple array.

Table 5.17: Overall Bias & ICC Values from Open Door, No Action vs. Open Door, Vent Window Comparisons of Post-Growth Data from each Interior Thermocouple Array

Open Door No Action vs. Vent Window	Post-Growth		
	Biases in Range	Overall Bias	Overall ICC
<i>Fire Room (1TC)</i>			
Furniture	5/5	1.11	0.08
Pallets	4/5	0.85	0.74
Pallets & OSB	5/5	0.97	0.82
<i>End Hall (2TC)</i>			
Furniture	2/3	0.83	0.02
Pallets	2/3	0.83	0.51
Pallets & OSB	2/3	0.84	0.47
<i>Start Hall (3TC)</i>			
Furniture	0/3	0.77	0.27
Pallets	2/3	0.85	0.54
Pallets & OSB	2/3	0.86	0.46

As the sole difference between the experiments in each comparison is the window that was opened, any significant differences between data sets can be attributed to the window vent significantly altering the local fire conditions. On the contrary, if post-growth comparisons between data sets revealed temperatures were indistinguishable between experiments, the window vent did not significantly impact the surrounding thermal conditions.

A consistent trend can be seen in the table of bias and ICC values calculated for comparisons of hallway temperatures between the open door, no action and open door, vent window experiments with each fuel package. All bias values from these comparisons are in the direction of more extreme temperatures during the open door, no action experiment. This is reasonable result considering the effect that opening a window has on the flow path of the fire environment.

The values from comparisons between post-growth data measured by fire room thermocouples indicate that the temperatures were indistinguishable between tests when either wood-based fuel was used. The fire room temperatures between experiments with the pallets and OSB fuel package were highly agreeable. The fire room temperatures between experiments with the pallets fuel load were on the border of the being considered highly agreeable, but with a bias equal to the limit of the measurement uncertainty at 0.85 and an ICC value of 0.74, the temperature data sets between experiments were categorized as only being agreeable. These values from the comparison of fire room temperatures between experiments with wood-based fuel packages indicate that venting the window did not significantly alter conditions in the fire room. The comparison of fire room tem-

peratures between furniture experiments, however, revealed a bias towards more severe conditions during the post-growth portion of the open door, vent window test compared to those over the same period of the open door, no action test. The bias and ICC values computed for the comparison imply that the difference in fire room temperatures between the experiments is significant.

These findings are a result of the larger energy content of the furniture fuel package compared to the wood-based fuel loads. Ventilation through the open door provided the wood-based fuel loads with enough oxygen for them to burn efficiently. It did not, however, provide enough oxygen for the furniture fuel load to burn with complete efficiency. Thus, when the second ventilation opening was introduced, O₂ concentrations within the fire room increased and combustion efficiency improved. This behavior is displayed in Figure 5.19, which contains plots of the oxygen concentration data collected during the open door, no action and open door, vent window tests with the furniture fuel package.

Visual observations during the formation of the neutral plane at the hallway door as the fire grew were noted during the open door, no action tests for each fuel load. There was variation in height of the fully-developed neutral plane between fuel loads, as shown by the images and BDP plots in Figure 5.20. The neutral plane was consistently lowest during the furniture tests. Of the two wood-based fuel loads, the neutral plane generated by the pallets and OSB fuel load was lower than that created by the pallets fuel load.

When the window was opened to supply additional ventilation to the developed fire during the open door, vent window experiments, the initial response of the neutral plane was similar between the experiment with the furniture fuel load and those with wood-based fuel loads. Figure 5.21 contains a side-by-side comparison of stills from exterior thermal imager recordings one second before, 30 seconds after, and 60 seconds after the window was opened to alter ventilation during experiments with the pallets and OSB fuel load and furniture fuel load. Notice, the initial response in each case was similar; the neutral plane rose after the window was opened, as shown by the video stills 30 seconds after the window was opened compared to the corresponding stills one second before the window was opened. After 60 seconds, the neutral plane remained elevated during the pallets and OSB test, while during the furniture test, it eventually descended after rising as the fire burned more efficiently due to the new ventilation source. Previous research has shown that a brief rise of the neutral plane followed by a descent is the expected response in the case of supplying ventilation to a fuel-rich fire — the type often encountered by firefighters in structure fires containing fuels composed of synthetic materials and foam plastics [5].

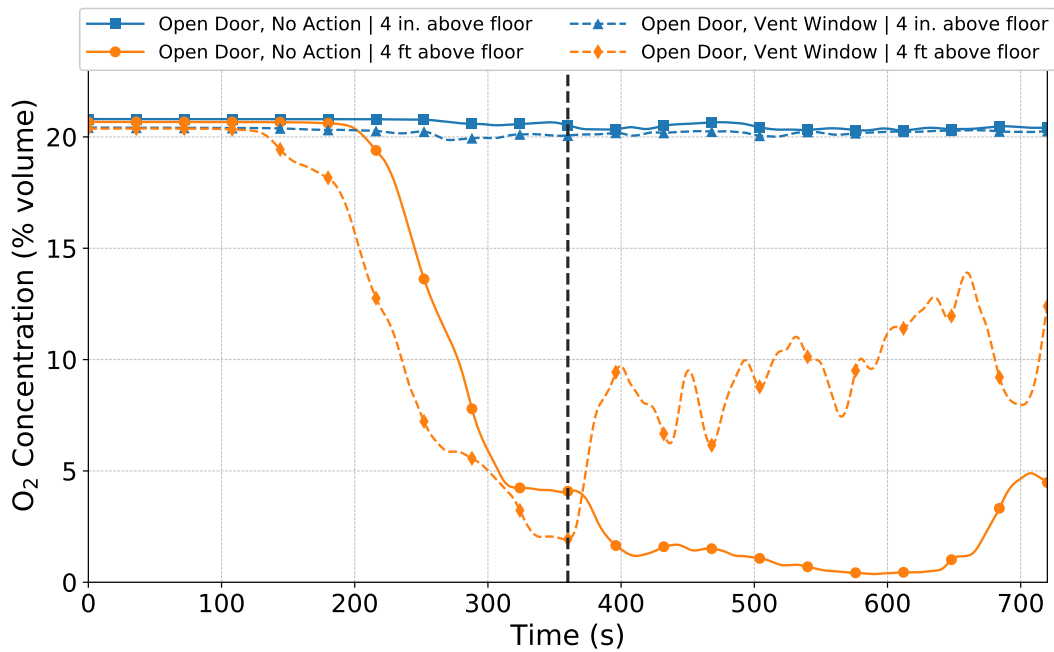
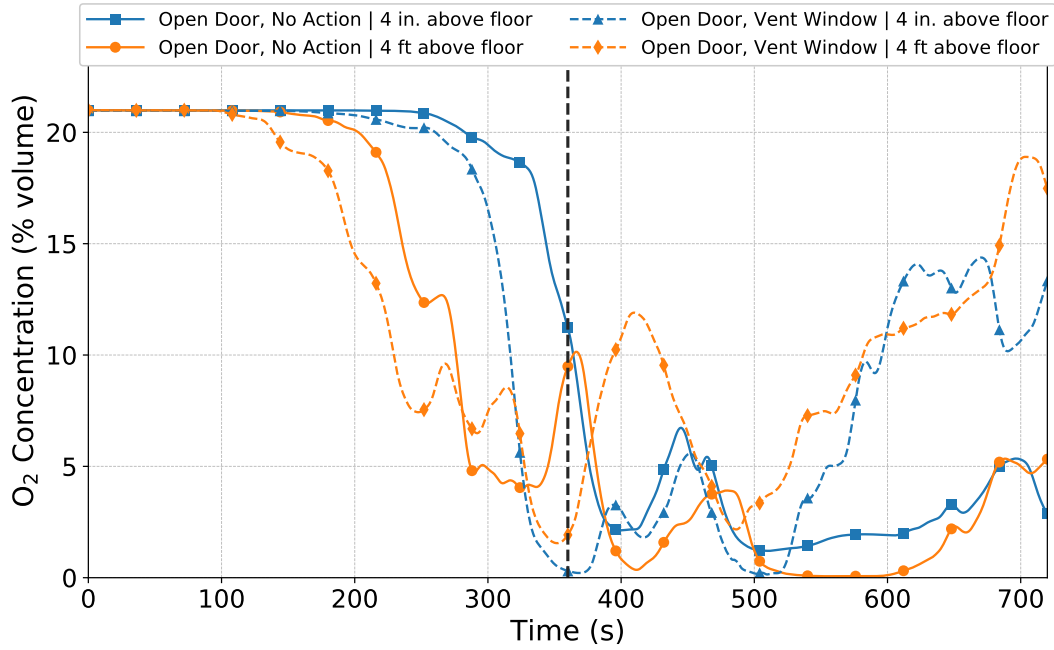


Figure 5.19: Plots of the O₂ concentrations from the open door, no action and open door, vent window tests with the furniture fuel load. The top graph is of the data collected near the fire room window, and the bottom graph is of the data collected near the fire room doorway. Data from 4.0 in. (10.2 cm) above the floor are plotted with solid lines, and data from 4.0 ft (1.2 m) above the floor are plotted with dashed lines. The black dashed line marks the time at which the window was opened during the open door, vent window test.

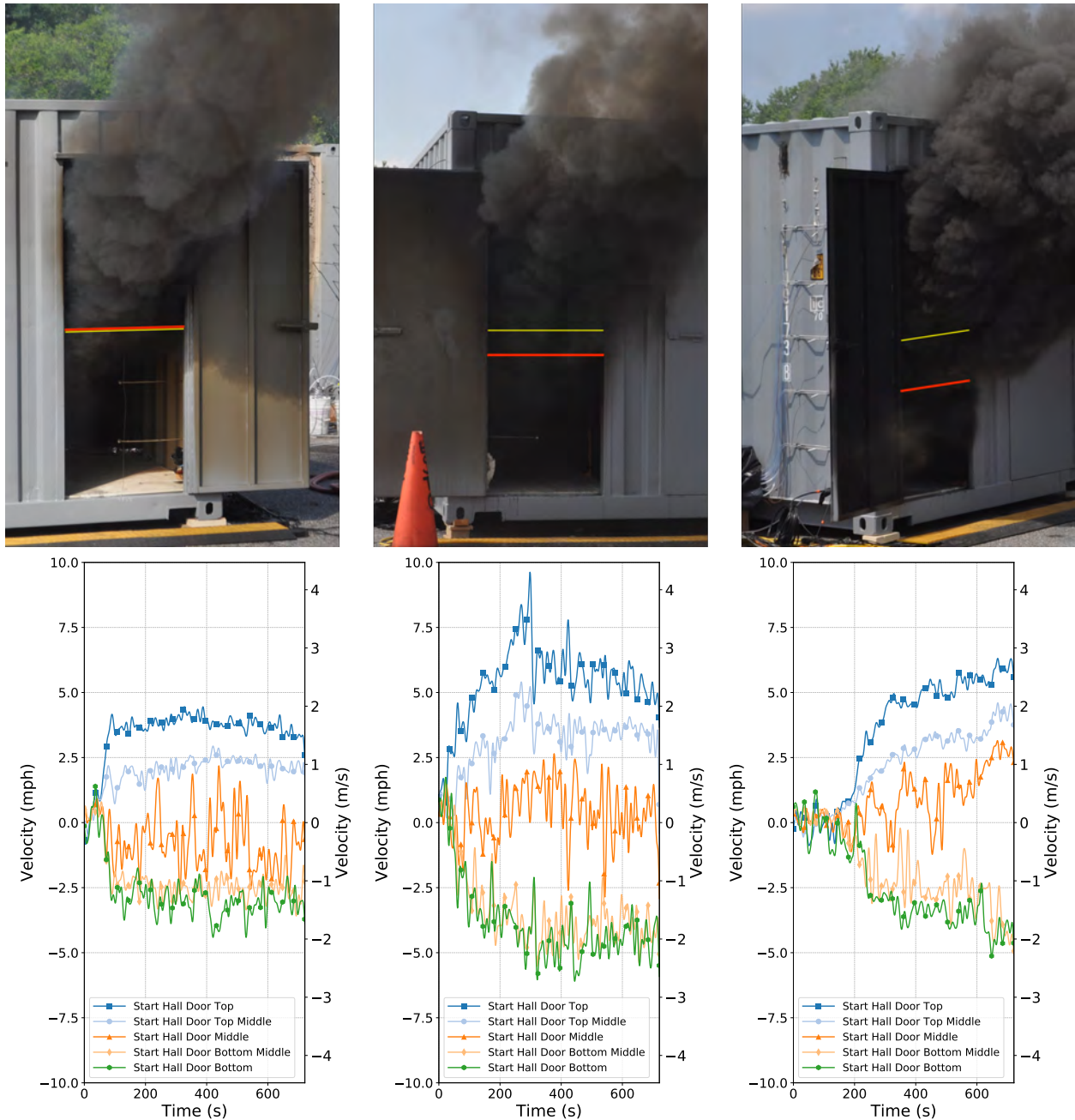


Figure 5.20: Neutral plane at the doorway after fire development of the pallets (left); pallets and OSB (middle); and furniture (right) fuel packages. A yellow line marks the approximate height of the door handle to provide a reference point in each photo, and the red line marks the approximate height of the neutral plane based on the smoke in the photo and the BDP data. The BDP data measured in the doorway over the period after the hall door was opened in each test is included under each image.

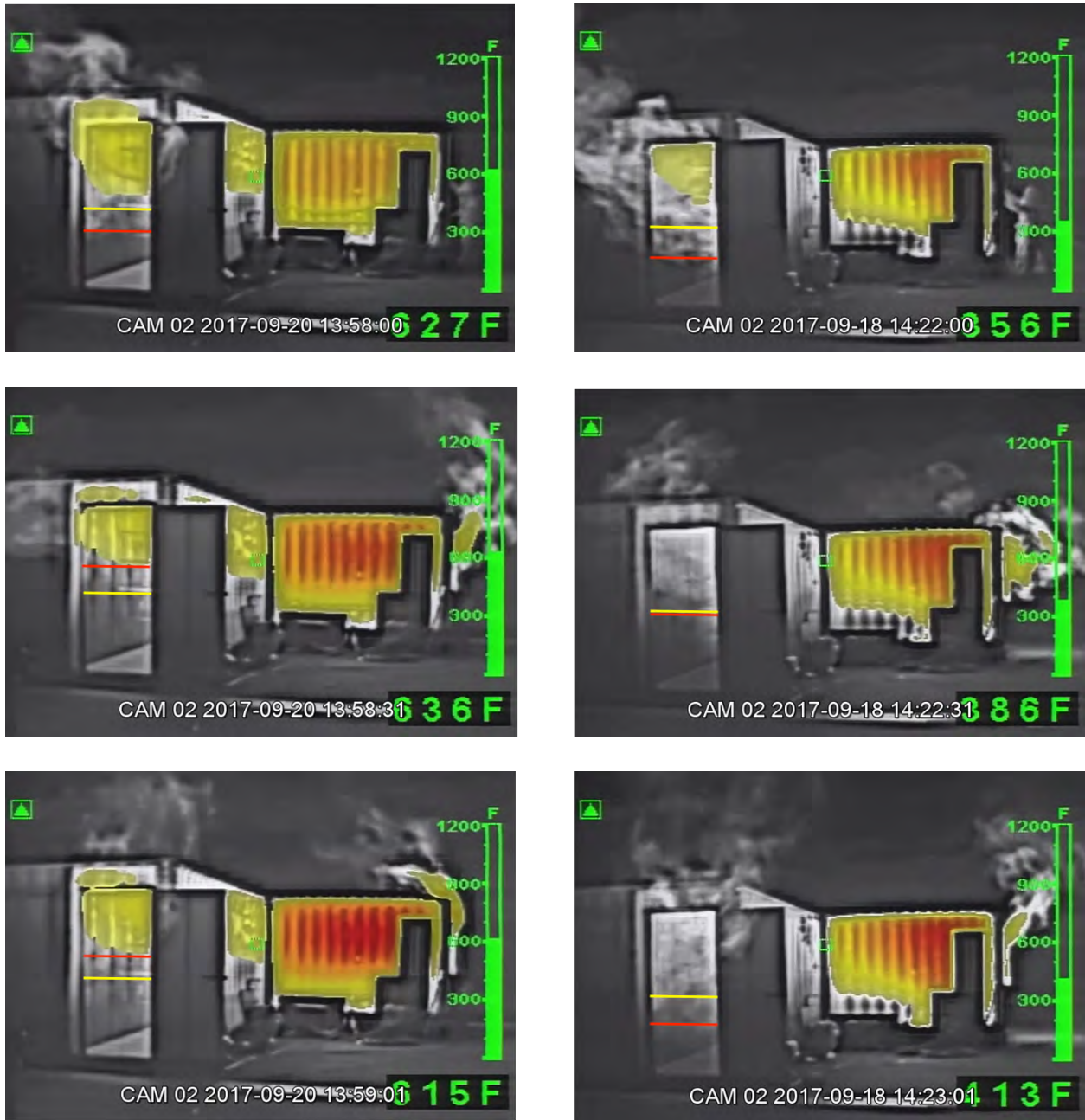


Figure 5.21: Still images from thermal imager video of the Metal Prop exterior one second before (top row), 30 seconds after (middle row), and 60 seconds after (bottom row) the window was opened during tests with the pallets and OSB (left side) and furniture (right side) fuel loads. A red line marks the approximate height of the neutral plane and a yellow line marks the height of the door handle to provide a similar reference point in each image.

Being able to correctly relate visual cues from smoke conditions during the progression of neutral planes and flow paths to specific characteristics of fire dynamics allows firefighters to make better-informed decisions on the fireground. Thus, the differences between flow path and neutral plane development with wood-based fuels compared to modern fuels should be acknowledged and discussed during fire training.

5.7 Suppression Effects

Three experiments, one per prop, were conducted to study the effects of interior suppression in each type of prop. The pallets and OSB fuel package was used for each test. The fuel was ignited with the fire room window closed and the hall door opened, and suppression was initiated approximately 360 seconds later. The vent openings remained unchanged (hall door open and window closed) over the duration of the experiments to maintain a constant ventilation configuration. This ensured that changes in conditions during the time of firefighter operation were independent of changes to the ventilation profile of the prop.

The thermal exposure to the firefighter performing suppression was measured by two gauges equipped to the firefighter's helmet: one positioned on the front to measure the incident heat flux in the horizontal direction (labeled HF1) and one positioned on the top to measure the incident heat flux in the vertical direction (labeled HF2). Plots of the heat flux measured by these sensors around the time of suppression during each experiment are presented in Figure 5.22.

The plots in the two charts are of similar shape. In the time leading up to suppression, the data remain relatively steady at slightly elevated values because the firefighter was positioned with the hoseline near the open doorway. A few seconds before suppression, the plots sharply increase as the firefighter enters the prop to begin suppression. Shortly thereafter, the plots change direction and rapidly decline as the intensity of the fire environment is mitigated due to suppression. The horizontal and vertical maximum heat flux values from the Metal Prop and Insulated Metal Prop tests are indistinguishable from the gauge's measurement uncertainty, which is represented by error bars on the plots. Both values from the Gypsum Prop tests, however, are drastically smaller than those measured during the Metal Prop and Insulated Metal Prop tests.

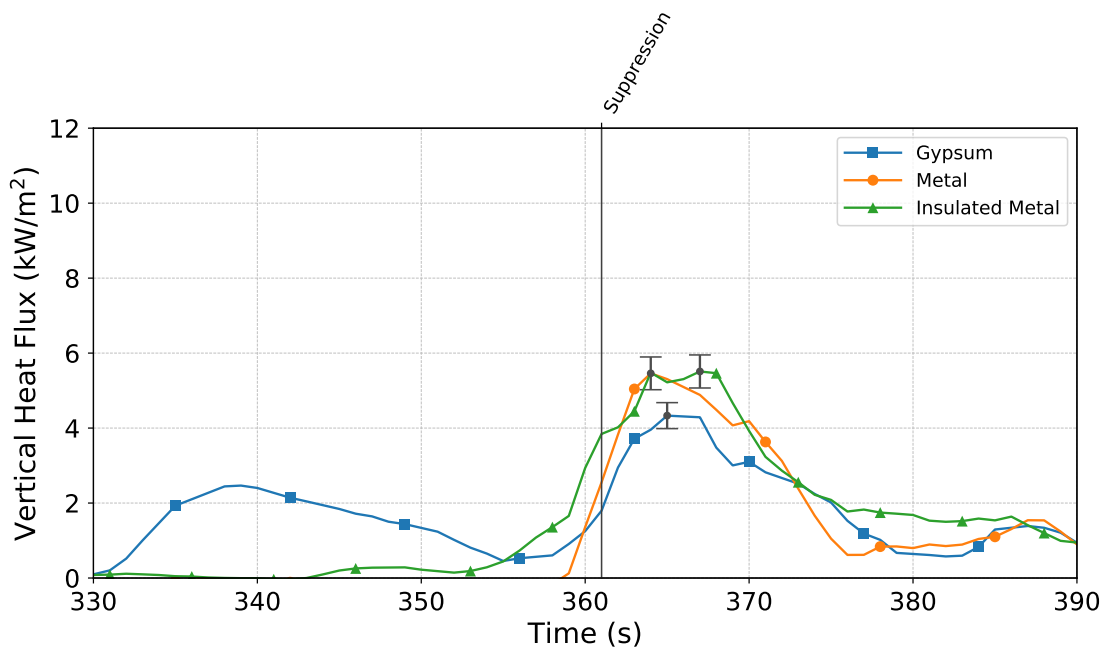
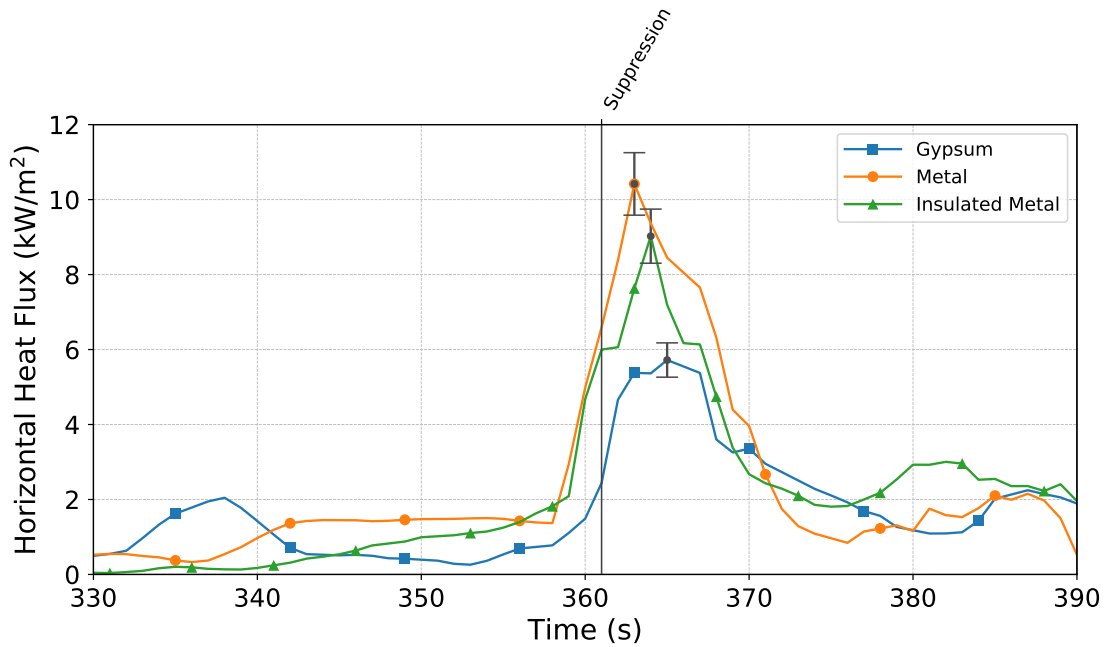


Figure 5.22: Plot of the incident heat flux to the firefighter around the time of suppression during the suppression effects tests. The top chart contains horizontal heat flux data measured in front of the firefighter, and the bottom chart contains vertical heat flux data measured above the firefighter.

Further analysis of the experimental data was performed to determine if this discrepancy was simply a result of the firefighter entering a thermal environment in the Gypsum Prop that was less intense than that encountered during the Metal Prop and Insulated Metal Prop experiments. Temperatures measured 4.0 ft (1.2 m) below the ceiling at the end hall and start hall array locations

during each test are plotted in Figure 5.23 to provide insight into how thermal conditions near the height of a crawling firefighter varied between tests.

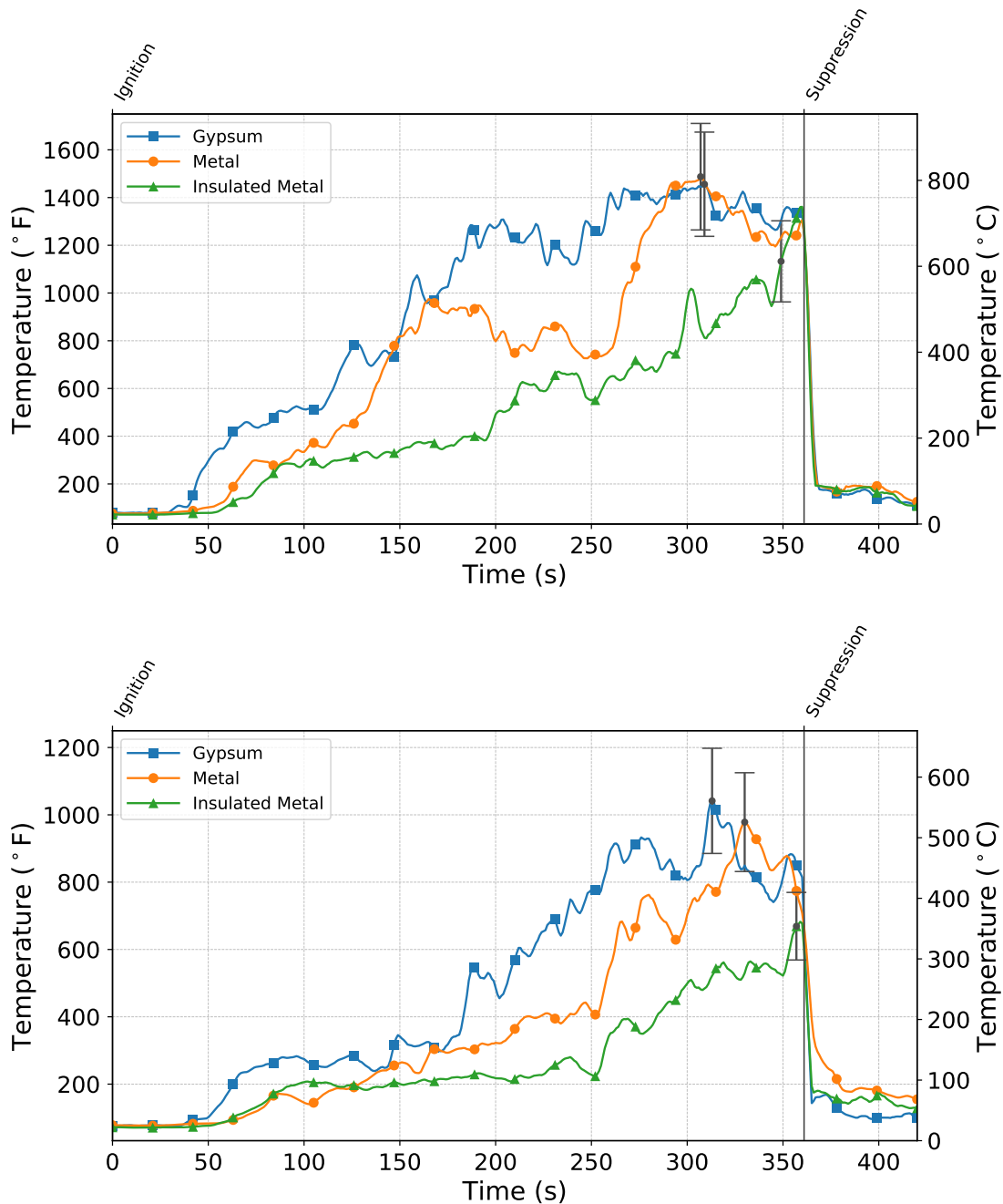


Figure 5.23: Temperatures measured 4.0 ft (1.2 m) below the ceiling at the end hall (top) and start hall (bottom) locations plotted over the duration of each suppression effects test.

Looking at the charts, specifically around the time shortly before the start of interior suppression, the end hall temperatures are indistinguishable from the measurement uncertainty between all tests, and the start hall temperatures during the Insulated Metal Prop are noticeably less severe than those

from the Metal Prop and Gypsum Prop tests, which are indistinguishable from one another. So, this suggests that if the difference in heat flux data collected by the helmet sensors was due to varying intensities of the thermal environments at the time of entry, the heat flux measurements from the Insulated Metal Prop test would be less than those from the Metal Prop and Gypsum Prop tests. As previously discussed, this was not the case; the measured incident heat flux to the firefighter was less intense during the Gypsum Prop test than during the tests in the metal props.

As mentioned in Section 3.3, the hallway thermocouple arrays were moved against the wall and the corresponding heat flux gauges were removed entirely for the suppression effects tests to eliminate potential obstructions for the firefighter performing interior suppression. To approximate the horizontal heat flux exposure at firefighter level near the doorway around the time of suppression, the heat flux measured 3.0 ft (0.9 m) above the floor at the start hall location during the open door, no action test with the pallets and OSB fuel load in the Metal Prop can be used. This heat flux averaged $3.7 \text{ kW/m}^2 \pm 0.3 \text{ kW/m}^2$ from 330 s to 390 s after ignition and is plotted with the HF1 helmet data from the suppression effects tests in Figure 5.24.

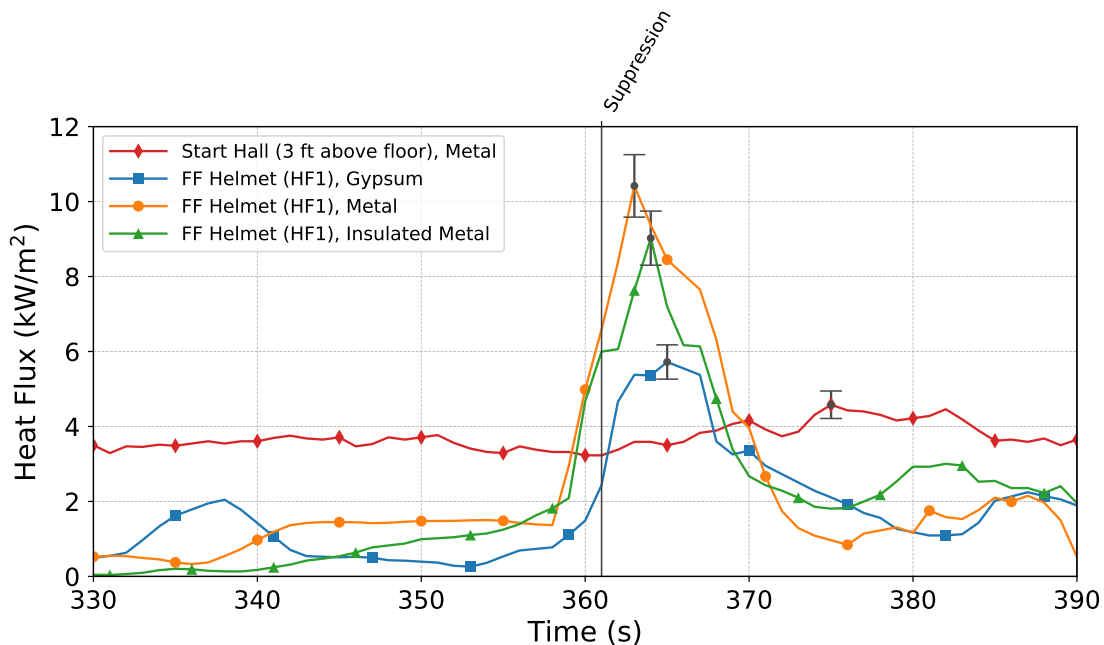


Figure 5.24: Start hall heat flux measured over the period from 330 s to 390 s after ignition of the pallets and OSB fuel load during the open door, no action test plotted with the HF1 helmet data over the same period of each suppression effects test. Note, the sharp increase in the couple seconds before suppression that occurs in the HF1 data plots is due to the firefighter entering the prop before initiating suppression.

If the increase in heat flux measured by the sensor on the firefighter’s helmet after the start of suppression was solely the result of the firefighter entering the interior thermal environment, the maximum recorded value shouldn’t be much larger than this average value. However, it was significantly larger during the Metal Prop and Insulated Metal Prop tests, suggesting something may have happened during these tests that did not occur during the Gypsum Prop test as the firefighter

entered the environment and initiated suppression.

The difference in heat flux exposure during the first moments of suppression are suspected to be at least partially due to the conversion of water into steam. The interior of both metal props were lined with steel, a material with a thermal conductivity drastically higher than that of gypsum. This difference in thermal conductivity resulted in more water being converted to steam as it contacted the wall during suppression in the Insulated Metal Prop and Metal Prop experiments than in the Gypsum Prop experiment. This difference is not only manifested in the heat flux data but also in qualitative evidence from the firefighter performing suppression, who stated that the environments in the metal props were “noticeably more uncomfortable” than in the Gypsum Prop.

The results discussed above indicate the thermal exposure to firefighters in a metal container prop during interior suppression can differ significantly from a typical structure, possibly due to steam conversion. It should be noted the applicability of this result is limited exclusively to the tested scenarios. Additional experiments need to be performed with varying parameters (prop size and layout, suppression technique, etc.) to obtain a more complete understanding of suppression effects within metal container props. It's possible that increasing the interior volume of the training prop or using a certain suppression tactic could mitigate the measurable differences in thermal exposure to firefighters between training props constructed from metal shipping containers and those constructed from other materials, like the Gypsum Prop. Despite its limitations, this result should be taken into consideration and discussed before conducting fire training exercises in any prop with metal interior wall linings, as the interior walls of modern-day structures are typically lined with a non-metal material, like gypsum board.

6 Considerations

Important findings resulting from the analysis of experimental data presented and discussed in Chapter 5 are outlined in the following sections of this chapter. Data and/or experience(s) are provided to support each consideration regarding the implementation of different prop constructions and fuel loads in live-fire training exercises and demonstrations.

Unlike the tactical considerations from previous UL FSRI reports [5–7, 27], which focused on the fire dynamics in single-family dwellings and the application of fireground tactics, such as ventilation and suppression, these considerations focus on the use of props constructed from steel shipping containers for live-fire training. The prior studies identified changes in construction and contents of homes that have caused present-day residential structure fires to vary drastically from those typically created during live-fire training. Through the use of the following training considerations, it is possible to quantify this gap and safely replicate ventilation-controlled fires. Application of these considerations should always coincide with local and regional training laws/protocols, specifically those described in *NFPA 1403*.

6.1 Training Considerations

The ability to represent pieces of ventilation-controlled fire environments in metal props provides instructors with a tool to effectively demonstrate and reproduce some principles of fire dynamics applicable to present-day residential structure fires. Understanding the limitations and their practical impact on training is essential to ensuring that the most accurate message is transmitted to students. The training considerations in Sections 6.1.1–6.1.6 further elaborate on the limitations and safety considerations associated with reproducing fire dynamics principles in metal containers.

6.1.1 Specific Aspects of Ventilation-Controlled Fires can be Generated in Metal Props

Of the fires studied for this report, those in the Gypsum Prop with the furniture fuel load were considered to be the most similar to what is typically encountered by firefighters in the field. These fires occurred in a structure with interior walls lined with gypsum board overtop wood studs and fiberglass insulation, similar to the construction of many residential dwellings, and also had a fuel load of modern furnishings composed of synthetic materials and foam plastics. Comparing experimental data from these tests in the Gypsum Prop to data from similar tests in the Metal Prop and Insulated Metal Prop revealed both similarities and differences between the three props.

Following ignition with all ventilation openings (i.e., the hall door and fire room window) closed, the fire in every prop became ventilation-limited, entered a decay state, and regrew after a vent

was opened. As an example, plots of the fire room temperatures during tests with the furniture fuel load in the Gypsum Prop and Metal Prop are shown in Figure 6.1.

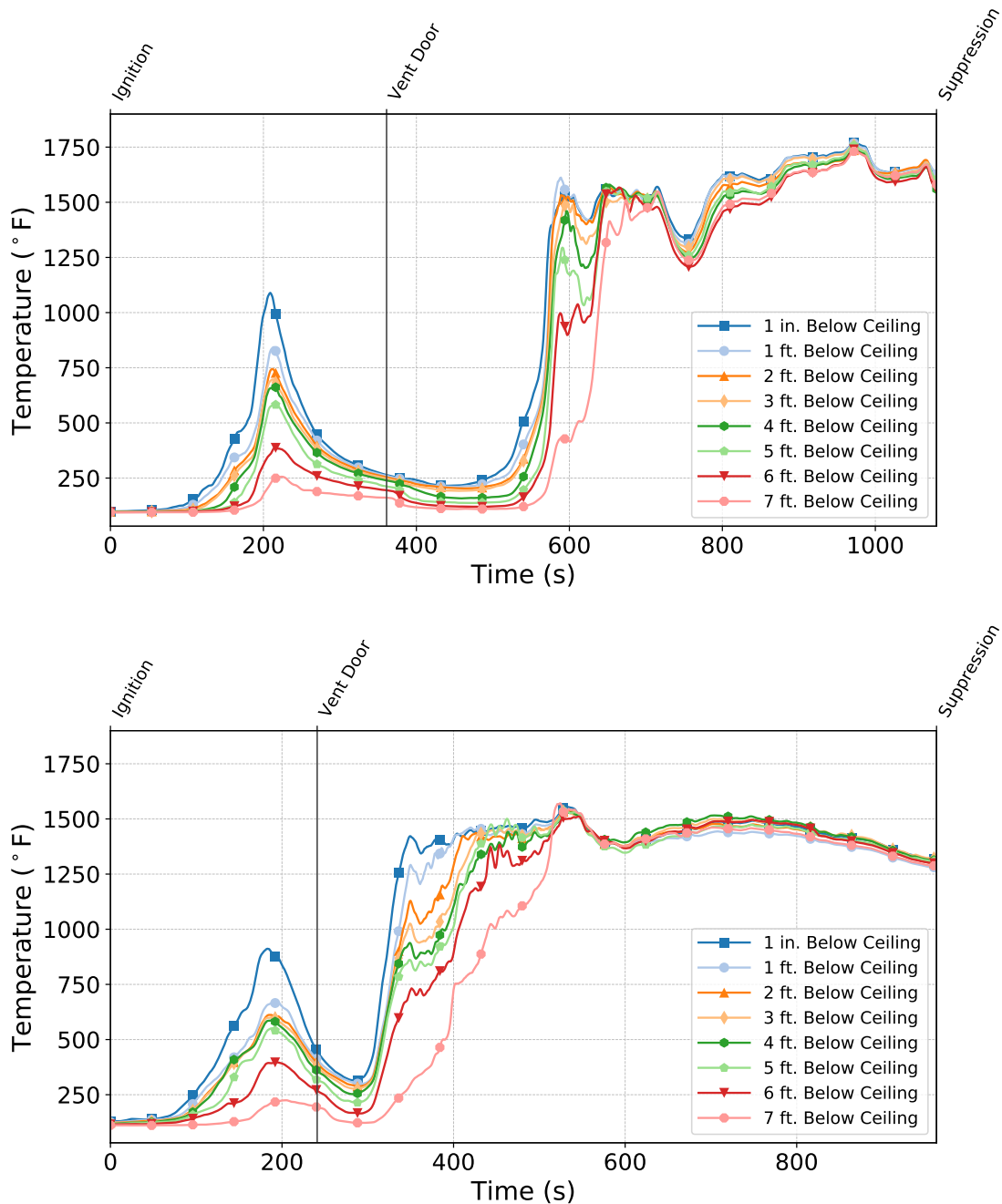


Figure 6.1: Temperatures from the fire room thermocouple array during tests with the furniture fuel load in the Gypsum Prop (top) and Metal Prop (bottom).

The two charts show that the overall fire development was similar between the props — the fire became ventilation-limited shortly after ignition, regrew after the door was opened, and then progressed to flashover. However, the door had to be opened at 240 seconds after ignition in the Metal

Prop to prevent the fire from extinguishing due to lack of oxygen, whereas in the Gypsum Prop, opening the door 360 seconds after ignition resulted in fire regrowth.

The inability to produce fire regrowth by opening the door at 360 seconds in the metal props may be due to the differences between the interior wall linings. The interior wall linings of the props constructed from shipping containers were composed of steel, a heat conductor, while the interior walls of the Gypsum Prop were composed of gypsum, a heat insulator. As a result, the heat generated during initial fire growth was transferred from the environment to the walls of the prop at a quicker rate in the metal props than in the Gypsum Prop. When the door was opened at 360 seconds after ignition in the metal props, too much heat may have been transferred from the environment for the fire to regrow.

Thermal conditions generated by fires in the Metal Prop and Insulated Metal Prop were consistently less intense than those in the Gypsum Prop. Consider the heat flux measurements from the end hall and start hall locations (shown in Figure 6.2) during tests with the furniture fuel load in the Gypsum Prop and Metal Prop plotted in Figure 6.3. The figure contains data over the period following the opening of the hall door, which provided sufficient ventilation to the fire, allowing it to regrow and reach a fully-developed state for the new ventilation configuration.

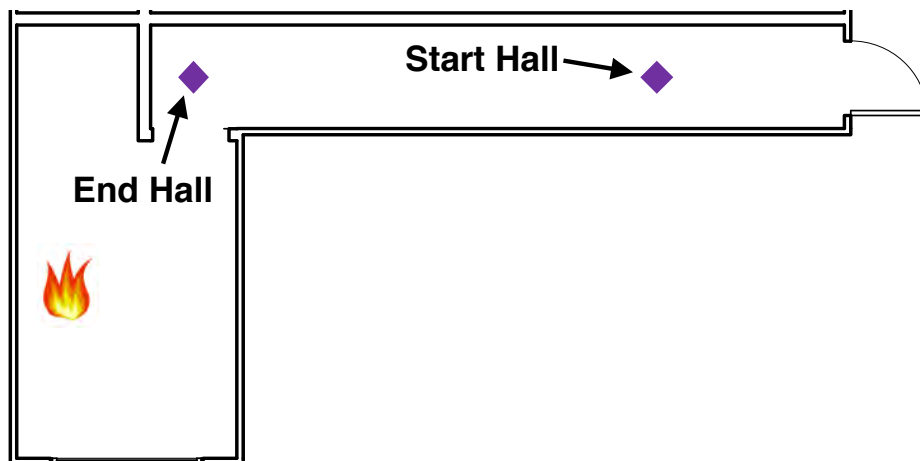


Figure 6.2: Floor plan showing the end hall and start hall heat flux gauge locations. Both were positioned 3.0 ft (0.9 m) above the floor to measure the heat flux in the horizontal direction. The end hall gauge was centered in the fire room doorway and between the hall walls, and the start hall gauge was centered in the hallway and located 8.0 ft (2.4 m) inside the doorway.

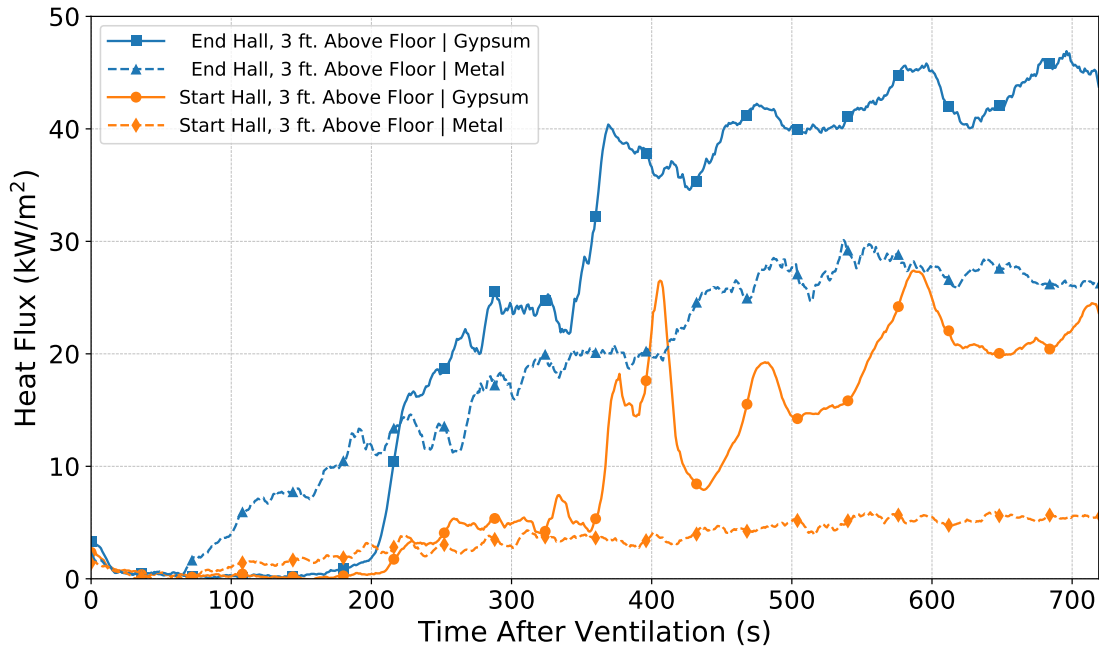


Figure 6.3: Heat flux measured at the end hall (blue lines) and start hall (orange lines) locations after ventilation occurred via the hall door during tests with the furniture fuel load in the Gypsum Prop (solid lines) and Metal Prop (dashed lines).

The plots in Figure 6.3 show that the thermal environment produced by the furniture fuel load in the Metal Prop was less intense than that in the Gypsum Prop. Additionally, the rise in the end hall heat flux due to fire regrowth was more gradual in the Metal Prop than in the Gypsum Prop.

Initially, the inability of fires in the Metal Prop and Insulated Metal Prop to fully replicate conditions produced in the Gypsum Prop may seem like a disadvantage of using metal props for live-fire training. However, the differences in wall construction did not change *how* the fire developed in response to ventilation. In regards to decreasing the thermal hazard faced by trainees, the less intense fire may be considered an advantage of using metal props.

6.1.2 NFPA 1403-Compliant Fuels can Produce Ventilation-Limited Conditions in Metal Props

Previous research has illustrated the importance of understanding how fires respond to ventilation [5–8]. Residential structure fires are typically fuel-rich and in a ventilation-limited, decay state by the time firefighters arrive at the scene, meaning that introducing additional ventilation to the environment has the potential to cause rapid and intense fire growth. To more effectively teach firefighters about the potential effects of ventilation on compartment fires, ventilation-limited fires should be generated during training. Safely creating such fires while maintaining compliance with *NFPA 1403* allows instructors to educate students on this important principle of fire dynamics in

the training environment.

The behavior of such fires is shown by the idealized ventilation-controlled fire curve. Figure 6.4 highlights the similarities between the shape of the idealized curve and the shape of the fire room temperature data plots from an experiment in the Gypsum Prop with the furniture fuel package, which was designed to replicate ventilation-controlled fire behavior in residential structures.

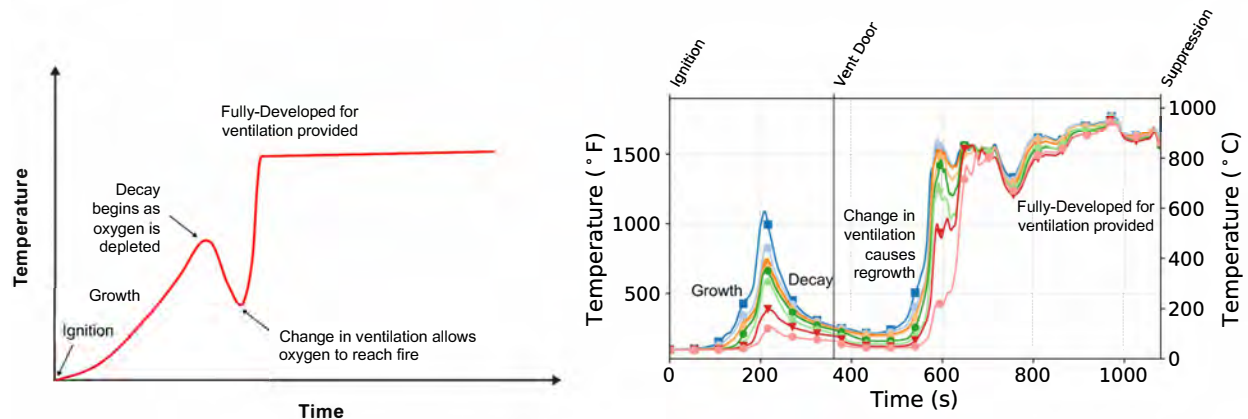


Figure 6.4: Ventilation-controlled fire curve (left), which describes the growth of fires that occur in fuel-rich structures with insufficient ventilation at ignition. The fire grows until oxygen concentrations drop below levels needed for flaming combustion, at which point it decays and enters a ventilation-limited state. If enough ventilation is provided to the fire via a new opening, like a door or window, it will rapidly regrow and reach a fully-developed state for the new ventilation configuration. Notice the similarities between the modern fire curve and the fire room temperature data (right) from a fire with the furniture fuel load in the Gypsum Prop.

It can be difficult to produce training fires that become ventilation-limited and decay in many concrete training structures. This limitation of such training fires to replicate ventilation-controlled fire behavior has been noted by articles published in fire service publications [23]. As shown by the fire room temperature plots in Figure 6.5, ventilation-limited conditions were able to be created by both wood-based training fuel loads in the Metal Prop.

The fires with *NFPA 1403*-compliant fuel loads were not only able to enter a ventilation-limited state with decay but were also able to transition from said state to a fully-developed state after the hall door was opened. Opening the door caused the fire to regrow, increasing the intensity of thermal conditions. This response to ventilation is similar to that of present-day residential structure fires, but there's still a significant difference in the magnitude of the response with training fuels compared to modern furnishings. Unlike the furniture fuel load, neither wood-based fuel package caused the fire room to flashover, as exhibited by the fire room temperature data plotted in Figure 6.5. However, fires with the wood-based fuel loads still created hazardous conditions in certain areas of the prop, specifically within and immediately outside the fire room. More details about this topic are presented and discussed in Section 6.1.4.

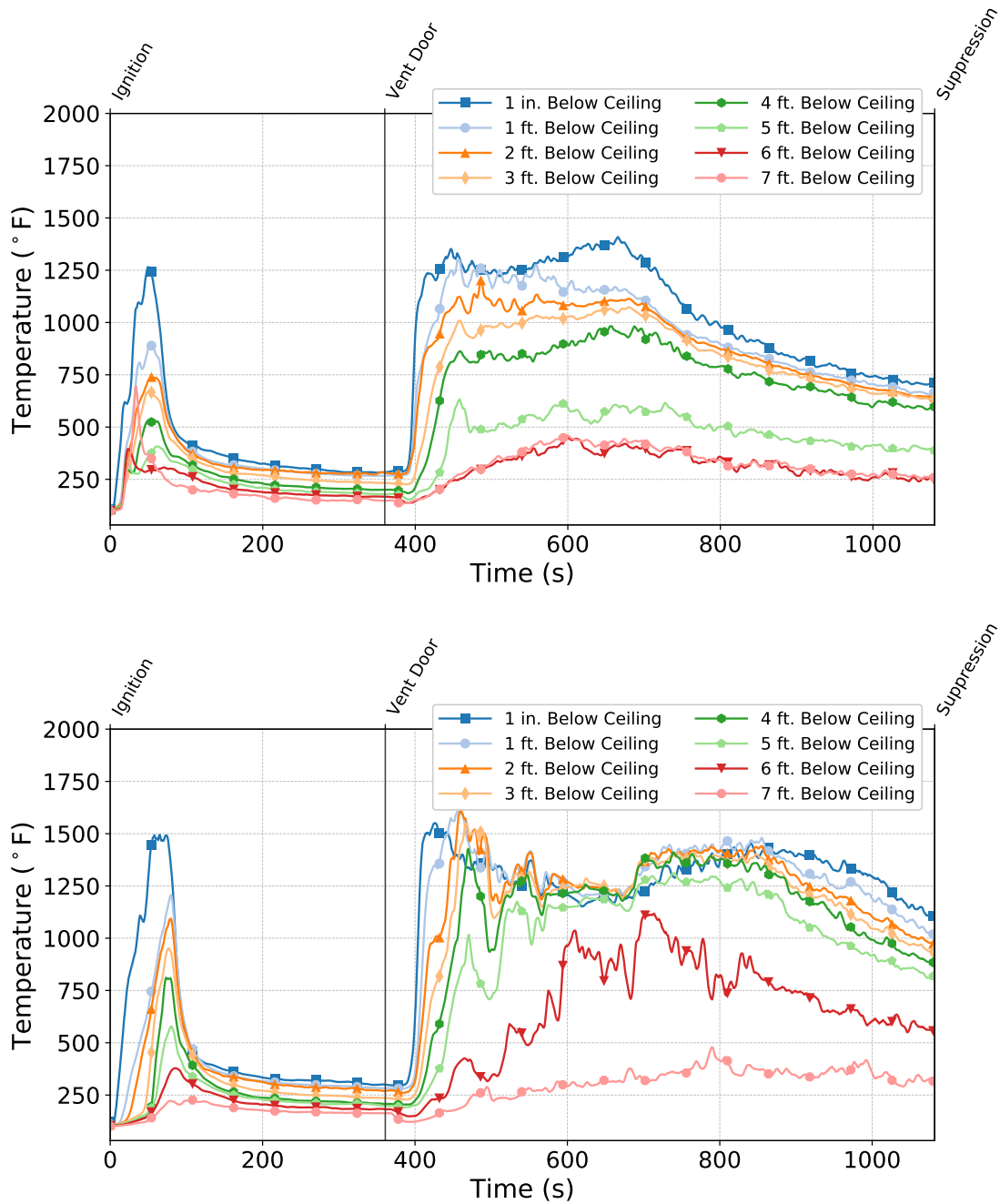


Figure 6.5: Temperatures measured in the fire room during tests with pallets fuel load (top) and pallets and OSB fuel load (bottom) in Metal Prop. For both wood-based fuel loads, the fire entered a ventilation-limited state, as indicated by the initial temperature rise followed by decay shortly after ignition. After ventilation was introduced via the opening of the hall door, the fire quickly regrew to a fully-developed state for the new ventilation configuration.

To minimize leakage of metal container props, users should refrain from cutting significant holes in the prop. Regularly inspect the prop for any large gaps, which should be filled with high-

temperature, insulating foam sealant. If a prop develops enough leakage, whether through custom modifications or natural degradation from repeated use, the ability of fires to transition to a ventilation-limited, decay state could diminish.

6.1.3 NFPA 1403-Compliant Fuels can be used to Demonstrate Flow Path & Neutral Plane Development in L-Shaped Props

Flow path and neutral plane development are important concepts for firefighters to understand. By having knowledge of such topics, they are able to make more informed decisions on the fire-ground. Turbulence and thickness of smoke can also provide information about the intensity of fire conditions and stage of fire development.

After ventilation was provided to a decayed, ventilation-controlled fire via the opening of the hall door, a neutral plane formed in the hallway and descended to a steady level as a flow path was established between the doorway and fire room. Images of the smoke conditions immediately after the door was opened and once a flow path was established during fires with each fuel load in the Metal Prop are presented in Figure 6.6.

Looking at the top row of images, the smoke color immediately after opening the hall door was drastically different during fires with wood-based fuels compared to fires with the furniture fuel package; the smoke from wood-based fuels was brown, and the smoke from the furniture fuel load was black. As the fires regrew and reached a fully-developed stage for the new ventilation configuration, the smoke from wood-based fuels eventually resembled the smoke from the furniture fire, as shown by the bottom row of images in Figure 6.6. Also note the heights of the neutral plane at the hall door during the fully-developed fires and how they varied based on the fuel load. The neutral plane was consistently lowest during the furniture tests. Of the two *NFPA 1403*-compliant fuel loads, the neutral plane generated by the pallets and OSB fuel load was lower than that created by the pallets fuel load. This difference is thought to be due to the variation in heat release rate potential between the fuel packages.



Figure 6.6: Images of the smoke conditions immediately after the hall door was opened (top row) and after the neutral plane developed at the doorway (bottom row) during tests with the pallets (left side); pallets and OSB (middle); and furniture (right side) fuel packages. A red line marks the approximate height of the neutral plane and a yellow line marks the height of the door handle to provide a similar reference point in the photos along the bottom row.

Experiments that involved opening the window to supply additional ventilation to a fire after that had grown to a fully-developed state with the hall door opened were also conducted. Figure 6.7 contains a side-by-side comparison of stills from exterior thermal imager recordings one second before, 30 seconds after, and 60 seconds after the window was opened during these experiments with the pallets and OSB fuel load and with the furniture fuel load. Notice the rise of the neutral plane in response to the window vent by comparing the video stills one second before the window was opened to those 30 seconds after. This initial response of the neutral plane was similar for

all three fuel loads. After 60 seconds, the neutral plane remained elevated during the pallets and OSB test, while during the furniture test, it descended after the initial rise as the fire burned more efficiently due to the new ventilation source. Previous research has shown that a brief rise of the neutral plane followed by a descent is the expected response in the case of supplying ventilation to a fuel-rich fire — the type often encountered by firefighters in structure fires containing fuels composed of synthetic materials and foam plastics [5].

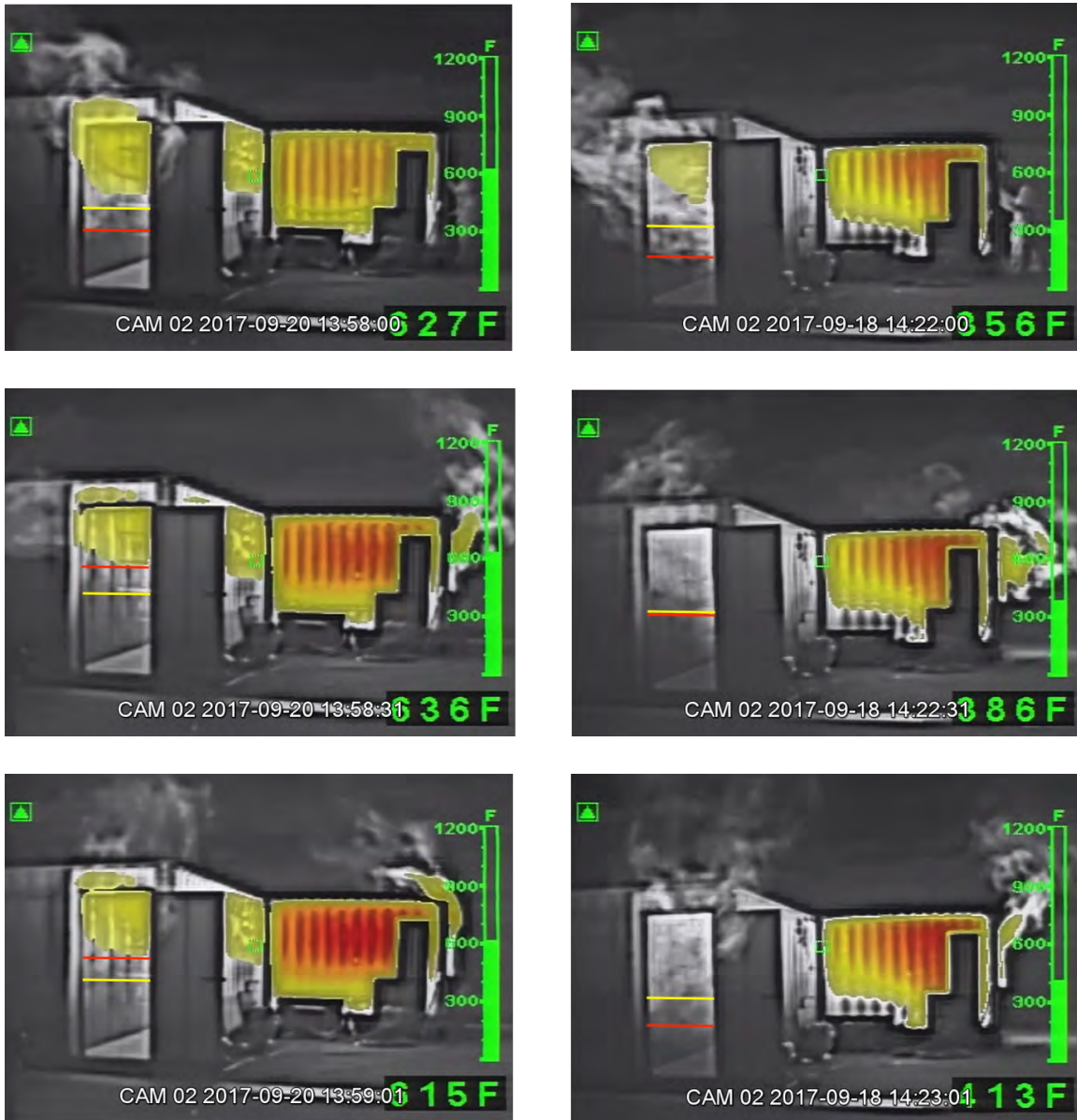


Figure 6.7: Still images from thermal imager video of the Metal Prop exterior one second before (top row), 30 seconds after (middle row), and 60 seconds after (bottom row) the window was opened during tests with the pallets and OSB (left side) and furniture (right side) fuel loads. A red line marks the approximate height of the neutral plane and a yellow line marks the height of the door handle to provide a similar reference point in each photo.

The behavior of a neutral plane can provide firefighters with a visual cue about the current stage of fire development. A descending neutral plane is often indicative of a growing fire; as the intensity of a fire increases, so does the pressure within the compartment, causing gases to exhaust from the structure. Alternatively, a rising neutral plane can be caused by a decrease in pressure, possibly due to the fire decaying or a change in ventilation. When the neutral plane remains constant, the fire is likely at a relatively steady state for its given ventilation configuration.

As shown in Figure 6.7, a rising neutral plane isn't always an indication of a decaying fire; it could be produced by a change in ventilation to the fire environment. During the experiment with the furniture fuel package, the neutral plane rose after the window was ventilated then quickly descended thereafter as the fire in the compartment grew and reached a steady state for the new ventilation configuration.

The visual differences between fires with wood-based fuels and those with fuels composed of synthetic materials and foam plastics should be acknowledged and discussed when wood-based fuels are used during training to demonstrate flow path and neutral plane development. Being able to correctly relate visual cues from smoke conditions during the progression of neutral planes and flow paths to specific characteristics of fire dynamics allows firefighters to make better-informed decisions on the fireground.

6.1.4 NFPA 1403-Compliant Fuels can Produce Conditions with the Potential to Cause Thermal Injury to Firefighters in Full PPE

A 2017 NIST grant/contract report by Horn et al. [44] stated that visible thermal damage (cracking, bubbling, grazing) was observed on SCBA facepiece lenses after 90 seconds of exposure to 10 kW/m². Additionally, a 2013 study by NIST [45] revealed that an SCBA facepiece lens can develop holes when exposed to 15 kW/m² for durations ranging from 30 to 300 seconds. The study also found that the surface of the lens reached its glass transition temperature, or temperature at which the material transitions from a hard plastic to a soft pliable material, after being exposed to 15 kW/m² for approximately 30 seconds. In response to these findings, *NFPA 1981: Standard on Open-Circuit SCBA for Emergency Services* was updated to require SCBA facepieces maintain positive pressure throughout an exposure to 500 °F (260 °C) for 300 seconds and throughout an exposure to 15 kW/m² for 300 seconds [46]. During tests with wood-based fuel loads inside the metal props, measurements at different locations in the fire room and hallway exceeded these limits. Thus, although they were less severe than those with modern furnishings, fires with wood-based fuels still created an atmosphere in certain areas of the prop that was immediately dangerous to life and health (IDLH)¹ for firefighters in full PPE.

Figure 6.8 contains plots of the heat flux and temperature measured in the hallway during experiments with the pallets fuel load and the pallets and OSB fuel load in the Metal Prop. The plotted data were collected at the end hall and start hall locations, which are shown and described in Fig-

¹Defined by NFPA as “any condition that would pose an immediate or delayed threat to life, cause irreversible adverse health effects, or interfere with an individual’s ability to escape unaided from a hazardous environment.” [53]

ure 6.9, at heights corresponding to the approximate levels of a crawling/crouching firefighter's facepiece.

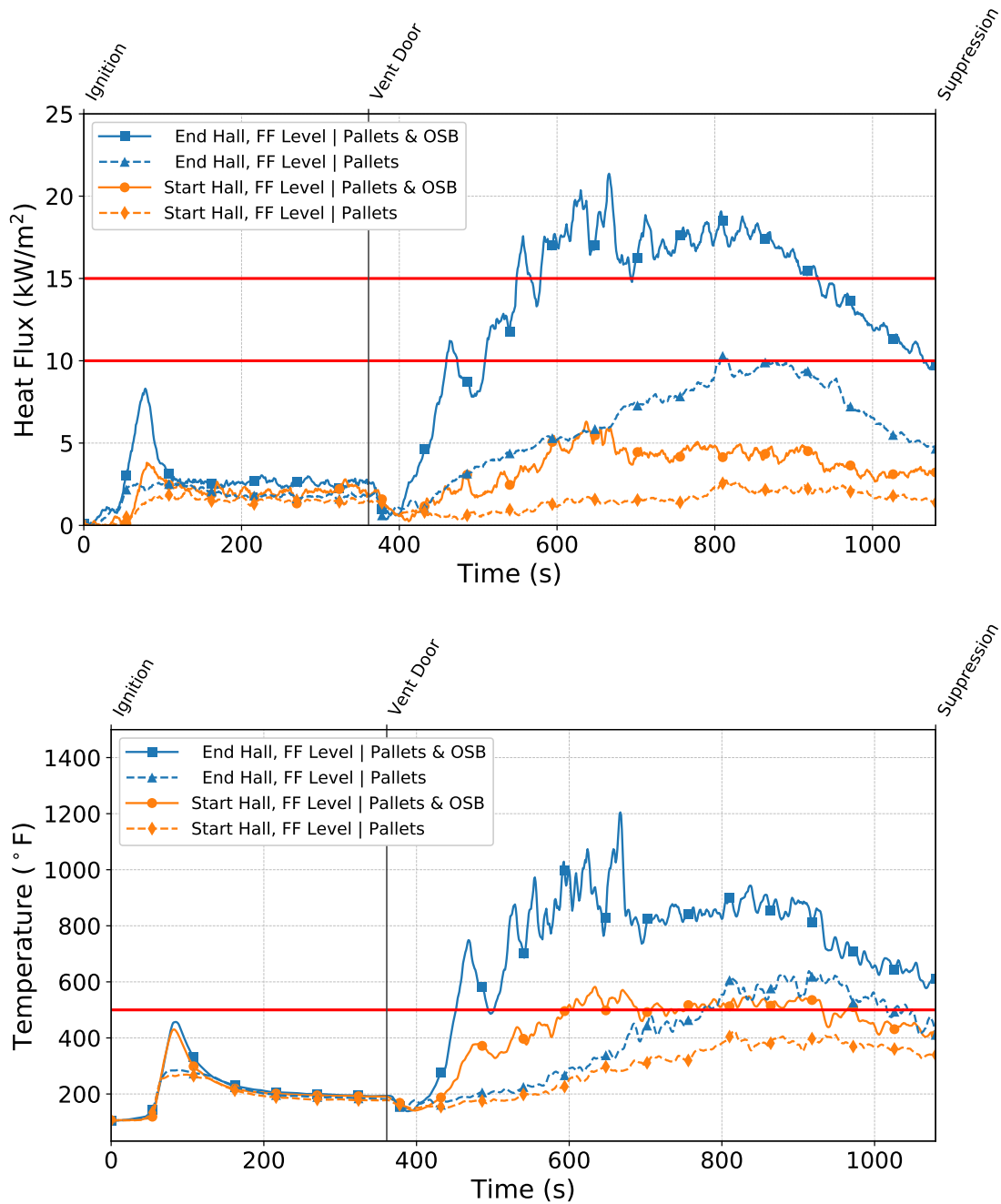


Figure 6.8: Plots of the heat flux (top) and temperature (bottom) measured at the end hall (blue lines) and start hall (orange lines) locations during tests using the pallets and OSB fuel load (solid lines) and the pallets fuel load (dashed lines) in the Metal Prop. The exposure thresholds mentioned in the beginning of this section are marked on the graphs by solid red lines.

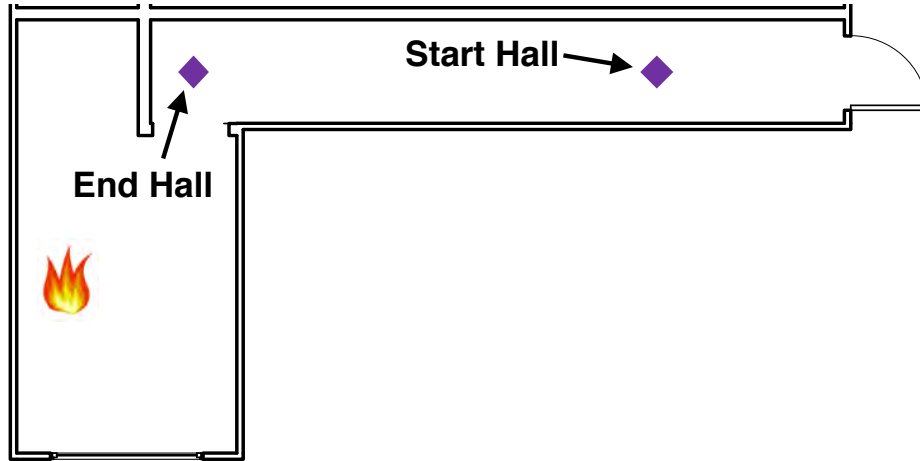


Figure 6.9: Floor plan showing the locations of the start hall and end hall thermocouple array and heat flux gauge pairs. The end hall pair was centered in the fire room doorway and between the hall walls. Likewise, the start hall pair was centered in the hallway and located approximately 8.0 ft (2.4 m) from the hall doorway.

Notice from Figure 6.8 that the end hall heat flux exceeded 15 kW/m^2 for more than 300 consecutive seconds (from around 580 s to 915 s) during the test with the pallets and OSB fuel load. Additionally, the start hall temperature exceeded $500 \text{ }^\circ\text{F}$ ($260 \text{ }^\circ\text{C}$) over approximately the same duration, and the end hall temperature exceeded the same threshold for more than 600 consecutive seconds from around 450 s until suppression at 1080 s. Hallway conditions during the experiment with the pallets fuel package were significantly less severe — the end hall heat flux and temperature surpassed exposure limit values but never for longer than the duration stated at the beginning of this section.

Recall that these measurements were collected at approximate heights of a crawling/crouching firefighter's facepiece. Thus, whenever the plots approach or exceed exposure limits, firefighters near the corresponding measurement location would be at risk of being injured and/or having their PPE damaged unless water was effectively applied for suppression. Anyone located at higher elevations (e.g., standing instead of crouching) around these areas or closer to the fire (e.g., in the fire room) would be exposed to even more severe conditions and would have less time before experiencing PPE damage and/or personal injuries.

The fact that wood-based fuels can create an IDLH atmosphere outside the fire room suggests that caution should be used when determining the fuel load size for training exercises, especially when they involve extended periods of exposure to the fire environment, like in a fire behavior demonstration. Extra caution should be employed when adding OSB to the fuel package, as the addition of three sheets to the pallets fuel load generated potentially hazardous conditions around the level of a crouching/crawling firefighter's facepiece over the majority of the hallway.

In addition to fuel load size, ventilation also dictates the intensity of the environment created by a fire. Thermal conditions at the peak levels of severity for a given fuel load will only be realized during a fire if a sufficient supply of oxygen is provided to the fire throughout its development.

Both the fuel load size and ventilation configurations used during live-fire training should be selected by instructors. Those conducting the training are responsible for creating and maintaining a fire environment that's at an appropriate level of intensity for the given training scenario. This appropriate level should be based on a number of factors, including the experience of the participants and goal(s) of the exercise. This can be accomplished through proper selection of the fuel load size and certain alterations to ventilation patterns throughout the fire environment.

6.1.5 NFPA 1403-Compliant Fuels can Create Repeatable Fire Behavior

The growth and regrowth of the wood-based fuel packages were consistent across replicate experiments. For example, consider Figure 6.10, which contains plots of the temperature 1.0 in. (25 mm) below the fire room ceiling during replicate tests with the pallets fuel load and with the pallets and OSB fuel load. The periods of initial growth and regrowth after ventilation are shaded for each plot.

Looking at the plots, notice how all the vertical lines marking the start of fire growth and regrowth except the orange line on the top chart are virtually indistinguishable from one another. Also notice how the growth and regrowth start times are less than 60 seconds from their causal event in every case. Finally, the growth and regrowth periods — the shaded portions of each plot — are of similar length across replicate experiments.

The ability to produce predictable and repeatable fire dynamics is important for live-fire training evolutions, especially in regards to peak thermal exposure and rate of change (growth) of the thermal environment in which students are operating. Fuel loads that create environments in which the thermal exposure to instructors is similar to that of students allow for a margin of safety. Instructors can use the predictability of training fires to achieve the objectives of fire dynamics education. When fire development is not predictable, it becomes a challenge to complete lesson objectives and also unnecessarily increases risk during live-fire training.

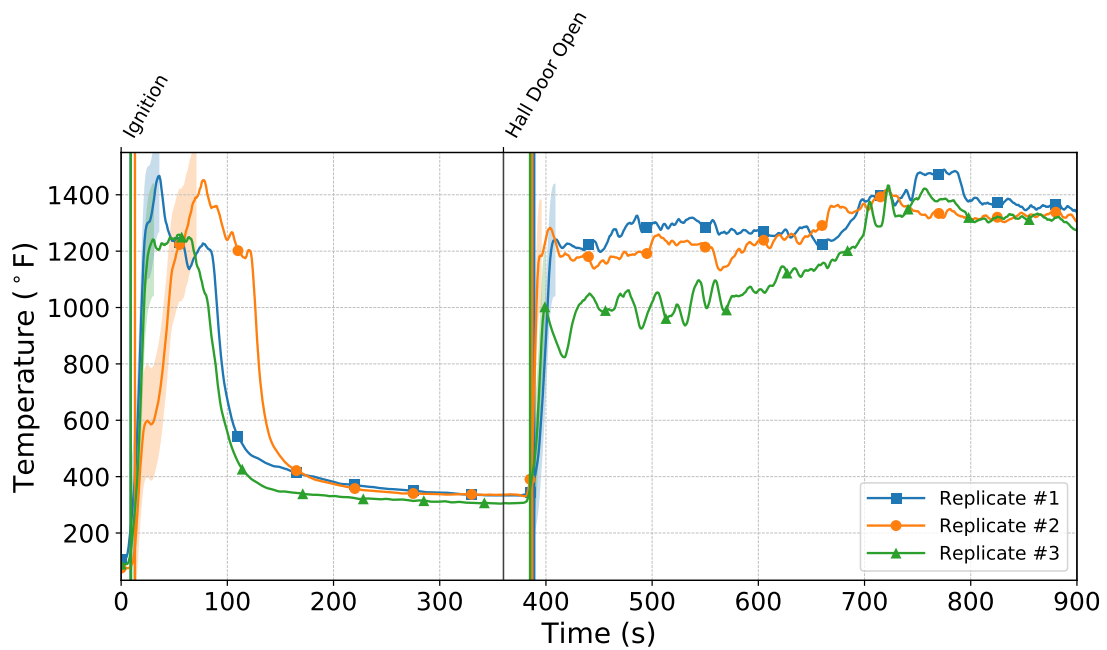
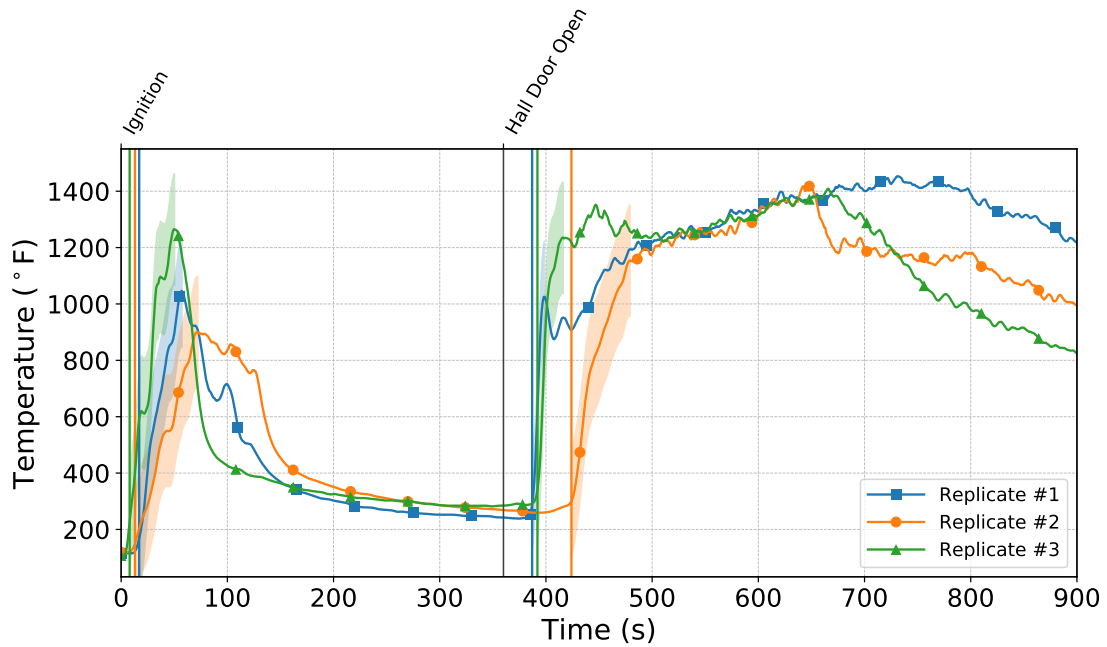


Figure 6.10: Plots of the fire room ceiling temperature from three replicate tests with the pallets fuel load (top chart) and pallets and OSB fuel load (bottom chart). The growth and regrowth periods of each replicate test are shaded in colors corresponding to their respective plots, and the vertical lines mark the start of these periods.

6.1.6 Thermal Exposures Experienced During Interior Suppression may Differ Between the Gypsum Prop & Metal Props

One test with interior suppression was performed in each of the three props. The pallets and OSB fuel package was used for each test. The fuel was ignited with the fire room window closed and the hall door opened, and suppression (flow and move down hallway) was initiated approximately 360 seconds later. In addition to the data collected by fixed instrumentation throughout the prop, a sensor was attached to the suppression firefighter's helmet to measure the heat flux encountered by the advancing suppression crew.

The incident heat flux to the suppression crew was higher immediately following the start of suppression during tests in the Metal and Insulated Metal Props than in the Gypsum Prop, as shown in Figure 6.11, which contains the heat flux plotted over the approximate range of 30 seconds before to 30 seconds after the start of suppression in each test.

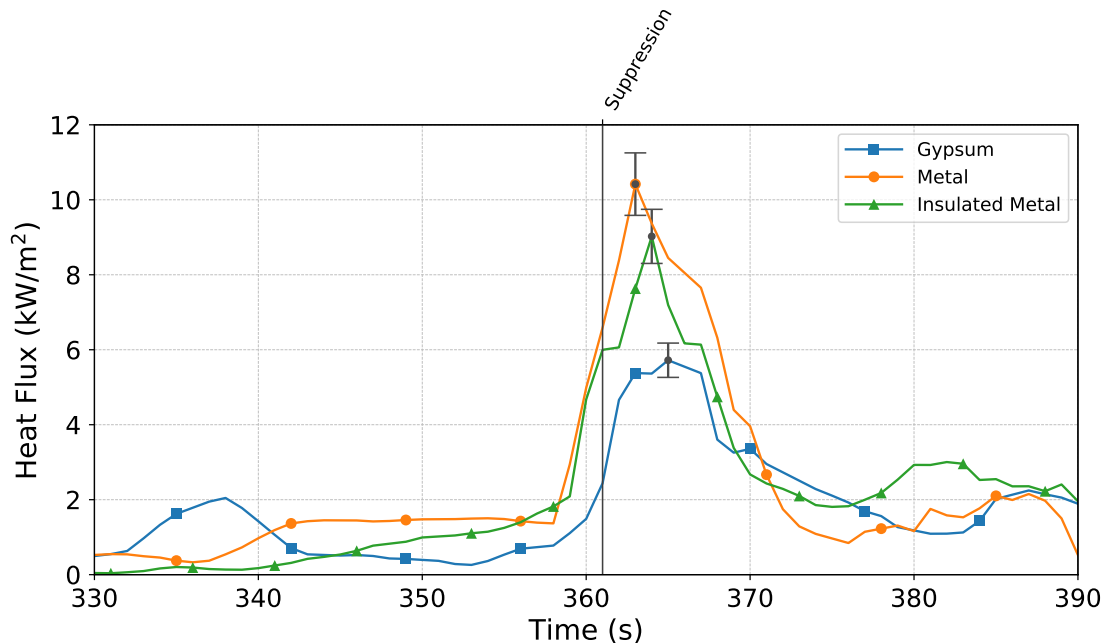


Figure 6.11: Heat flux measured by the sensor on the helmet of the firefighter performing suppression plotted over the period approximately 30 seconds before to 30 seconds after the start of interior suppression. Note, the slightly elevated heat flux before suppression is a result of the firefighter being in position outside the hallway door before the start of suppression.

This result indicates that the thermal exposure to the firefighters was more severe in the Metal and Insulated Metal Props than in the Gypsum Prop for a brief period of time (less than 10 seconds) after the start of suppression. Furthermore, the maximum heat flux values recorded during the brief period of the Metal Prop and Insulated Metal Prop tests are alike, suggesting that the effect of suppression on the firefighters' local environment was similar between these two props.

The higher heat fluxes measured shortly after the start of suppression in the metal props are sus-

pected to be at least partially due to steam production. When liquid water is heated to its boiling point temperature, 212 °F (100 °C), it converts to steam. Consider what happens when a hot metal cooking pan is removed from a stovetop and immediately placed under a sink faucet that's flowing water. As water comes into contact with the hot metal surface, heat stored in the metal is transferred to the liquid water, causing its temperature to increase to its boiling point and convert to steam. This same phenomenon occurred as water contacted the hot steel walls of the metal props during the first moments of suppression. In the Gypsum Prop, water was also converted into steam in the first seconds of suppression. However, the rate at which it was converted was significantly less due to the different wall lining material — heat transfer occurs at a drastically faster rate through steel than through gypsum.

Although it was only over a brief period of time, the firefighter who performed the interior suppression during the experiments stated that the environments in the metal props were “noticeably more uncomfortable” than in the Gypsum Prop. The results discussed above indicate the thermal exposure to firefighters in a metal container prop during interior suppression can differ significantly from what would occur in a gypsum-lined structure. It should be noted, however, that the applicability of this result is limited exclusively to the tested scenarios. Additional experiments need to be performed with varying parameters (prop size, prop layout, suppression technique, etc.) to obtain a more complete understanding of suppression effects within metal container props. It's entirely possible that increasing the interior volume of the training prop or using a certain suppression tactic could mitigate the measurable differences in thermal exposure to firefighters between training props constructed from metal shipping containers and those constructed from other materials, like the Gypsum Prop.

Regardless, the results from the suppression effects experiments exhibit that firefighters could potentially be exposed to more severe conditions at the beginning of suppression inside props constructed from metal shipping containers compared to those encountered in a prop constructed like the Gypsum Prop. The interior walls of modern-day structures are typically lined with a non-metal material, such as gypsum board, so conducting live-fire training in metal container props could expose participants to an experience where water application doesn't immediately improve conditions. Such an experience contradicts previous research on residential fire suppression that identified the need to cool as a crew advances towards a fire to provide a tenable space for the advancing suppression crew [27]. Training instructors should understand and be able to explain the differences in environments during suppression between various types of structures utilized for fire training so that students understand the limitations of their training experience.

6.2 Prop Durability & Performance Considerations

6.2.1 Awareness of Prop Degradation is Important

The temperatures measured at locations throughout the Gypsum Prop were consistently greater than those measured throughout the metal props during experiments with the same fuel package

and event timeline. Theoretically, because the thermal environments created by the wood-based fuel loads were more intense during tests in the Gypsum Prop compared to the Metal Props, conducting live-fire training exercises in the Gypsum Prop might have the potential to create what “feels” closer to the environment encountered inside a structure fire, while still using fuels that adhere to *NFPA 1403*. Additionally, gypsum is used as an interior wall lining in present-day structures much more often than metal.

The interior lining of the Gypsum Prop had to be completely replaced at the end of every fire experiment. Because the interior would have to be reconstructed after every fire, the prep time needed between groups of firefighters participating in the training would be drastically longer for the Gypsum Prop than either of the metal props. Pictures of the Gypsum Prop interior are presented in Figure 6.12 to show the damage caused by a single fire with the pallets and straw fuel load, the least severe of the three fuel loads utilized for this project.



Figure 6.12: Images of the damage in the fire room (left) and hallway (right) of the Gypsum Prop after a single training fire with the pallets fuel load. The damage was caused by the fire and overhaul operations conducted to completely suppress the fire. After every fire, the gypsum board lining the inside needed to be replaced.

Compared to the Gypsum Prop, the metal props were more durable. However, degradation still occurred in both types of metal props. The first experiments conducted in each side of the Metal Prop and Insulated Metal Prop were labeled as “Burn In” tests after discovering that certain visual observations noted during the initial tests were not observed during tests that followed, like the fire spread to the exterior of the prop pictured in Figure 6.13.



Figure 6.13: Image of fire spread along the exterior surface of the Metal Prop during the Burn In experiment.

Significant changes to the physical structure of the metal props from before and after the Burn In tests were also documented. Fire damage to the exterior side of the corrugated walls in the Metal Prop was evident after the Burn In experiments. The most damaged portions of the exterior sides were along the upper parts of the fire room walls, in line with the hottest areas inside the prop during the experiment. A still frame from the TIC video recording of the Metal Prop exterior during the Burn In is presented next to an image of the exterior after the Burn In experiment in Figure 6.14 as an example of this trend.

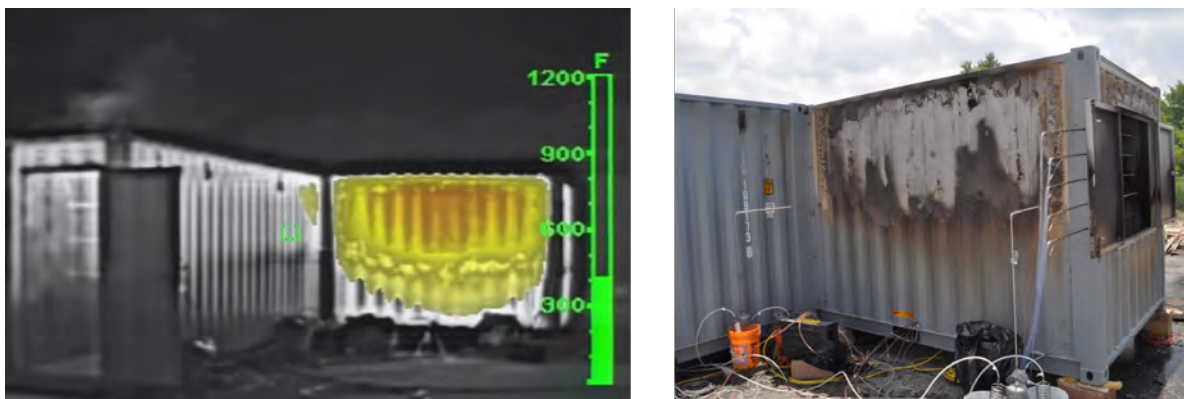


Figure 6.14: Still frame of the Metal Prop exterior from a TIC video recording of the Burn In test (left) and a picture of the exterior damage from after the Burn In test (right). Notice how the colored (hottest) areas from the TIC video correspond to the most damaged portions of the exterior.

There was minimal visible damage along the exterior of the Insulated Metal Prop after the Burn In

tests because the insulation prevented the exterior side from reaching the autoignition temperature of the paint. However, visible damage inside the prop was still observed after the experiments. A number of the welds that fused the metal sheets overtop the insulation were broken due to the expansion of the sheets as they absorbed heat produced by the fire. In fact, enough welds along the hinge of the left window shutter broke during one Burn In test that the shutter became completely detached from the prop as it was opened at the end of the experiment. Figure 6.15 contains images of the damage caused by the Burn In experiments in the Insulated Metal Prop.



Figure 6.15: Images of the Insulated Metal Prop before (left side) and after (right side) the Burn In test. The top images are of the exterior side of the fire room window, and the bottom images are looking at welds along the edge of a steel sheet on the interior side near the window. The left window shutter became detached from the prop and multiple interior welds were broken as a result of the Burn In experiment.

In addition to the visual differences, significant differences were observed in experimental measurements from before, during, and after the initial tests in the metal props. One of the most

prevalent trends was seen in the comparison of the fire room temperature data over the initial growth period of the Burn In tests to that of corresponding replicate tests conducted afterward. The temperatures recorded during the initial growth period of each replicate test tended to reach greater magnitudes compared to those from the respective Burn In. Figure 6.16 shows the fire room temperatures measured 1.0 in. (25 mm), 2.0 ft (0.6 m), and 4.0 ft (1.2 m) below the ceiling during the initial growth periods of a Burn In test and the replicate conducted afterwards as an example of the trend.

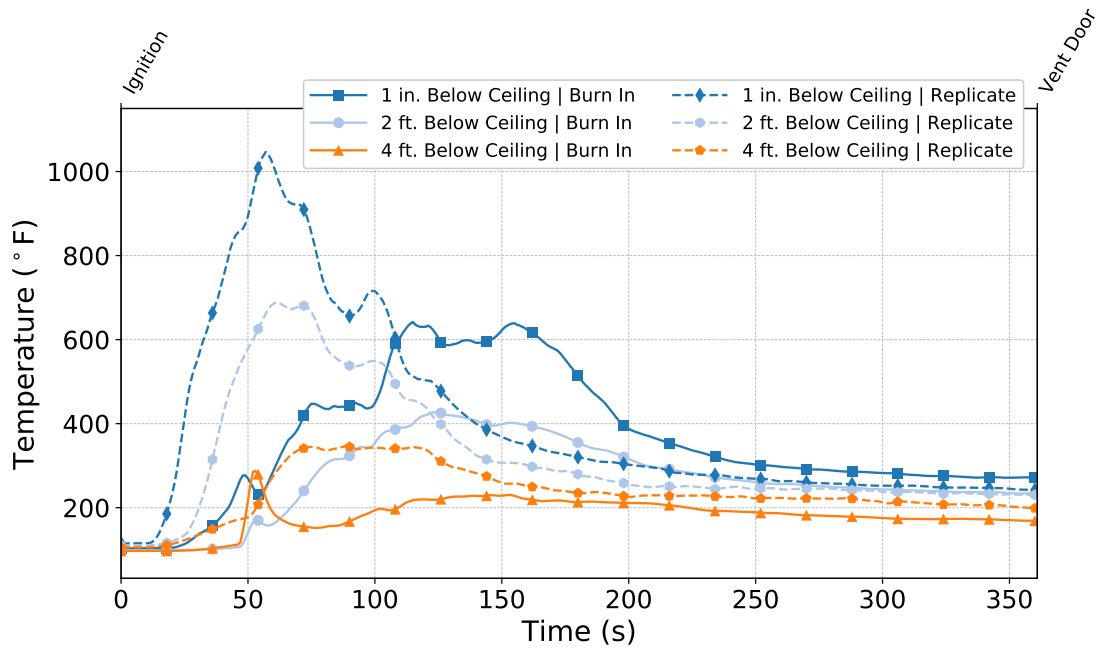


Figure 6.16: Temperatures measured 1.0 in. (25 mm), 2.0 ft (0.6 m), and 4.0 ft (1.2 m) below the ceiling of the fire room plotted over the initial growth period of a Burn In test (solid lines) and the replicate conducted afterwards (dashed lines) in the Metal Prop with the pallets fuel load.

The temperatures reached greater magnitudes during the replicate tests partially, if not entirely, because the prop was “leakier” after each Burn In test. A system designed to measure the leakage of a structure was used to quantify the leakage associated with each side of the metal props before and after the Burn In experiments. The measurement is reported in air changes per hour at 50 Pa (ACPH50) and was obtained by using a fan to pressurize the prop. The unit ACPH50 represents the number of times the total volume of air in the prop changes in one hour as a result of pressurizing the prop interior to 50 Pa with the fan. The results from the leakage tests are presented in Figure 6.17.

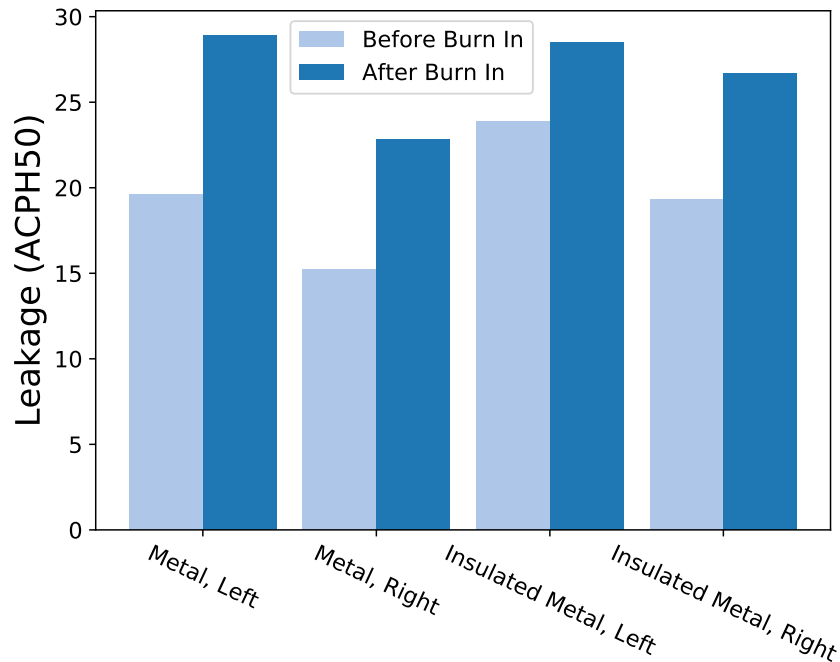


Figure 6.17: Bar graph of prop leakage measured before and after each Burn In test. The initial fire in each side of the metal props increased the prop leakage in all four cases.

Based on the permanent damage sustained by the metal props as a result of the initial experiment and how it affected fire conditions during portions of tests that followed, at least one fire should be ignited and allowed to burn inside a metal container prop so that the permanent damage is incurred before the prop is used for live-fire training. It is recommended that several evolutions of burns be performed prior to interior operations, as the initial fire may not be representative of conditions that occur in subsequent burns.

To control prop leakage, modifications that significantly increase leakage, such as cutting holes in the exterior walls, should not be made to the metal props. Furthermore, regularly inspecting the prop for potential repairs is recommended. Some components may need to be rewelded or bolted, and any large gaps or openings should be sufficiently covered or plugged. If not properly maintained, a prop could develop enough leakage that fuel packages of a specific type and size may lose the ability to generate ventilation-controlled conditions.

Note, the most fires ignited in one side of either container prop was 16, and minor repairs, such as filling gaps with high-temperature, insulating foam sealant and rewelding a detached window shutter, were performed to minimize the effects of degradation on leakage. It is quite possible that more than 16 training fires could be ignited in a metal container prop throughout a single day of training. Thus, the degradation results described here are limited in their scope being that they pertain to a short period of use. Additionally, prop degradation may vary from what's outlined above depending on the design of the prop and the duration and severity of fires ignited in the prop. For example, if fires are burned within a metal container prop for shorter periods and/or produce less severe conditions during their development, prop degradation may occur at a slower

rate. Additionally, a metal container prop with a more robust design may not show initial signs of degradation to the extent observed after the Burn In experiments, like the window shutter becoming detached from the prop.

6.2.2 Insulating the Metal Prop did not Noticeably Change the Overall Thermal Environment

Uncertainty exists at varying degrees in virtually every type of experimental measurement. Based on published research studies and previous experience, the total uncertainty for thermocouples, the devices used to measure temperature, was estimated as $\pm 15\%$, and the total uncertainty for heat flux gauges was estimated as $\pm 8\%$. For example, if a temperature of $100\text{ }^{\circ}\text{C}$ was measured by a thermocouple, the actual temperature value is between $85\text{ }^{\circ}\text{C}$ and $115\text{ }^{\circ}\text{C}$. Two measurements with uncertainty ranges that overlap cannot be considered completely distinguishable from each other. If the two ranges do not overlap, the measurements are considered to be measurably different.

Previous research has found that insulating a metal container prop may affect the thermal environment created by a fire in the compartment [26]. However, based on thermal measurements collected throughout the Metal Prop and the Insulated Metal Prop during comparable experiments (i.e., the same fuel package and event timeline), the environments tended to be, on average, indistinguishable from each other. This consistent trend suggests that thermal conditions were similar between experiments in the Metal Prop and Insulated Metal Prop.

As an example of indistinguishable measurements, Figure 6.18 shows the temperatures measured 3.0 ft (0.9 m) below the ceiling and the heat flux data 3.0 ft (0.9 m) above the floor at the start of the hallway 8.0 ft (2.4 m) inside the doorway over the duration of a comparable test with the pallets and OSB fuel load in the Metal Prop and Insulated Metal Prop. The uncertainty range of each plot is represented by the shaded areas. Notice how the shaded area from the Metal Prop temperatures overlaps with the shaded area from the Insulated Metal Prop temperatures for the majority of the test duration.

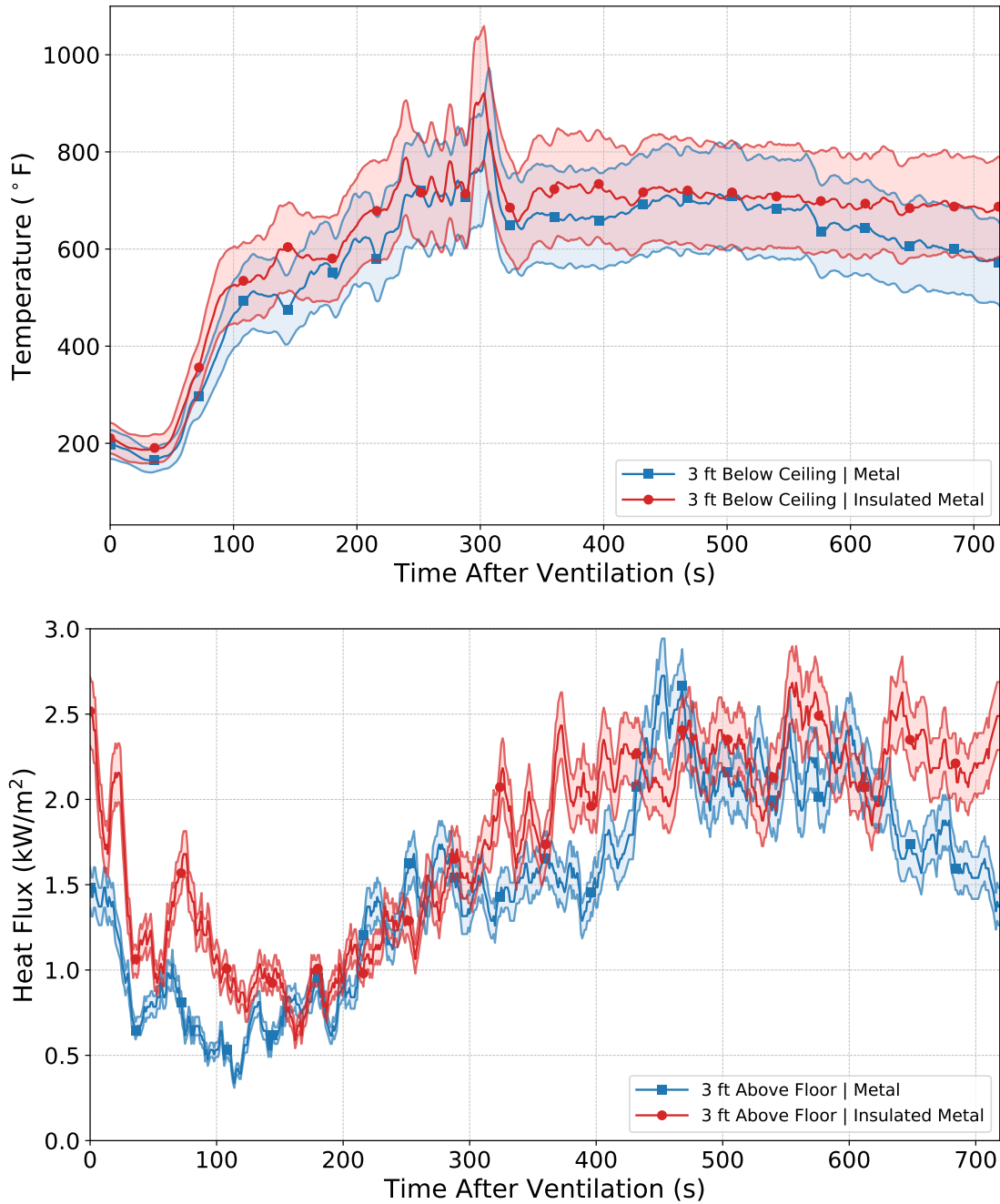


Figure 6.18: Plots containing temperatures measured 3.0 ft (0.9 m) below the ceiling (top graph) and heat flux data collected 3.0 ft (0.9 m) above the floor (bottom graph) at the start of the hallway 8.0 ft (2.4 m) inside the entrance doorway after ventilation in the Metal Prop (blue plot) & Insulated Metal Prop (red plot) with the pallets & OSB fuel package. The shaded area represents the uncertainty range of the measurements.

The indistinguishable conditions may be due to the effectiveness of air as an insulator. In the Metal Prop, the air surrounding the prop acted as an insulator, slowing the rate at which heat was

transferred from the wall to the exterior environment. In the Insulated Metal Prop, the mineral wool insulation between the layers of metal added an extra layer of insulation in addition to the air around the prop, slowing the rate of heat transfer to the exterior environment to an even greater extent. As fires grew and burned near their peak HRR, the difference in heat transfer rate from the interior environment through the two wall configurations became insignificant compared to the HRR of the fire, and therefore, thermal conditions over this period were indistinguishable between props. Comparisons between data collected during similar experiments in the Metal Prop and Insulated Metal Prop revealed that insulating the Metal Prop had no significant effect on the thermal environment produced throughout fire growth and development.

6.2.3 Insulating the Metal Prop Increased the Cooling Time of the Prop

Although thermal conditions were indistinguishable between the metal props through the fully-developed stage of fire growth, the interior of the Insulated Metal Prop cooled at a slower rate than the Metal Prop as the fire decayed and after it was extinguished. This difference in cooling time was noted by those involved with suppression and interior cleanup after the fires. Additionally, comparisons of temperature data between tests in each prop were consistent with this difference.

During a number of experiments, the fire was not suppressed until 12 minutes after ventilation (18 minutes after ignition). By this time during tests with either wood-based fuel package, the fire was in a fuel-limited state and was decaying due to a depleted fuel supply. As a result, interior temperatures measured throughout the prop were in decline over the minutes leading up to suppression. Comparisons of temperature decline over this period reveals that the interior of the Metal Prop cooled at a quicker rate than that of the Insulated Metal Prop.

Table 6.1 lists the rate of temperature decline over the 90 seconds before suppression averaged across the upper thermocouples (those 3.0 ft (0.9 m) or less from the ceiling) in the fire room and at the end of the hallway for each wood-based fuel load test in the Metal Prop and Insulated Metal Prop. Looking at the table, the average cooling rate in the Metal Prop is consistently greater in magnitude compared to that of the Insulated Metal Prop. The rates associated with the Metal Prop range from being nearly two times greater in magnitude (fire room, pallets) to being four times greater in magnitude (end hall, pallets and OSB) than those of the Insulated Metal Prop.

Table 6.1: Average Rate of Temperature Decline Across Upper Thermocouples in Fire Room & End Hall Arrays During Final 90 seconds of Wood-Based Fuel Load Tests in Metal & Insulated Metal Props

Thermocouple Array	Average Cooling Rate (°F/s)			
	Pallets		Pallets & OSB	
	Metal	Insulated	Metal	Insulated
Fire Room	-1.5 ± 0.2	-0.8 ± 0.1	-1.9 ± 0.3	-0.5 ± 0.2
End Hall	-1.1 ± 0.1	-0.4 ± 0.2	-1.2 ± 0.2	-0.3 ± 0.1

If a training structure or prop is not given time to cool between fires, excessive heat can be retained within the interior environment, drastically increasing the severity of thermal environments during evolutions that follow. At least one LODD has been attributed to the failure of PPE after exposure to extreme heat in the burn room of a training structure that wasn't allowed sufficient time to cool between training evolutions [14]. The time necessary to cool a training structure after a live-fire exercise can dictate the turnaround time between evolutions, and it is often one of the factors that limits the number of training exercises able to be conducted over a set period of time.

7 Summary

The goal of fire service training is to prepare students for the conditions and challenges that they will encounter on the fireground. The modern fire environment is constantly evolving as homes become more tightly sealed and are filled with contents that present larger potential fuel loads for fire. It is important that fire training keeps up with the trends to properly prepare firefighters for what is encountered in the field. At the same time, live-fire training needs to be conducted in a safe and knowledgeable fashion, as several firefighter LODDs caused by excessive thermal exposure during training evolutions have occurred [13–15]. Developing an understanding of ventilation-controlled fires in the training environment and in residential structure fires is critical for instructors to effectively prepare students for their jobs.

The use of props constructed from steel shipping containers for live-fire training has increased in popularity throughout the fire service over the last few decades. Additionally, some have suggested building props from materials more commonly used in residential construction, such as dimensional lumber and gypsum board [20]. Like many training tools, these props can be used incorrectly, potentially resulting in dangerous training scenarios and/or students developing techniques that are ineffective, perhaps even counterproductive, when applied on the fireground. Thirty-seven fire experiments were conducted in L-shaped training props to better understand the limitations associated with the props so that improper use can be avoided. Thermal environments produced by three fuel loads — one composed of modern furnishings and two composed of wood-based fuels compliant with *NFPA 1403* — were studied and compared between L-shaped props with the following interior wall constructions: lightweight gypsum board over insulation, a single layer of corrugated steel, and rolled steel sheeting over mineral wool insulation with corrugated steel as its backing.

Comparing data from the initial tests in the metal container props to data from replicate tests conducted afterwards revealed that the thermal insult from training fires can significantly increase the leakage of the prop and as a result, increase the amount of ventilation available to a fire inside the prop. It may be necessary to perform maintenance (e.g., welding, filling/covering major holes or gaps, etc.) on the metal container props to prevent the leakage from reaching a level that makes it difficult to attain ventilation-controlled fire conditions with training fuels. The results mentioned in this report regarding prop degradation over time are limited in the sense that the most fire experiments conducted in a single side of either metal container prop was 16.

Fifteen tests were used to quantify the repeatability of and differences between fire conditions in each type of prop with the three different fuel loads. Temperature and heat flux measurements from locations throughout the training props were compared between three groups of replicate tests to evaluate the repeatability of fire conditions in each prop with the different fuel packages. From the analysis, it was determined that fire conditions following fire growth were able to be consistently replicated in each type of prop with the different fuel packages. The time corresponding to the start of fire regrowth after ventilation varied significantly more between replicate tests with the furniture fuel load than those with the wood-based fuel loads. Note, this result was produced using

a consistent ignition location and fuel package geometry and is by no means a general representation of all comparisons between fires with wood-based fuel packages and those with fuel packages containing synthetic materials and foam plastics, like those found in furniture.

Experimental data were compared to quantify the differences in thermal conditions produced by the fuel loads between the different props. Overall, the results indicated that conditions in the Gypsum Prop were more intense than in either of the metal props. This difference in severity is thought to be due to the variation in wall construction between props. The innermost layer of the walls in both metal props was steel, a heat conductor, while in the Gypsum Prop, the innermost layer was gypsum, a heat insulator. This likely caused more total heat to be transferred from the thermal environment to the prop walls during fires in the metal props compared to that transferred to the walls during similar fires in the Gypsum Prop.

Between the metal props, the data measured during comparable tests were indistinguishable from one another as a whole, indicating there was no significant difference in thermal environments between the two props during fire development. However, once the environment began to cool as the fire became fuel-limited and after it was suppressed at the end of the experiment, the interior of the Insulated Metal Prop returned to ambient conditions at a much slower rate than the interior of the Metal Prop. This is significant because live-fire training structures must be allowed time to cool between training evolutions that are performed in succession.

Measurement data were also compared between tests with different fuel loads to determine the extent to which thermal conditions varied. Unsurprisingly, the furniture fuel package produced the most extreme conditions, and the pallets and OSB fuel load produced a more intense thermal environment than the pallets fuel load. Comparisons between heat flux and temperature data revealed that in some areas remote from the fire room, the environment produced by the pallets and OSB fuel package more closely resembled that generated during experiments with the furniture fuel load than that generated during experiments with the pallets fuel load. Thus, although it has the potential to create more realistic conditions, extra caution should be exhibited when considering the use of OSB in the fuel load for training fires due to the increase in the amount of heat generated and potential for injury.

Results from comparisons between experiments with different ventilation configurations were analyzed to better understand the effects of ventilation on the thermal environment throughout the props. When the fire room window and hall door were closed at ignition, the fire initially grew and then decayed as it became ventilation-limited, regardless of the prop and fuel load combination. In nearly every case, opening the door or window after the fire became ventilation-limited resulted in the fire regrowing and burning until extinguishment. There was a significant difference between the effect on fire conditions caused by venting the door compared to that caused by venting the window, most notably during the experiments with furniture due to the higher energy content and location of the fuel load in the room. In almost all cases, the fire environment created after venting the door was overall more severe than that produced after venting the window. Additionally, there was typically more variance in the thermal conditions throughout the prop after the window was opened compared to after the door was opened, indicating the fuel loads burned at a steadier rate as a result of the door vent compared to the window vent. In other words, the door was a more

efficient means to get air needed for combustion to the fire room.

Data comparisons between tests where the door was in the open position at the time of ignition were made to study the impact of opening the window six minutes after ignition on the environment of an already developed fire. The effect was, like the other ventilation configuration comparison, most evident during experiments with furniture due to the higher energy content of the fuel. Thermal conditions in the fire room during tests with wood-based fuels were not drastically affected by the window vent. Additionally, the neutral plane at the hallway door initially rose in response to the window vent with all three fuel loads. During the experiment with the furniture fuel package, the initial rise of the neutral plane was followed by a descent due to increased fire growth. This behavior did not occur during experiments with wood-based fuel packages.

Three tests were conducted to study the impact of interior suppression on the fire environment inside each prop, namely the local thermal environment of the suppression crew. One test with the pallets and OSB fuel load was conducted within each prop. The thermal insult from the fire environment to the firefighter was measured by two heat flux gauges mounted to the firefighter's helmet. The measurements obtained by the sensors around the time of suppression were compared between the three tests. The results showed that significantly higher heat fluxes were briefly experienced by the firefighter immediately after the start of suppression in the metal props than in the Gypsum Prop. The brief duration of high heat flux is suspected to be at least partially due to the conversion of water to steam. The metal linings are thought to have caused more steam production than the gypsum lining due to their drastically higher thermal conductivity. This is an important result that should be considered and discussed during live-fire training exercises in metal-lined props because the interior of modern-day structures are typically lined with non-metallic materials, like gypsum.

The insights that have emerged from these experiments will provide firefighters with more information about ventilation-controlled fire behavior in L-shaped training props. However, further research is needed to determine the applicability of these findings to scenarios with metal container props that are outside the scope of this project. Namely, future studies should investigate the variation in fire behavior between metal container props of different layouts and sizes; the effects of additional ventilation configurations on thermal conditions in such props; and the extent to which different suppression tactics affect the thermal exposure to firefighters within such props. Examination of these topics will deepen the understanding of the benefits and limitations associated with live-fire training in props constructed from metal shipping containers.

References

- [1] S. Wertman. F2010-10: One Career Firefighter/paramedic Dies and a Part-Time Firefighter/-Paramedic is Injured When Caught in a Residential Structure Flashover — Illinois. Report, National Institute for Occupational Safety and Health, March 2010.
- [2] M. Loflin. F2014-09: Lieutenant and Firefighter Die and 13 Firefighters Injured in a Wind-Driven Fire in a Brownstone — Massachusetts. Report, National Institute for Occupational Safety and Health, March 2014.
- [3] S. Wertman. F2013-04: Two Career Lieutenants Killed and Two Career Firefighters Injured Following a Flashover at an Assembly Hall Fire — Texas. Report, National Institute for Occupational Safety and Health, February 2013.
- [4] M. Loflin J. Tarley, S. Miles and T. Merinar. F2011-02: Volunteer Firefighter Caught in a Rapid Fire Event During Unprotected Search Dies After Facepiece Lens Melts — Maryland. Report, National Institute for Occupational Safety and Health.
- [5] S. Kerber. Impact of Ventilation on Fire Behavior in Legacy and Contemporary Residential Construction. Report, Underwriters Laboratories, Northbrook, Illinois, December 2010.
- [6] S. Kerber. Study of the Effectiveness of Fire Service Vertical Ventilation and Suppression Tactics in Single Family Homes. Report, Underwriters Laboratories, Northbrook, Illinois, June 2013.
- [7] R. Zevotek and S. Kerber. Study of the Effectiveness of Fire Service Positive Pressure Ventilation During Fire Attack in Single Family Homes Incorporating Modern Construction Practices. Technical Report, UL Firefighter Safety Research Institute, Columbia, MD, 2016.
- [8] D. Madrzykowski and C. Weinschenk. Understanding and Fighting Basement Fires. Technical report, UL Firefighter Safety Research Institute, Columbia, Maryland, March 2018.
- [9] D. Trump. Plymouth Firefighters Use Their DIY Skills to Construct a Live Burn Training Site. *Plymouth Magazine*, October 2015.
- [10] S. Levenstein. Smoke & Mirrors: Fire Training Facilities To Beat The Heat. *WebUrbanist*, April 2011. <https://weburbanist.com/2011/04/10/smoke-mirrors-fire-training-facilities-to-beat-the-heat/>.
- [11] K. Lambert. Live Fire Training: Benefits and Risks. *Compartment Fire Behavior Training, Belgium*, October 2013.
- [12] National Fire Protection Association. NFPA 1403: Standard on Live Fire Training Evolutions, 2018.

- [13] J. Tarley. F2007-09: Career Probationary Firefighter Dies While Participating in a Live-Fire Training Evolution at an Acquired Structure — Maryland. Report, National Institute for Occupational Safety and Health, February 2007.
- [14] S. Berardinelli. F2005-31: Career Officer Injured During a Live Fire Evolution at a Training Academy Dies Two Days Later — Pennsylvania. Report, National Institute for Occupational Safety and Health, October 2005.
- [15] J. Tarley and T. Mezzanotte. F2001-38: Volunteer fire fighter dies and two others are injured during live-burn training - New York. Report, National Institute for Occupational Safety and Health, September 2001.
- [16] Ed Hartin. Training Fires and “Real” Fires. <http://cfbt-us.com/wordpress/?p=485>, May 2009.
- [17] National Fire Protection Association, Quincy, Massachusetts. *NFPA 1001, Standard for Fire Fighter Professional Qualifications*, 2013.
- [18] S. Bernadelli N.T. Romano, J. Tarley. Career Lieutenant and Firefighter Die in a Flashover During a Live-Fire Training Evolution — Florida. Report, National Institute for Occupational Safety and Health, July 2002.
- [19] G. Fisher. Conducting NFPA 1403-Compliant Live Burn Training in Acquired Structures. *Fire Engineering*, March 2015.
- [20] K. Garcia and R. Kauffman. Realistic Live Burn Training You Can Afford. *Fire Engineering*, May 2009.
- [21] W. Goldfeder. “Avoidable — Nevada Training Accident Followup”. October 2012. <http://www.firefighterclosecalls.com/avoidable-nevada-training-accident-followup/>.
- [22] F. Reeder. The NFPA 1403 Debate. *FireRescue Magazine*, July 2013.
- [23] D. Rhodes. The Burn Building Limits. *FireRescue Magazine*, April 2018.
- [24] Irish National Directorate for Fire and Emergency Management, Dublin, Ireland. *Guidance for Compartment Fire Behaviour Training*, June 2010.
- [25] D. Madryzkowski. Fatal Training Fires: Fire Analysis for the Fire Service. Report, National Institute of Standards and Technology, Gaithersburg, MD, 2007.
- [26] A. Back. Fire development in insulated compartments: Effects from improved thermal insulation. Master’s thesis, Department of Fire Safety Engineering and Systems Safety, Lund University, Sweden, 2012.
- [27] R. Zevotek, K. Stakes, and J. Willi. Impact of Fire Attack Utilizing Interior and Exterior Streams on Firefighter Safety and Occupant Survival: Full Scale Experiments. Technical report, UL Firefighter Safety Research Institute, Columbia, MD, 2017.

- [28] B.N. Taylor and C.E. Kuyatt. Guidelines for Evaluating and Expressing the Uncertainty of NIST Measurement Results. NIST Technical Note 1297, National Institute of Standards and Technology, Gaithersburg, Maryland, 1994.
- [29] Omega Engineering Inc., Stamford, Connecticut. *The Temperature Handbook*, 2004.
- [30] L.G. Blevins. Behavior of bare and aspirated thermocouples in compartment fires. In *National Heat Transfer Conference, 33rd Proceedings*, pages 15–17, 1999.
- [31] W.M. Pitts, E. Braun, R. Peacock, H. Mitler, E. Johnson, P. Reneke, and L.G. Blevins. Temperature uncertainties for bare-bead and aspirated thermocouple measurements in fire environments. *ASTM Special Technical Publication*, 1427:3–15, 2003.
- [32] Medtherm Corporation, Huntsville, Alabama. *64 Series Heat Flux Transducers*, 2003.
- [33] W.M. Pitts, A.V. Murthy, J.L. de Ris, J. Filtz, K. Nygård, D. Smith, and I. Wetterlund. Round robin study of total heat flux gauge calibration at fire laboratories. *Fire Safety Journal*, 41(6):459–475, 2006.
- [34] Setra Systems, Boxborough, Massachusetts. *Setra Model 264 Very Low Pressure Transducer Data Sheet Rev E.*, 2002.
- [35] R.A. Bryant. A comparison of gas velocity measurements in a full-scale enclosure fire. *Fire Safety Journal*, 44:793–800, 2009.
- [36] M. Bundy, A. Hamins, E.L. Johnsson, S.C. Kim, G.H. Ko, and D.B. Lenhart. Measurements of Heat and Combustion Products in Reduced-Scale Ventilated-Limited Compartment Fires. NIST Technical Note 1483, National Institute of Standards and Technology, Gaithersburg, MD, 2007.
- [37] A. Lock, M. Bundy, E.L. Johnsson, A. Hamins, G.H. Ko, C. Hwang, P. Fuss, and R. Harris. Experimental study of the effects of fuel type, fuel distribution, and vent size on full-scale underventilated compartment fires in an ISO 9705 room. NIST Technical Note 1603, National Institute of Standards and Technology, Gaithersburg, MD, 2008.
- [38] Stanley Hand Tools, New Britain, Connecticut. *User Manual TLM 100*, 2013.
- [39] T. Butcher, S. Cook, L. Crown, and R. Harshman. NIST Handbook 44: Specifications, Tolerances, and Other Technical Requirements for Weighing and Measuring Devices. *National Institute of Standards, Gaithersburg, MD*, 2012.
- [40] Ohaus Corporation, Pine Brook, New Jersey. *Manual for SD Series Bench Scale*, 2000.
- [41] Retrotec, Everson, WA. *Retrotec 5101 Classic Blower Door Specifications*, 2017.
- [42] ASTM International, ASTM International, West Conshohocken, PA. *ASTM E779-10, Standard Test Method for Determining Air Leakage Rate by Fan Pressurization*, 2010. www.astm.org.

- [43] Badger Meter, Milwaukee, Wisconsin. *M-Series M2000 Electromagnetic Flow Meter*, MAG-DS-01047-EN-06 edition, 2015.
- [44] G. Horn, R. Kesler, J. Regan, and D. Madrzykowski. A Study on the Effect of Repeat Moderate Intensity Radiant Exposures on SCBA Facepiece Properties. NIST GCR 17-014, National Institute of Standards and Technology, Gaithersburg, Maryland, July 2017.
- [45] A. Putorti, A. Mensch, N. Bryner, and G. Braga. Thermal Performance of Self-Contained Breathing Apparatus Facepiece Lenses Exposed to Radiant Heat Flux. Technical Report NIST TN 1785, National Institute of Standards and Technology, Gaithersburg, MD, 2013.
- [46] National Fire Protection Association, Quincy, Massachusetts. *NFPA 1981, Standard on Open-Circuit Self Contained Breathing Apparatus for Fire and Emergency Services*, 2013.
- [47] National Fire Protection Association, Quincy, Massachusetts. *NFPA 1971, Standard on Protective Ensembles for Structural Fire Fighting and Proximity Fire Fighting*, 2013.
- [48] P.F. Watson and A. Petrie. Method Agreement Analysis: A Review of Correct Methodology. *Therriogenology*, 73(9):1167–1179, 2010.
- [49] M.J. Hurley. *SFPE Handbook of Fire Protection Engineering*, chapter Appendix 2: Thermo-physical Property Data. Springer, New York, 5th edition, 2016.
- [50] S. L. Manzello, S. Park, T. Mizukami, and D. P. Bentz. Measurement of Thermal Properties of Gypsum Board at Elevated Temperatures. In *Proceedings of the Fifth International Conference Structures in Fire*, pages 656–665. Nanyang Technological University, Singapore: Organising Committee, Fifth International Conference Structures in Fire (SiF'08), May 28-30 2008.
- [51] J. Regan and R. Zevotek. Study of the Fire Service Training Environment: Safety and Fidelity in Concrete Live Fire Training Buildings. Technical report, UL Firefighter Safety Research Institute, Columbia, MD, 2018.
- [52] G. Rein. *SFPE Handbook of Fire Protection Engineering*, chapter Ch. 19: Smoldering Combustion. Springer, New York, 5th edition, 2016.
- [53] National Fire Protection Association, Quincy, Massachusetts. *NFPA 1404, Standard for Fire Service Respiratory Protection Training*, 2018.

Appendix A Example of Sample Set Comparison & Bias/ICC Calculation

The following example outlines the process used to compare temperature data sets between experiments to determine the extent to which the data sets varied.

Consider the temperature data collected at the same location during identical tests in the Metal Prop and Insulated Metal Prop plotted in Figure A.1.

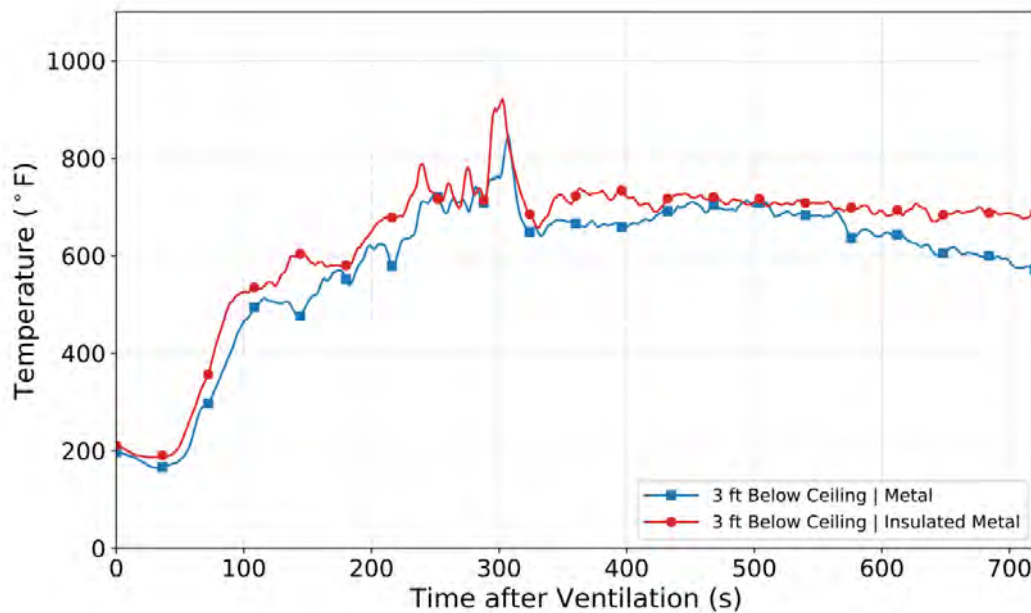


Figure A.1: Temperature data collected 3 ft (0.9 m) below the ceiling at start hall location during similar tests in the Metal Prop (blue line) and Insulated Metal Prop (red line).

To determine the degree of variance between the two data sets, the measurements at each second are paired with one another. Instead of considering all 720 pairs that are formed by the sets, the upcoming steps and equations will focus on the five pairs highlighted in Figure A.2.

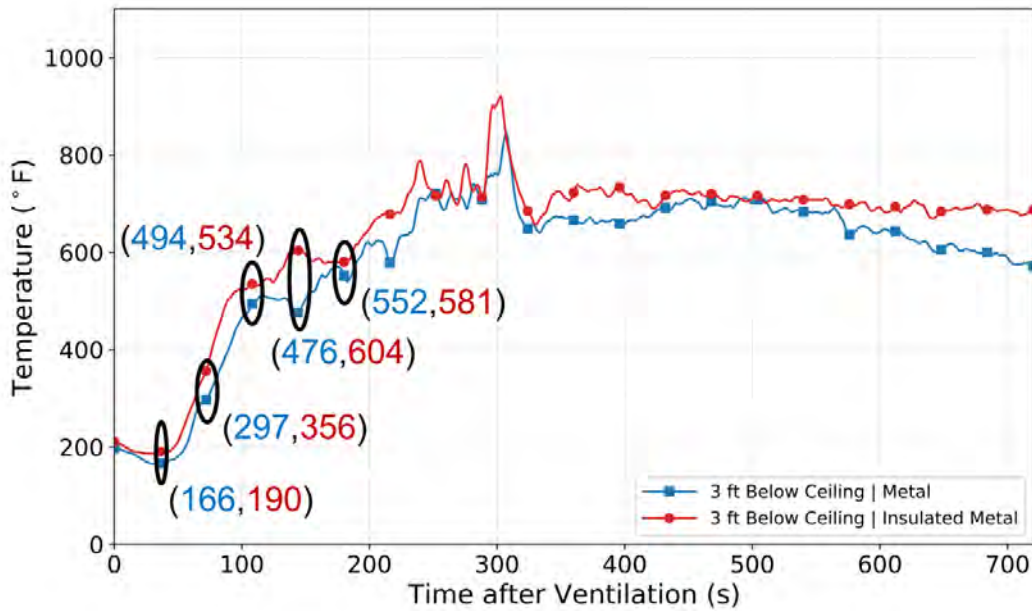


Figure A.2: Temperature data sets used for Bias & ICC calculation example with the five measurement pairs of focus highlighted.

After they are formed, the measurement pairs can be translated to a scatter plot. For example, a scatter plot of the five highlighted pairs is shown in Figure A.3, followed the complete scatter plot with all 720 measurement pairs in Figure A.4.

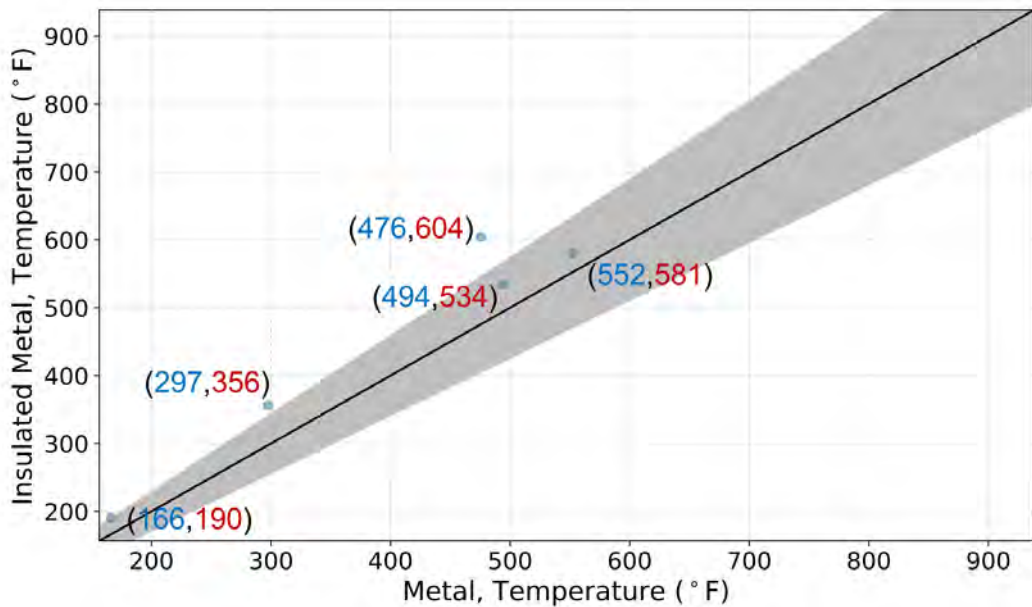


Figure A.3: Scatter plot of the five highlighted data pairs. The black line is the line of perfect agreement, and the gray area represents the range around the line that is within the thermocouple measurement uncertainty.

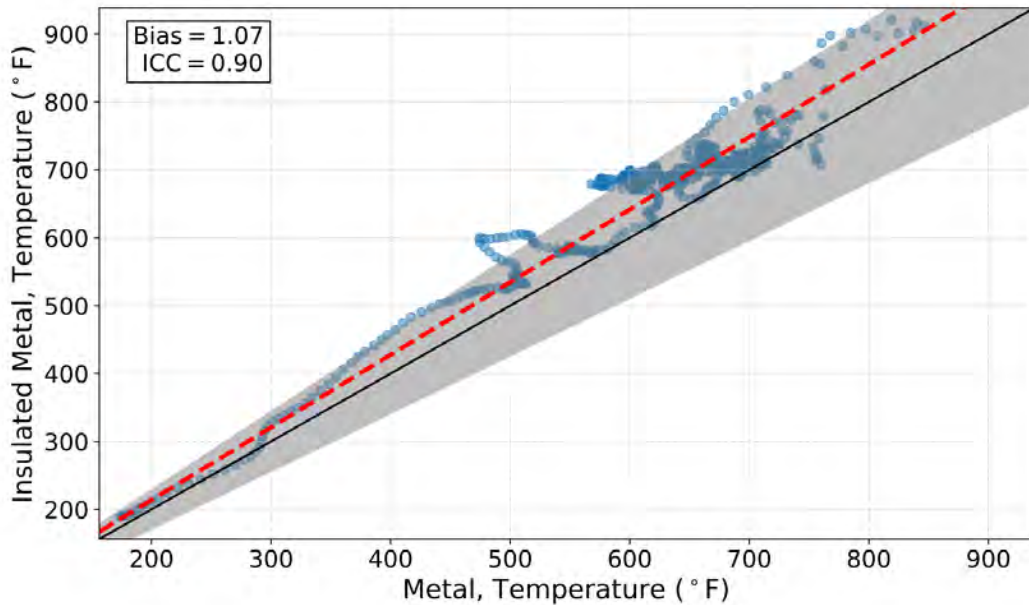


Figure A.4: Scatter plot of the 720 measurement pairs formed by the example data sets. The black line is the line of perfect agreement, the gray area represents the range around the line that is within the thermocouple measurement uncertainty, and the dashed, red line is the line of best fit across the data pairs.

The black line on the charts is the line of perfect agreement; if the data sets were identical, all points on the scatter plot would fall on this line. The gray area represents the range around the line of perfect agreement that is within the thermocouple measurement uncertainty, $\pm 15\%$. If a plotted measurement pair lies within this area, the difference between the two measurements is indistinguishable from the measurement uncertainty. The dashed, red line in Figure A.4 represents the line of best fit across the measurement pairs.

The values of the two statistical metrics used to quantify the overall agreement between the data sets also appear on Figure A.4. The bias, which is the slope of the best fit line, is a measure of the difference between the linear approximation line and the line of perfect agreement. The second parameter, the intraclass correlation coefficient (ICC), is a measure of the amount of variation between the measurement pairs. Visual representations of these definitions are denoted by the arrows that overlay the scatter plot in Figure A.5.

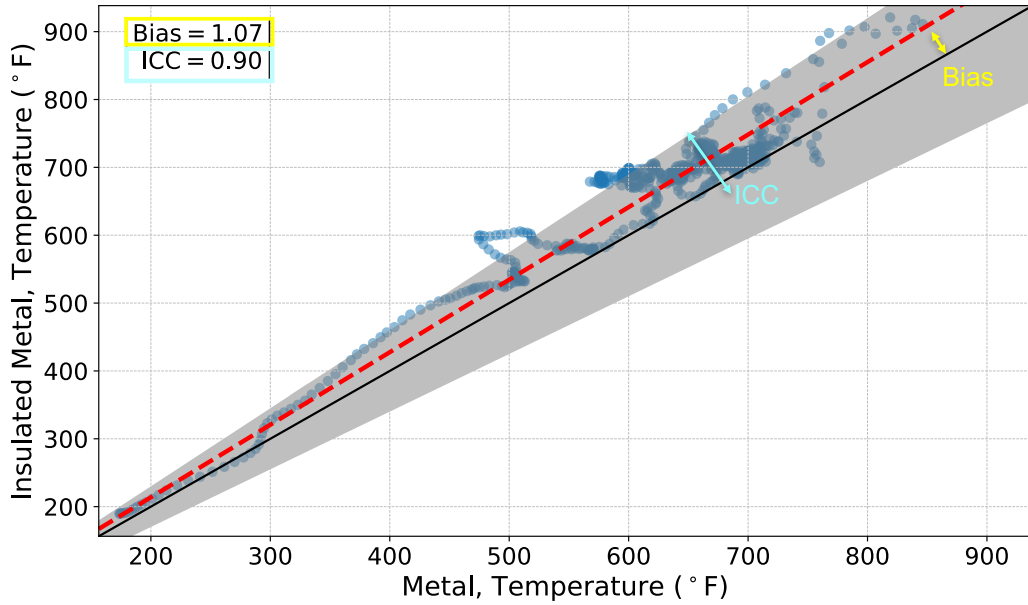


Figure A.5: Scatter plot of the 720 measurement pairs formed by the example data sets with arrows to provide a visual representation of the bias and ICC. The bias factor is a measure of the difference between the line of best fit and the line of perfect agreement, and the ICC is a measure of the variation between measurement pairs.

To calculate the ICC, two lists are created from the set of data pairs: a list of the sum of the values in each pair (L_a) and a list of the difference between the values in each pair (L_d),

$$L_a = \{ \dots, 166 + 190, \dots, 297 + 356, \dots, 494 + 534, \dots, 476 + 604, \dots, 552 + 581, \dots \}$$

$$\Rightarrow L_a = \{ \dots, 356, \dots, 653, \dots, 1028, \dots, 1080, \dots, 1133, \dots \}$$

$$L_d = \{ \dots, |166 - 190|, \dots, |297 - 356|, \dots, |494 - 534|, \dots, |476 - 604|, \dots, |552 - 581|, \dots \}$$

$$\Rightarrow L_d = \{ \dots, 24, \dots, 59, \dots, 40, \dots, 128, \dots, 29, \dots \}$$

Then, the ICC is computed using

$$ICC = \frac{\sigma_a^2 - \sigma_d^2}{\sigma_a^2 + \sigma_d^2 + \frac{2}{n} (n\bar{d}^2 - \sigma_d^2)}$$

where n is the number of measurement pairs formed by the two data sets, σ_a^2 is the variance of L_a , σ_d^2 is the variance of L_d , and \bar{d} is the mean of L_d .

Appendix B Bias & ICC Tables

B.1 Fuel Load Comparisons

Table B.1: Overall Bias & ICC Values for Comparisons of Post-Vent Data from each Thermocouple Array Between Fuel Loads in the Gypsum Prop

Comparison	Biases in Range	Post-Vent	
		Overall Bias	Overall ICC
<i>Furniture vs. Pallets</i>			
Fire Room Window (BDP1)	0/5	0.46	0.05
Fire Room (1TC)	2/5	0.75	0.24
End Hall (2TC)	0/3	0.58	0.09
Start Hall (3TC)	0/3	0.43	0.09
Hall Doorway (BDP2)	0/2	0.47	0.14
<i>Furniture vs. Pallets & OSB</i>			
Fire Room Window (BDP1)	0/5	0.77	0.28
Fire Room (1TC)	5/5	0.88	0.68
End Hall (2TC)	3/3	0.91	0.87
Start Hall (3TC)	3/3	0.88	0.79
Hall Doorway (BDP2)	1/2	0.85	0.82
<i>Pallets vs. Pallets & OSB</i>			
Fire Room Window (BDP1)	1/5	1.46	0.09
Fire Room (1TC)	3/5	1.12	0.23
End Hall (2TC)	0/3	1.53	0.11
Start Hall (3TC)	0/3	2.02	0.14
Hall Doorway (BDP2)	0/2	1.80	0.17

Table B.2: Overall Bias & ICC Values for Comparisons of Post-Vent Data from each Thermocouple Array Between Fuel Loads in the Insulated Metal Prop

Comparison	Biases in Range	Post-Vent	
		Overall Bias	Overall ICC
<i>Furniture vs. Pallets</i>			
Fire Room Window (BDP1)	4/5	0.88	0.74
Fire Room (1TC)	2/5	0.82	0.51
End Hall (2TC)	0/3	0.71	0.39
Start Hall (3TC)	0/3	0.73	0.52
Hall Doorway (BDP2)	0/2	0.73	0.50
<i>Furniture vs. Pallets & OSB</i>			
Fire Room Window (BDP1)	3/5	0.86	0.78
Fire Room (1TC)	4/5	0.90	0.76
End Hall (2TC)	3/3	0.91	0.55
Start Hall (3TC)	3/3	1.00	0.74
Hall Doorway (BDP2)	2/2	1.03	0.80
<i>Pallets vs. Pallets & OSB</i>			
Fire Room Window (BDP1)	5/5	0.99	0.92
Fire Room (1TC)	4/5	1.09	0.75
End Hall (2TC)	0/3	1.28	0.32
Start Hall (3TC)	0/3	1.35	0.39
Hall Doorway (BDP2)	0/2	1.37	0.30

Appendix C Experimental Data

Plots of data collected during each experiment by the different instrumentation throughout the prop are contained in this appendix. The labels that appear in the legends correspond to the shaded areas presented in Figure C.1.

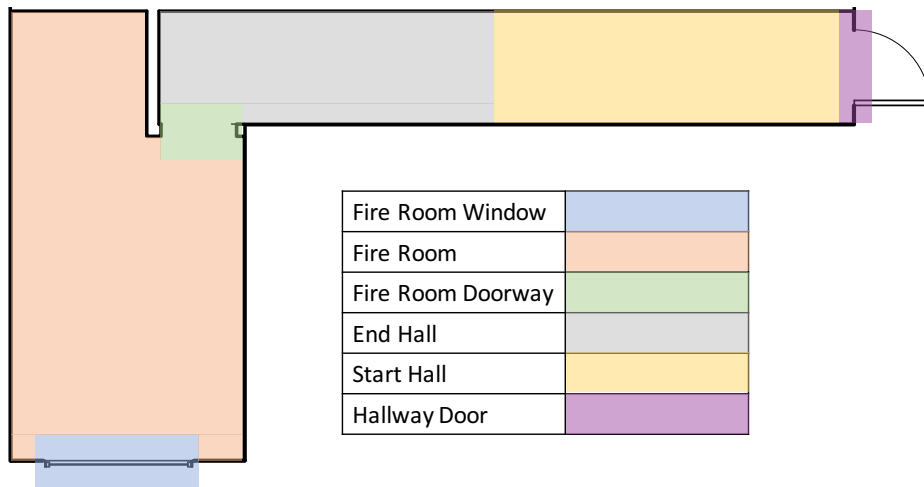


Figure C.1: Floor plan showing the standard locations of the instrumentation devices used to collect data from the fire environment during experiments.

C.1 Burn In Experiments

Test 1

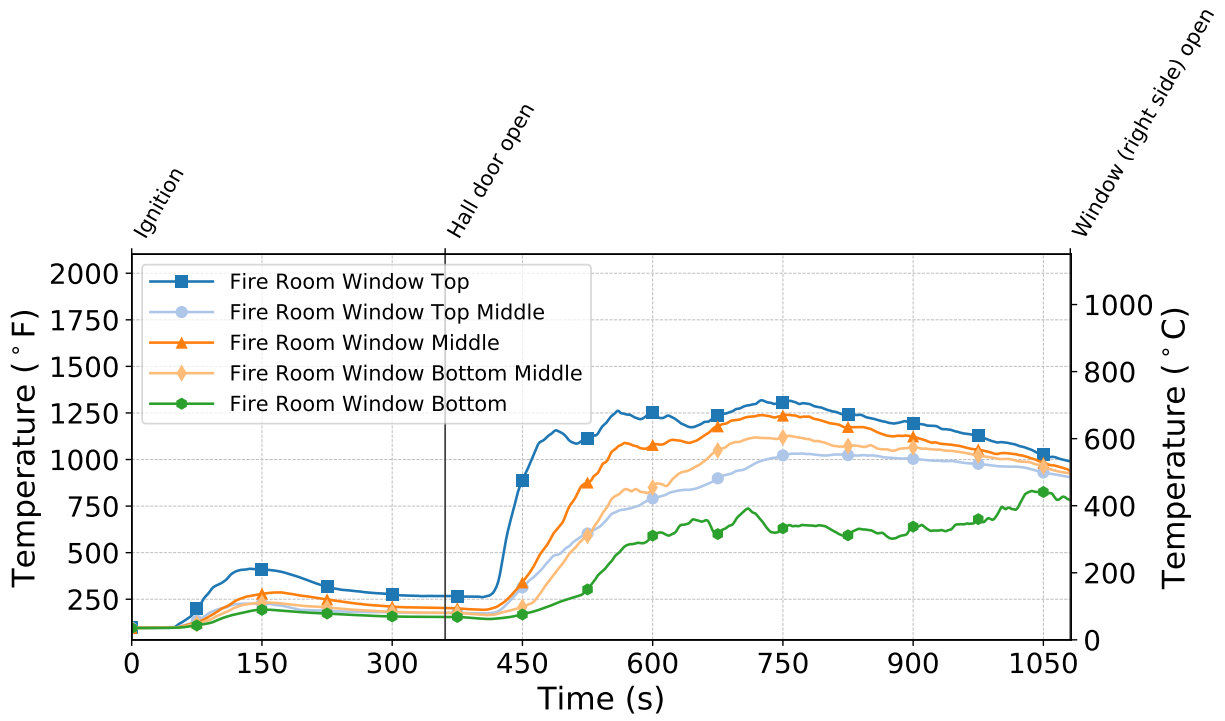


Figure C.2: Temperatures measured by the fire room window thermocouples during Test 1.

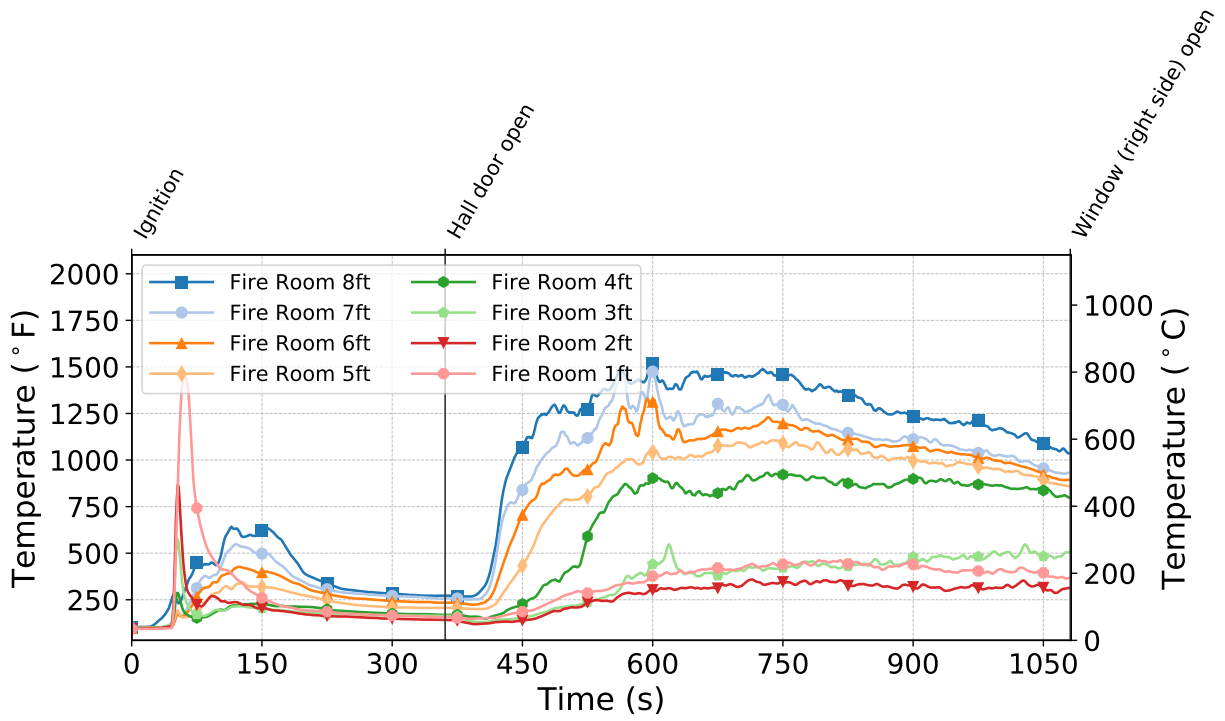


Figure C.3: Temperatures measured by the fire room thermocouples during Test 1.

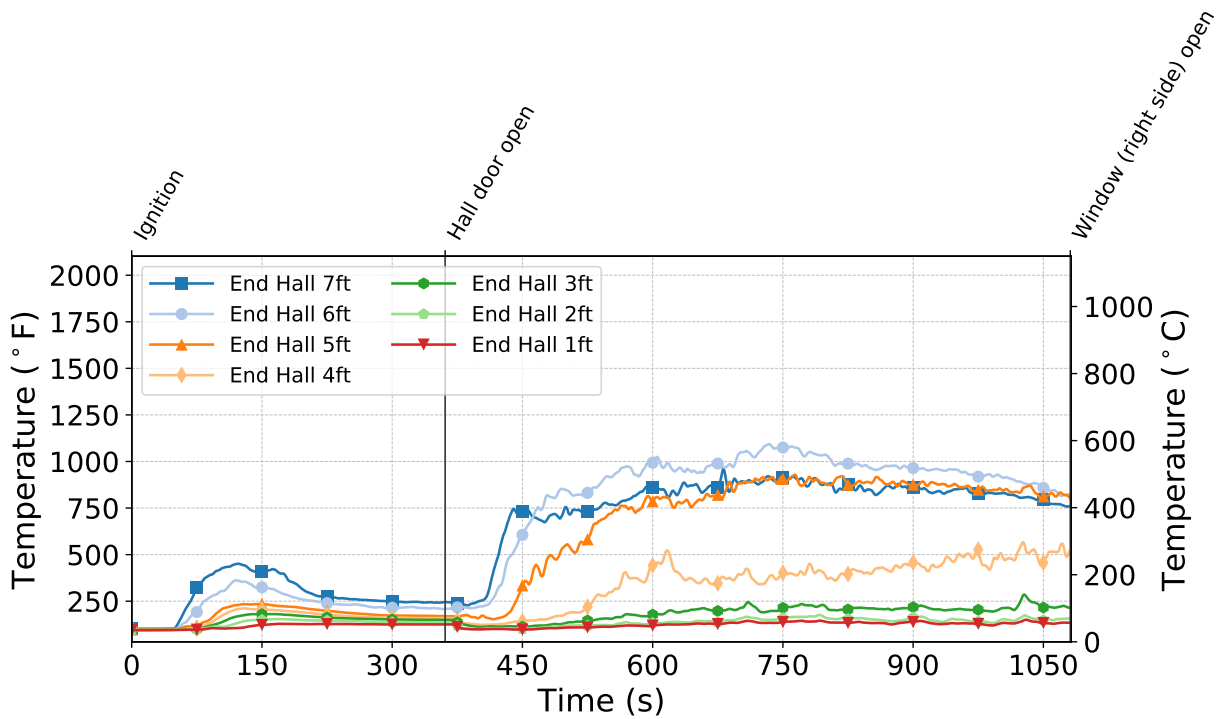


Figure C.4: Temperatures measured by the end hall thermocouples during Test 1.

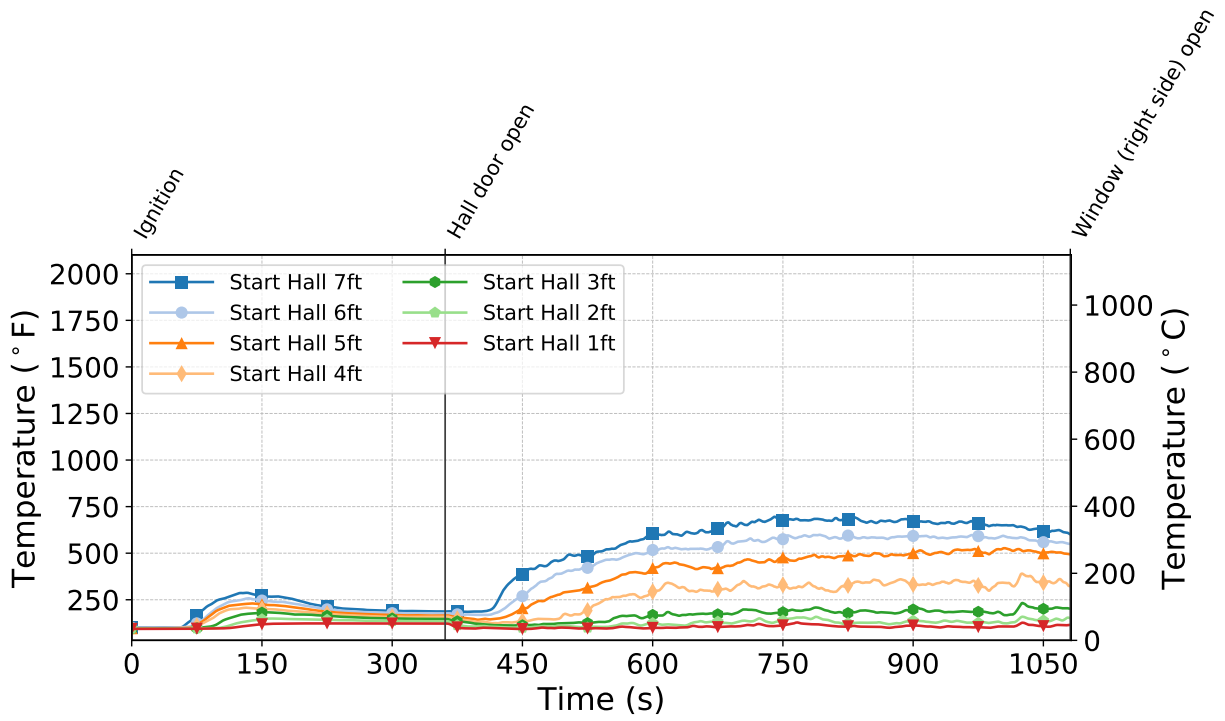


Figure C.5: Temperatures measured by the start hall thermocouples during Test 1.

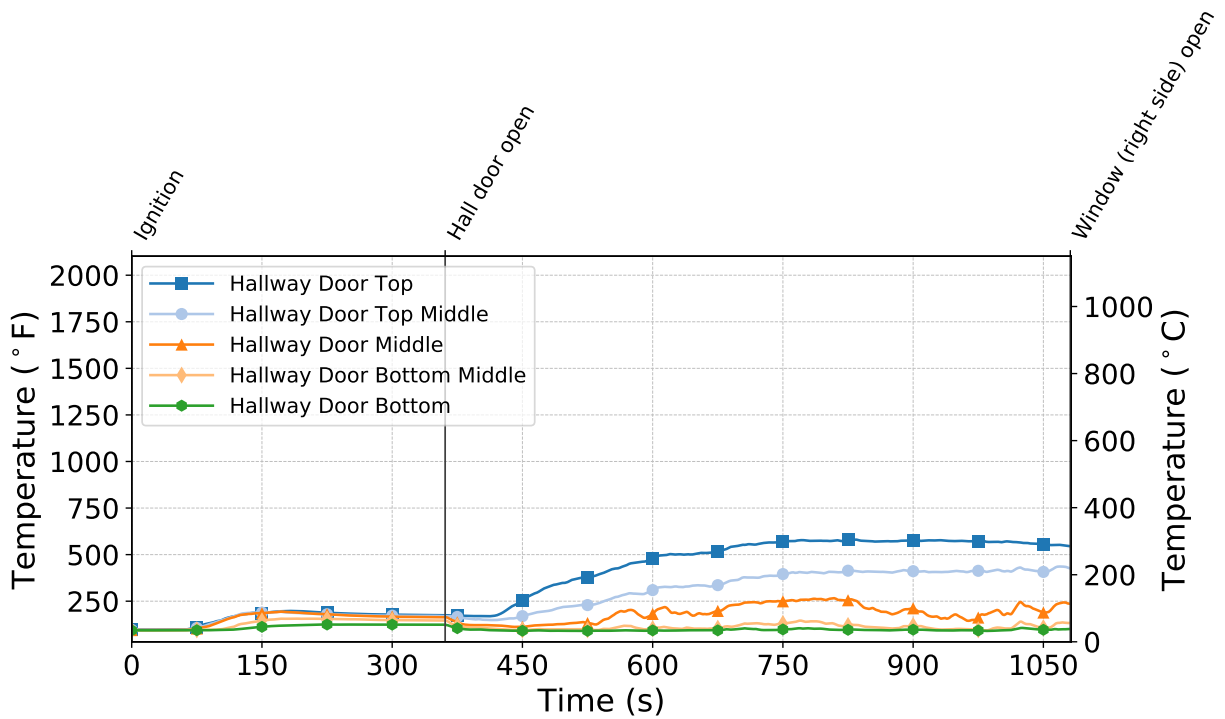


Figure C.6: Temperatures measured by the hallway door thermocouples during Test 1.

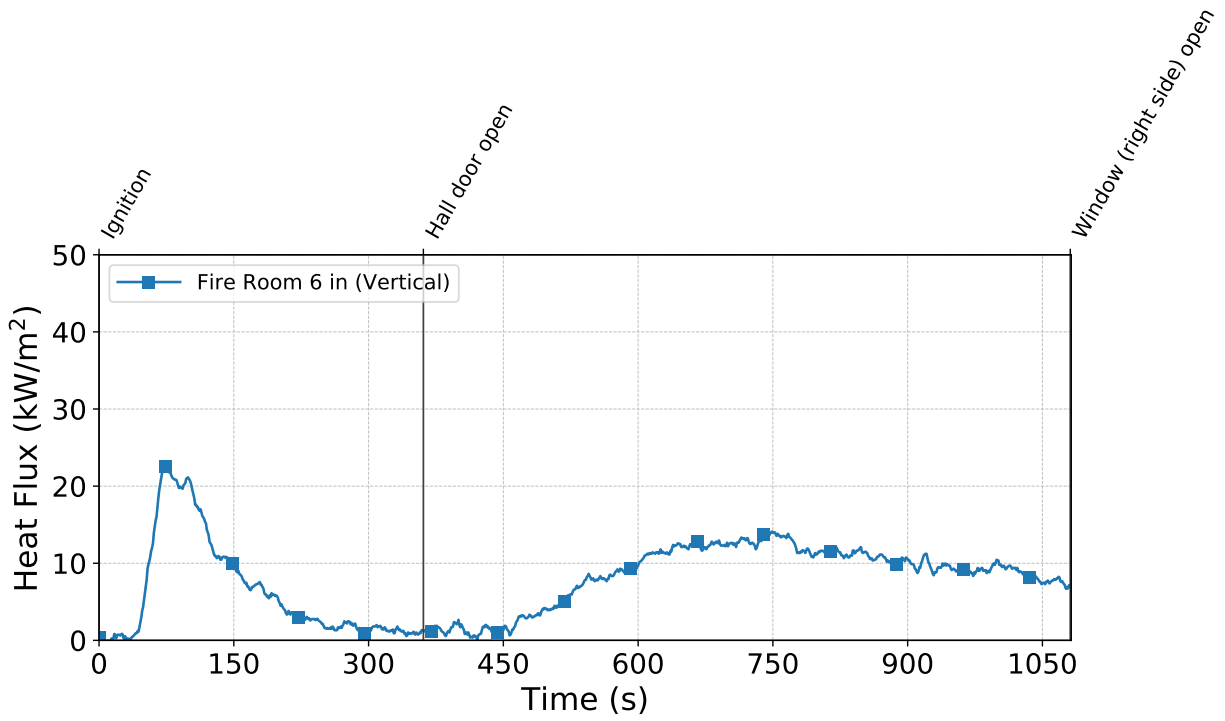


Figure C.7: Heat flux measured by the fire room gauge during Test 1.

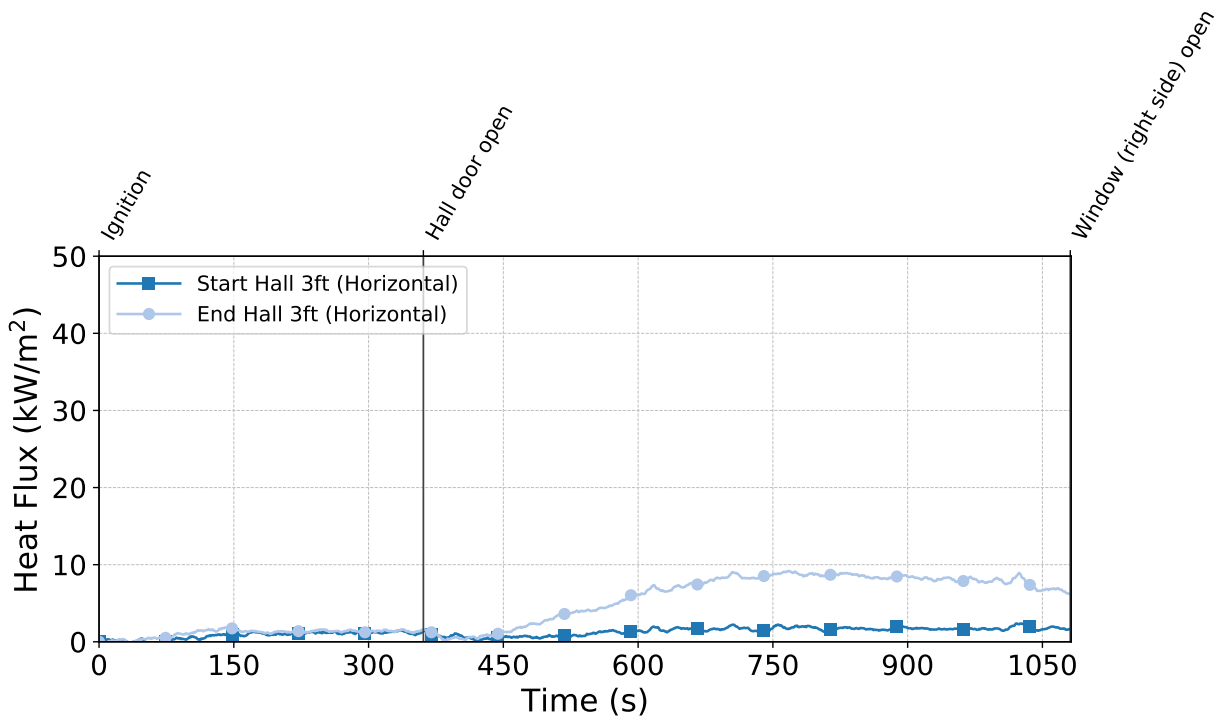


Figure C.8: Heat flux measured by the hallway gauges during Test 1.

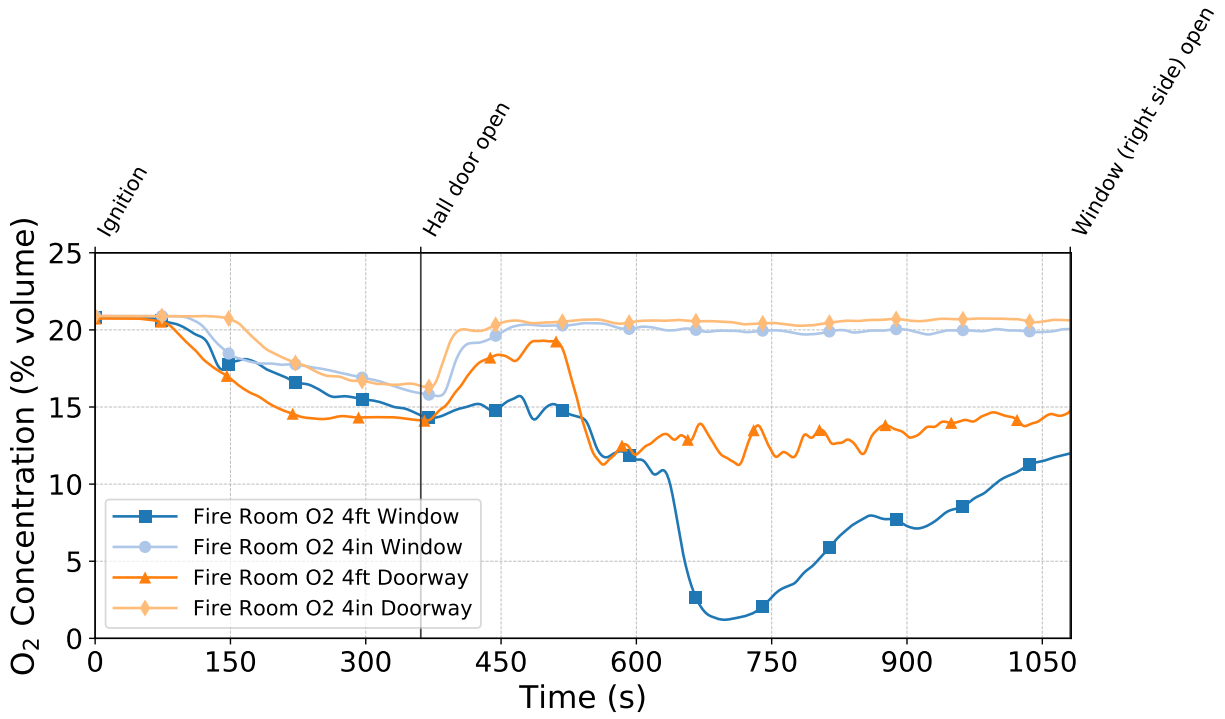


Figure C.9: Oxygen concentrations measured by the fire room gas sampling probes during Test 1.

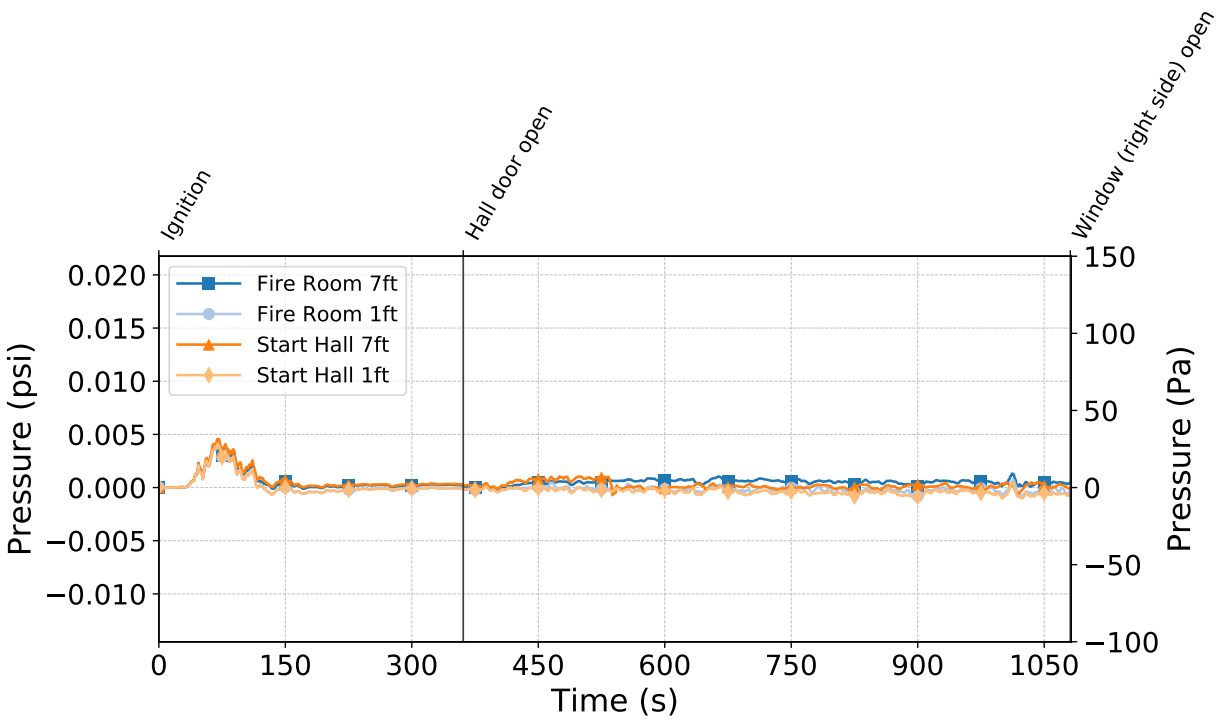


Figure C.10: Pressures measured by the fire room and hallway probes during Test 1.

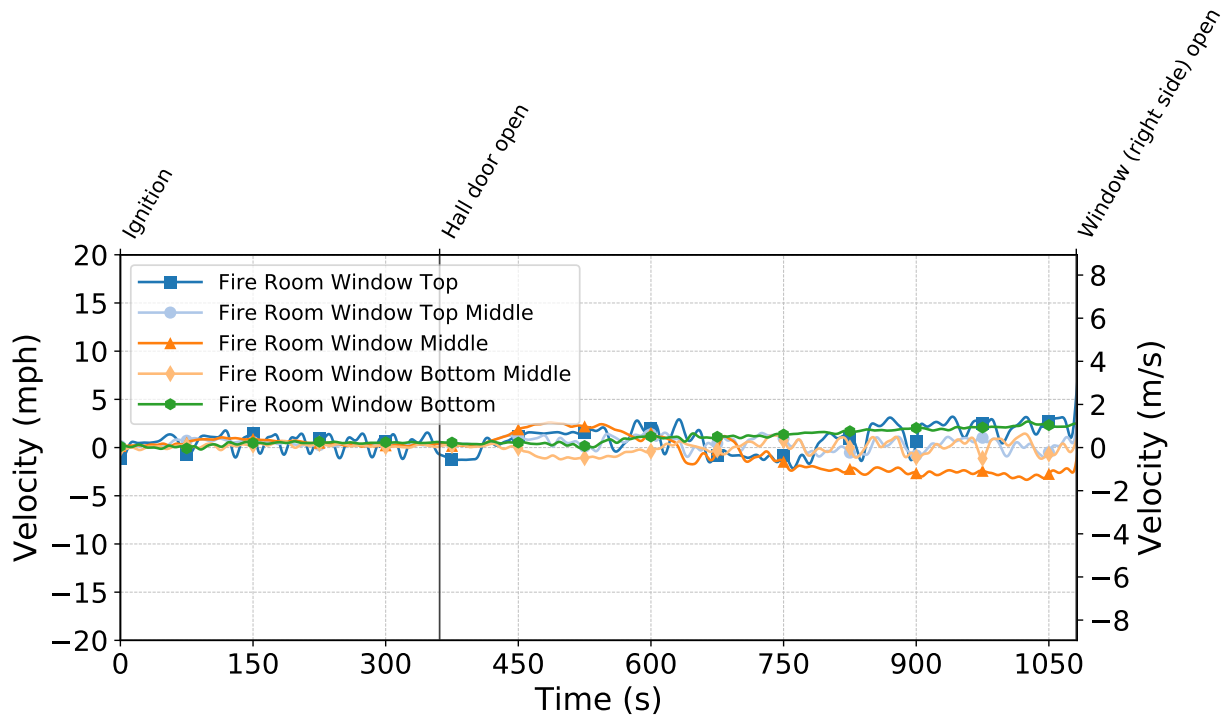


Figure C.11: Gas velocities measured by the fire room window bdps during Test 1.

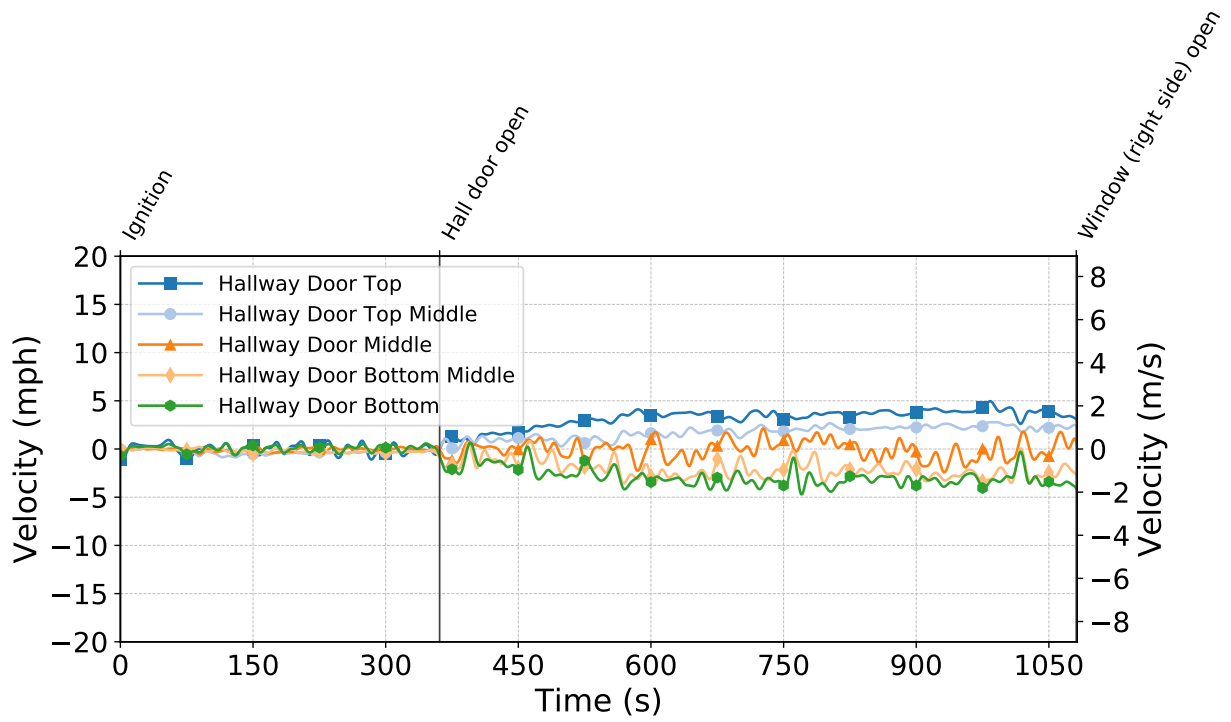


Figure C.12: Gas velocities measured by the hallway door bdps during Test 1.

Test 2

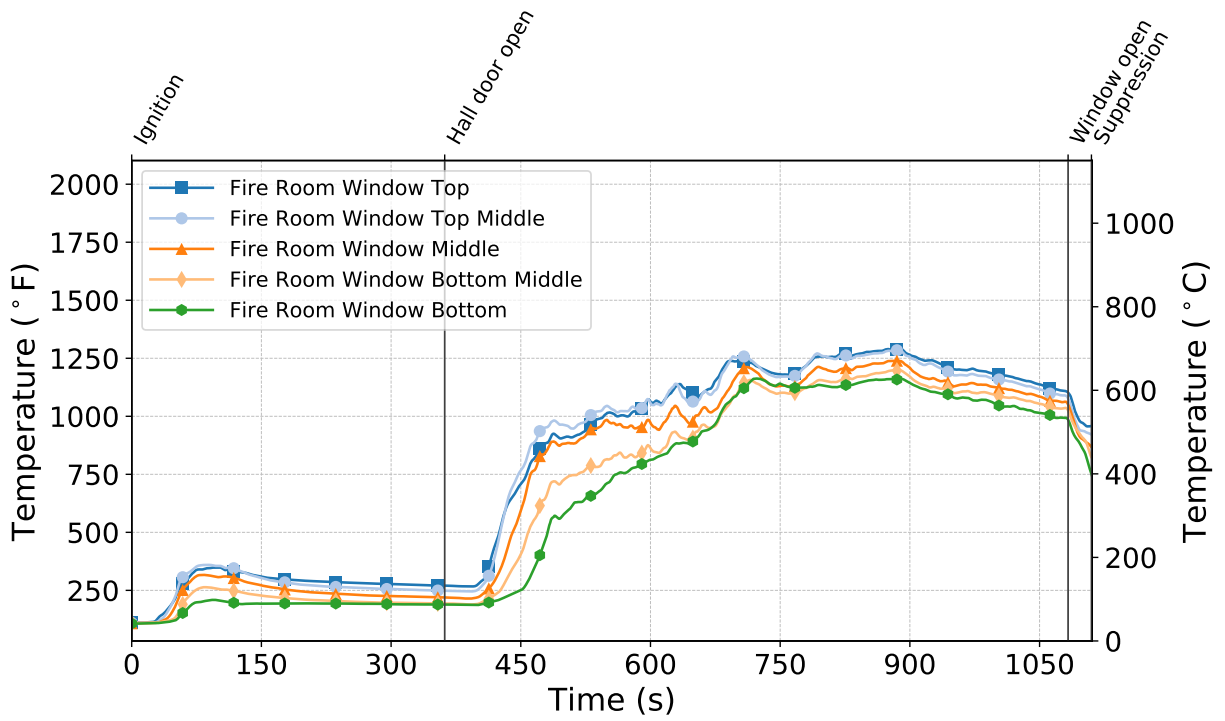


Figure C.13: Temperatures measured by the fire room window thermocouples during Test 2.

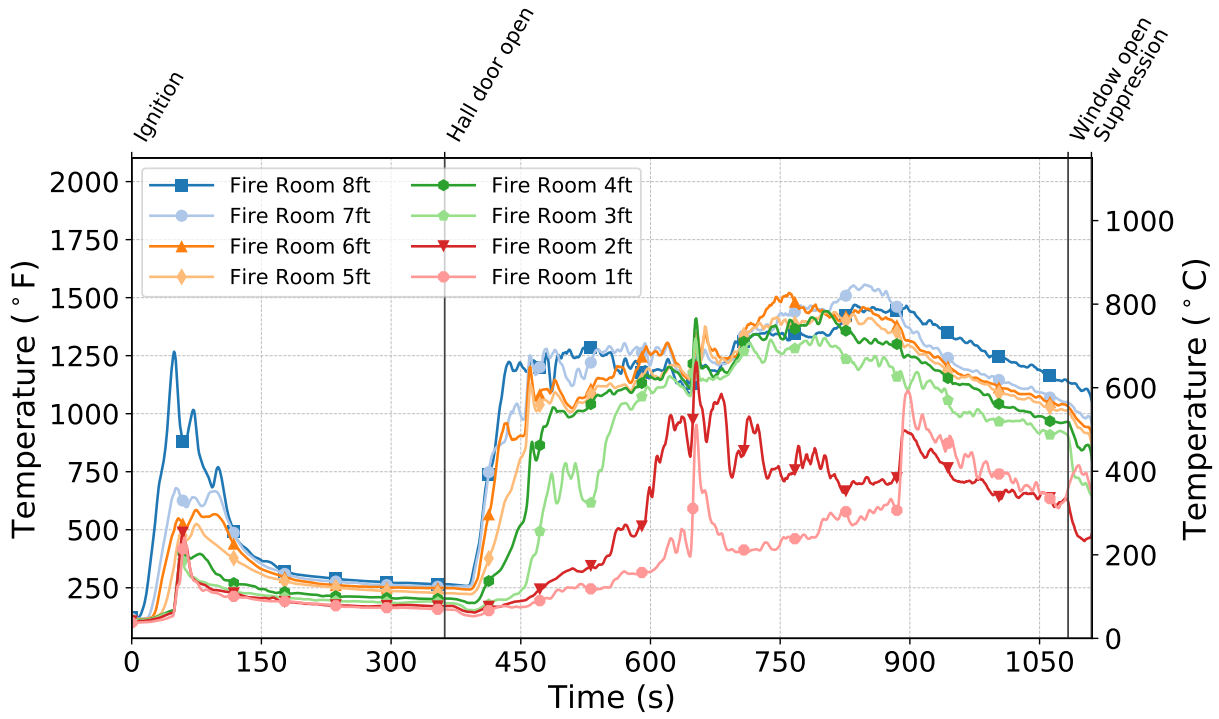


Figure C.14: Temperatures measured by the fire room thermocouples during Test 2.

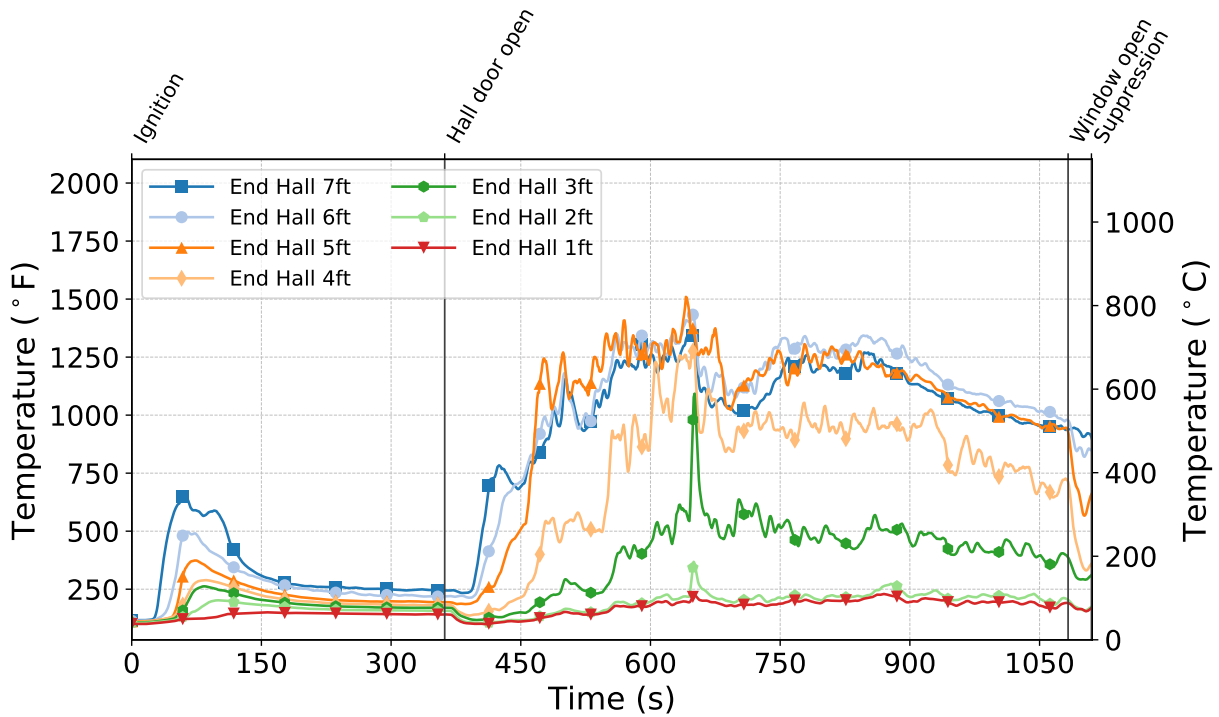


Figure C.15: Temperatures measured by the end hall thermocouples during Test 2.

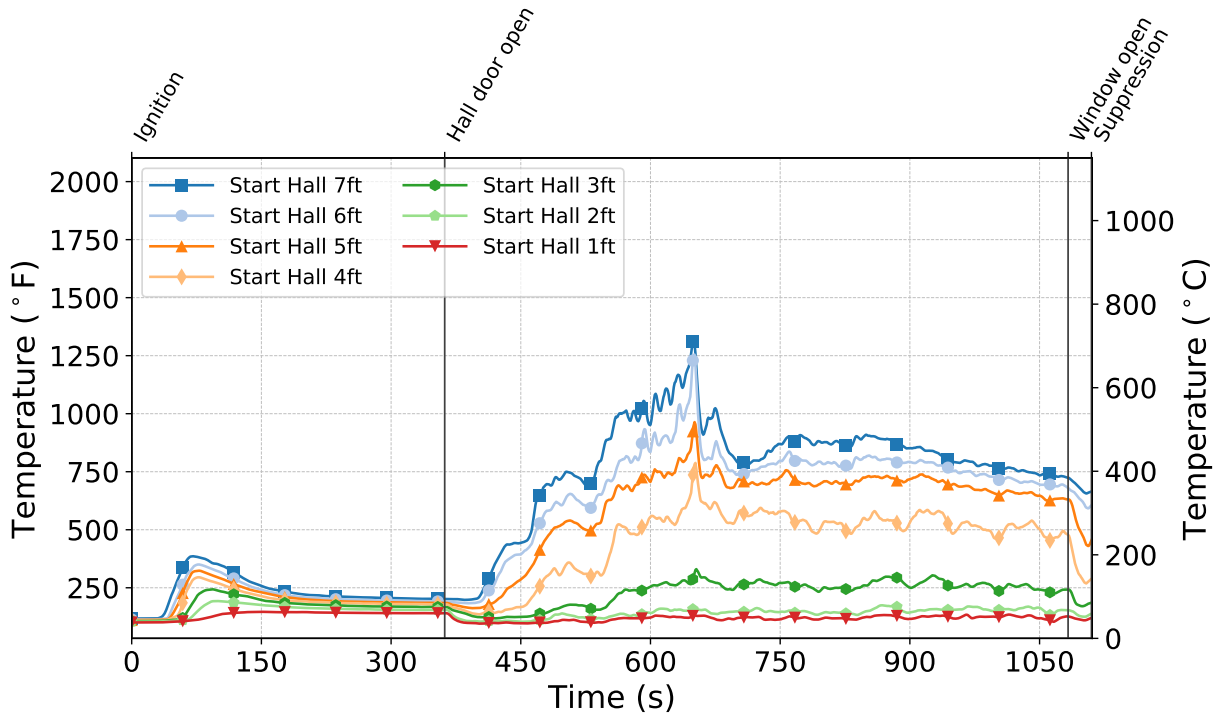


Figure C.16: Temperatures measured by the start hall thermocouples during Test 2.

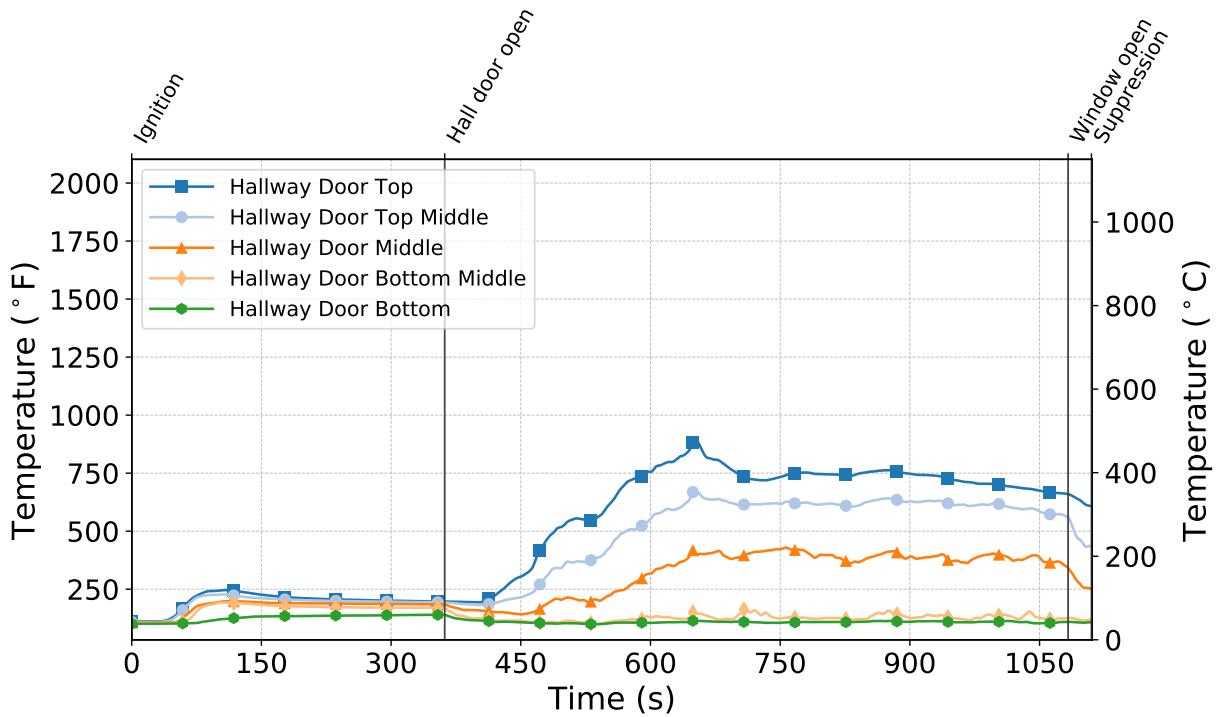


Figure C.17: Temperatures measured by the hallway door thermocouples during Test 2.

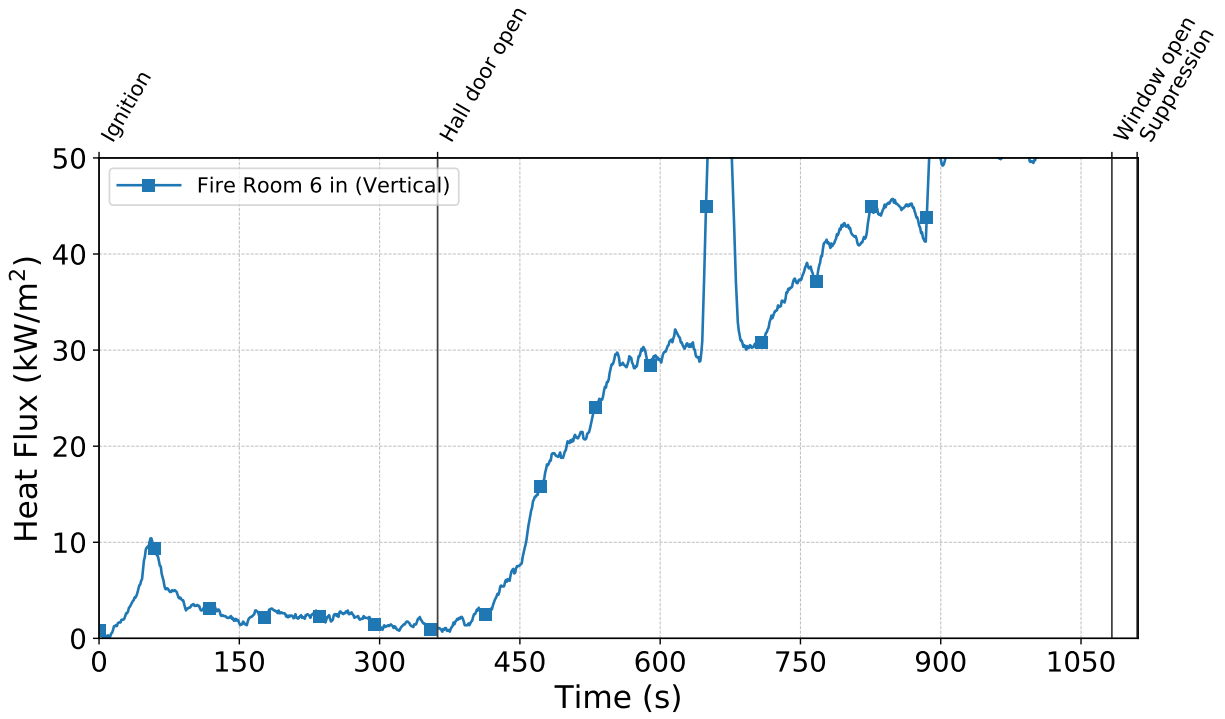


Figure C.18: Heat flux measured by the fire room gauge during Test 2.

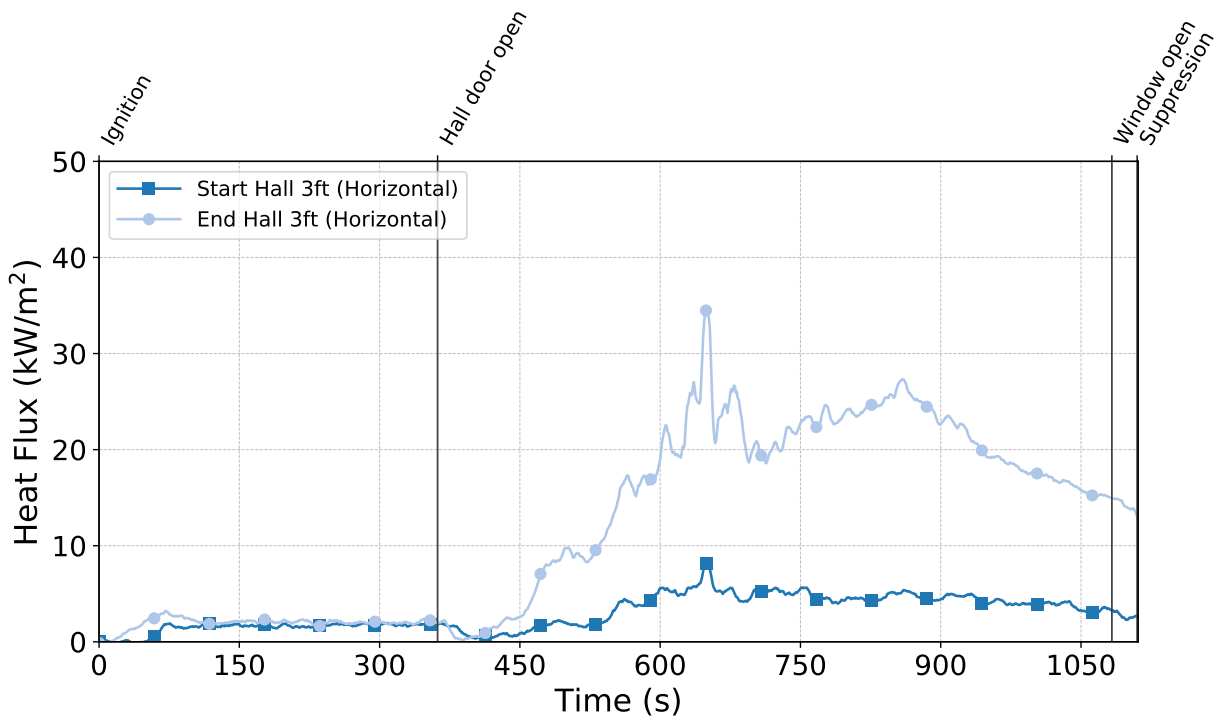


Figure C.19: Heat flux measured by the hallway gauges during Test 2.

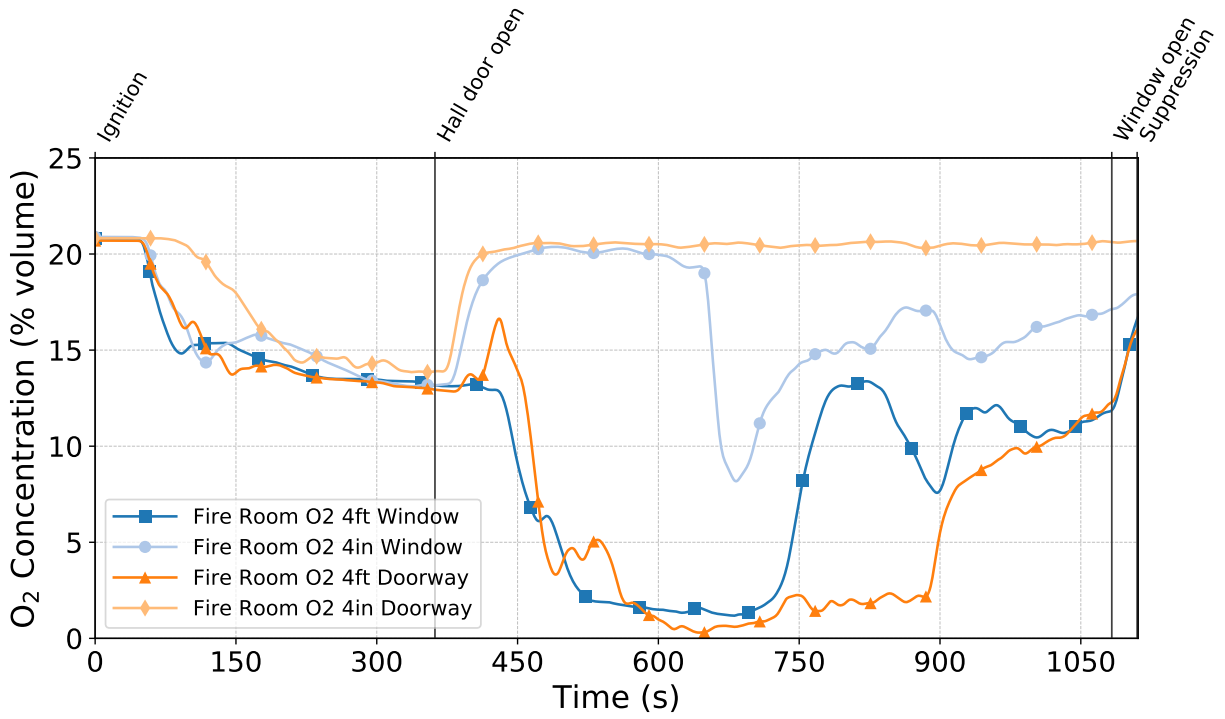


Figure C.20: Oxygen concentrations measured by the fire room gas sampling probes during Test 2.

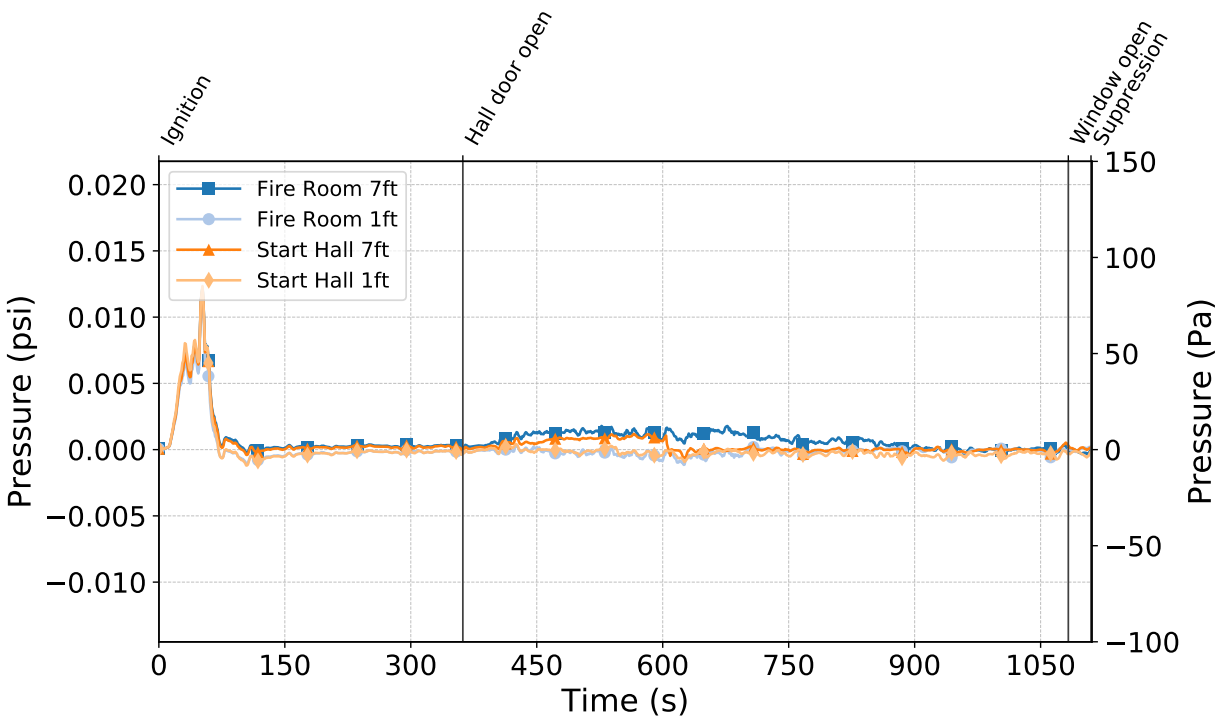


Figure C.21: Pressures measured by the fire room and hallway probes during Test 2.

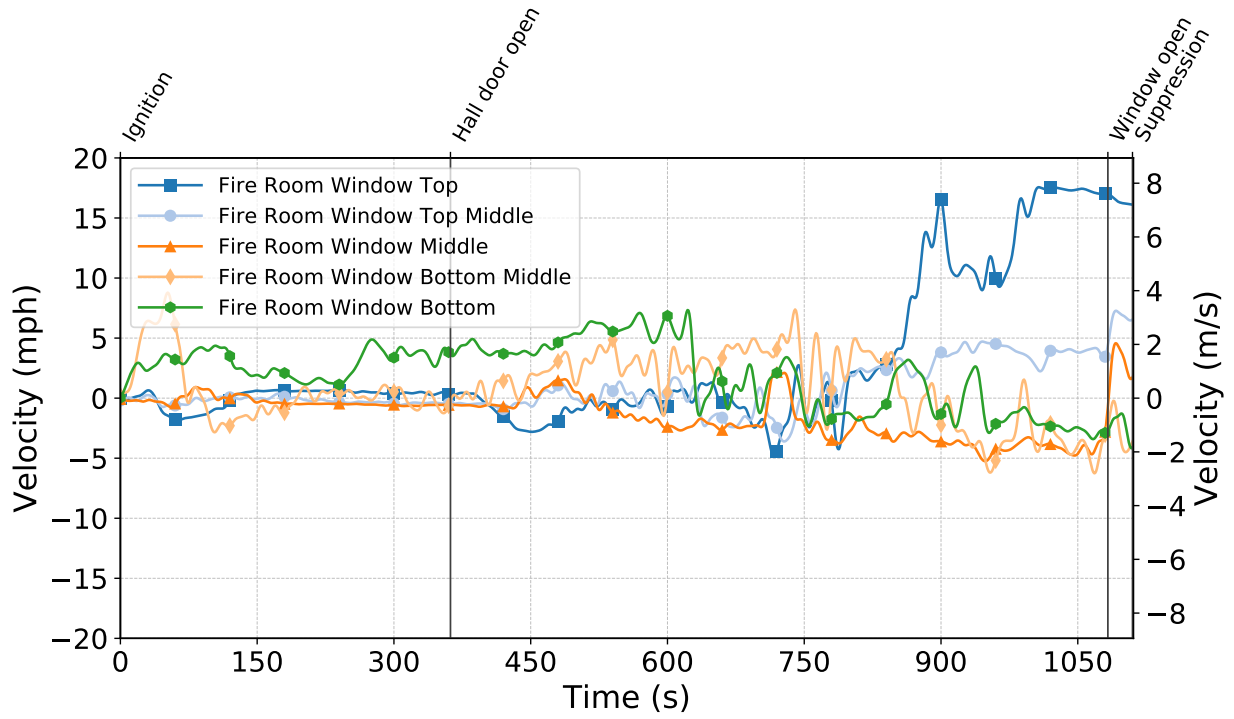


Figure C.22: Gas velocities measured by the fire room window bdps during Test 2.

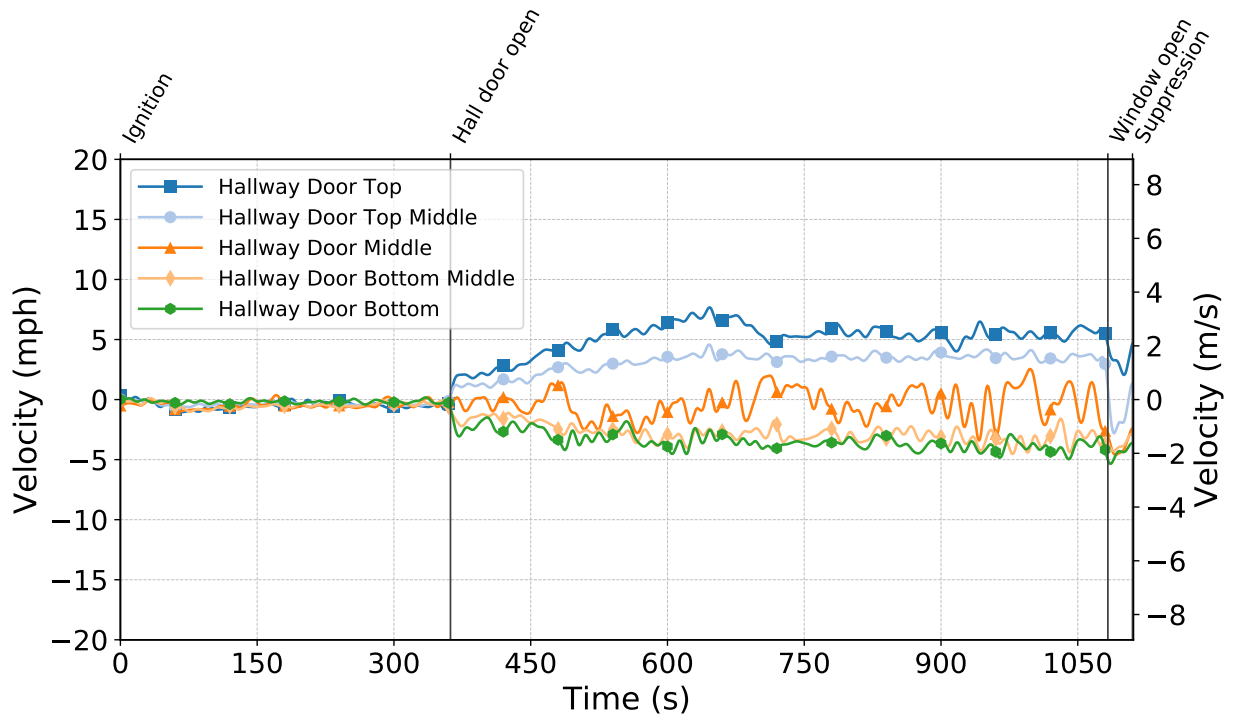


Figure C.23: Gas velocities measured by the hallway door bdps during Test 2.

Test 3

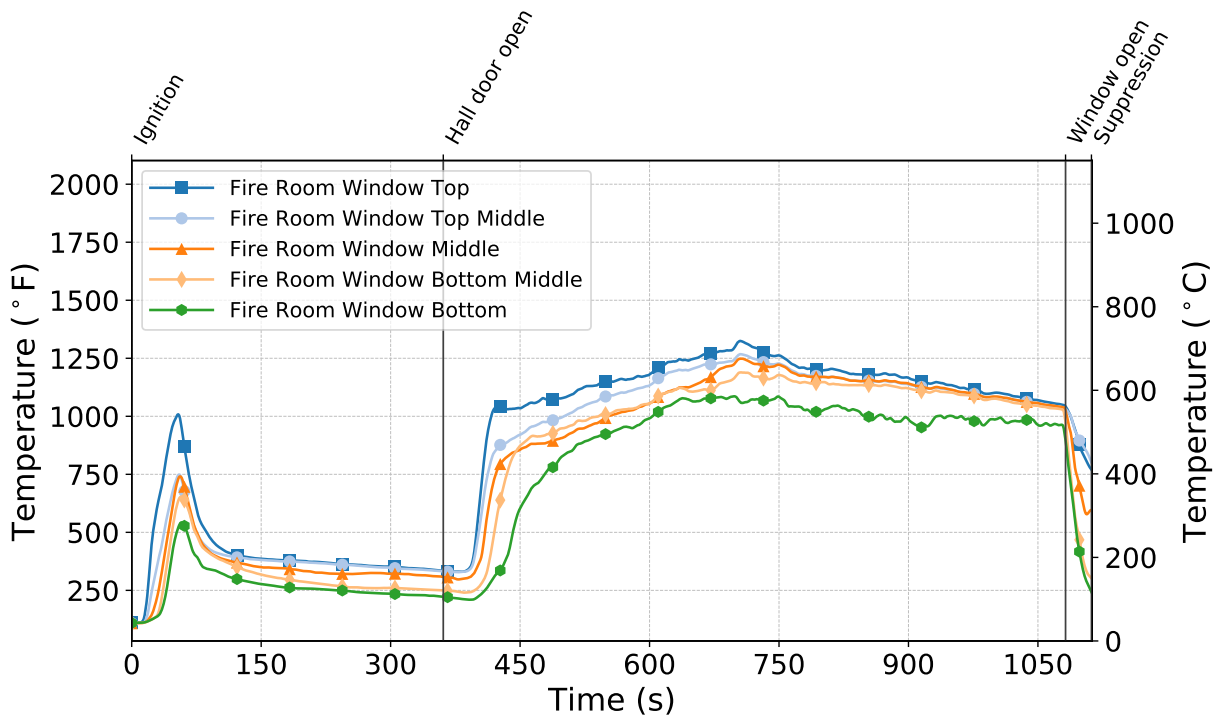


Figure C.24: Temperatures measured by the fire room window thermocouples during Test 3.

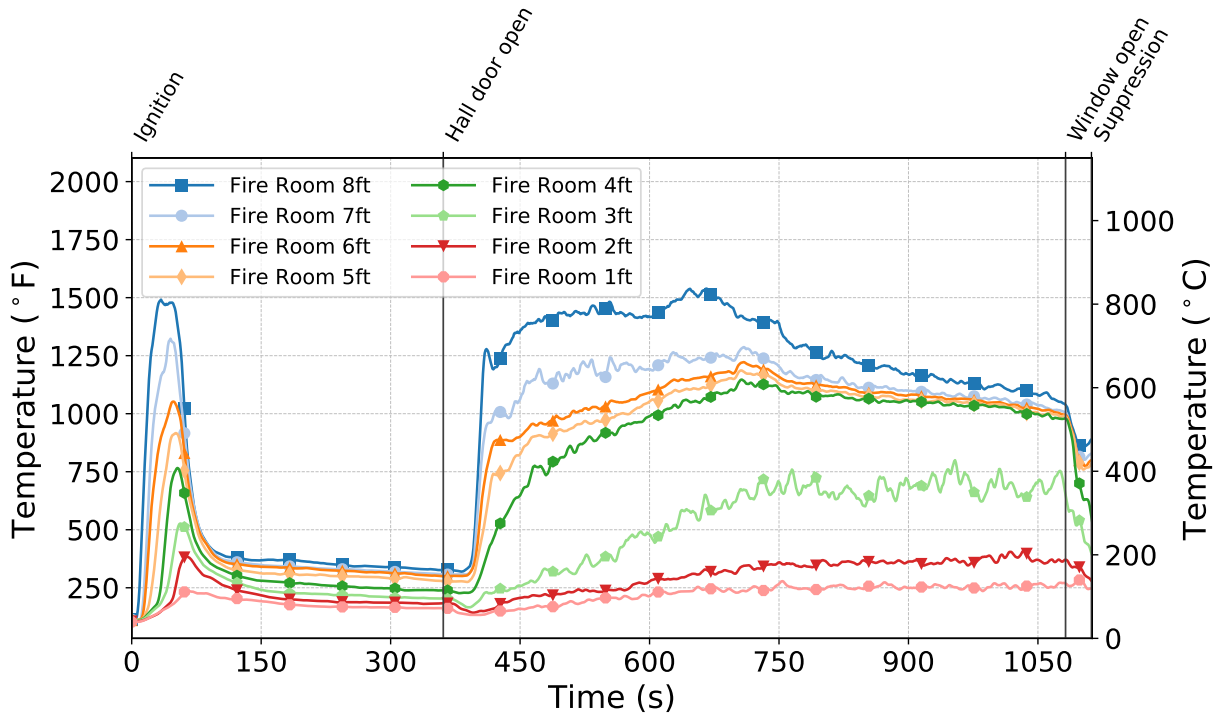


Figure C.25: Temperatures measured by the fire room thermocouples during Test 3.

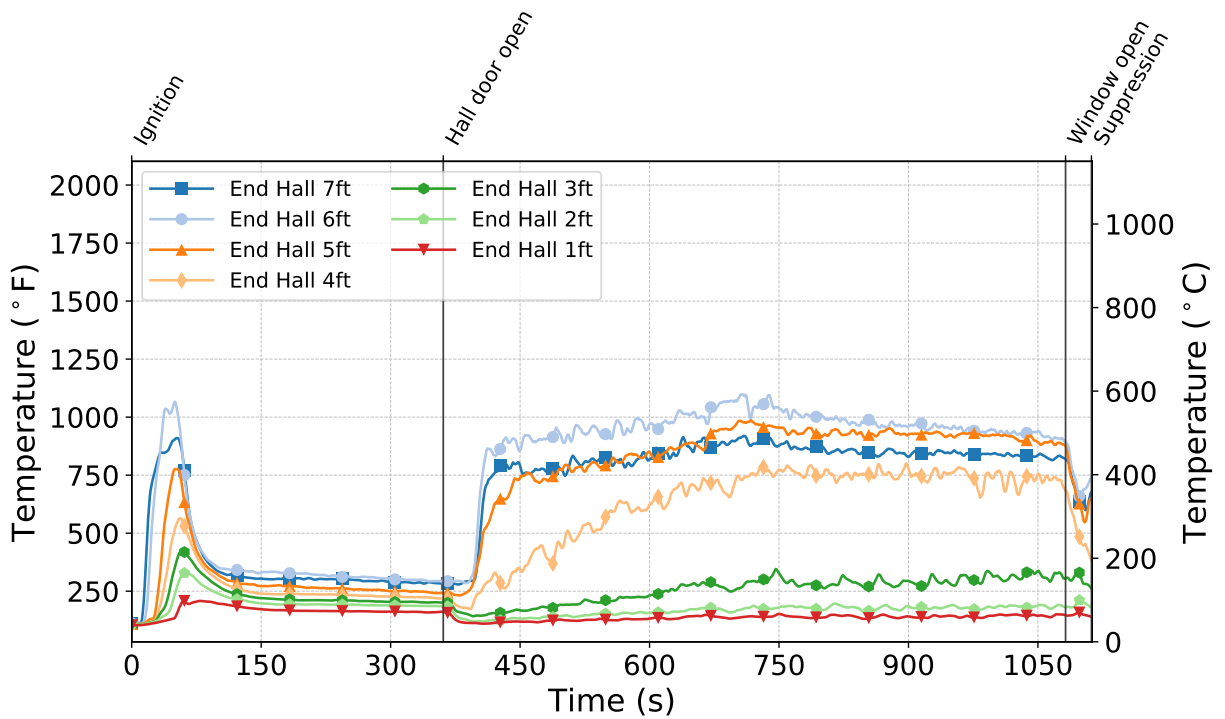


Figure C.26: Temperatures measured by the end hall thermocouples during Test 3.

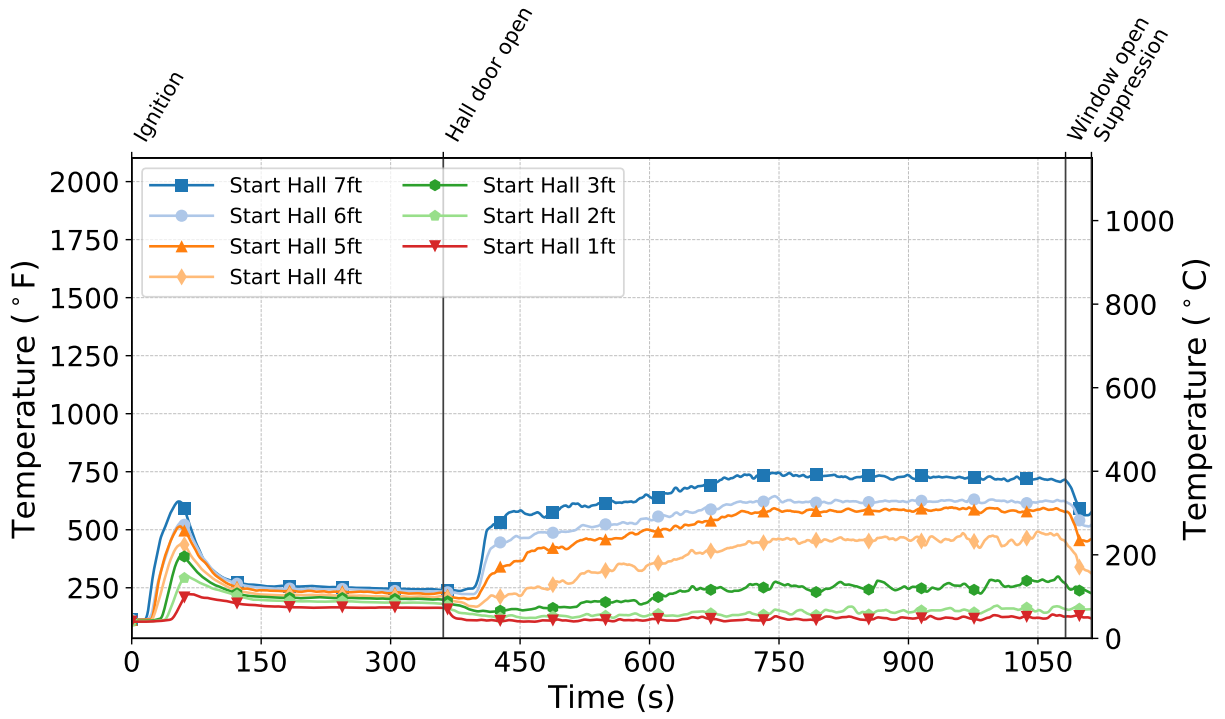


Figure C.27: Temperatures measured by the start hall thermocouples during Test 3.

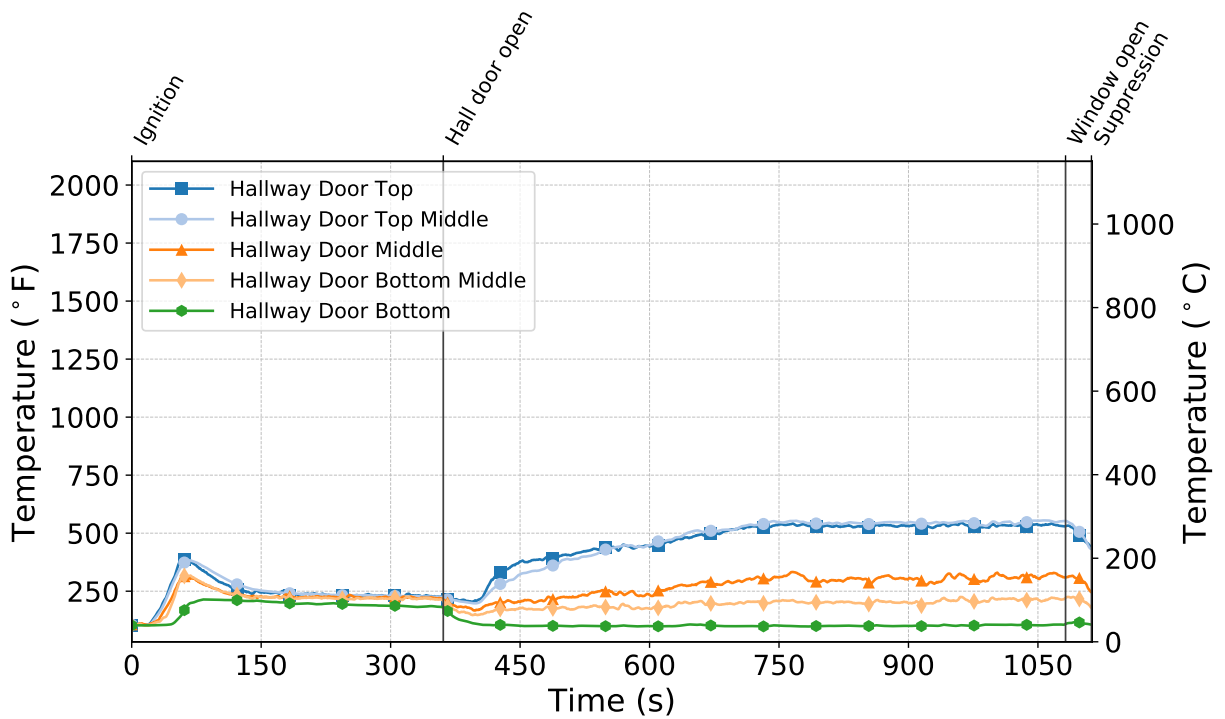


Figure C.28: Temperatures measured by the hallway door thermocouples during Test 3.

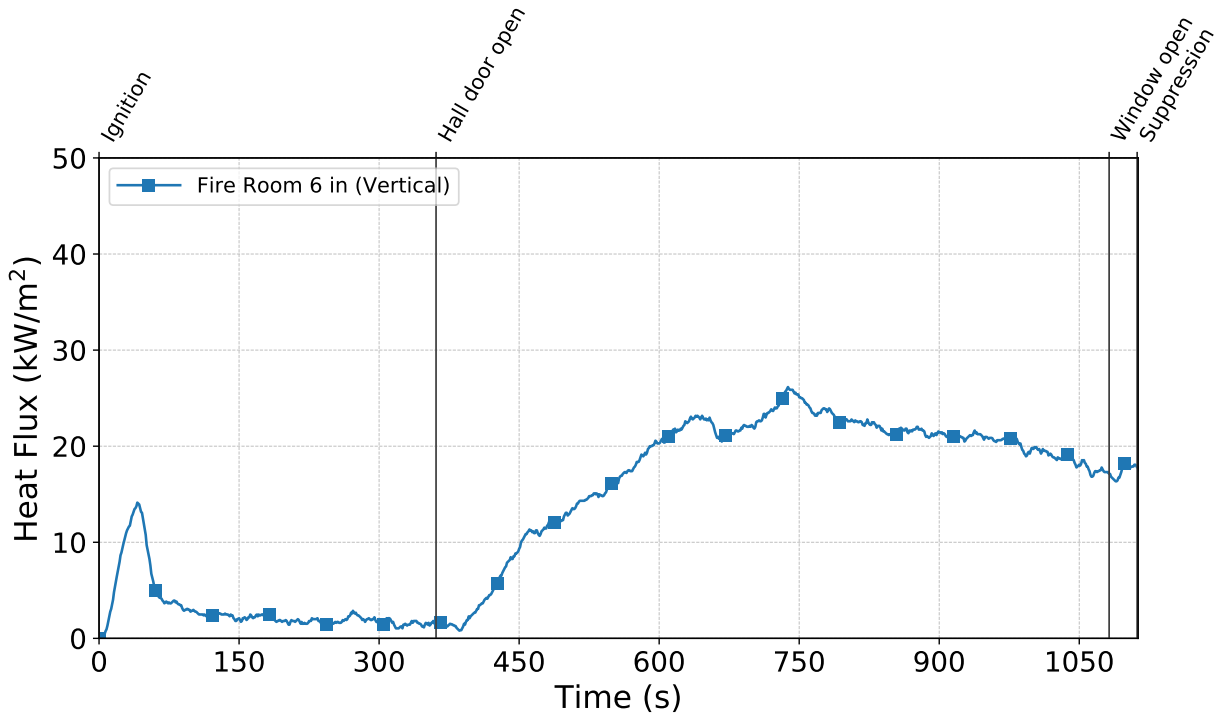


Figure C.29: Heat flux measured by the fire room gauge during Test 3.

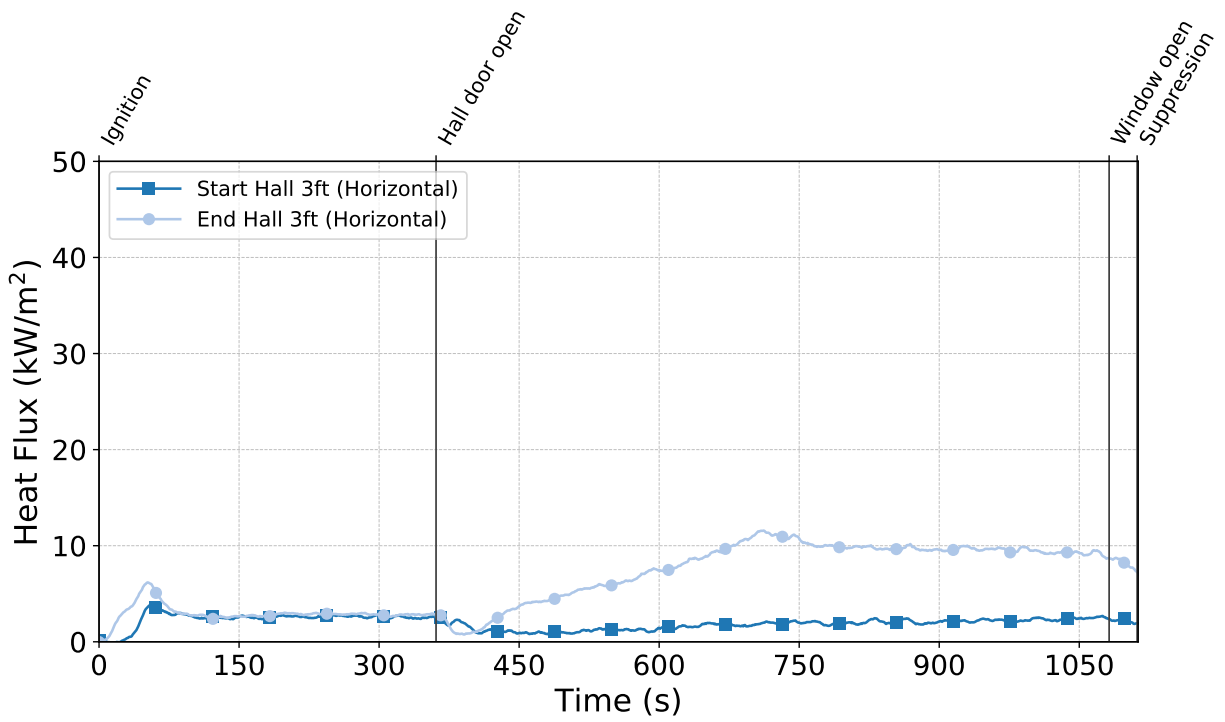


Figure C.30: Heat flux measured by the hallway gauges during Test 3.

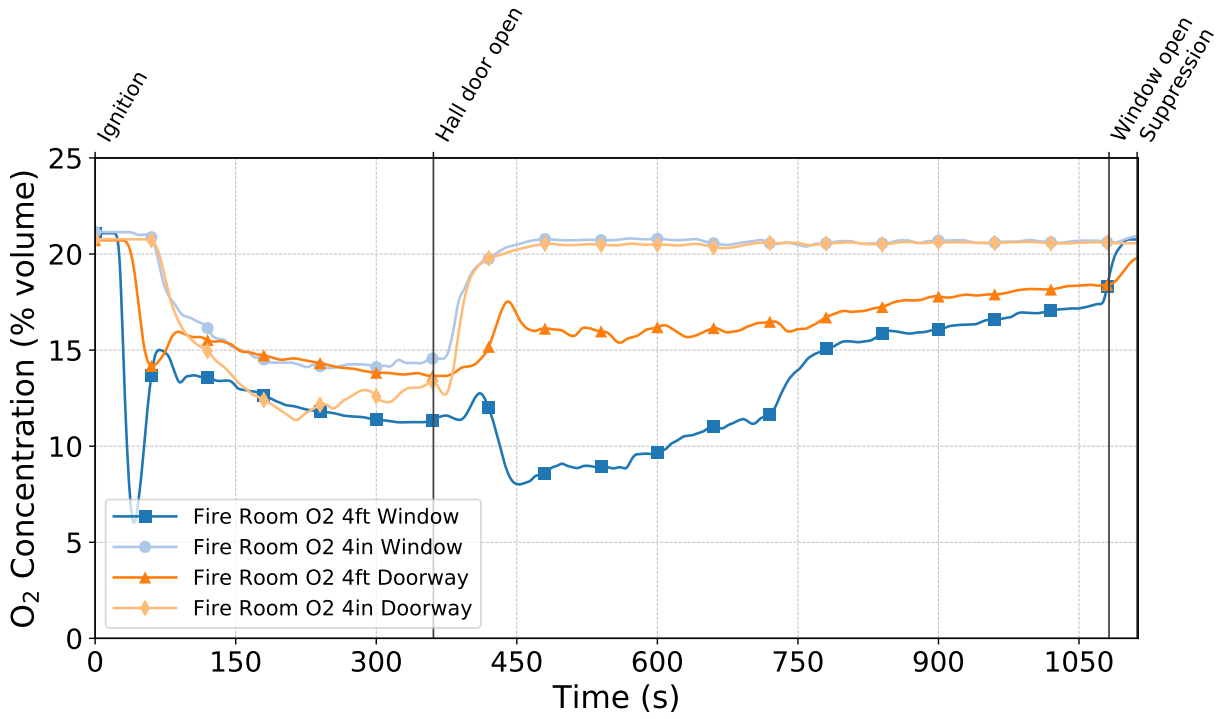


Figure C.31: Oxygen concentrations measured by the fire room gas sampling probes during Test 3.

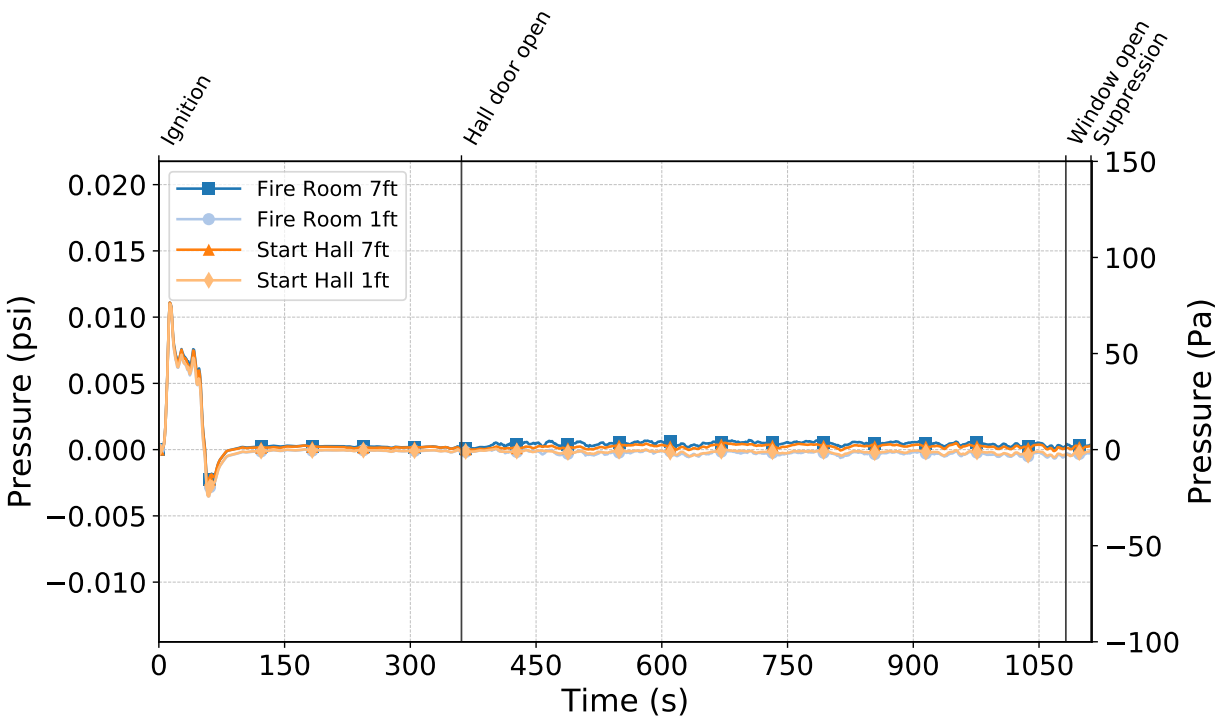


Figure C.32: Pressures measured by the fire room and hallway probes during Test 3.

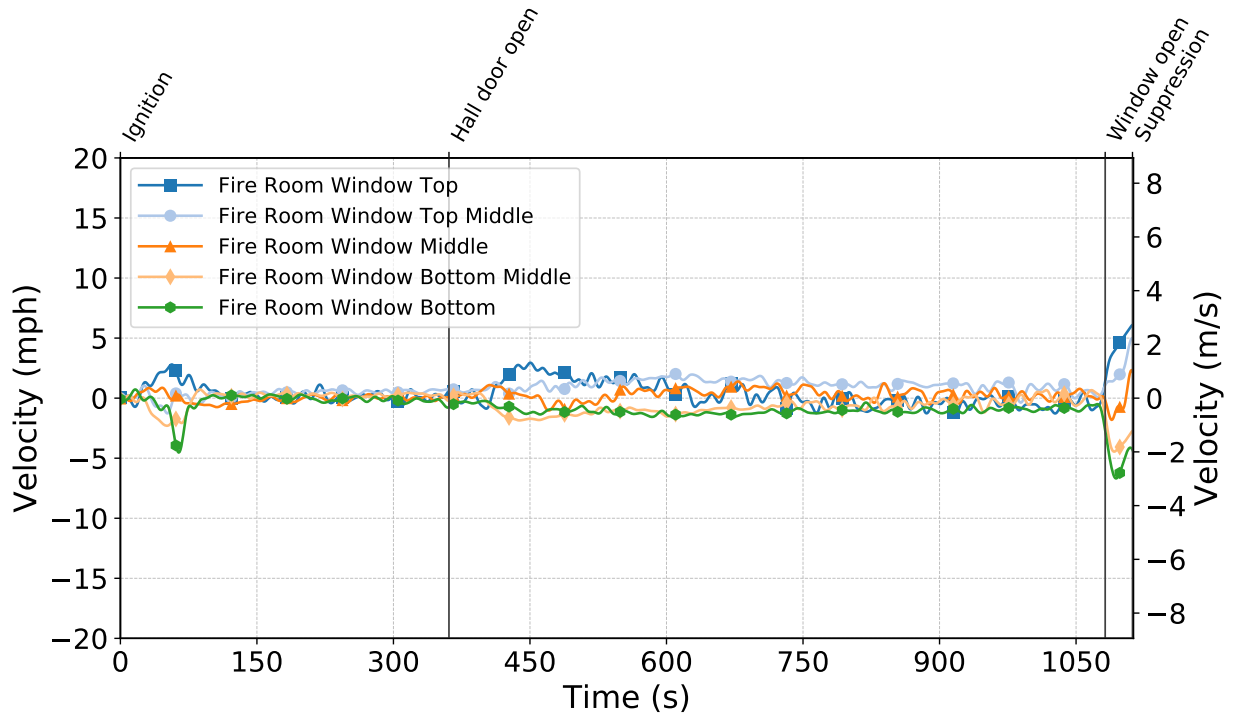


Figure C.33: Gas velocities measured by the fire room window bdps during Test 3.

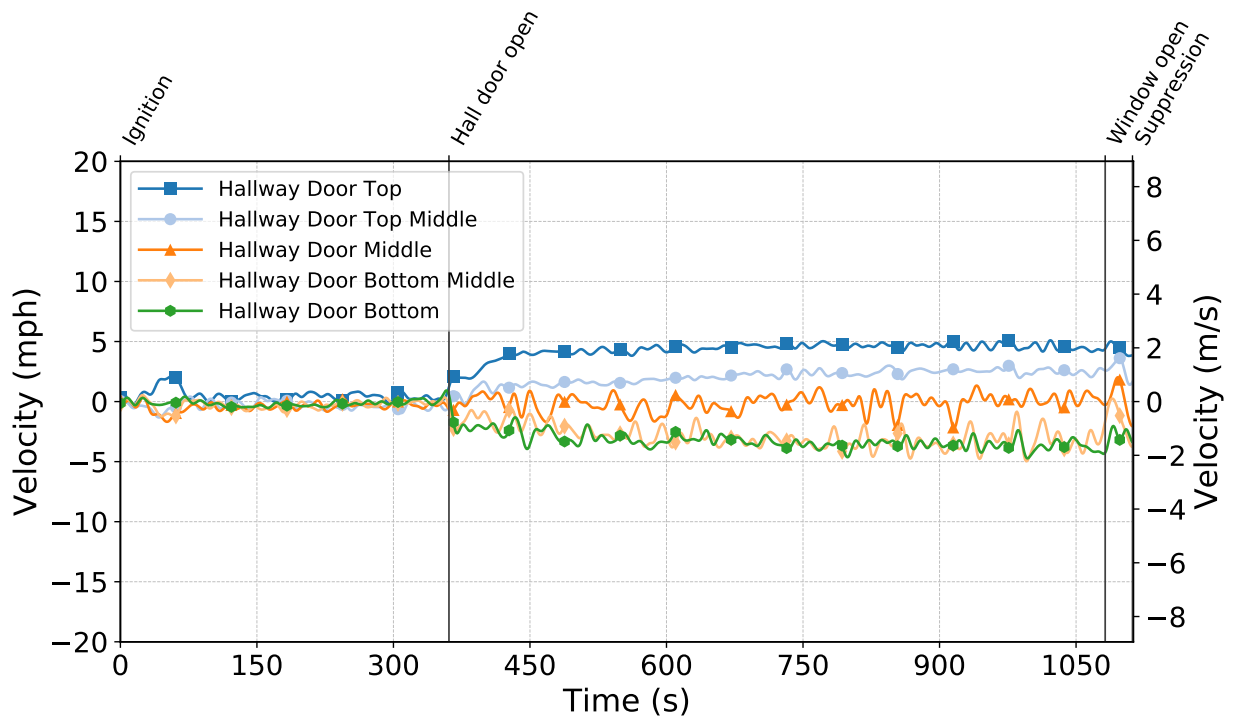


Figure C.34: Gas velocities measured by the hallway door bdps during Test 3.

Test 4

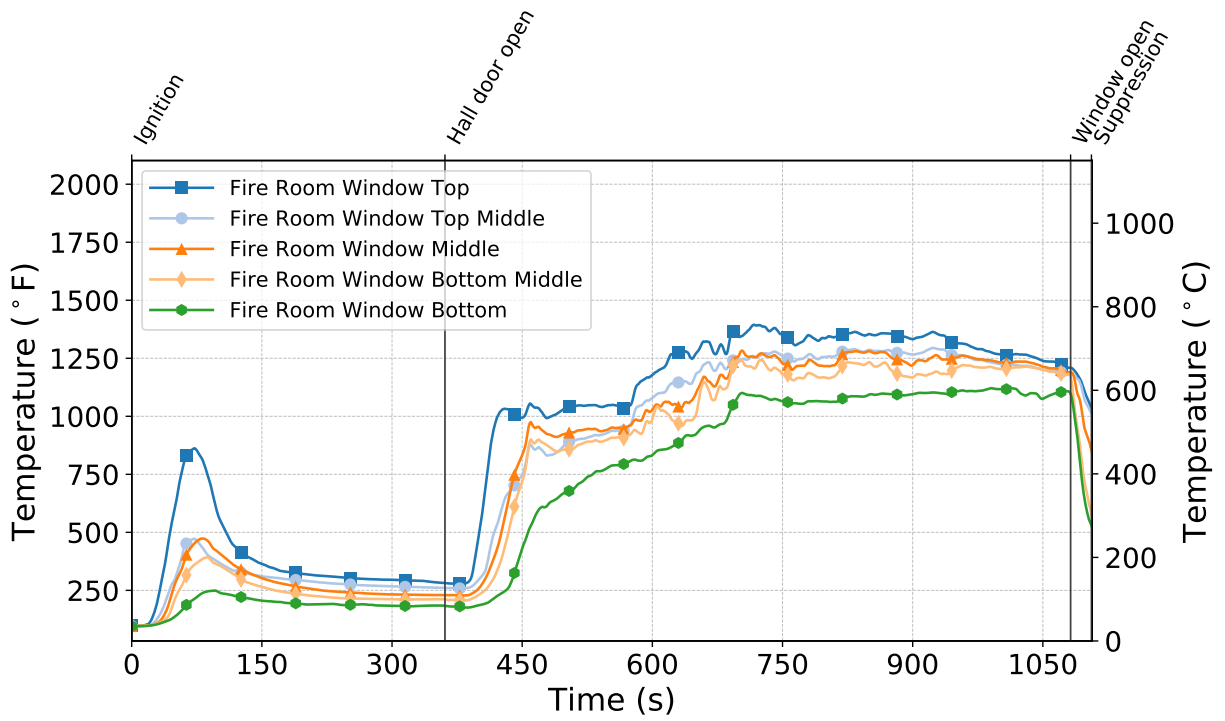


Figure C.35: Temperatures measured by the fire room window thermocouples during Test 4.

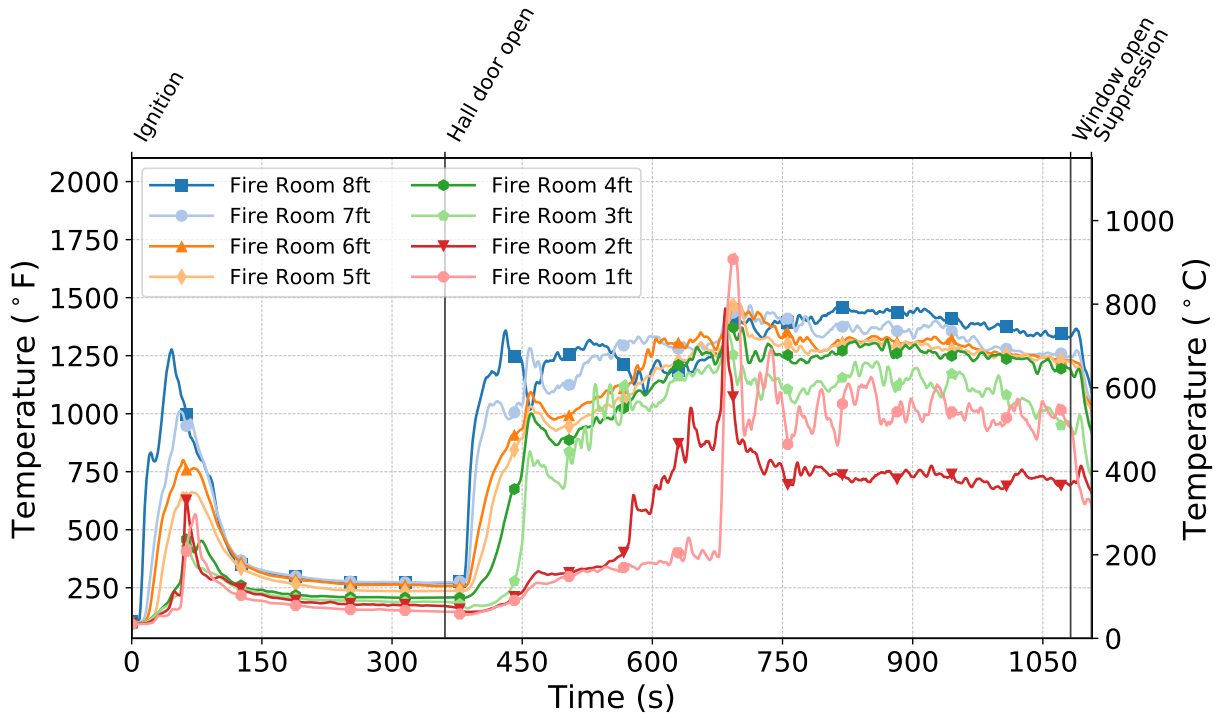


Figure C.36: Temperatures measured by the fire room thermocouples during Test 4.

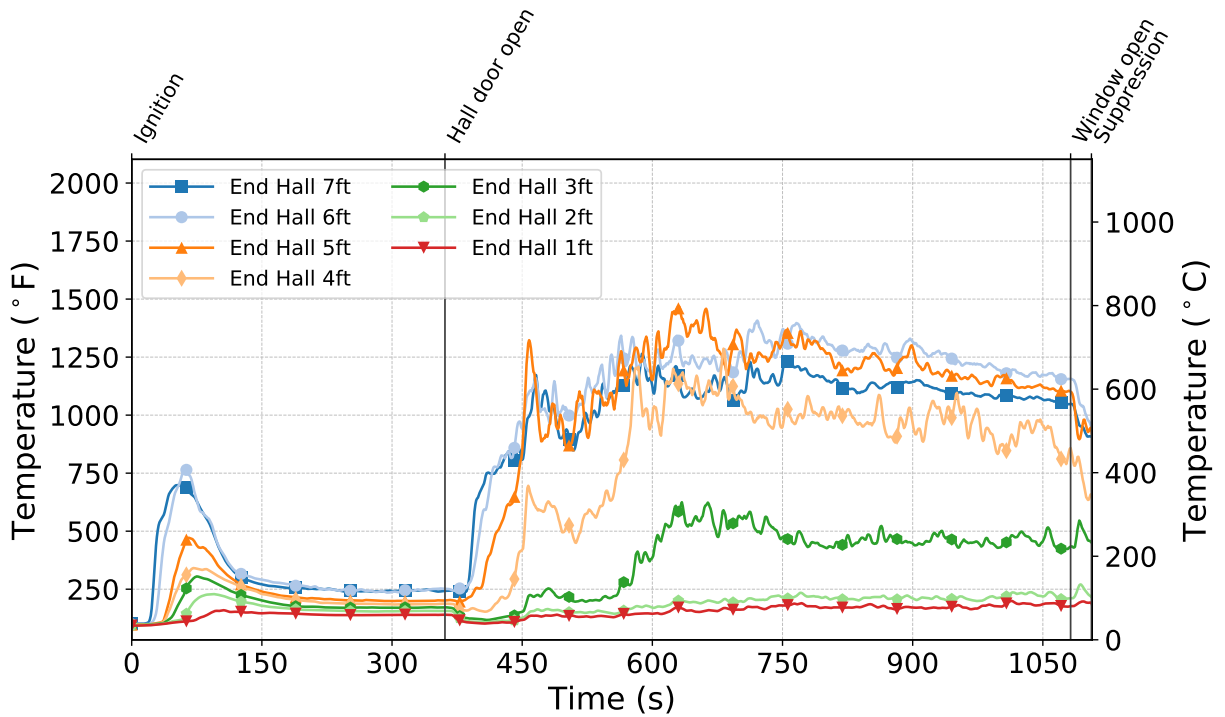


Figure C.37: Temperatures measured by the end hall thermocouples during Test 4.

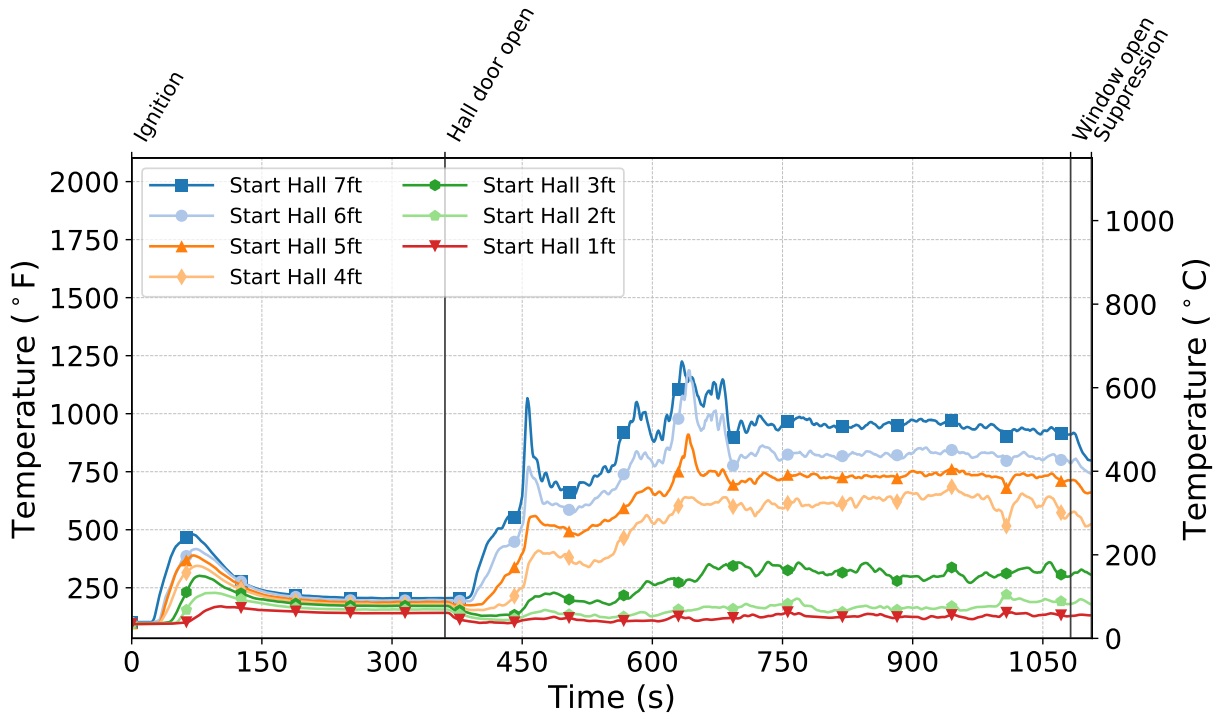


Figure C.38: Temperatures measured by the start hall thermocouples during Test 4.

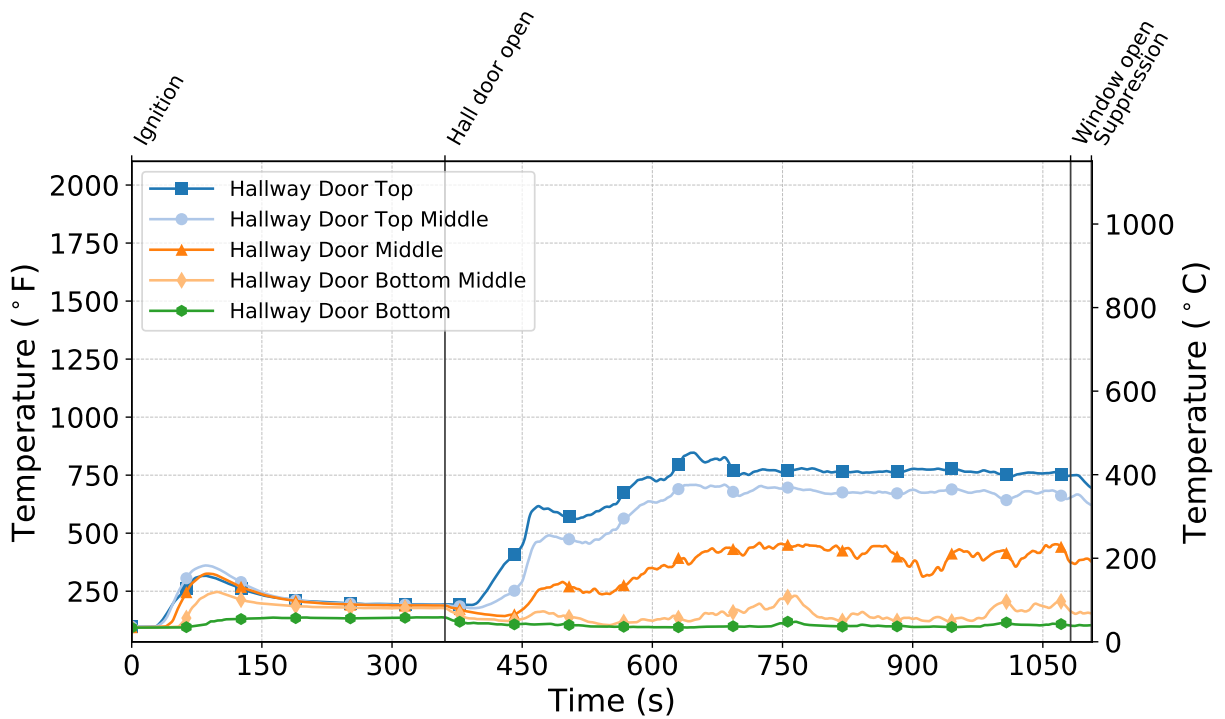


Figure C.39: Temperatures measured by the hallway door thermocouples during Test 4.

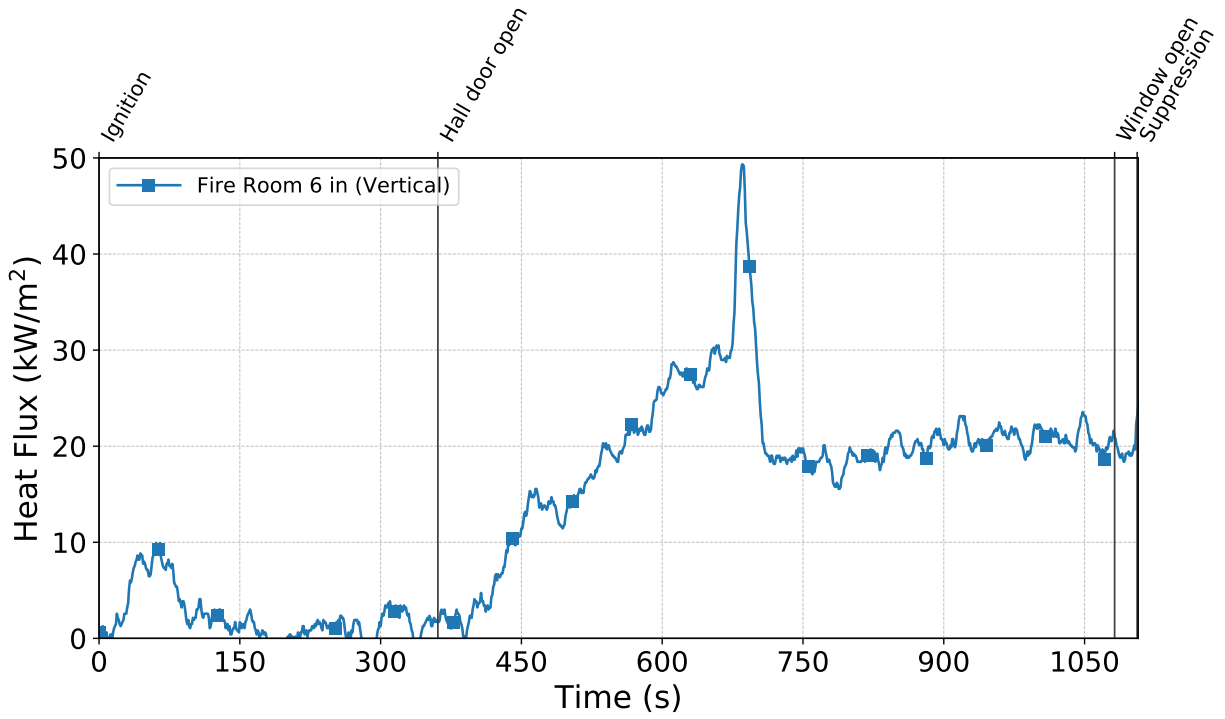


Figure C.40: Heat flux measured by the fire room gauge during Test 4.

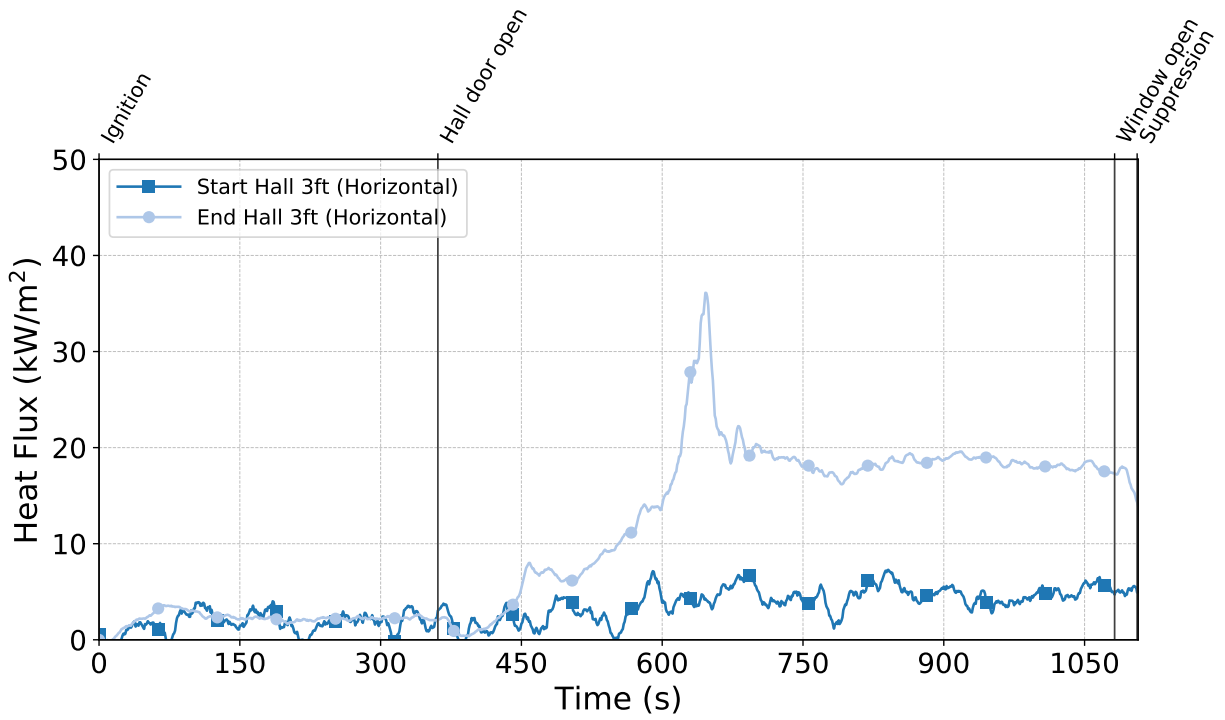


Figure C.41: Heat flux measured by the hallway gauges during Test 4.

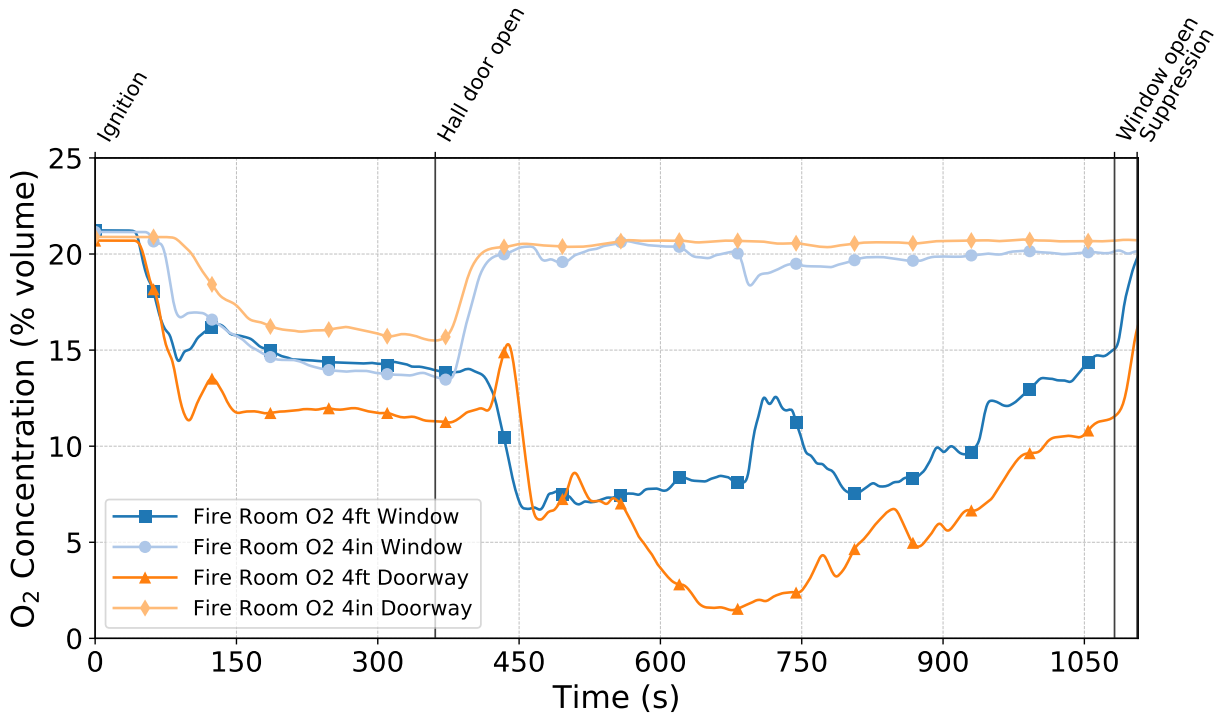


Figure C.42: Oxygen concentrations measured by the fire room gas sampling probes during Test 4.

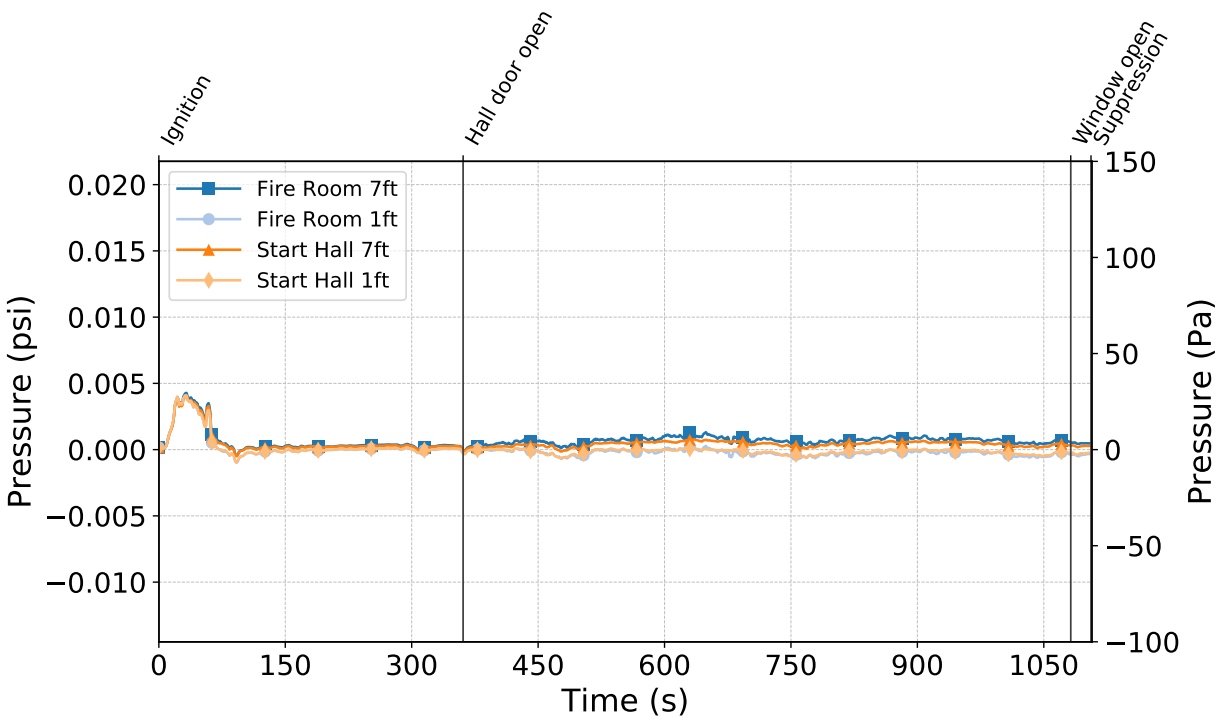


Figure C.43: Pressures measured by the fire room and hallway probes during Test 4.

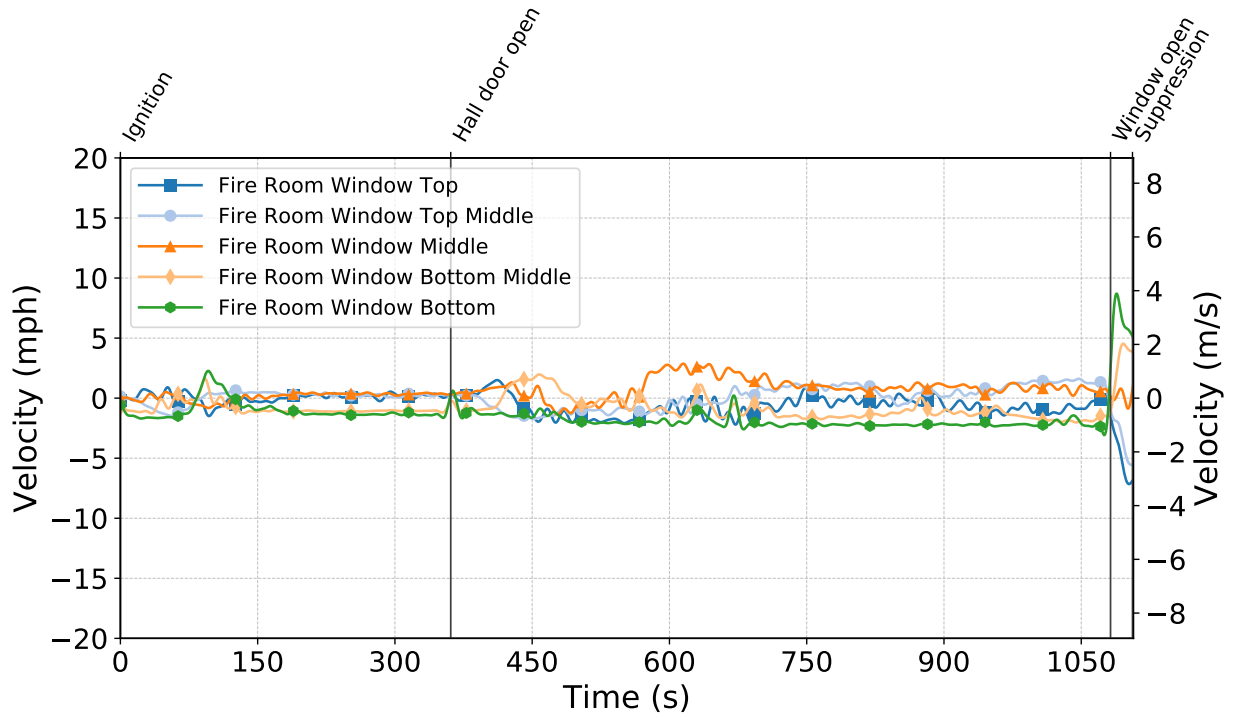


Figure C.44: Gas velocities measured by the fire room window bdps during Test 4.

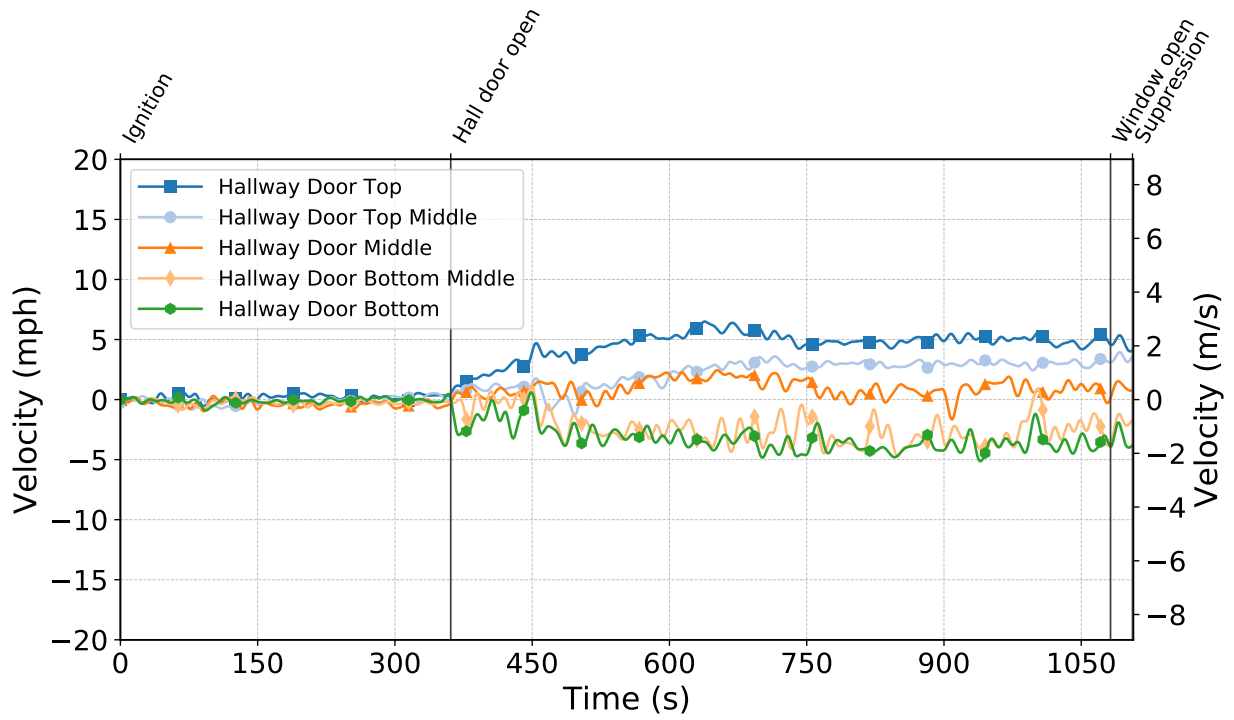


Figure C.45: Gas velocities measured by the hallway door bdps during Test 4.

C.2 Prop & Fuel Comparison Experiments

Test 5

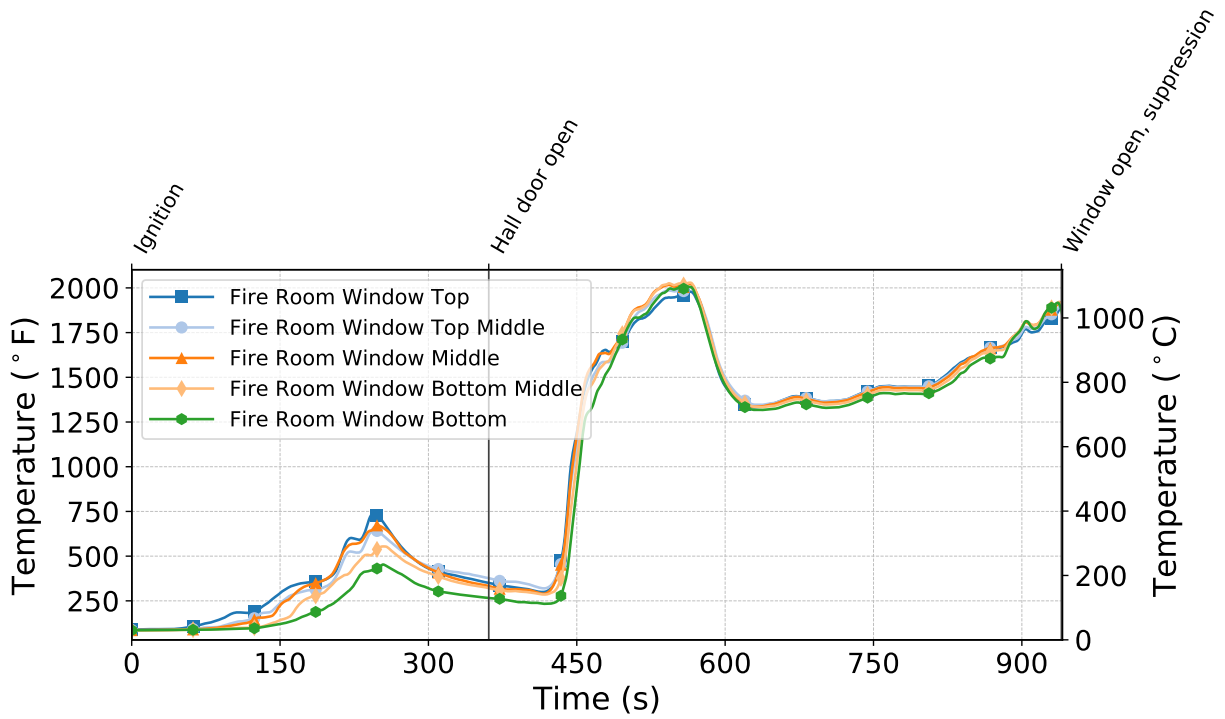


Figure C.46: Temperatures measured by the fire room window thermocouples during Test 5.

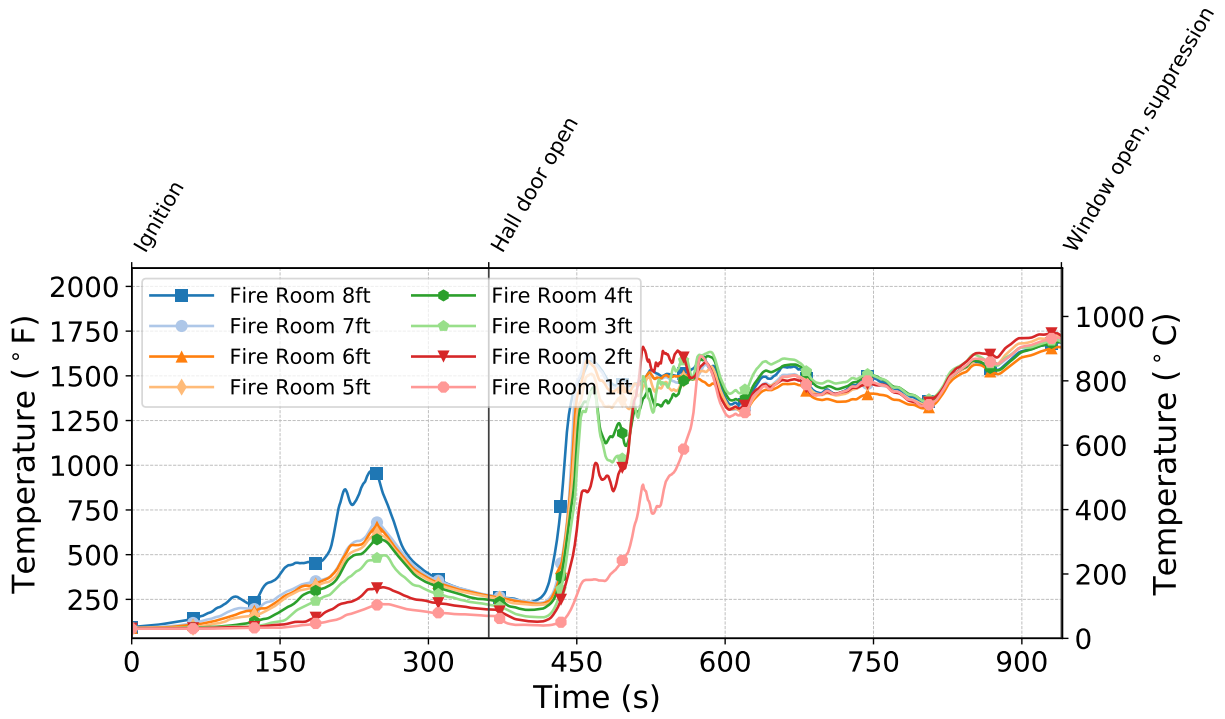


Figure C.47: Temperatures measured by the fire room thermocouples during Test 5.

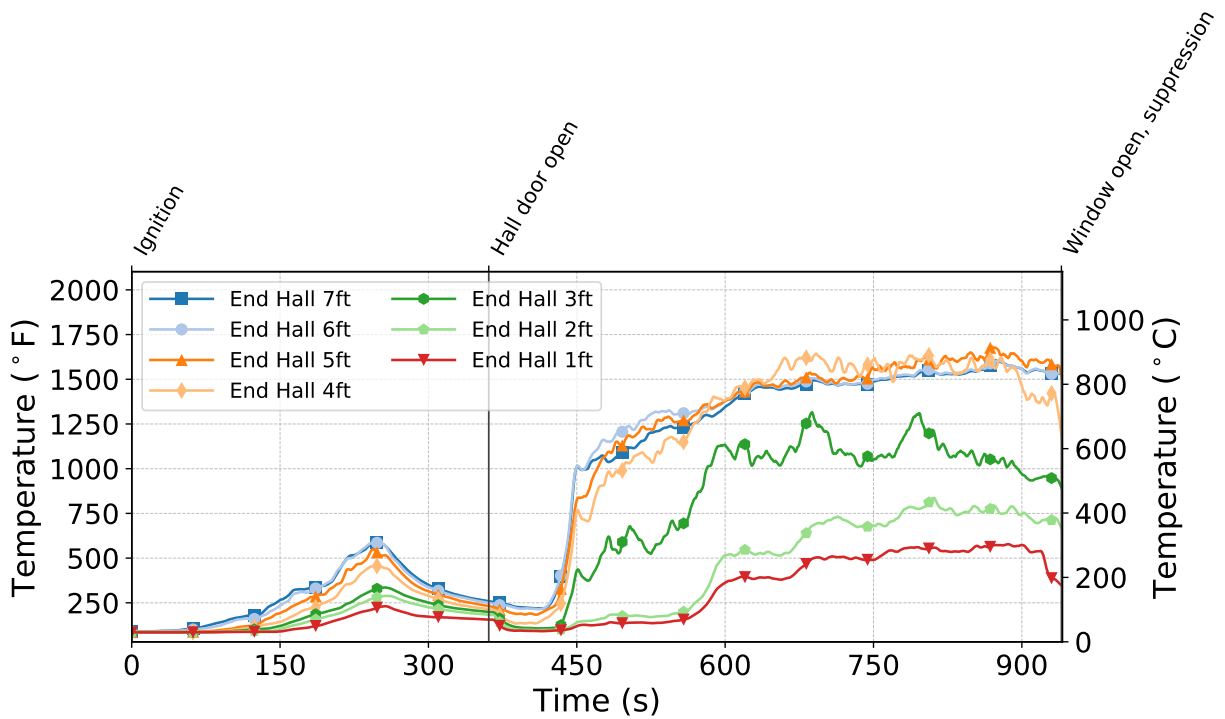


Figure C.48: Temperatures measured by the end hall thermocouples during Test 5.

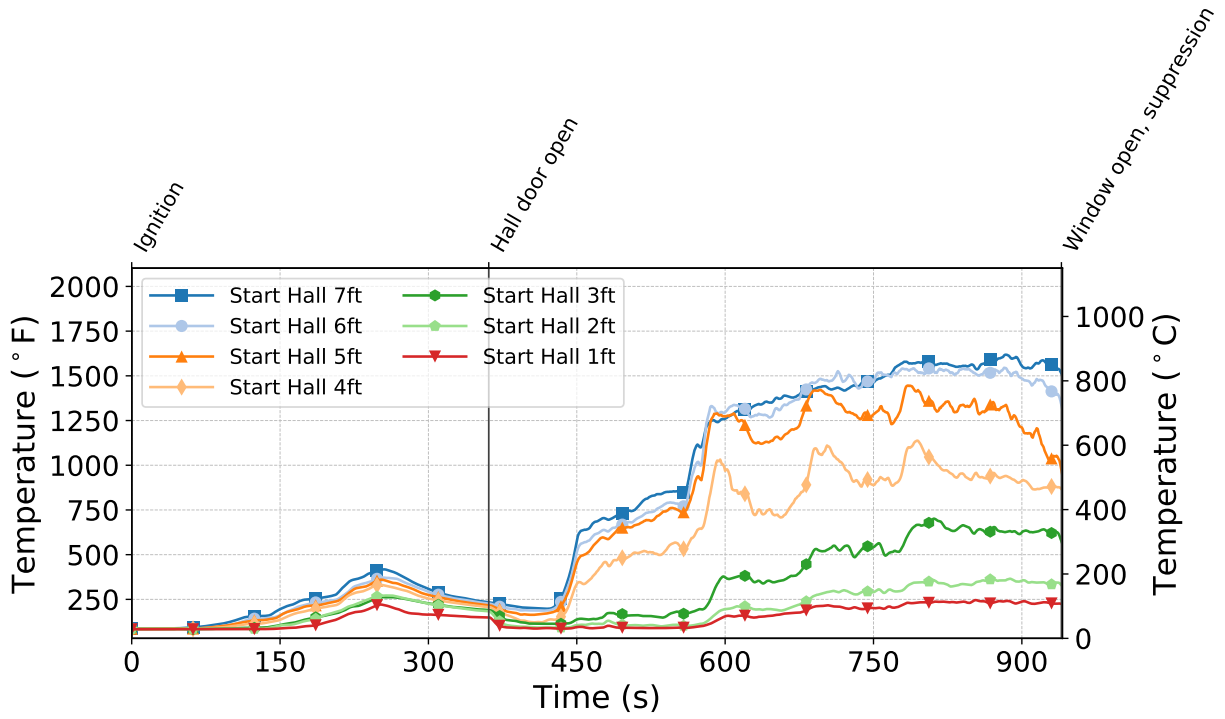


Figure C.49: Temperatures measured by the start hall thermocouples during Test 5.

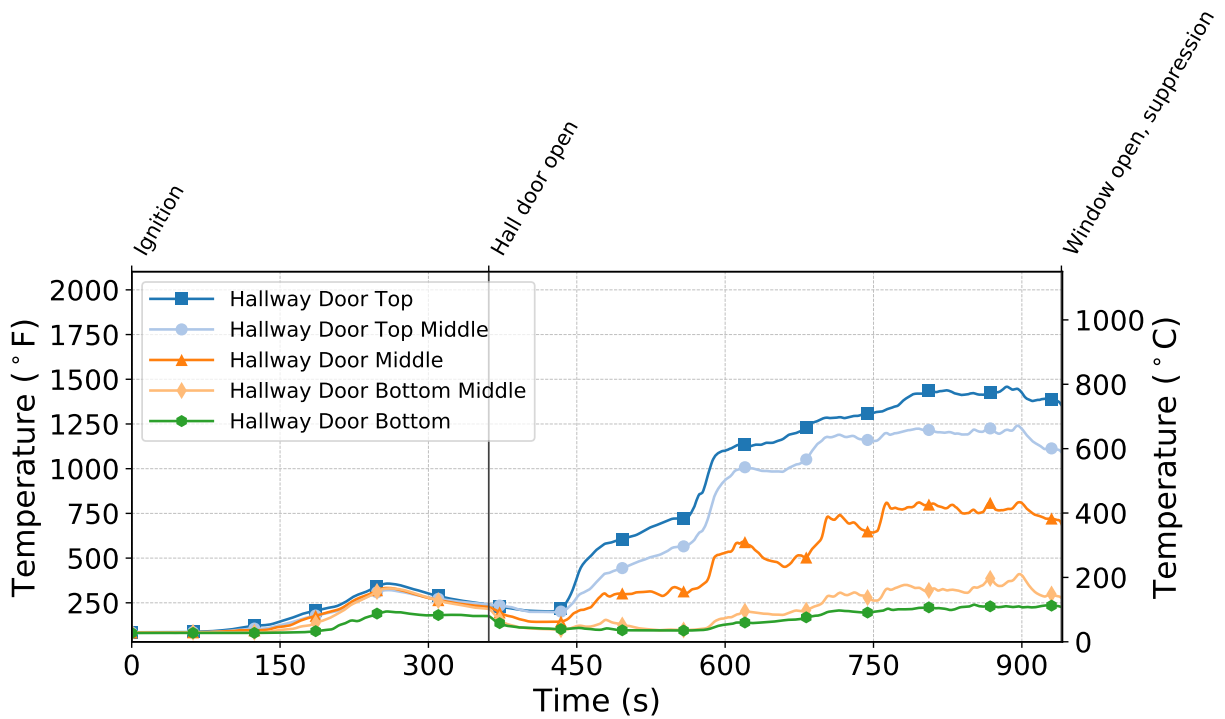


Figure C.50: Temperatures measured by the hallway door thermocouples during Test 5.

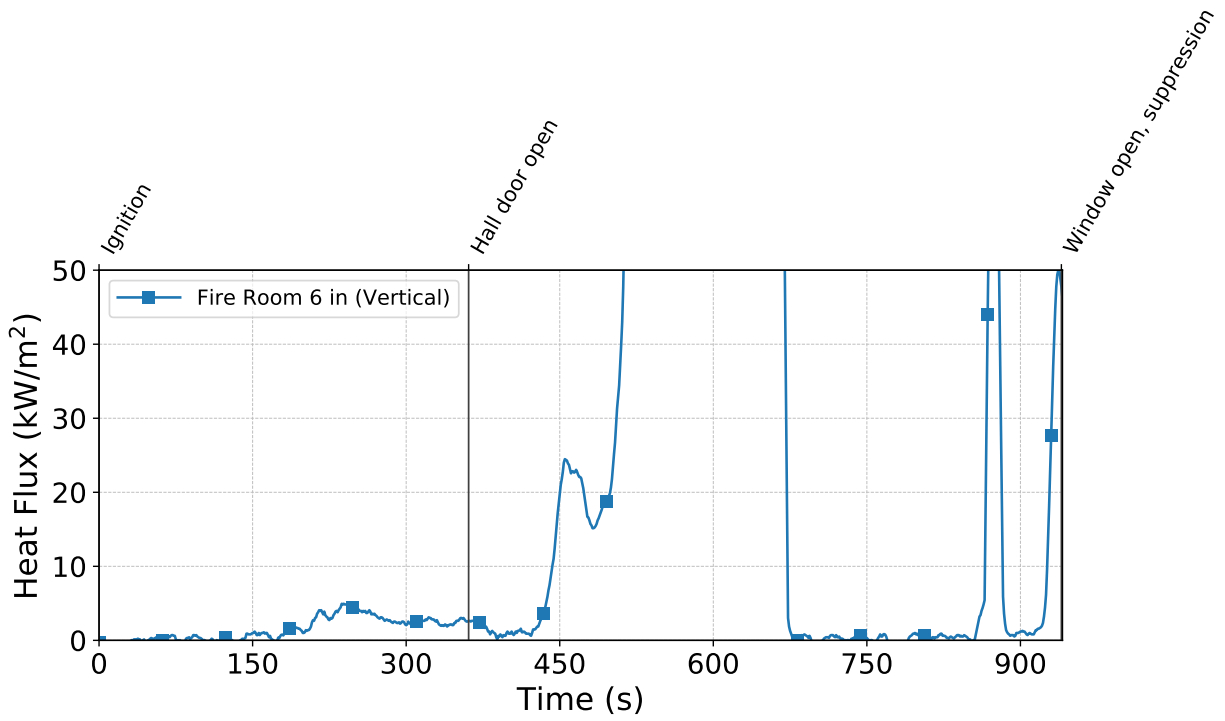


Figure C.51: Heat flux measured by the fire room gauge during Test 5.

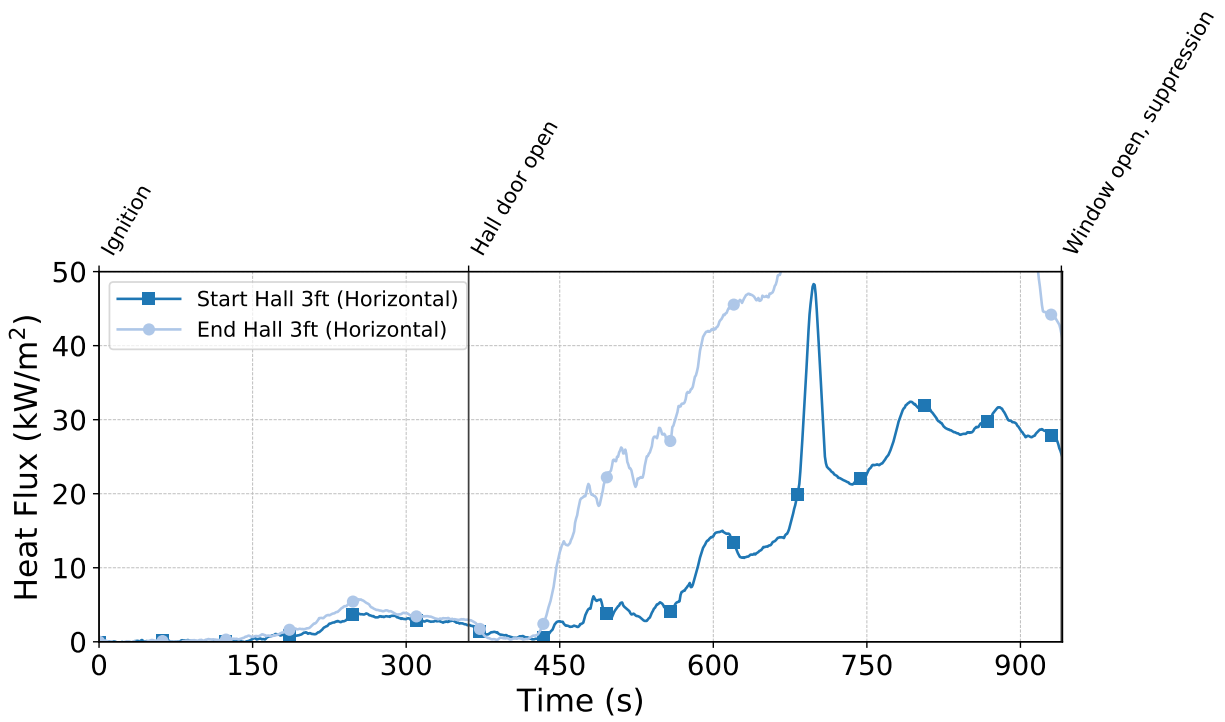


Figure C.52: Heat flux measured by the hallway gauges during Test 5.

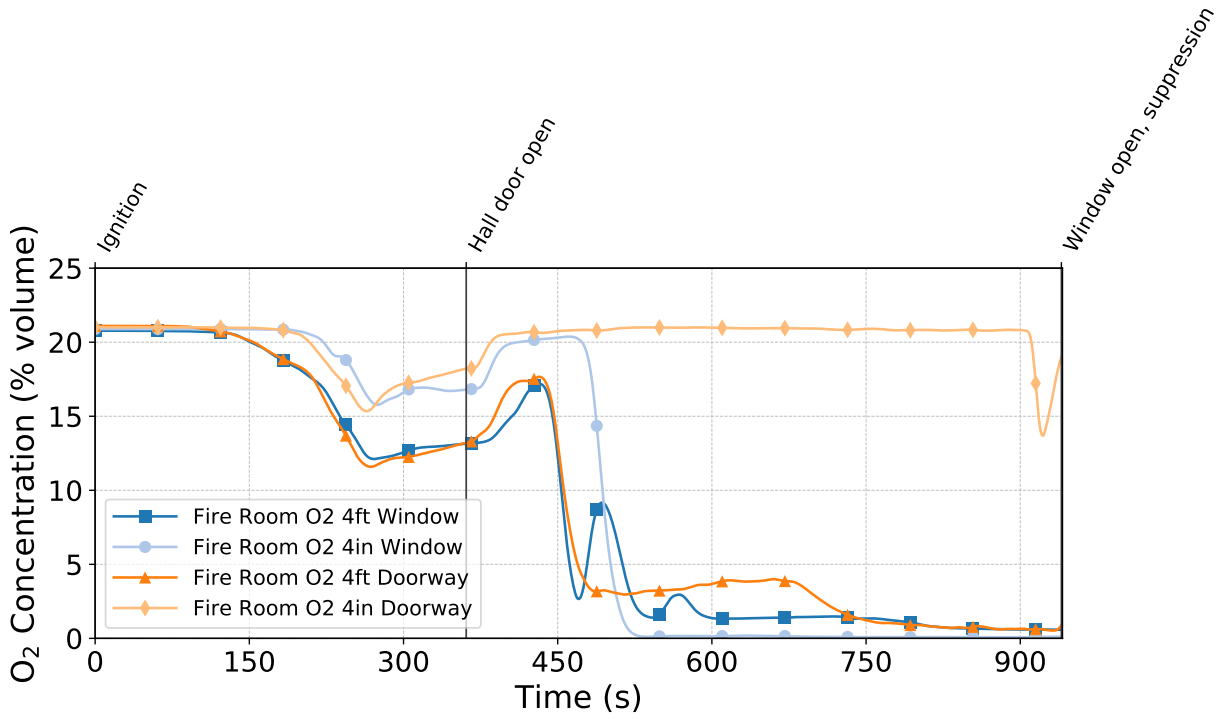


Figure C.53: Oxygen concentrations measured by the fire room gas sampling probes during Test 5.

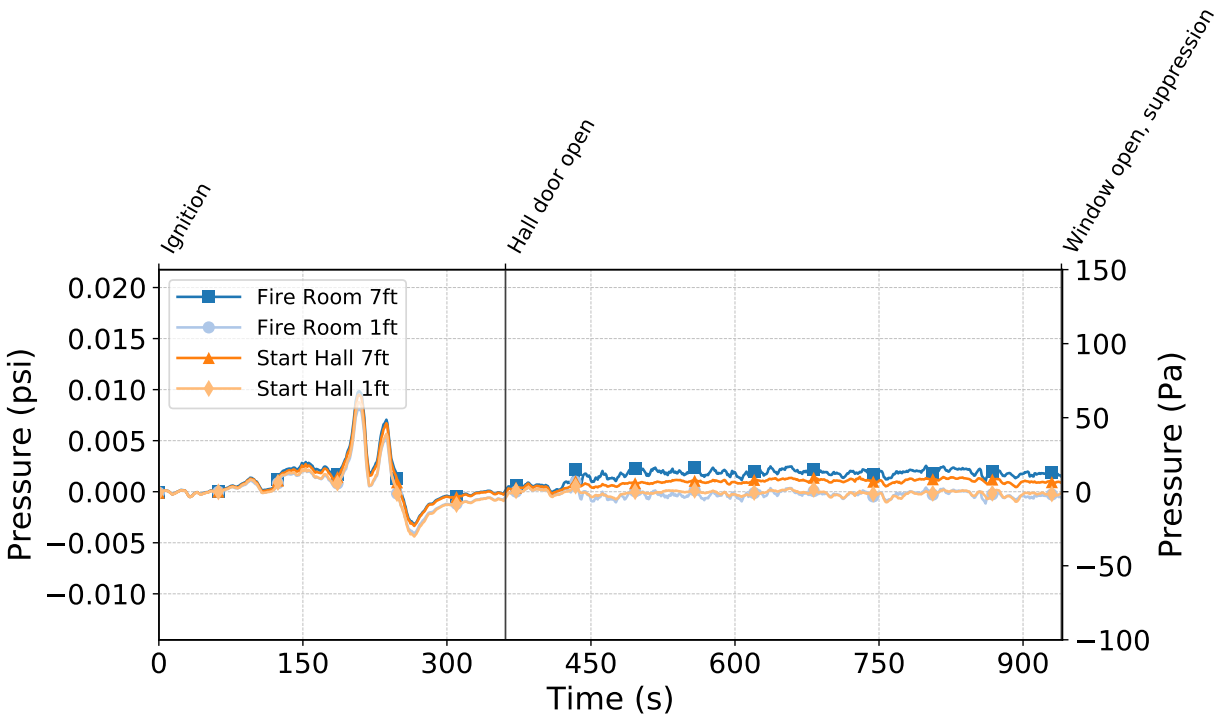


Figure C.54: Pressures measured by the fire room and hallway probes during Test 5.

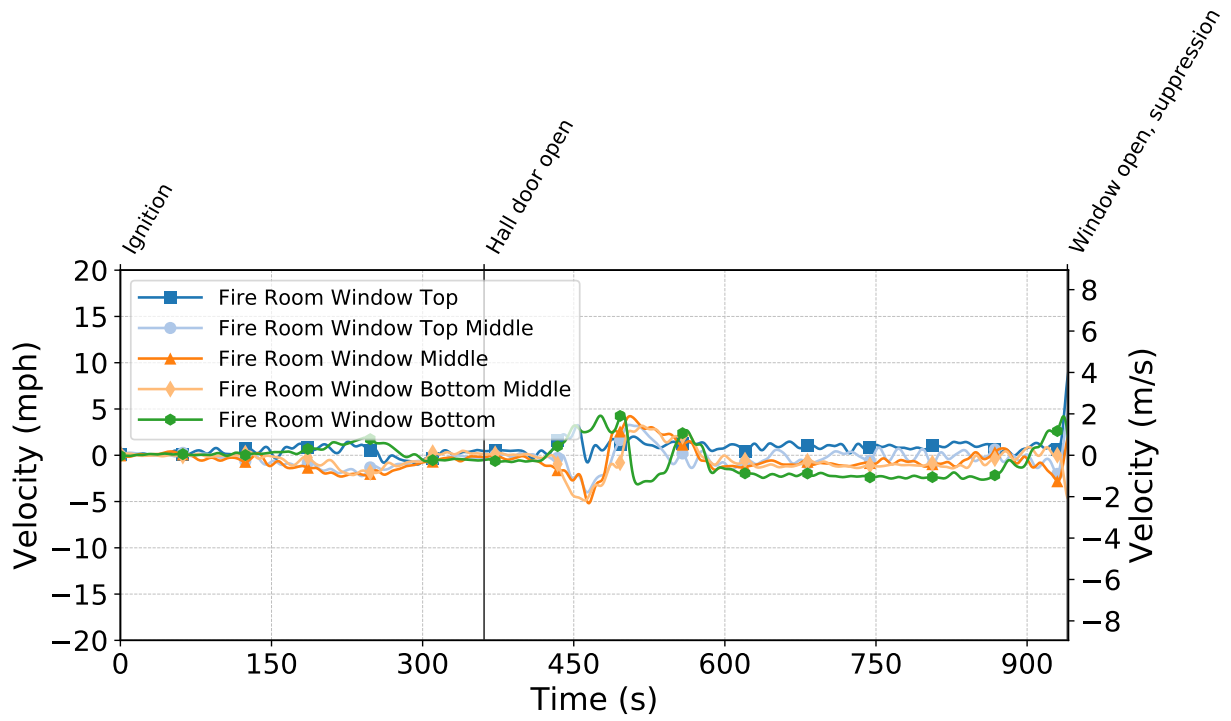


Figure C.55: Gas velocities measured by the fire room window bdps during Test 5.

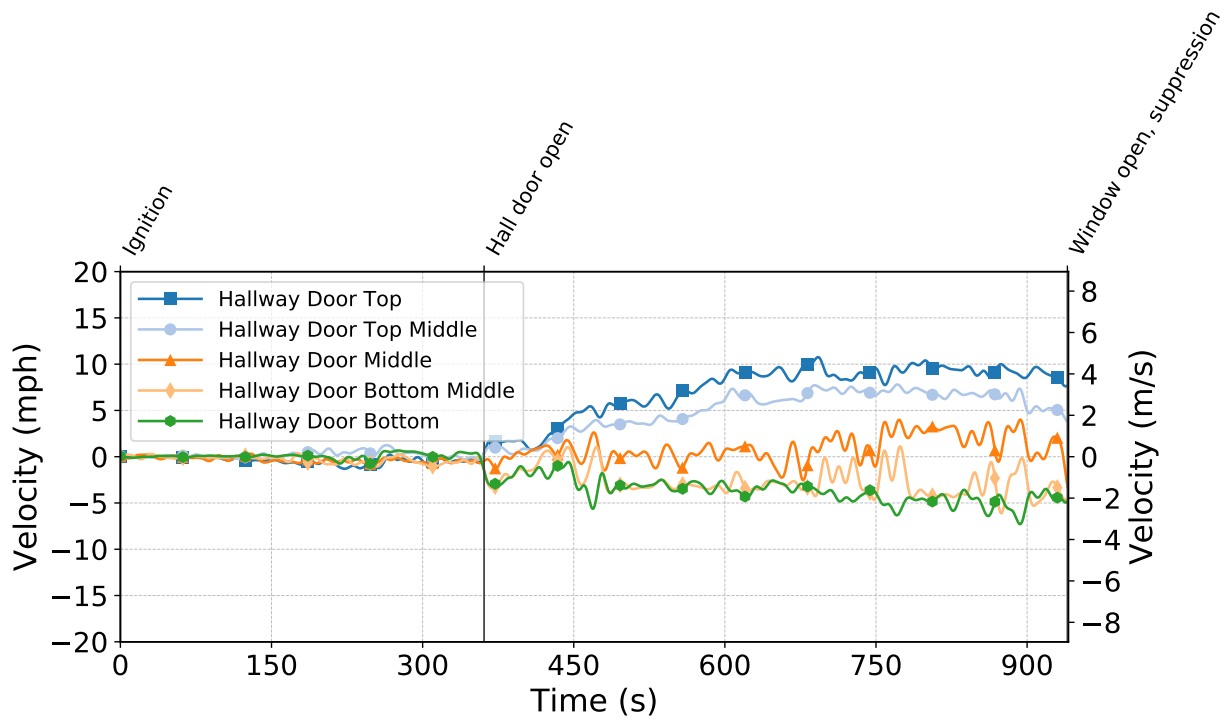


Figure C.56: Gas velocities measured by the hallway door bdps during Test 5.

Test 6

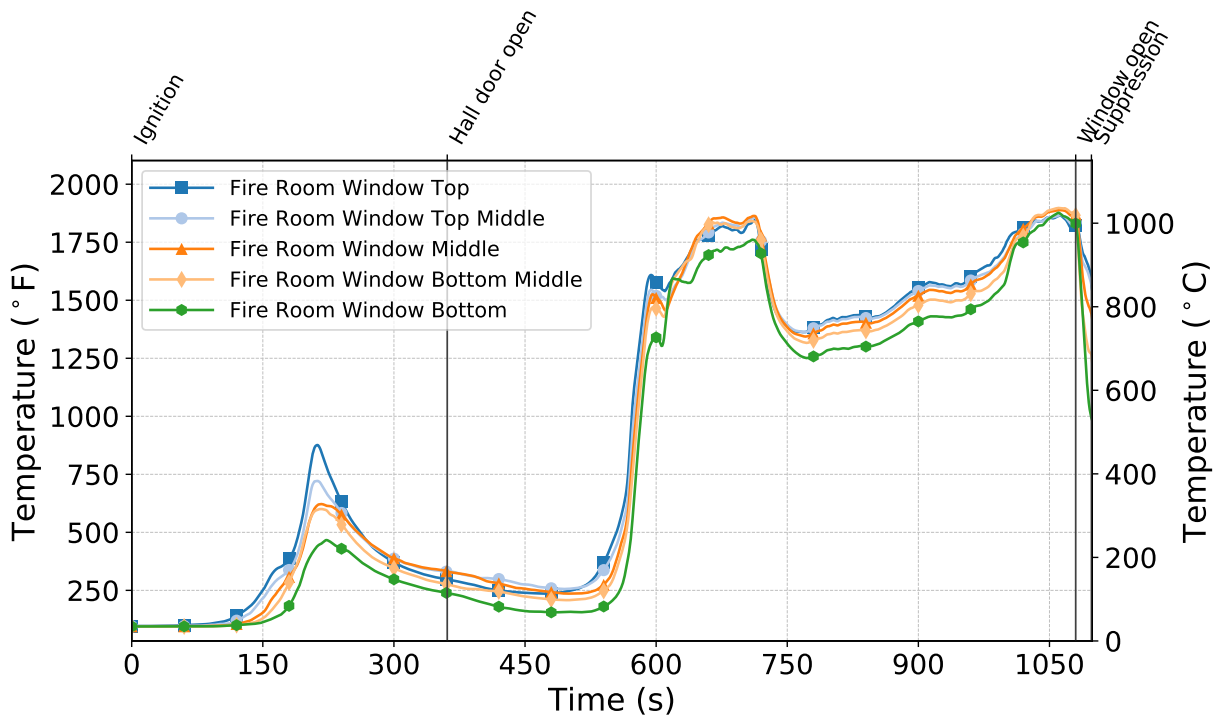


Figure C.57: Temperatures measured by the fire room window thermocouples during Test 6.

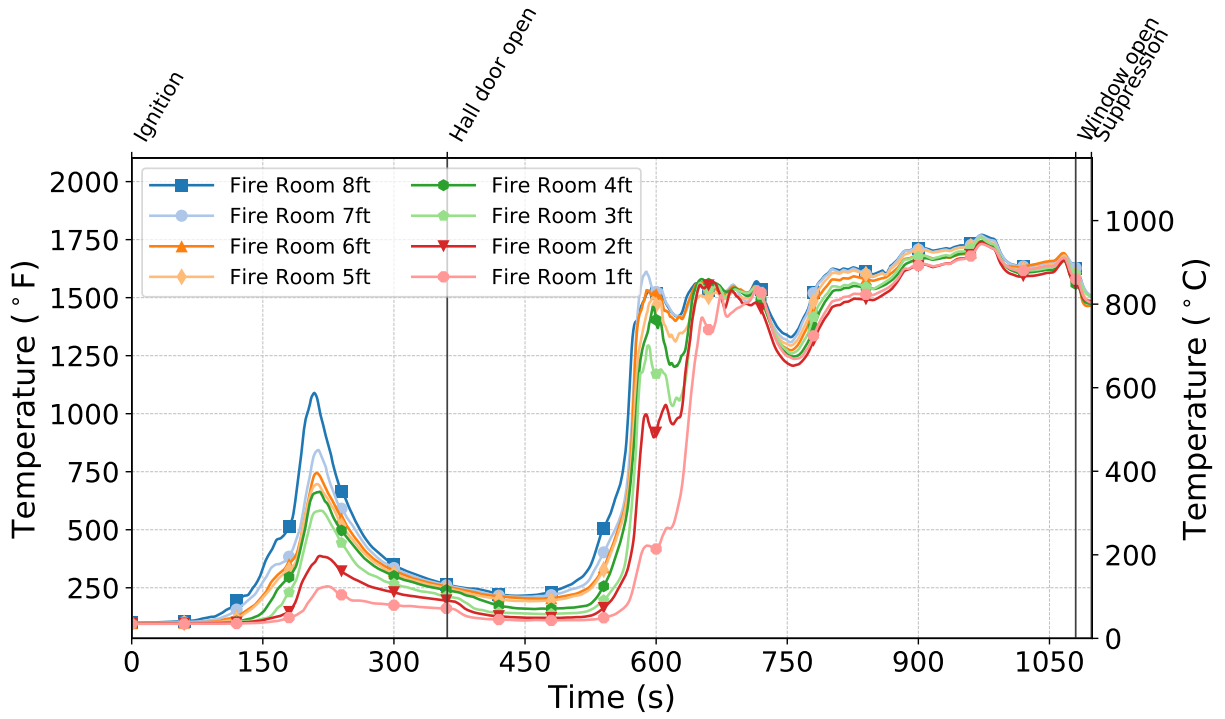


Figure C.58: Temperatures measured by the fire room thermocouples during Test 6.

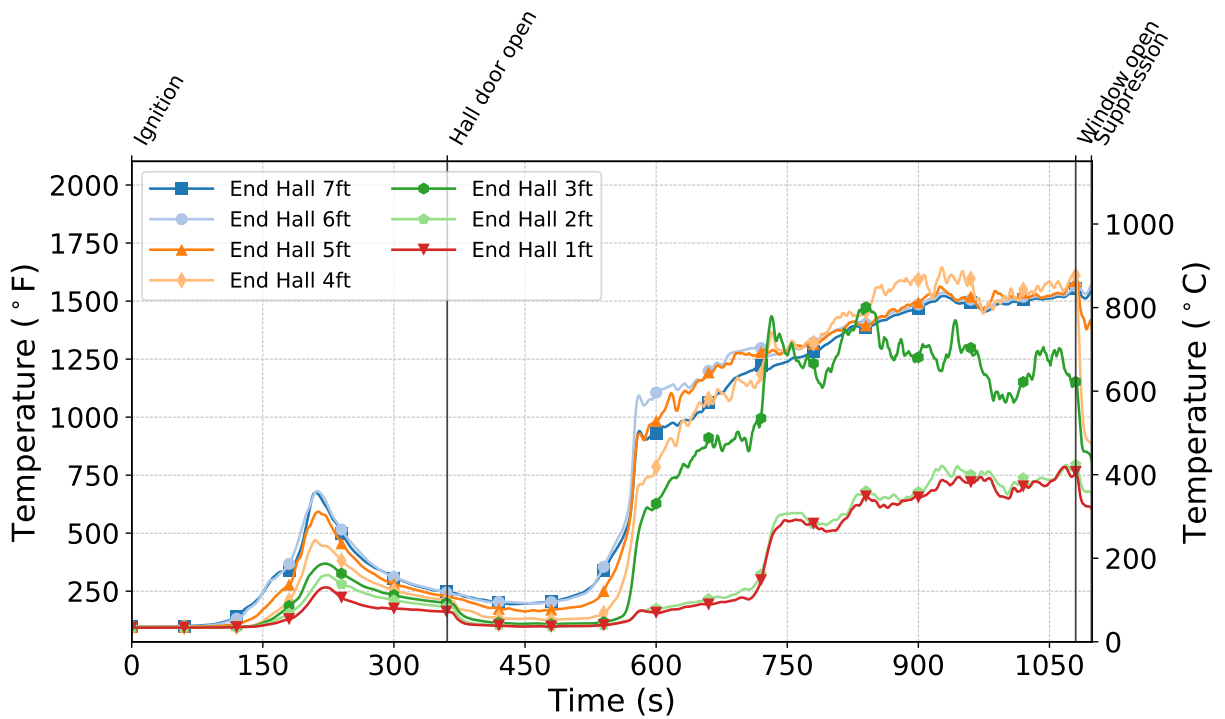


Figure C.59: Temperatures measured by the end hall thermocouples during Test 6.

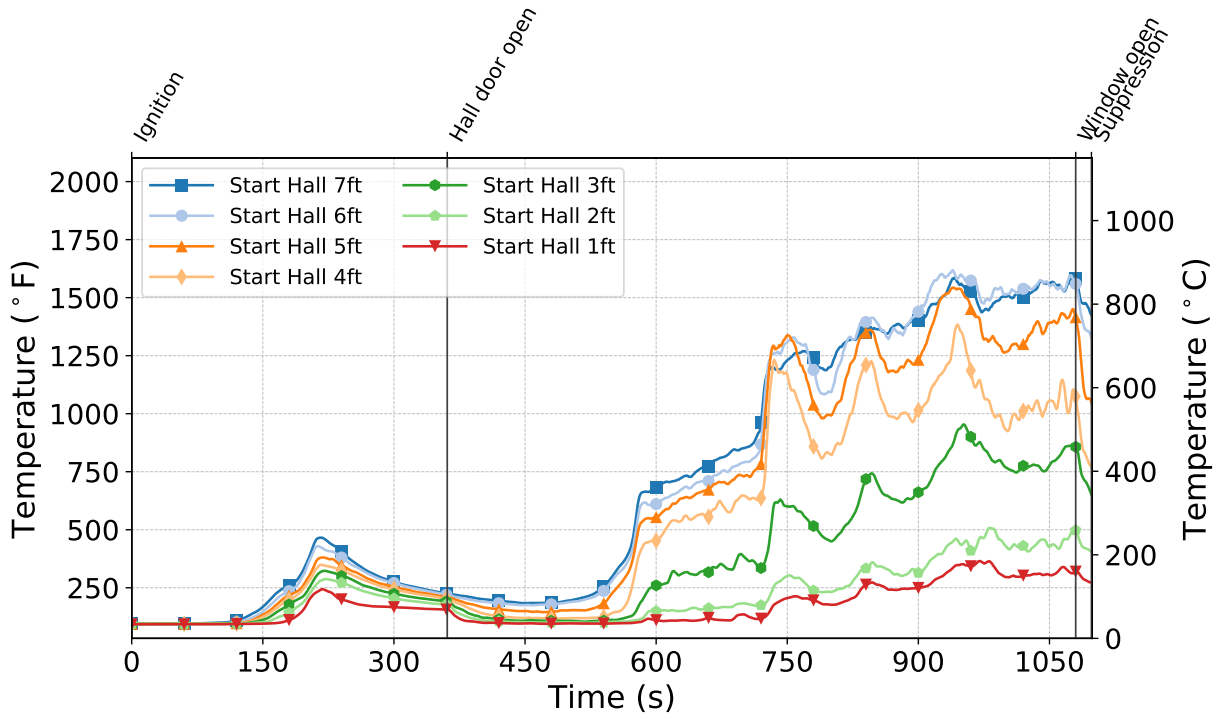


Figure C.60: Temperatures measured by the start hall thermocouples during Test 6.

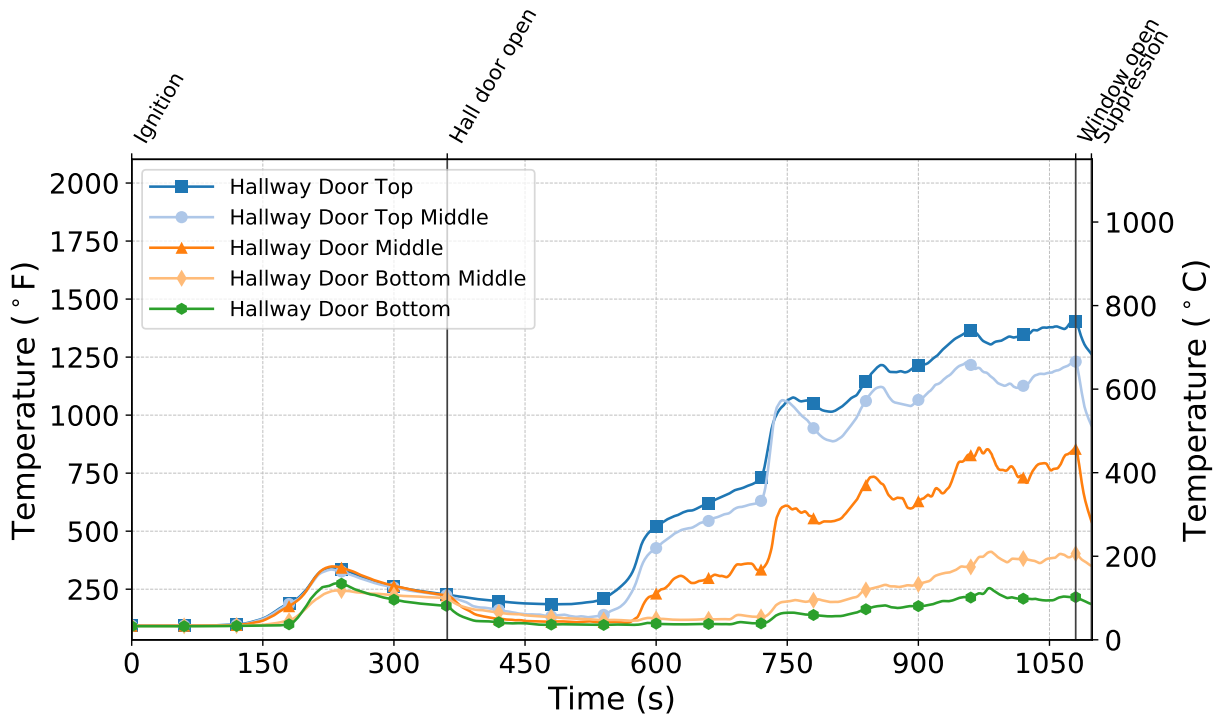


Figure C.61: Temperatures measured by the hallway door thermocouples during Test 6.

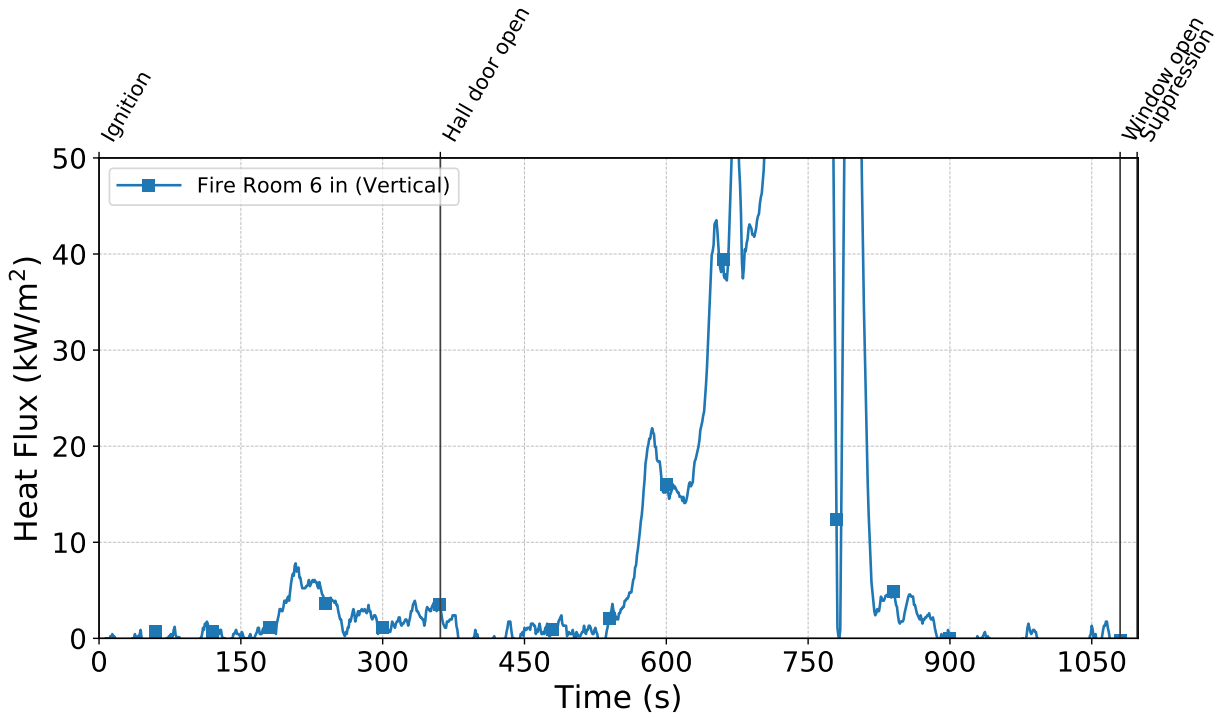


Figure C.62: Heat flux measured by the fire room gauge during Test 6.

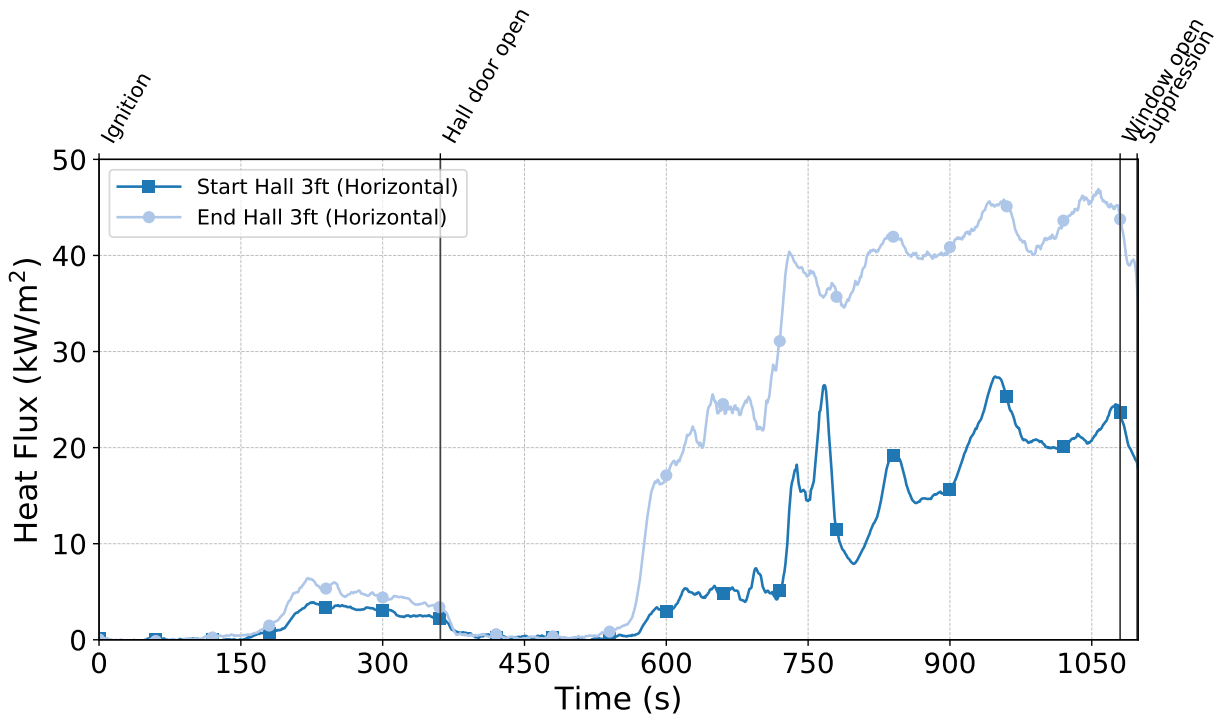


Figure C.63: Heat flux measured by the hallway gauges during Test 6.

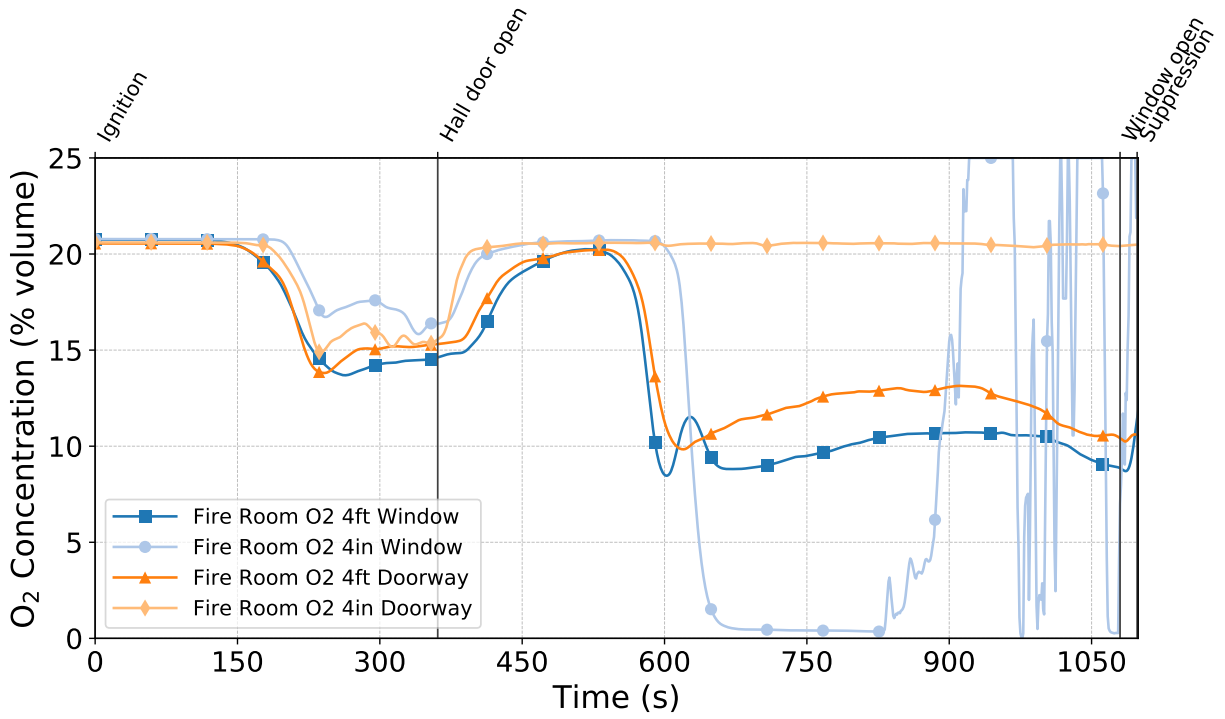


Figure C.64: Oxygen concentrations measured by the fire room gas sampling probes during Test 6.

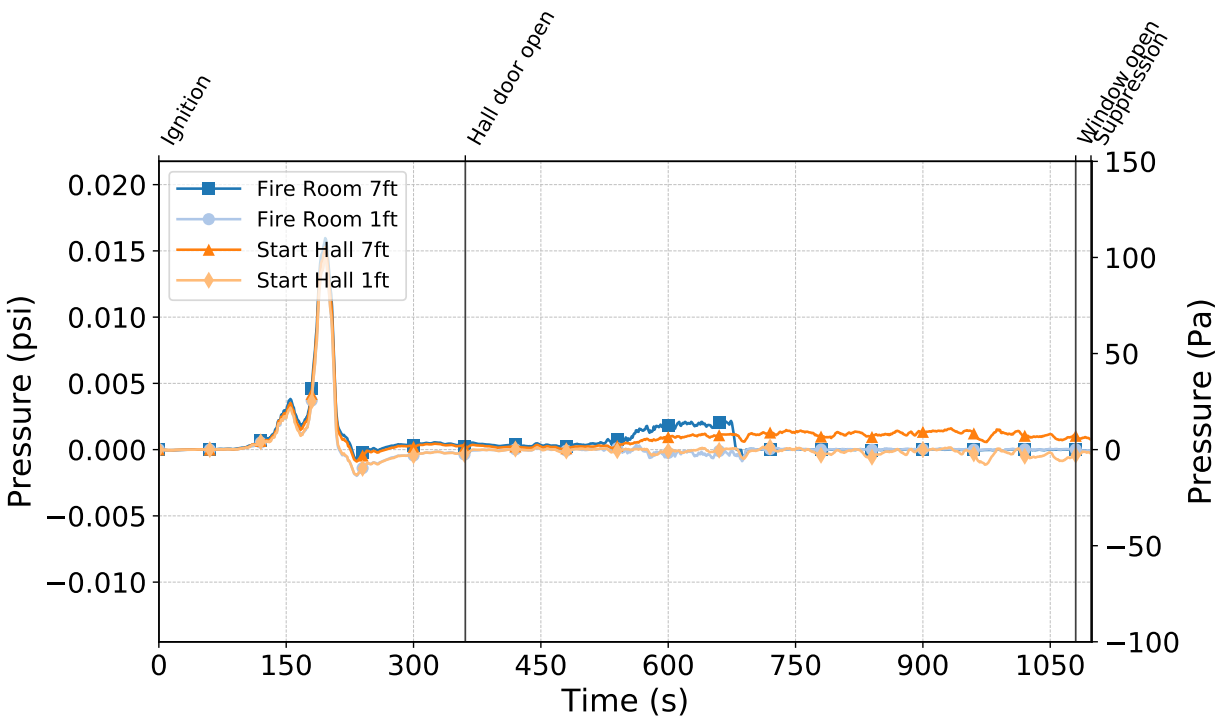


Figure C.65: Pressures measured by the fire room and hallway probes during Test 6.

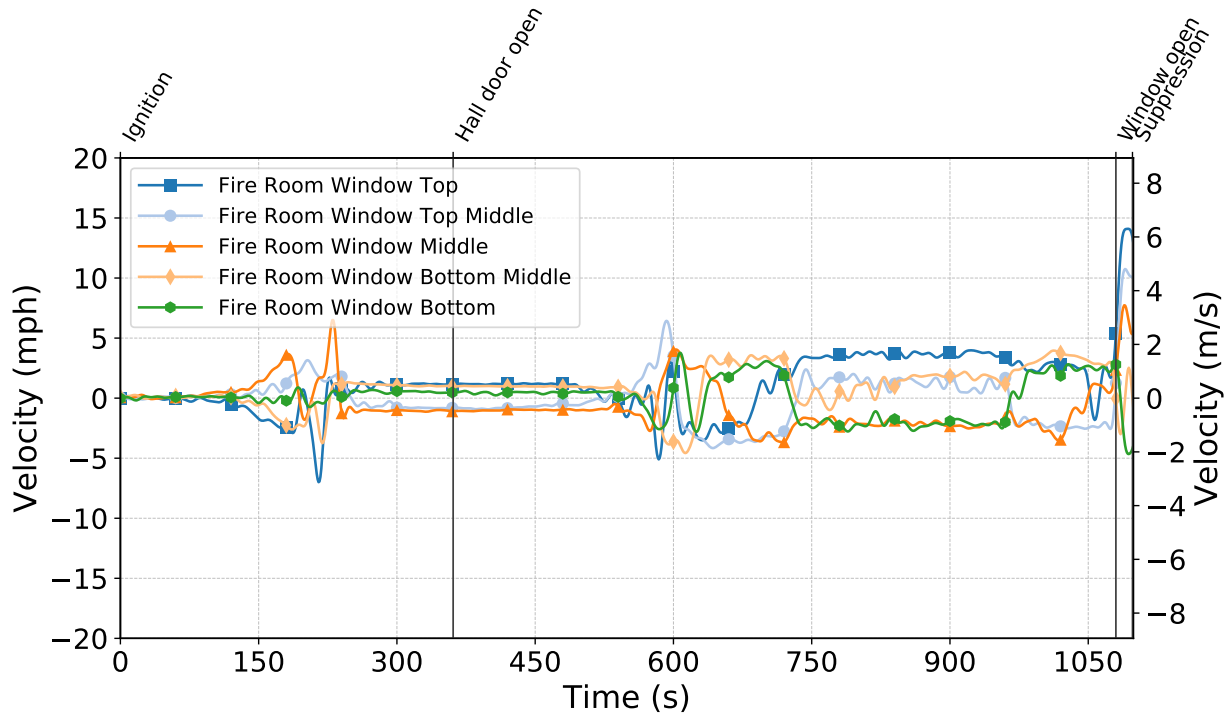


Figure C.66: Gas velocities measured by the fire room window bdp's during Test 6.

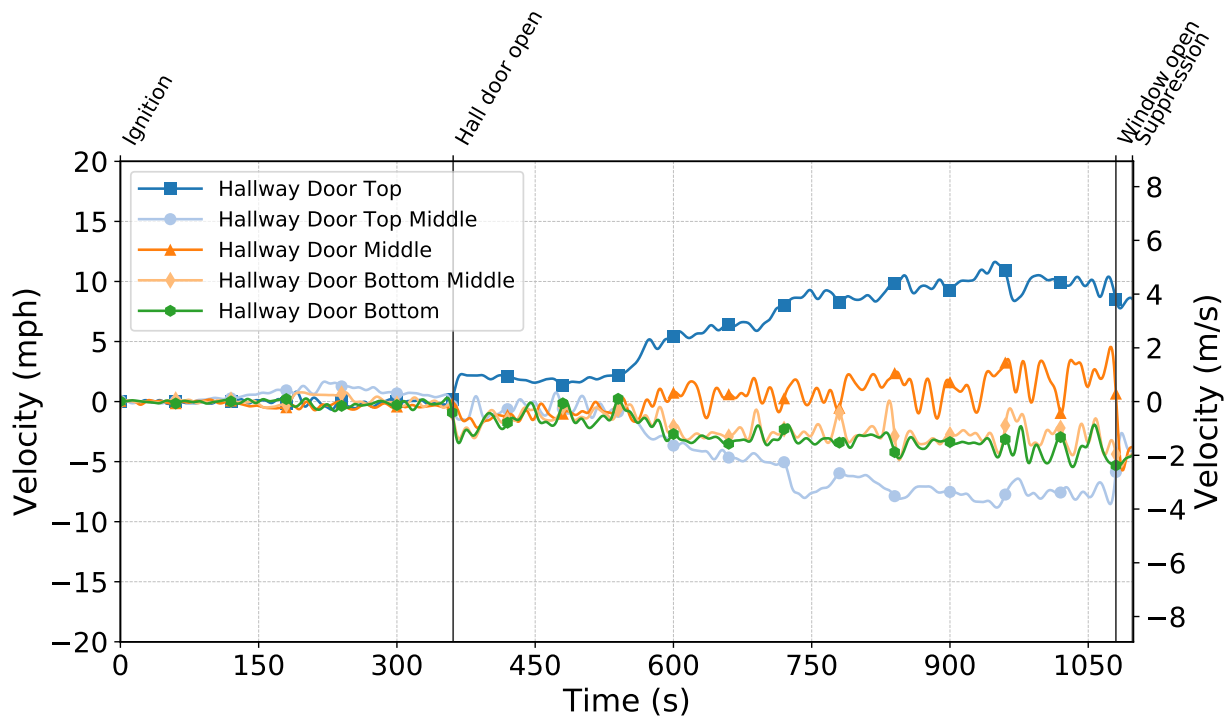


Figure C.67: Gas velocities measured by the hallway door bdp's during Test 6.

Test 7

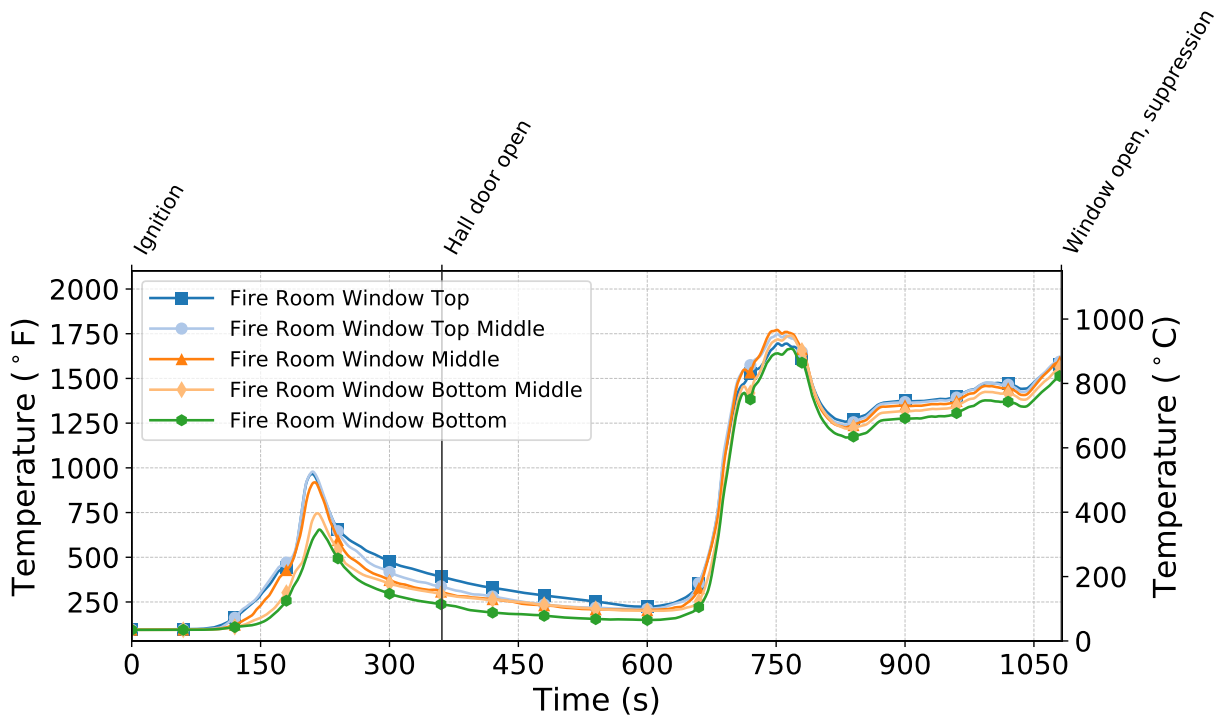


Figure C.68: Temperatures measured by the fire room window thermocouples during Test 7.

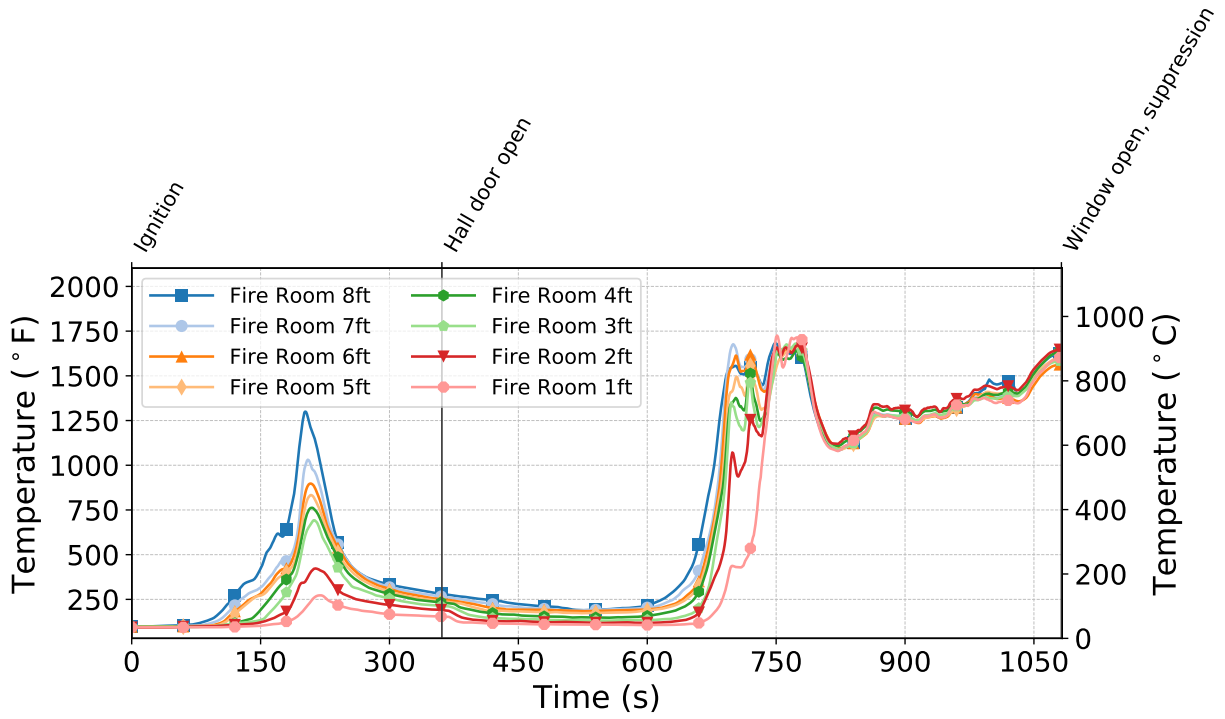


Figure C.69: Temperatures measured by the fire room thermocouples during Test 7.

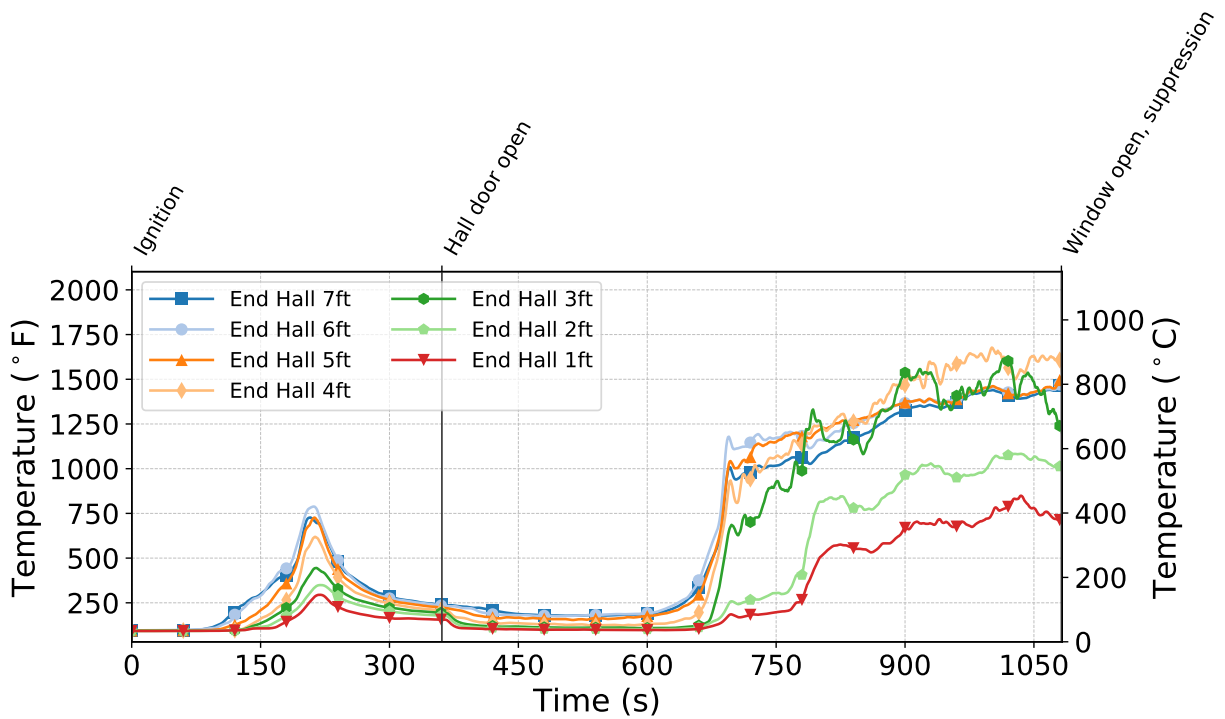


Figure C.70: Temperatures measured by the end hall thermocouples during Test 7.

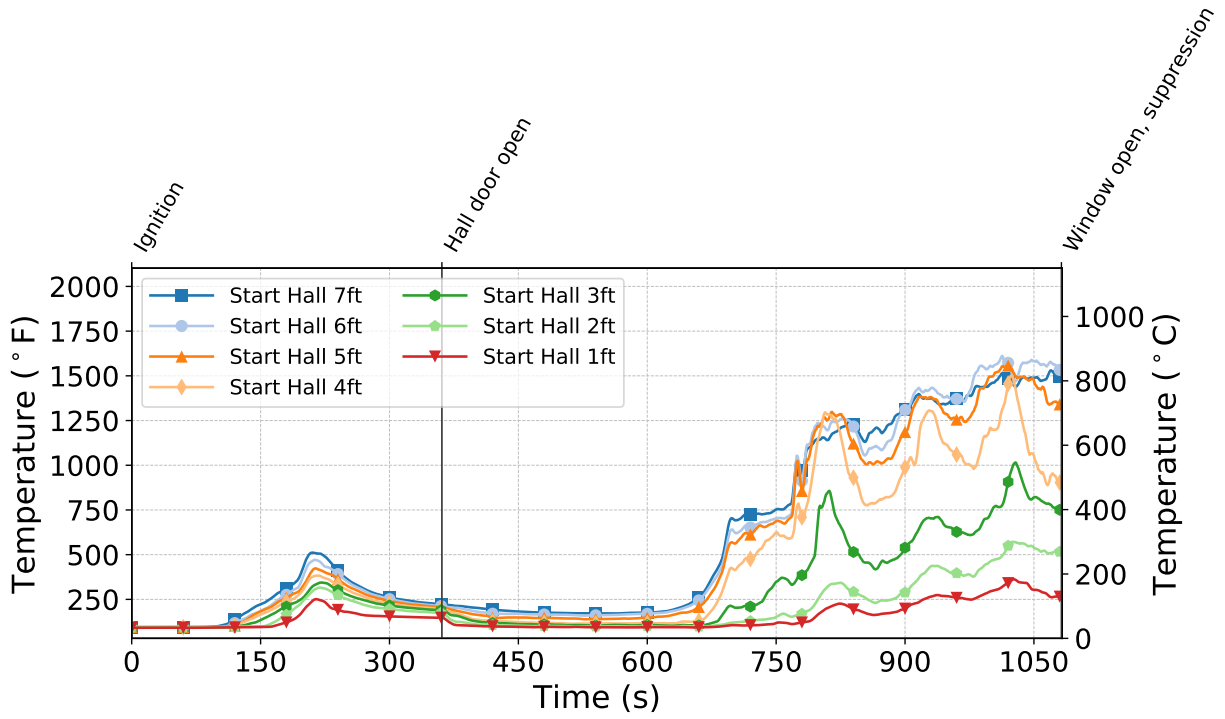


Figure C.71: Temperatures measured by the start hall thermocouples during Test 7.

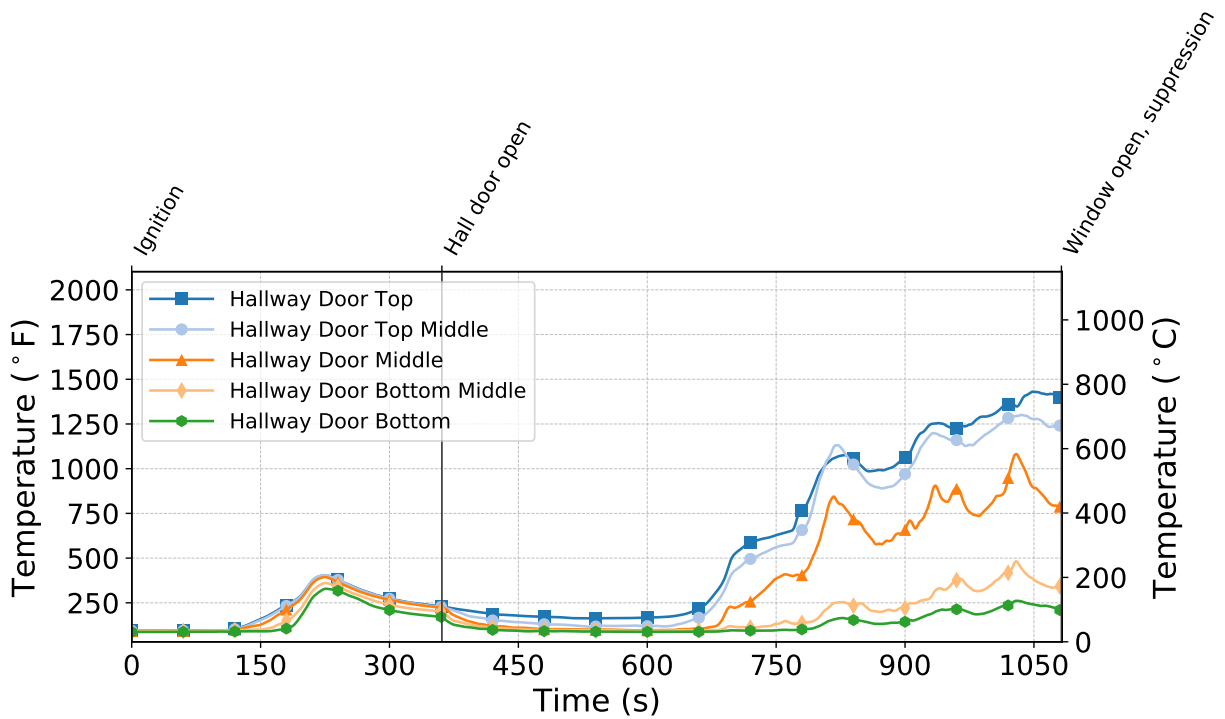


Figure C.72: Temperatures measured by the hallway door thermocouples during Test 7.

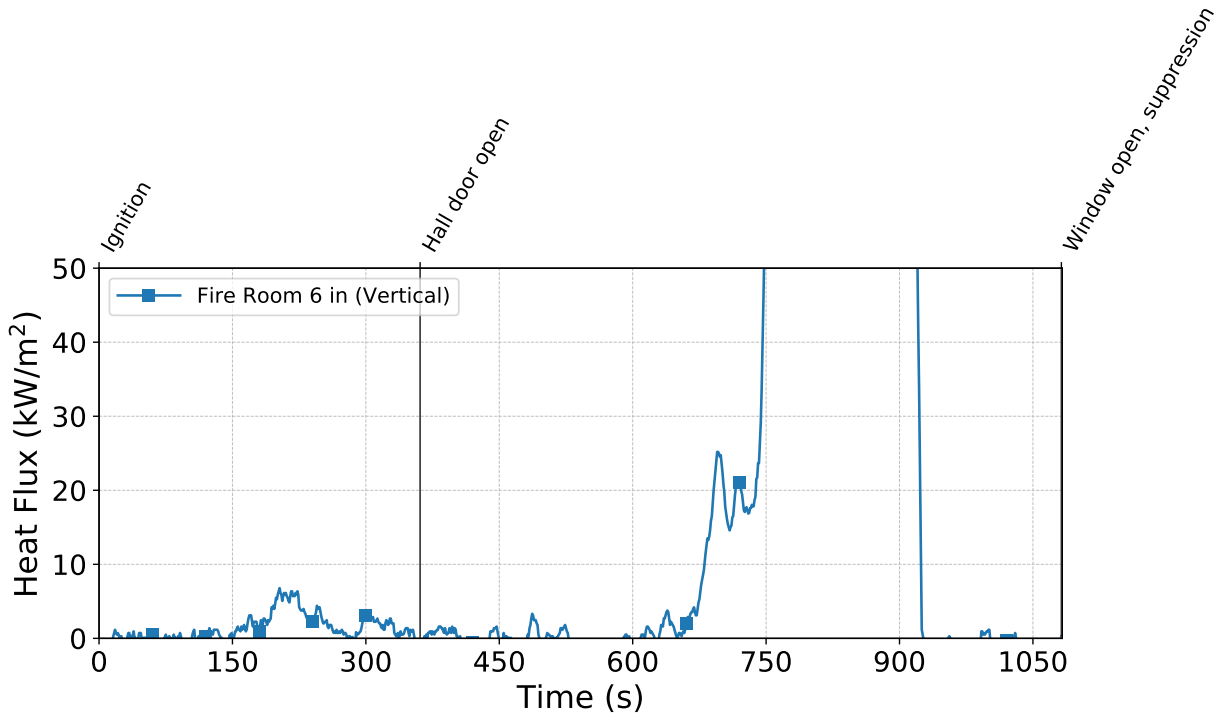


Figure C.73: Heat flux measured by the fire room gauge during Test 7.

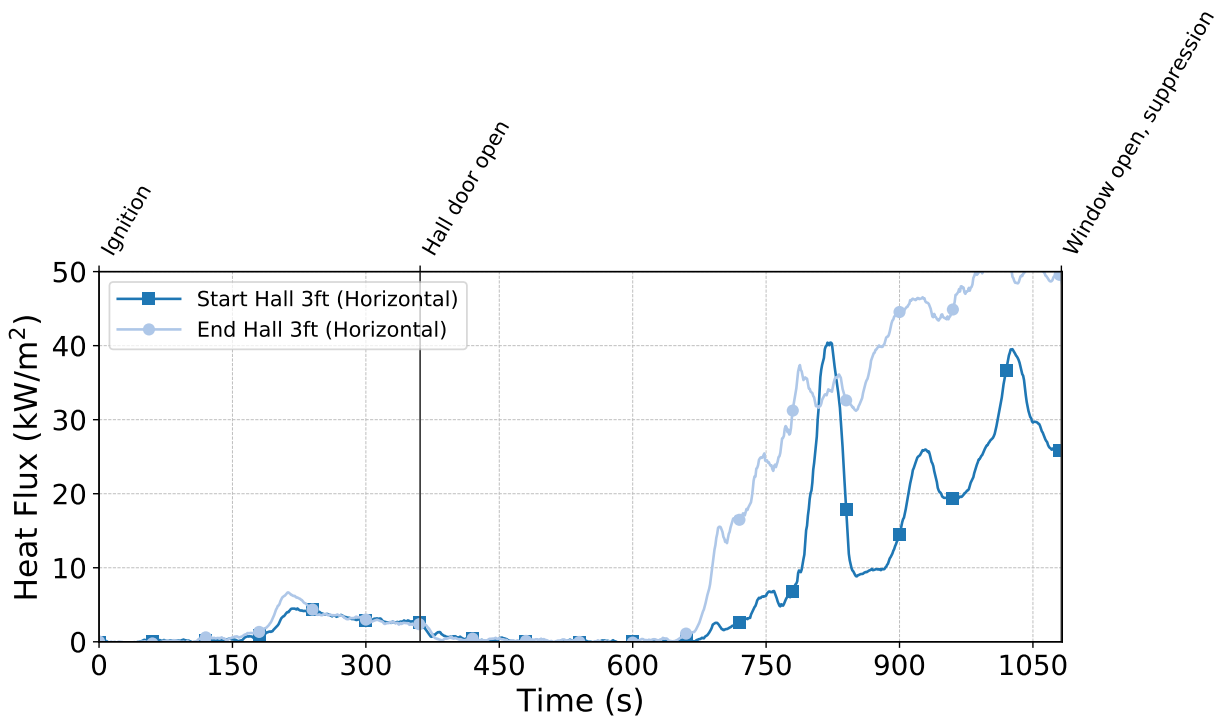


Figure C.74: Heat flux measured by the hallway gauges during Test 7.

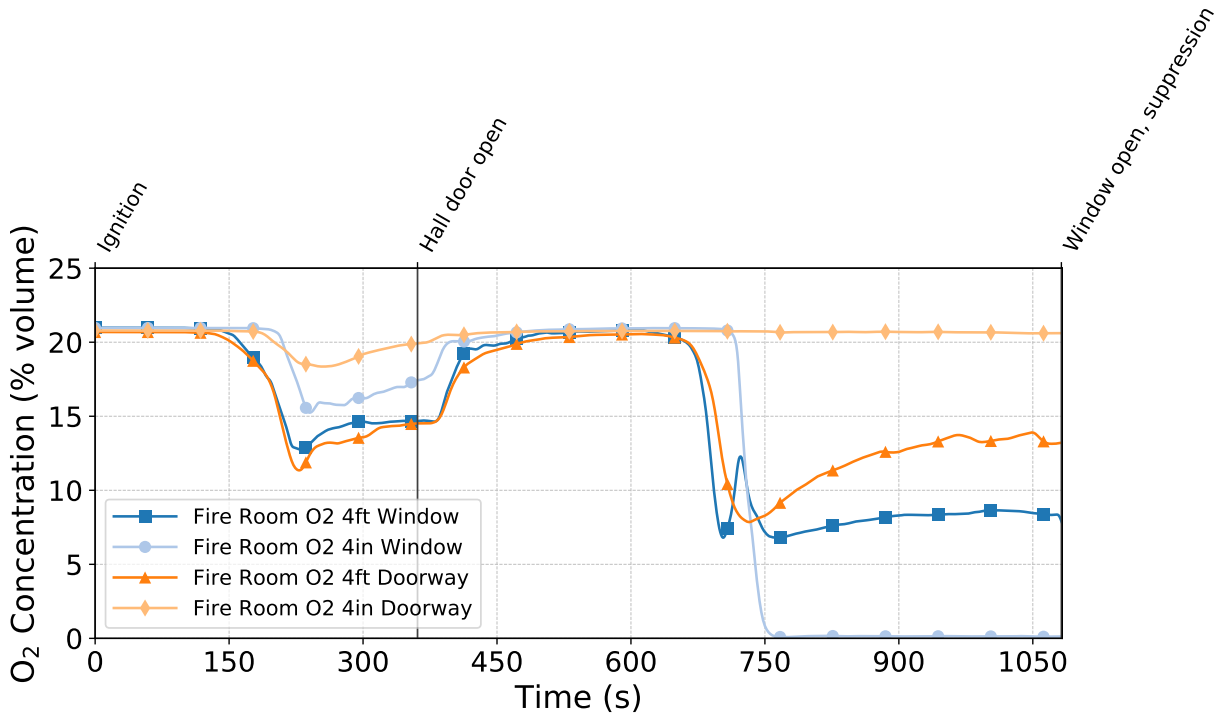


Figure C.75: Oxygen concentrations measured by the fire room gas sampling probes during Test 7.

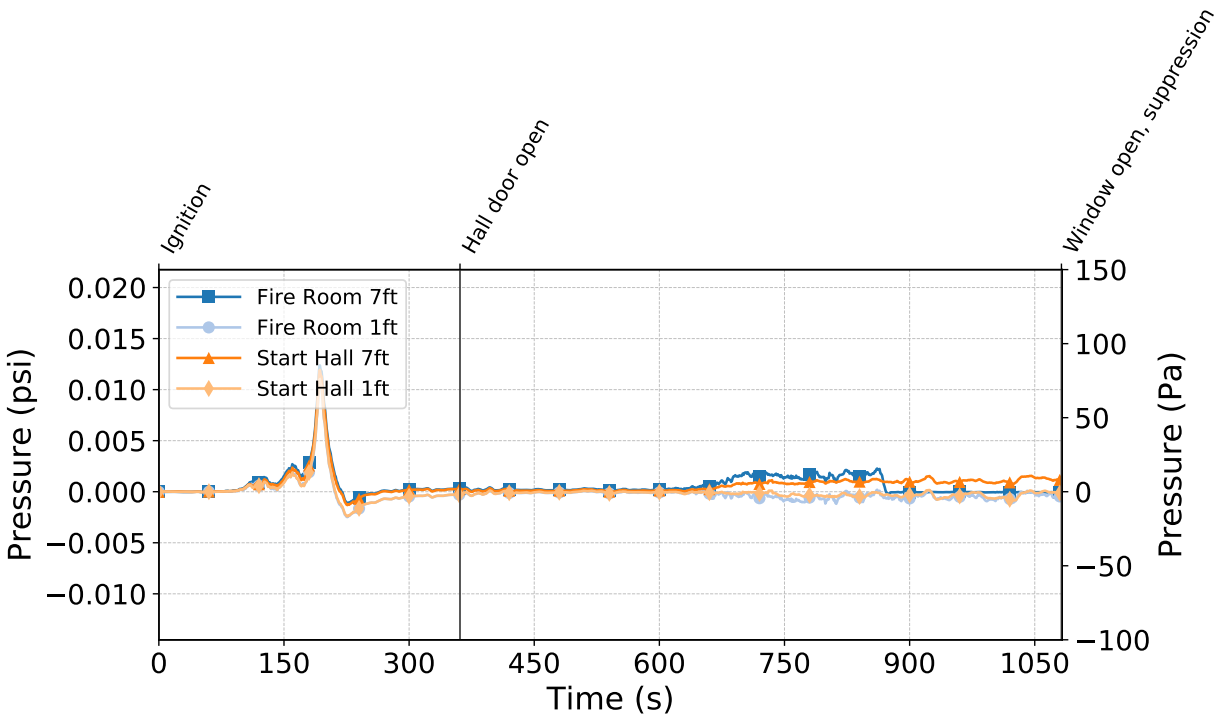


Figure C.76: Pressures measured by the fire room and hallway probes during Test 7.

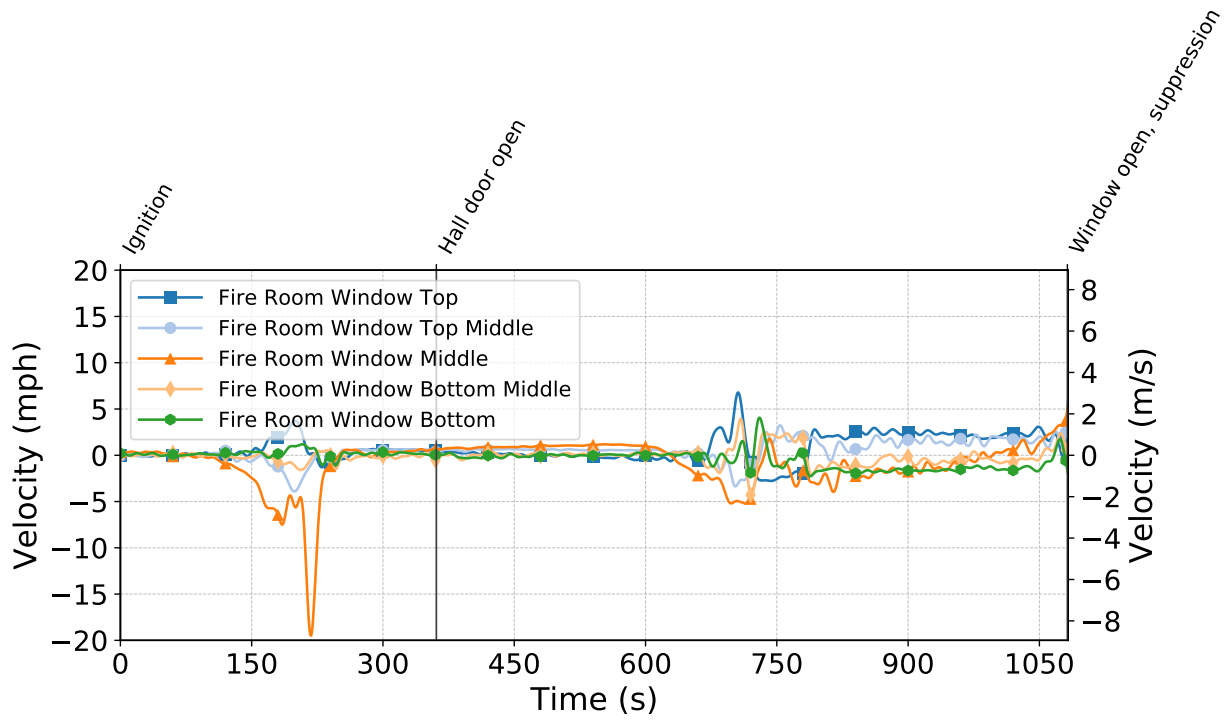


Figure C.77: Gas velocities measured by the fire room window bdps during Test 7.

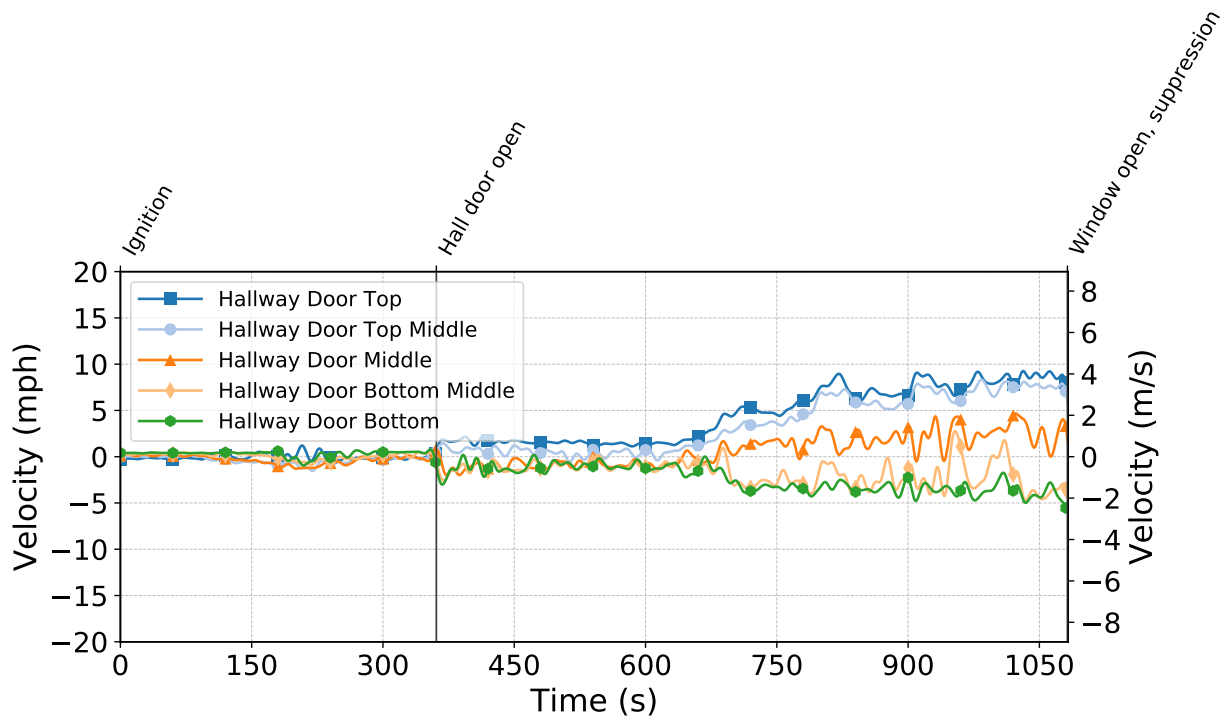


Figure C.78: Gas velocities measured by the hallway door bdps during Test 7.

Test 8

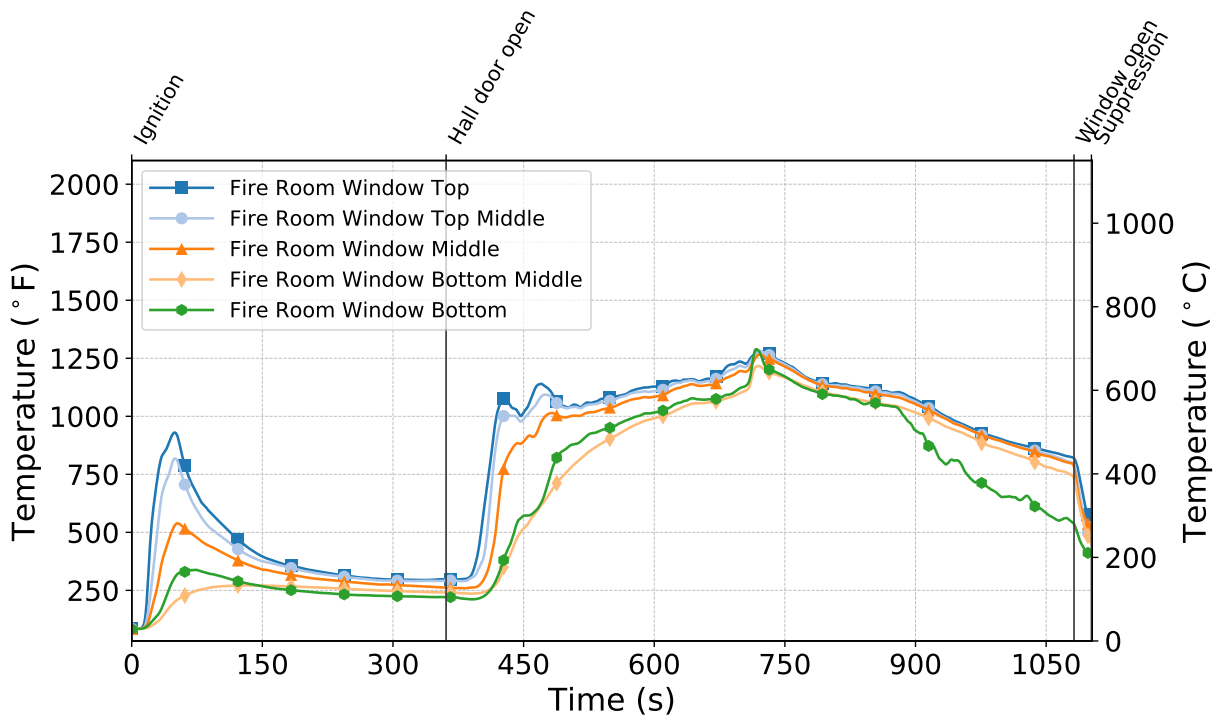


Figure C.79: Temperatures measured by the fire room window thermocouples during Test 8.

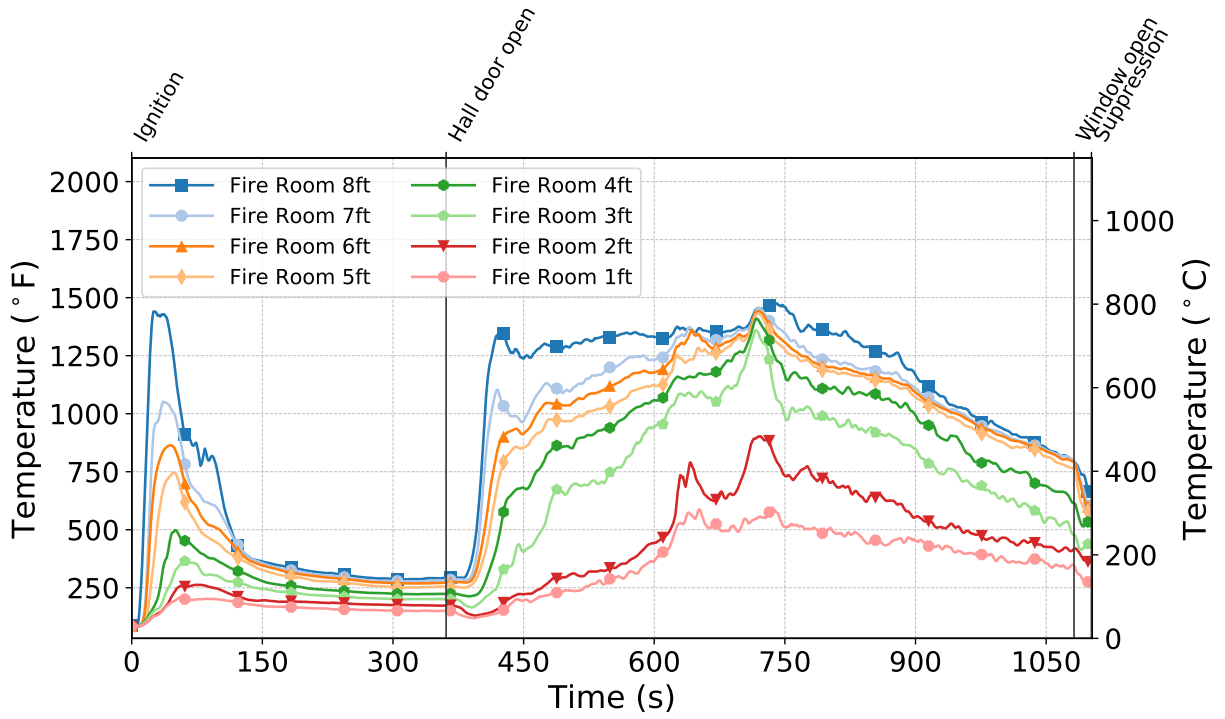


Figure C.80: Temperatures measured by the fire room thermocouples during Test 8.

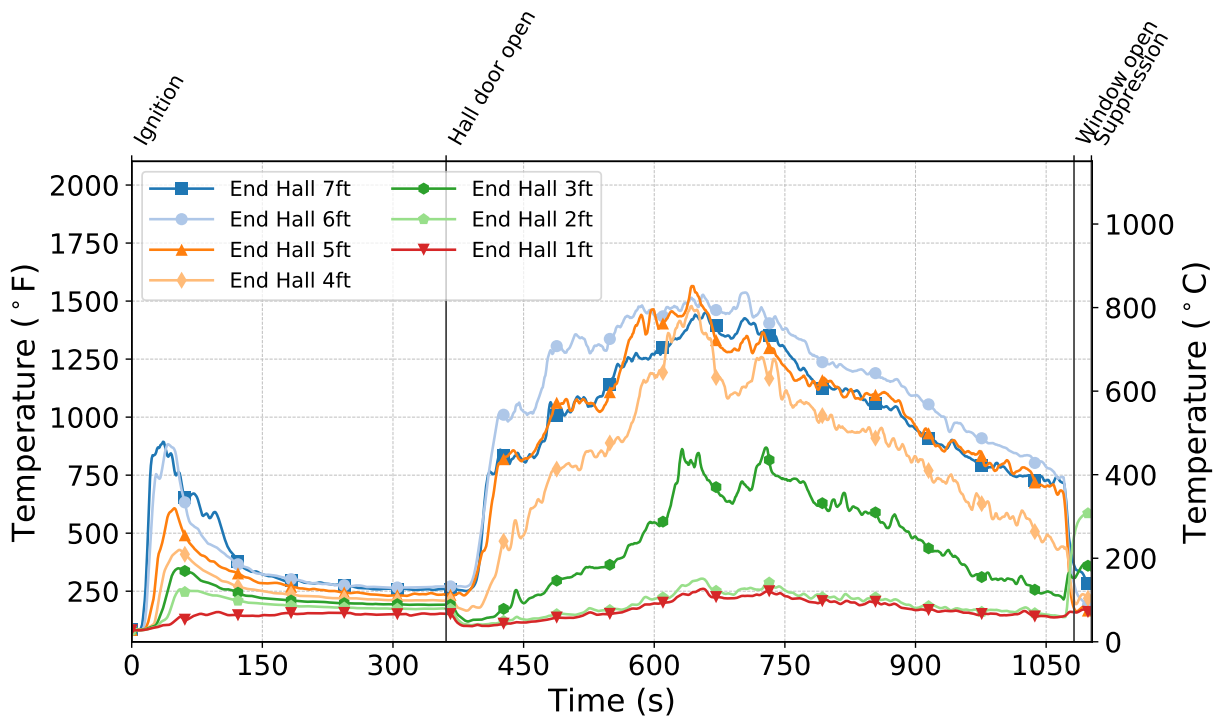


Figure C.81: Temperatures measured by the end hall thermocouples during Test 8.

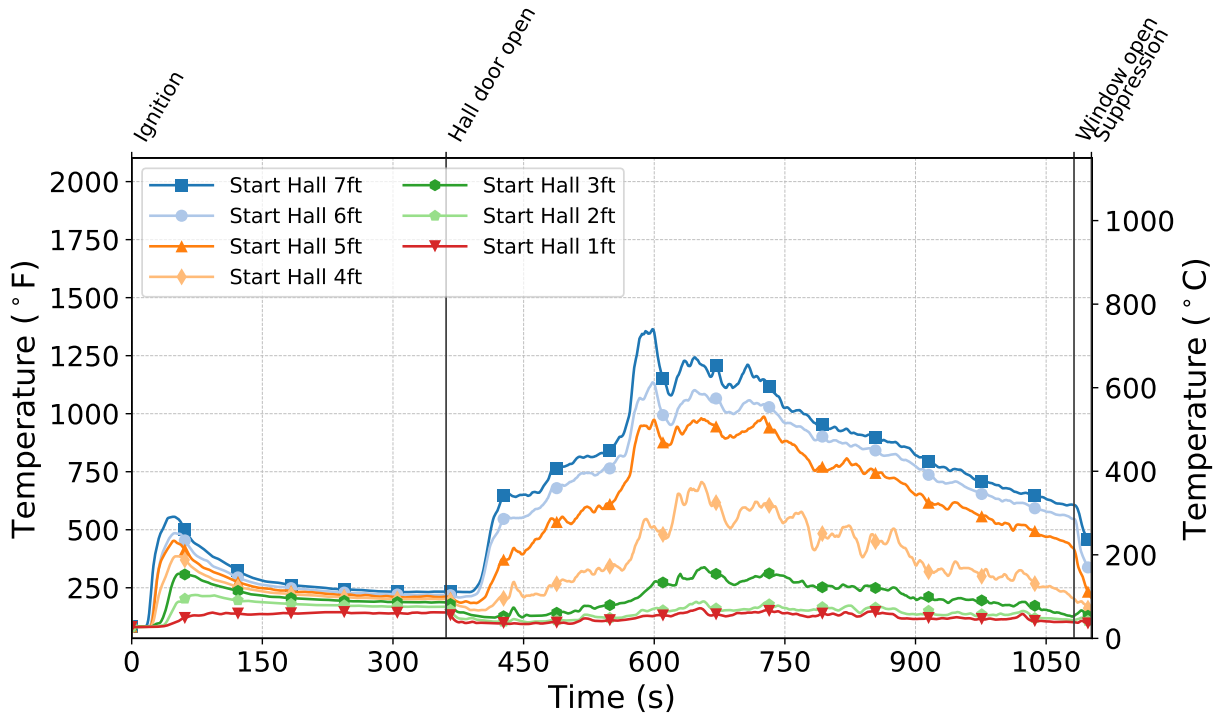


Figure C.82: Temperatures measured by the start hall thermocouples during Test 8.

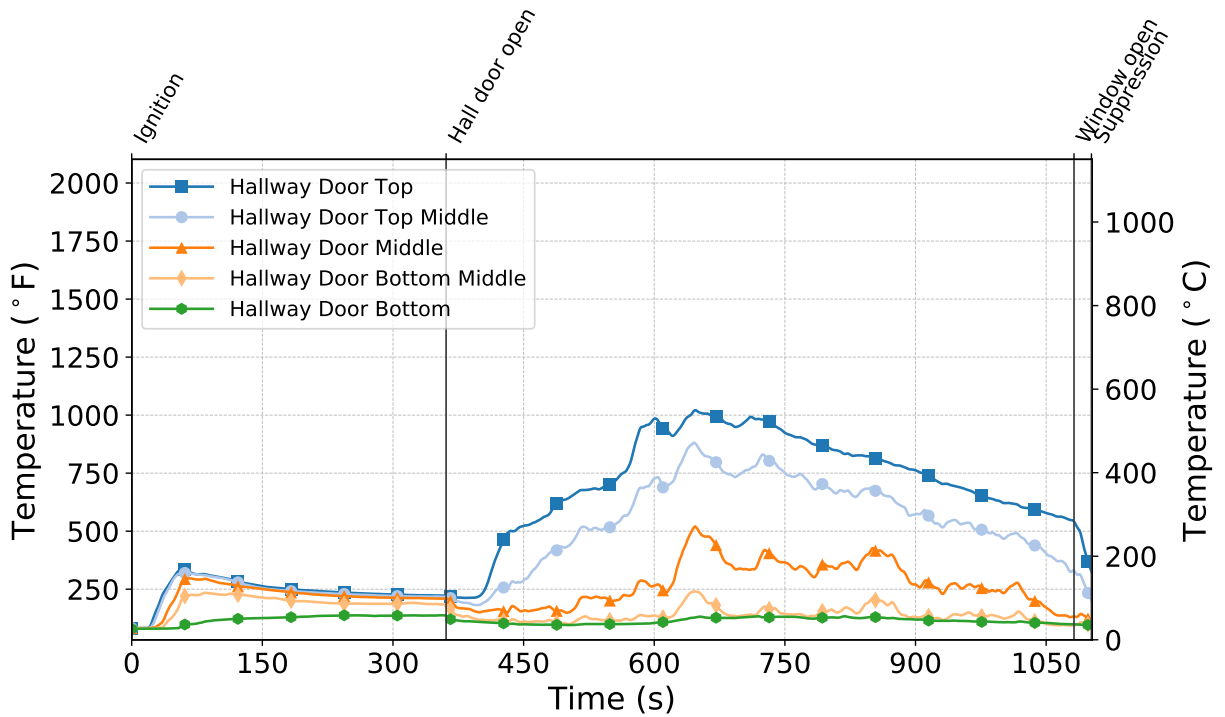


Figure C.83: Temperatures measured by the hallway door thermocouples during Test 8.

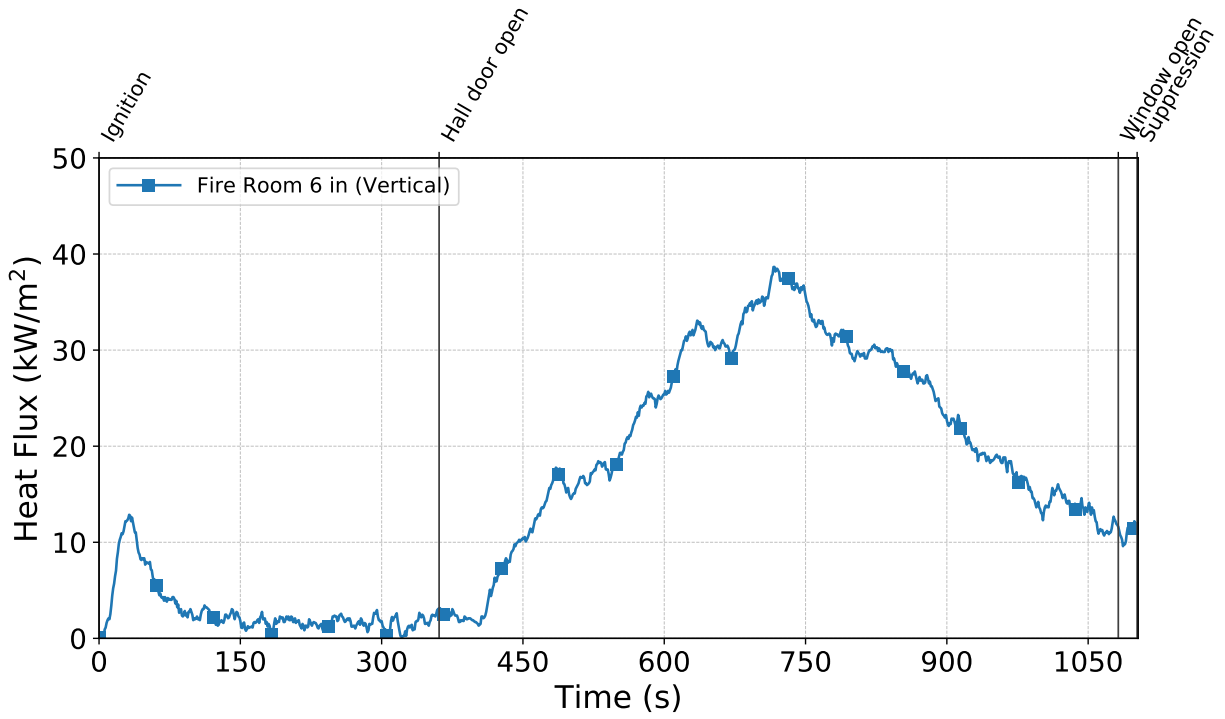


Figure C.84: Heat flux measured by the fire room gauge during Test 8.

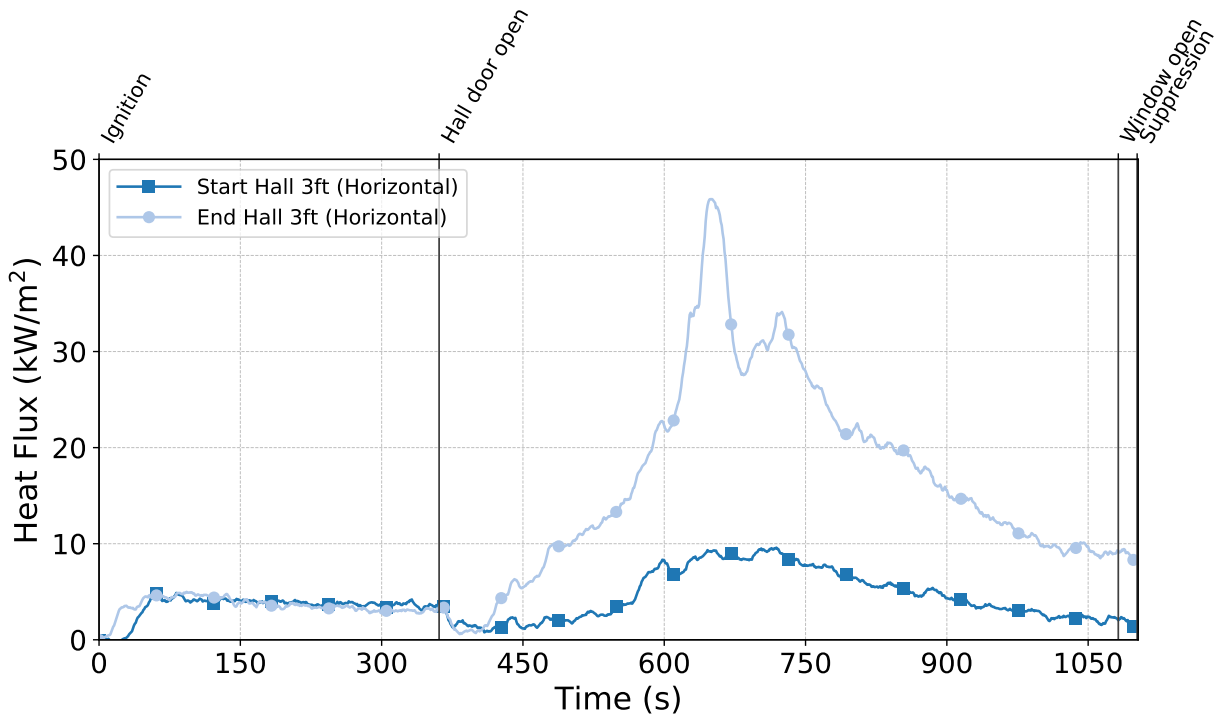


Figure C.85: Heat flux measured by the hallway gauges during Test 8.

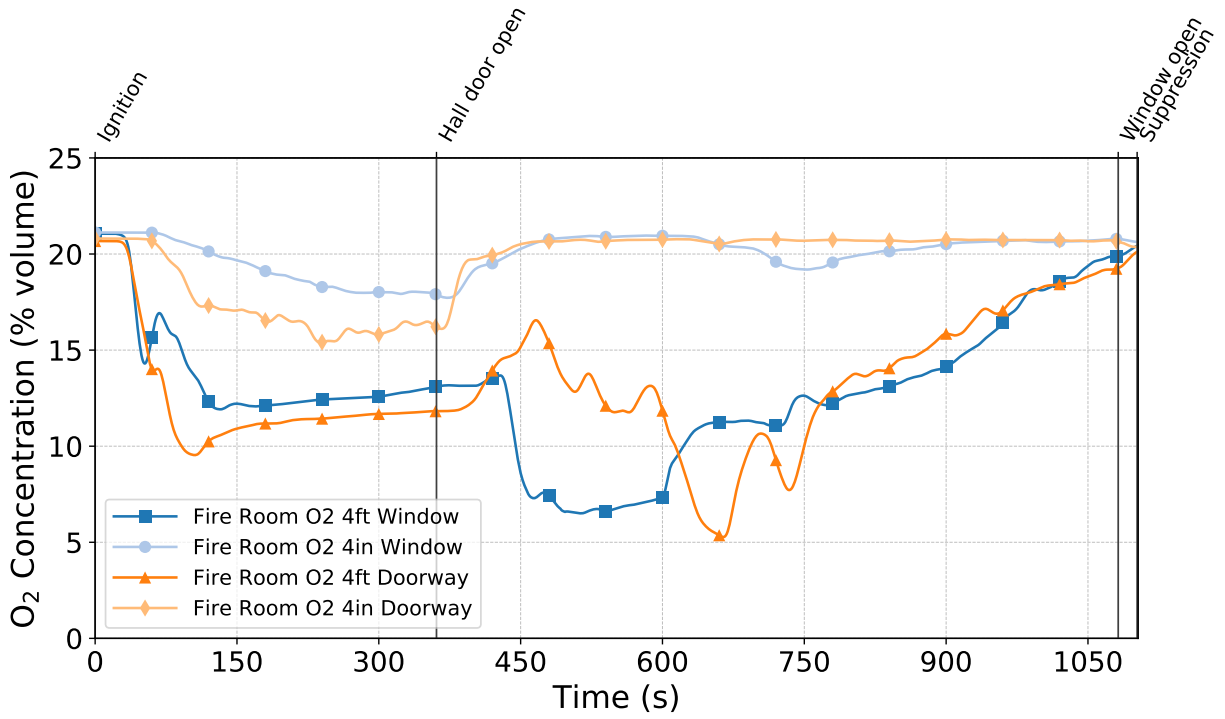


Figure C.86: Oxygen concentrations measured by the fire room gas sampling probes during Test 8.

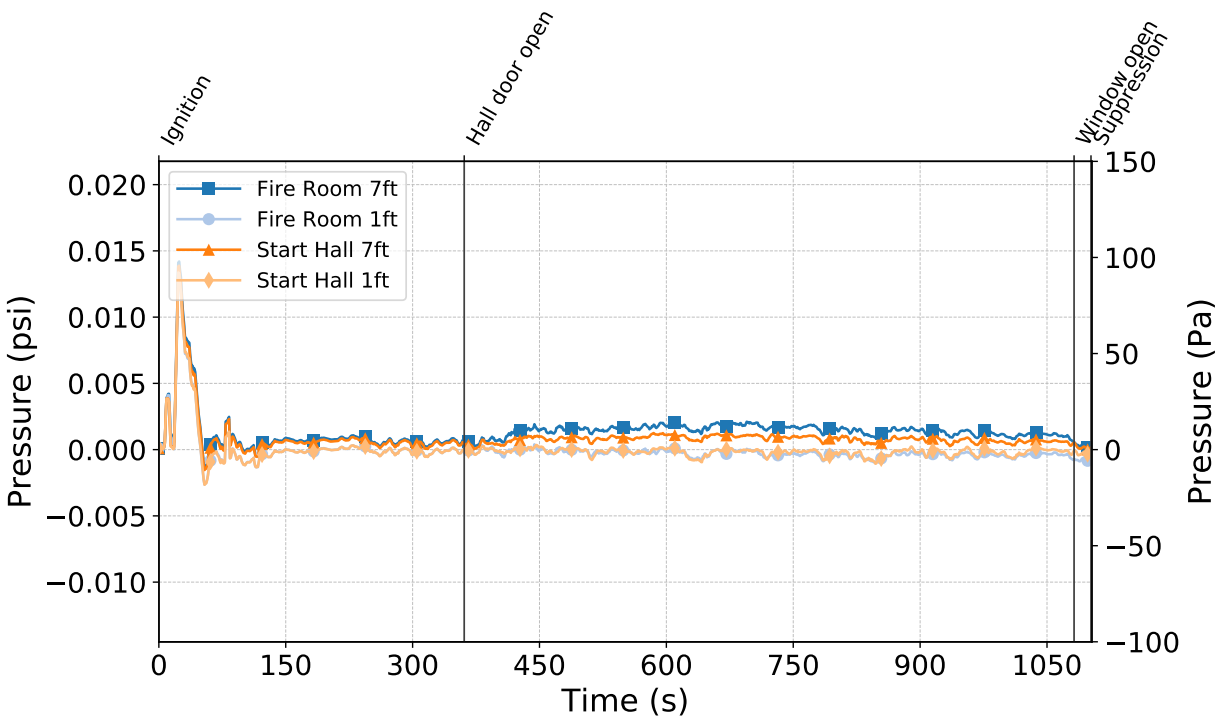


Figure C.87: Pressures measured by the fire room and hallway probes during Test 8.

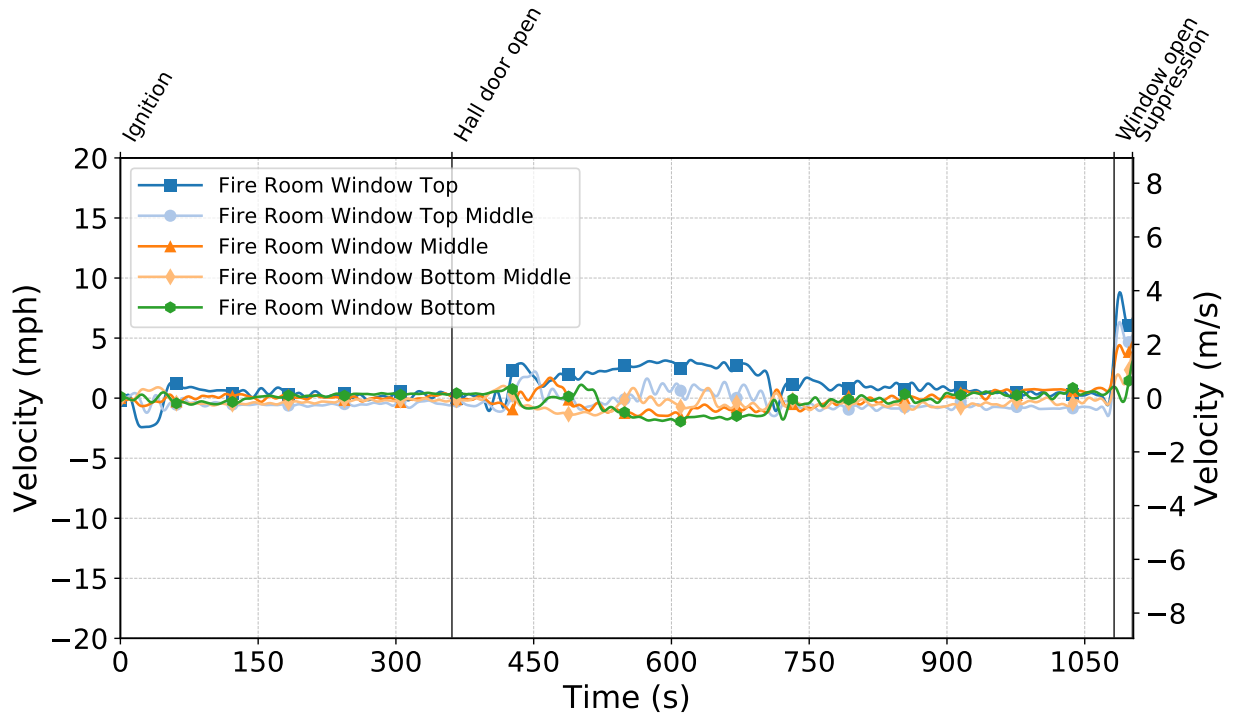


Figure C.88: Gas velocities measured by the fire room window bdps during Test 8.

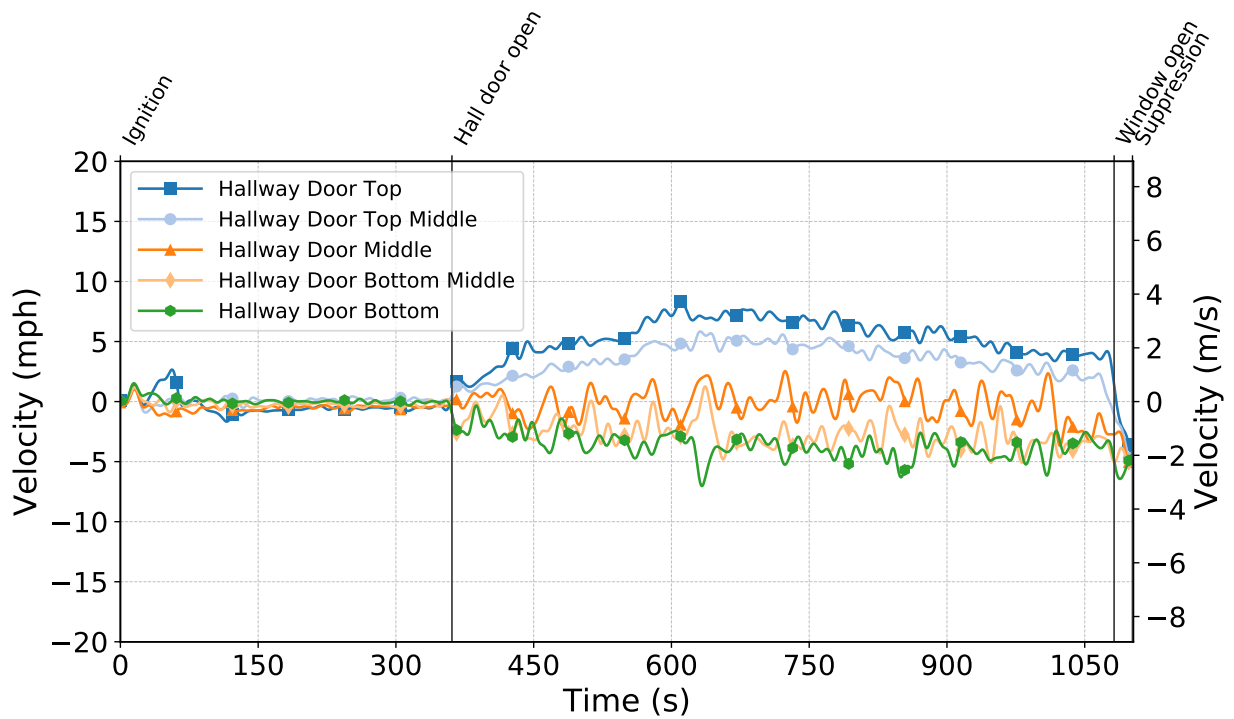


Figure C.89: Gas velocities measured by the hallway door bdps during Test 8.

Test 9

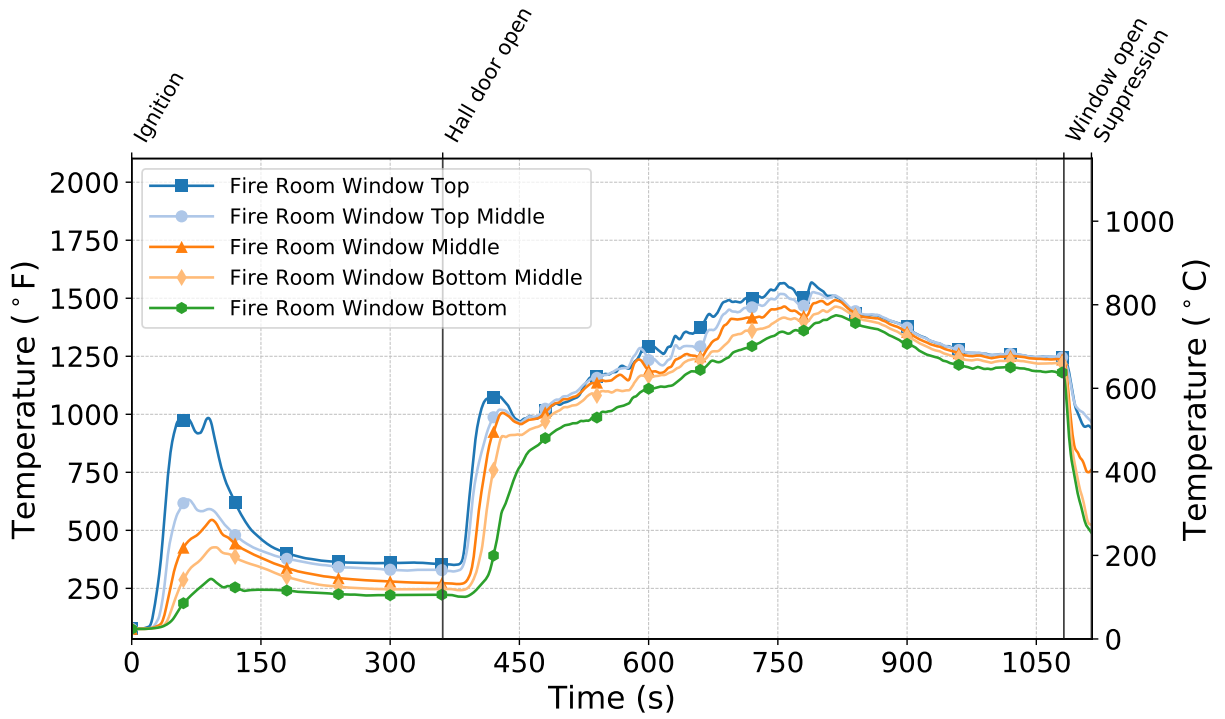


Figure C.90: Temperatures measured by the fire room window thermocouples during Test 9.

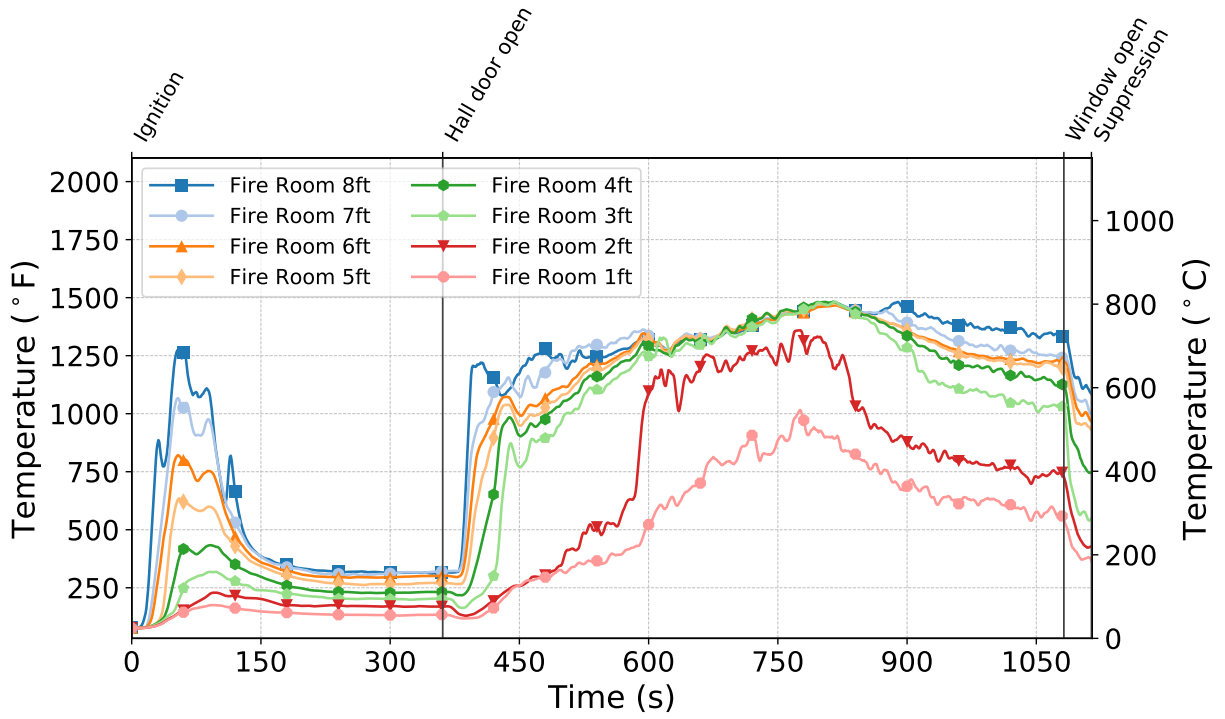


Figure C.91: Temperatures measured by the fire room thermocouples during Test 9.

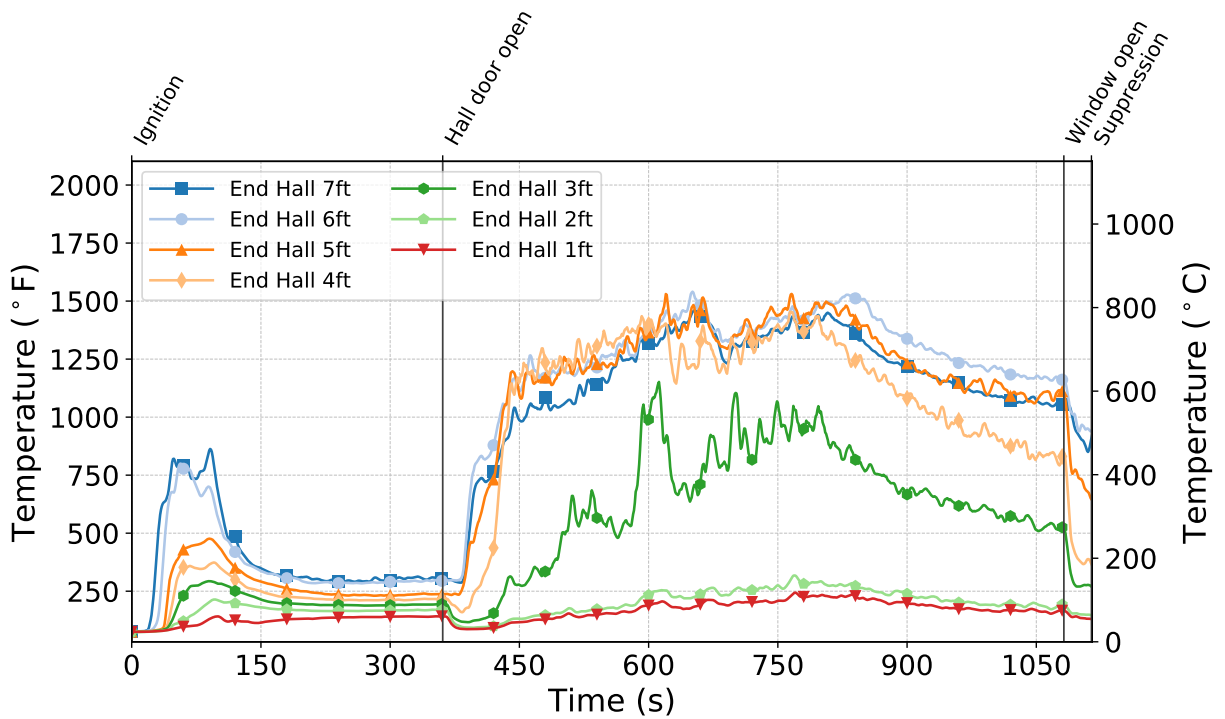


Figure C.92: Temperatures measured by the end hall thermocouples during Test 9.

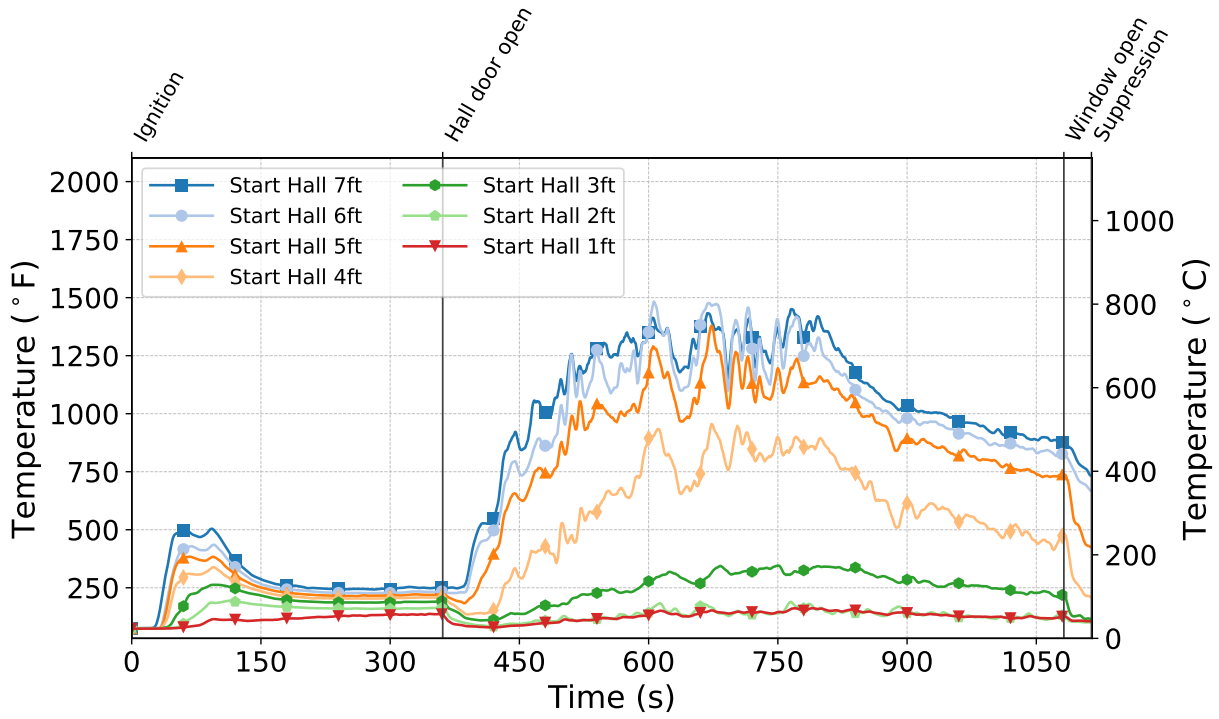


Figure C.93: Temperatures measured by the start hall thermocouples during Test 9.

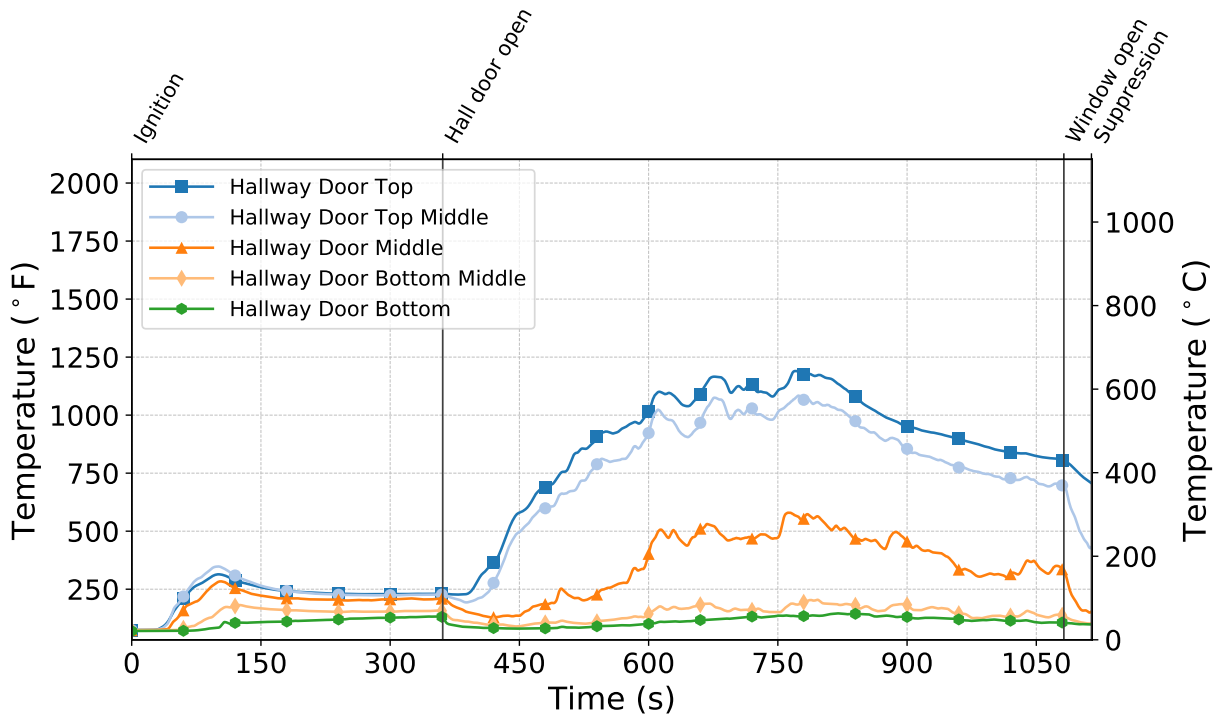


Figure C.94: Temperatures measured by the hallway door thermocouples during Test 9.

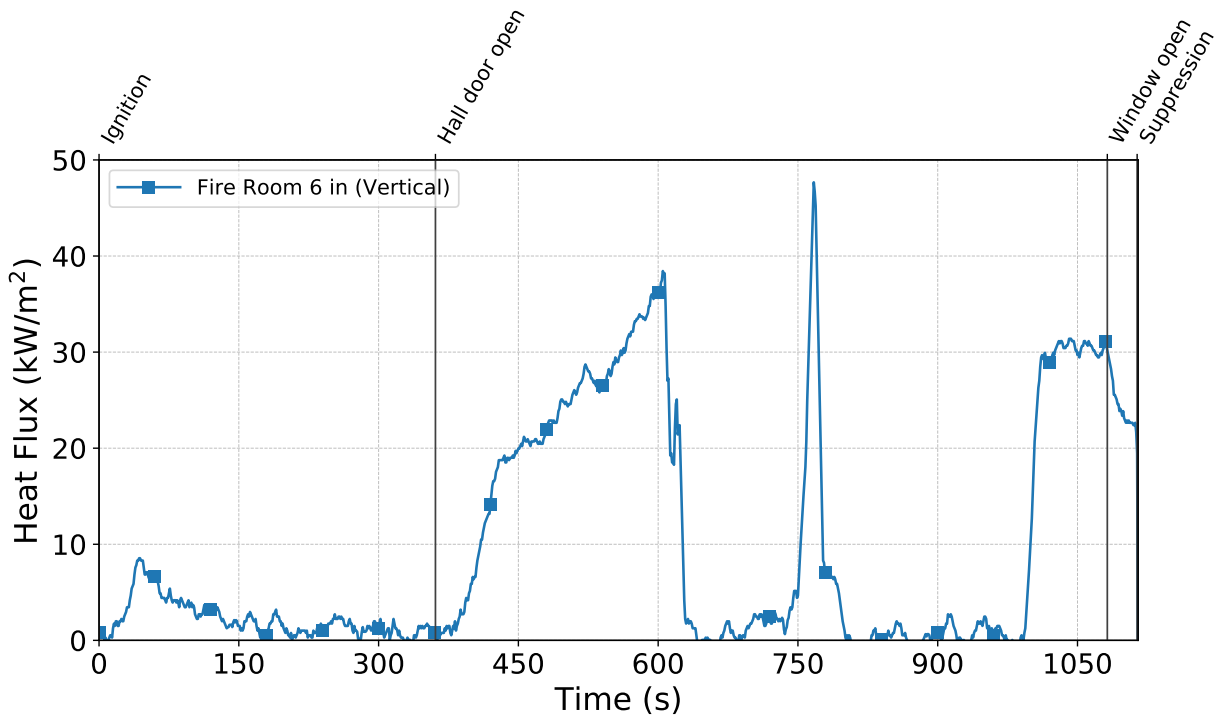


Figure C.95: Heat flux measured by the fire room gauge during Test 9.

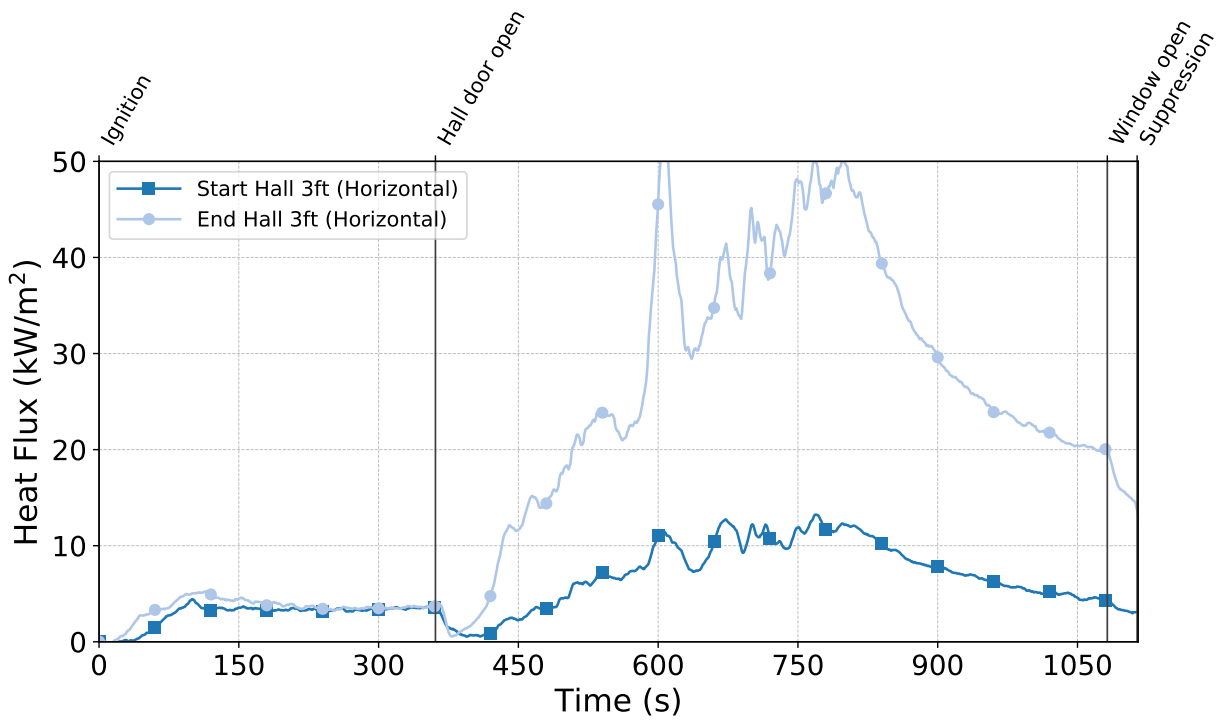


Figure C.96: Heat flux measured by the hallway gauges during Test 9.

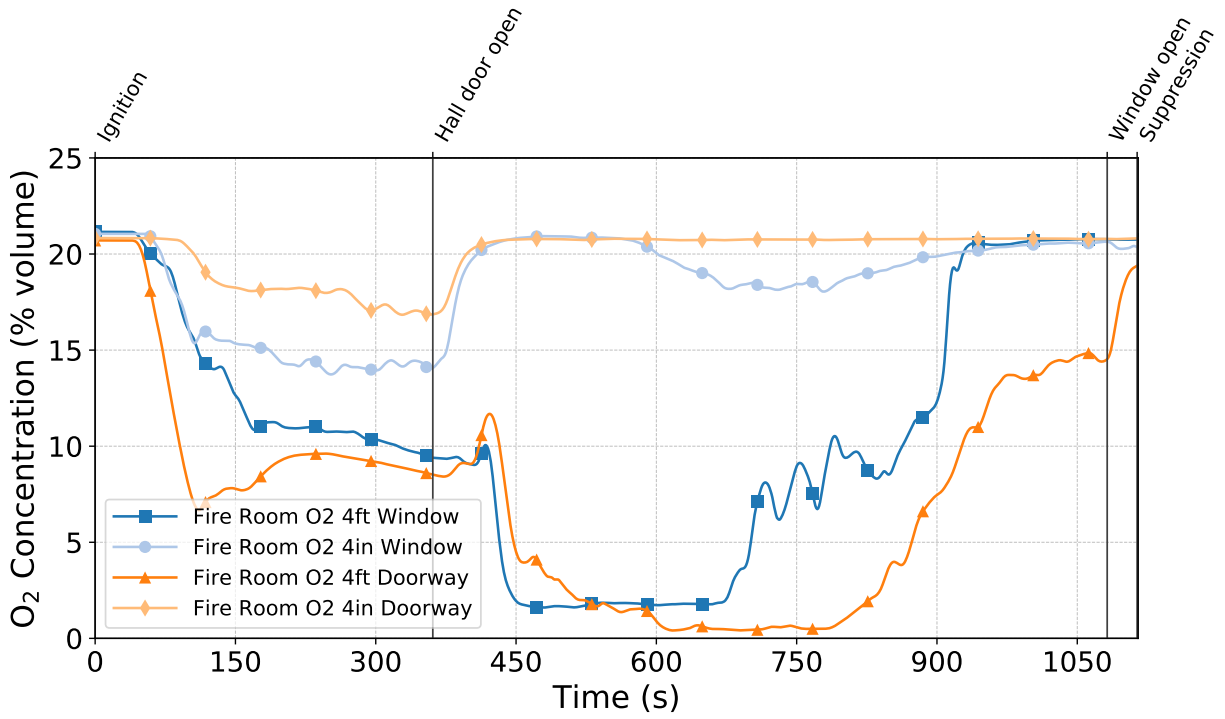


Figure C.97: Oxygen concentrations measured by the fire room gas sampling probes during Test 9.

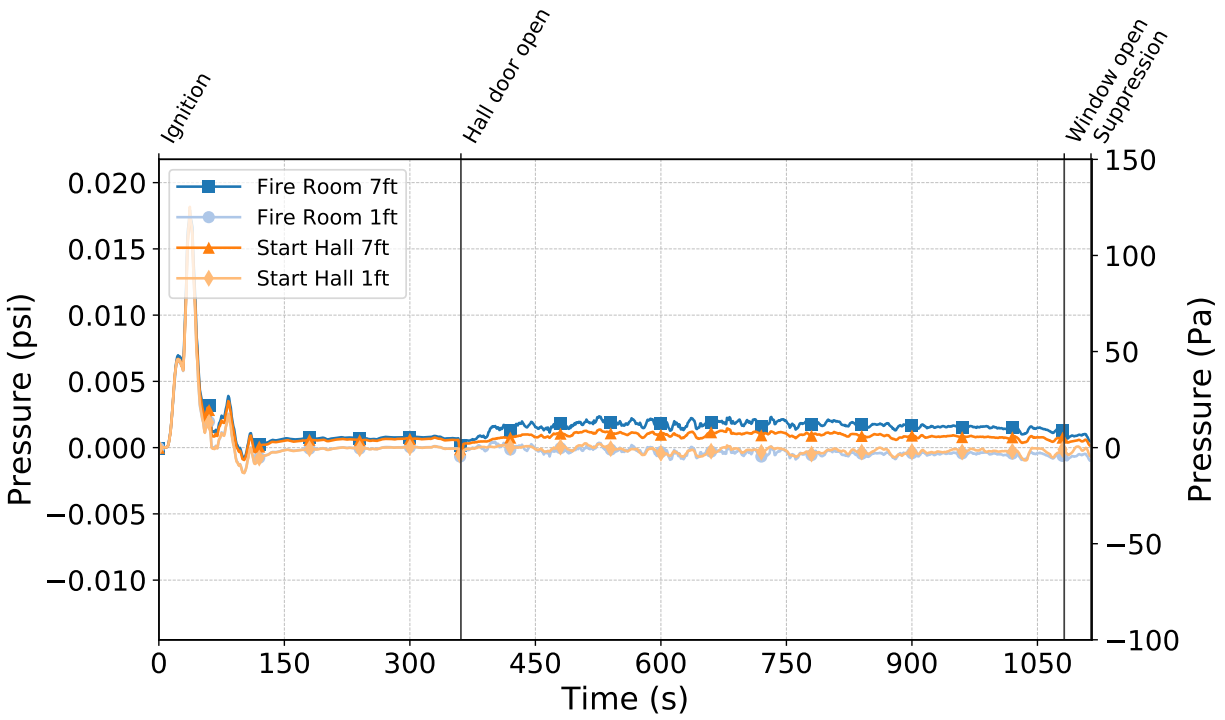


Figure C.98: Pressures measured by the fire room and hallway probes during Test 9.

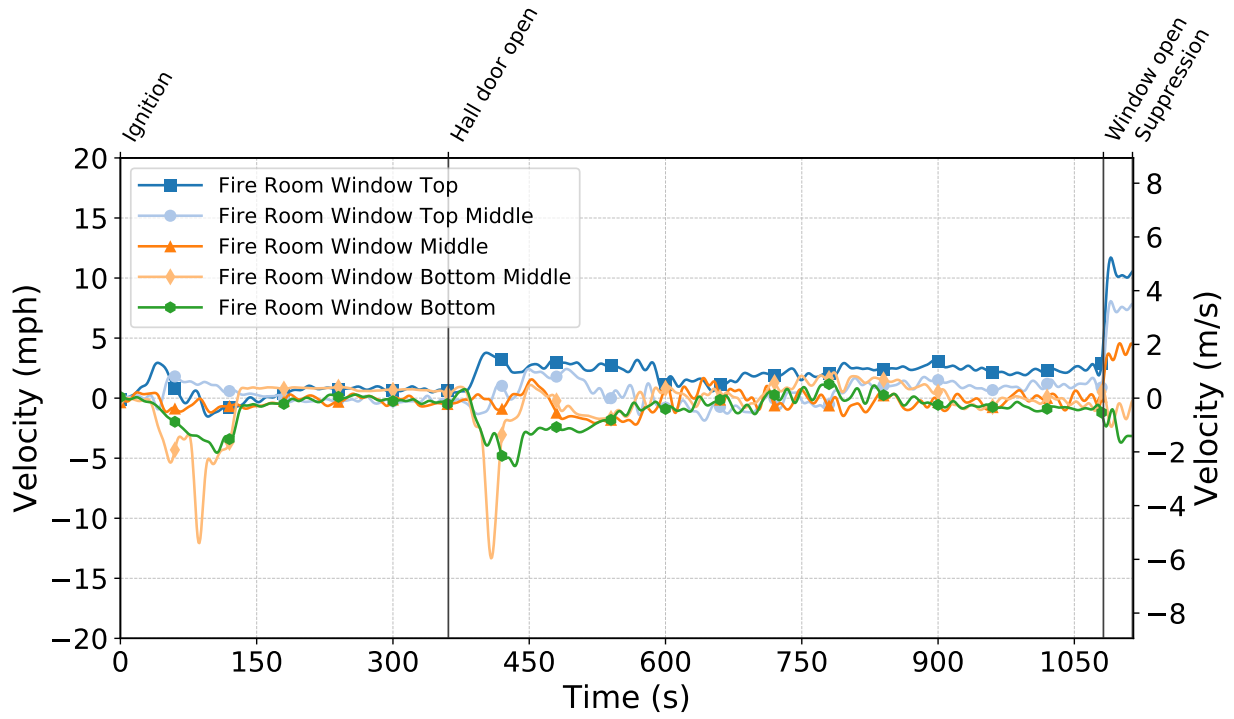


Figure C.99: Gas velocities measured by the fire room window bdp's during Test 9.

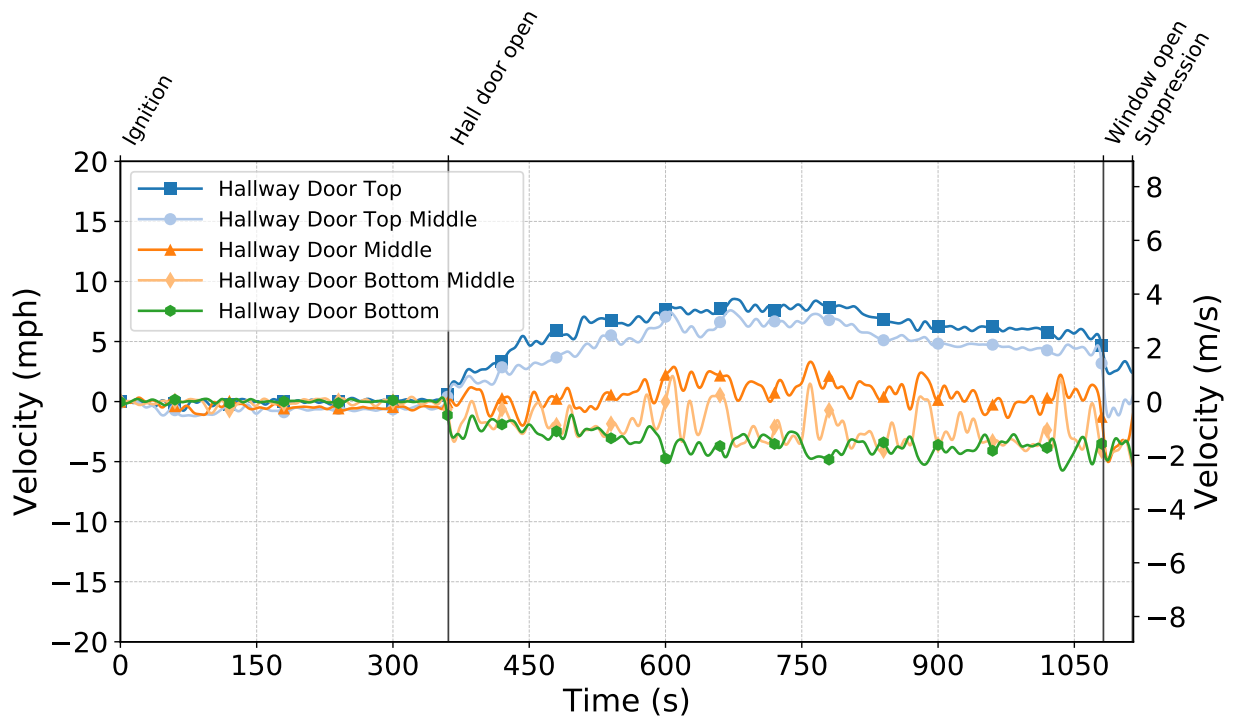


Figure C.100: Gas velocities measured by the hallway door bdp's during Test 9.

Test 10

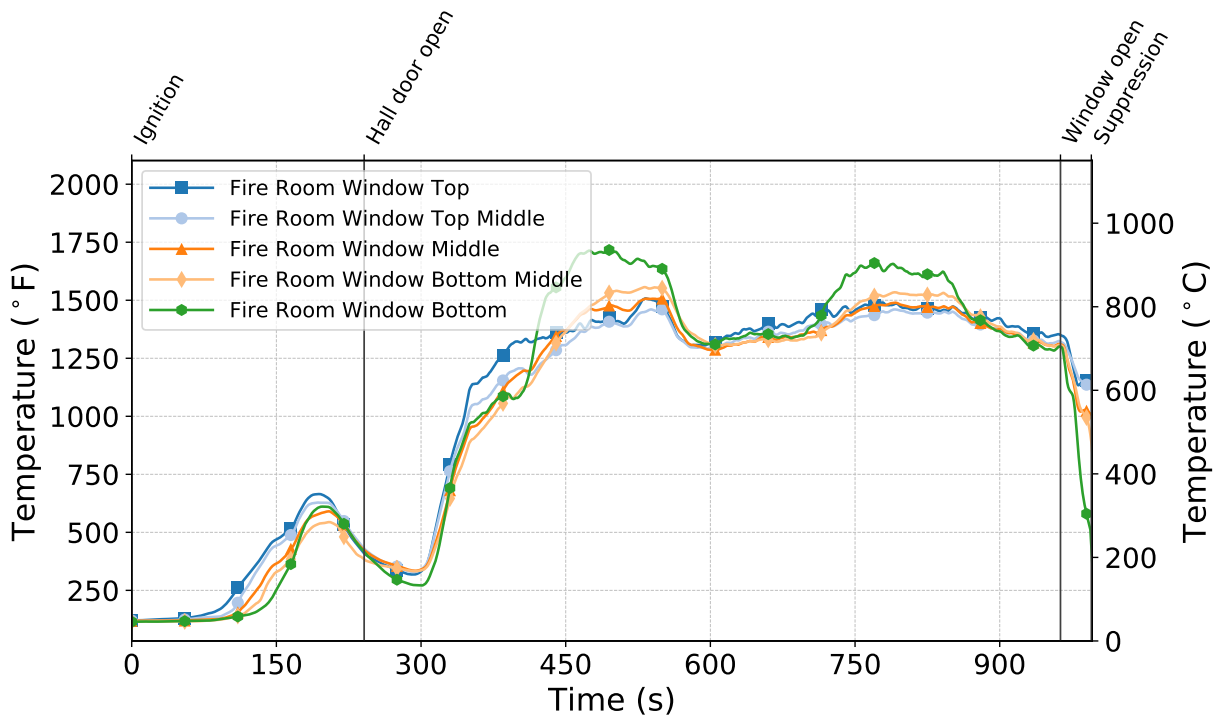


Figure C.101: Temperatures measured by the fire room window thermocouples during Test 10.

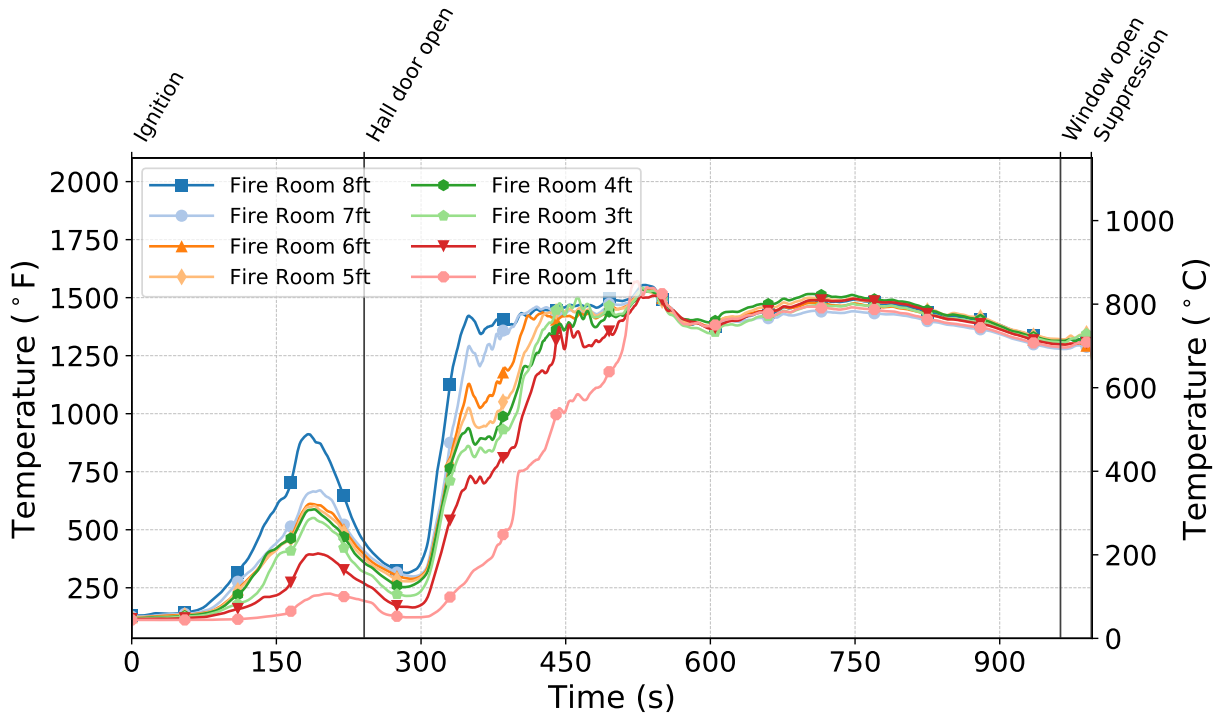


Figure C.102: Temperatures measured by the fire room thermocouples during Test 10.

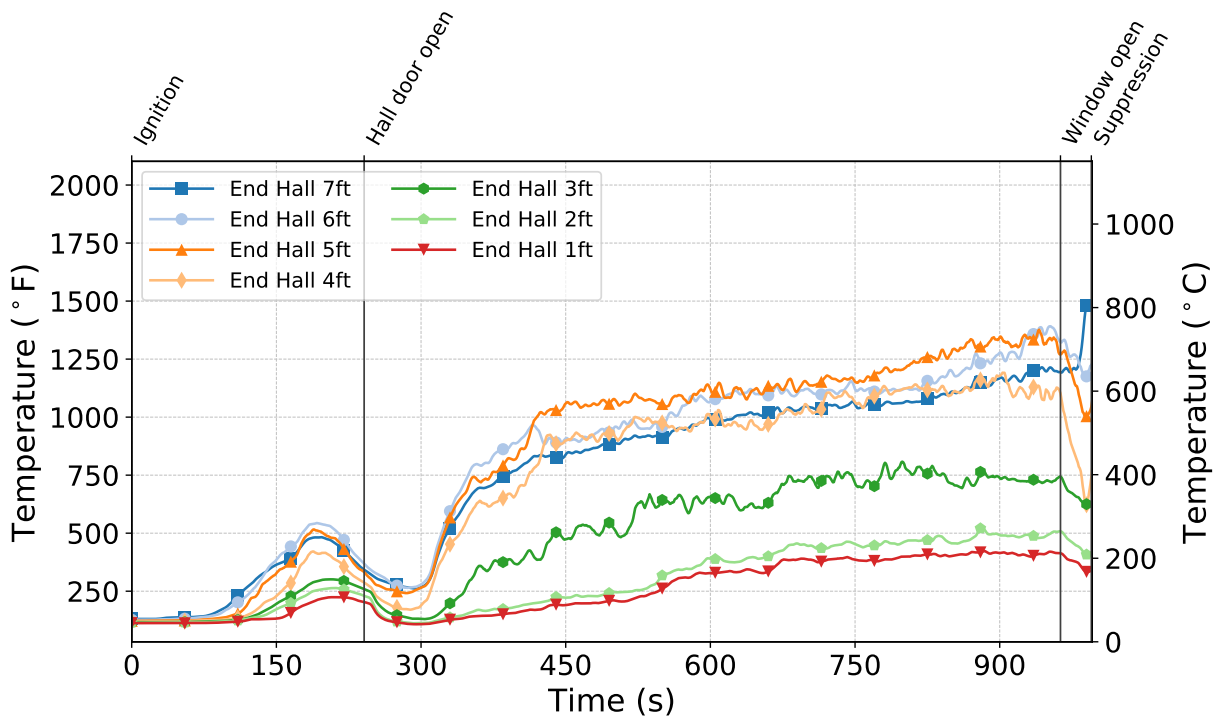


Figure C.103: Temperatures measured by the end hall thermocouples during Test 10.

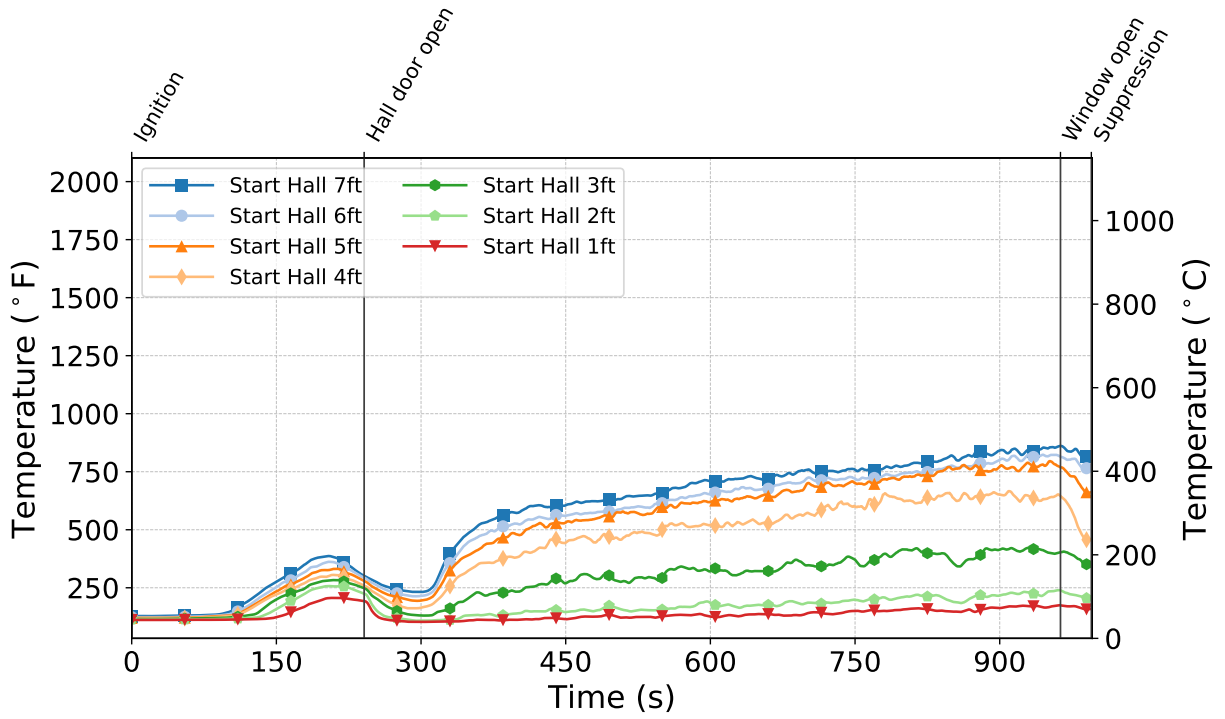


Figure C.104: Temperatures measured by the start hall thermocouples during Test 10.

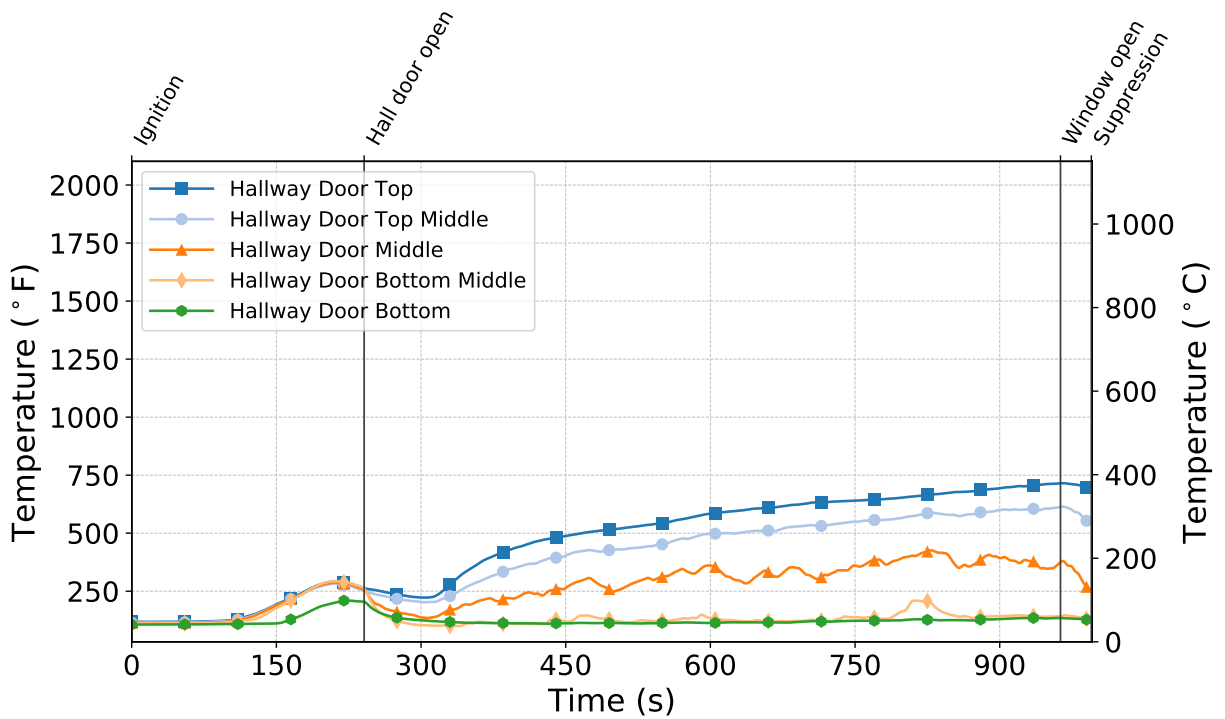


Figure C.105: Temperatures measured by the hallway door thermocouples during Test 10.

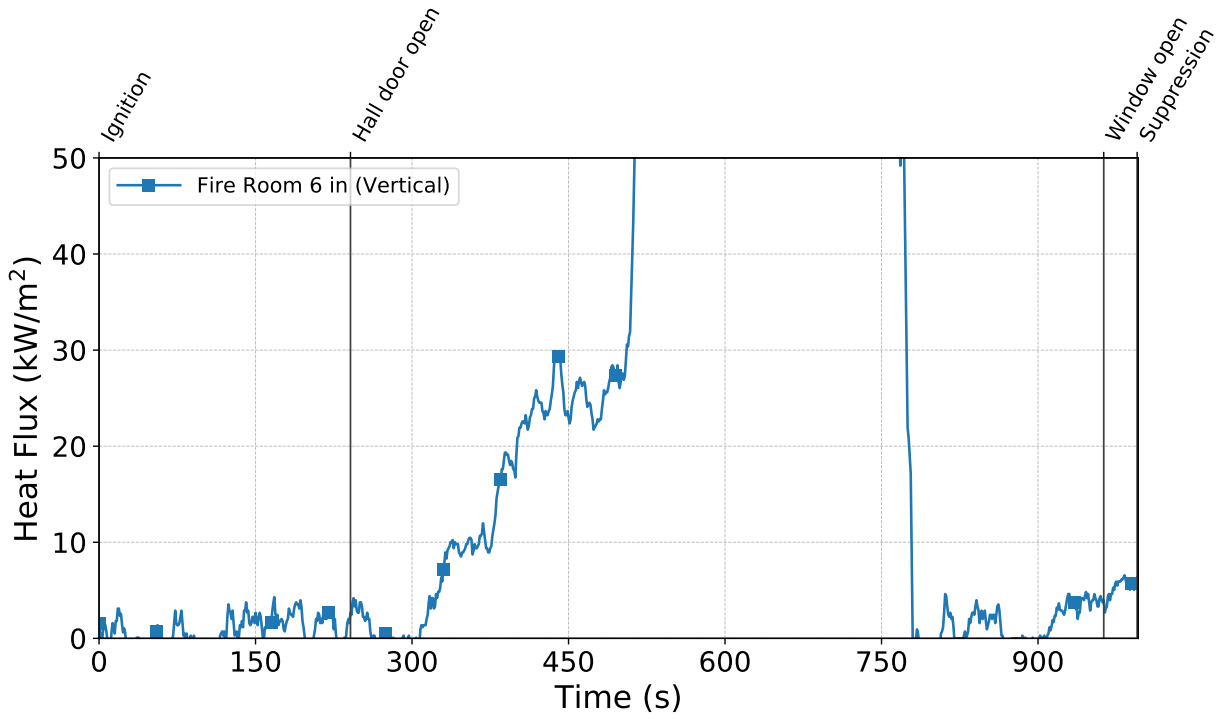


Figure C.106: Heat flux measured by the fire room gauge during Test 10.

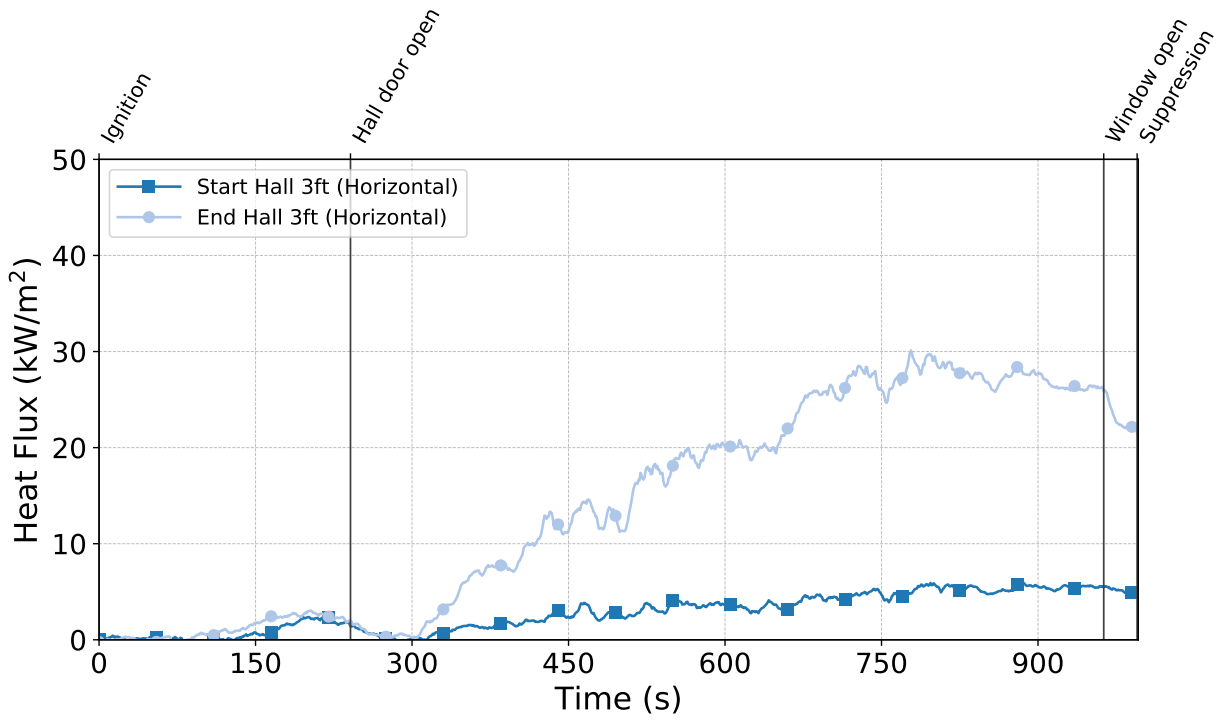


Figure C.107: Heat flux measured by the hallway gauges during Test 10.

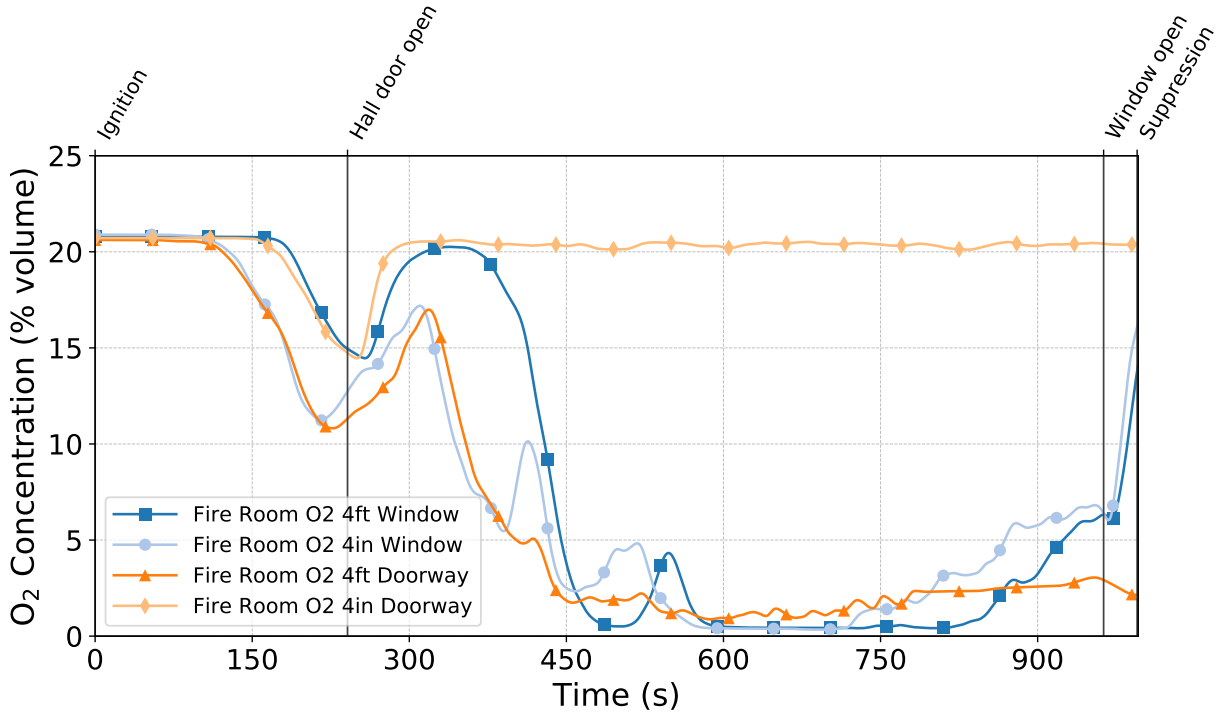


Figure C.108: Oxygen concentrations measured by the fire room gas sampling probes during Test 10.

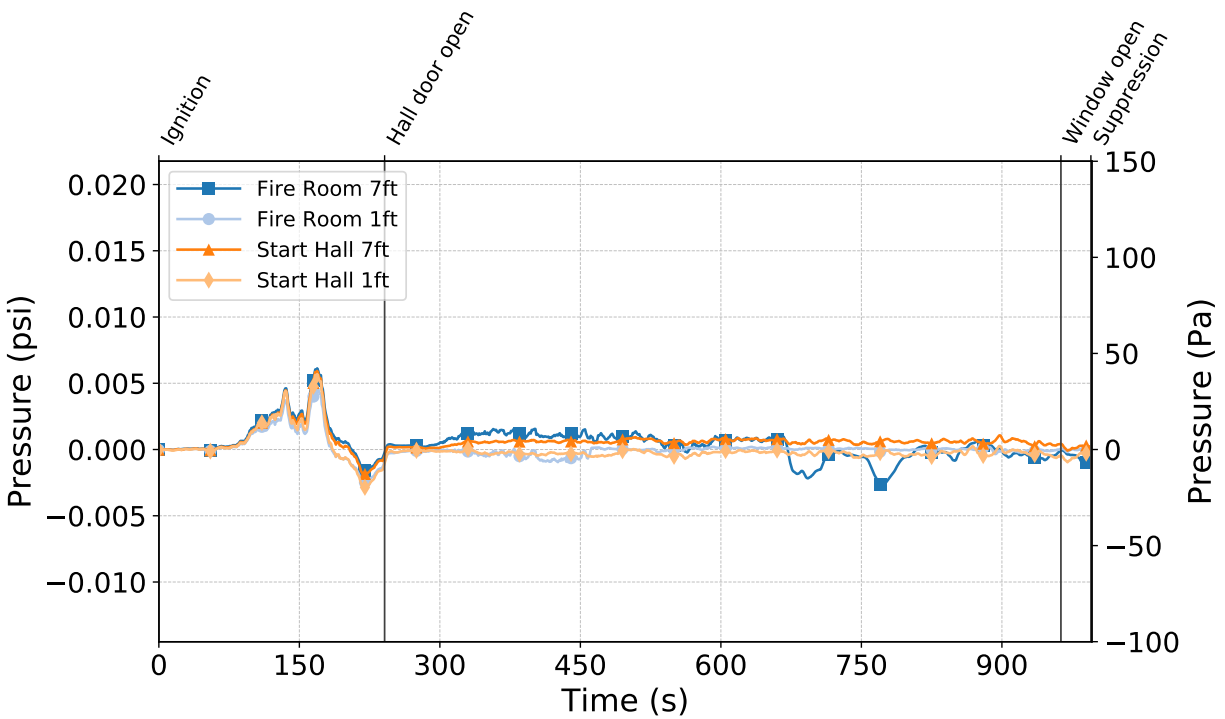


Figure C.109: Pressures measured by the fire room and hallway probes during Test 10.

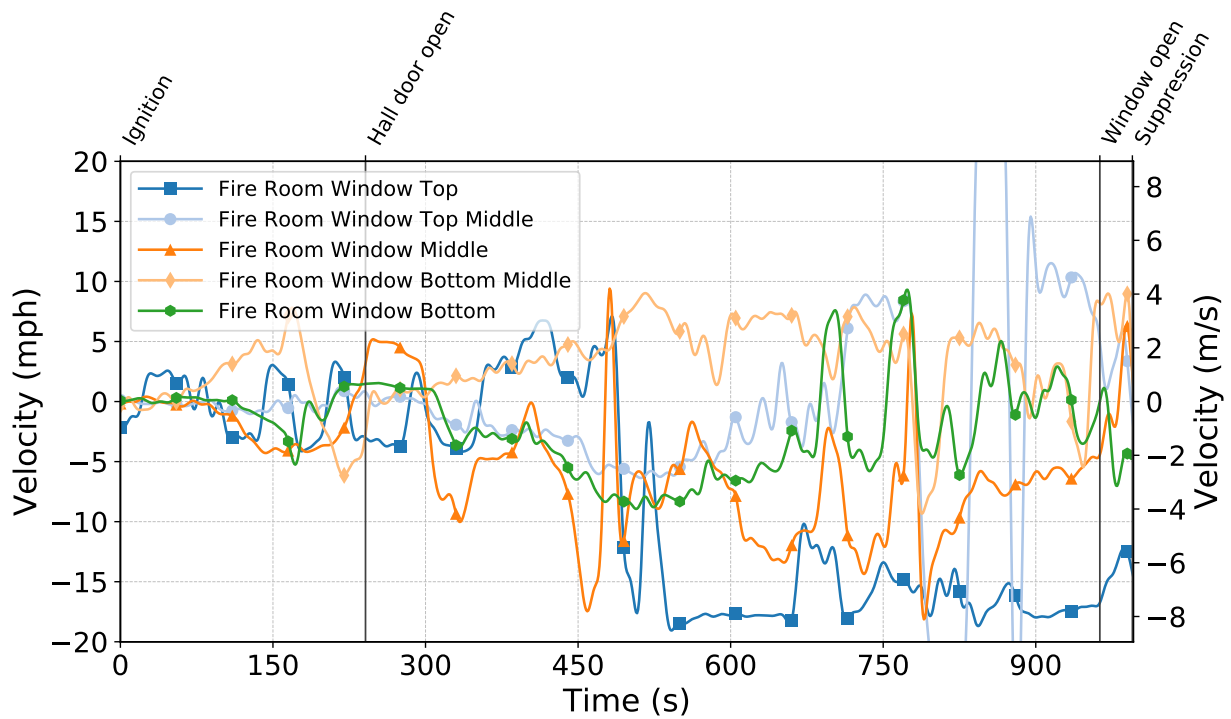


Figure C.110: Gas velocities measured by the fire room window bdps during Test 10.

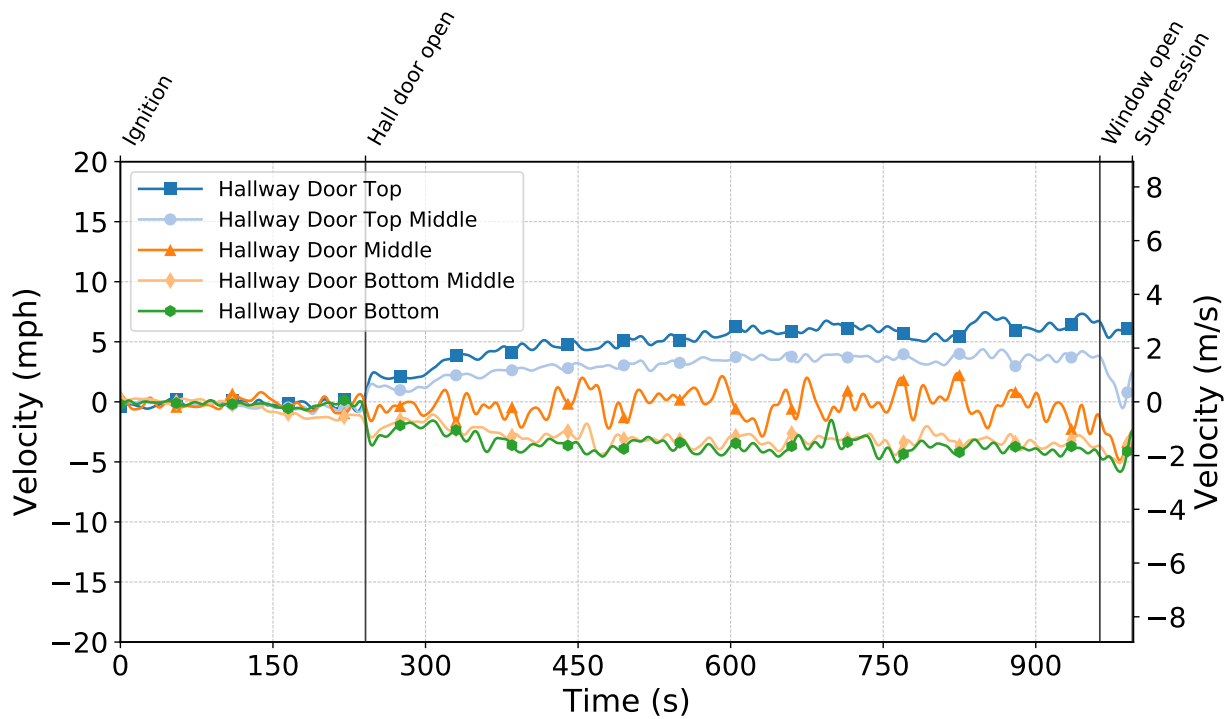


Figure C.111: Gas velocities measured by the hallway door bdps during Test 10.

Test 11

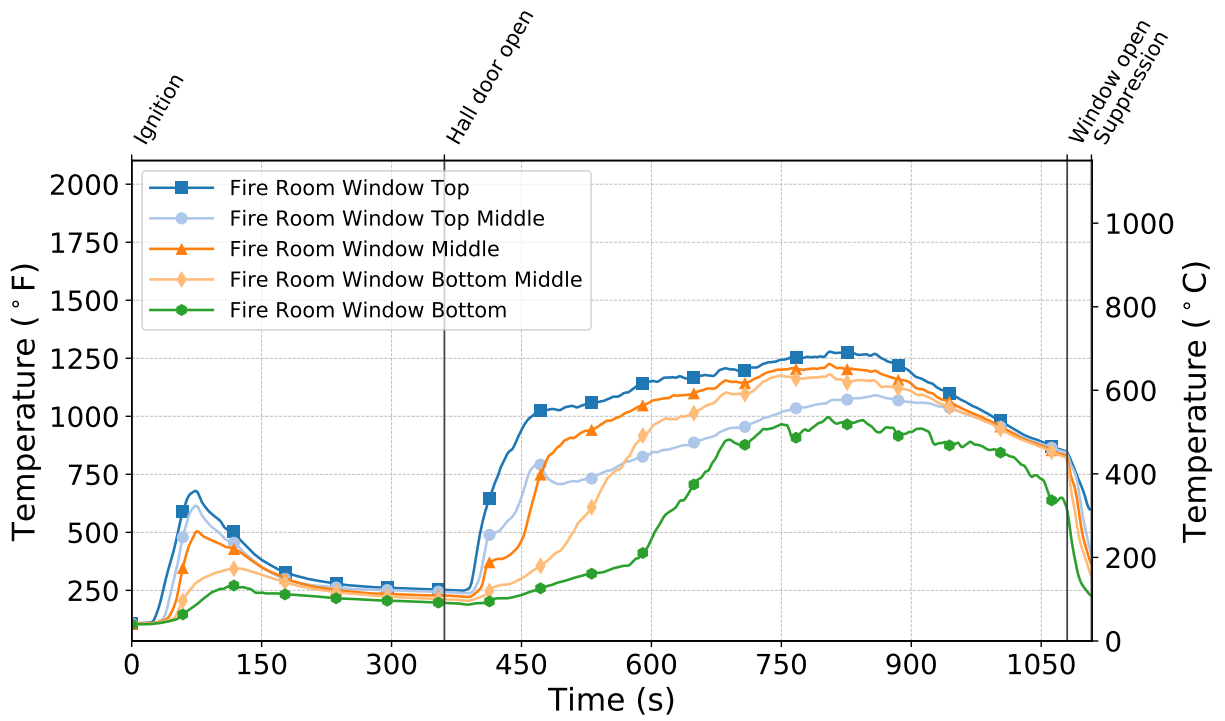


Figure C.112: Temperatures measured by the fire room window thermocouples during Test 11.

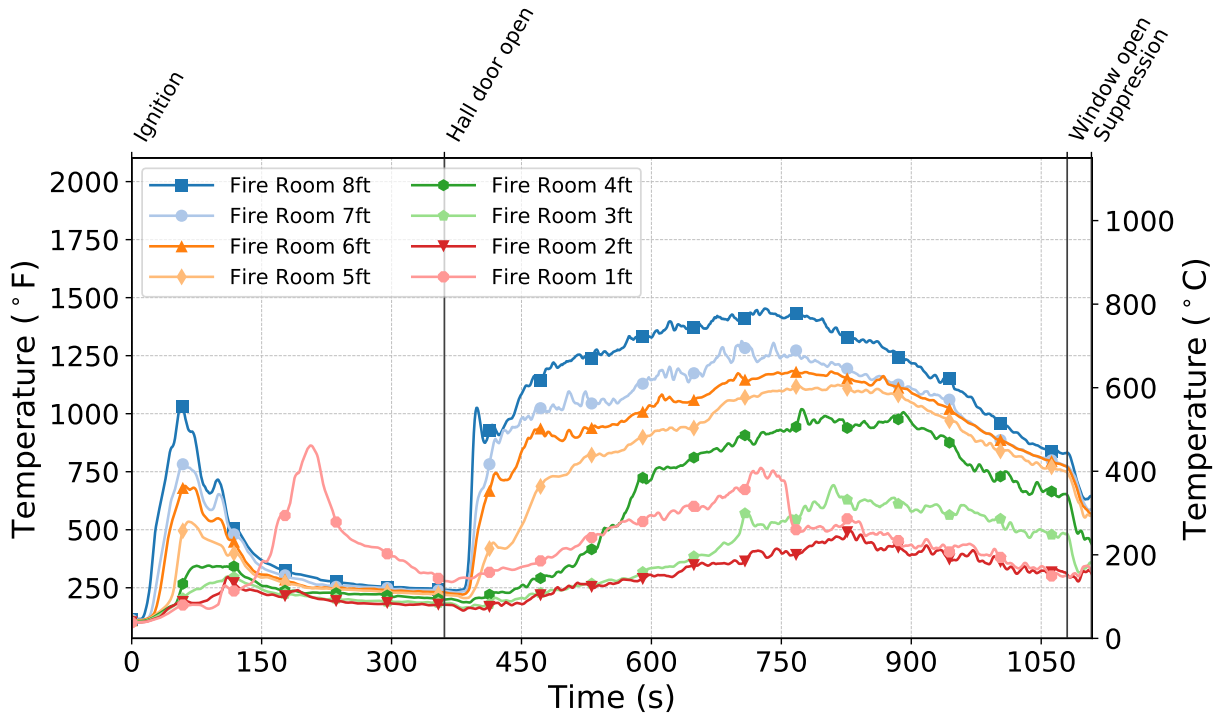


Figure C.113: Temperatures measured by the fire room thermocouples during Test 11.

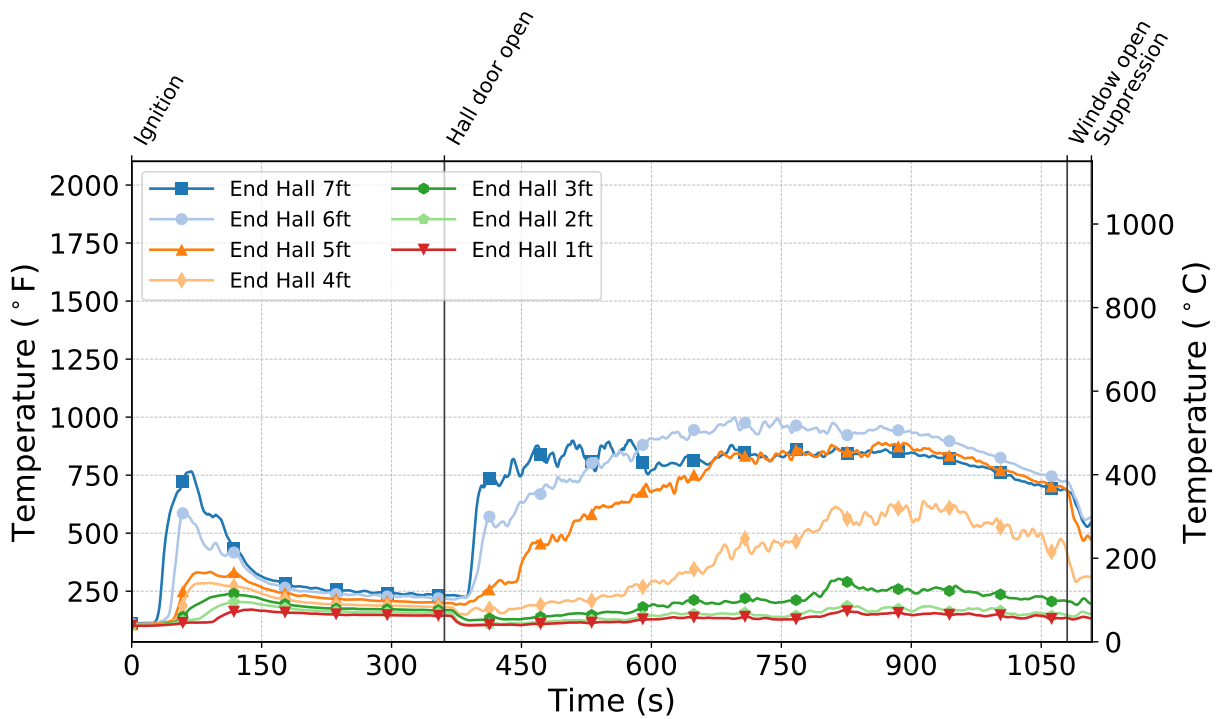


Figure C.114: Temperatures measured by the end hall thermocouples during Test 11.

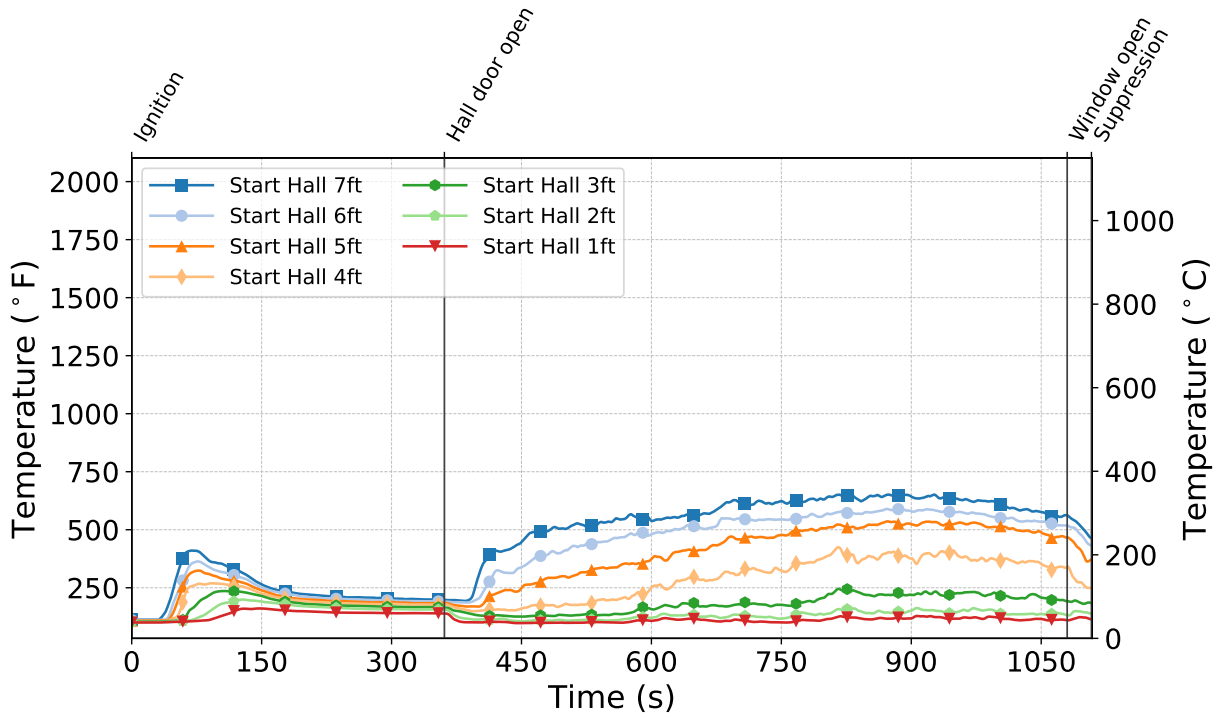


Figure C.115: Temperatures measured by the start hall thermocouples during Test 11.

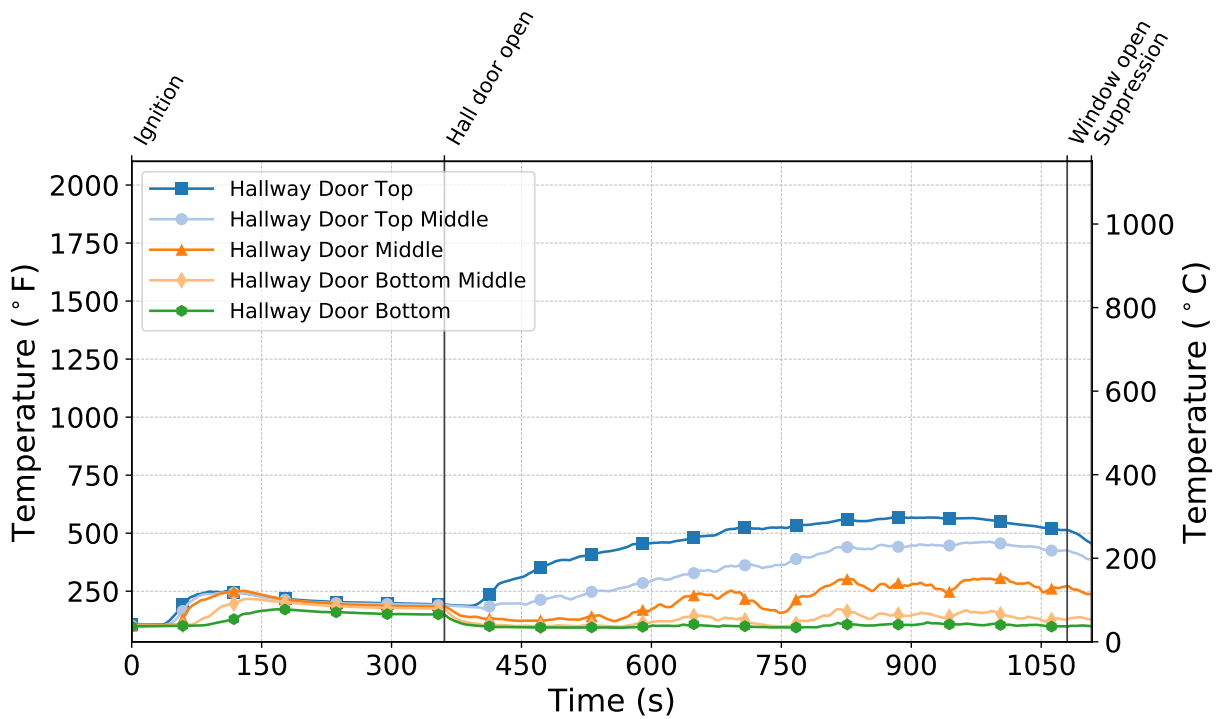


Figure C.116: Temperatures measured by the hallway door thermocouples during Test 11.

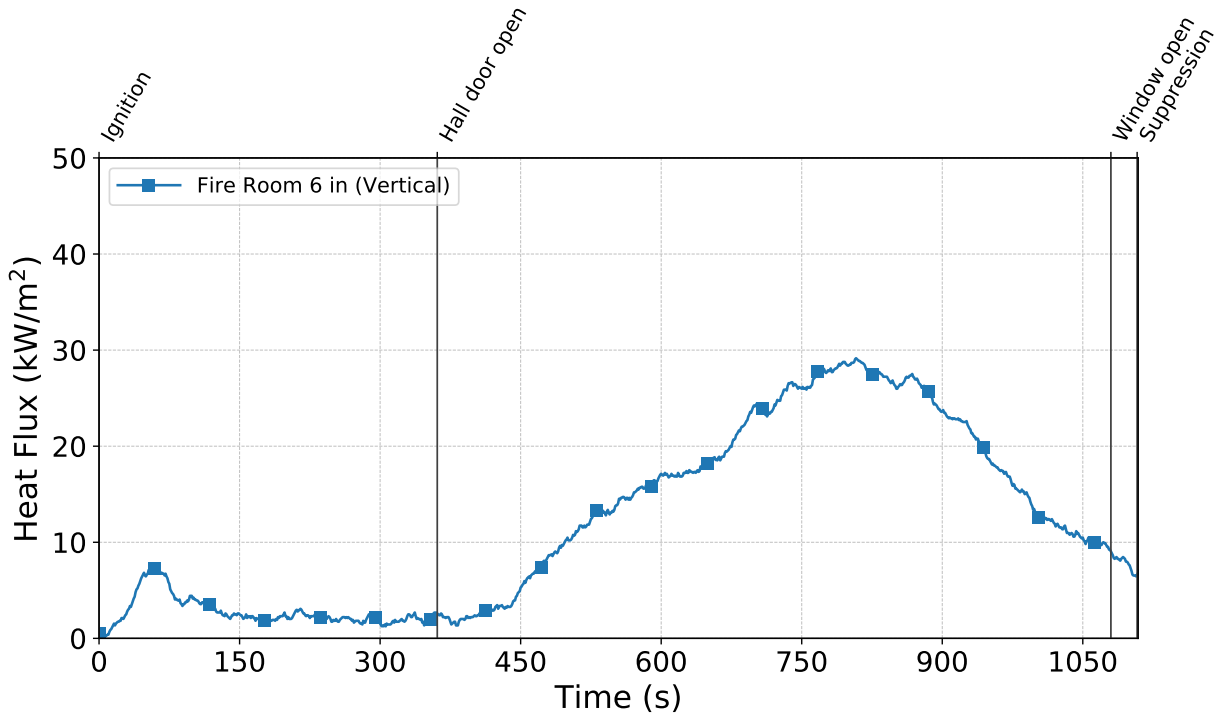


Figure C.117: Heat flux measured by the fire room gauge during Test 11.

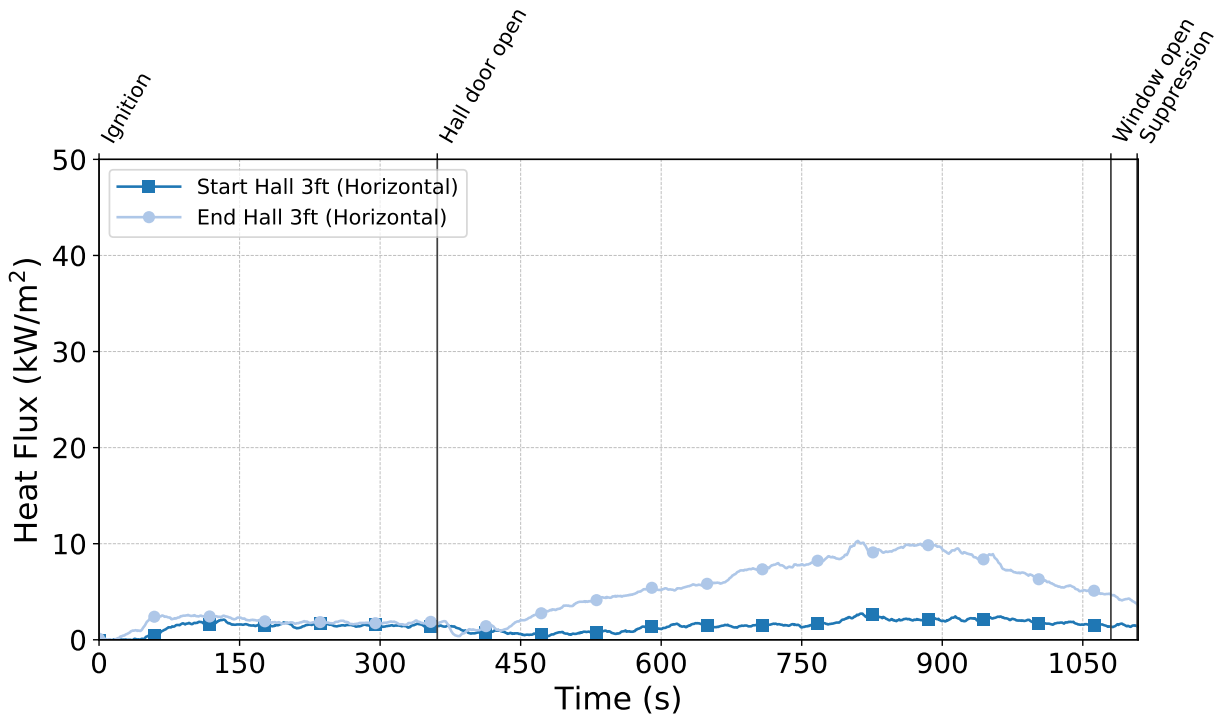


Figure C.118: Heat flux measured by the hallway gauges during Test 11.

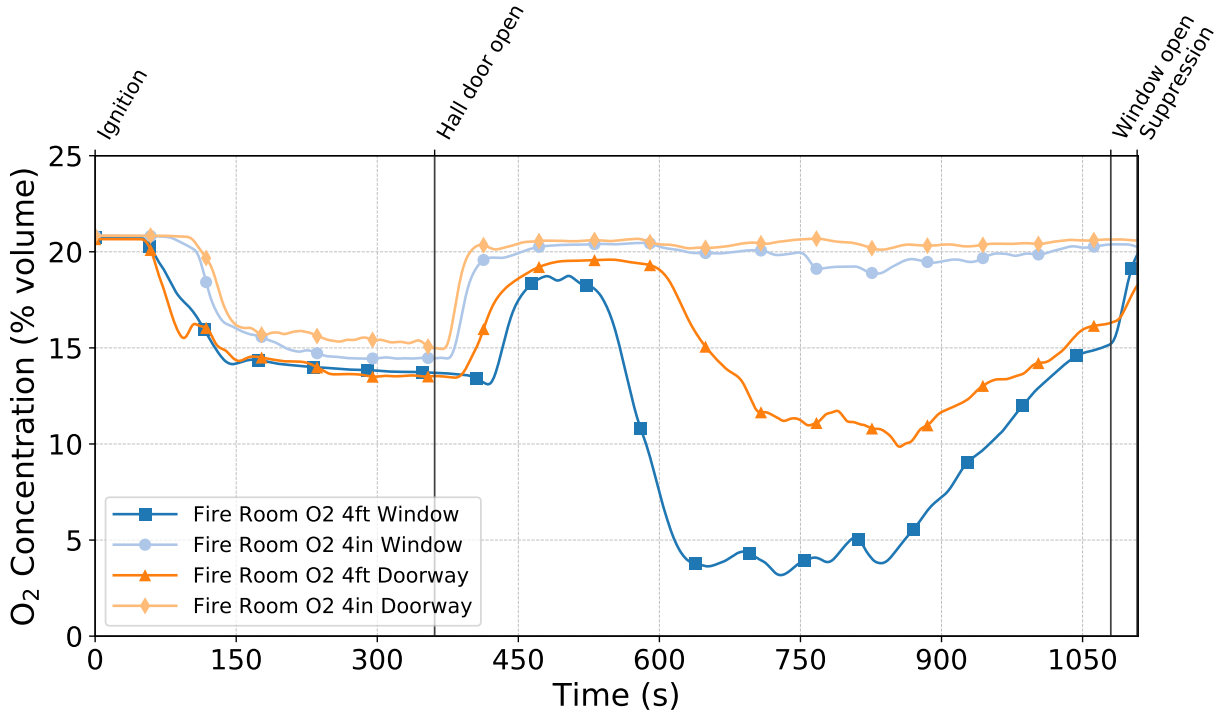


Figure C.119: Oxygen concentrations measured by the fire room gas sampling probes during Test 11.

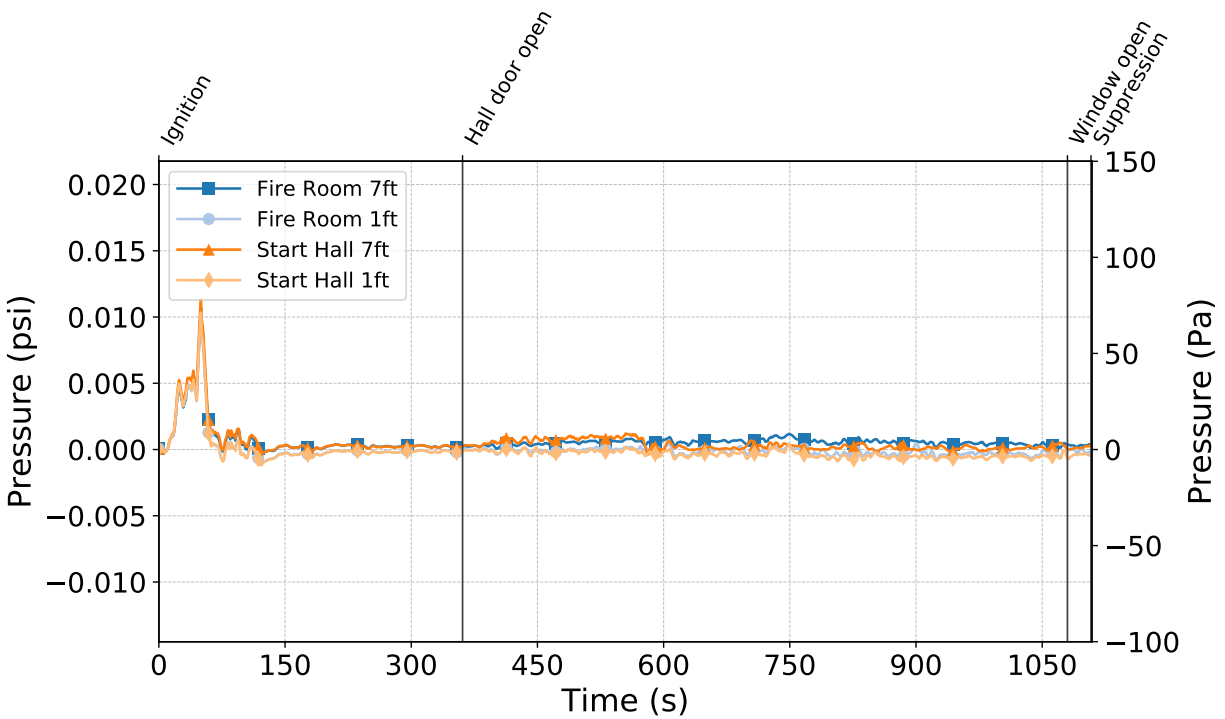


Figure C.120: Pressures measured by the fire room and hallway probes during Test 11.

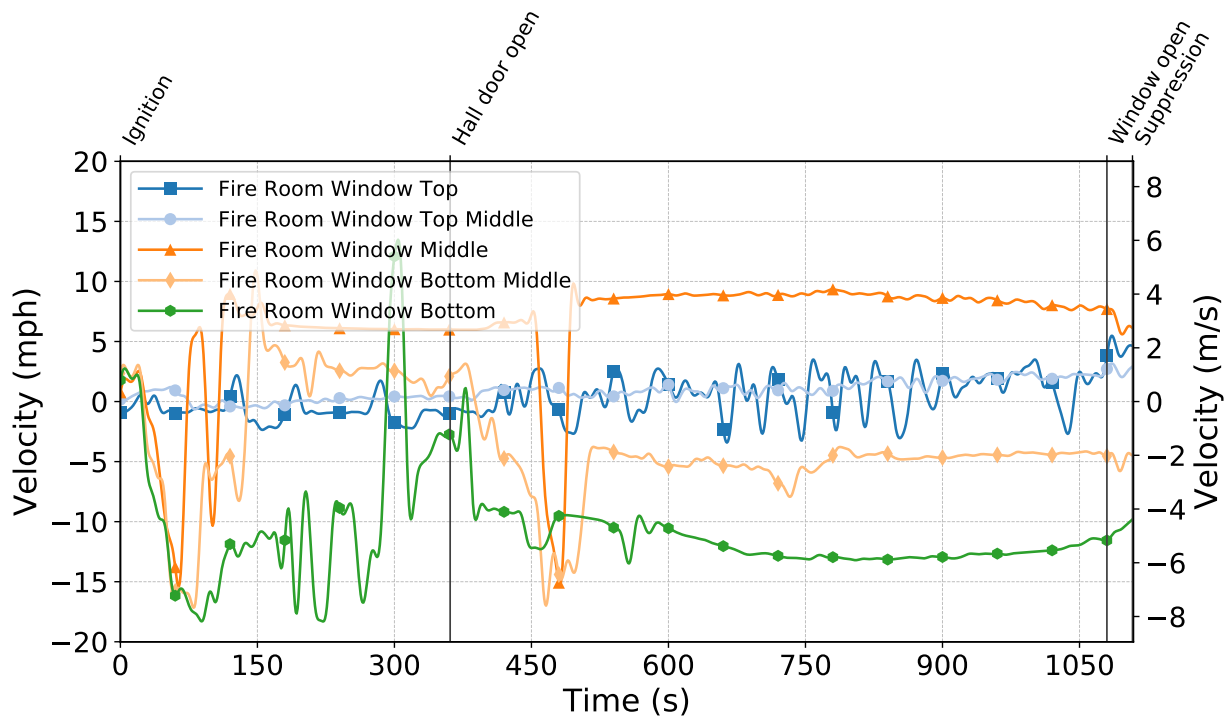


Figure C.121: Gas velocities measured by the fire room window bdps during Test 11.

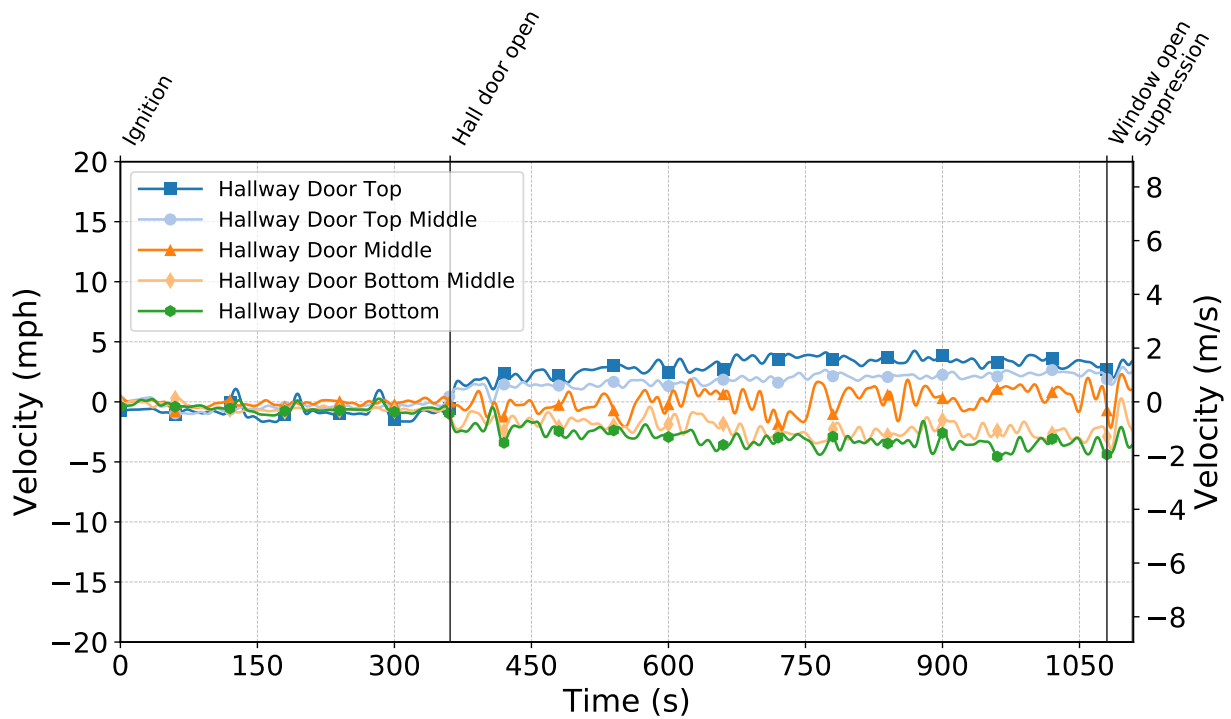


Figure C.122: Gas velocities measured by the hallway door bdps during Test 11.

Test 12

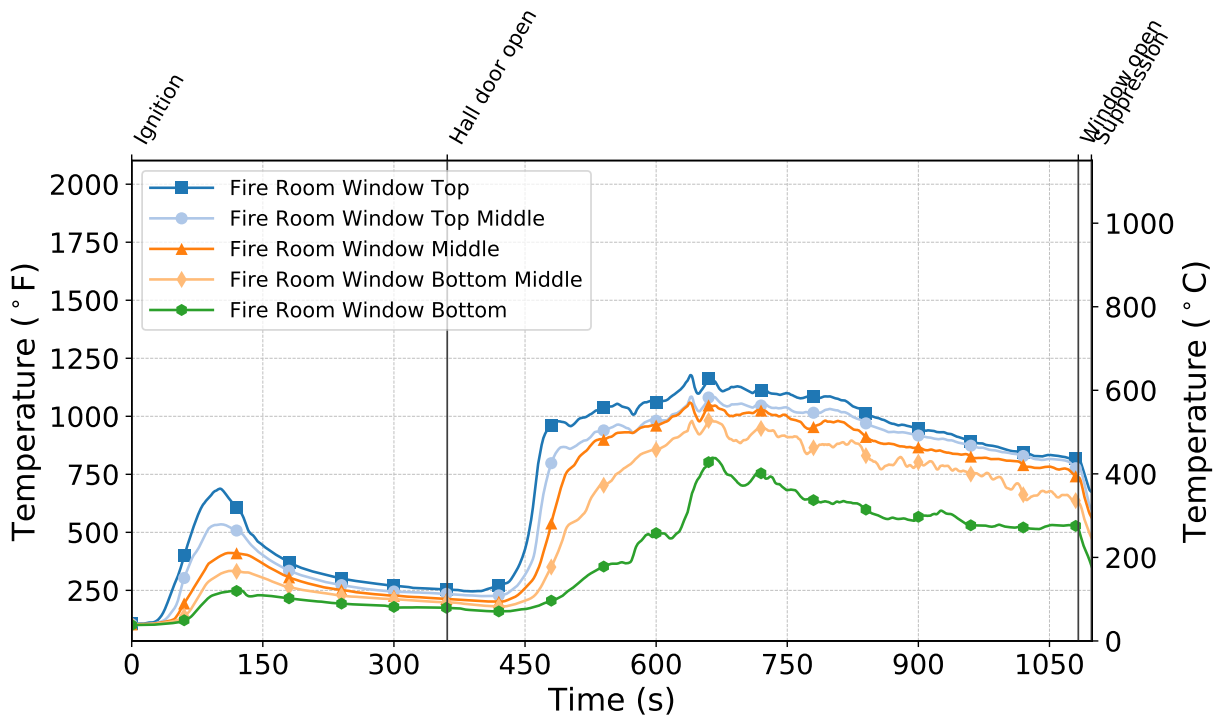


Figure C.123: Temperatures measured by the fire room window thermocouples during Test 12.

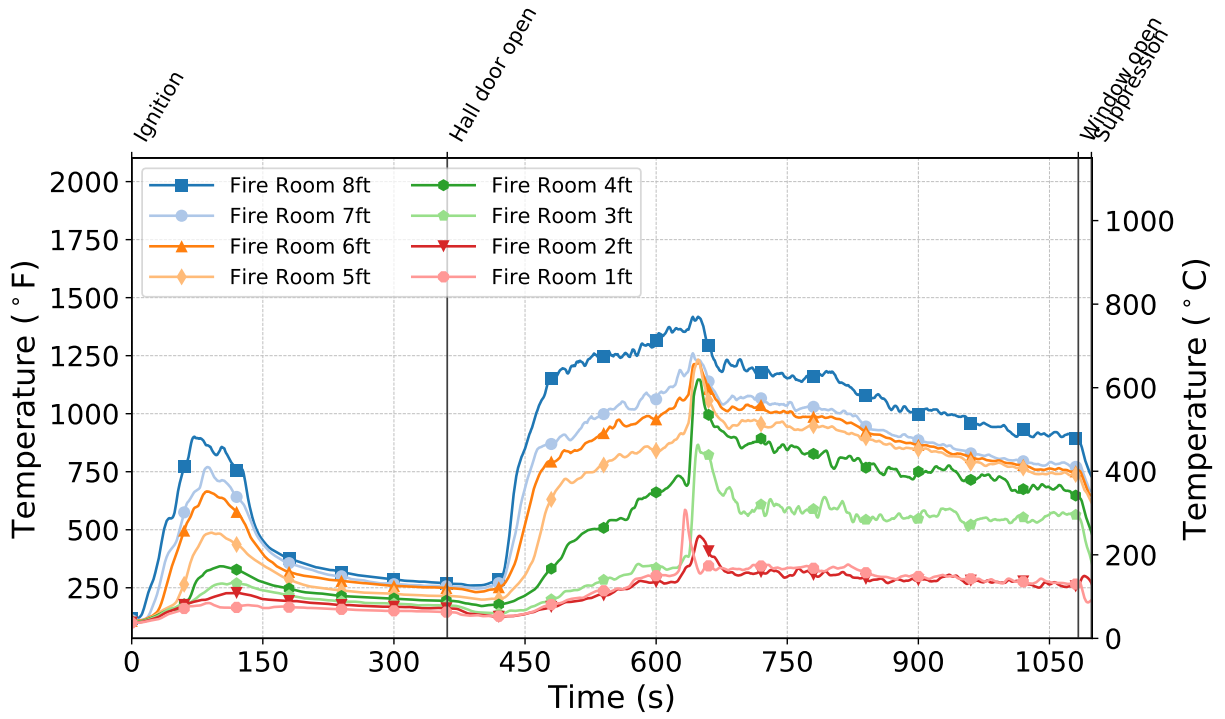


Figure C.124: Temperatures measured by the fire room thermocouples during Test 12.

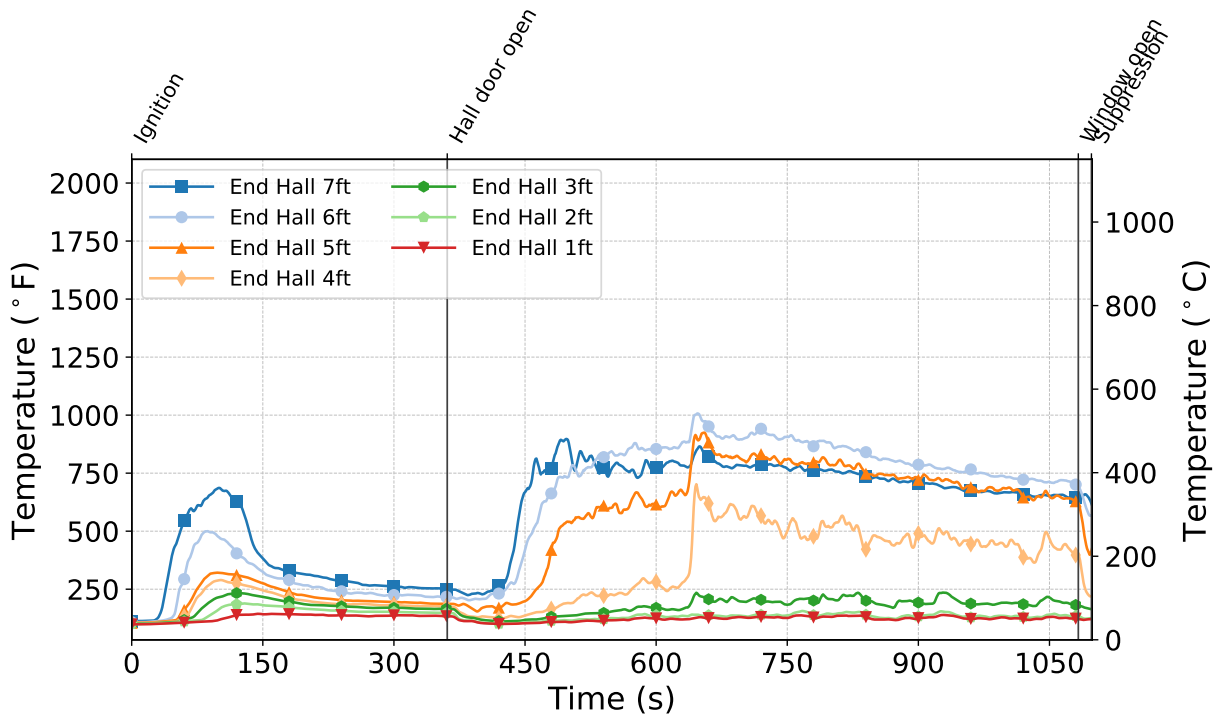


Figure C.125: Temperatures measured by the end hall thermocouples during Test 12.

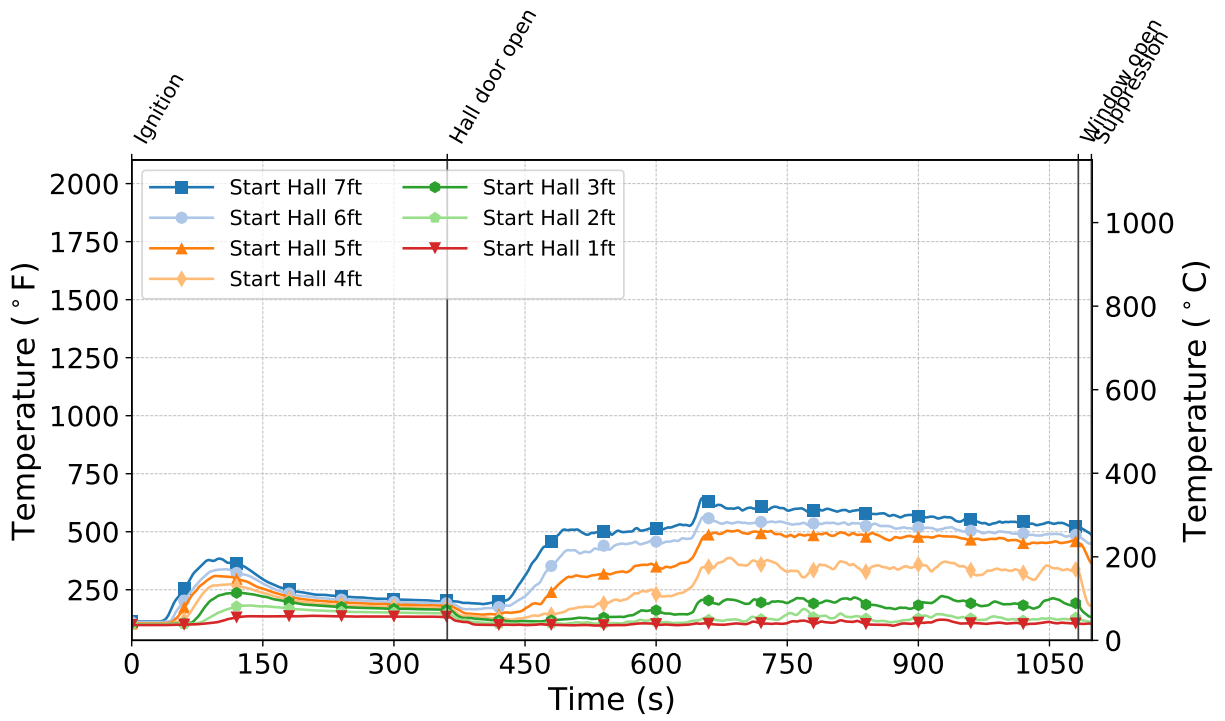


Figure C.126: Temperatures measured by the start hall thermocouples during Test 12.

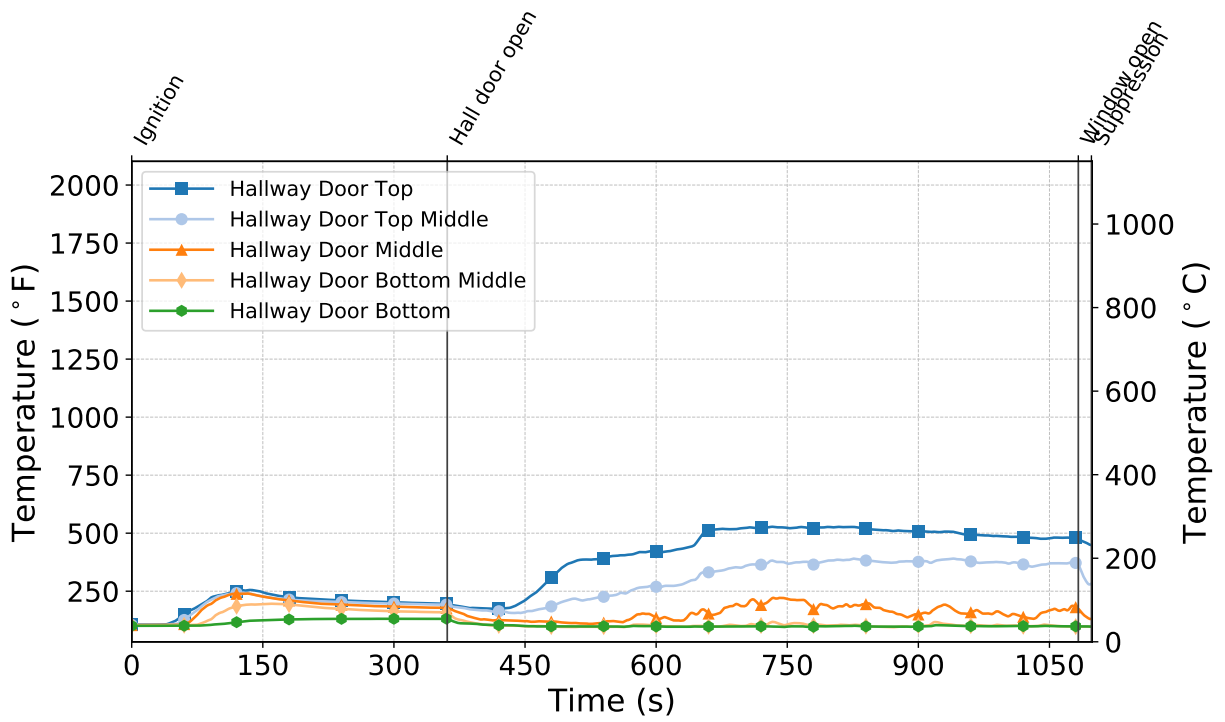


Figure C.127: Temperatures measured by the hallway door thermocouples during Test 12.

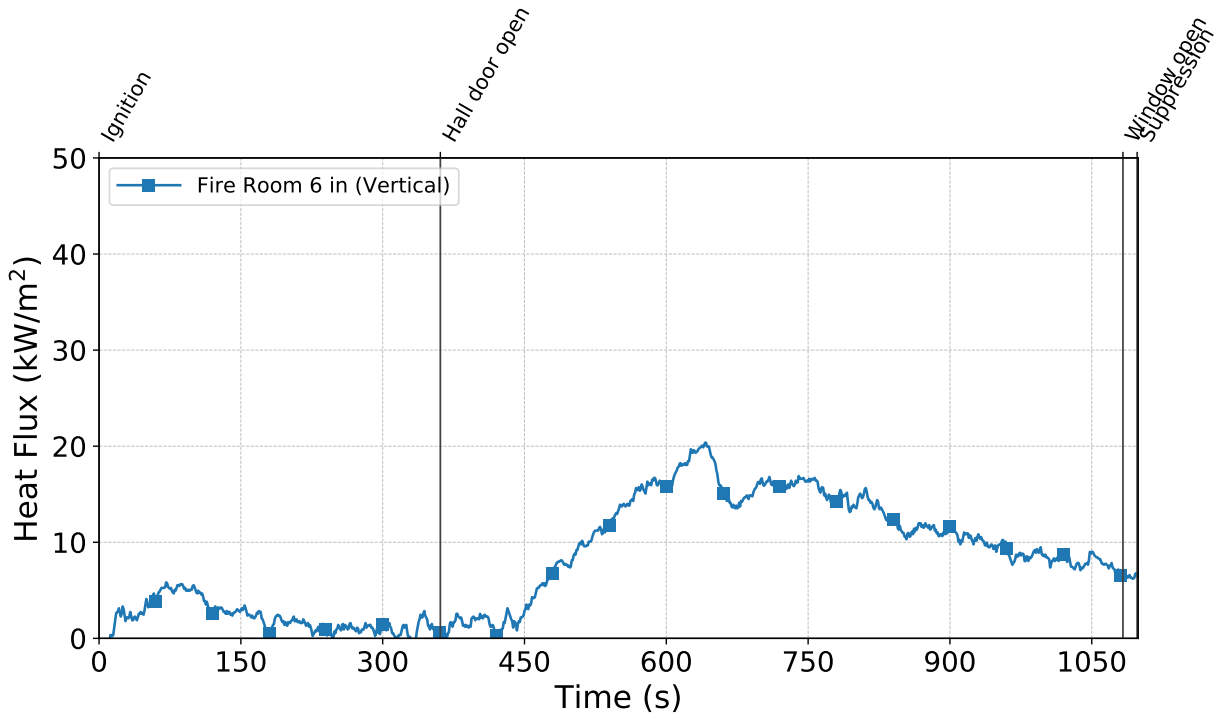


Figure C.128: Heat flux measured by the fire room gauge during Test 12.

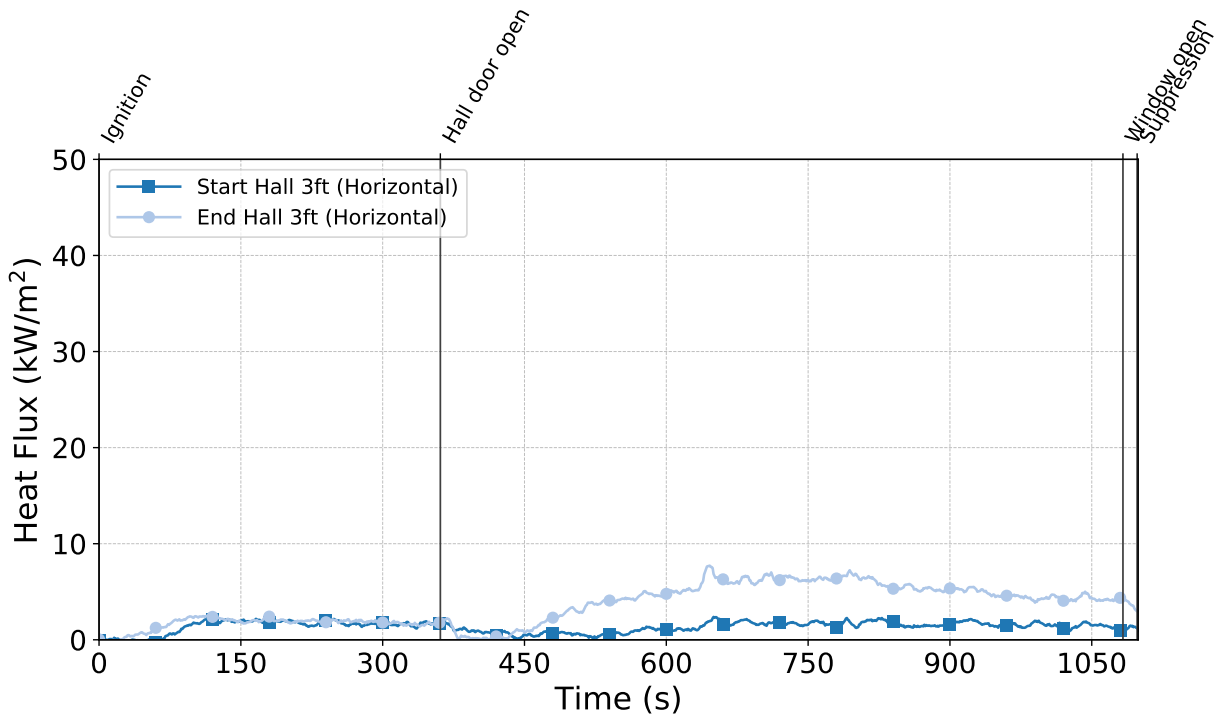


Figure C.129: Heat flux measured by the hallway gauges during Test 12.

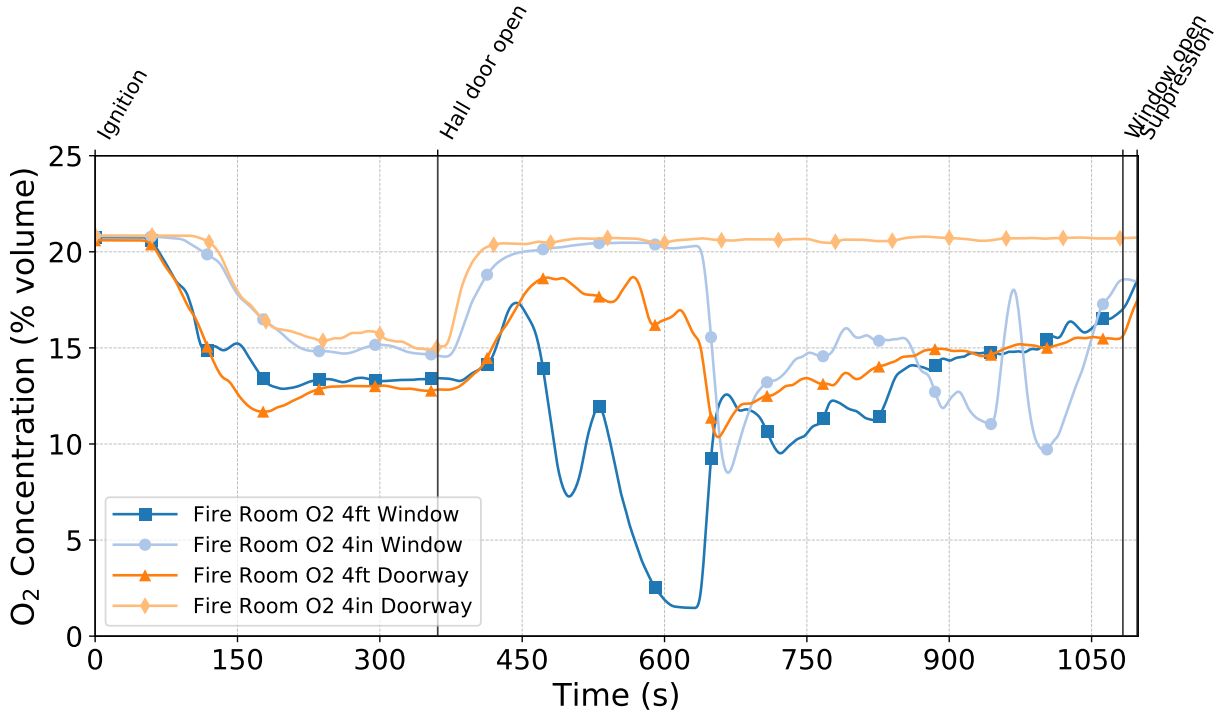


Figure C.130: Oxygen concentrations measured by the fire room gas sampling probes during Test 12.

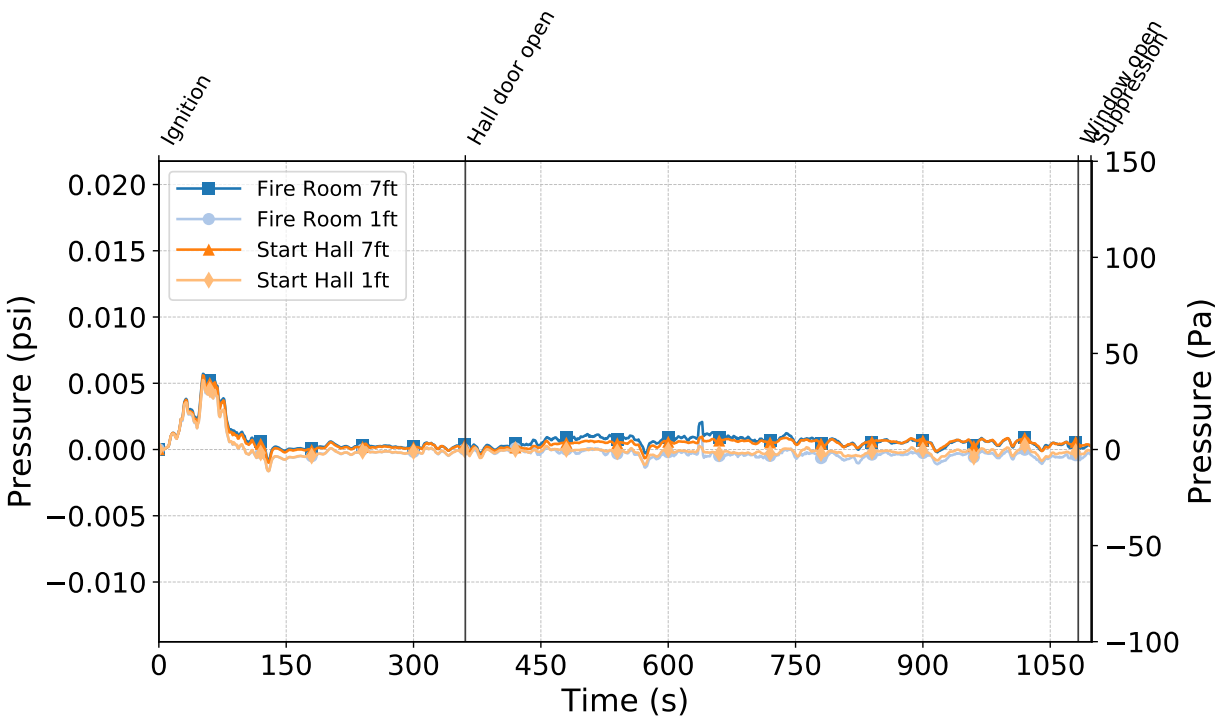


Figure C.131: Pressures measured by the fire room and hallway probes during Test 12.

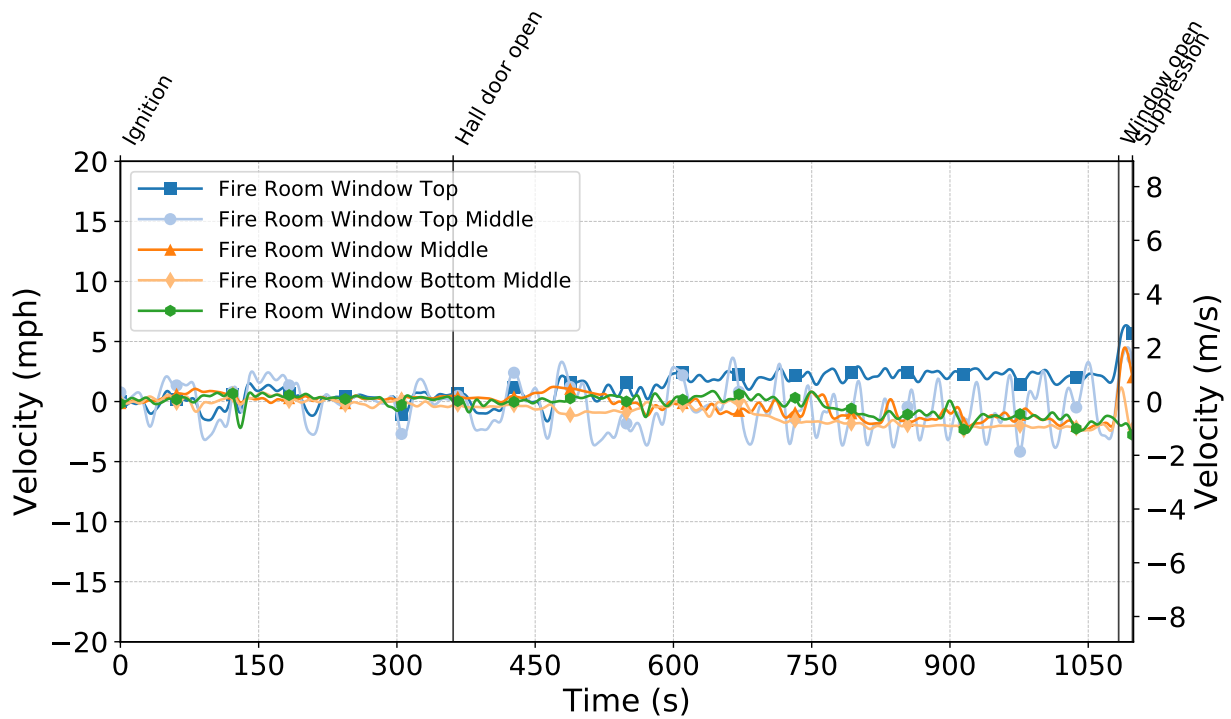


Figure C.132: Gas velocities measured by the fire room window bdps during Test 12.

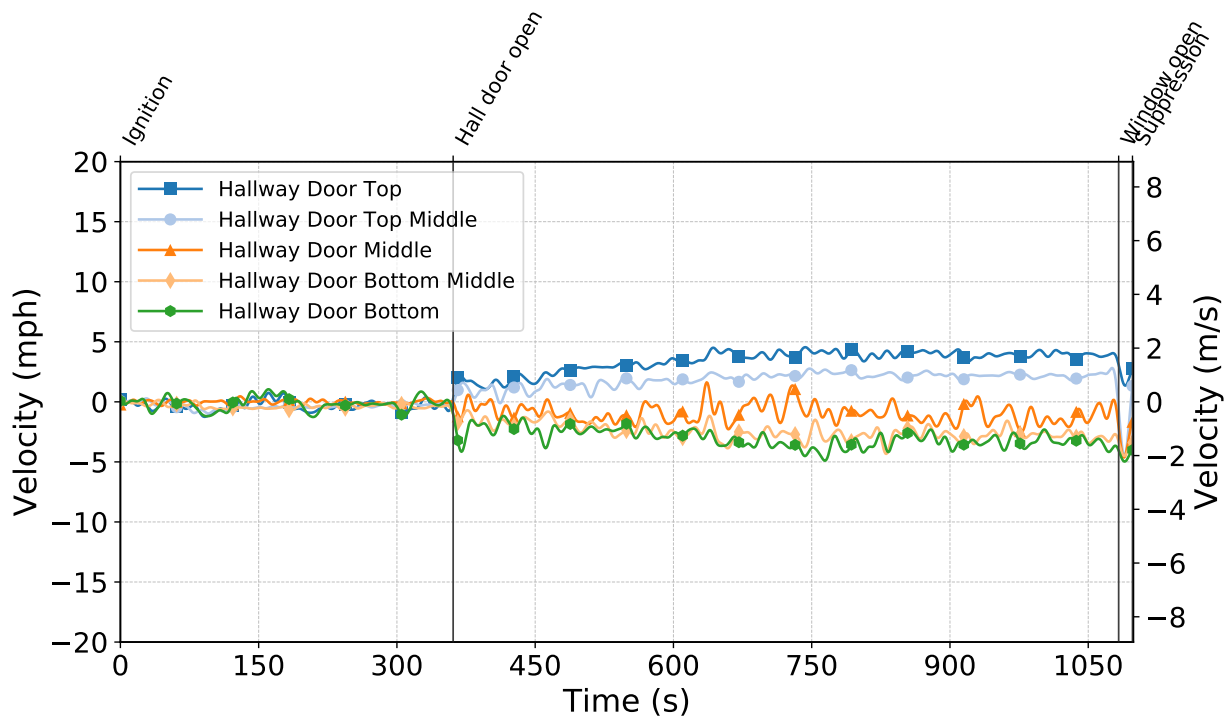


Figure C.133: Gas velocities measured by the hallway door bdps during Test 12.

Test 13

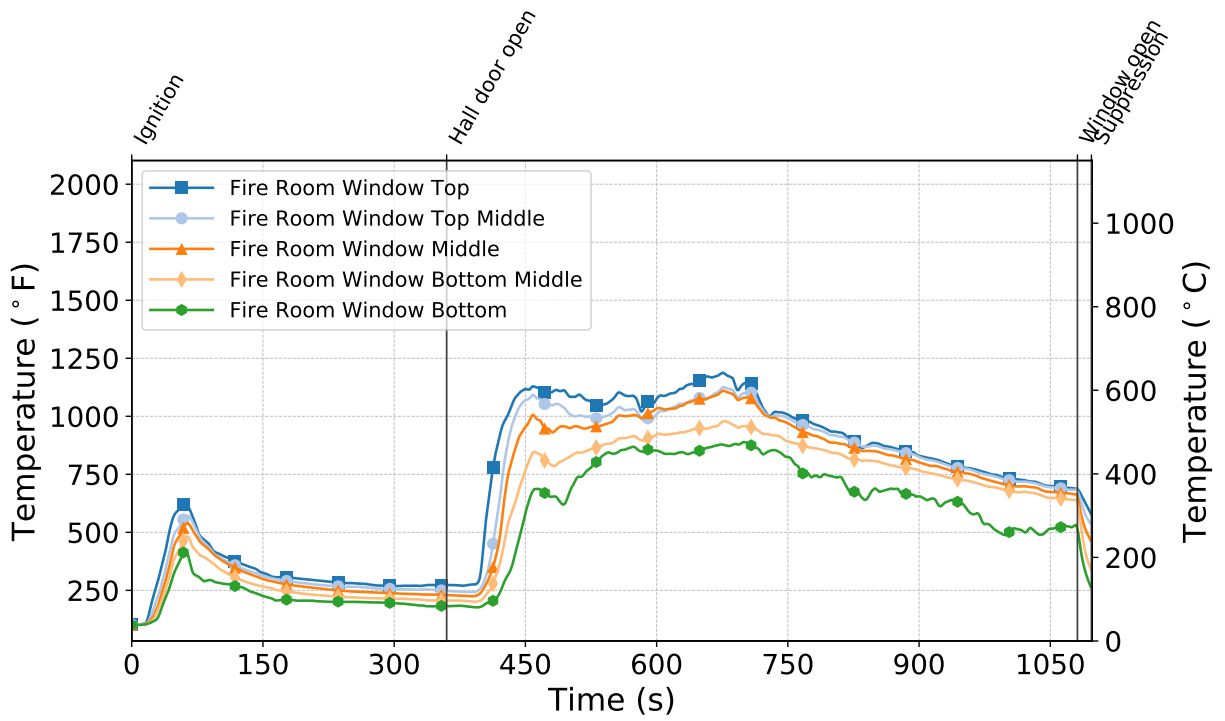


Figure C.134: Temperatures measured by the fire room window thermocouples during Test 13.

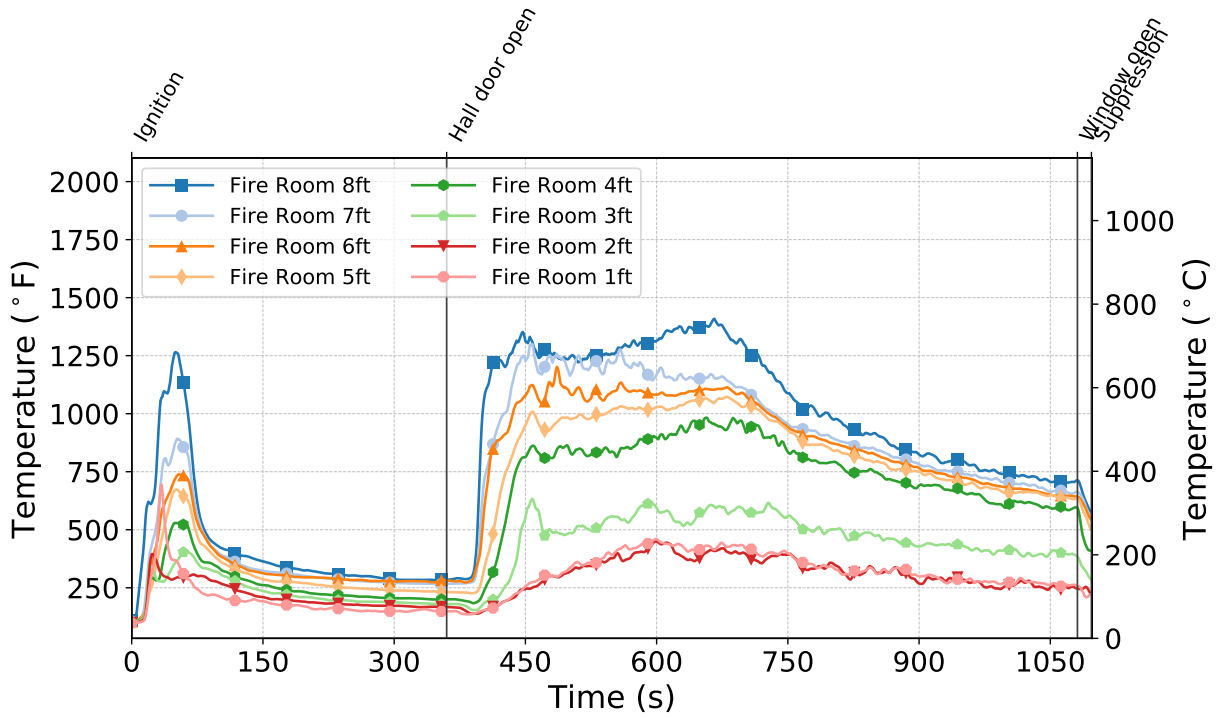


Figure C.135: Temperatures measured by the fire room thermocouples during Test 13.

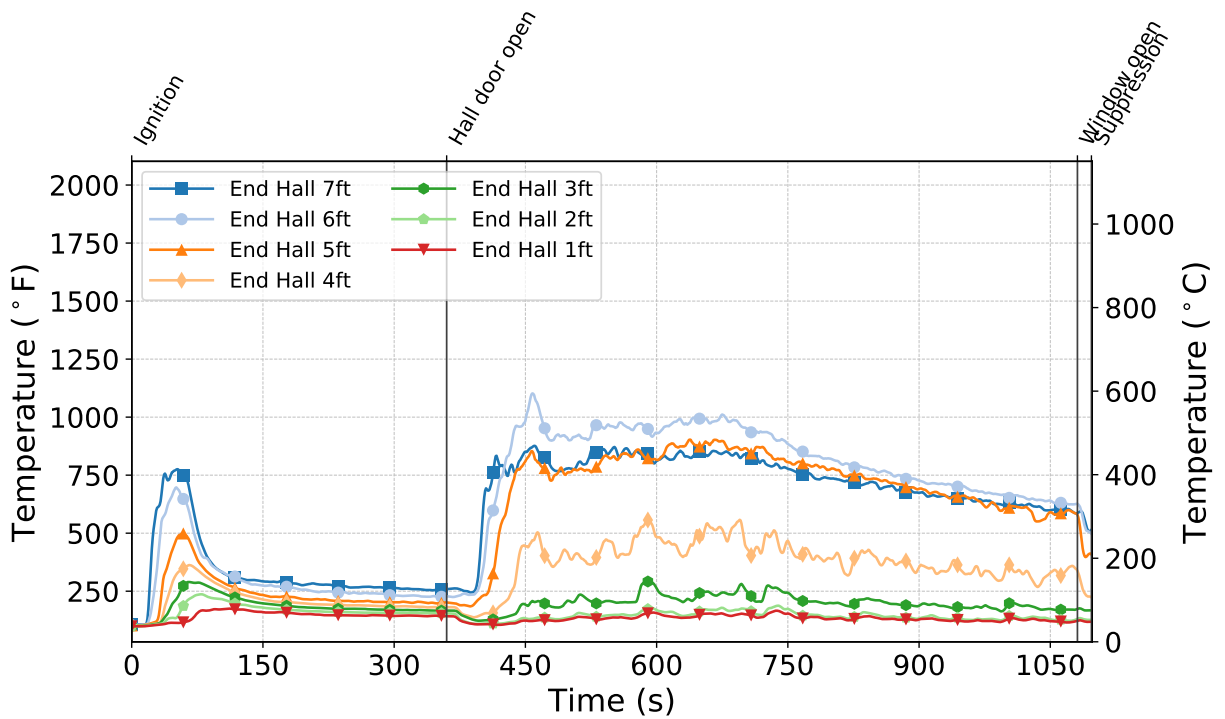


Figure C.136: Temperatures measured by the end hall thermocouples during Test 13.

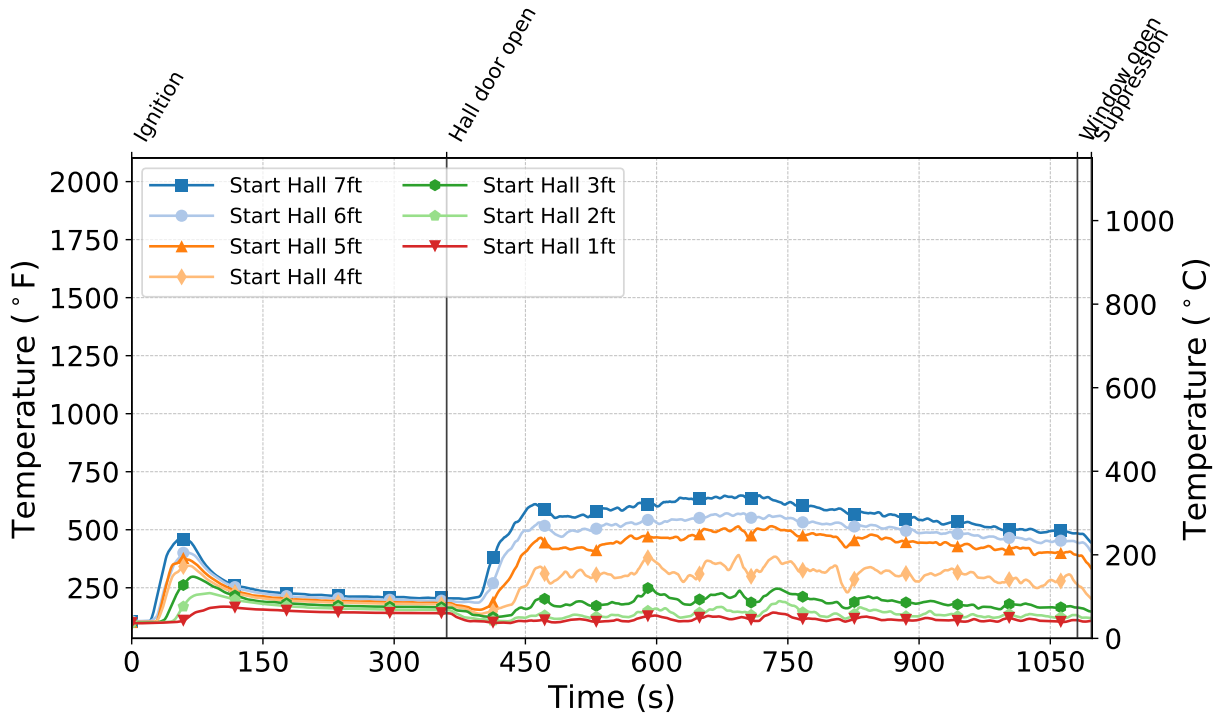


Figure C.137: Temperatures measured by the start hall thermocouples during Test 13.

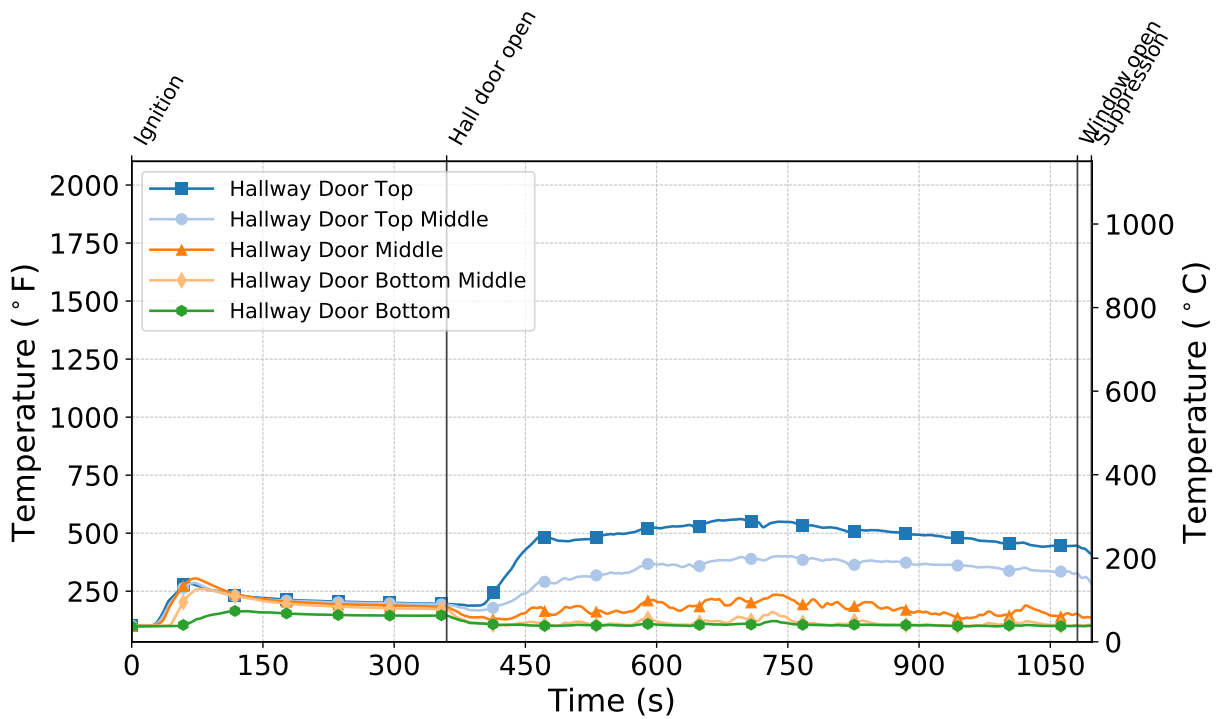


Figure C.138: Temperatures measured by the hallway door thermocouples during Test 13.

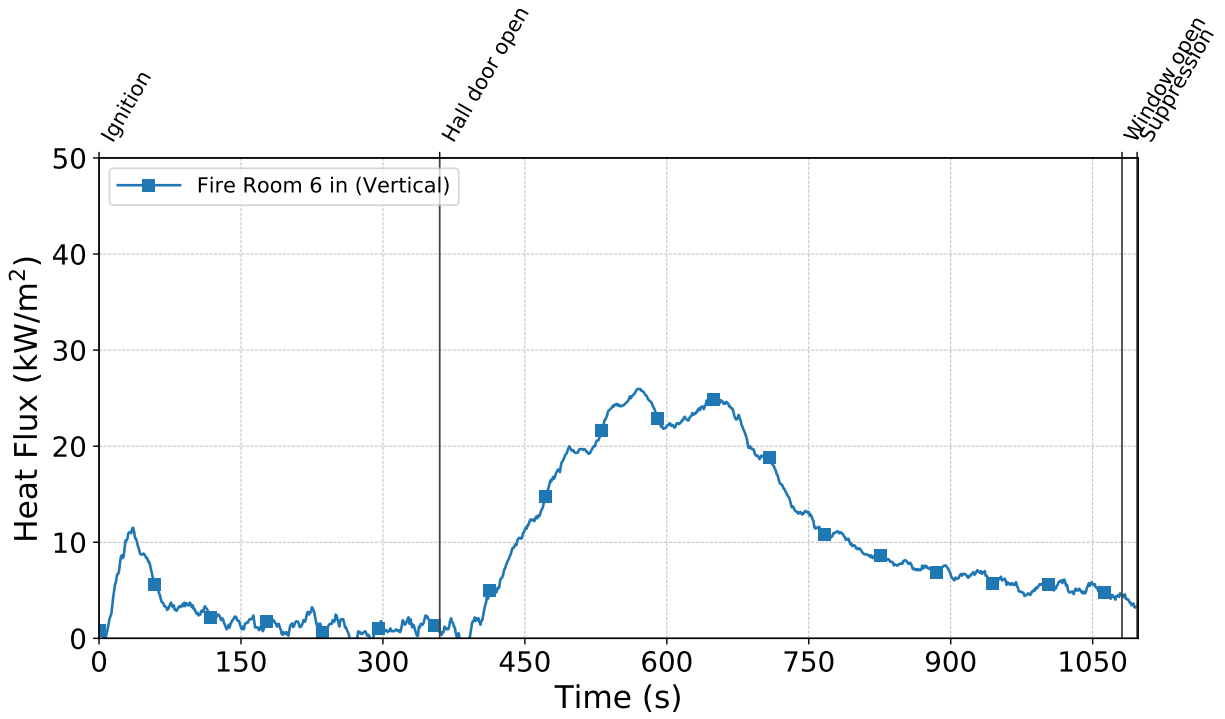


Figure C.139: Heat flux measured by the fire room gauge during Test 13.

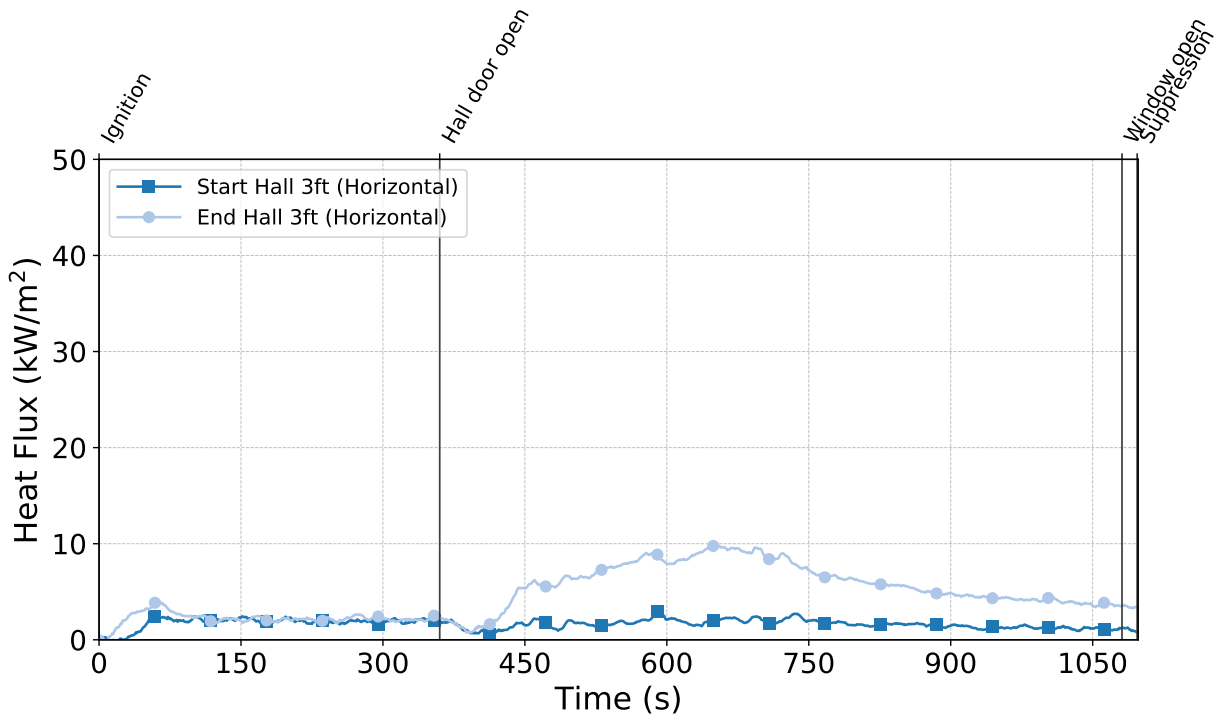


Figure C.140: Heat flux measured by the hallway gauges during Test 13.

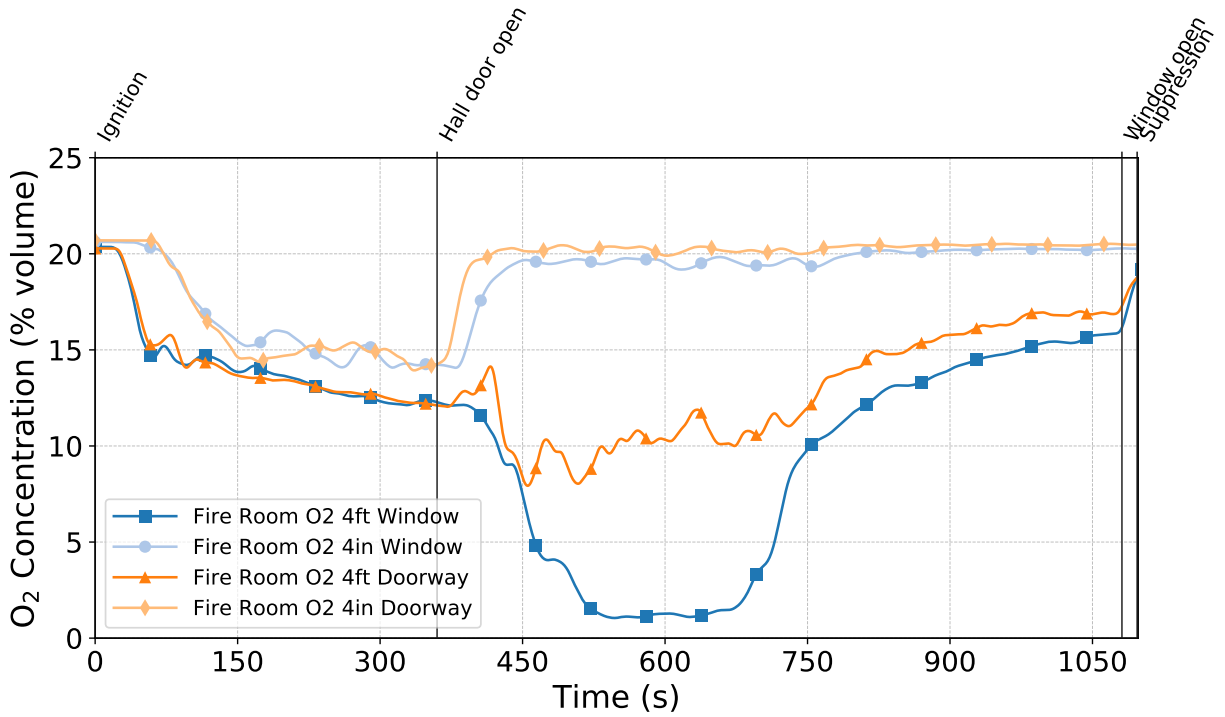


Figure C.141: Oxygen concentrations measured by the fire room gas sampling probes during Test 13.

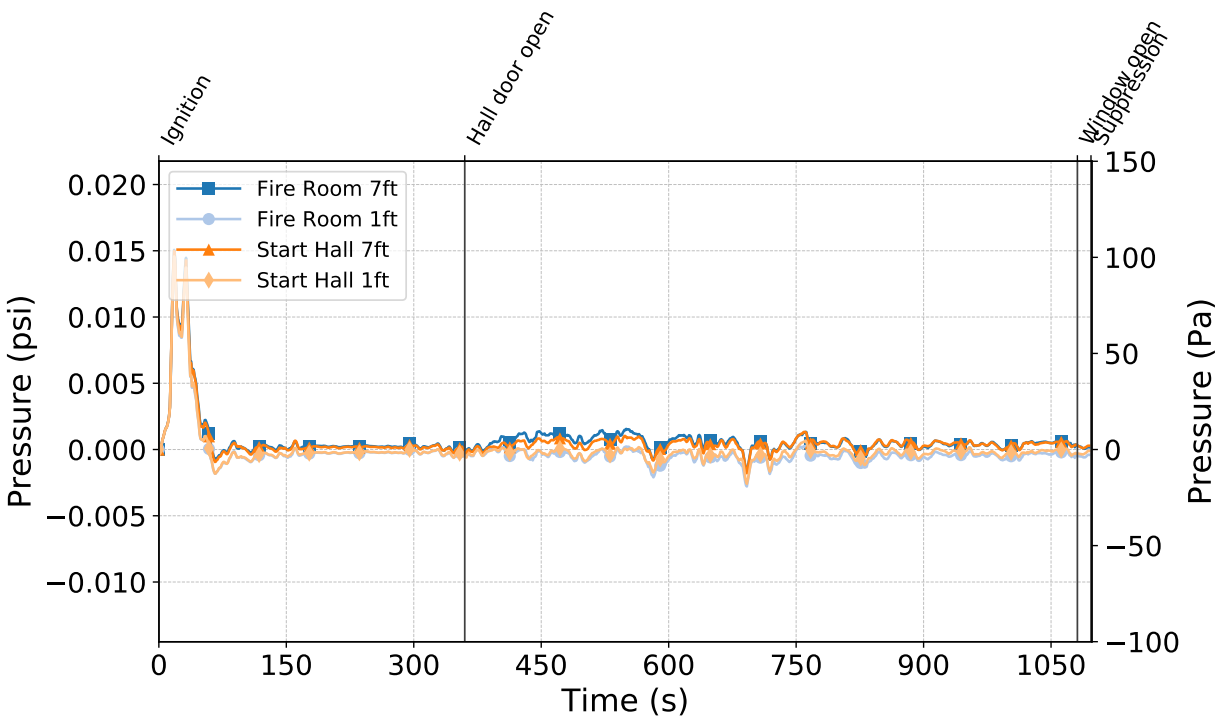


Figure C.142: Pressures measured by the fire room and hallway probes during Test 13.

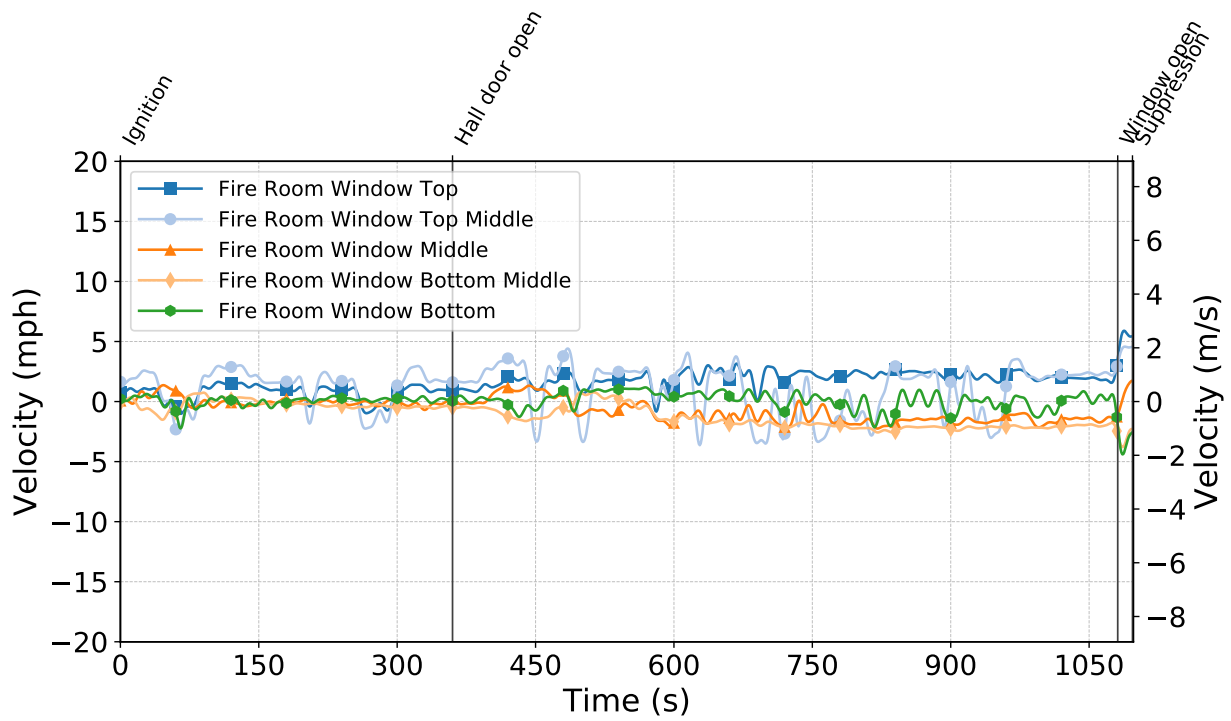


Figure C.143: Gas velocities measured by the fire room window bdps during Test 13.

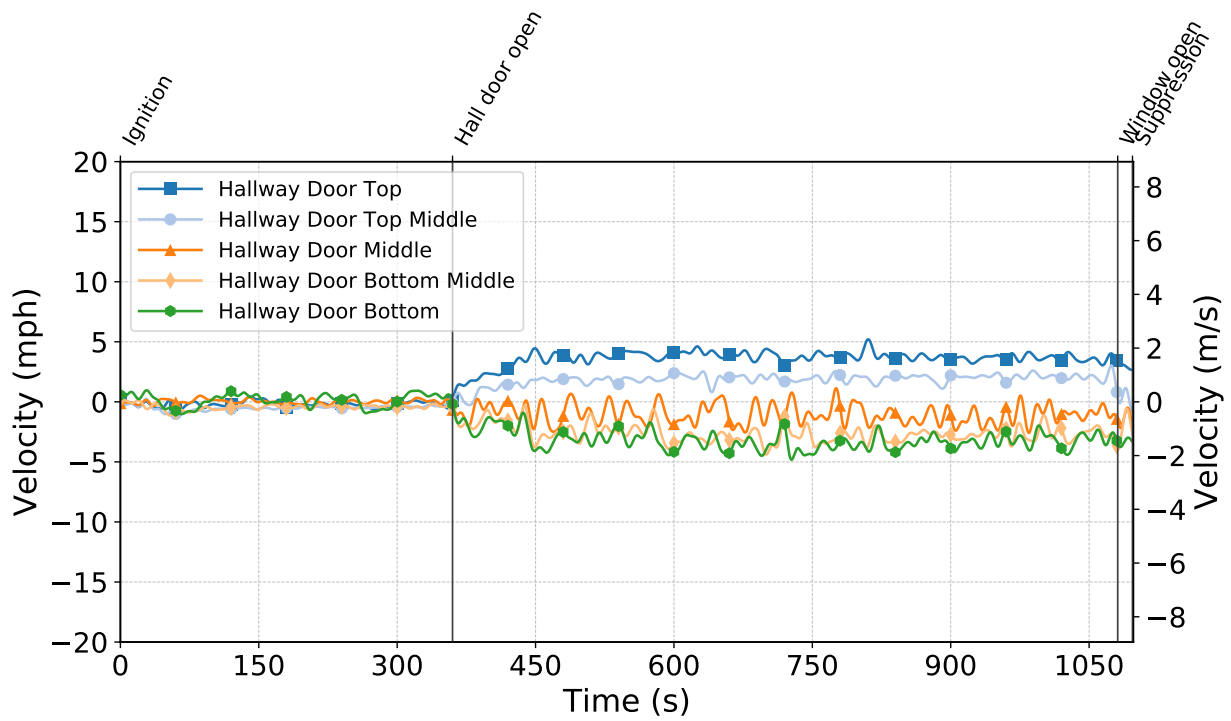


Figure C.144: Gas velocities measured by the hallway door bdps during Test 13.

Test 14

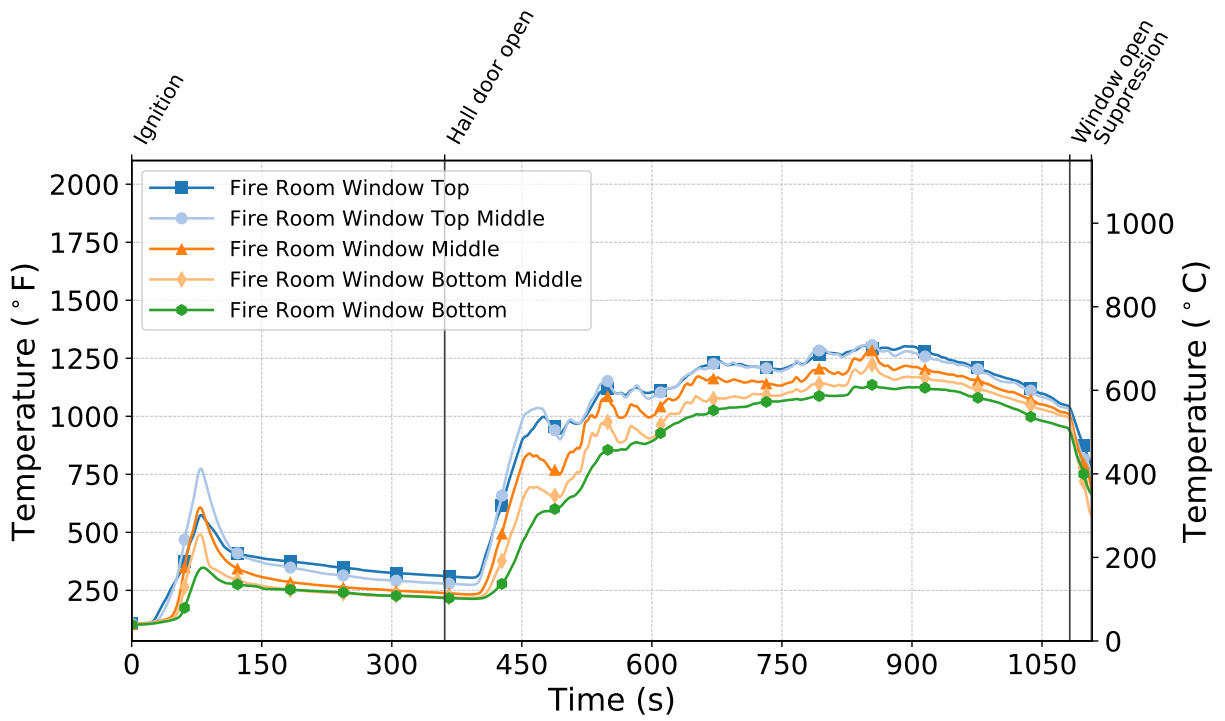


Figure C.145: Temperatures measured by the fire room window thermocouples during Test 14.

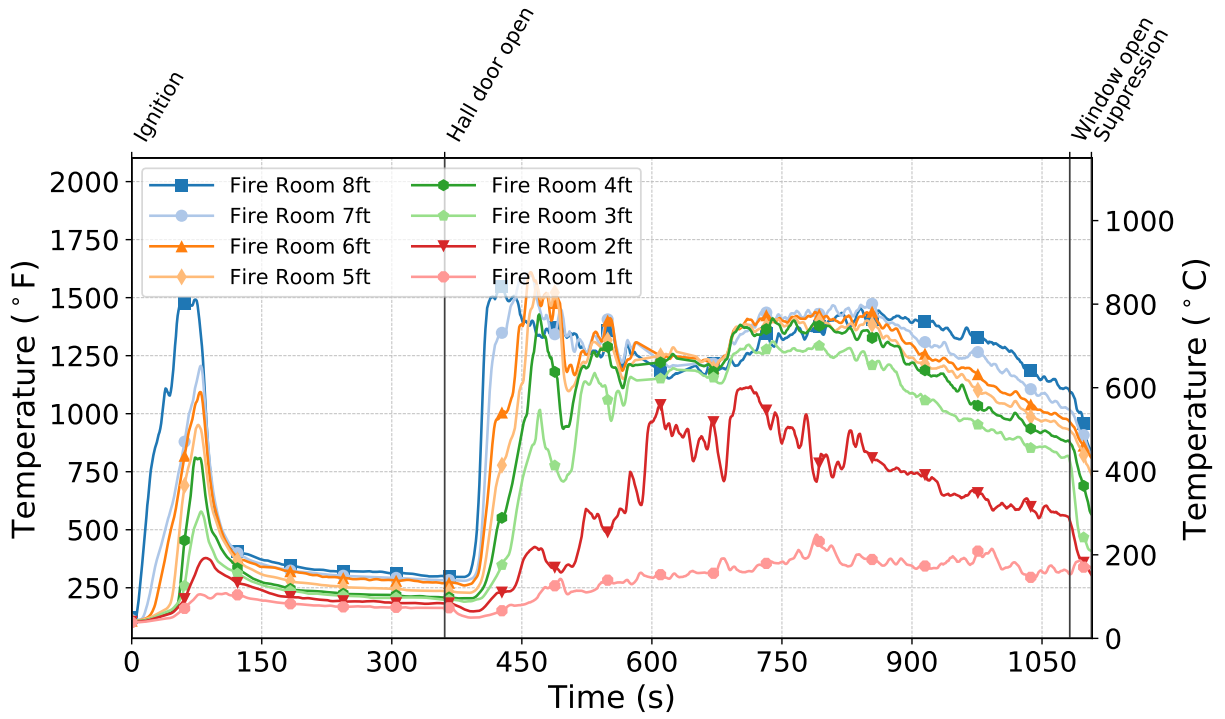


Figure C.146: Temperatures measured by the fire room thermocouples during Test 14.

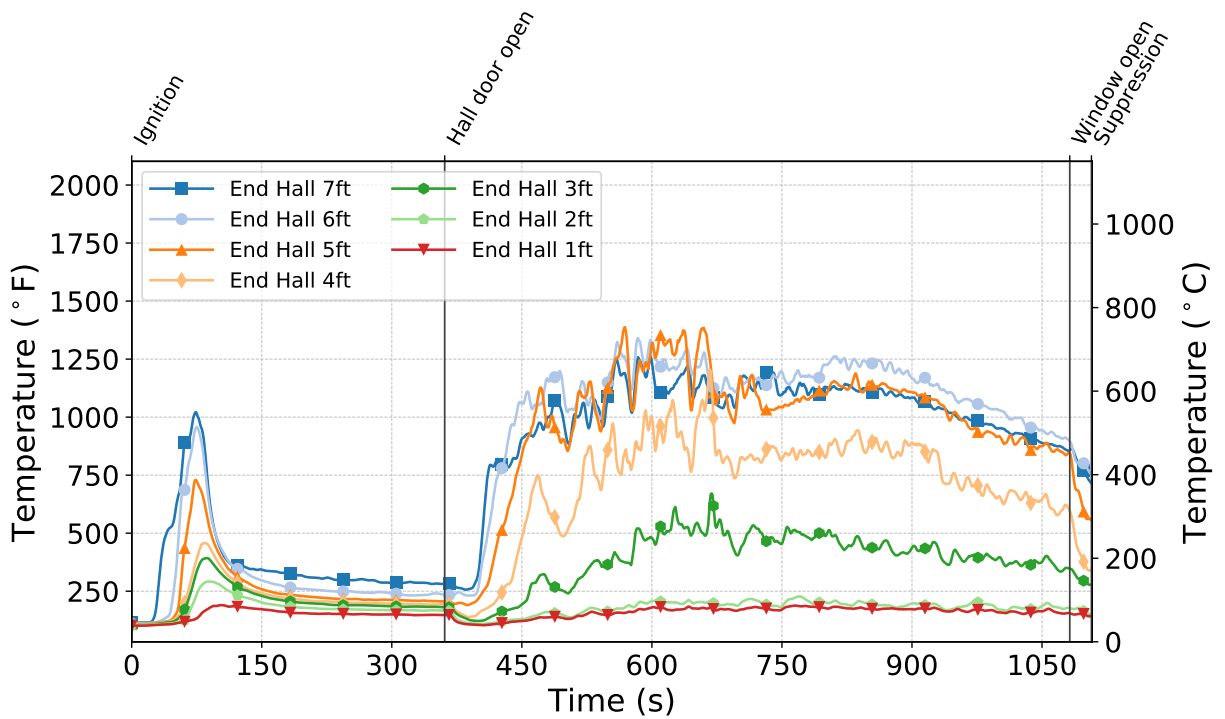


Figure C.147: Temperatures measured by the end hall thermocouples during Test 14.

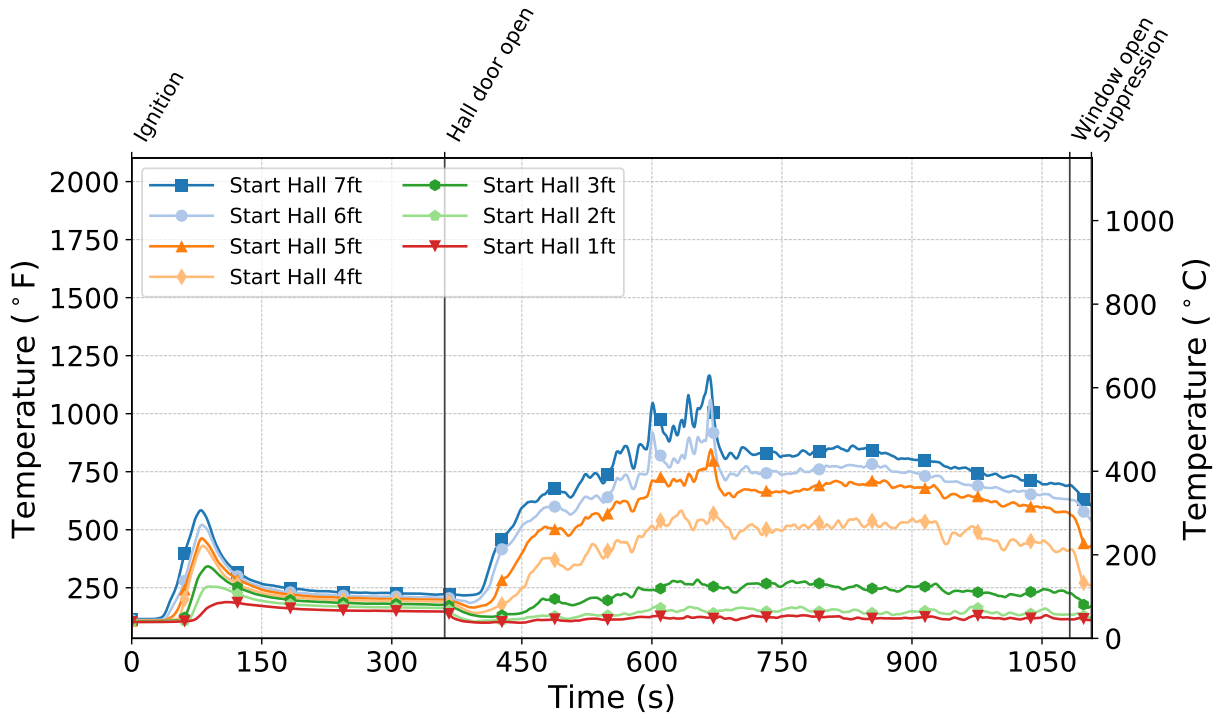


Figure C.148: Temperatures measured by the start hall thermocouples during Test 14.

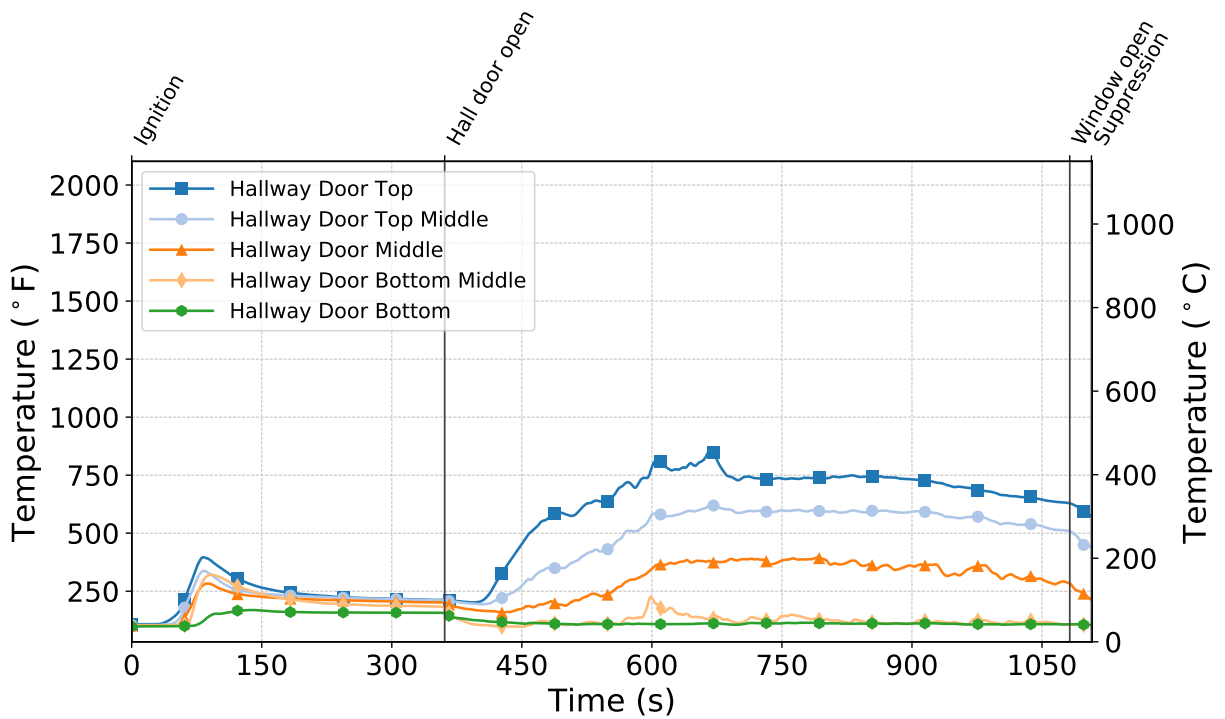


Figure C.149: Temperatures measured by the hallway door thermocouples during Test 14.

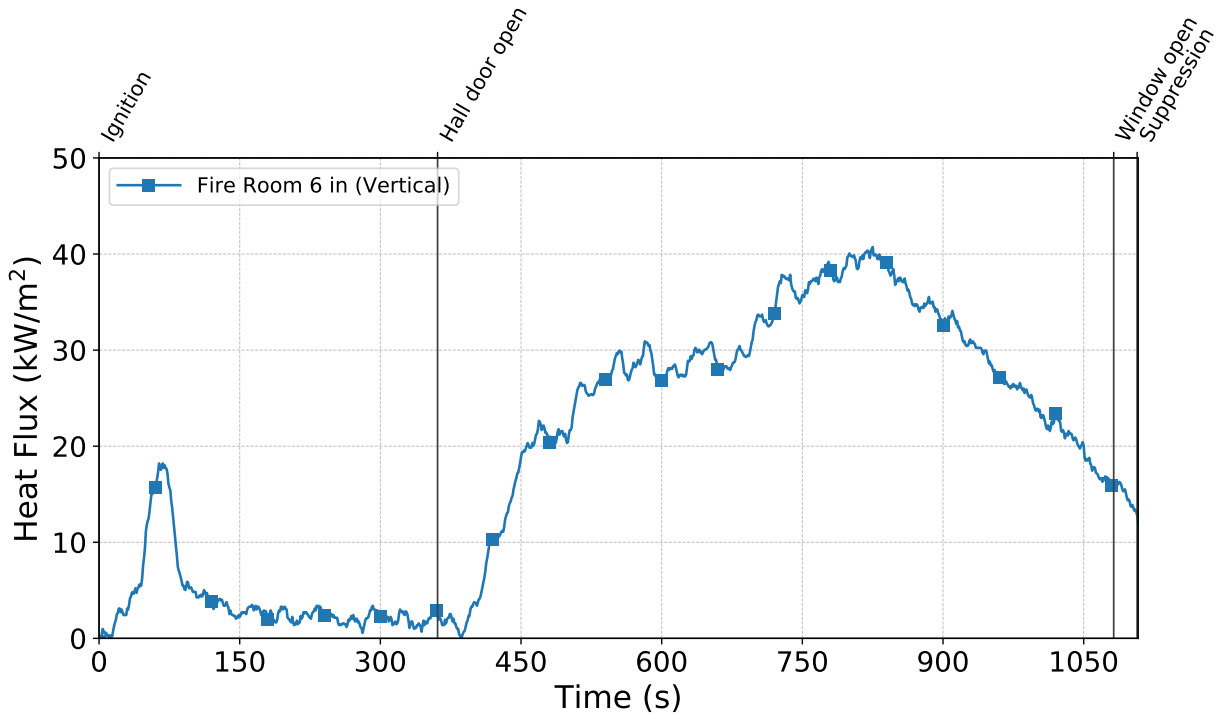


Figure C.150: Heat flux measured by the fire room gauge during Test 14.

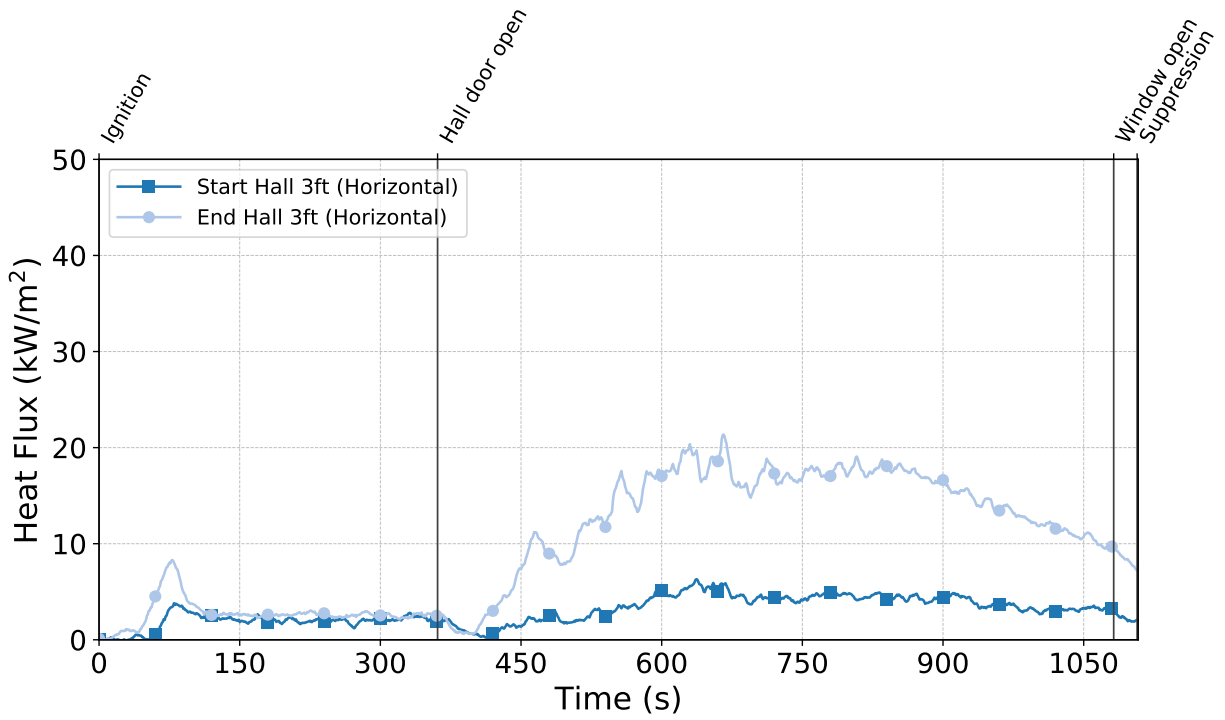


Figure C.151: Heat flux measured by the hallway gauges during Test 14.

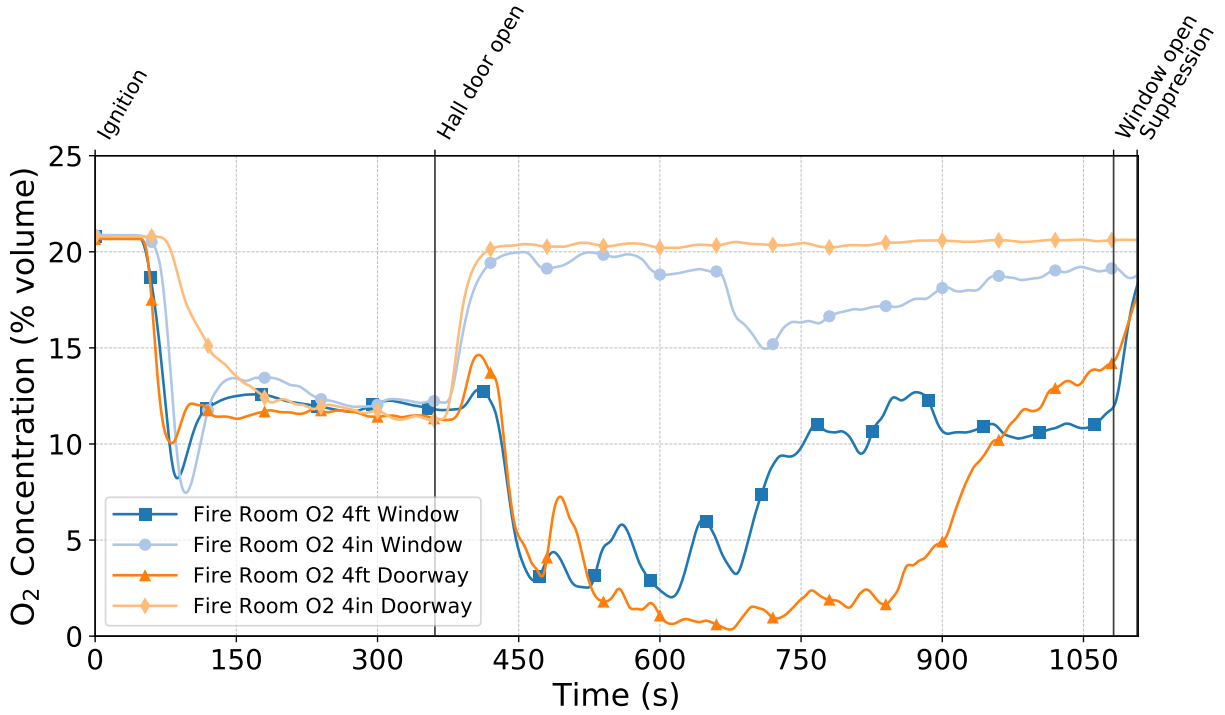


Figure C.152: Oxygen concentrations measured by the fire room gas sampling probes during Test 14.

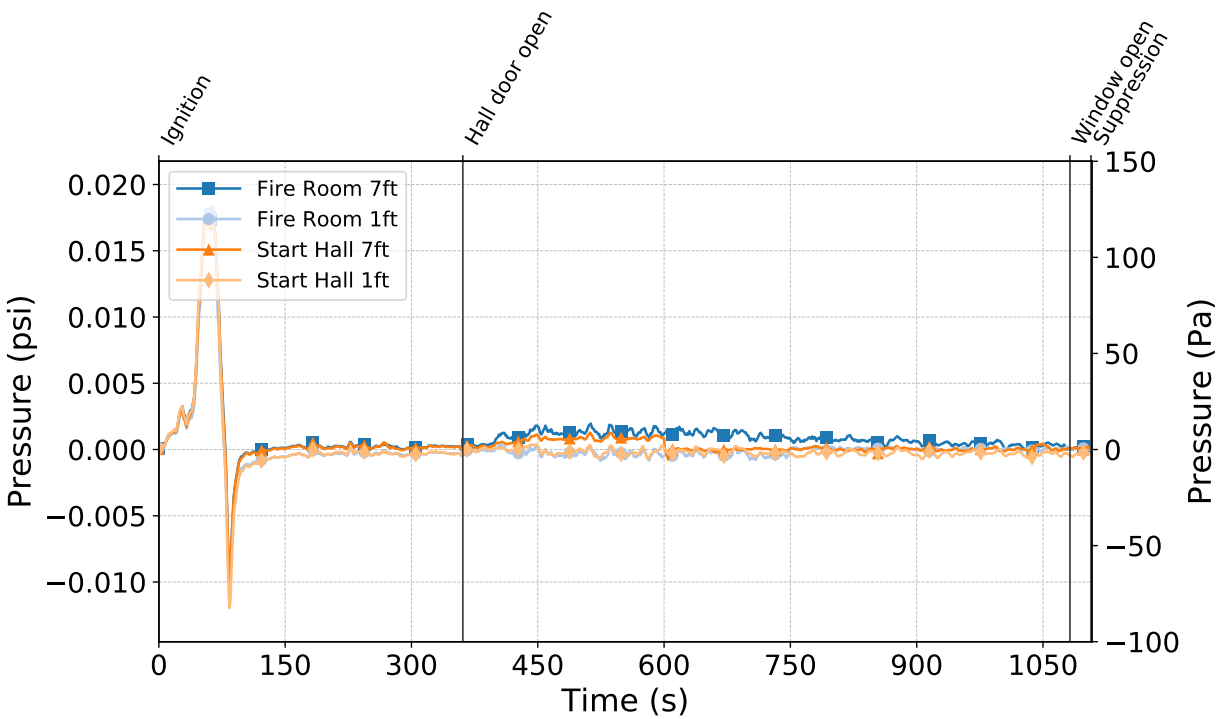


Figure C.153: Pressures measured by the fire room and hallway probes during Test 14.

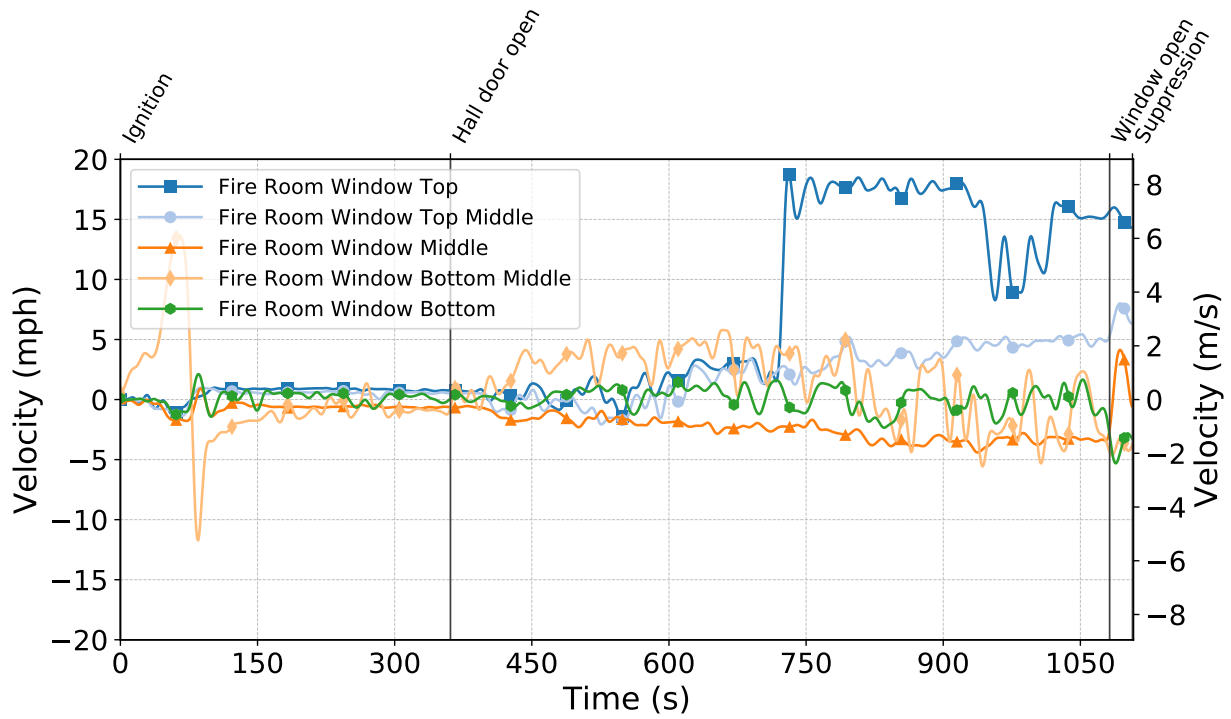


Figure C.154: Gas velocities measured by the fire room window bdp's during Test 14.

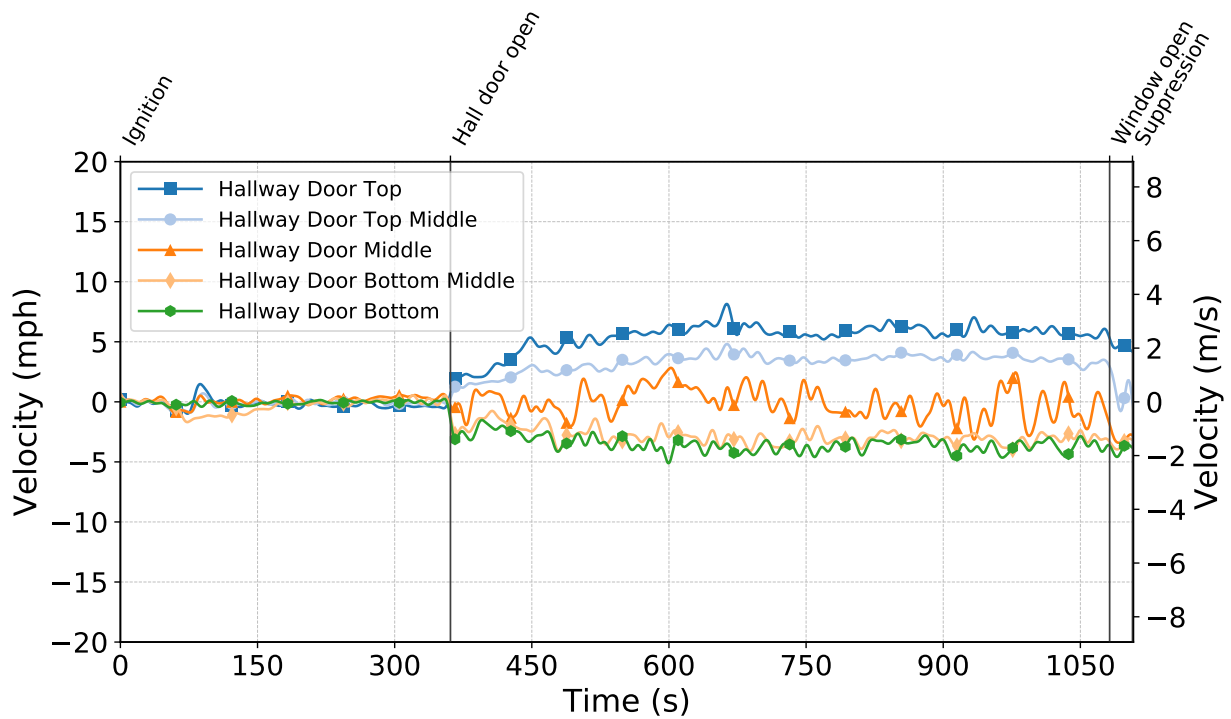


Figure C.155: Gas velocities measured by the hallway door bdp's during Test 14.

Test 15

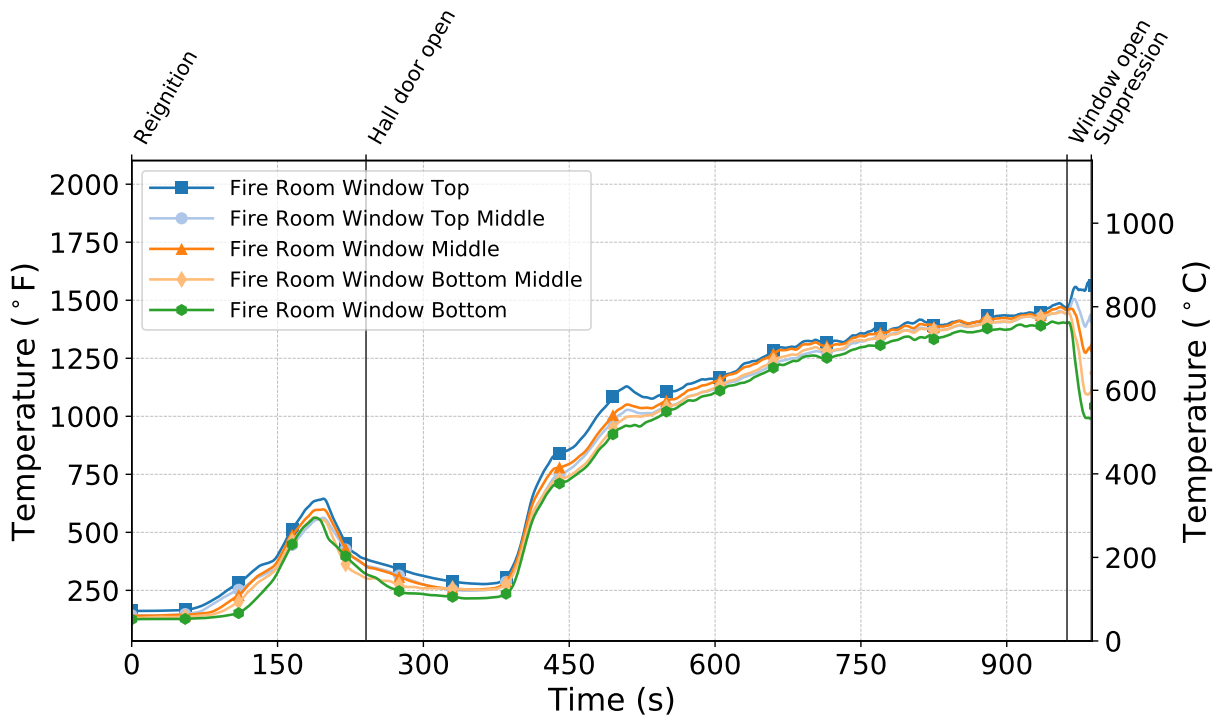


Figure C.156: Temperatures measured by the fire room window thermocouples during Test 15.

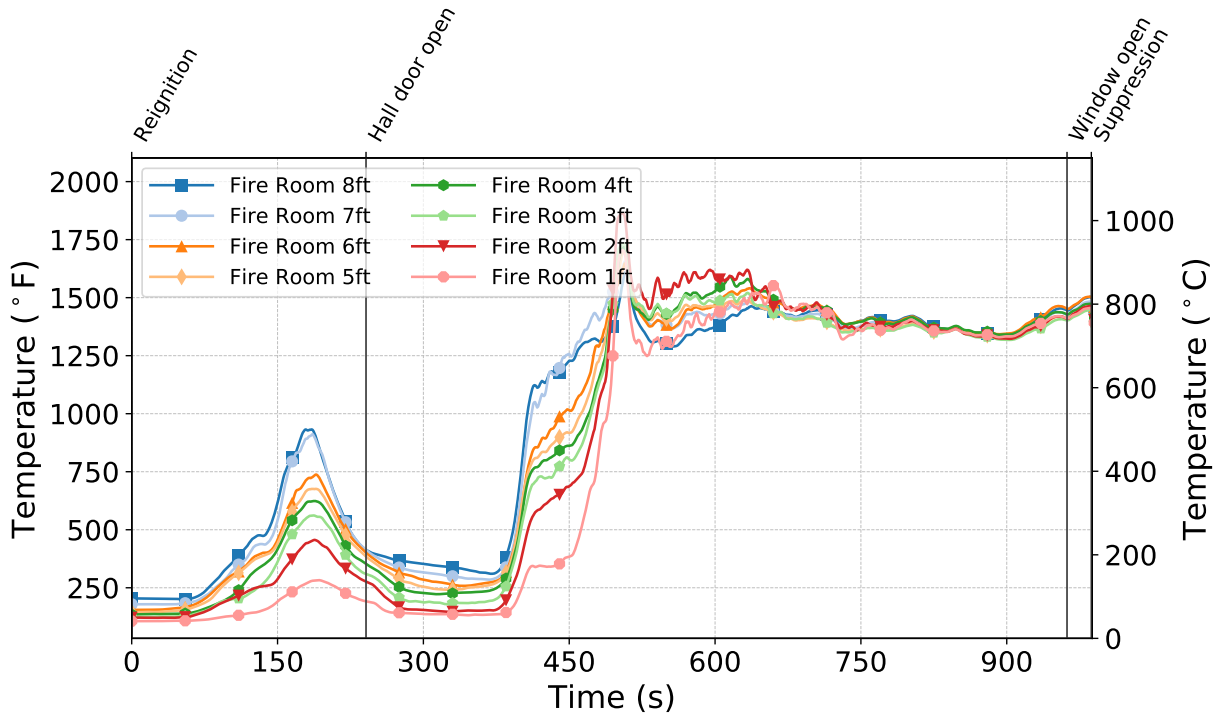


Figure C.157: Temperatures measured by the fire room thermocouples during Test 15.

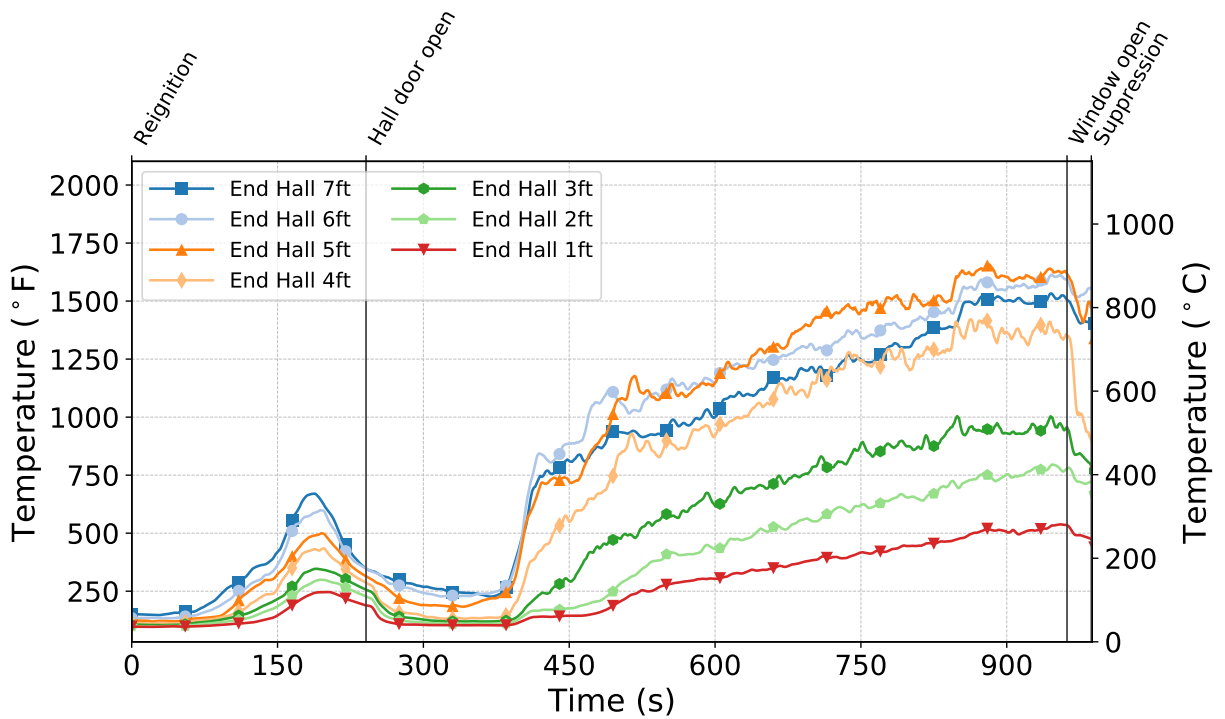


Figure C.158: Temperatures measured by the end hall thermocouples during Test 15.

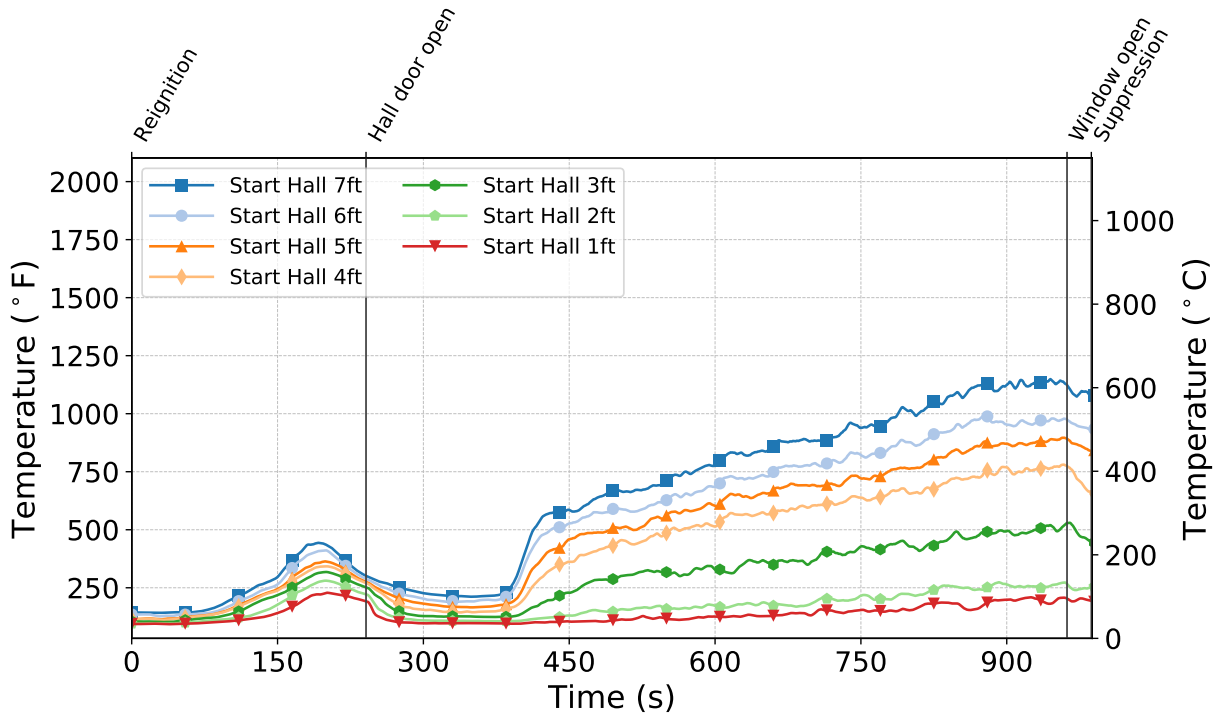


Figure C.159: Temperatures measured by the start hall thermocouples during Test 15.

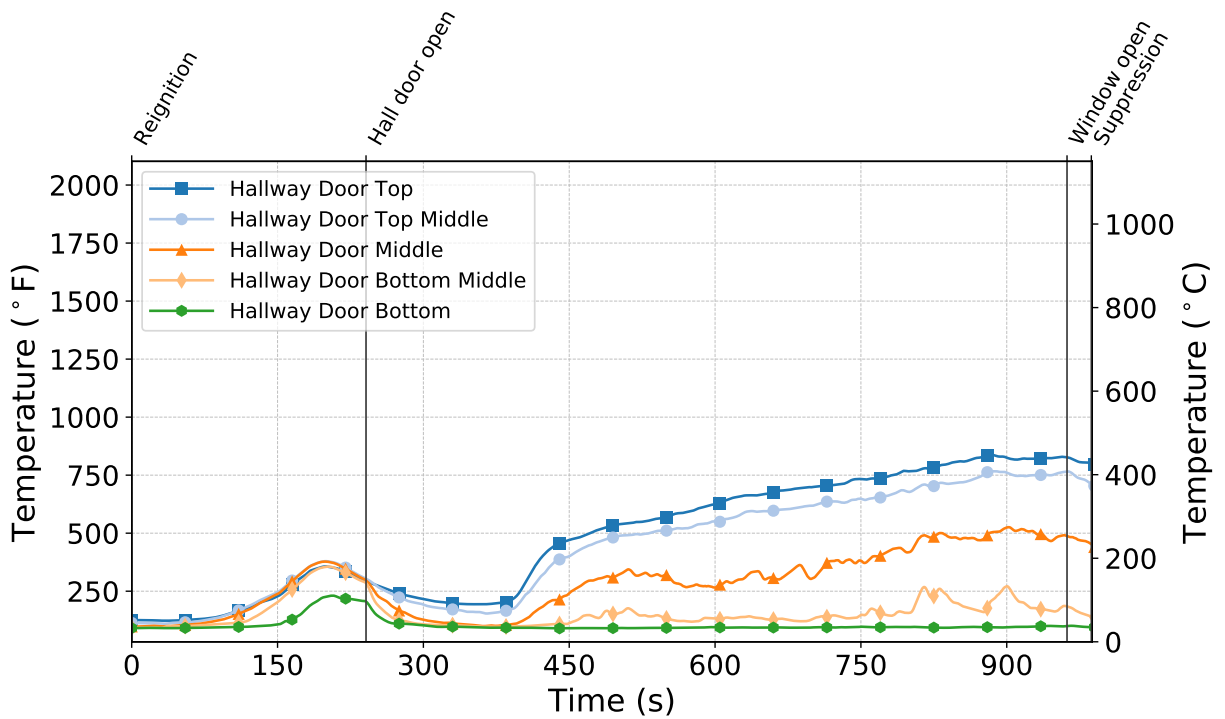


Figure C.160: Temperatures measured by the hallway door thermocouples during Test 15.

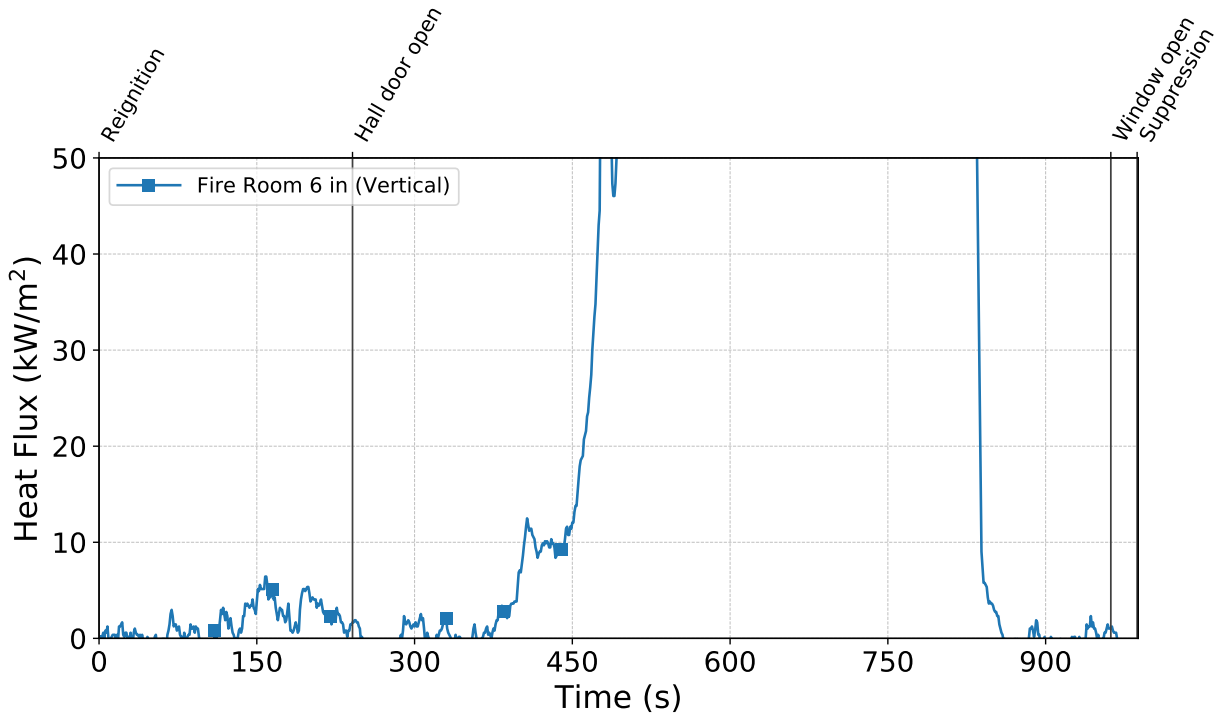


Figure C.161: Heat flux measured by the fire room gauge during Test 15.

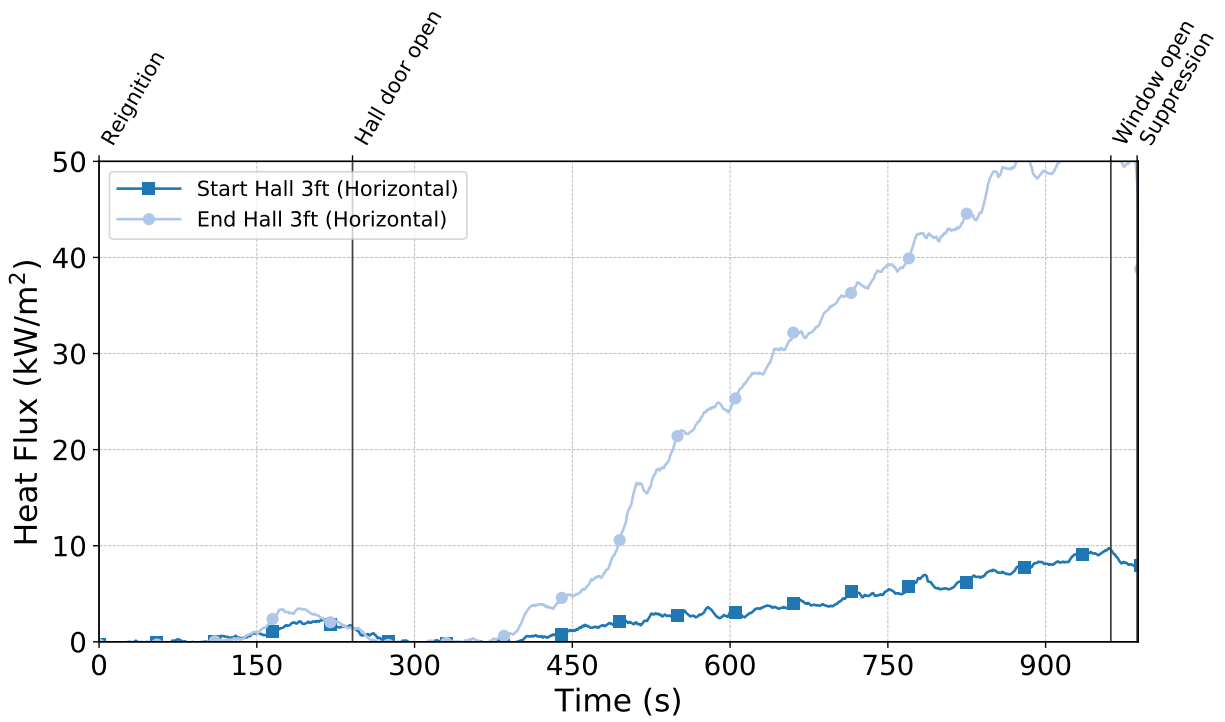


Figure C.162: Heat flux measured by the hallway gauges during Test 15.

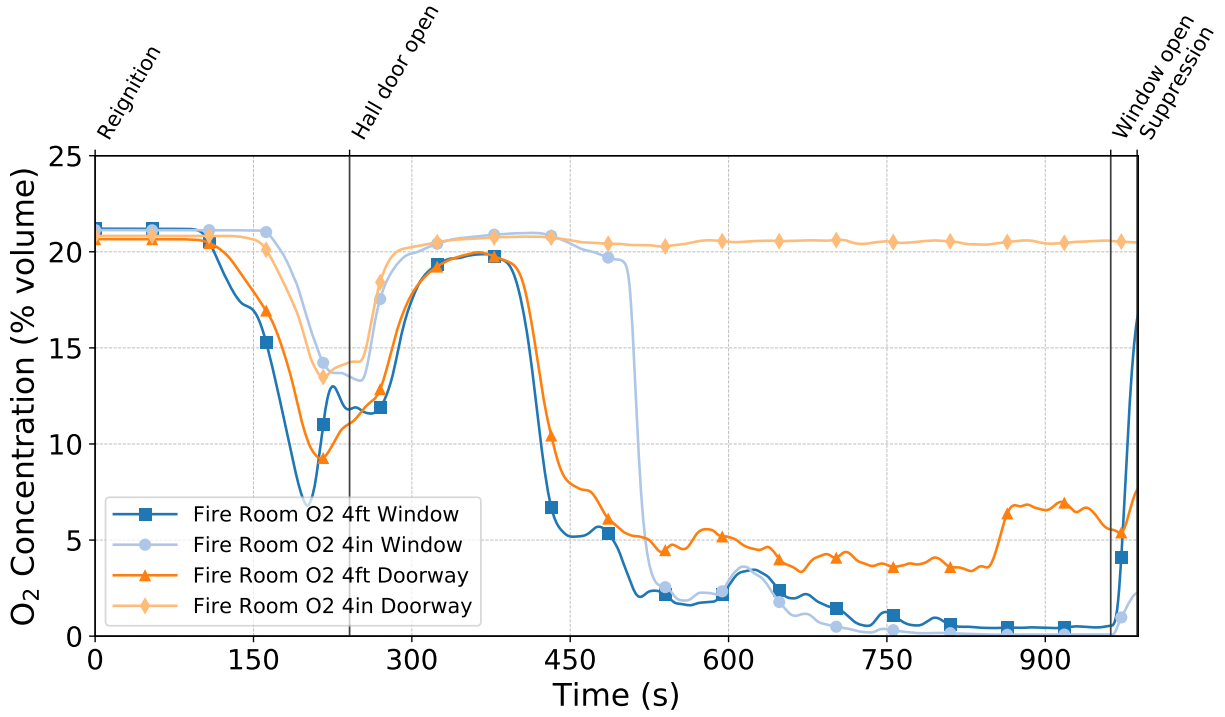


Figure C.163: Oxygen concentrations measured by the fire room gas sampling probes during Test 15.

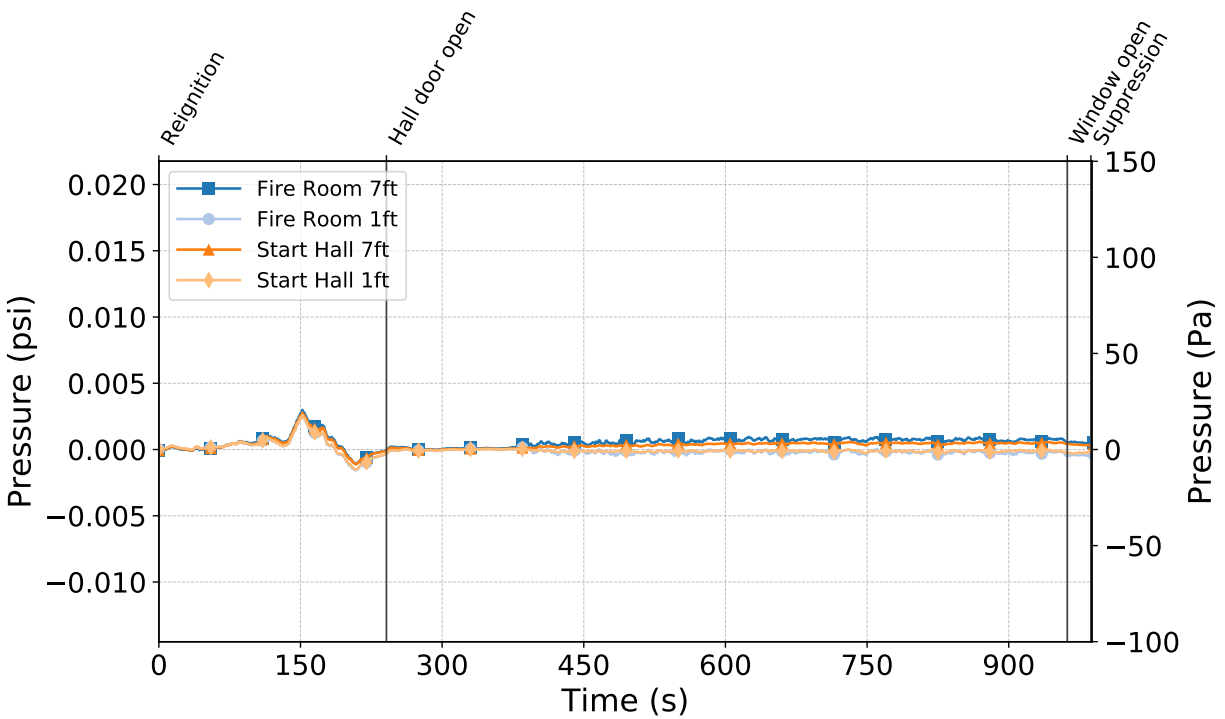


Figure C.164: Pressures measured by the fire room and hallway probes during Test 15.

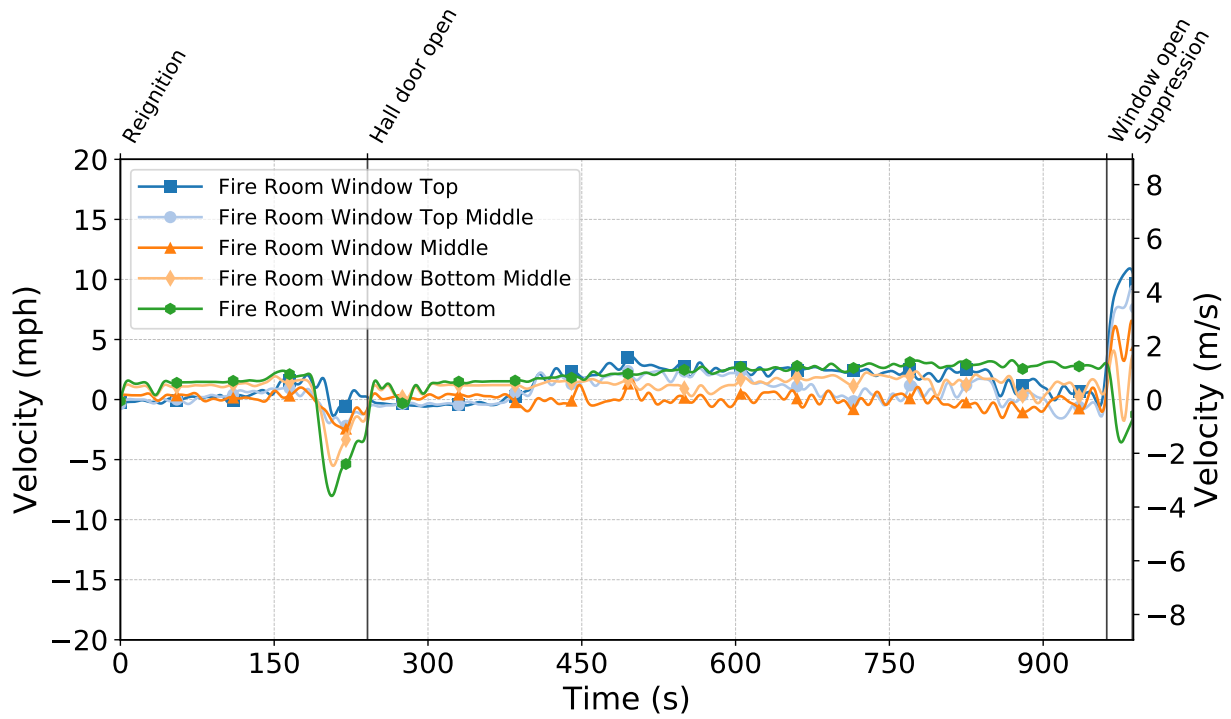


Figure C.165: Gas velocities measured by the fire room window bdps during Test 15.

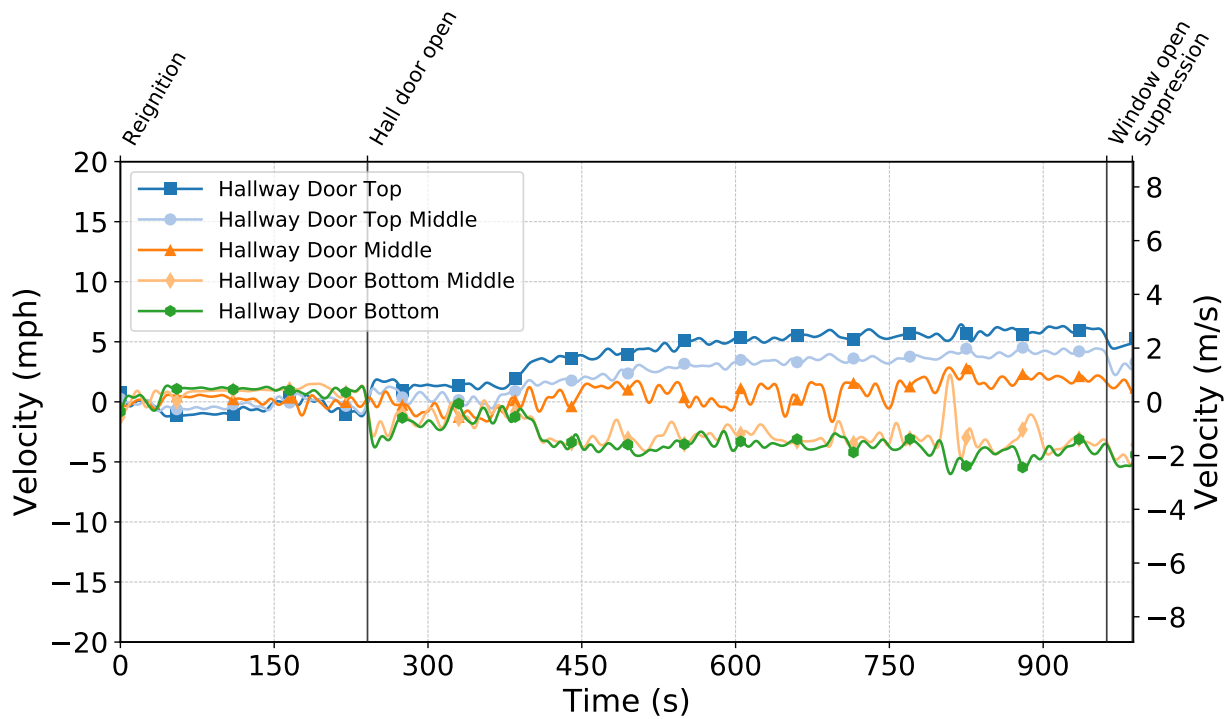


Figure C.166: Gas velocities measured by the hallway door bdps during Test 15.

Test 16

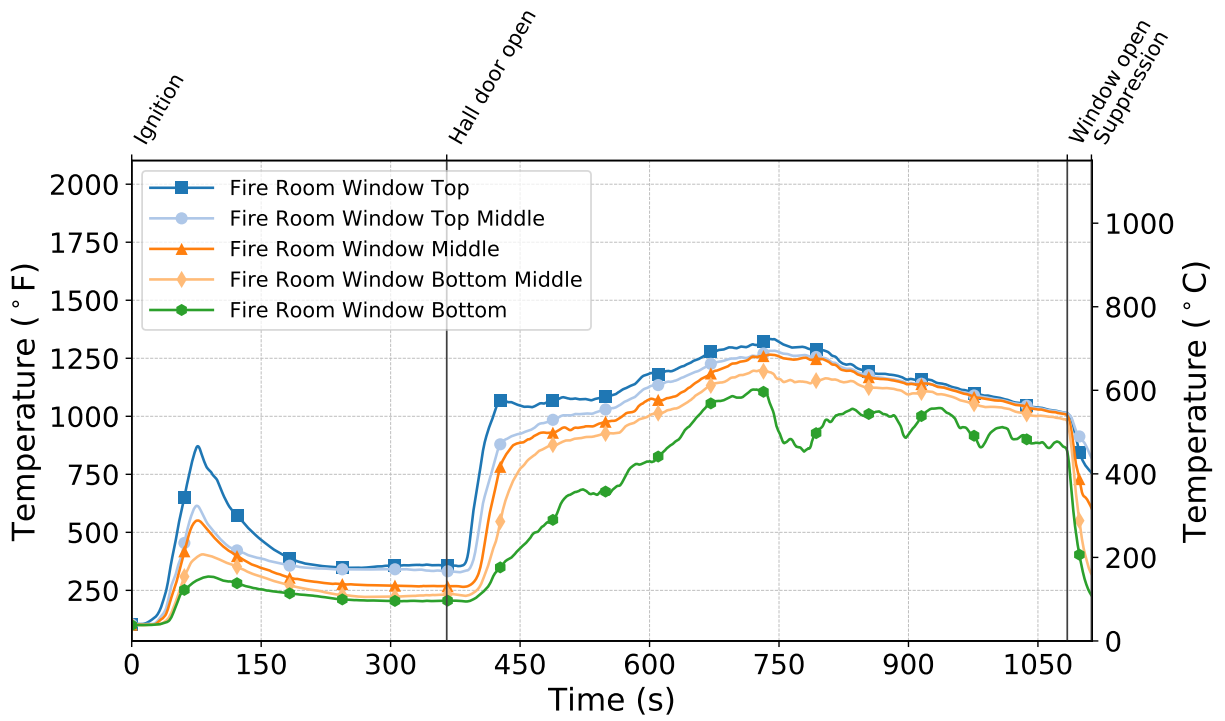


Figure C.167: Temperatures measured by the fire room window thermocouples during Test 16.

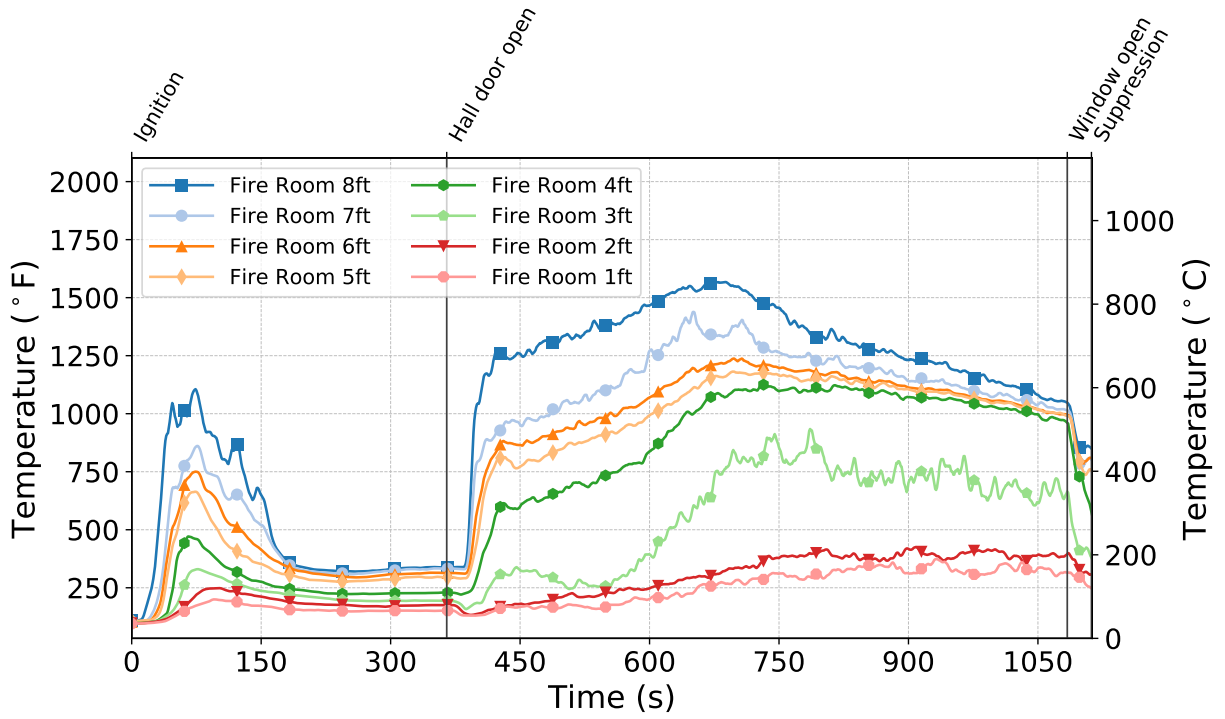


Figure C.168: Temperatures measured by the fire room thermocouples during Test 16.

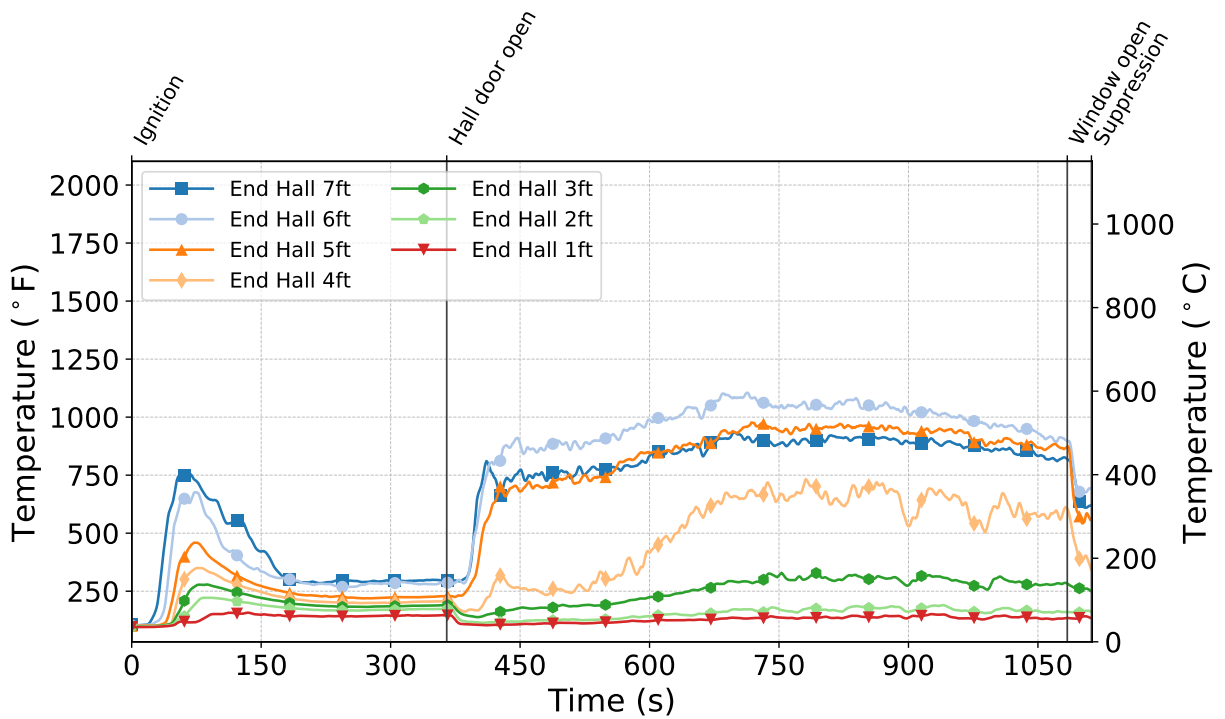


Figure C.169: Temperatures measured by the end hall thermocouples during Test 16.

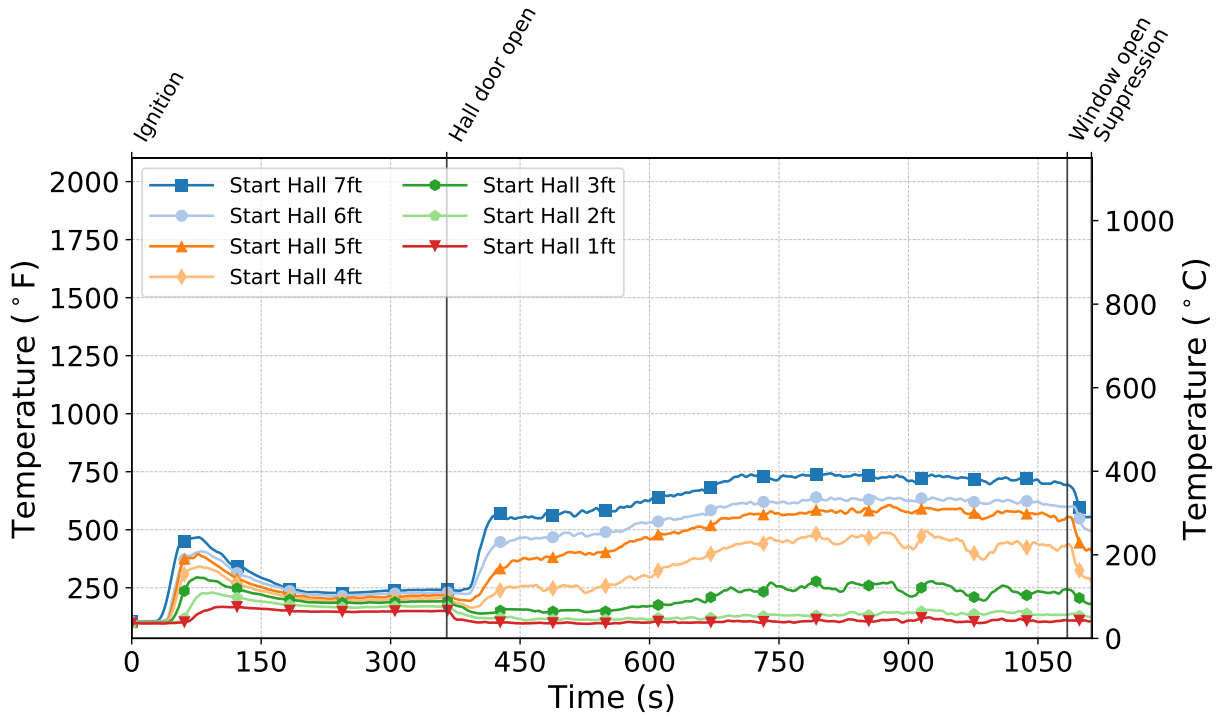


Figure C.170: Temperatures measured by the start hall thermocouples during Test 16.

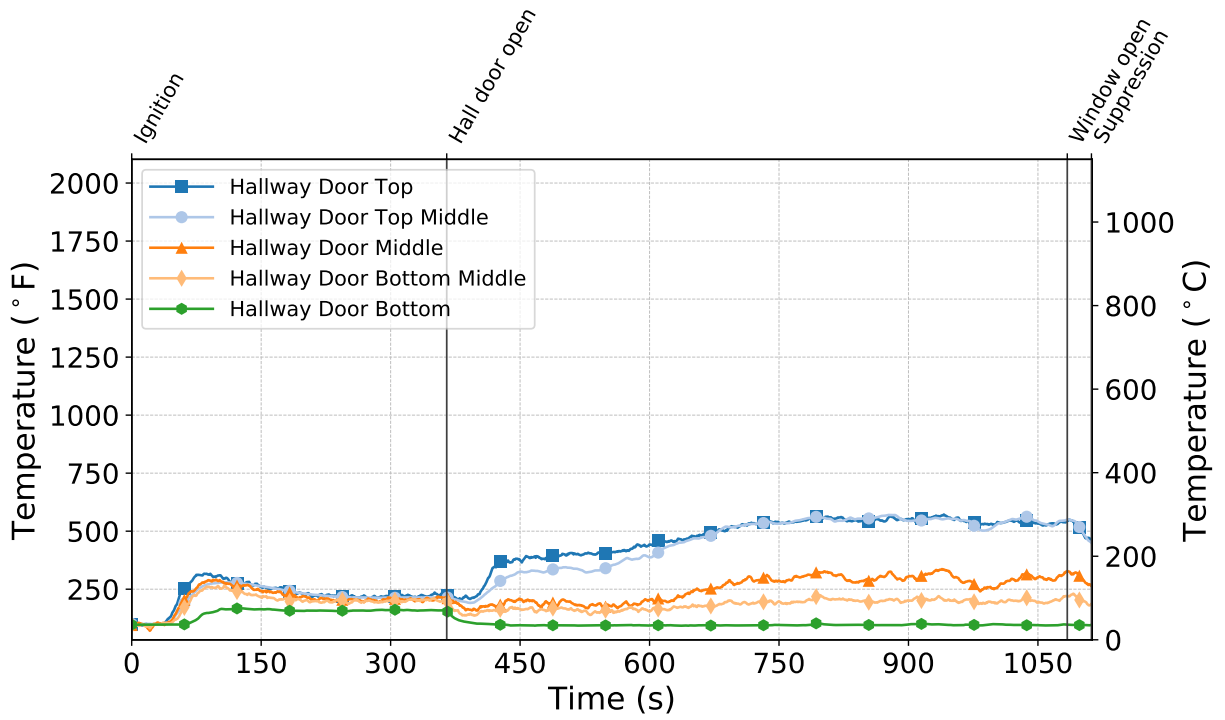


Figure C.171: Temperatures measured by the hallway door thermocouples during Test 16.

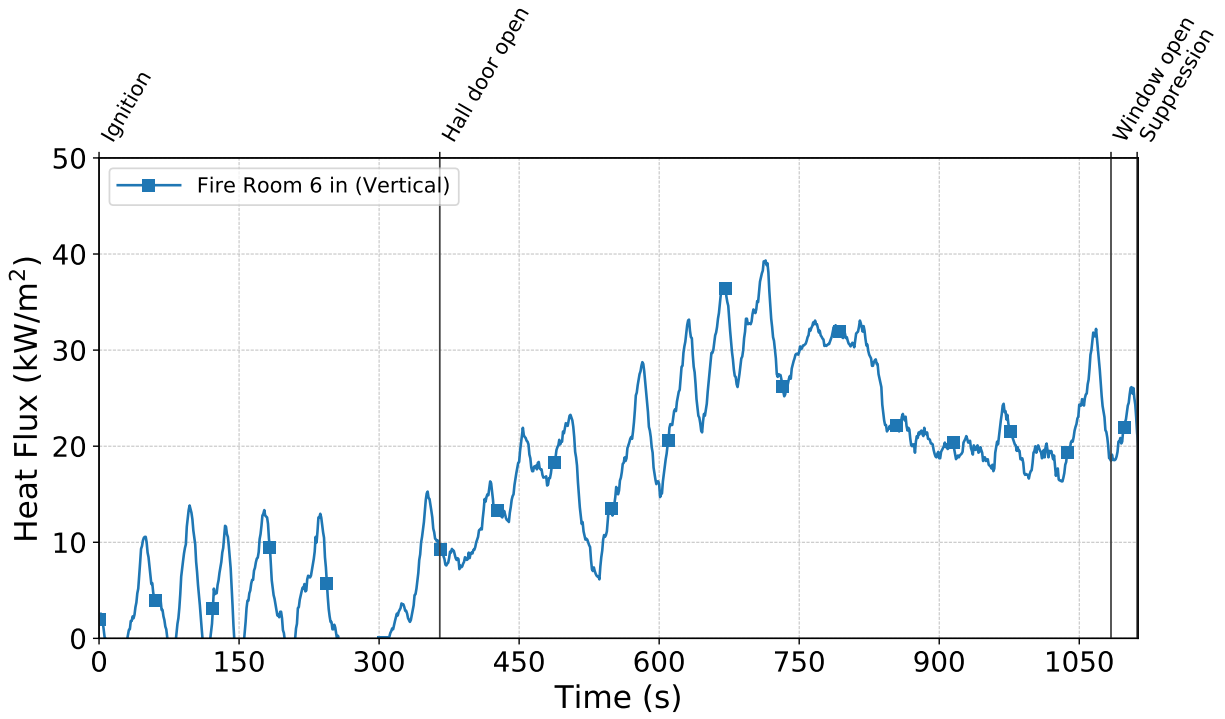


Figure C.172: Heat flux measured by the fire room gauge during Test 16.

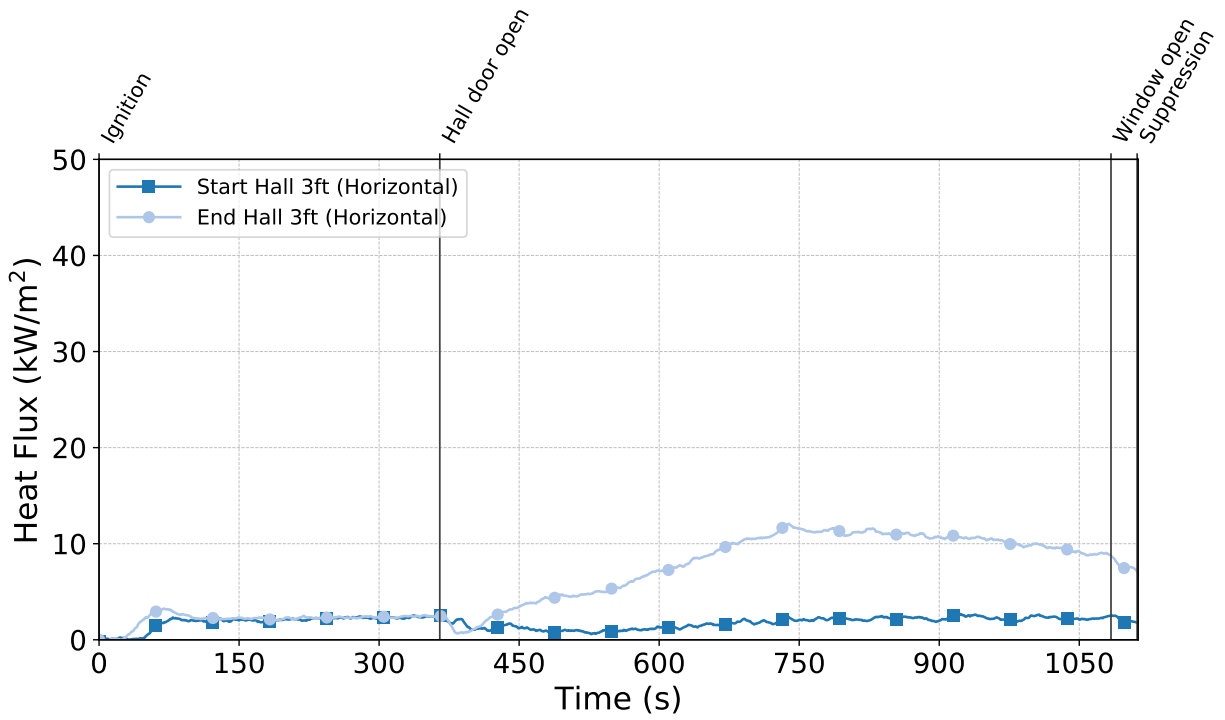


Figure C.173: Heat flux measured by the hallway gauges during Test 16.

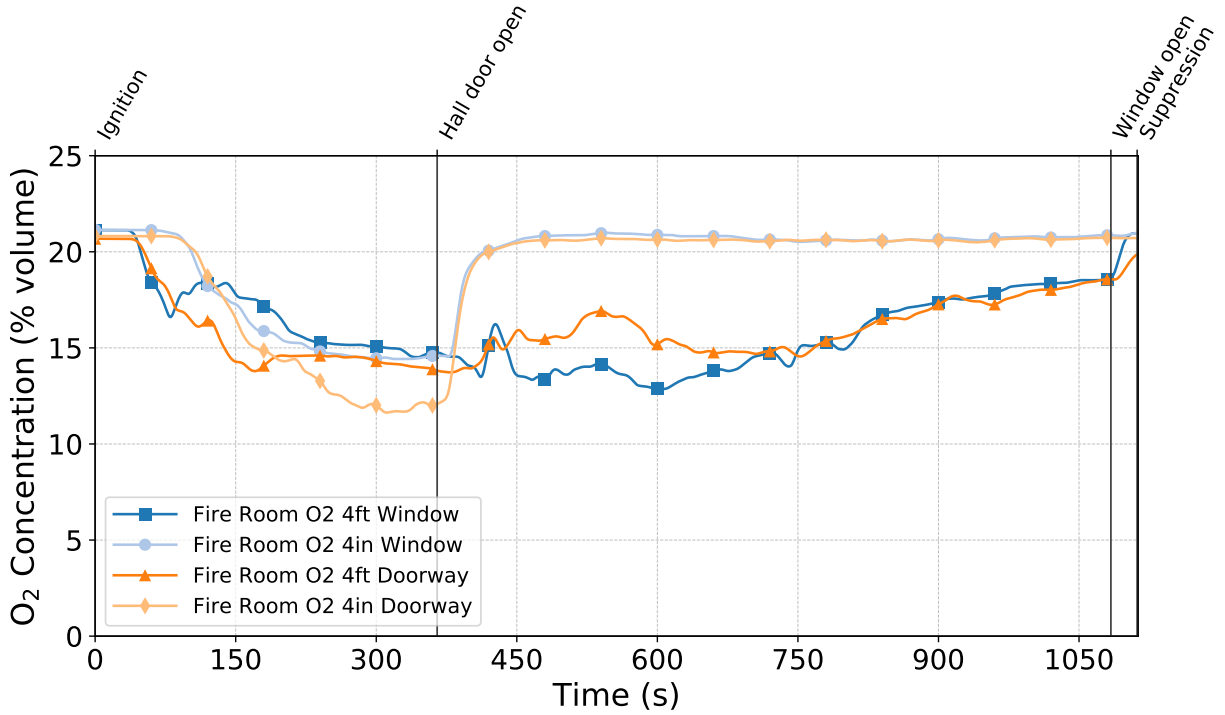


Figure C.174: Oxygen concentrations measured by the fire room gas sampling probes during Test 16.

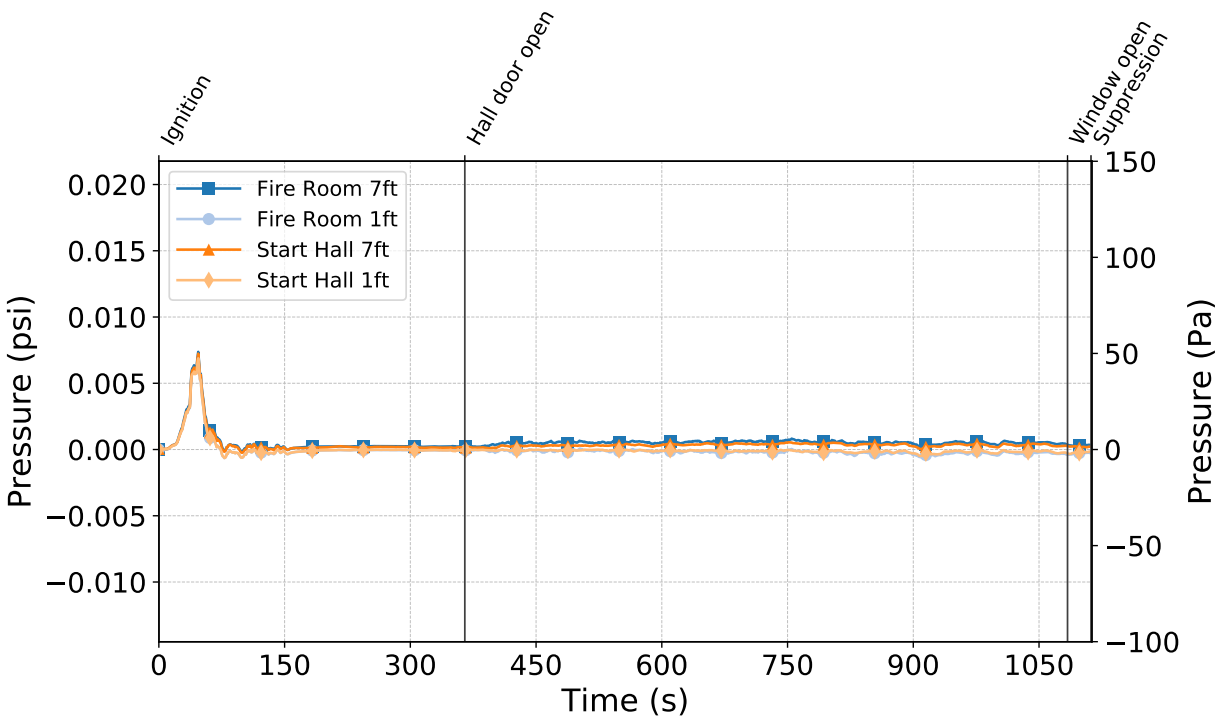


Figure C.175: Pressures measured by the fire room and hallway probes during Test 16.

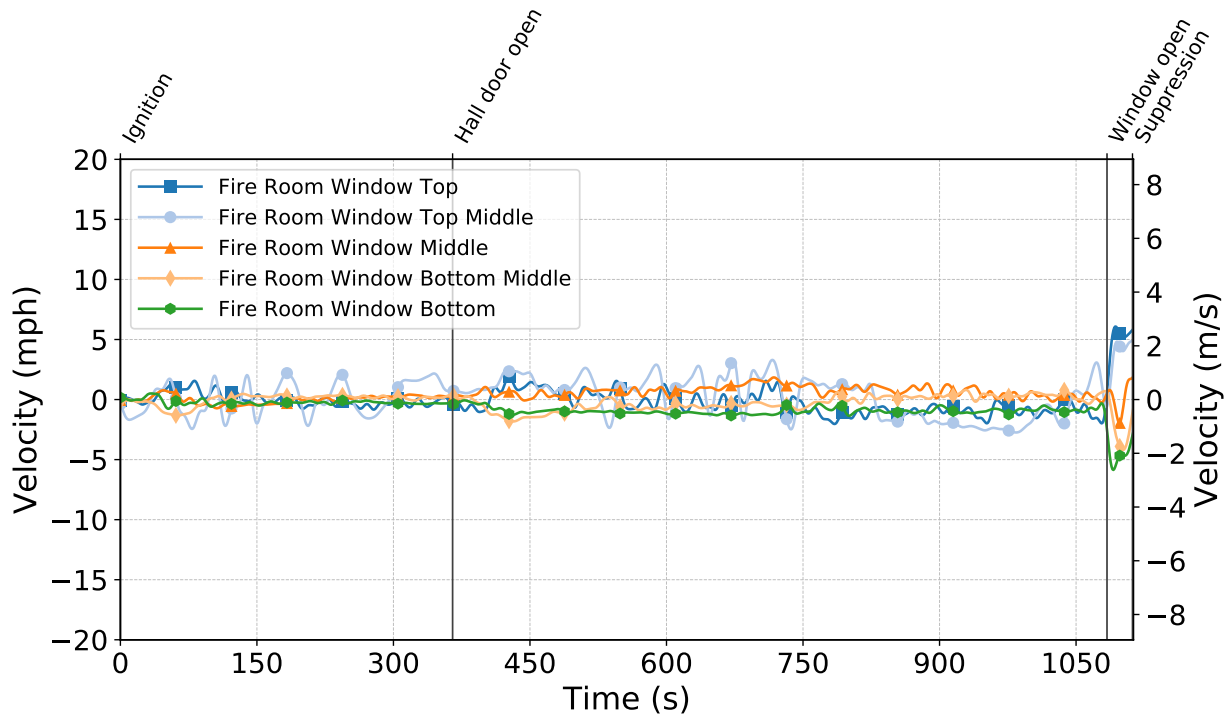


Figure C.176: Gas velocities measured by the fire room window bdps during Test 16.

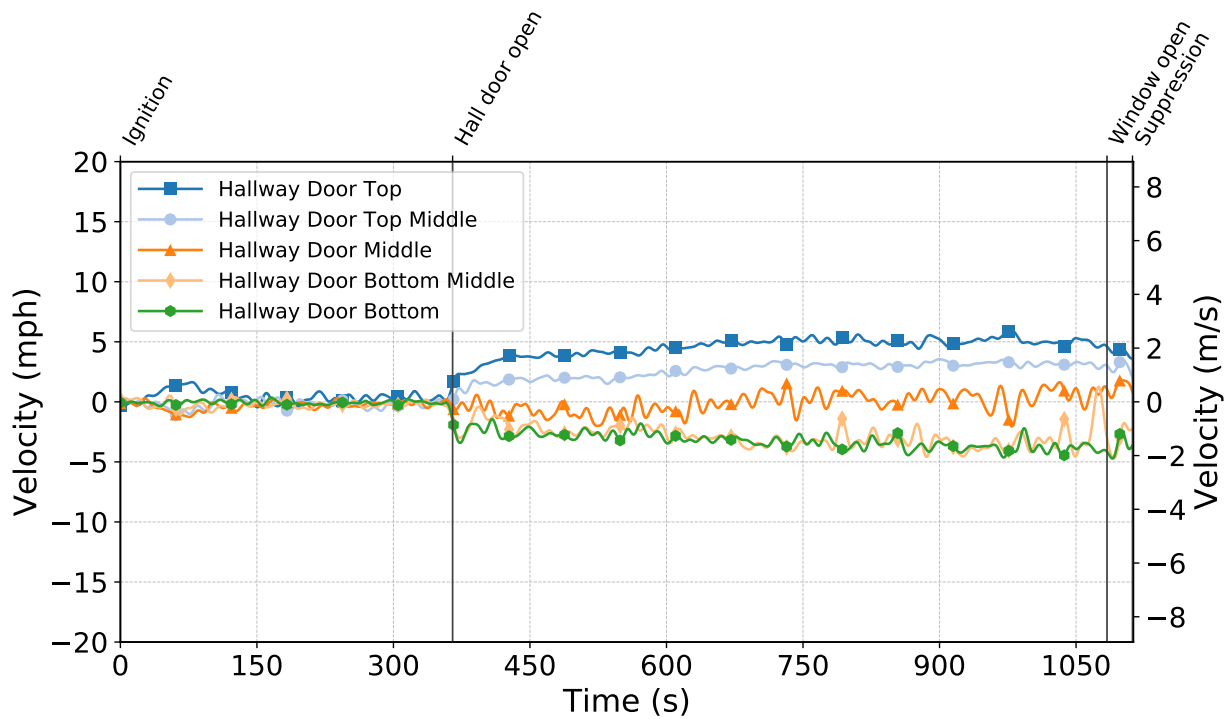


Figure C.177: Gas velocities measured by the hallway door bdps during Test 16.

Test 17

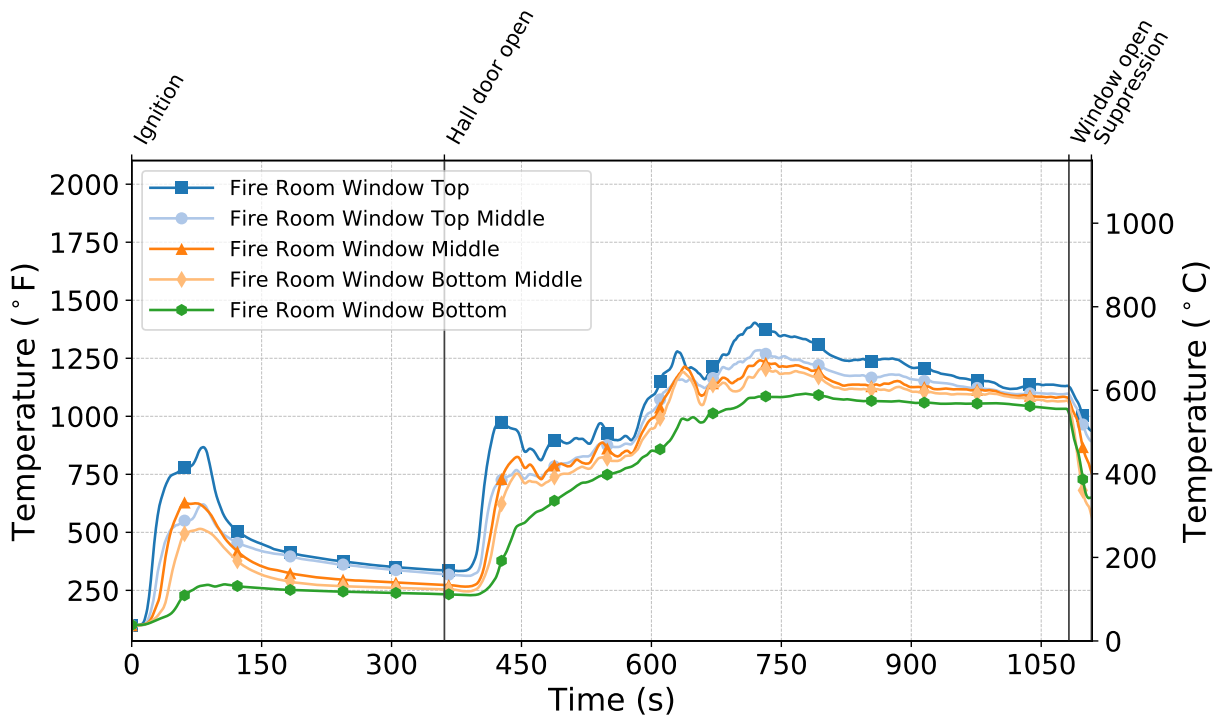


Figure C.178: Temperatures measured by the fire room window thermocouples during Test 17.

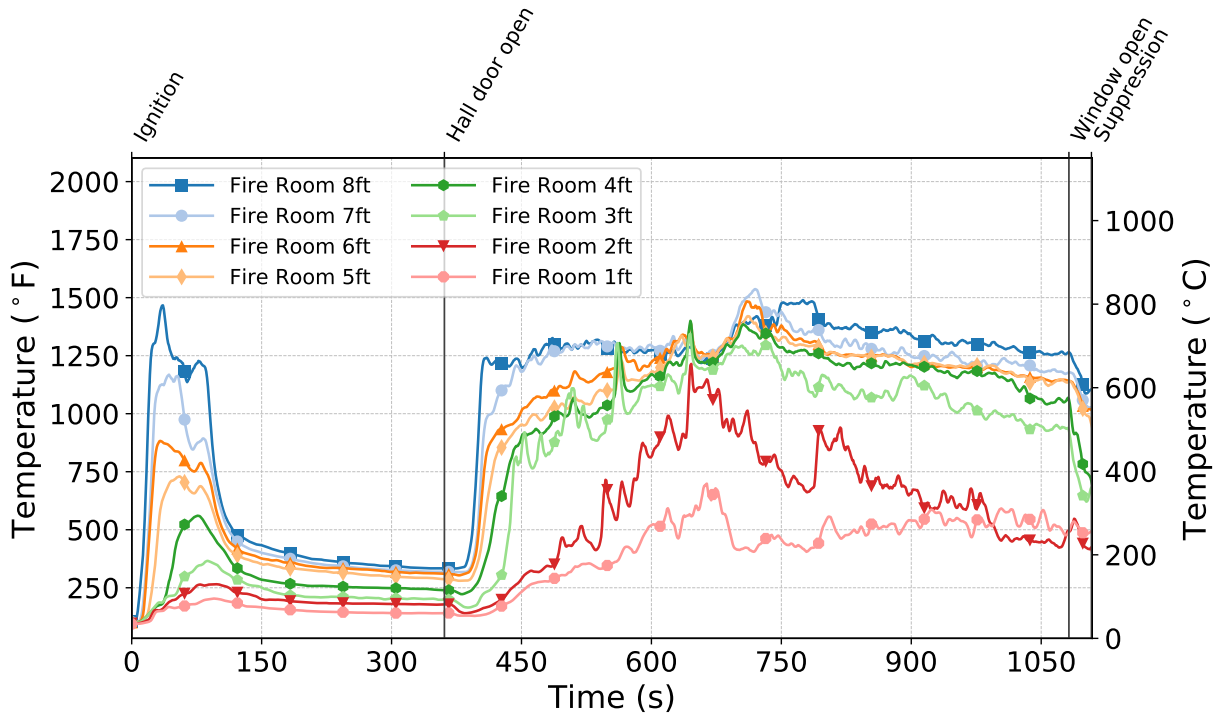


Figure C.179: Temperatures measured by the fire room thermocouples during Test 17.

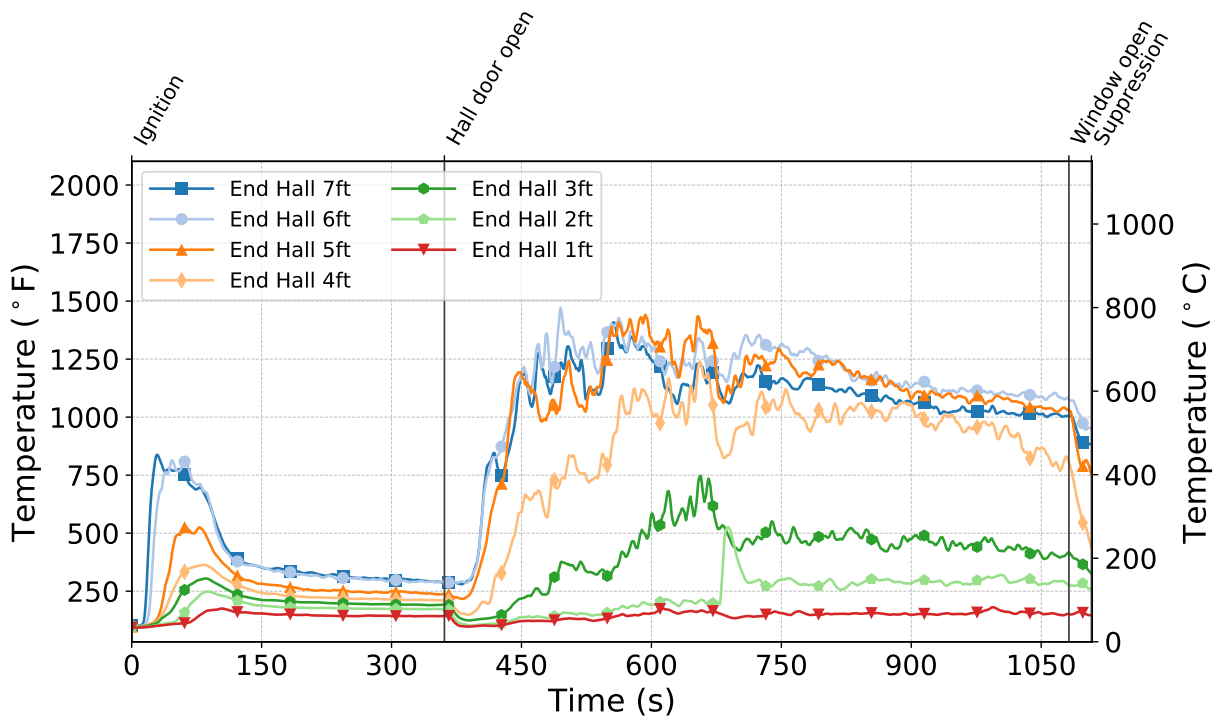


Figure C.180: Temperatures measured by the end hall thermocouples during Test 17.

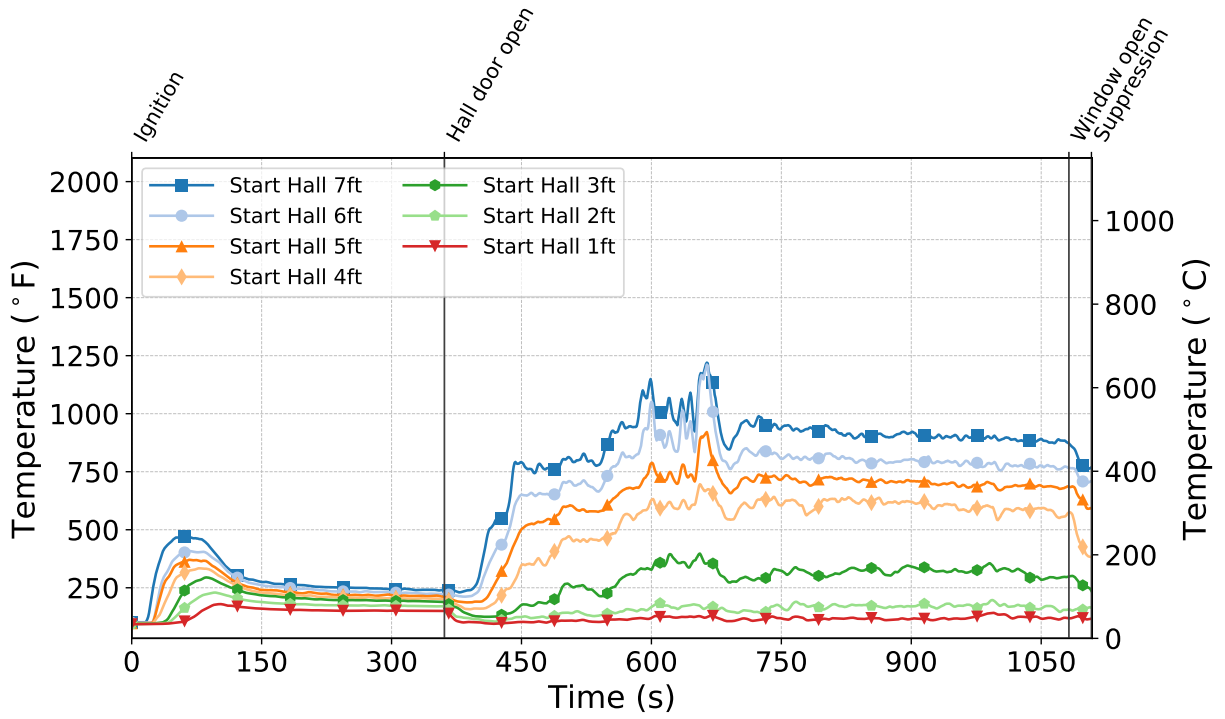


Figure C.181: Temperatures measured by the start hall thermocouples during Test 17.

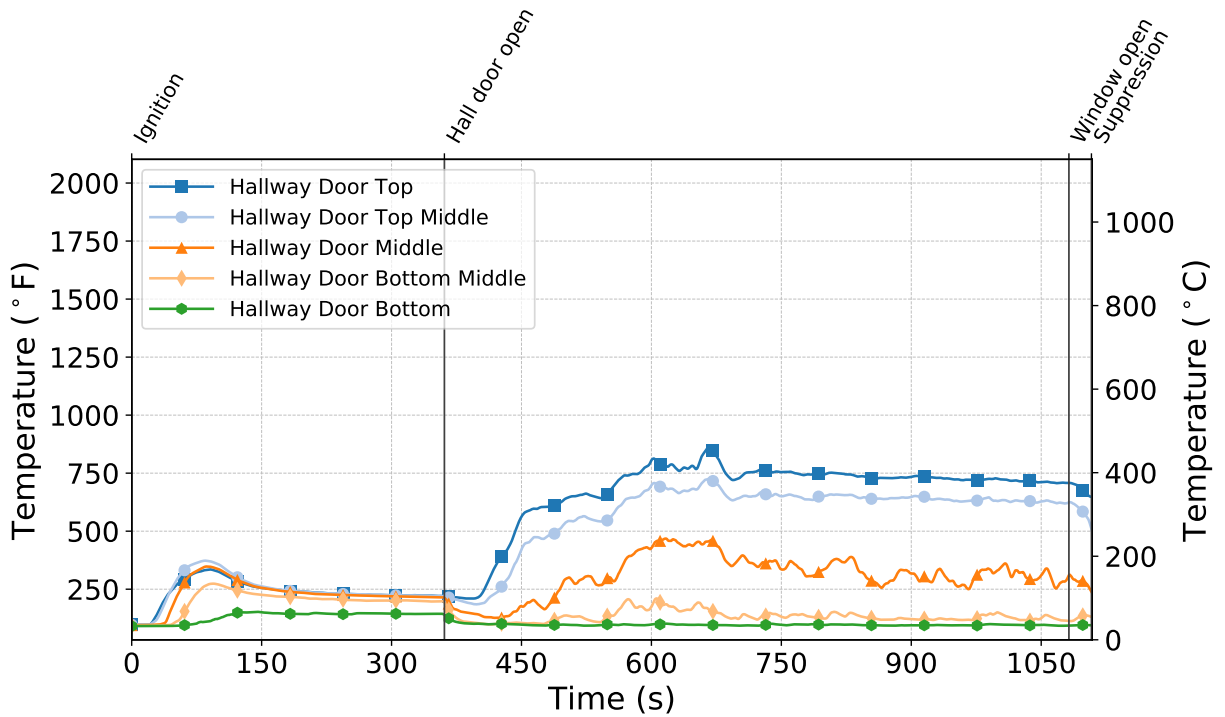


Figure C.182: Temperatures measured by the hallway door thermocouples during Test 17.

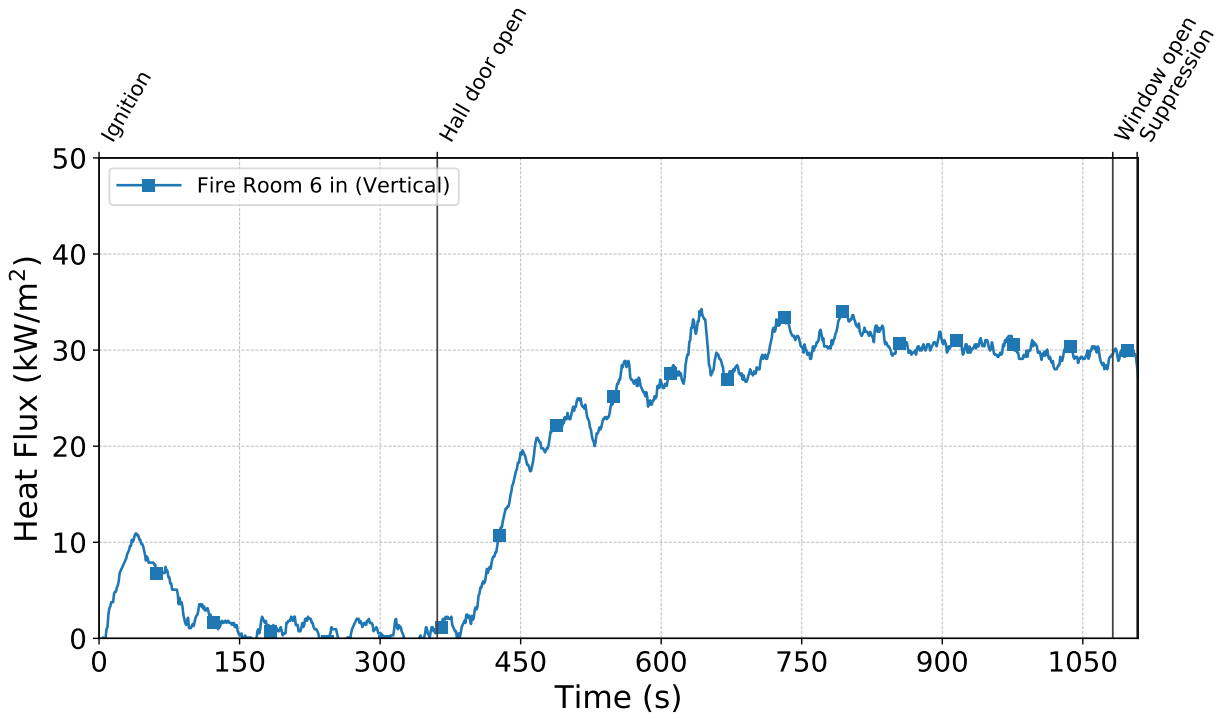


Figure C.183: Heat flux measured by the fire room gauge during Test 17.

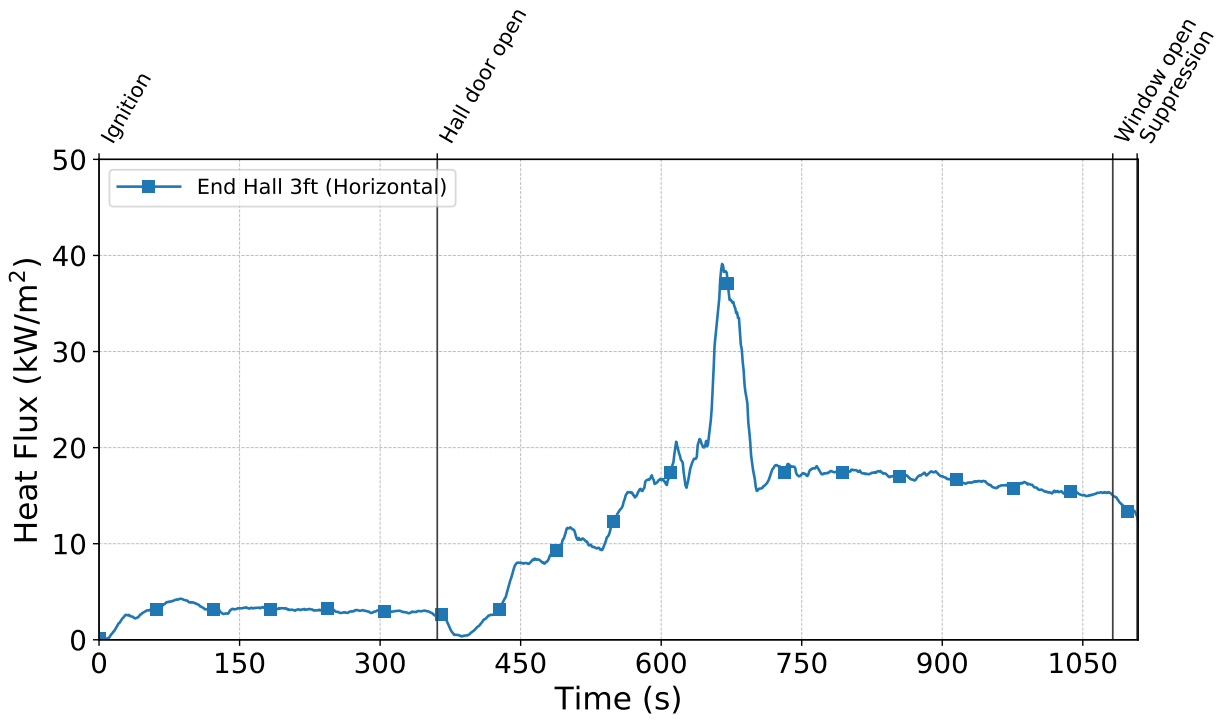


Figure C.184: Heat flux measured by the hallway gauges during Test 17.

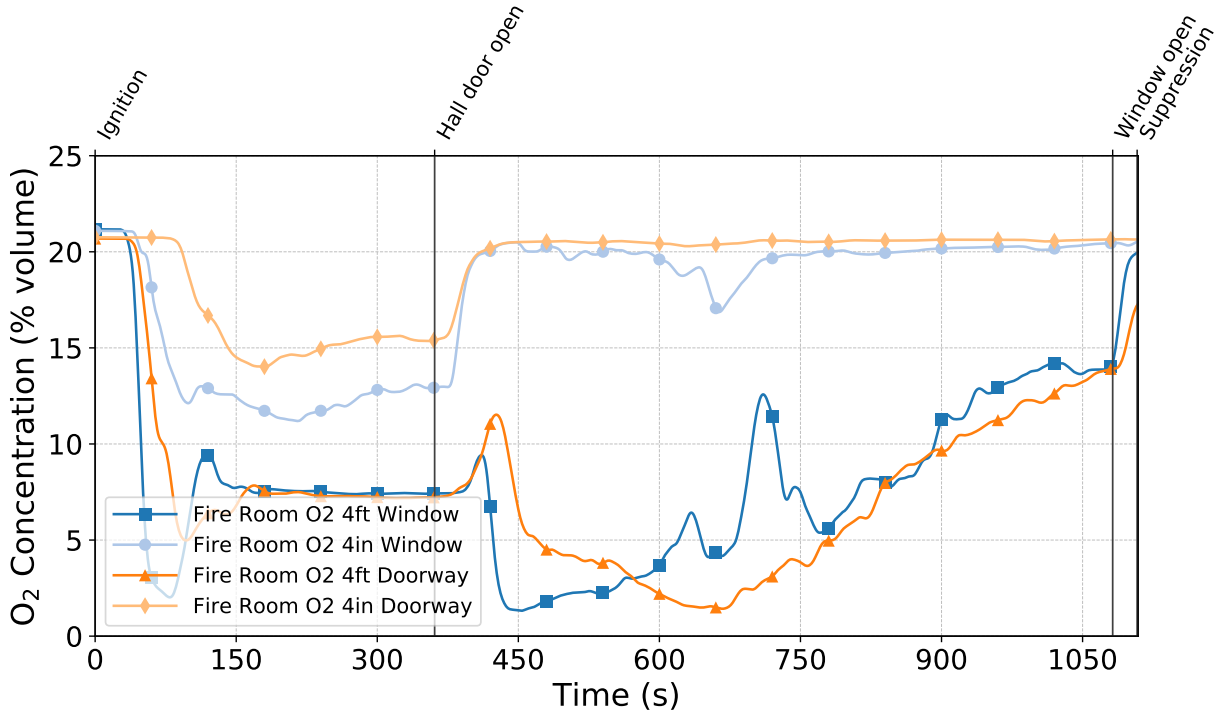


Figure C.185: Oxygen concentrations measured by the fire room gas sampling probes during Test 17.

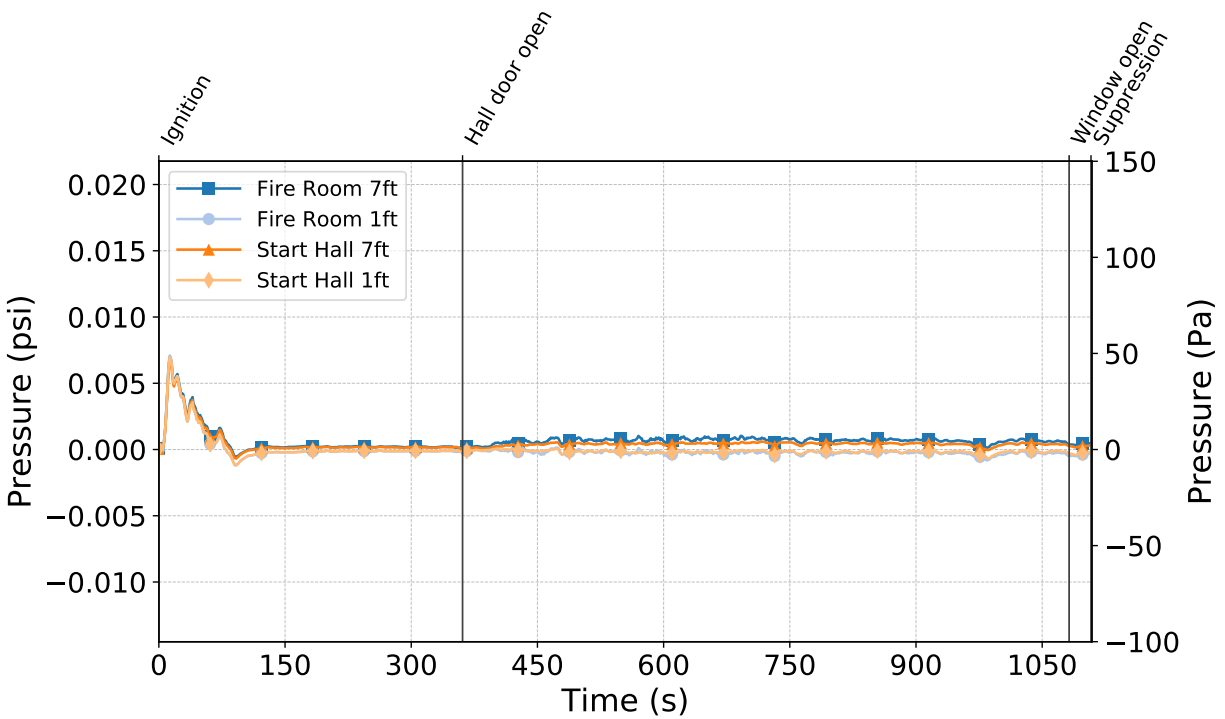


Figure C.186: Pressures measured by the fire room and hallway probes during Test 17.

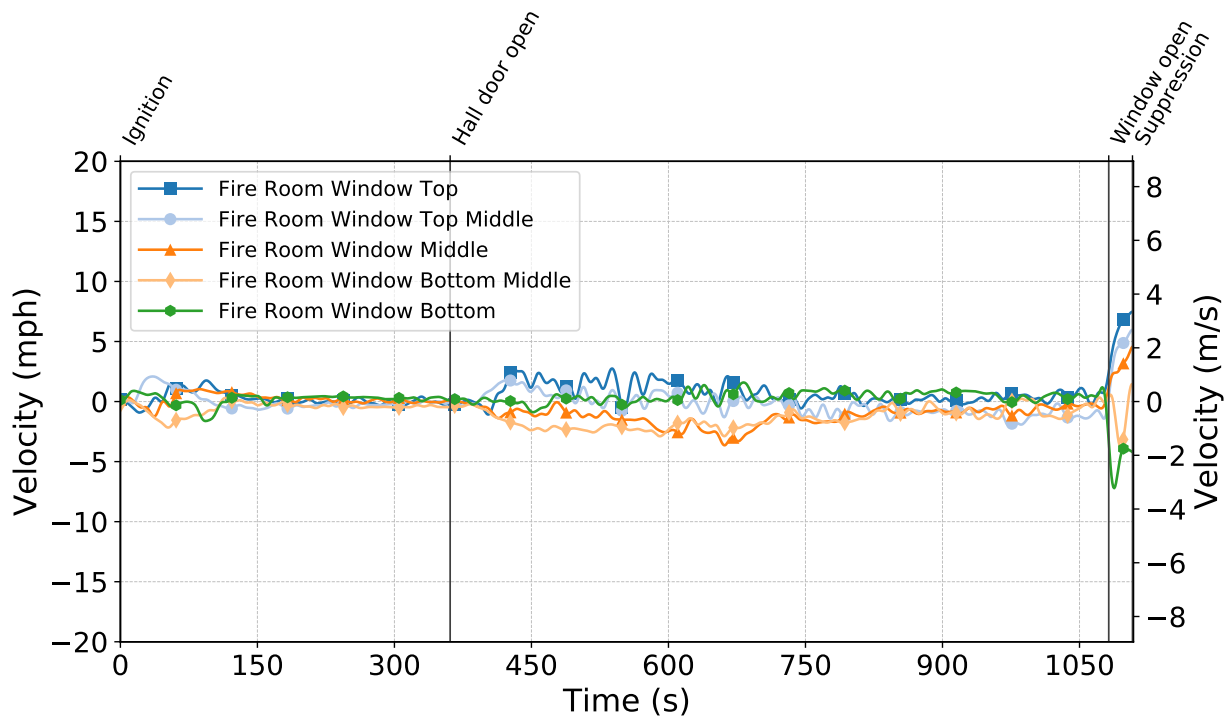


Figure C.187: Gas velocities measured by the fire room window bdps during Test 17.

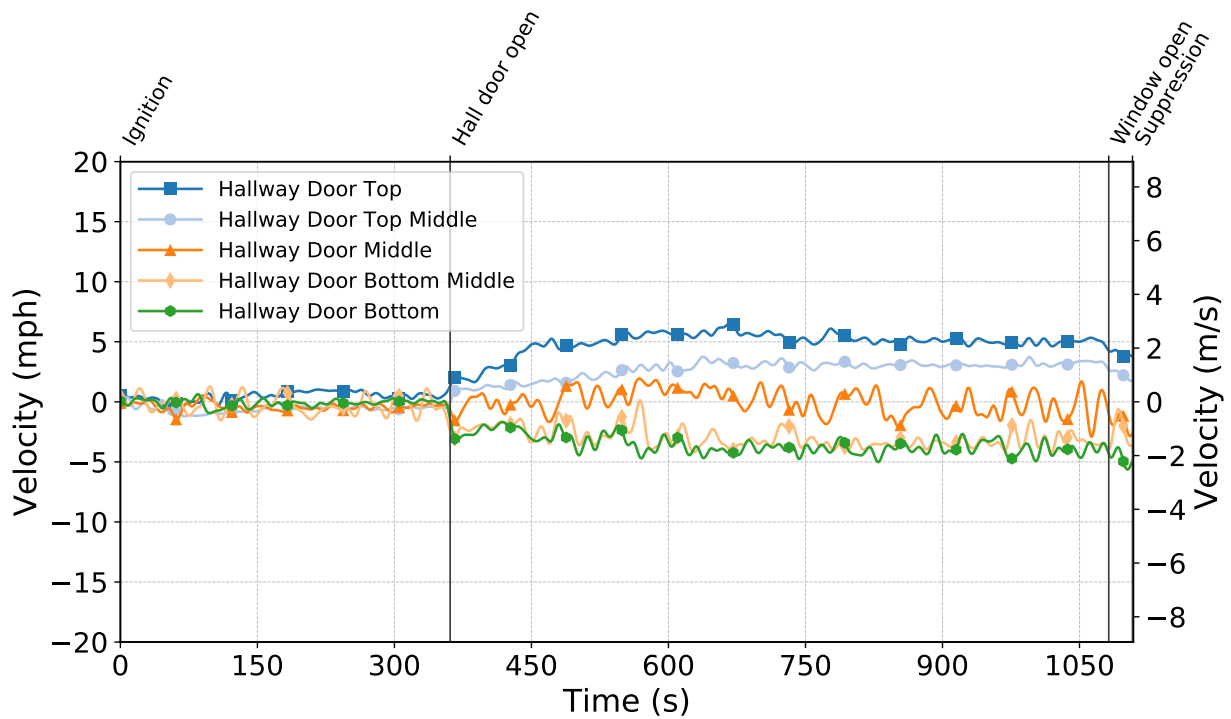


Figure C.188: Gas velocities measured by the hallway door bdps during Test 17.

Test 18

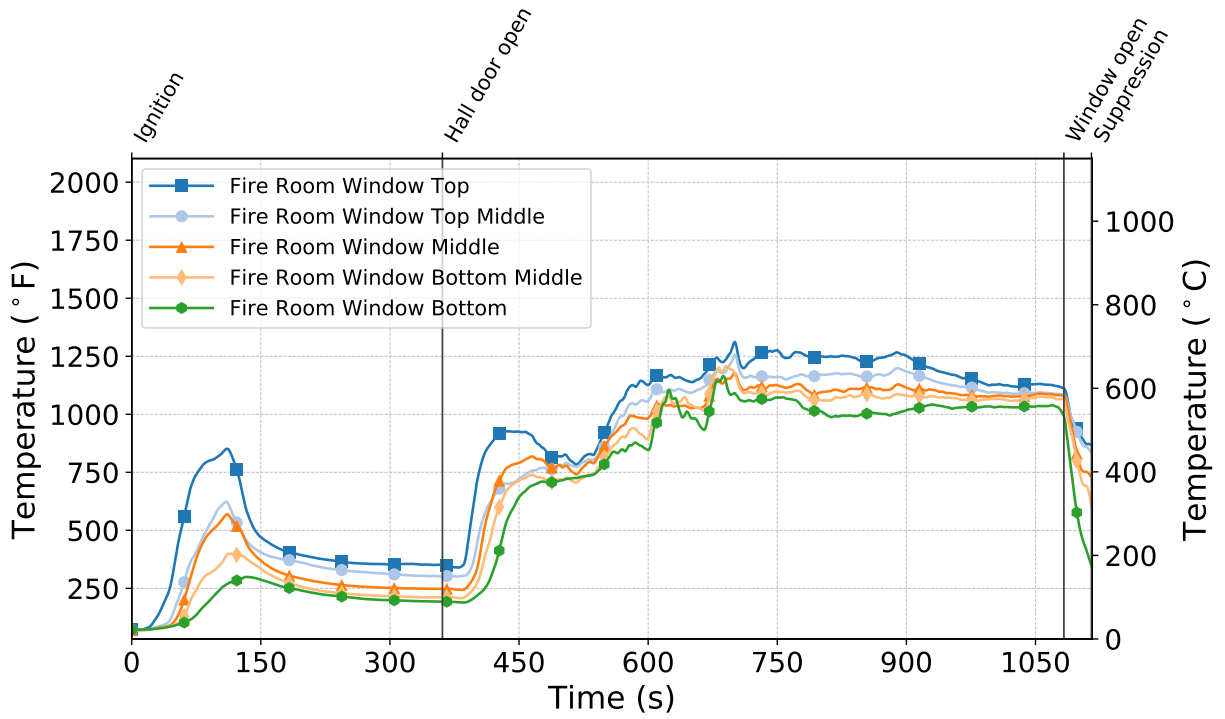


Figure C.189: Temperatures measured by the fire room window thermocouples during Test 18.

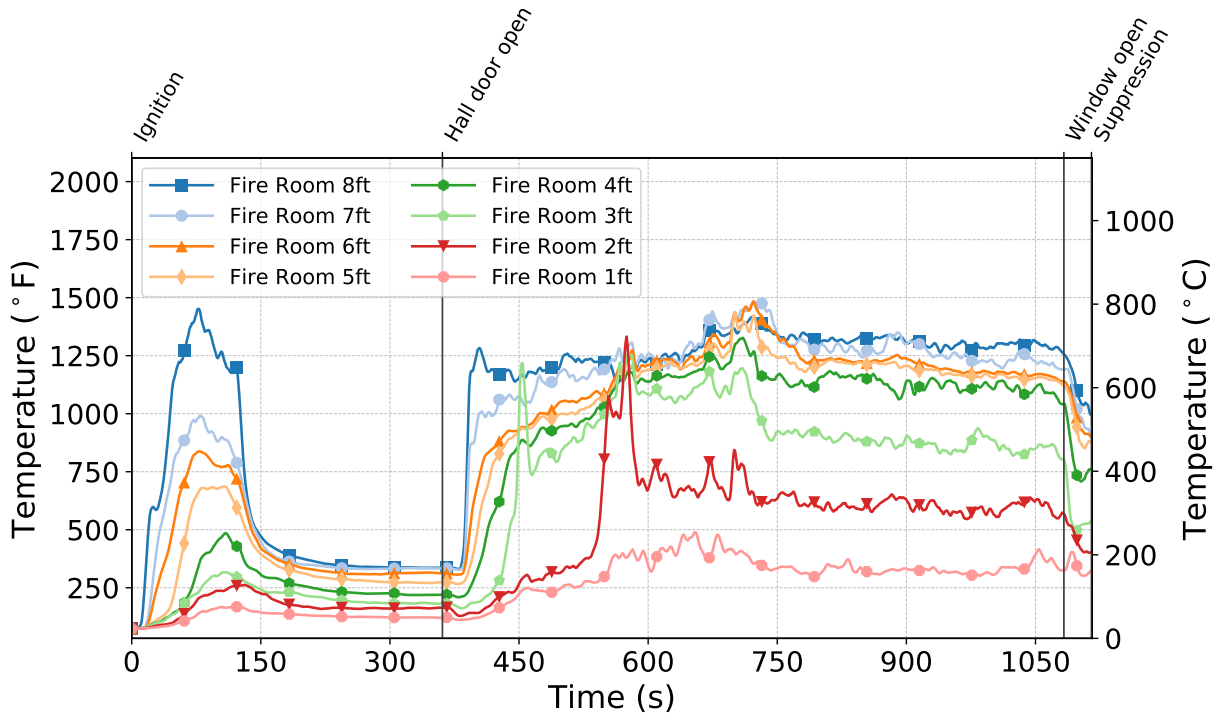


Figure C.190: Temperatures measured by the fire room thermocouples during Test 18.

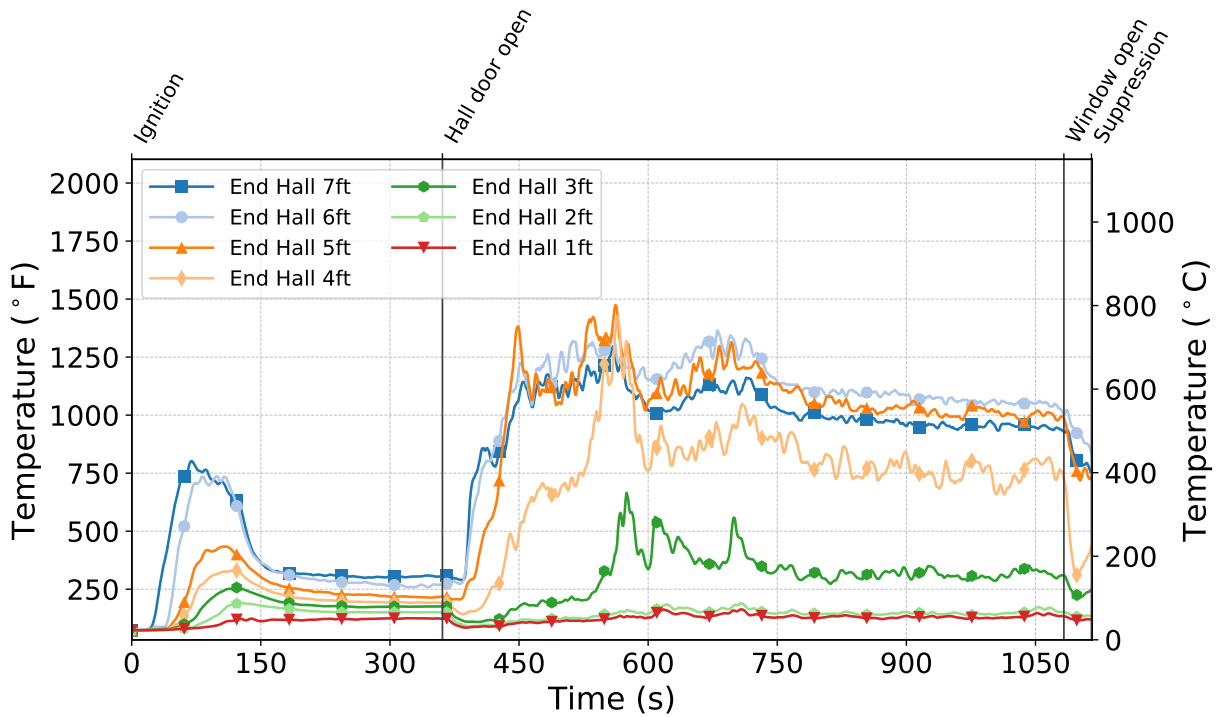


Figure C.191: Temperatures measured by the end hall thermocouples during Test 18.

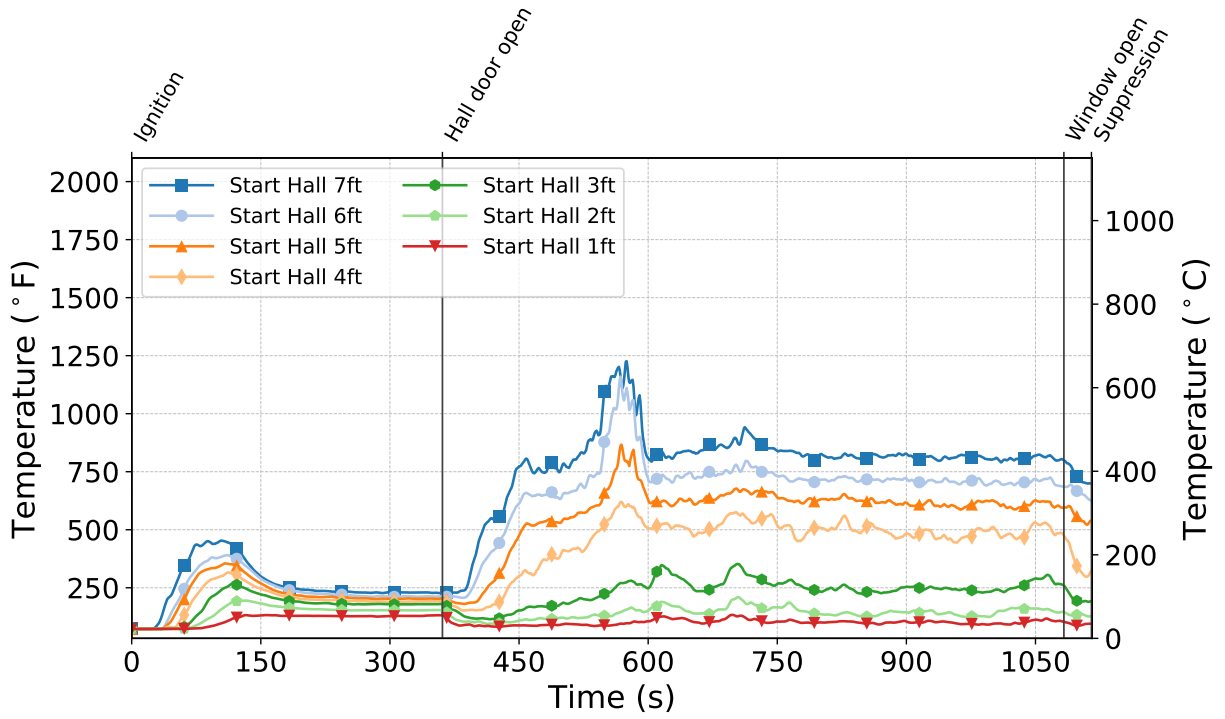


Figure C.192: Temperatures measured by the start hall thermocouples during Test 18.

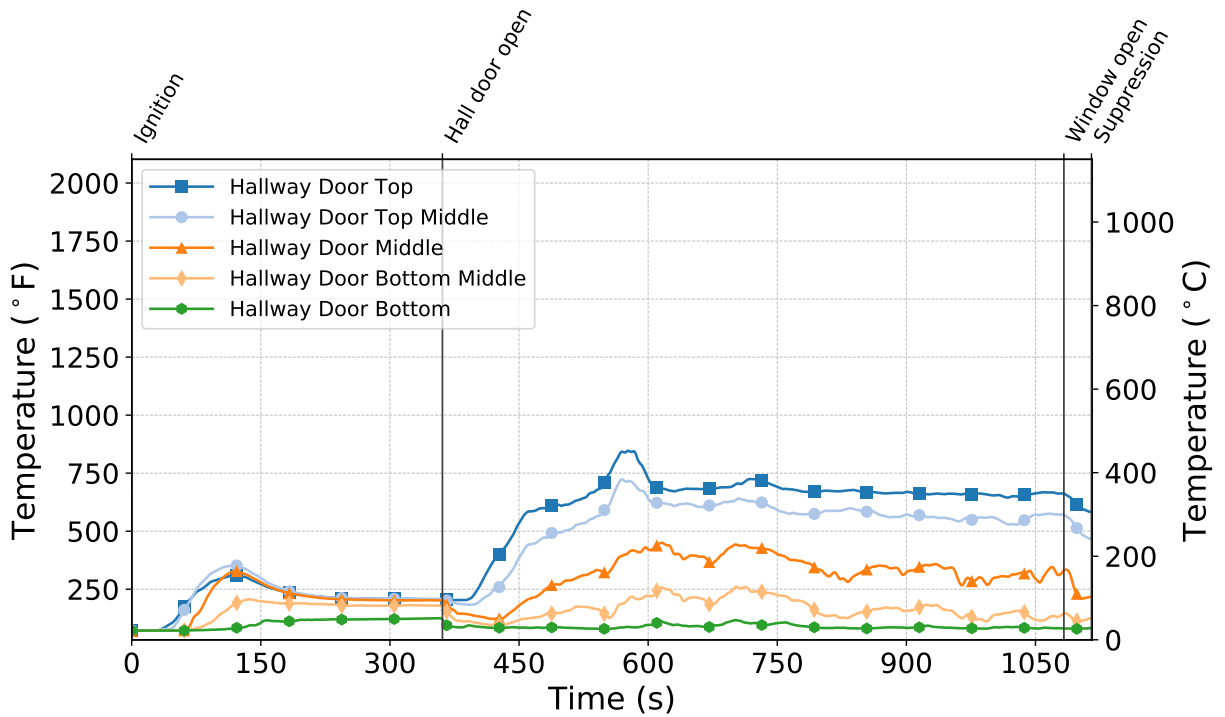


Figure C.193: Temperatures measured by the hallway door thermocouples during Test 18.

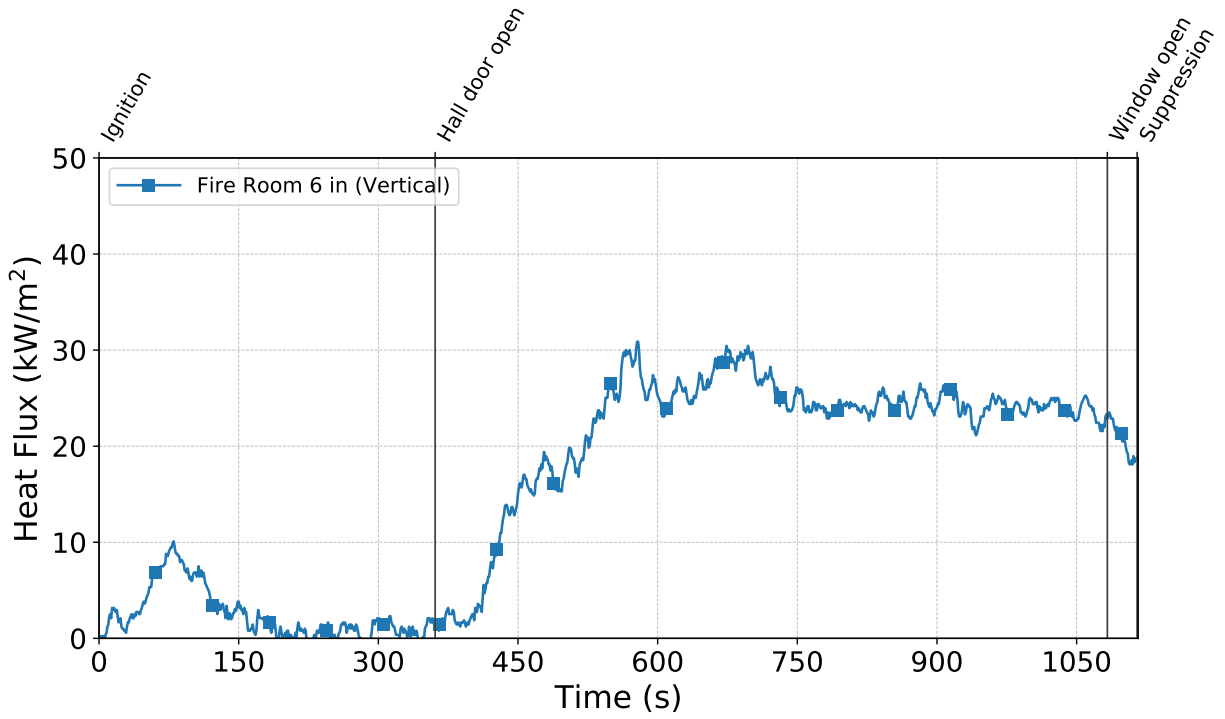


Figure C.194: Heat flux measured by the fire room gauge during Test 18.

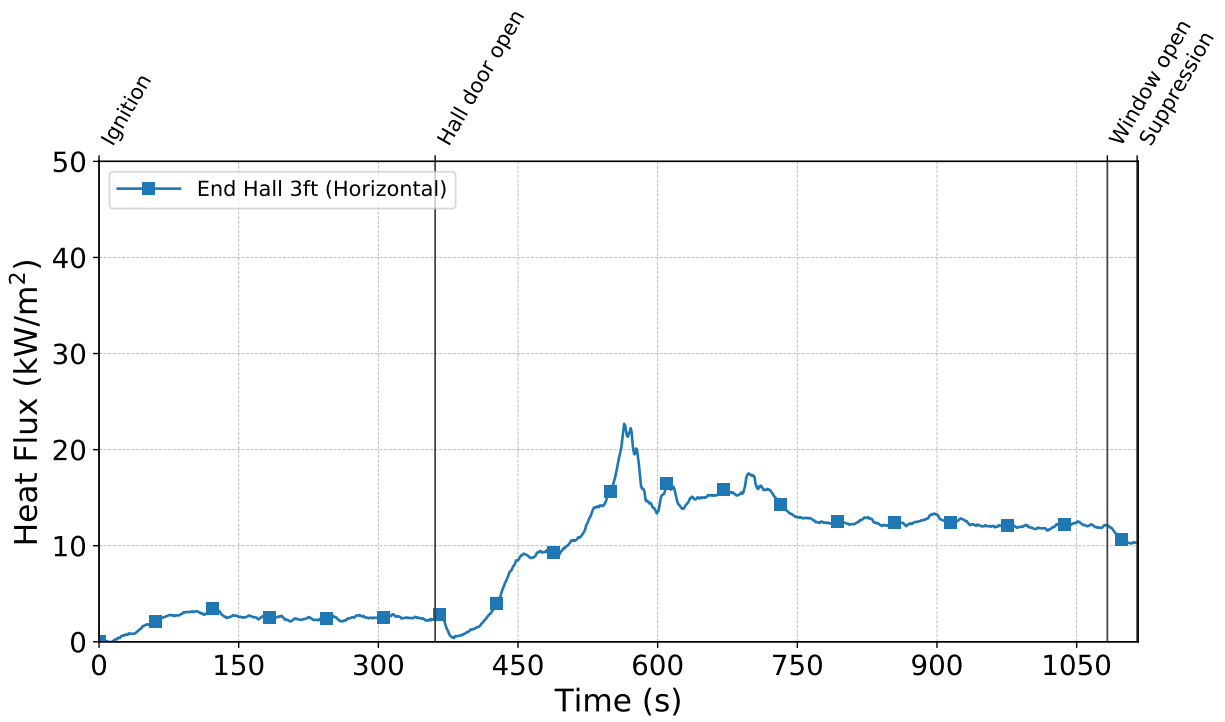


Figure C.195: Heat flux measured by the hallway gauges during Test 18.

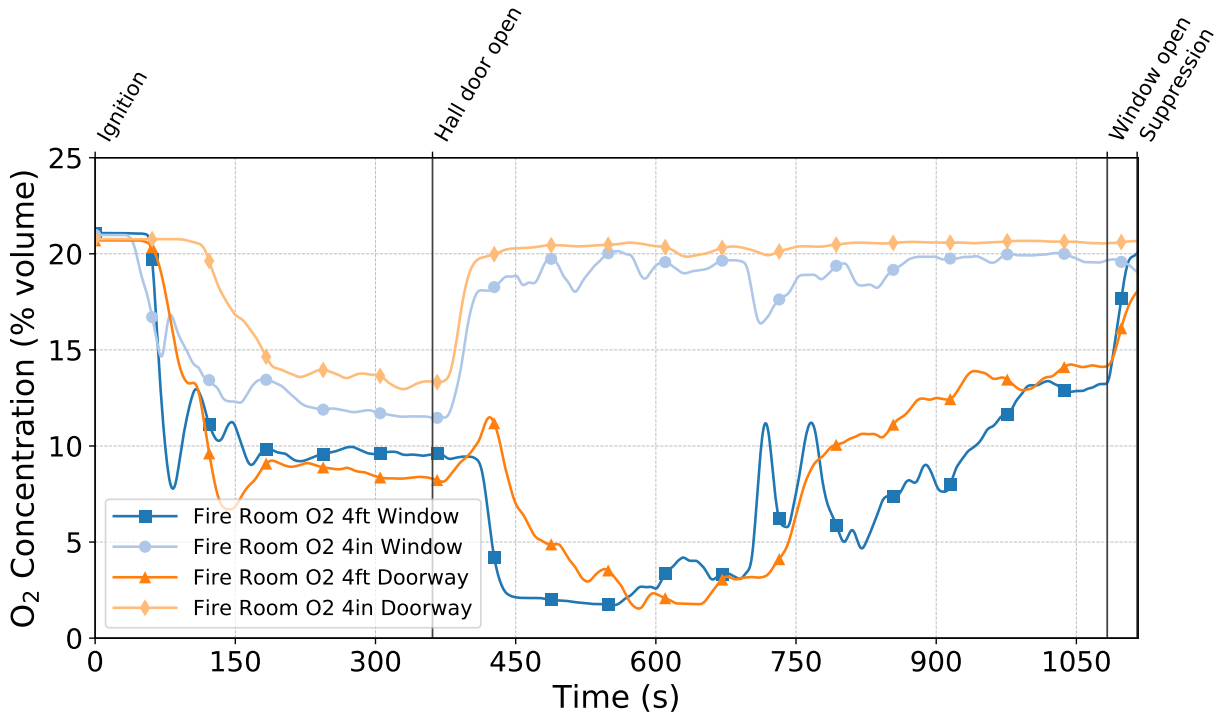


Figure C.196: Oxygen concentrations measured by the fire room gas sampling probes during Test 18.

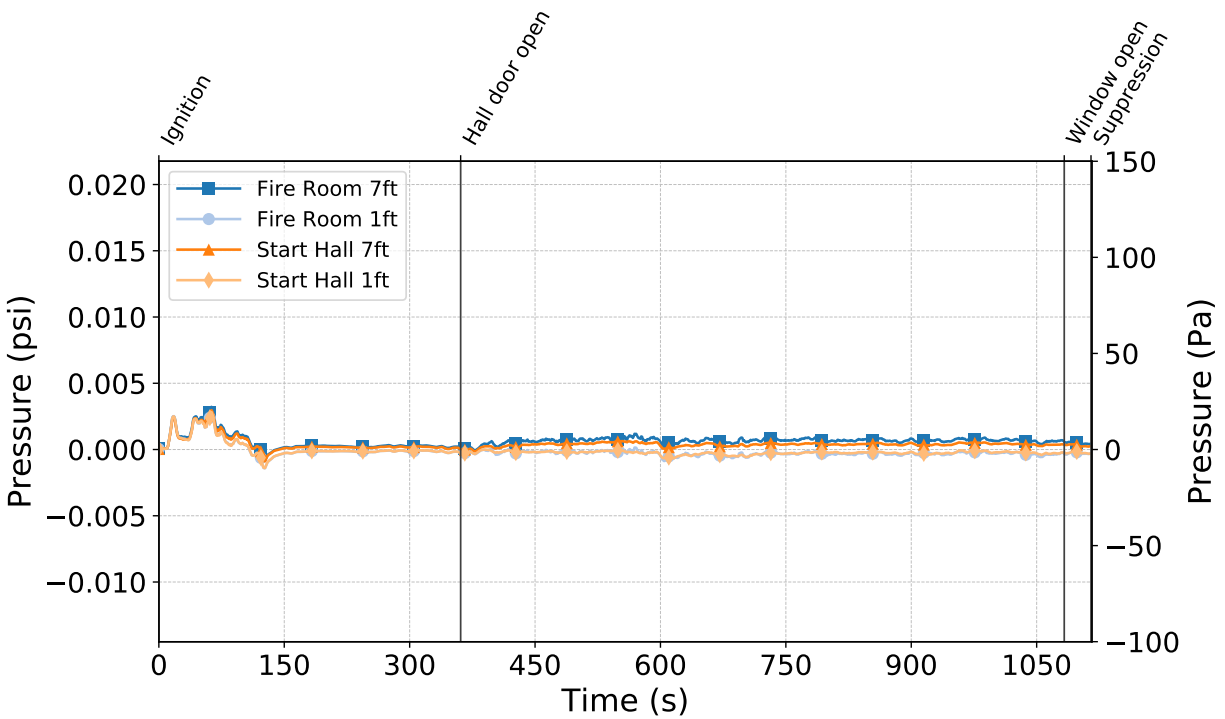


Figure C.197: Pressures measured by the fire room and hallway probes during Test 18.

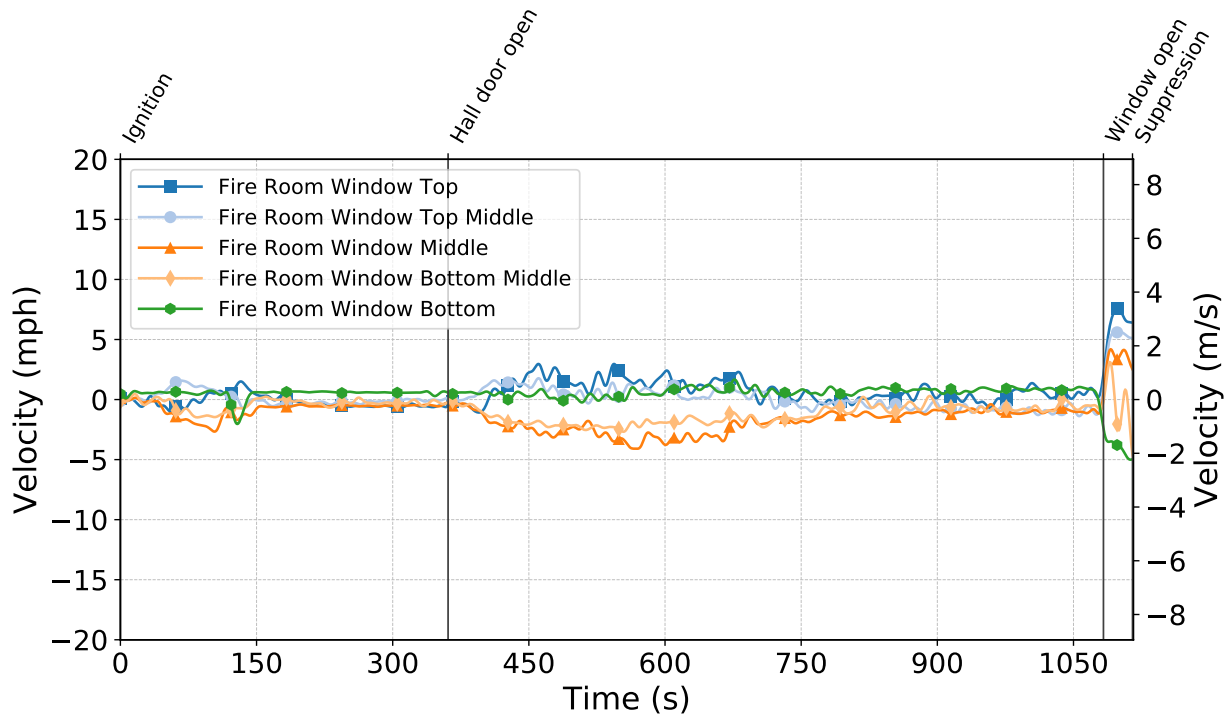


Figure C.198: Gas velocities measured by the fire room window bdps during Test 18.

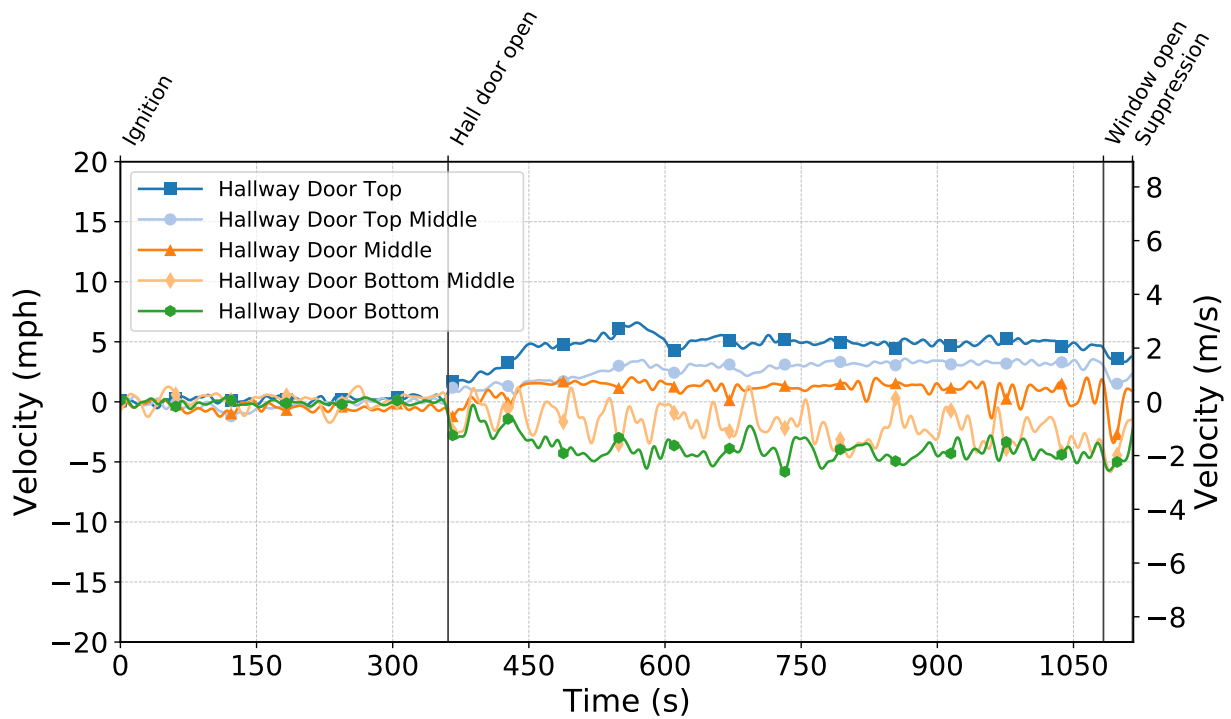


Figure C.199: Gas velocities measured by the hallway door bdps during Test 18.

Test 19

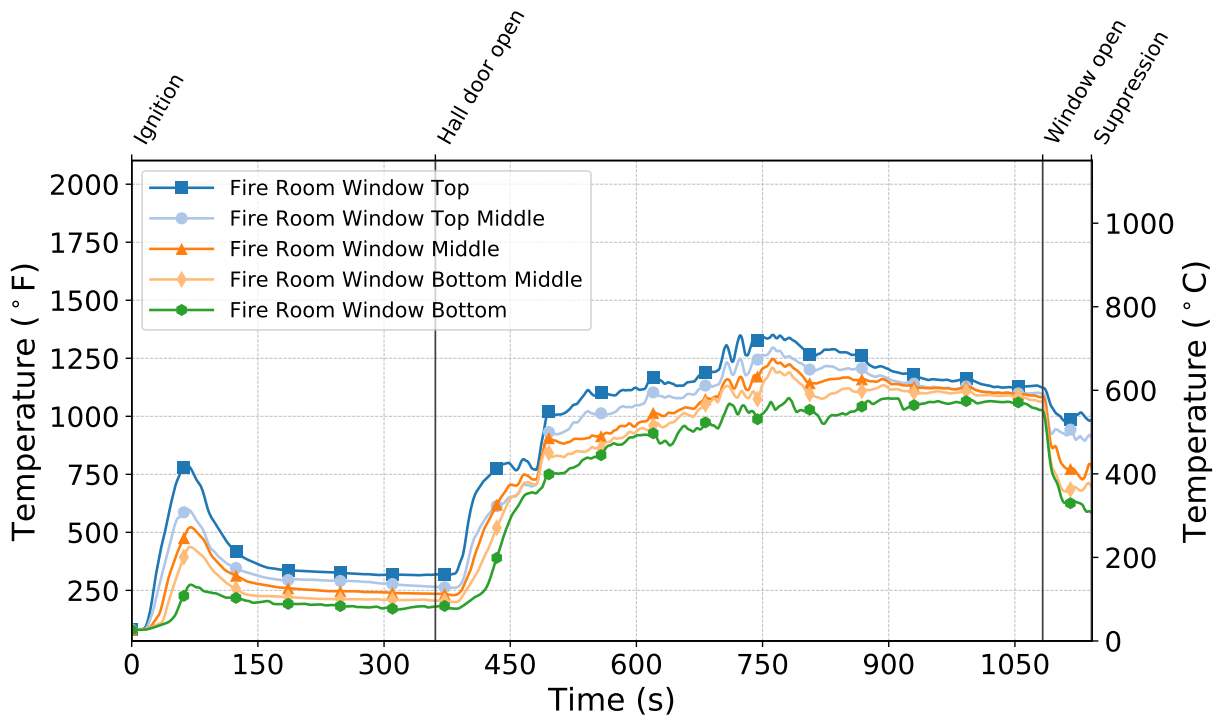


Figure C.200: Temperatures measured by the fire room window thermocouples during Test 19.

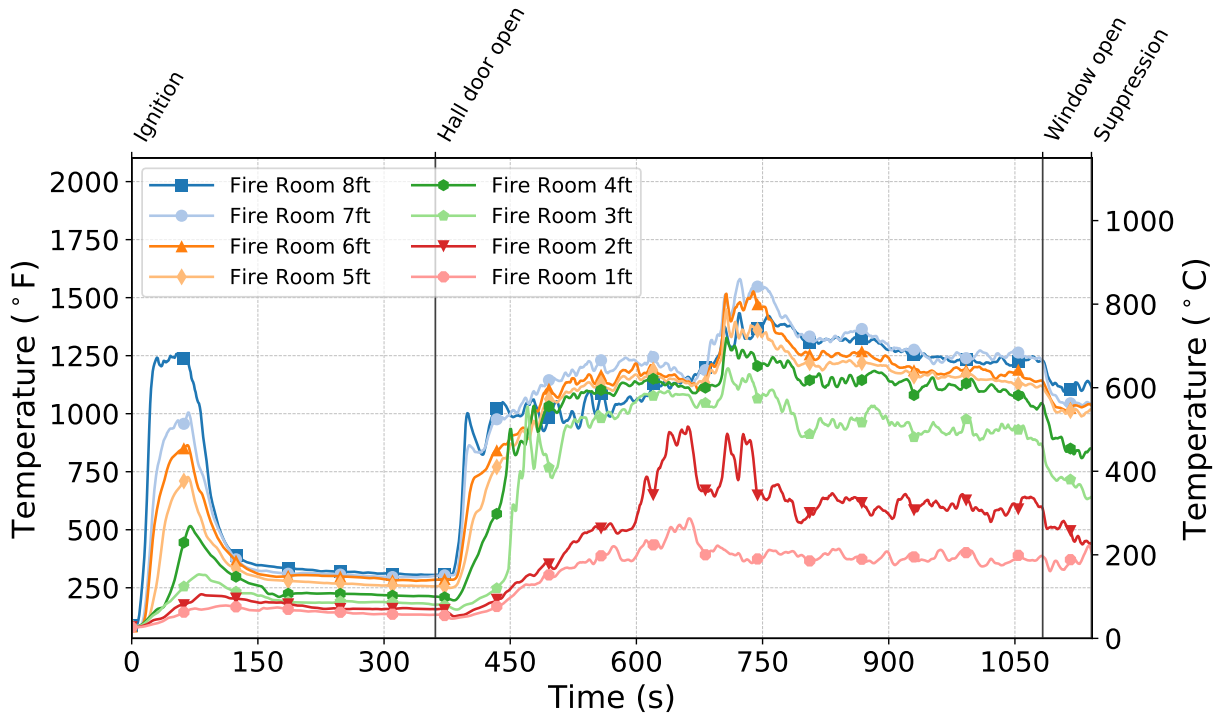


Figure C.201: Temperatures measured by the fire room thermocouples during Test 19.

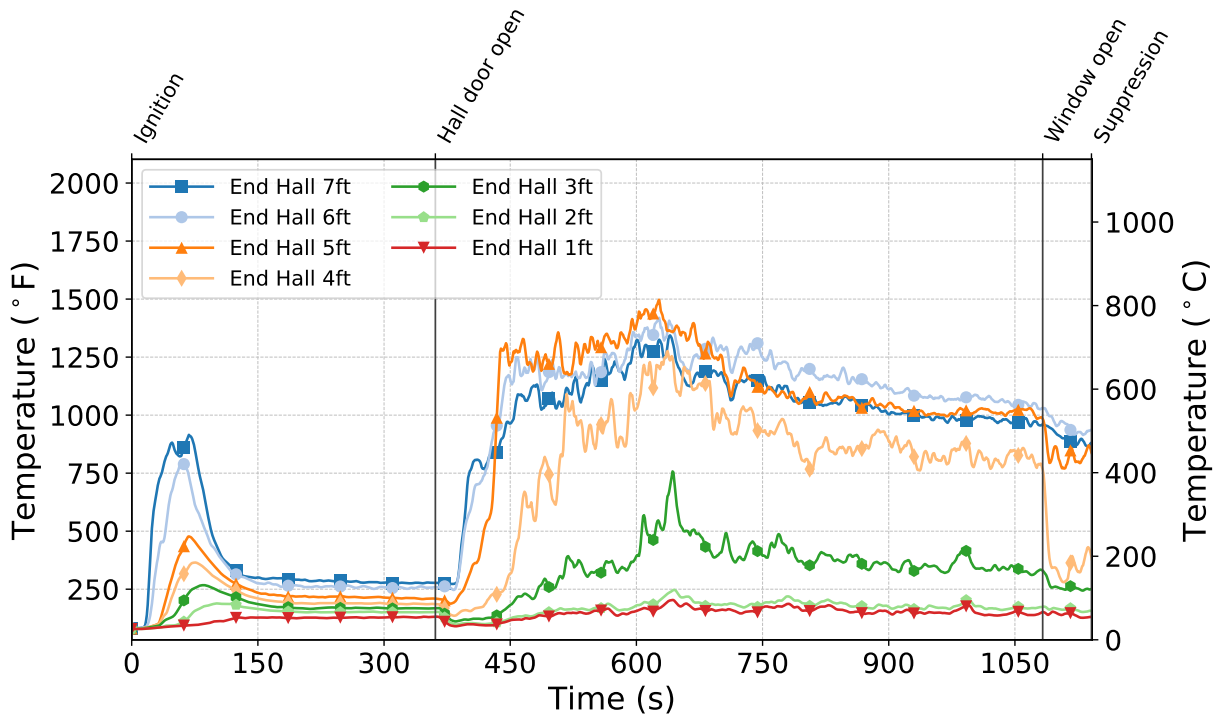


Figure C.202: Temperatures measured by the end hall thermocouples during Test 19.

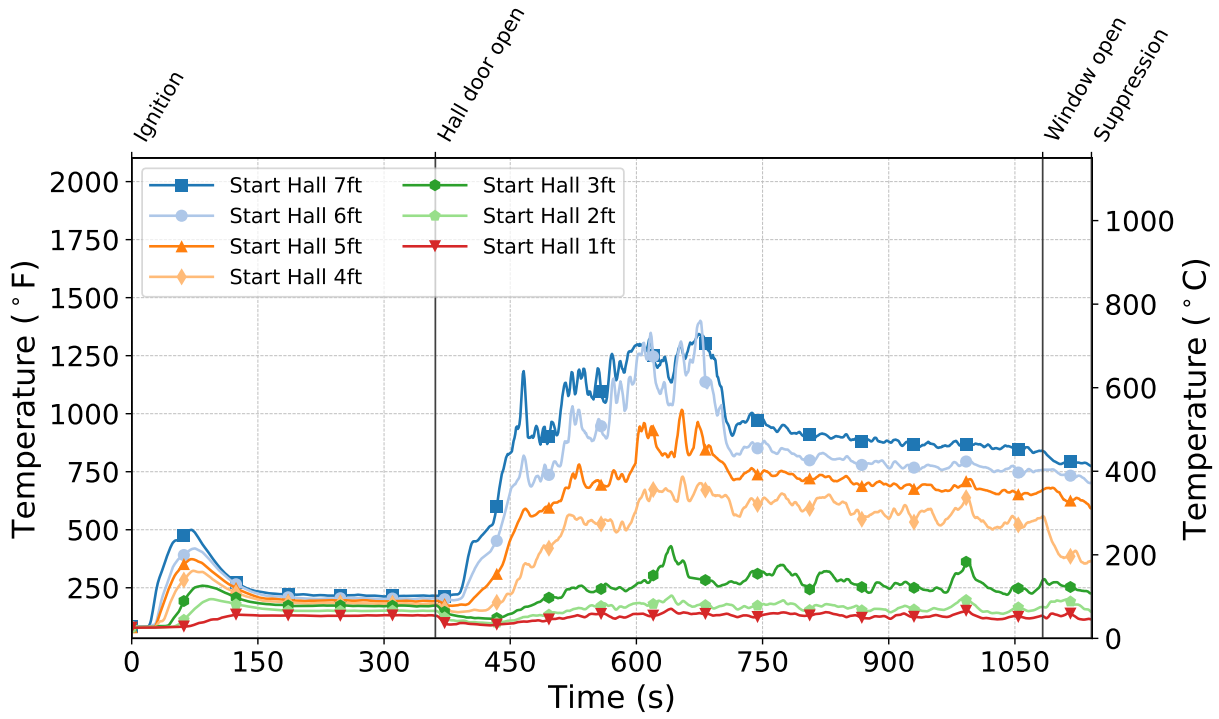


Figure C.203: Temperatures measured by the start hall thermocouples during Test 19.

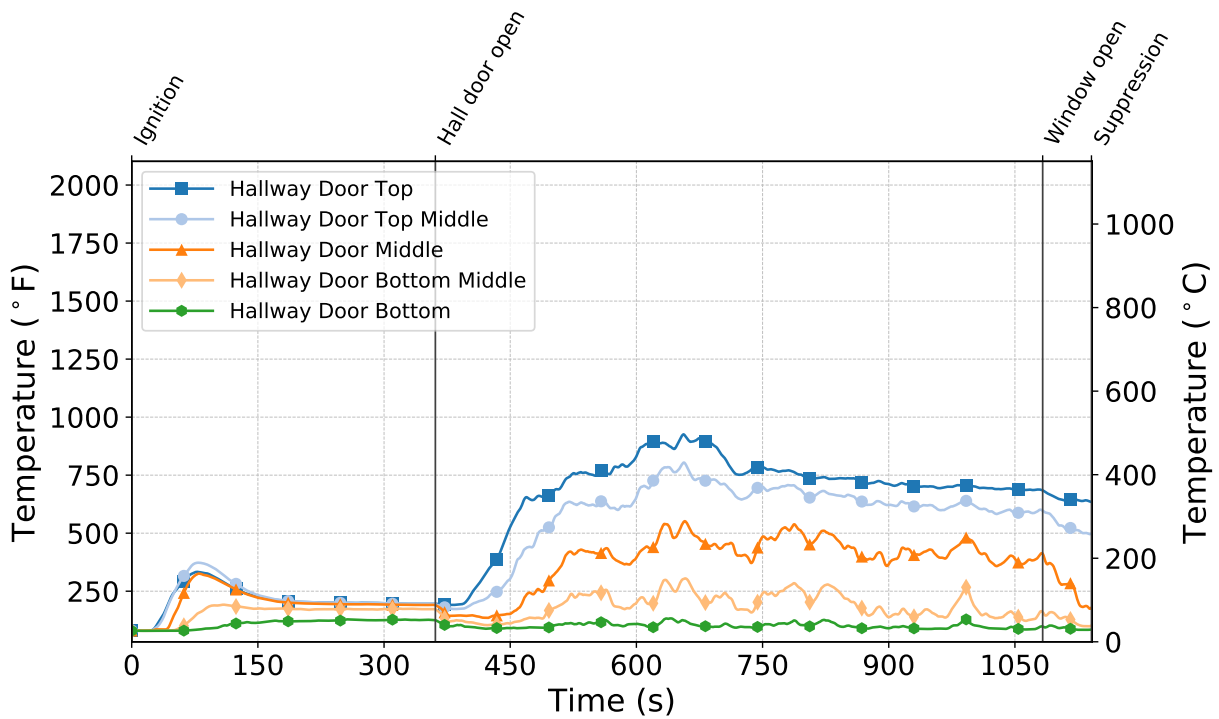


Figure C.204: Temperatures measured by the hallway door thermocouples during Test 19.

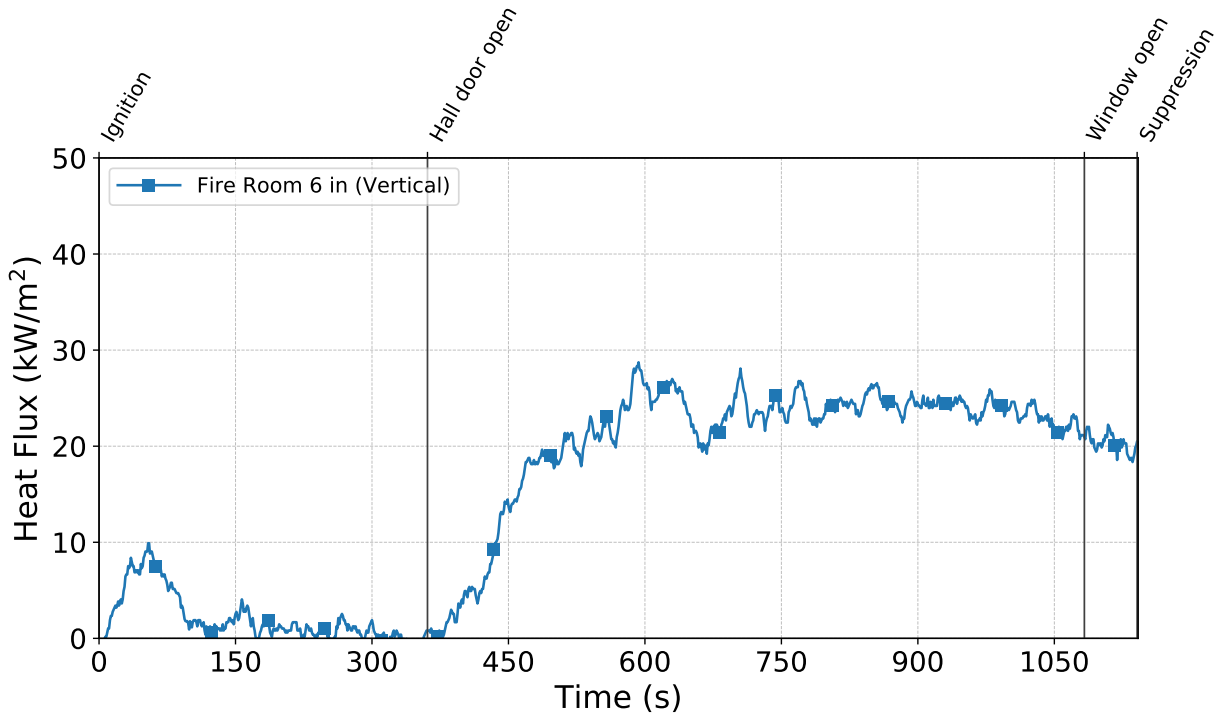


Figure C.205: Heat flux measured by the fire room gauge during Test 19.

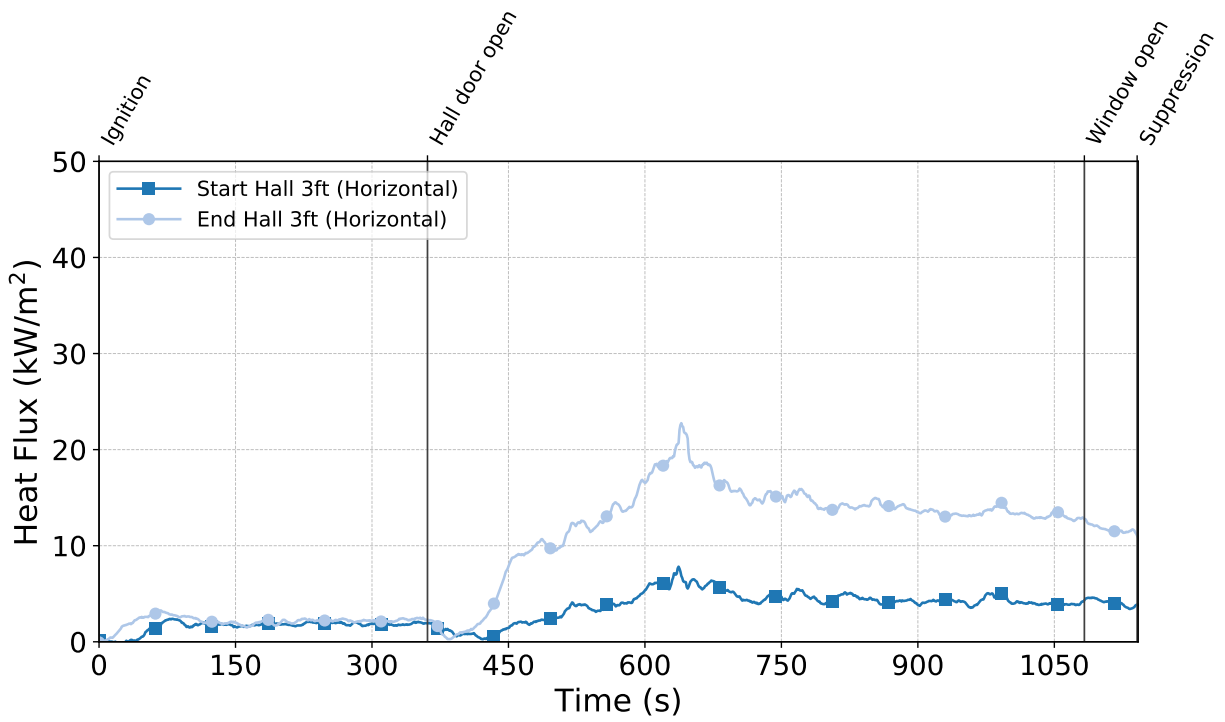


Figure C.206: Heat flux measured by the hallway gauges during Test 19.

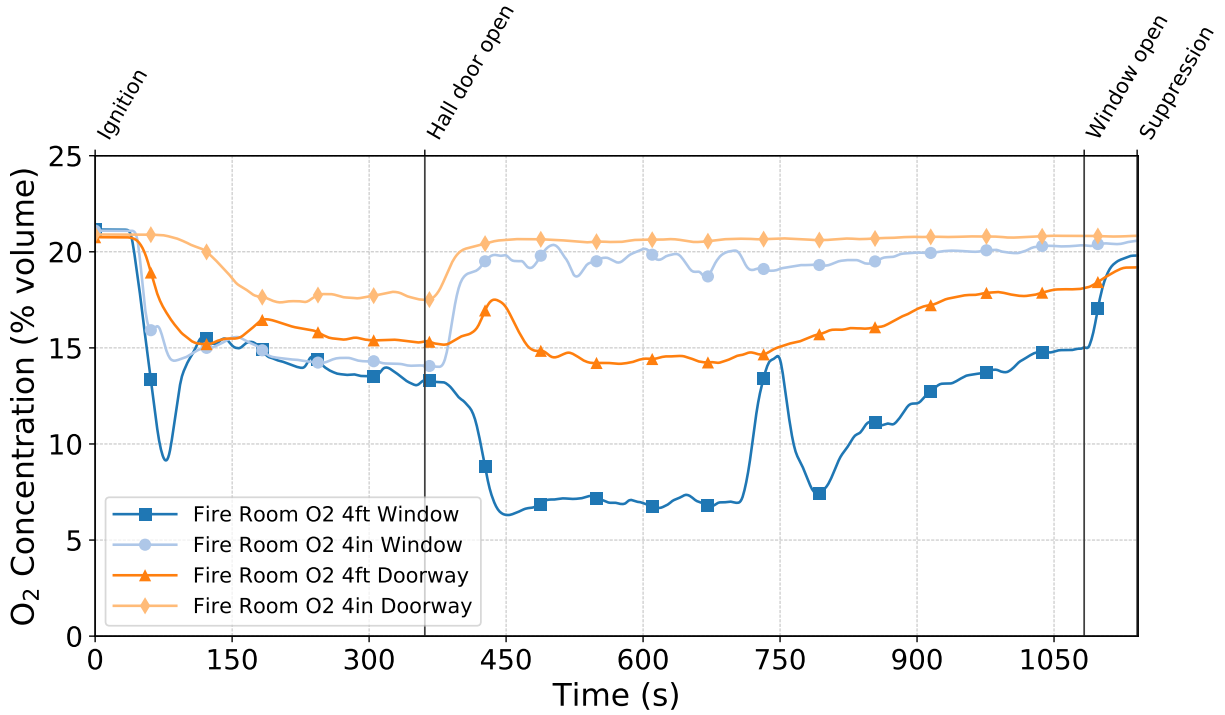


Figure C.207: Oxygen concentrations measured by the fire room gas sampling probes during Test 19.

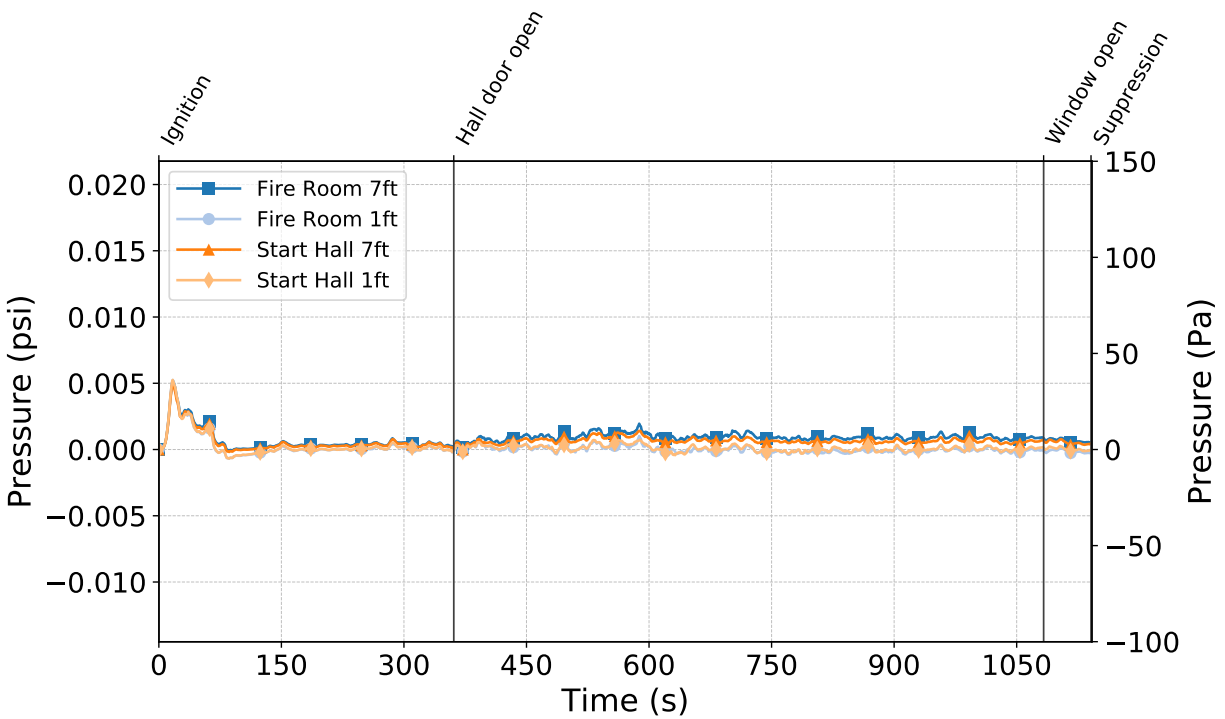


Figure C.208: Pressures measured by the fire room and hallway probes during Test 19.

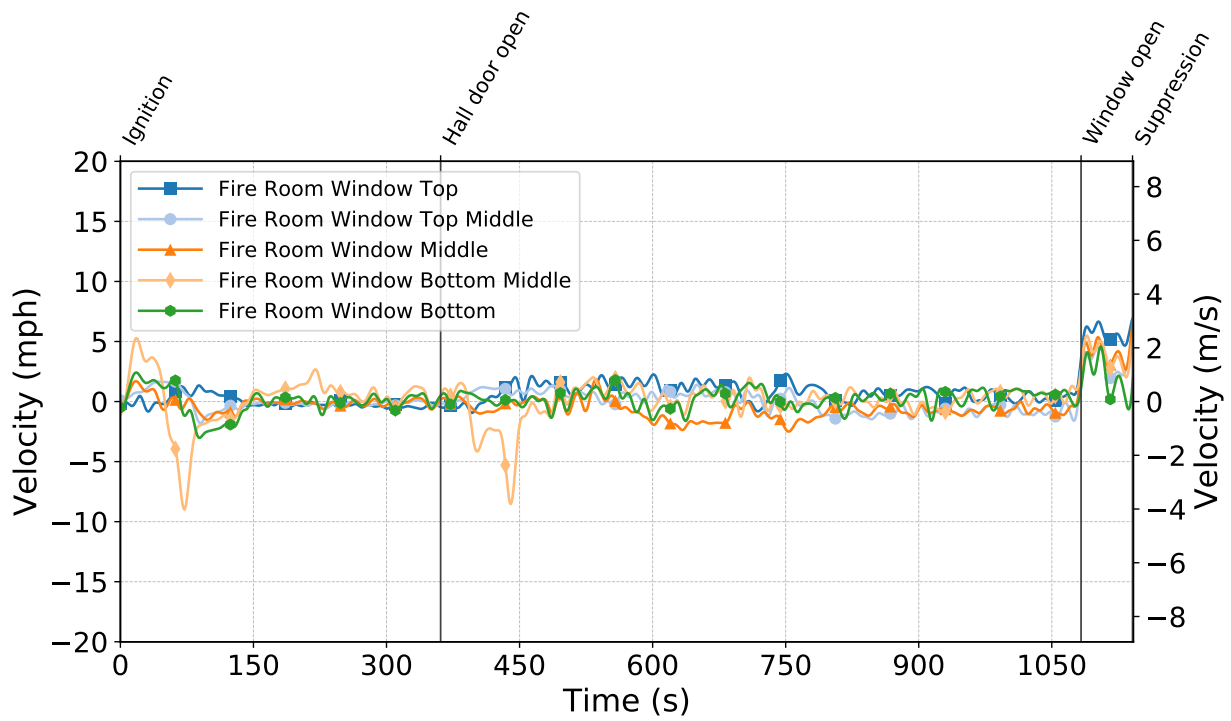


Figure C.209: Gas velocities measured by the fire room window bdps during Test 19.

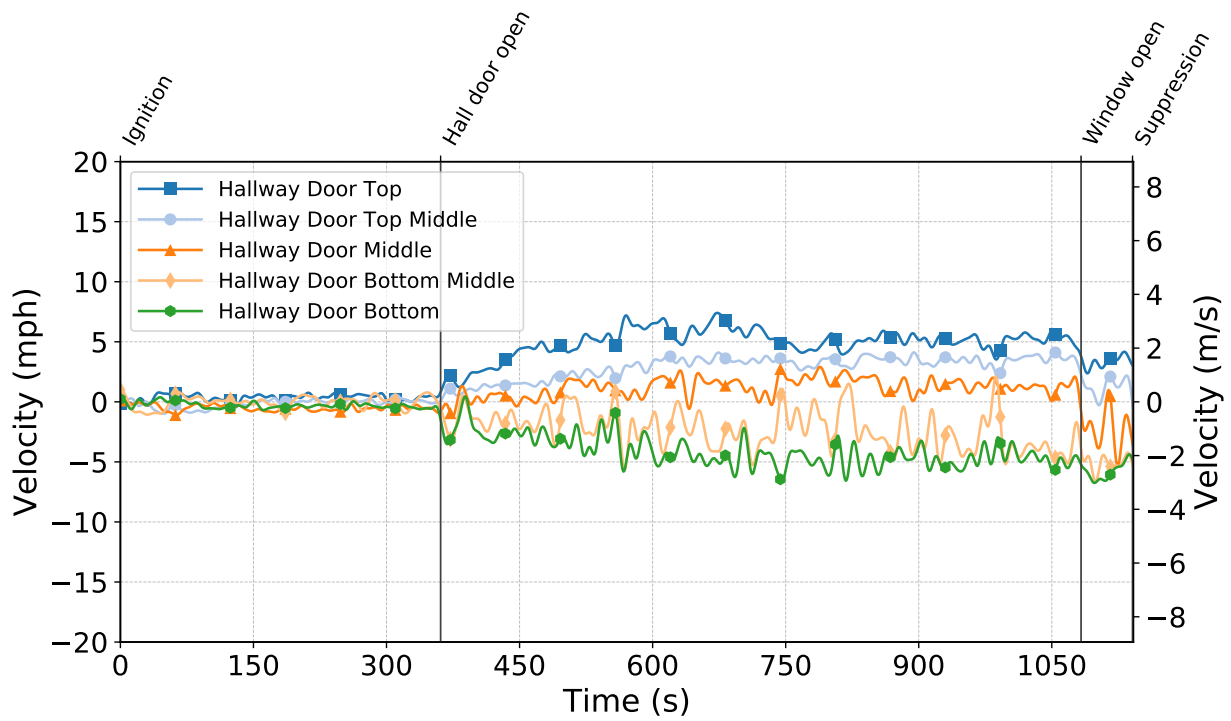


Figure C.210: Gas velocities measured by the hallway door bdps during Test 19.

C.3 Ventilation Effects Experiments

Test 20

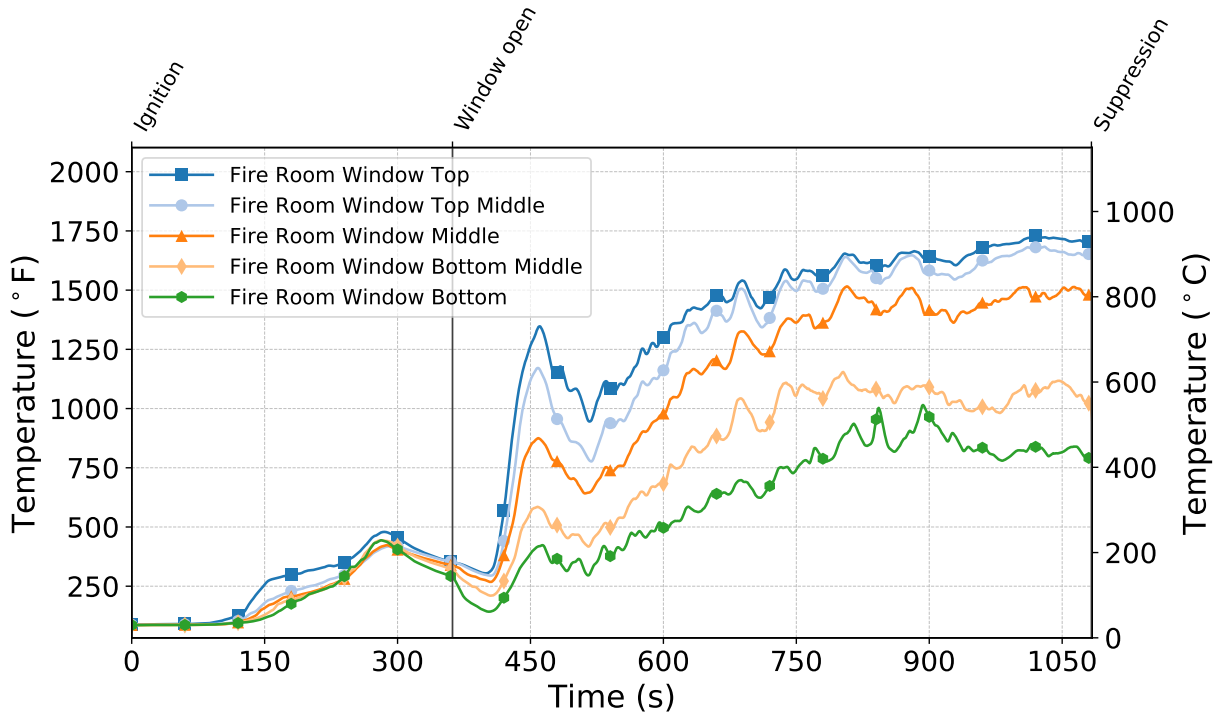


Figure C.211: Temperatures measured by the fire room window thermocouples during Test 20.

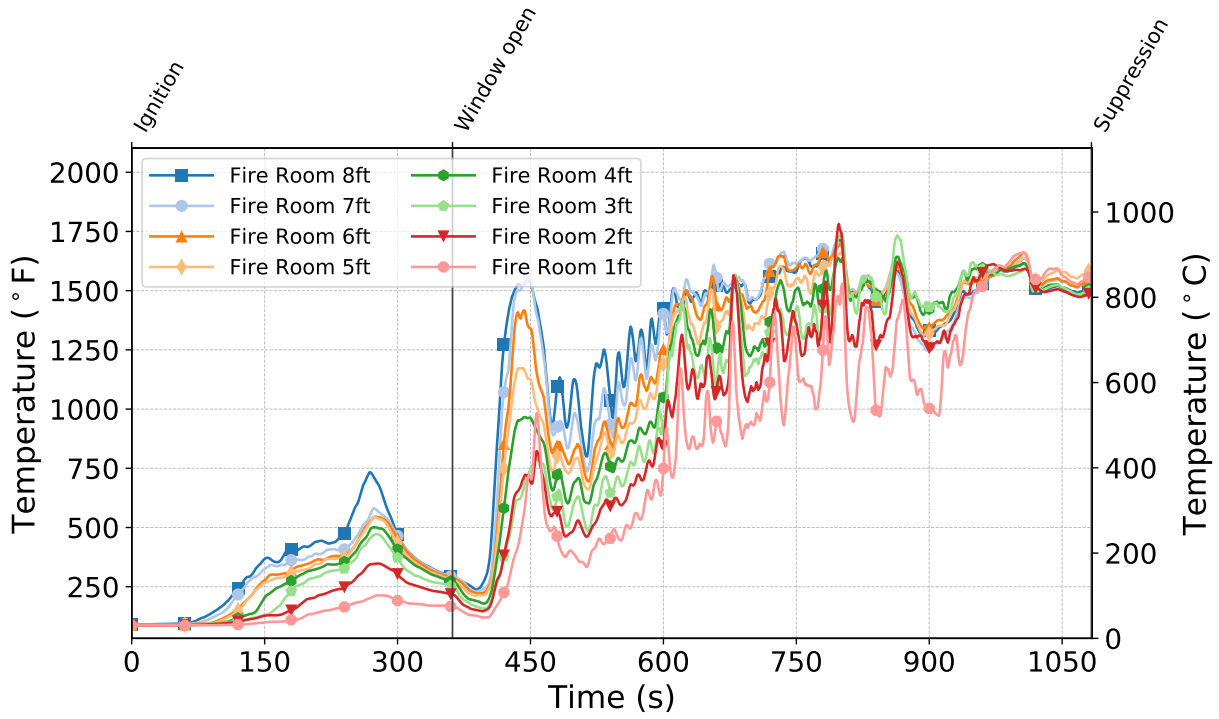


Figure C.212: Temperatures measured by the fire room thermocouples during Test 20.

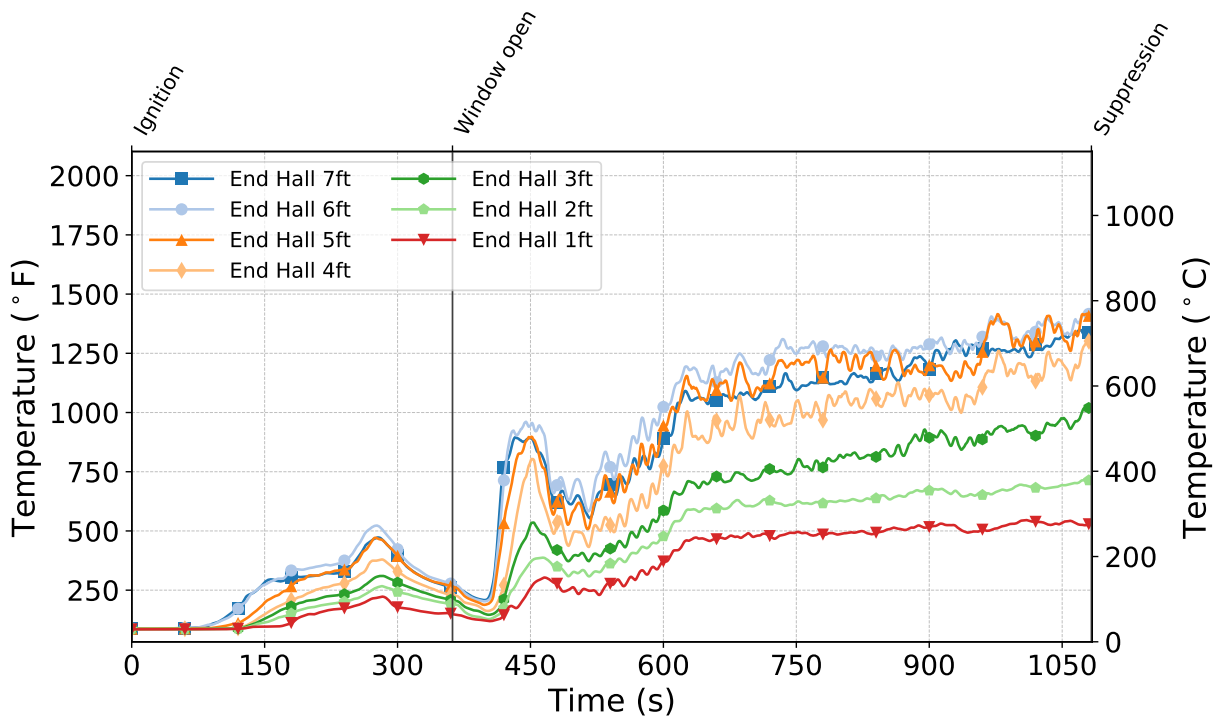


Figure C.213: Temperatures measured by the end hall thermocouples during Test 20.

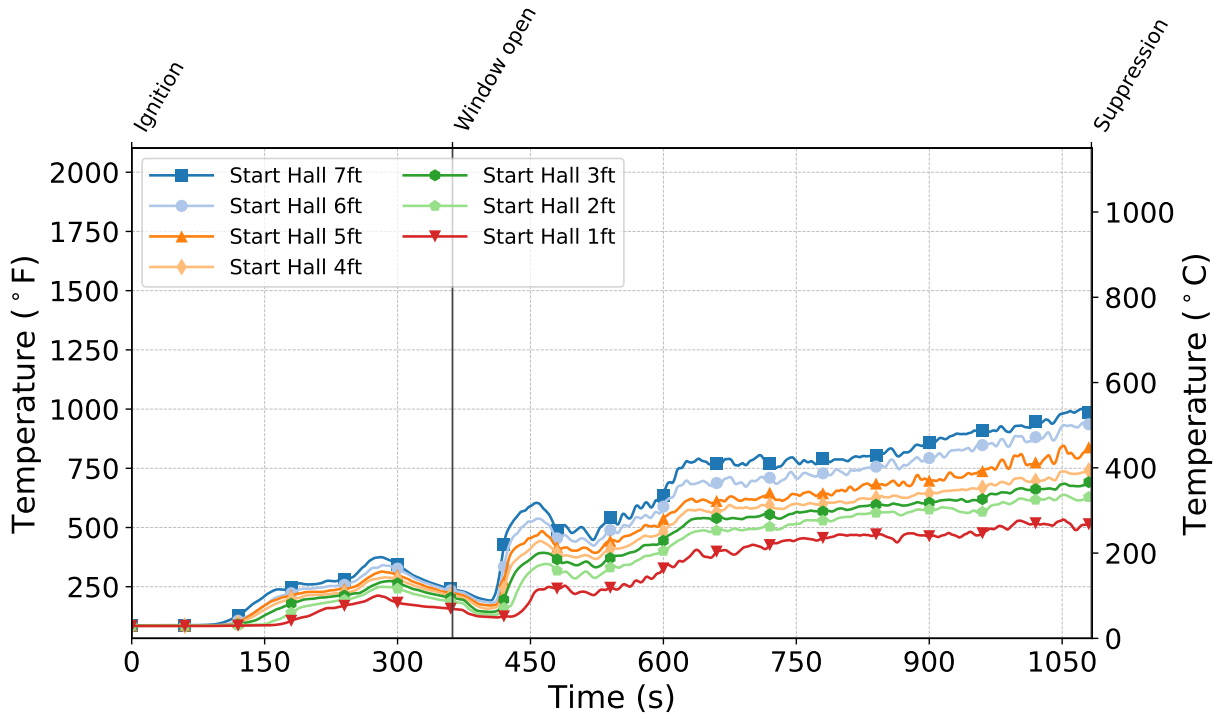


Figure C.214: Temperatures measured by the start hall thermocouples during Test 20.

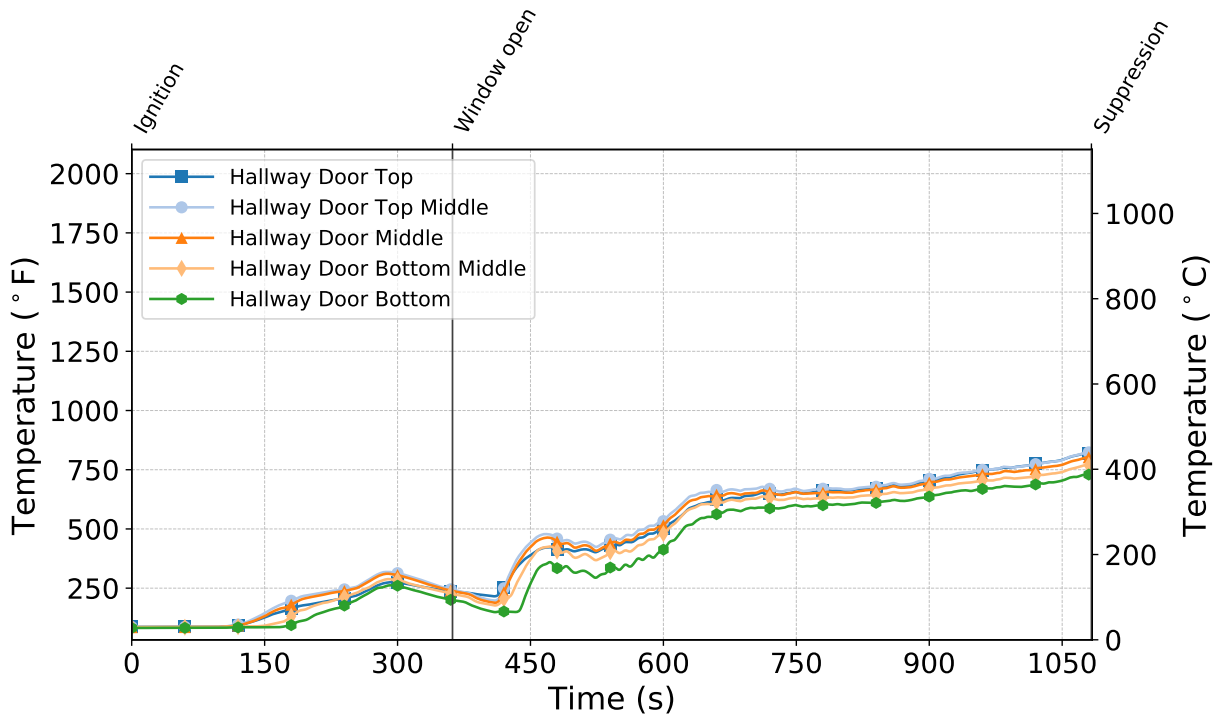


Figure C.215: Temperatures measured by the hallway door thermocouples during Test 20.

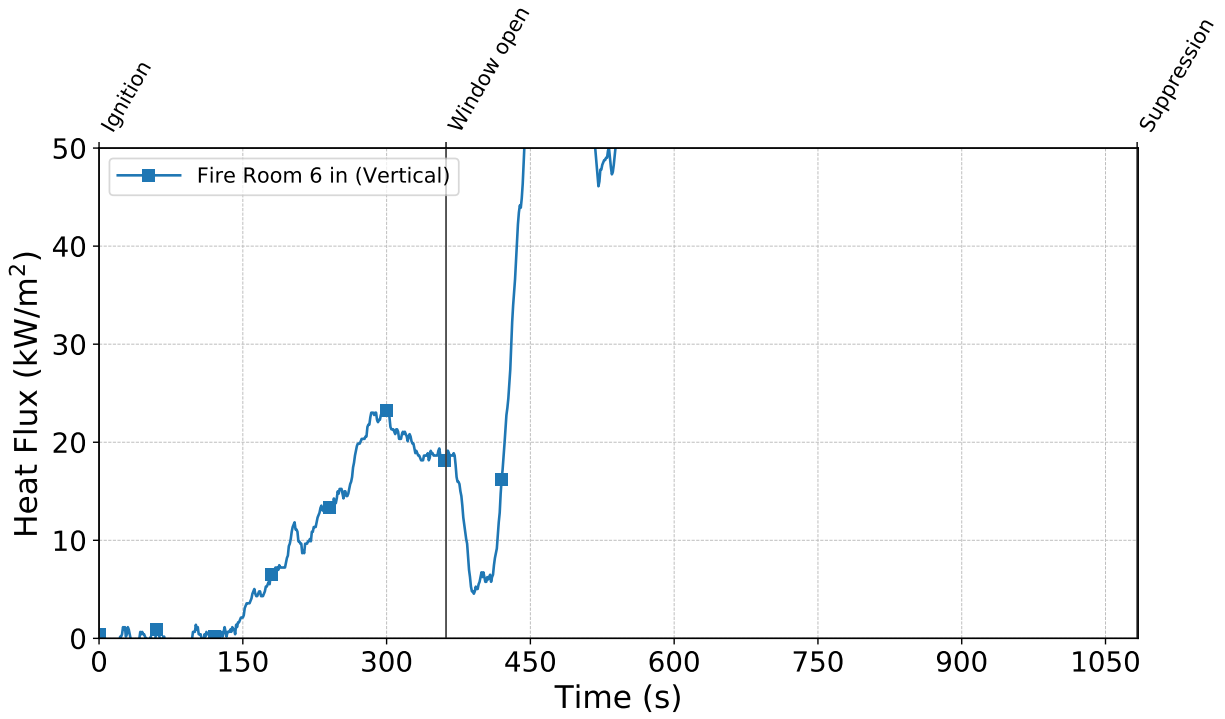


Figure C.216: Heat flux measured by the fire room gauge during Test 20.

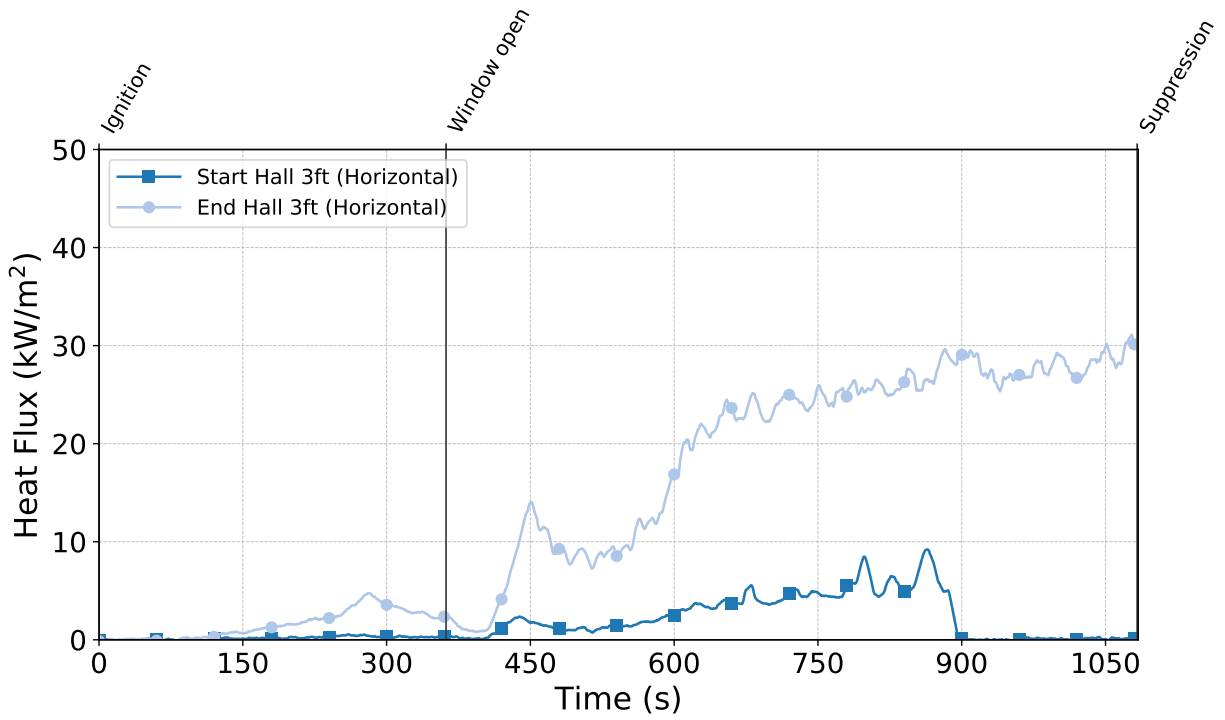


Figure C.217: Heat flux measured by the hallway gauges during Test 20.

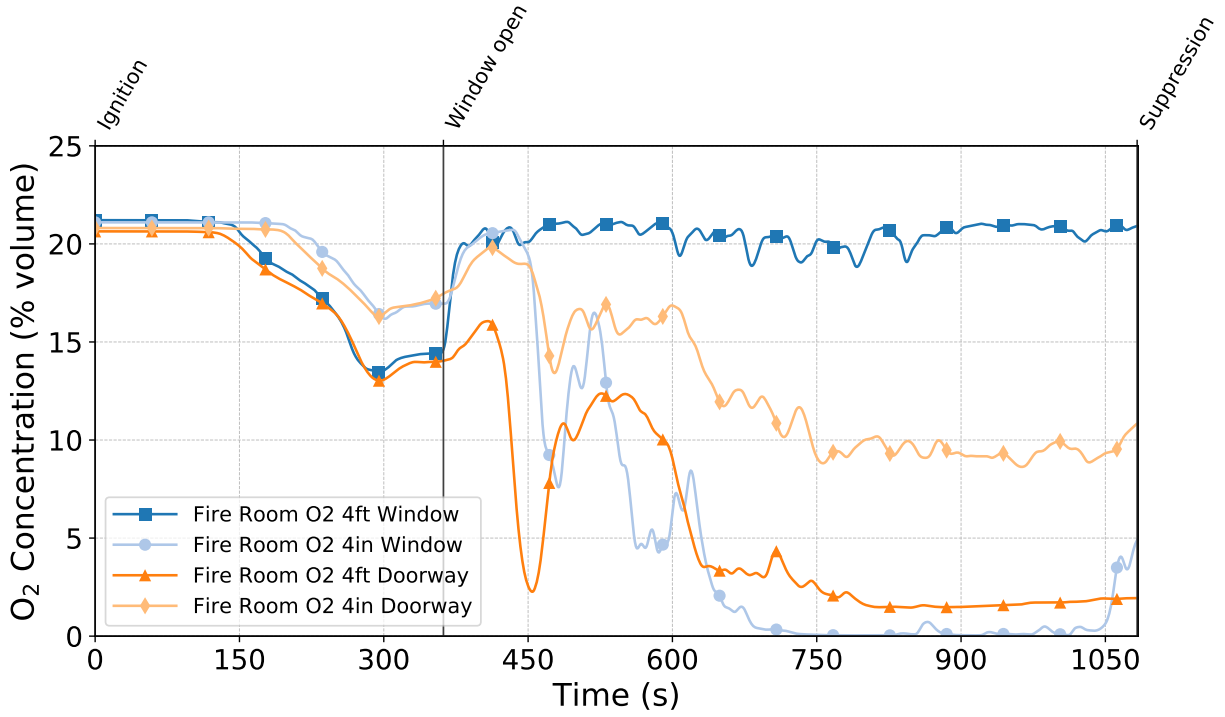


Figure C.218: Oxygen concentrations measured by the fire room gas sampling probes during Test 20.

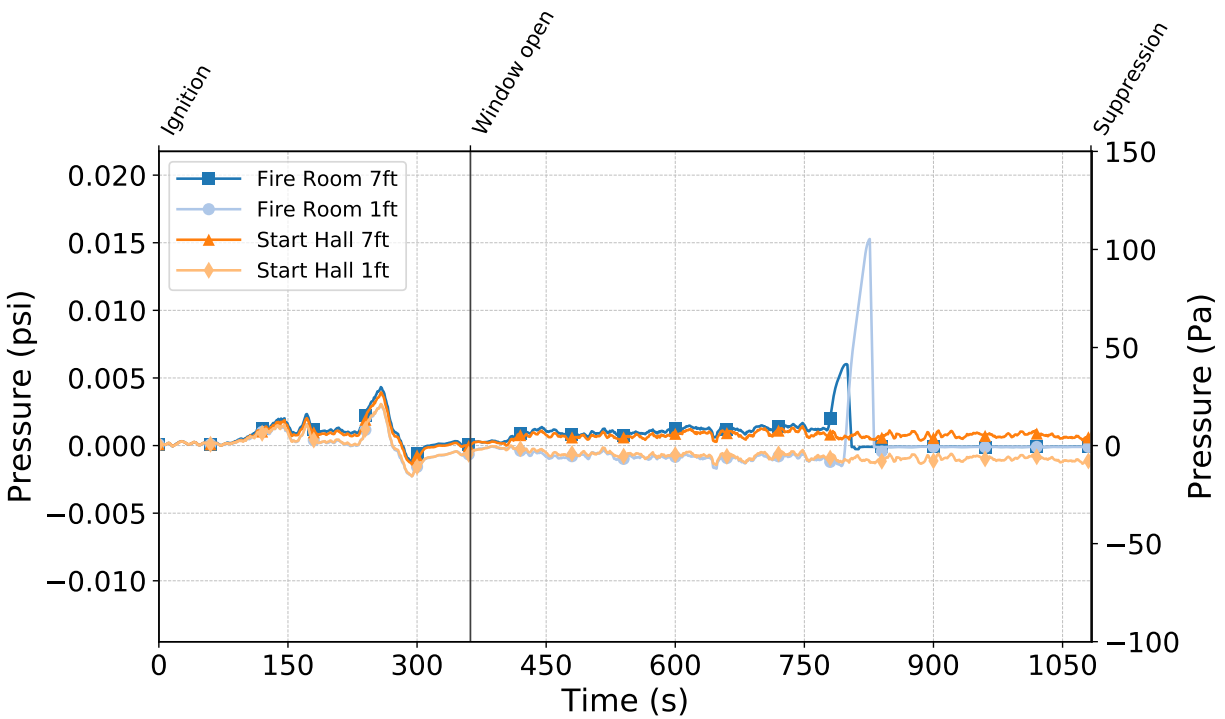


Figure C.219: Pressures measured by the fire room and hallway probes during Test 20.

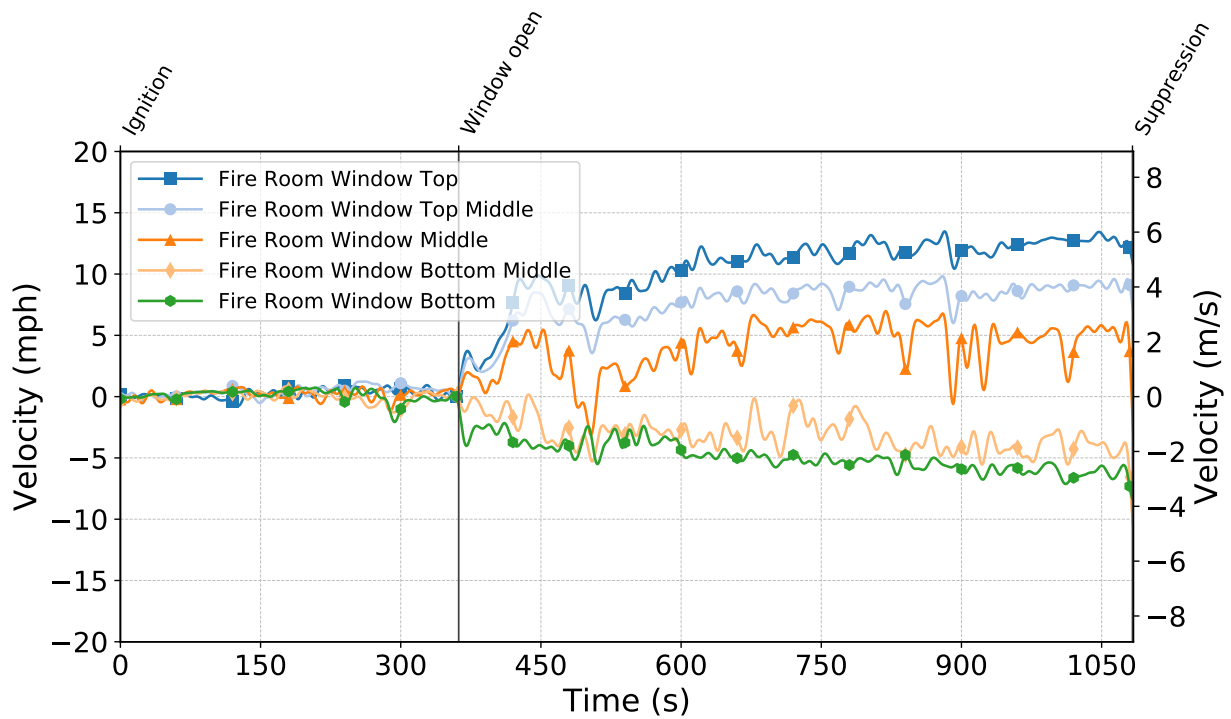


Figure C.220: Gas velocities measured by the fire room window bdps during Test 20.

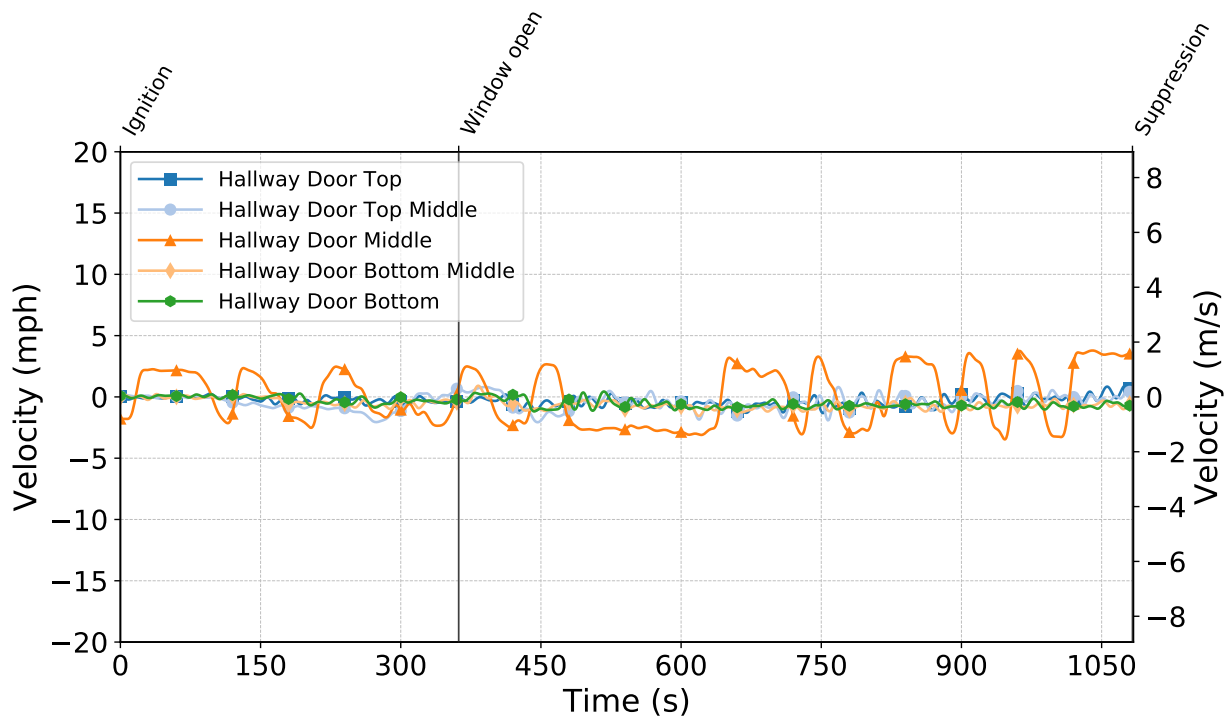


Figure C.221: Gas velocities measured by the hallway door bdps during Test 20.

Test 21

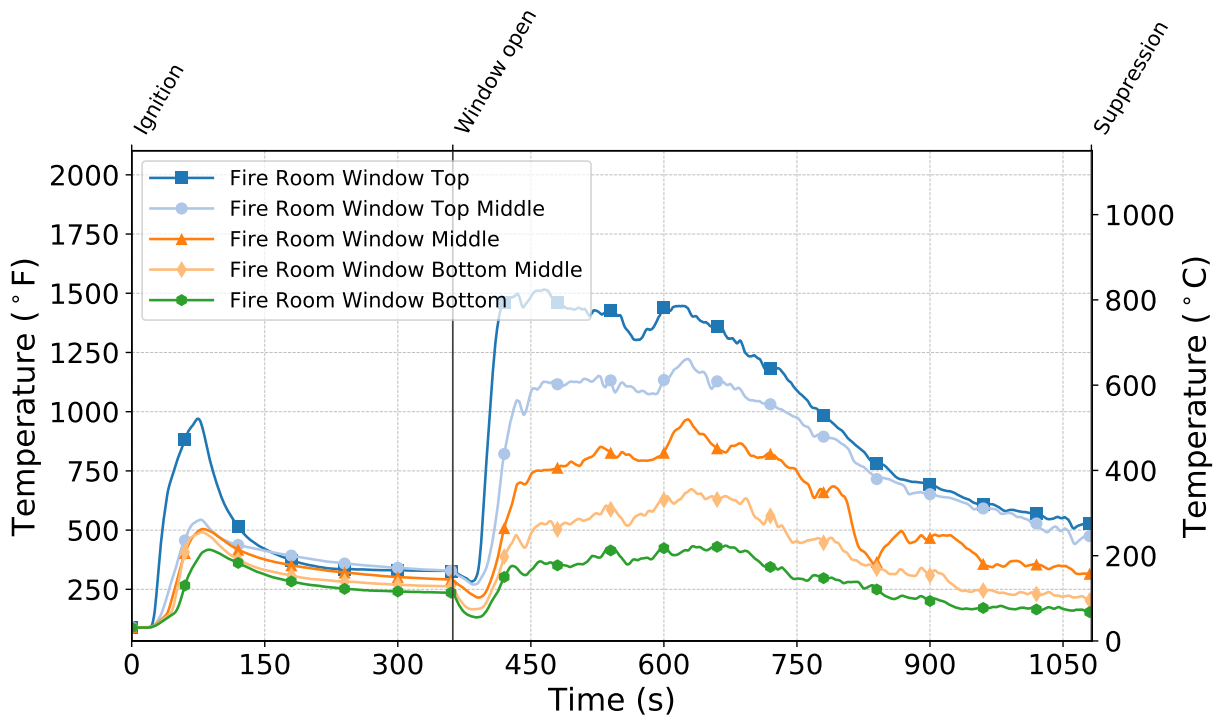


Figure C.222: Temperatures measured by the fire room window thermocouples during Test 21.

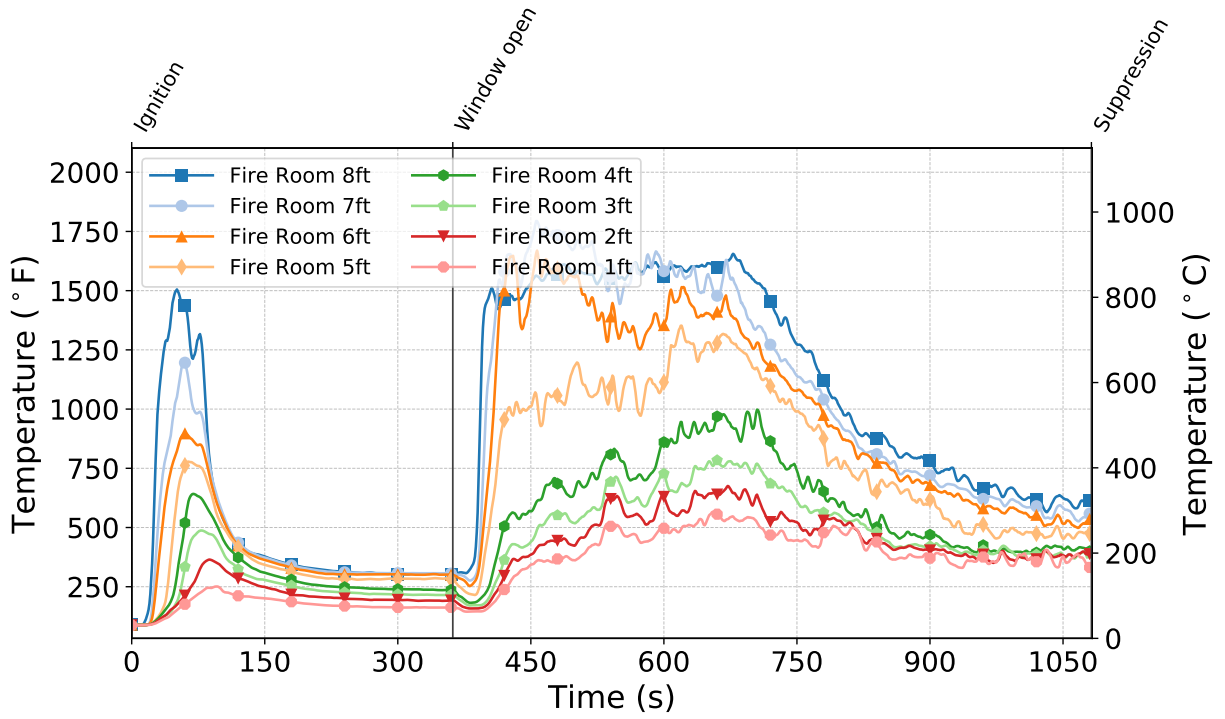


Figure C.223: Temperatures measured by the fire room thermocouples during Test 21.

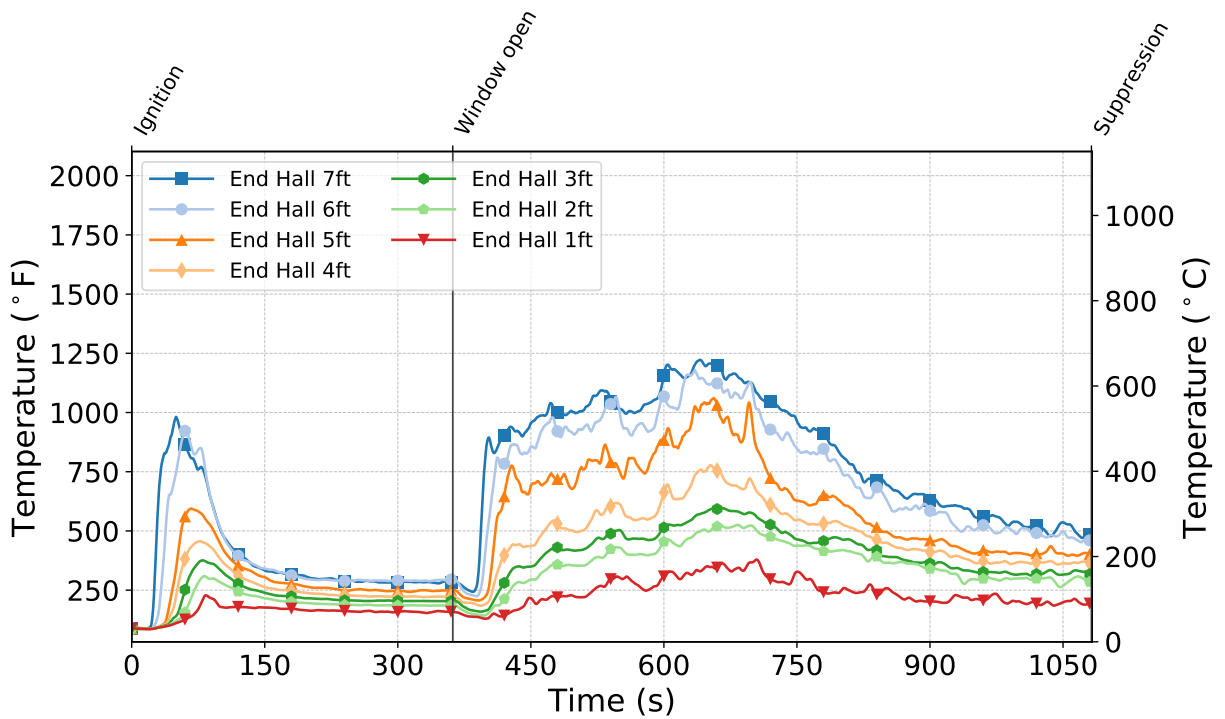


Figure C.224: Temperatures measured by the end hall thermocouples during Test 21.

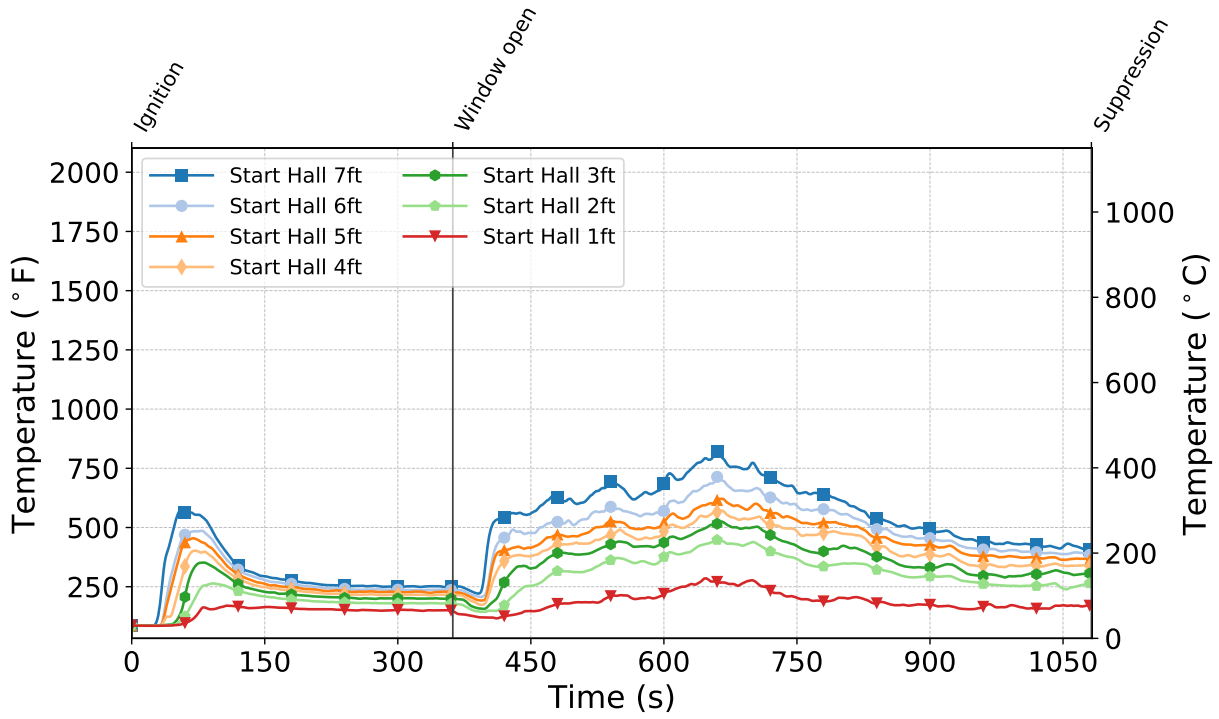


Figure C.225: Temperatures measured by the start hall thermocouples during Test 21.

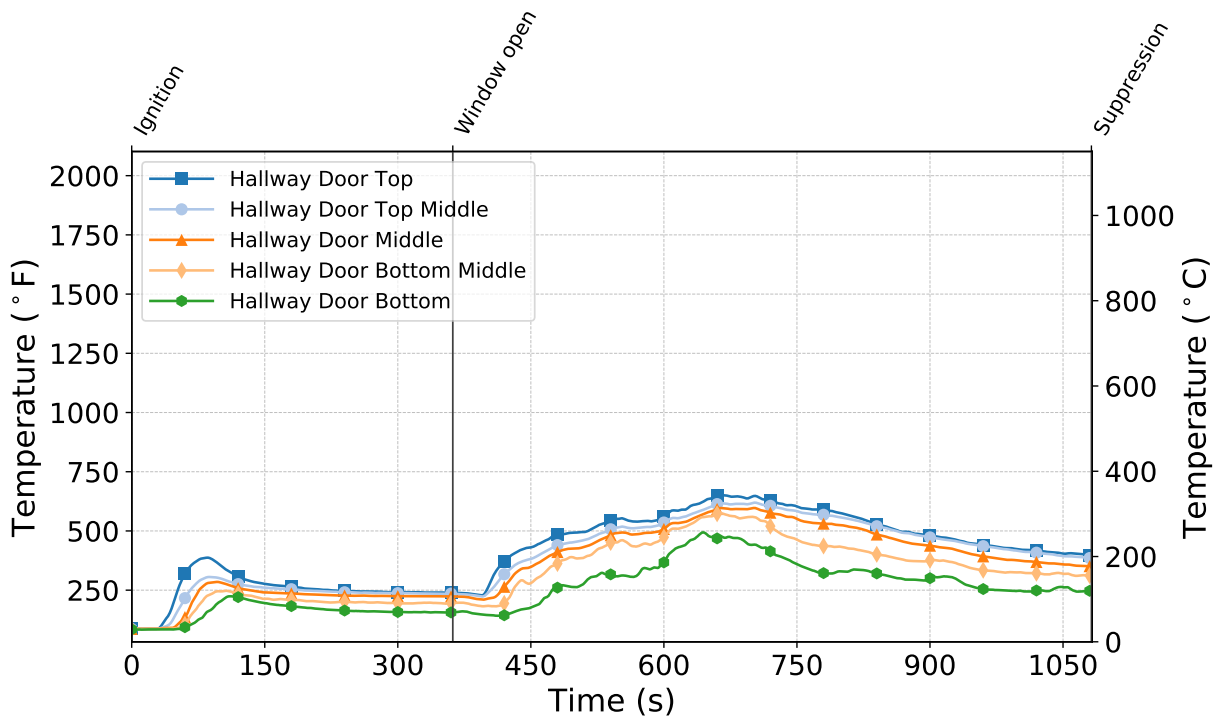


Figure C.226: Temperatures measured by the hallway door thermocouples during Test 21.

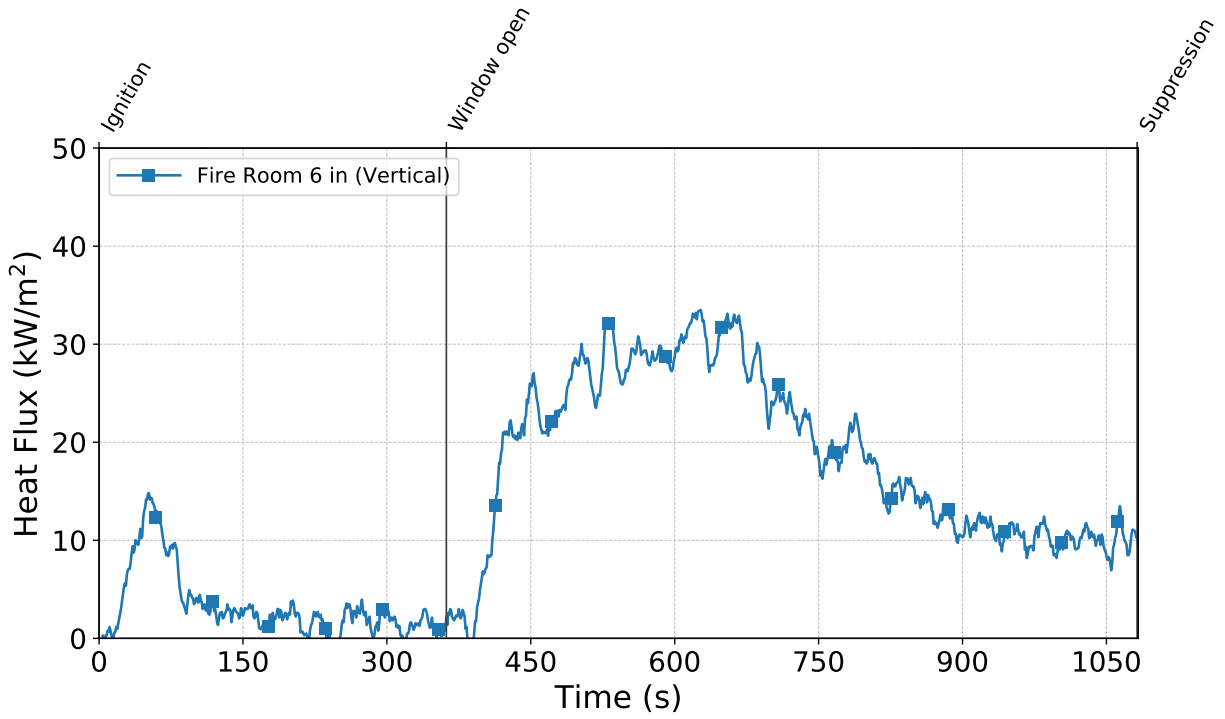


Figure C.227: Heat flux measured by the fire room gauge during Test 21.

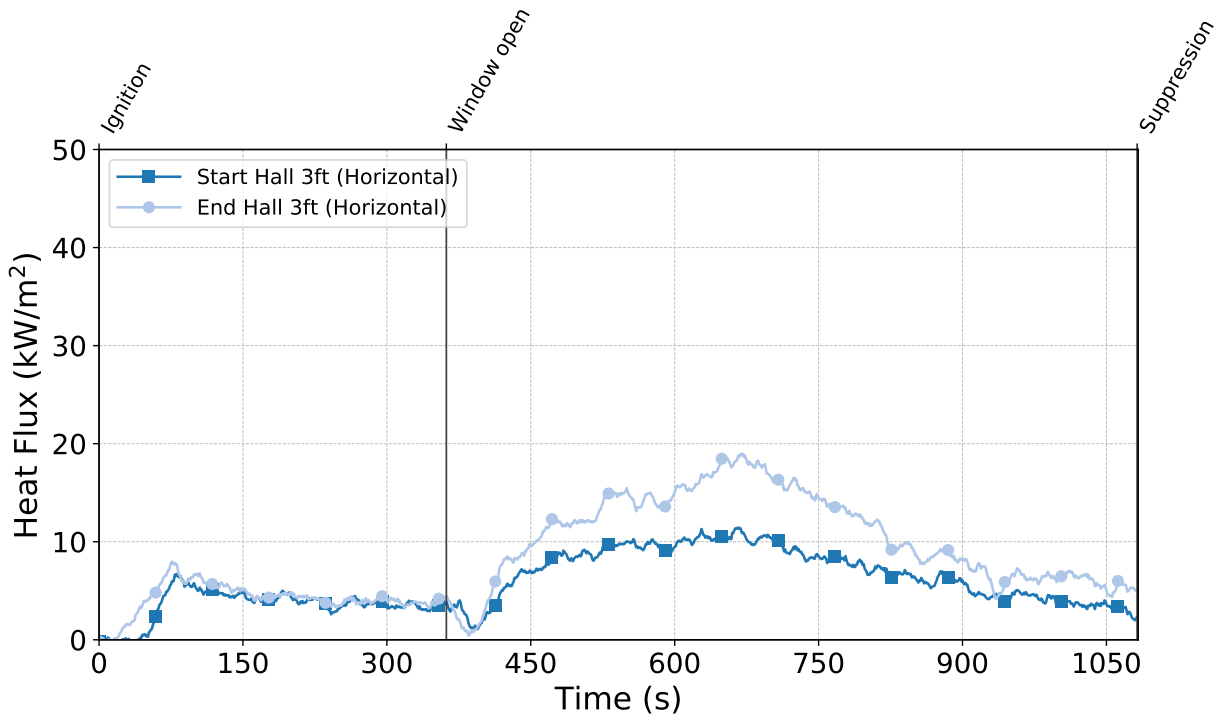


Figure C.228: Heat flux measured by the hallway gauges during Test 21.

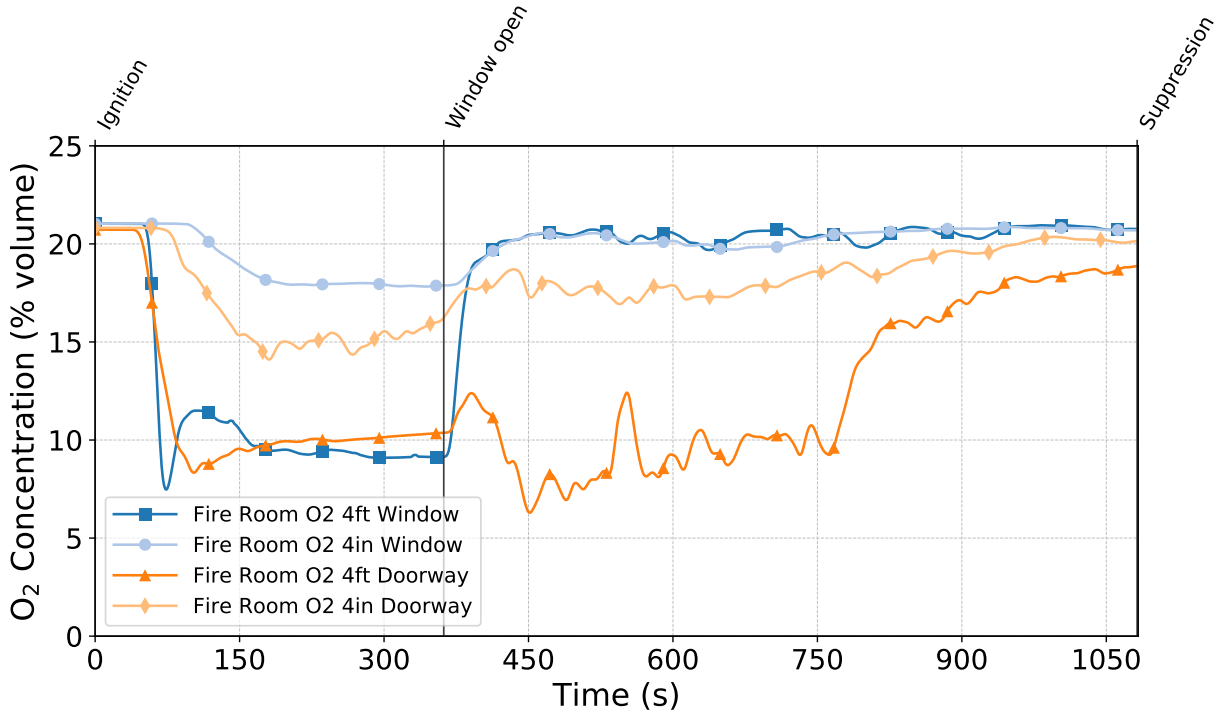


Figure C.229: Oxygen concentrations measured by the fire room gas sampling probes during Test 21.

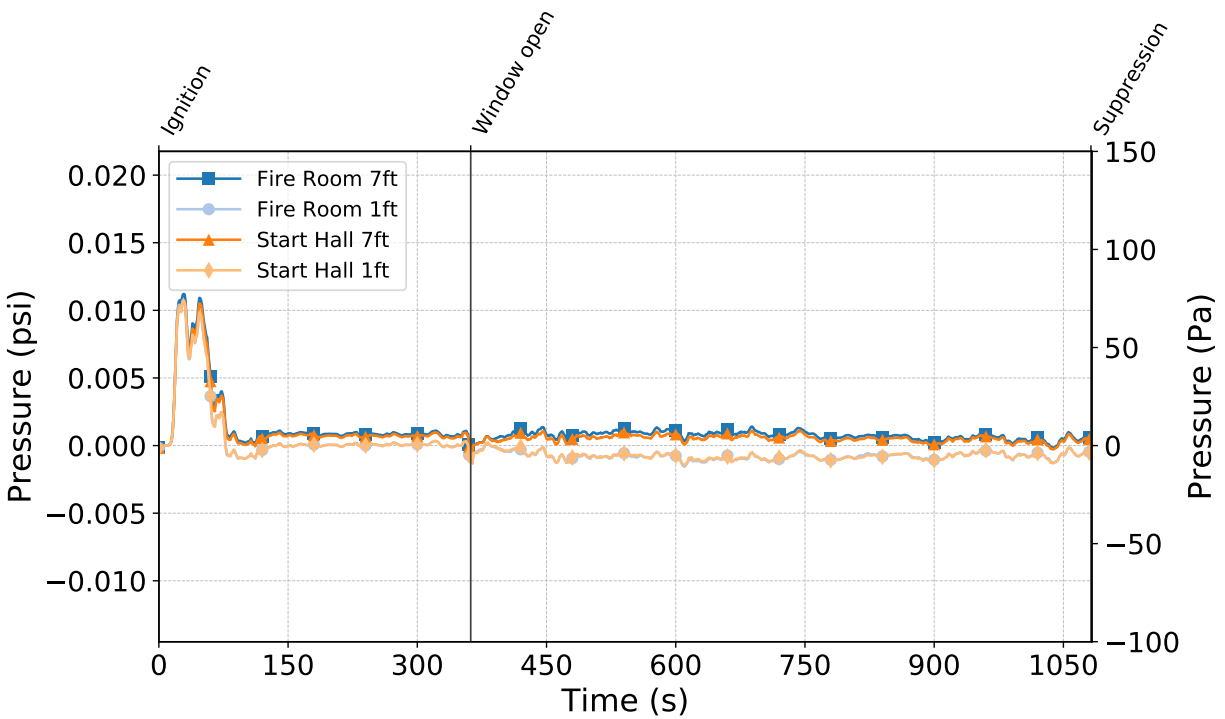


Figure C.230: Pressures measured by the fire room and hallway probes during Test 21.

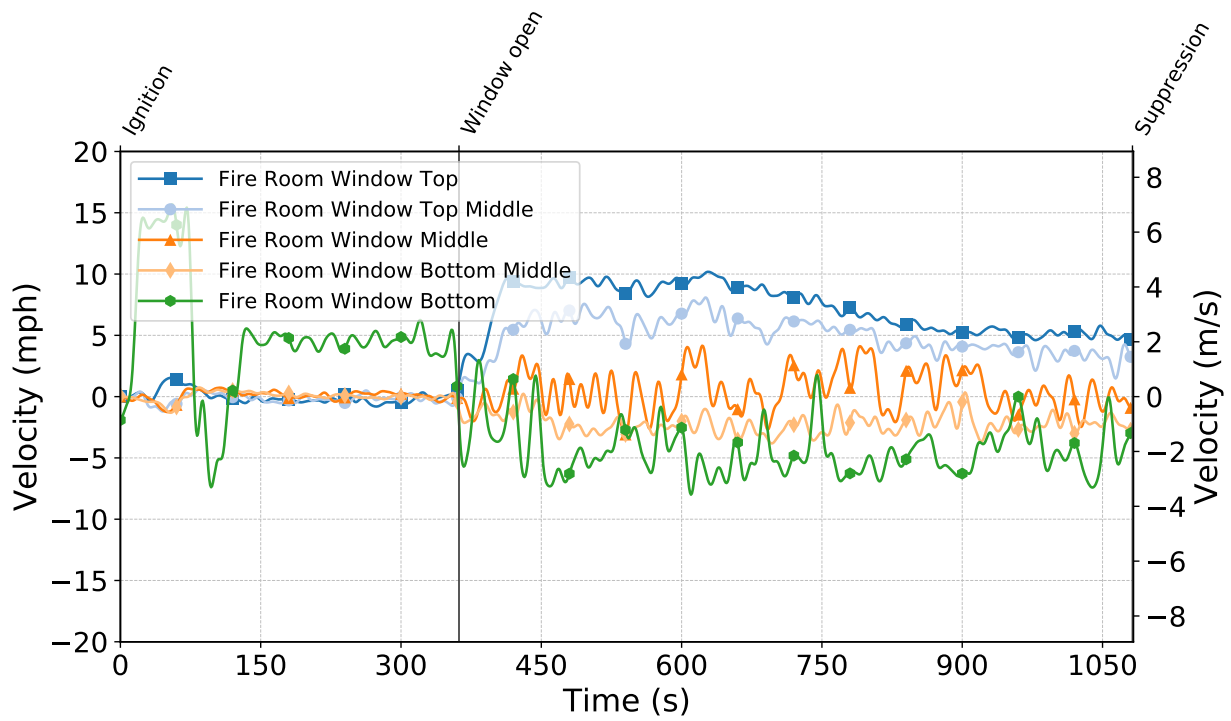


Figure C.231: Gas velocities measured by the fire room window bdp locations during Test 21.

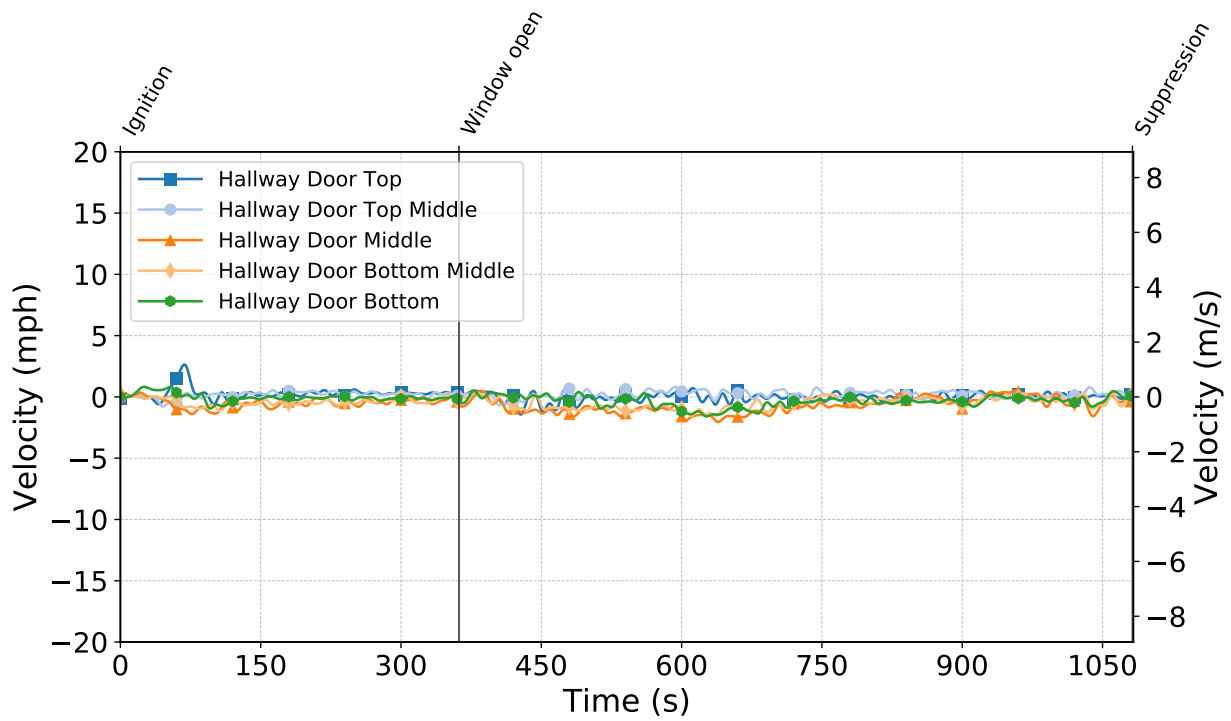


Figure C.232: Gas velocities measured by the hallway door bdp locations during Test 21.

Test 22

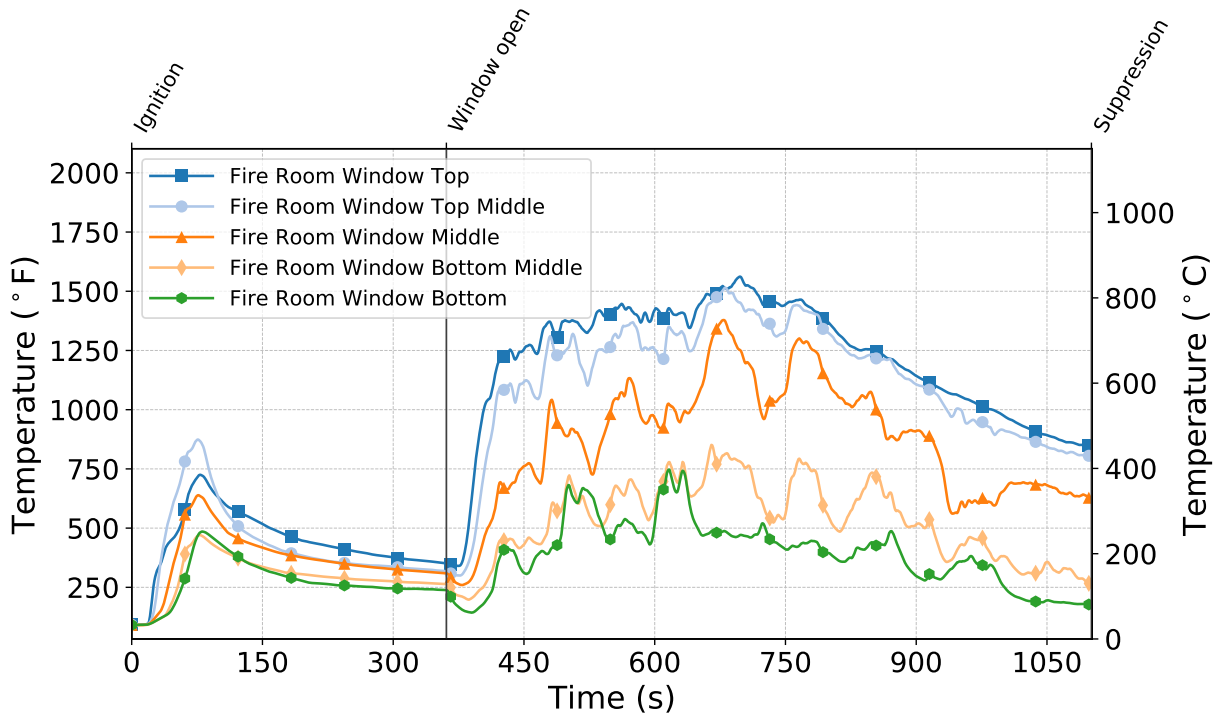


Figure C.233: Temperatures measured by the fire room window thermocouples during Test 22.

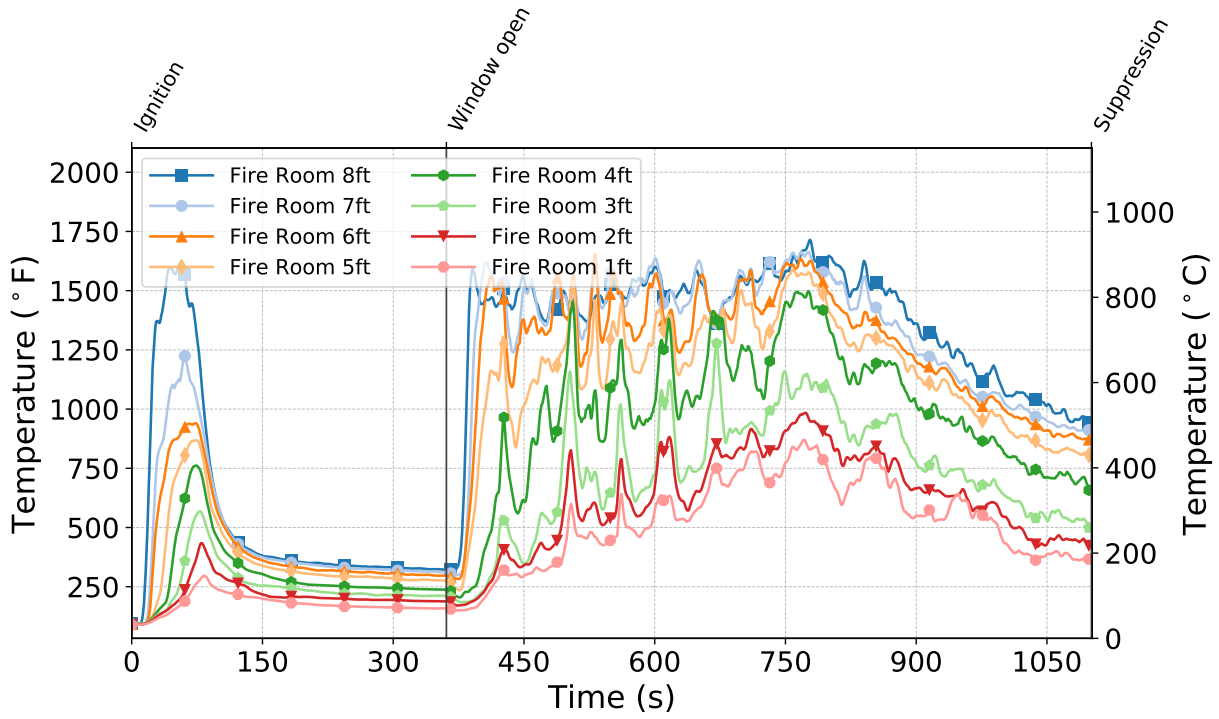


Figure C.234: Temperatures measured by the fire room thermocouples during Test 22.

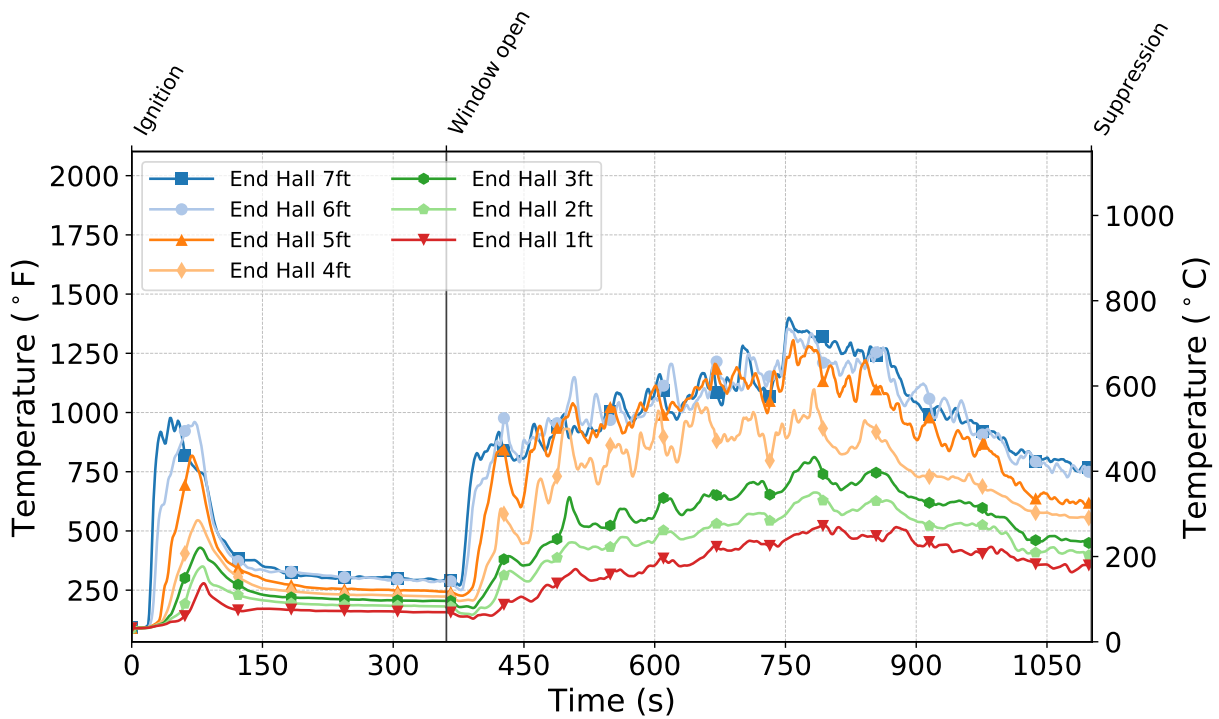


Figure C.235: Temperatures measured by the end hall thermocouples during Test 22.

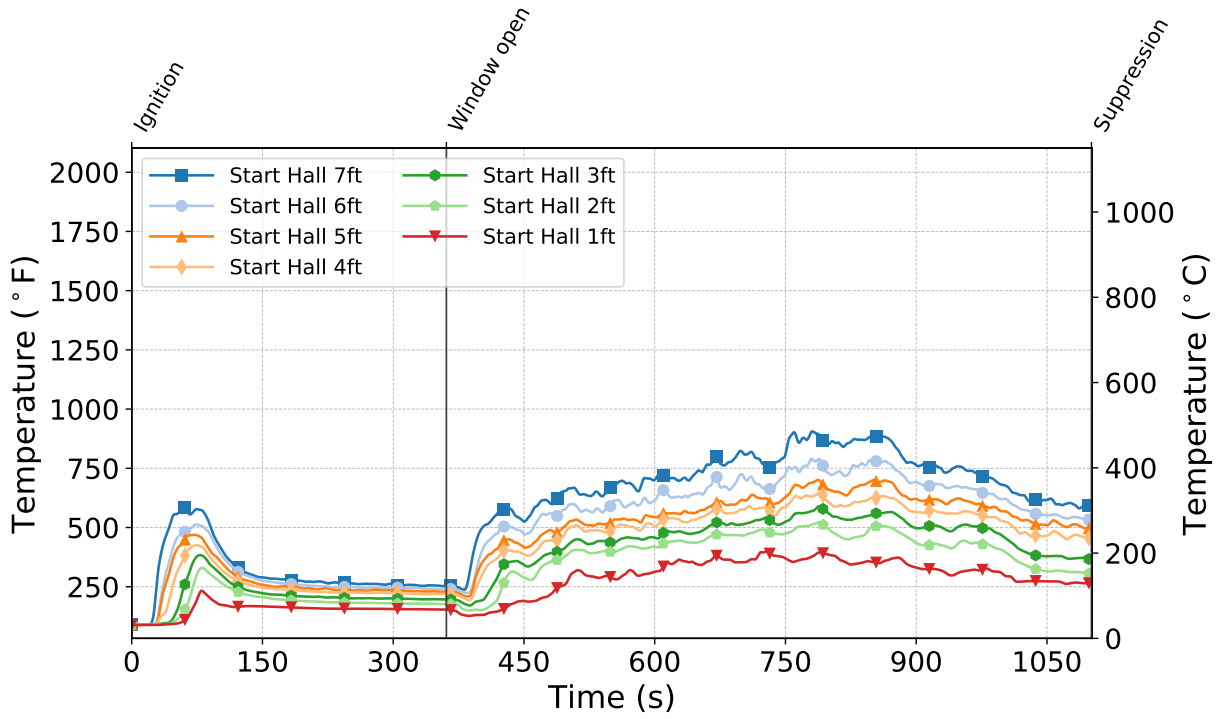


Figure C.236: Temperatures measured by the start hall thermocouples during Test 22.

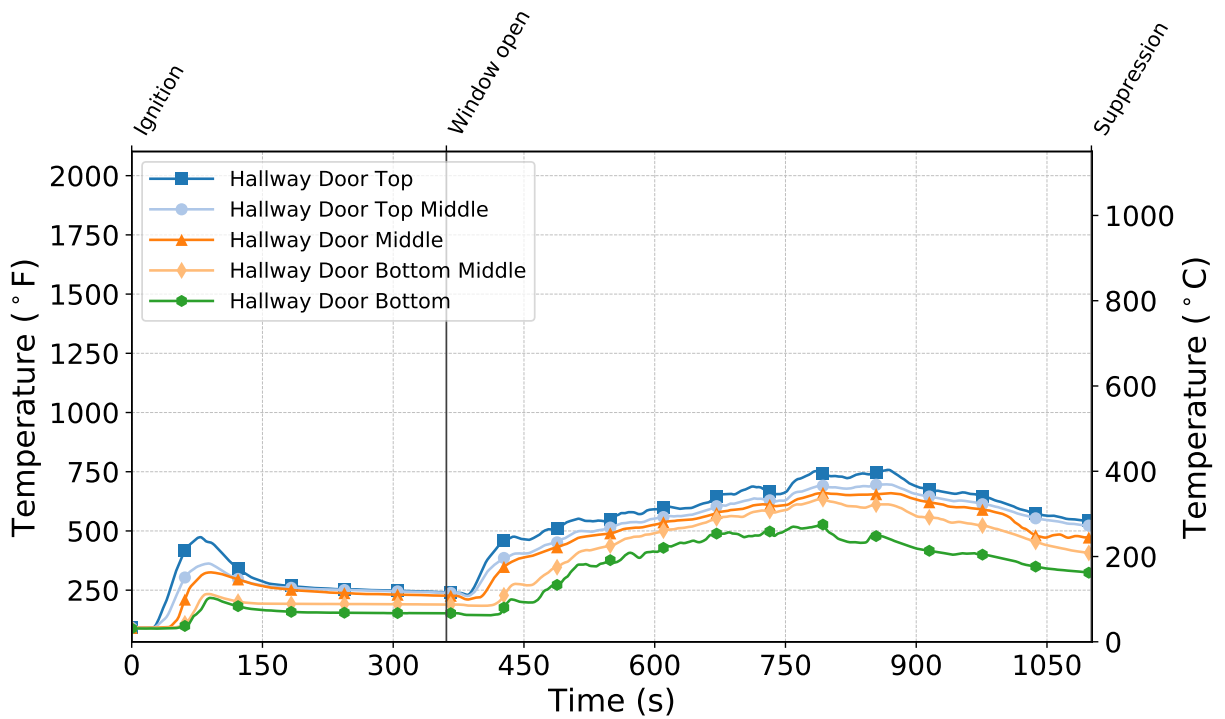


Figure C.237: Temperatures measured by the hallway door thermocouples during Test 22.

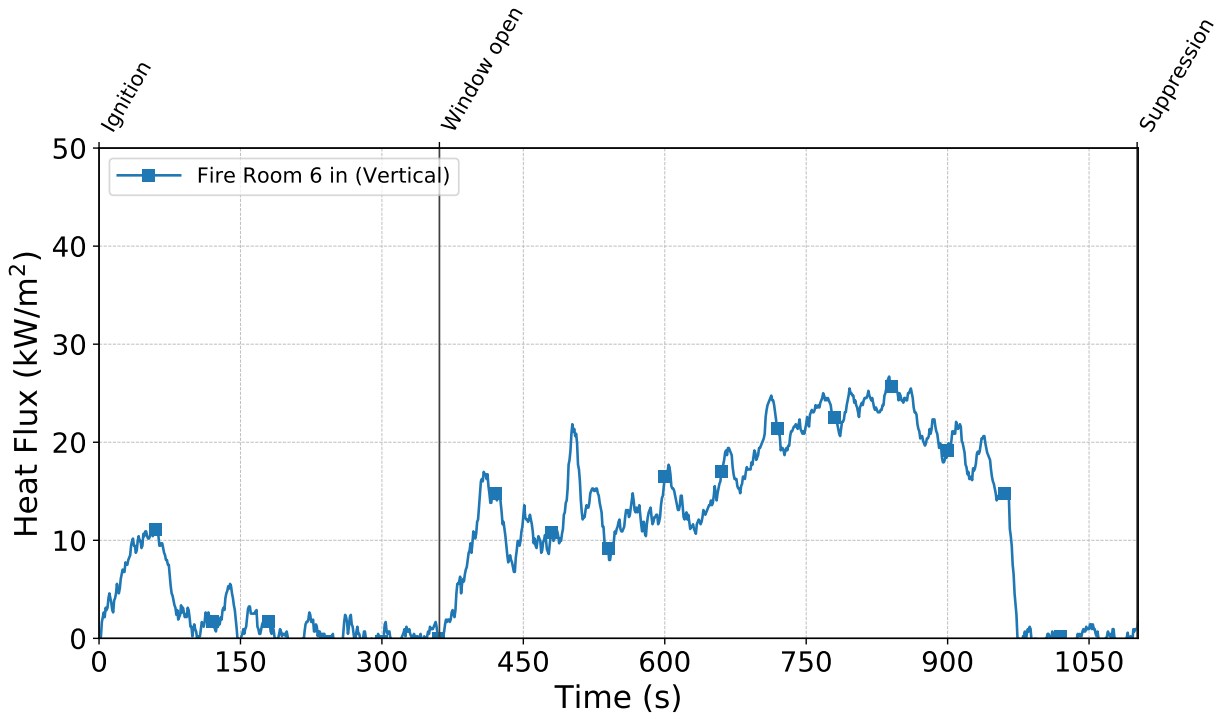


Figure C.238: Heat flux measured by the fire room gauge during Test 22.

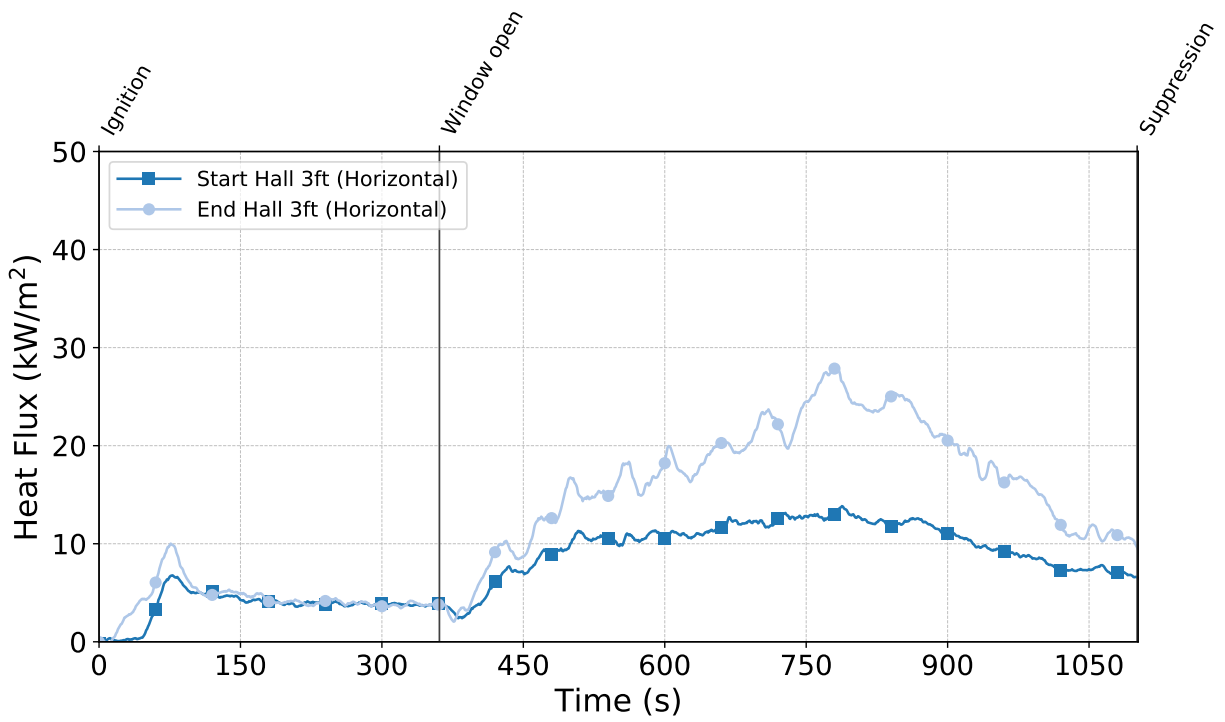


Figure C.239: Heat flux measured by the hallway gauges during Test 22.

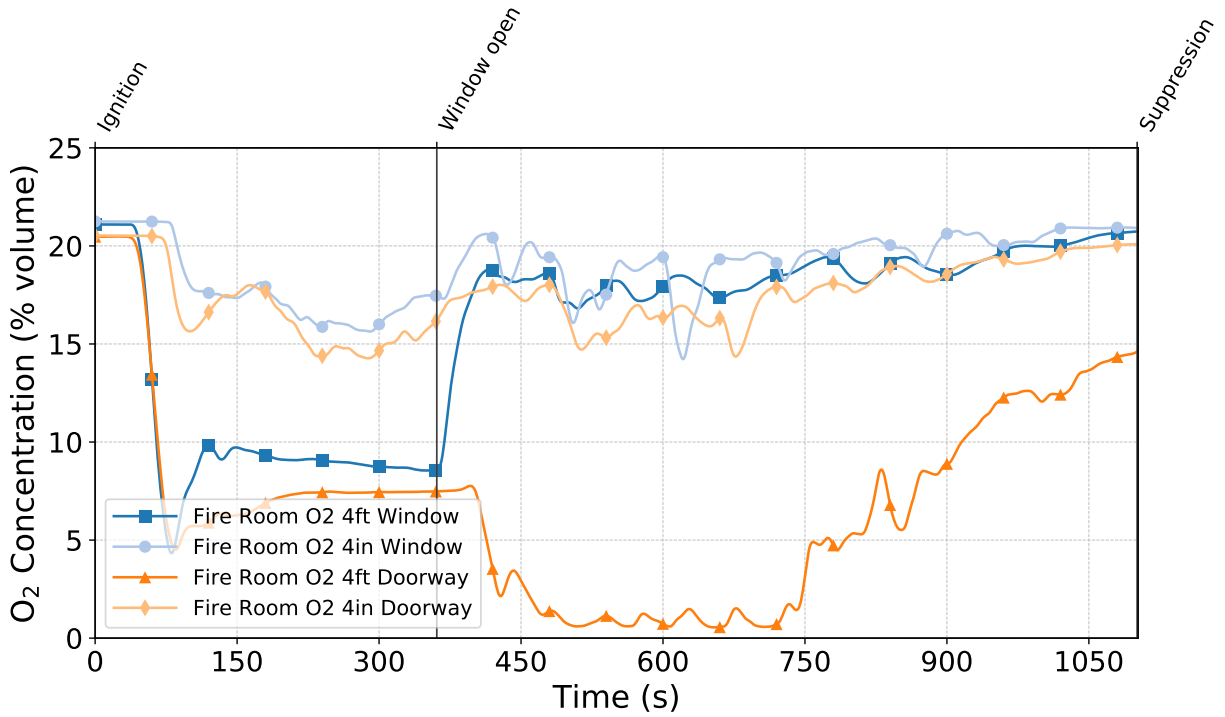


Figure C.240: Oxygen concentrations measured by the fire room gas sampling probes during Test 22.

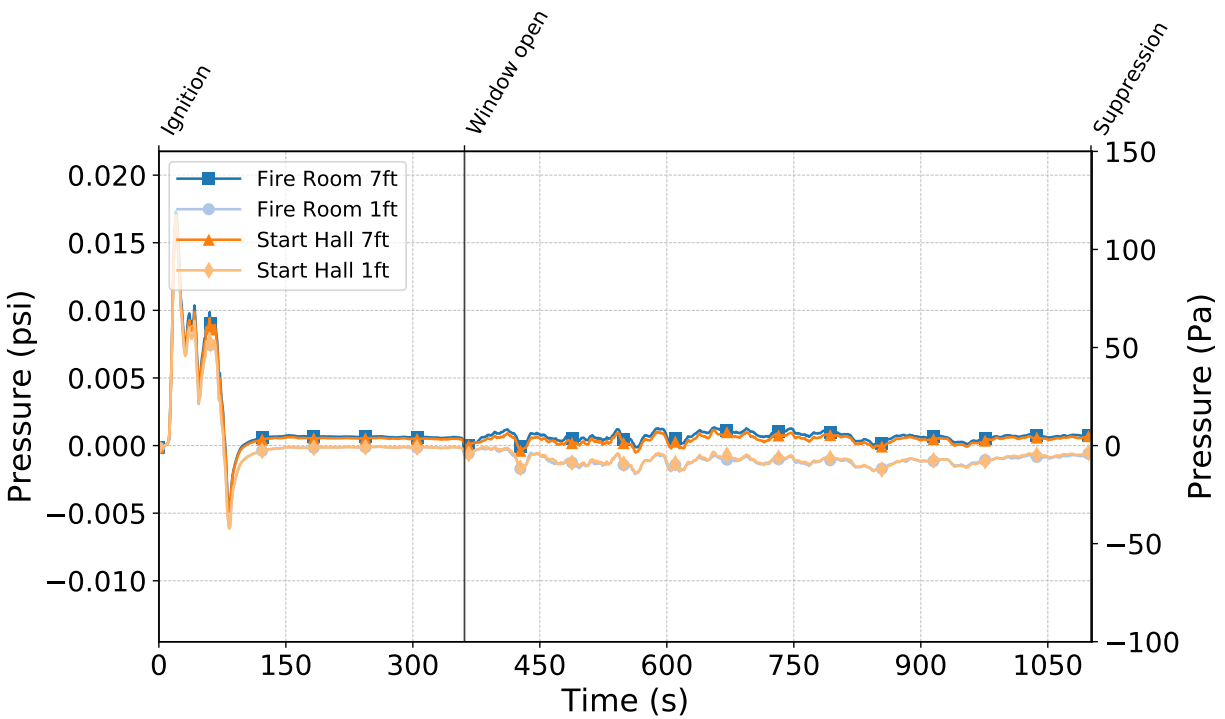


Figure C.241: Pressures measured by the fire room and hallway probes during Test 22.

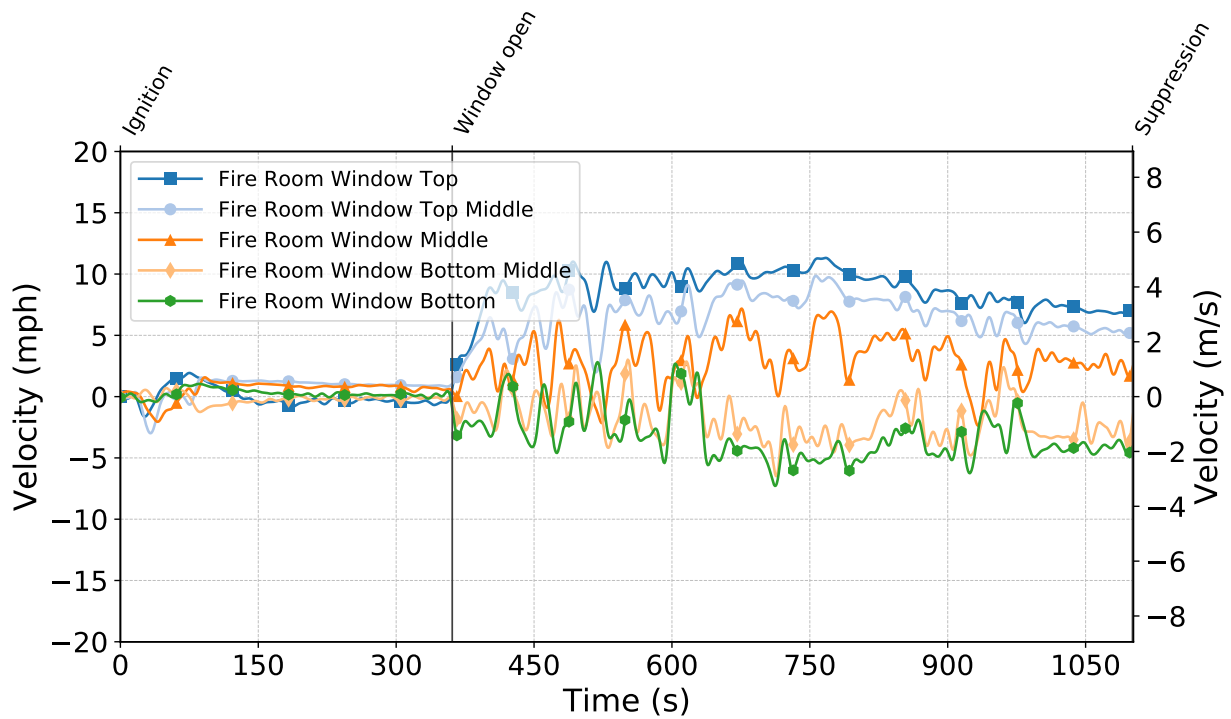


Figure C.242: Gas velocities measured by the fire room window bdps during Test 22.

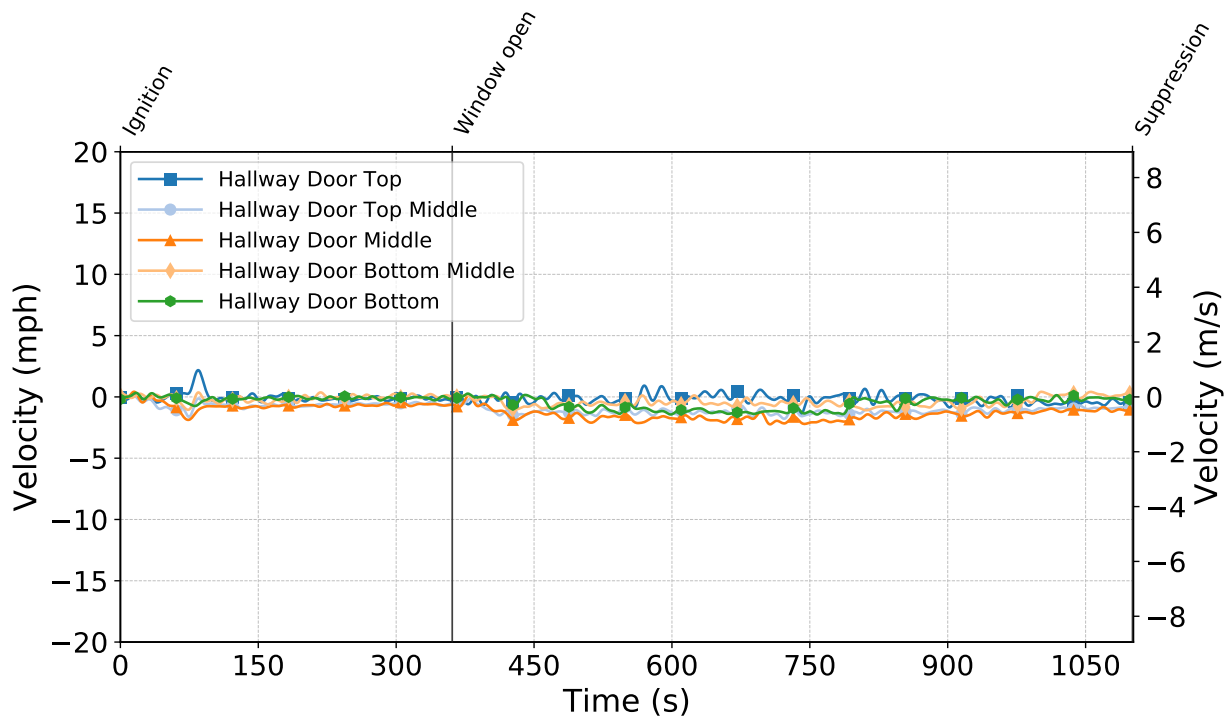


Figure C.243: Gas velocities measured by the hallway door bdps during Test 22.

Test 23

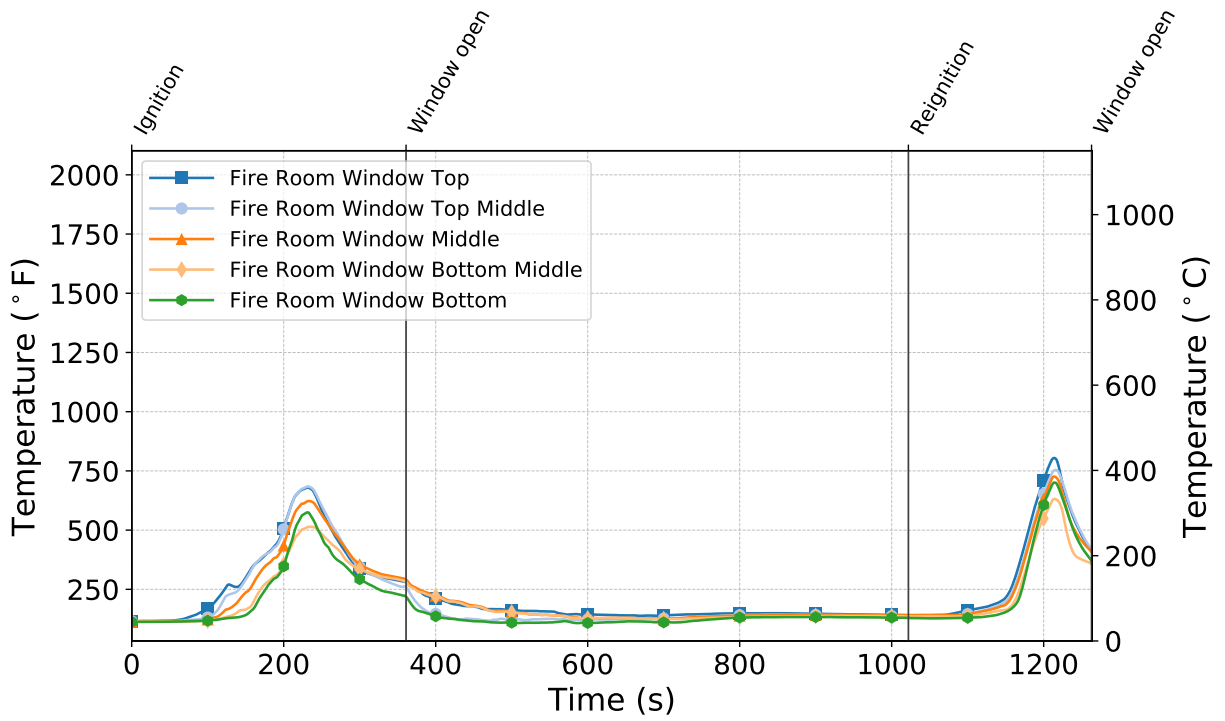


Figure C.244: Temperatures measured by the fire room window thermocouples during Test 23.

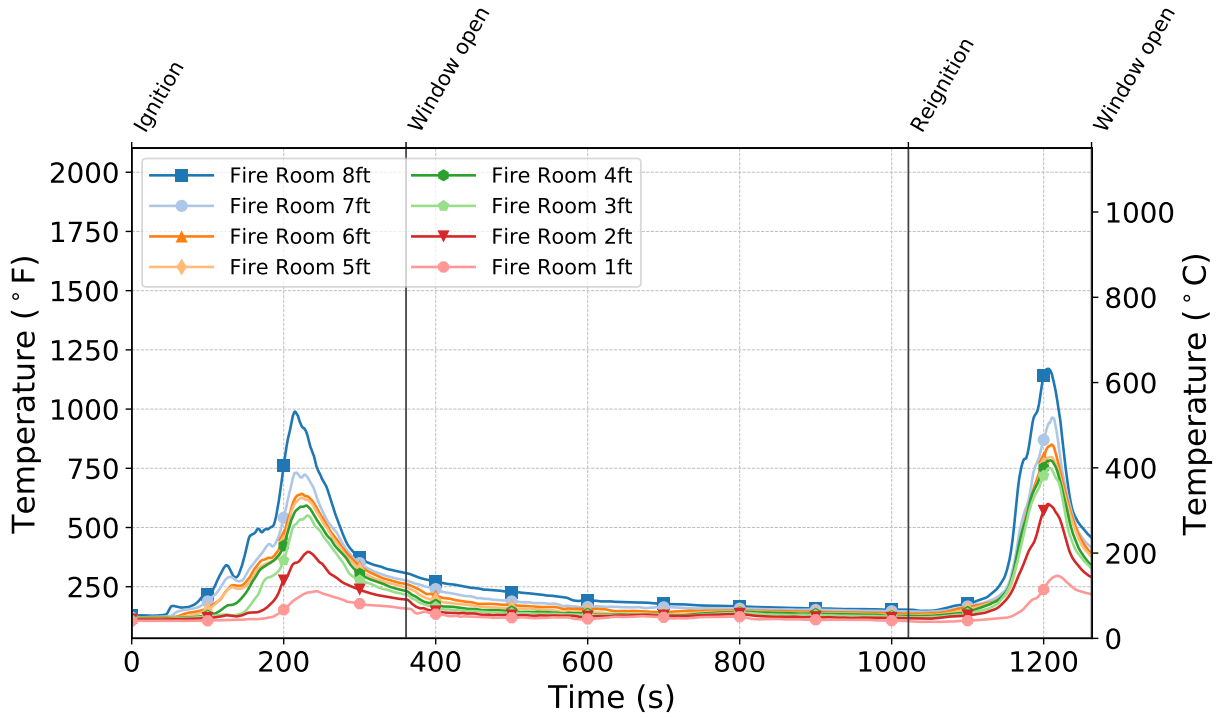


Figure C.245: Temperatures measured by the fire room thermocouples during Test 23.

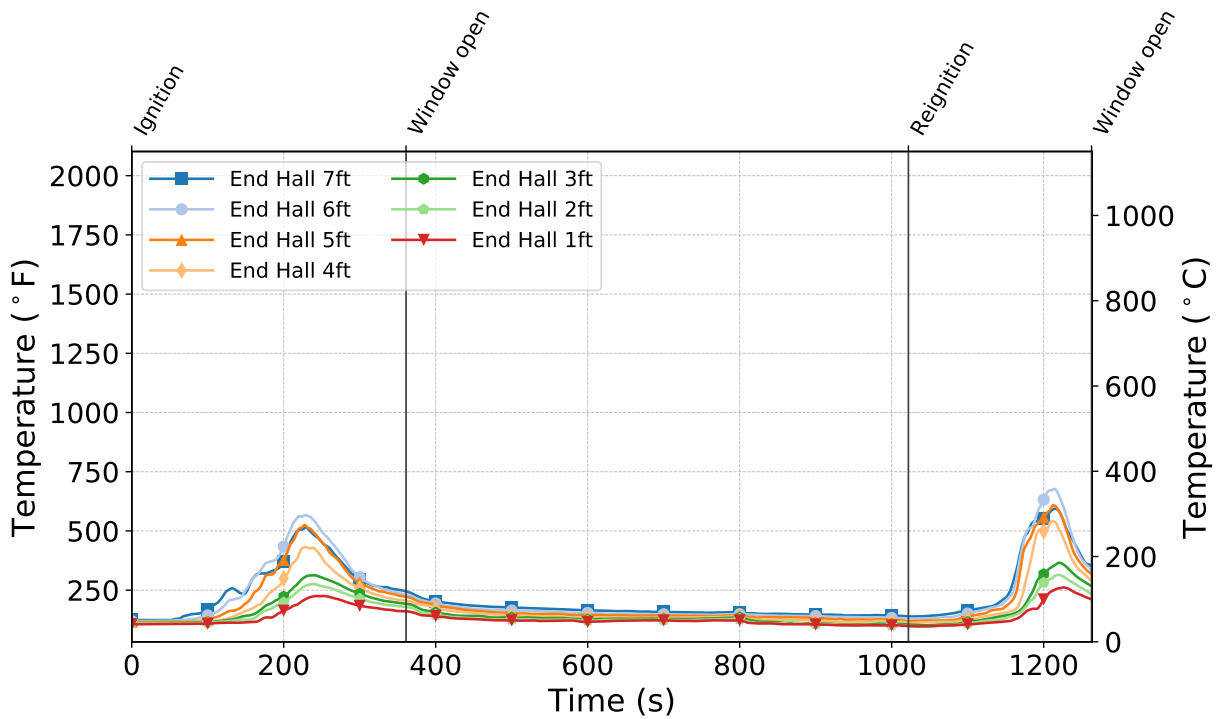


Figure C.246: Temperatures measured by the end hall thermocouples during Test 23.

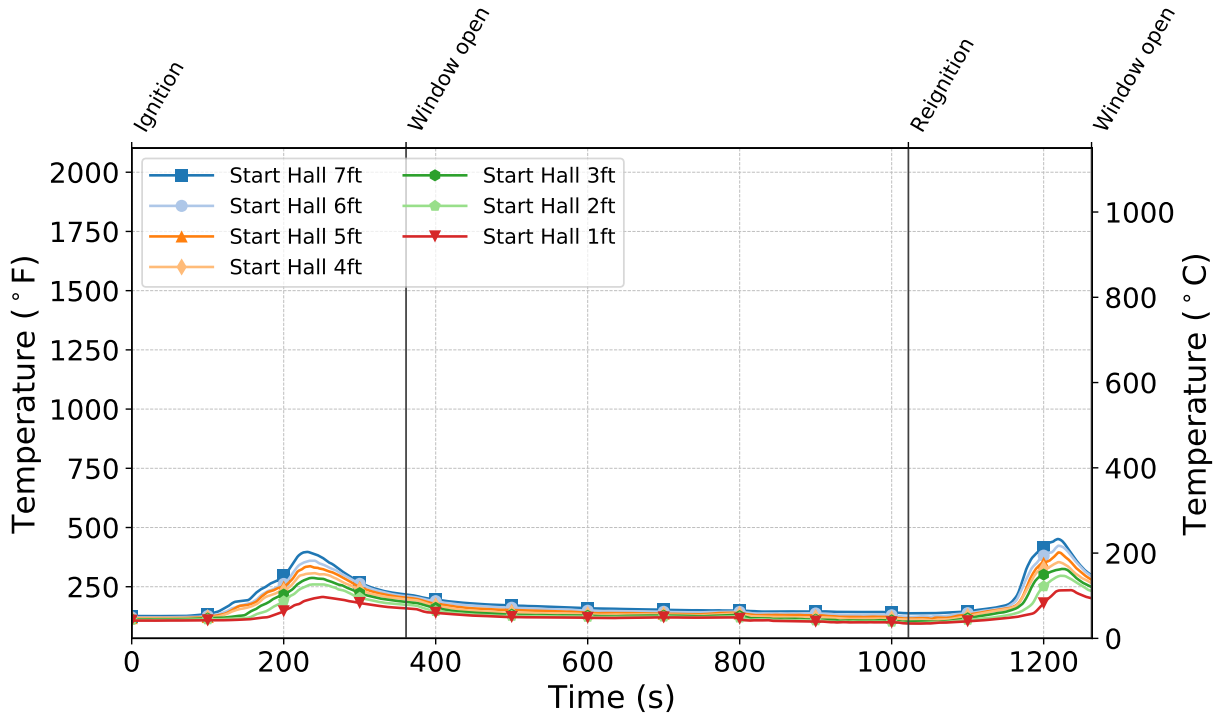


Figure C.247: Temperatures measured by the start hall thermocouples during Test 23.

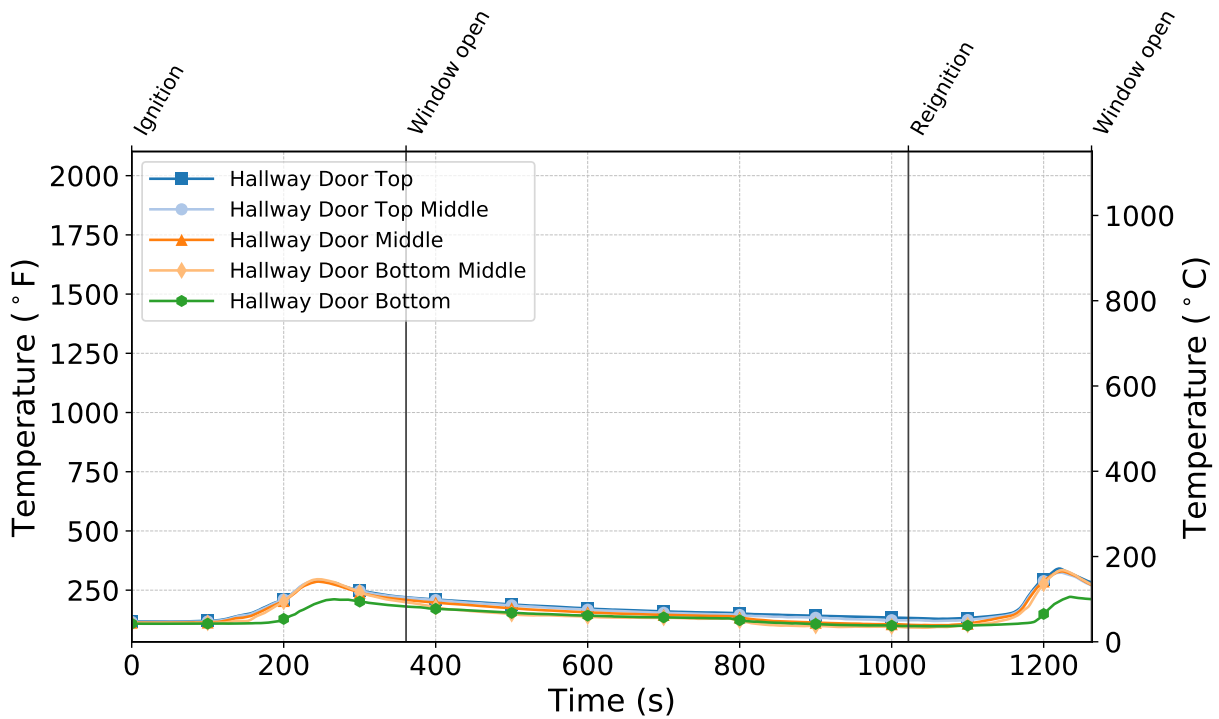


Figure C.248: Temperatures measured by the hallway door thermocouples during Test 23.

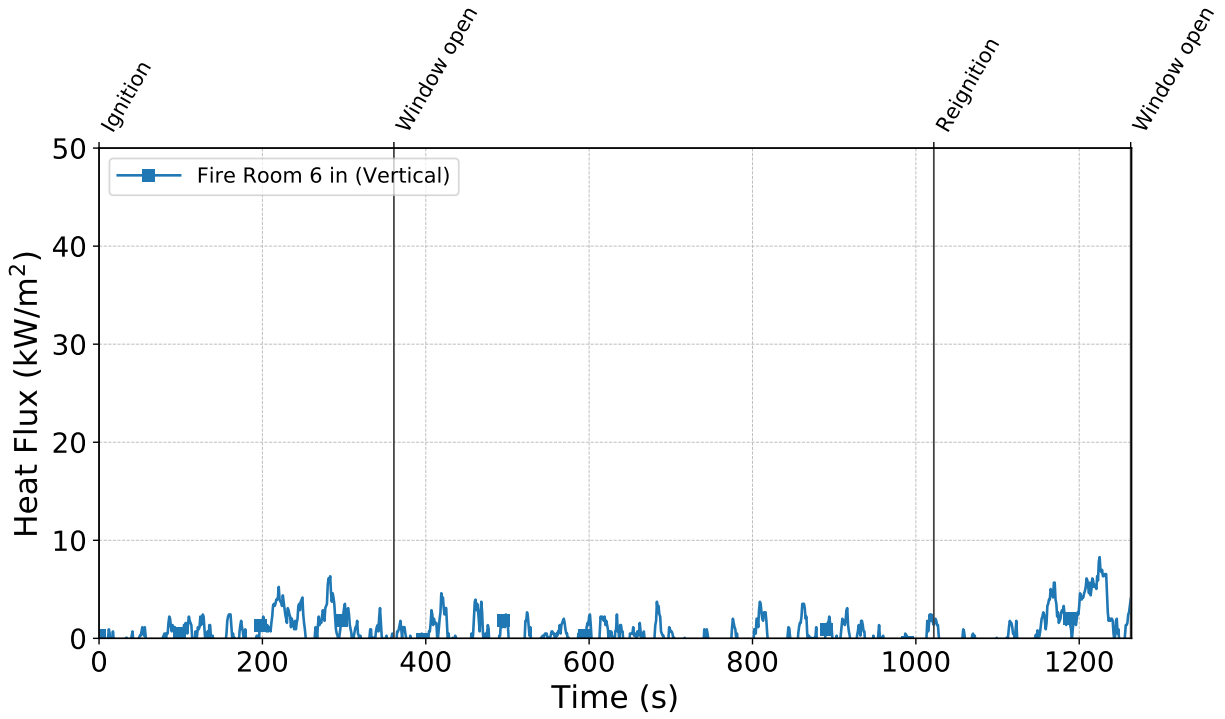


Figure C.249: Heat flux measured by the fire room gauge during Test 23.

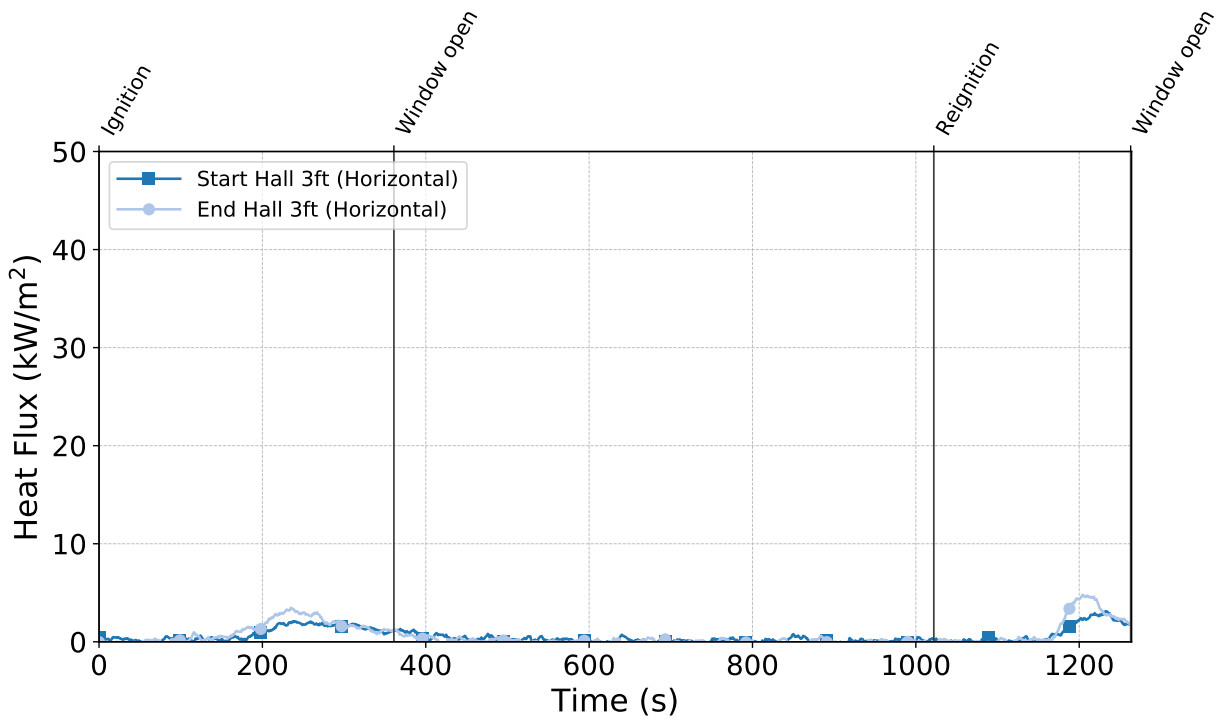


Figure C.250: Heat flux measured by the hallway gauges during Test 23.

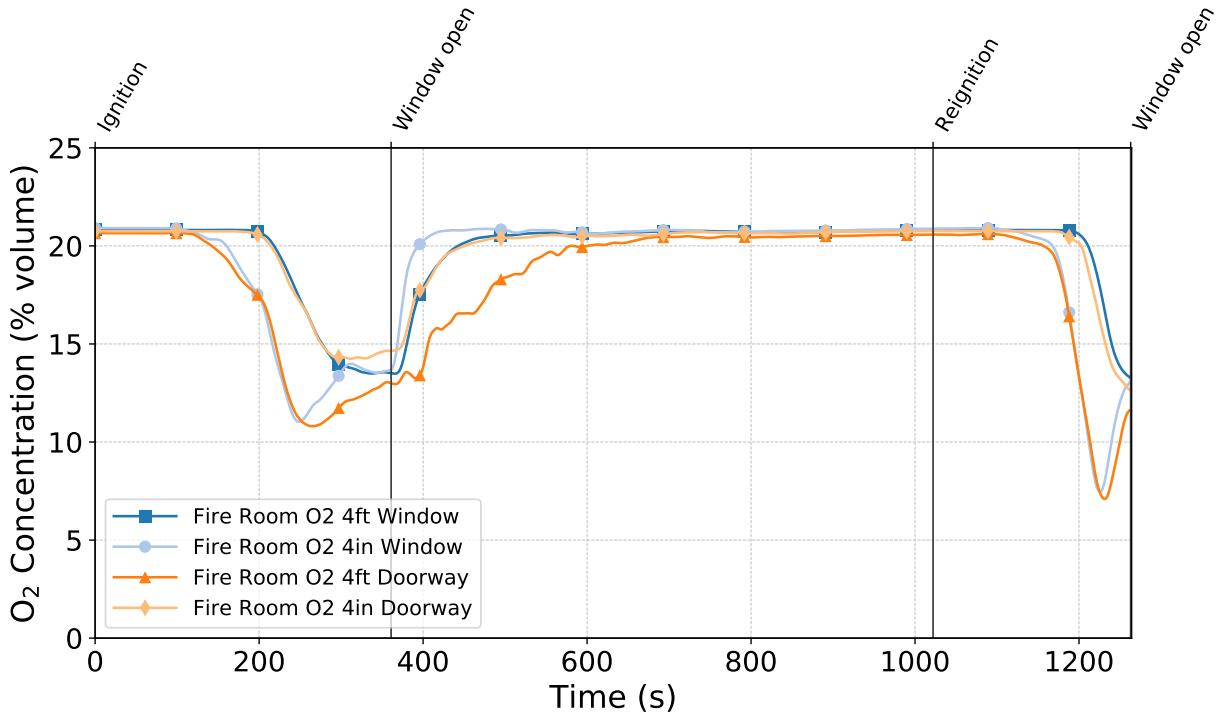


Figure C.251: Oxygen concentrations measured by the fire room gas sampling probes during Test 23.

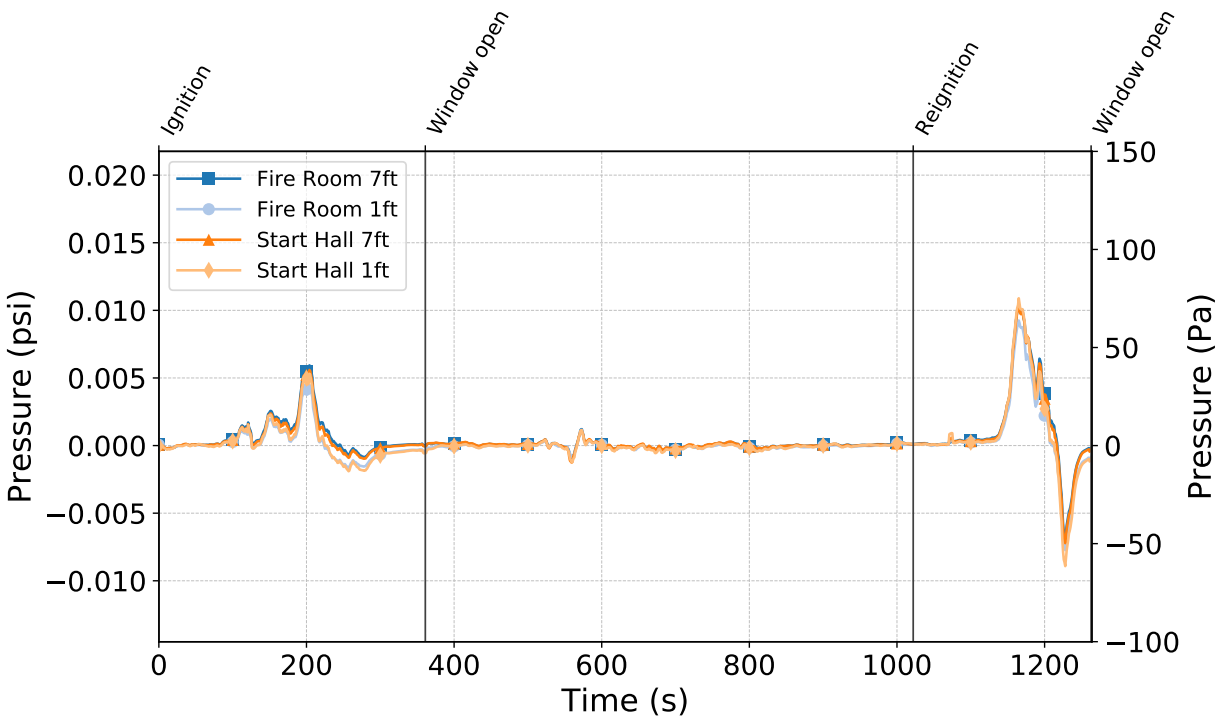


Figure C.252: Pressures measured by the fire room and hallway probes during Test 23.

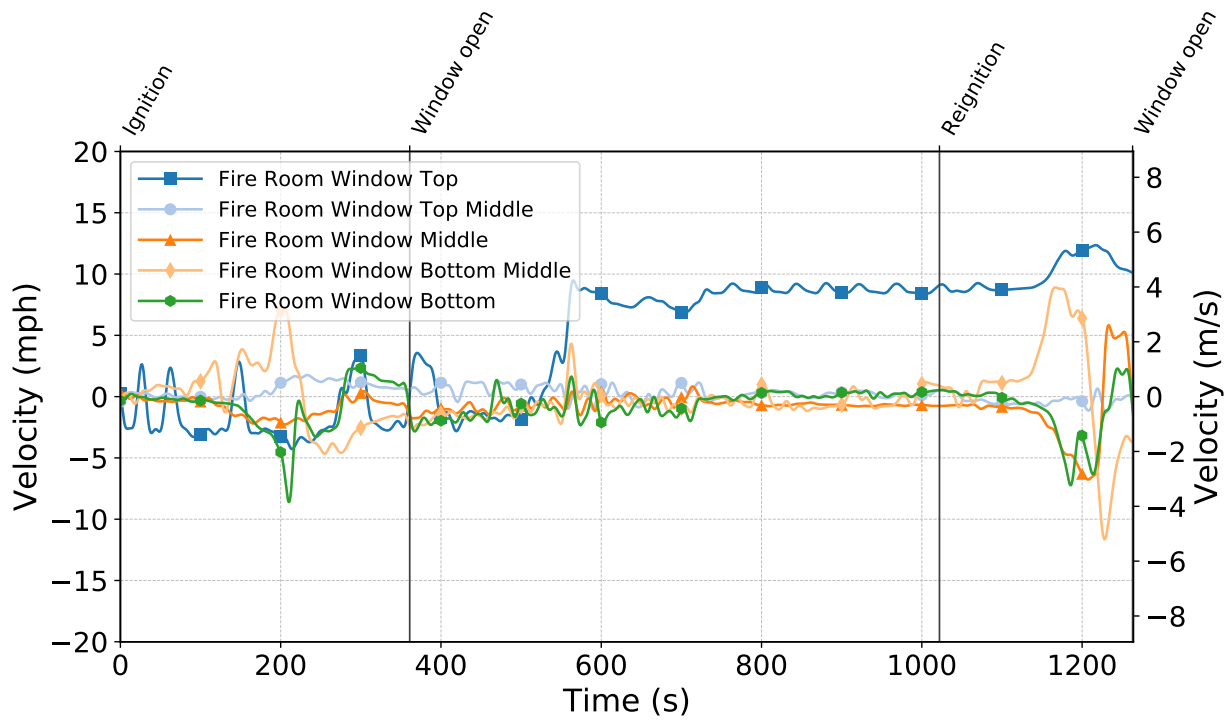


Figure C.253: Gas velocities measured by the fire room window bdp's during Test 23.

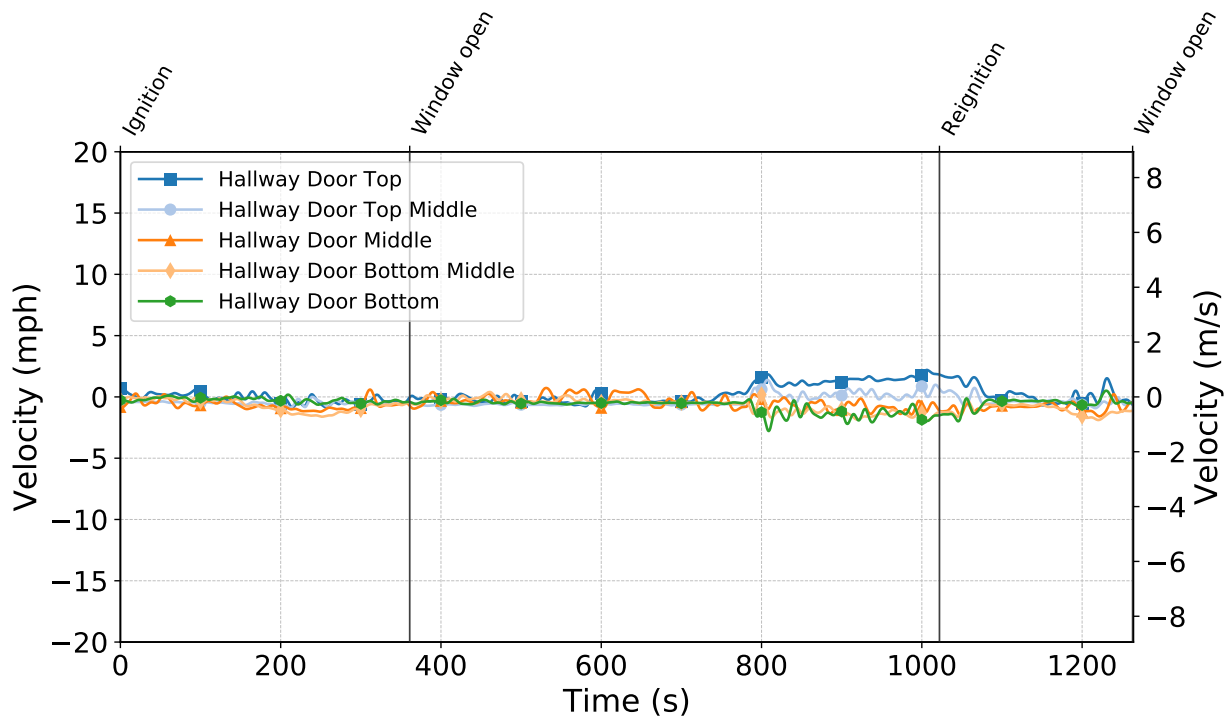


Figure C.254: Gas velocities measured by the hallway door bdp's during Test 23.

Test 24

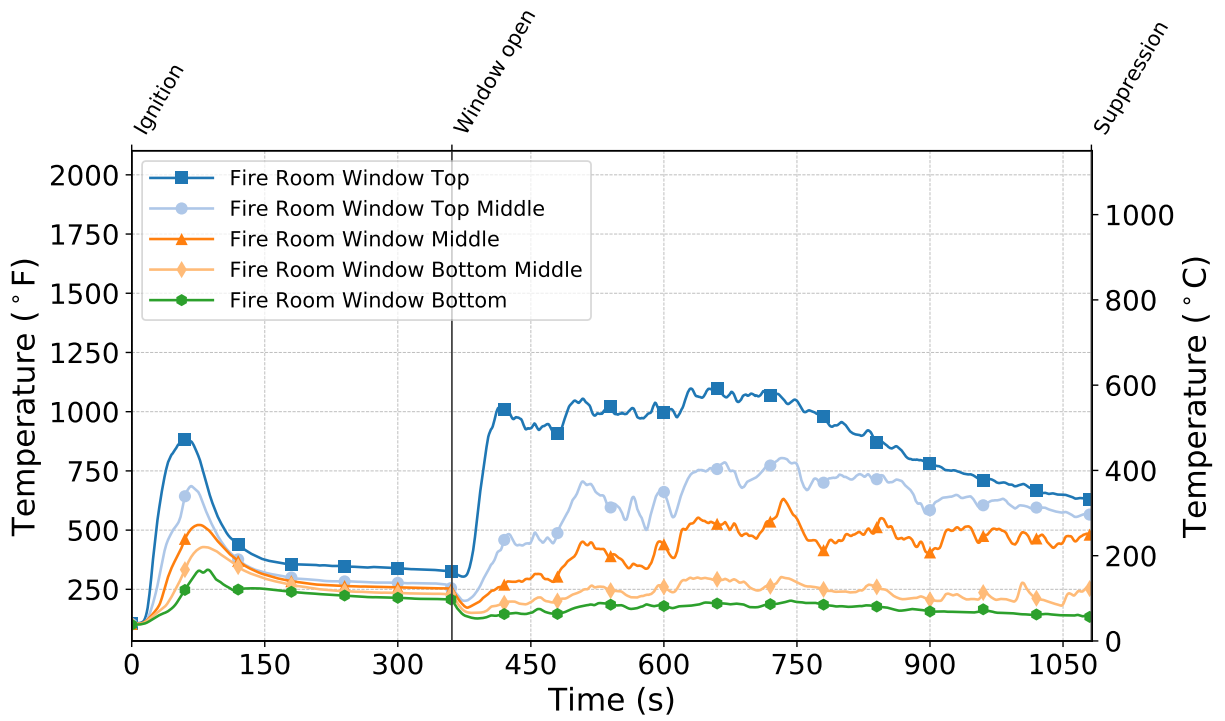


Figure C.255: Temperatures measured by the fire room window thermocouples during Test 24.

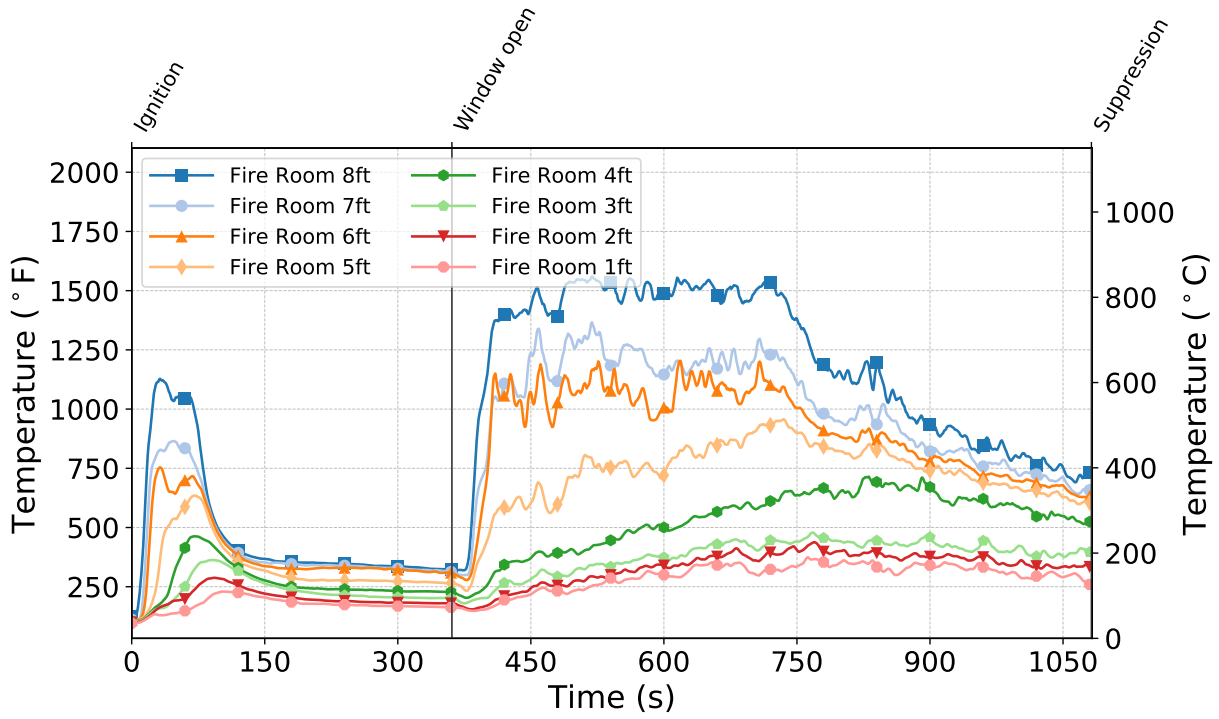


Figure C.256: Temperatures measured by the fire room thermocouples during Test 24.

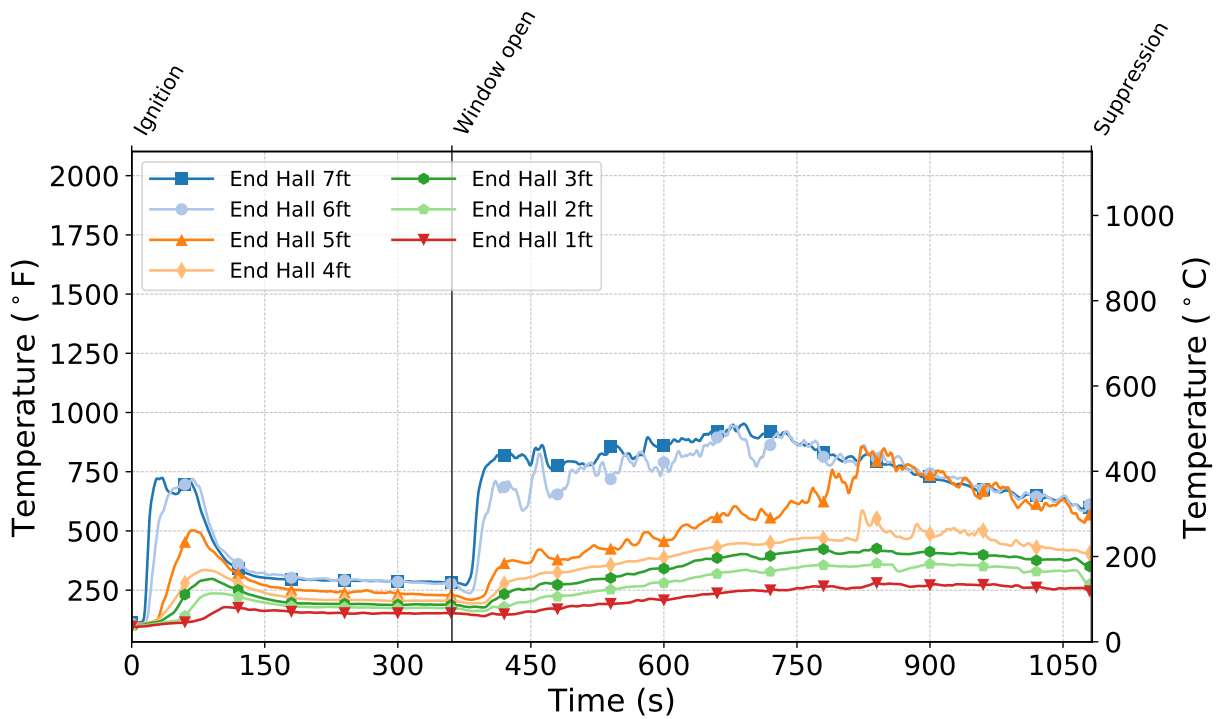


Figure C.257: Temperatures measured by the end hall thermocouples during Test 24.

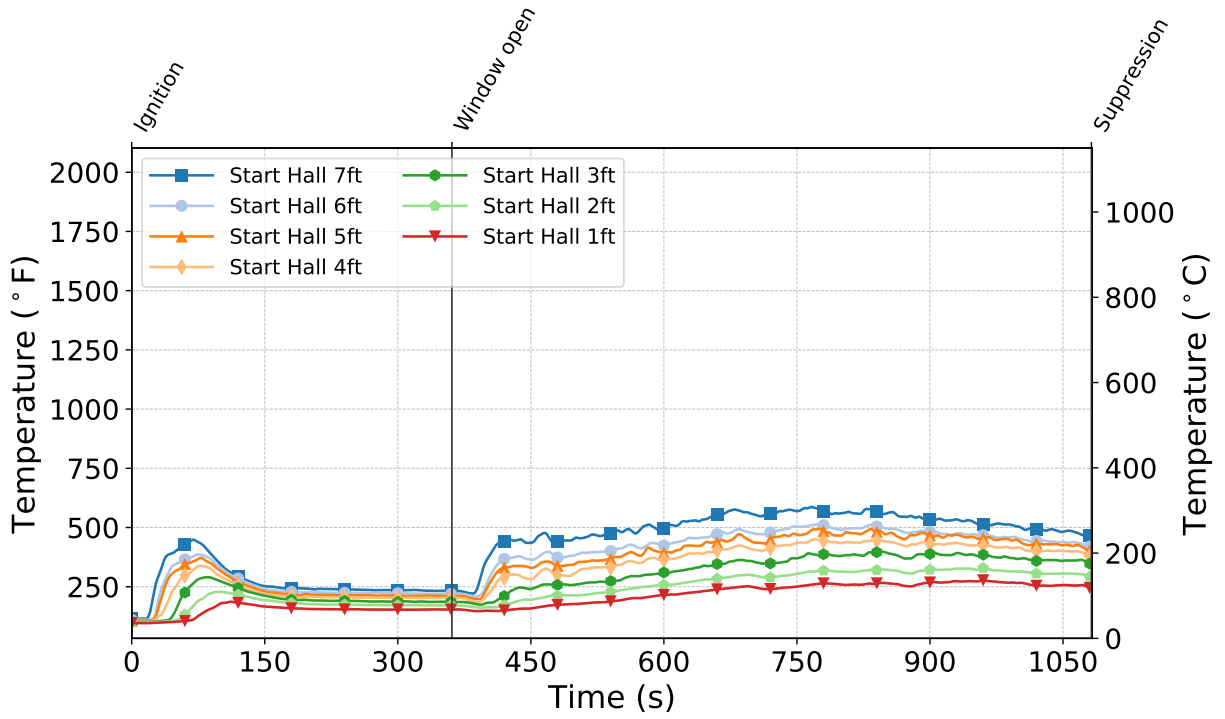


Figure C.258: Temperatures measured by the start hall thermocouples during Test 24.

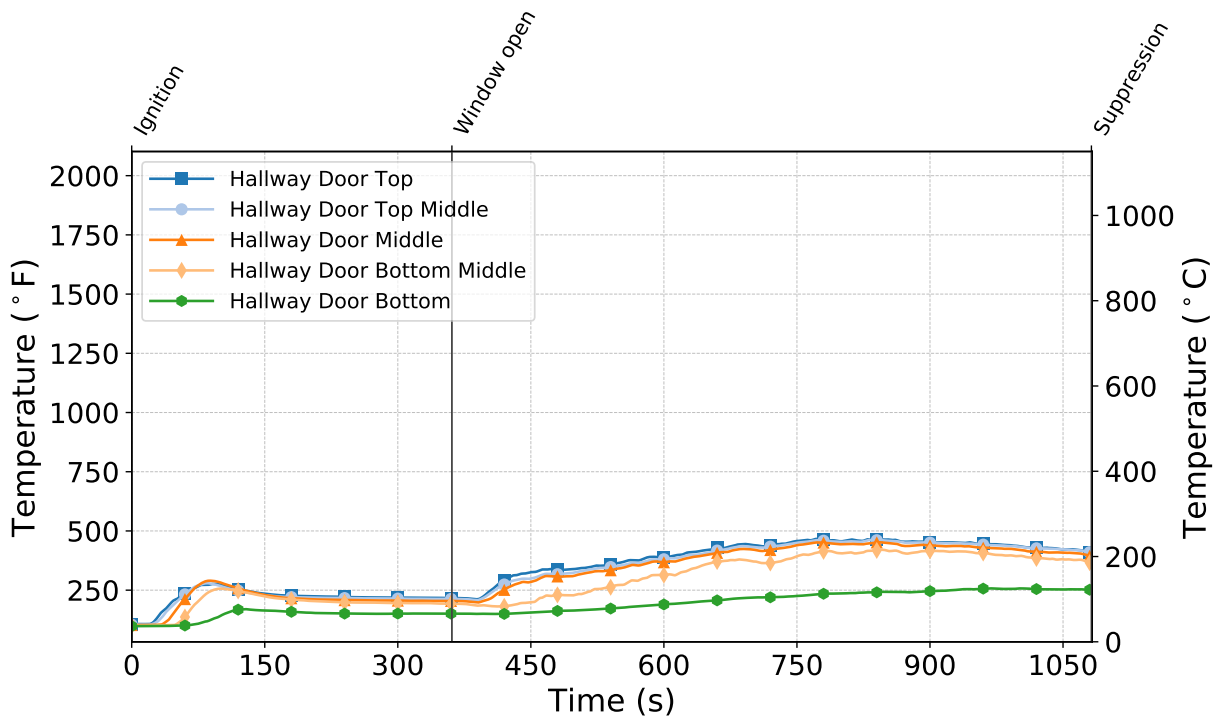


Figure C.259: Temperatures measured by the hallway door thermocouples during Test 24.

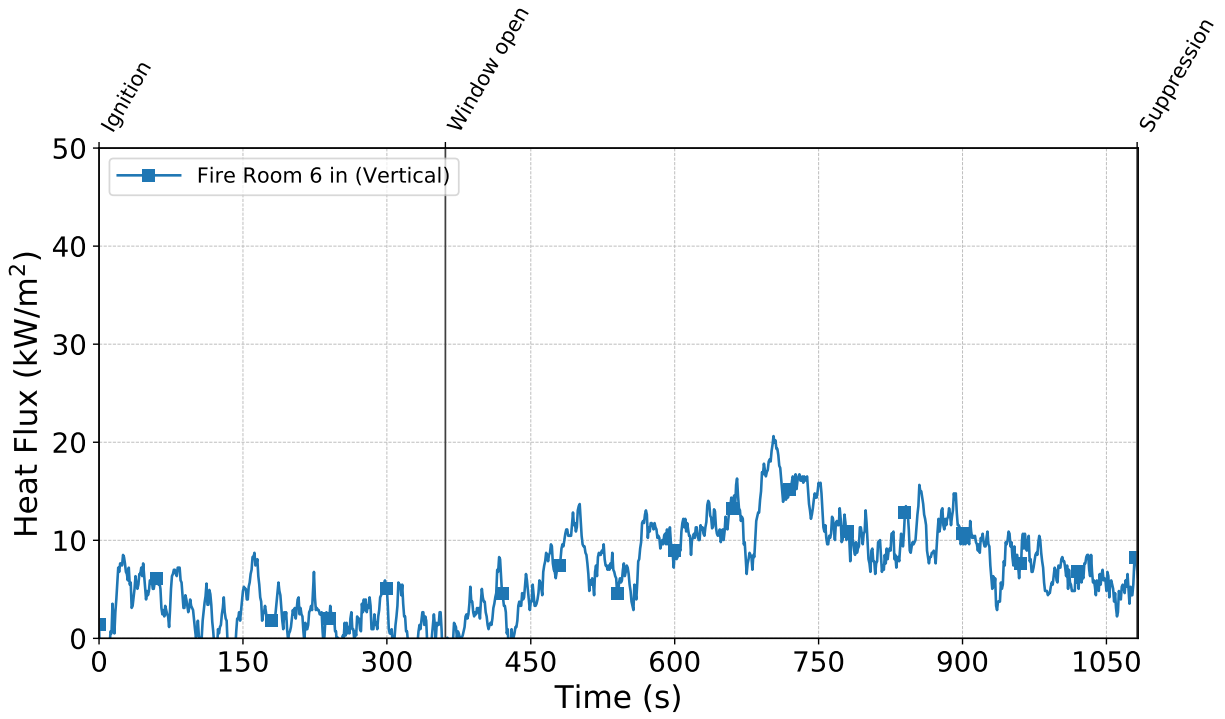


Figure C.260: Heat flux measured by the fire room gauge during Test 24.

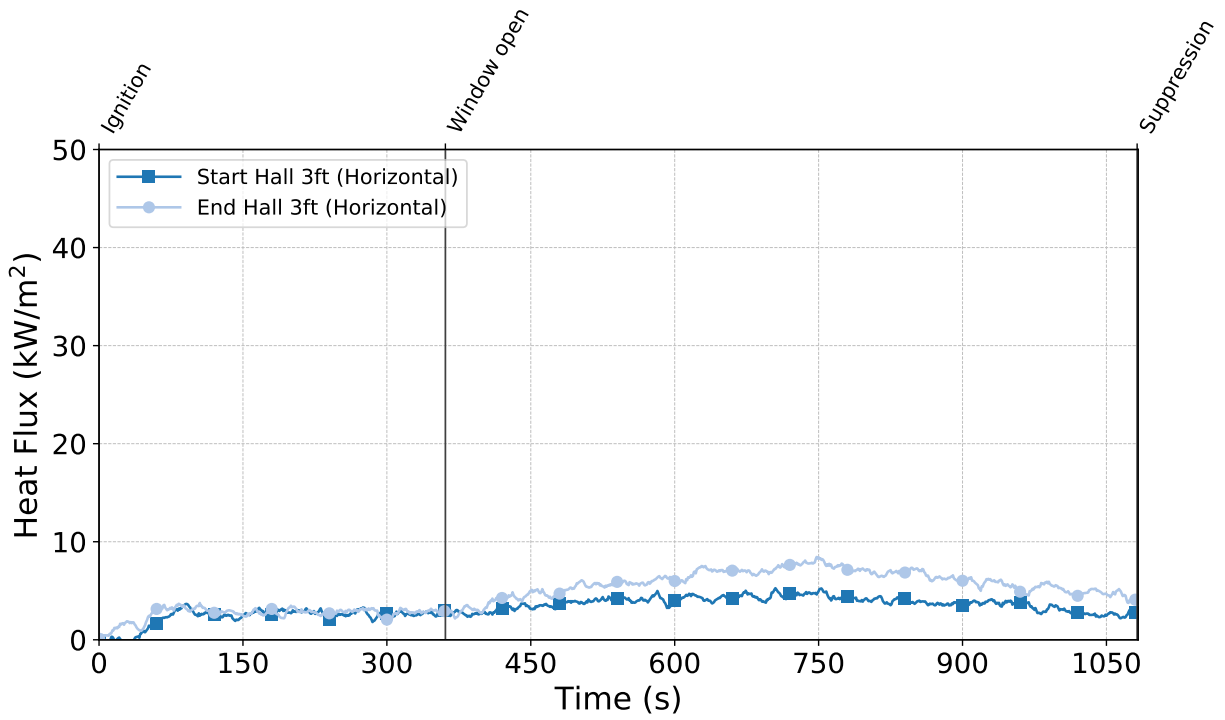


Figure C.261: Heat flux measured by the hallway gauges during Test 24.

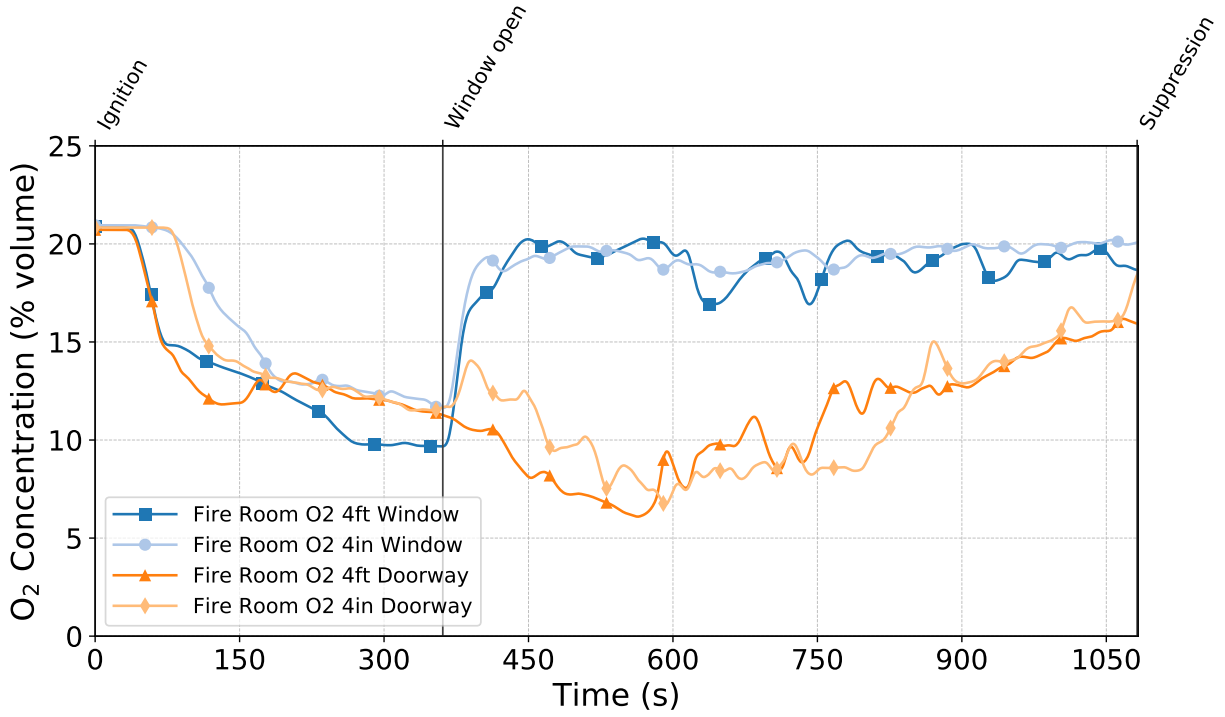


Figure C.262: Oxygen concentrations measured by the fire room gas sampling probes during Test 24.

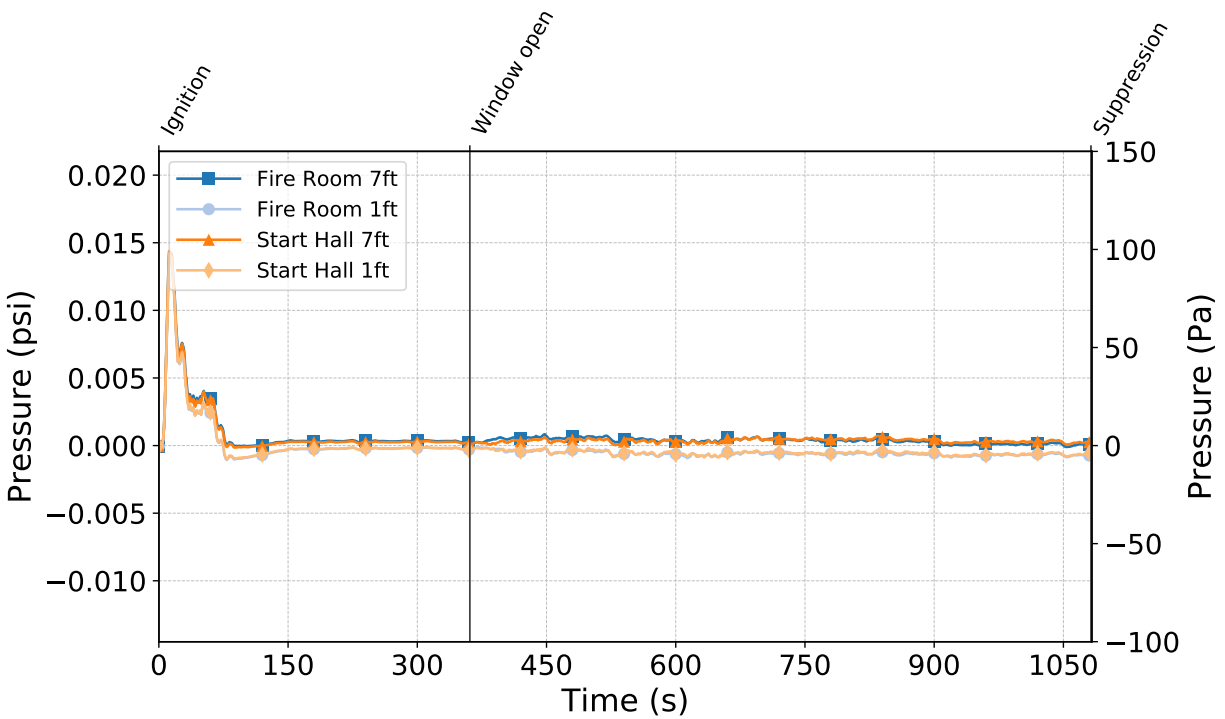


Figure C.263: Pressures measured by the fire room and hallway probes during Test 24.

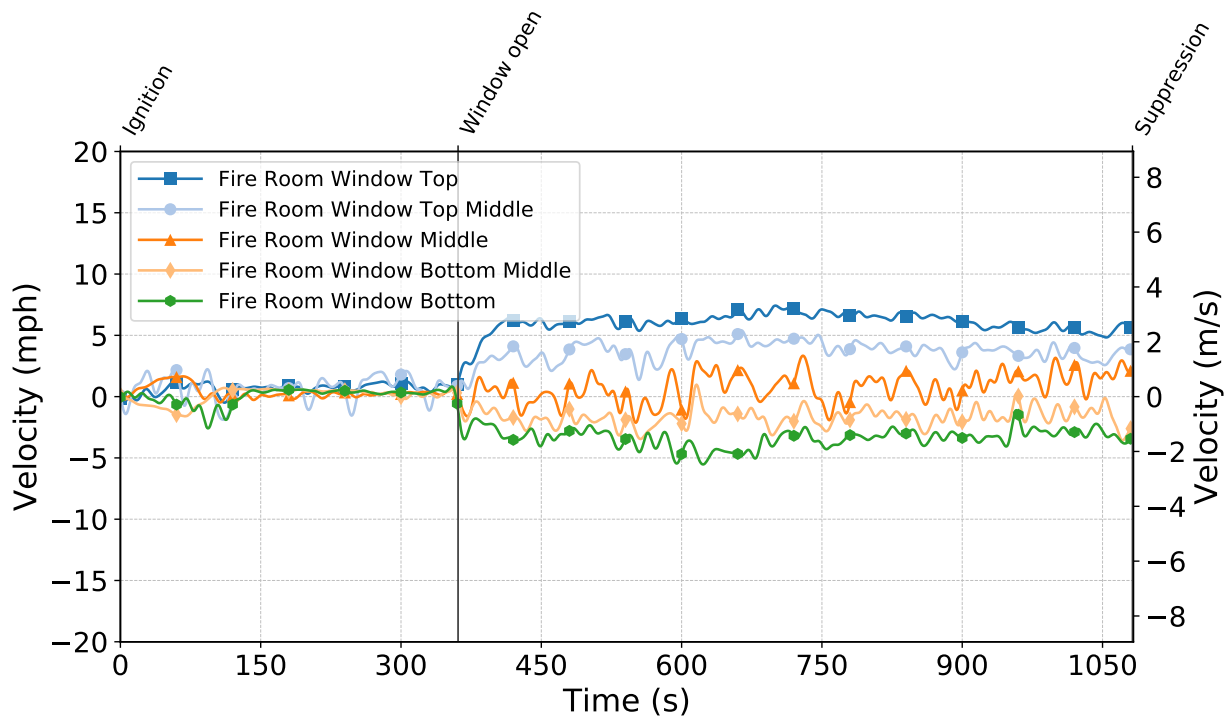


Figure C.264: Gas velocities measured by the fire room window bdps during Test 24.

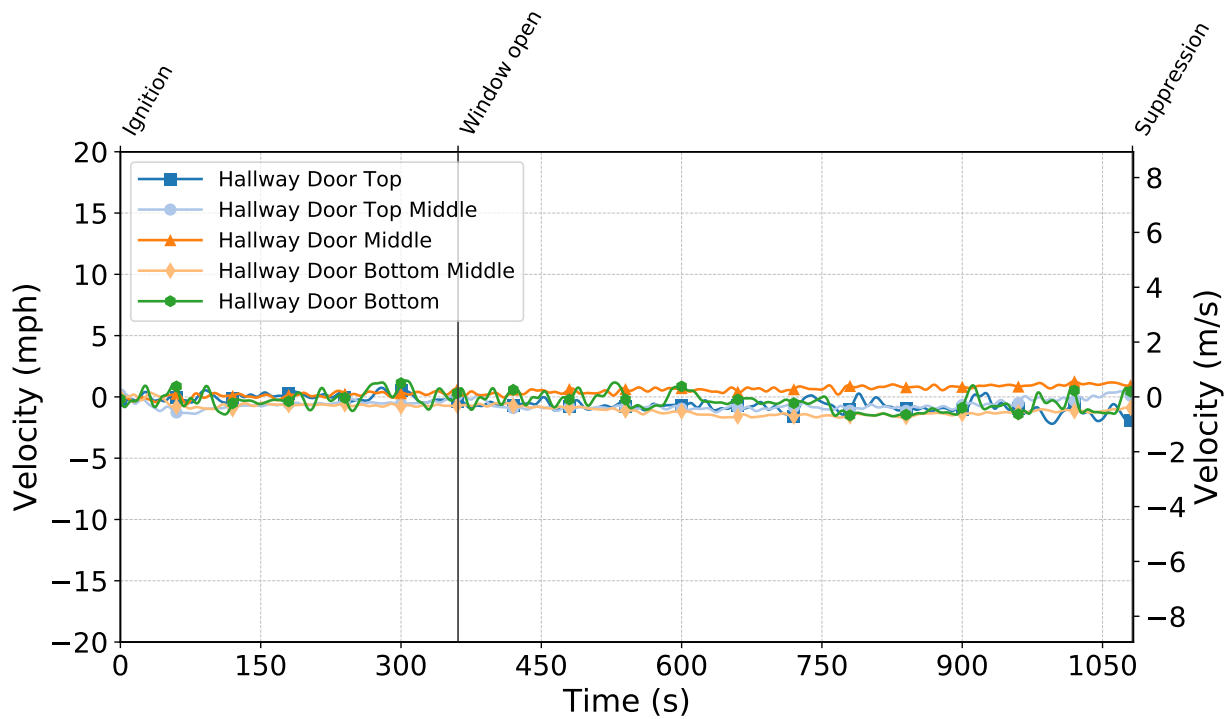


Figure C.265: Gas velocities measured by the hallway door bdps during Test 24.

Test 25

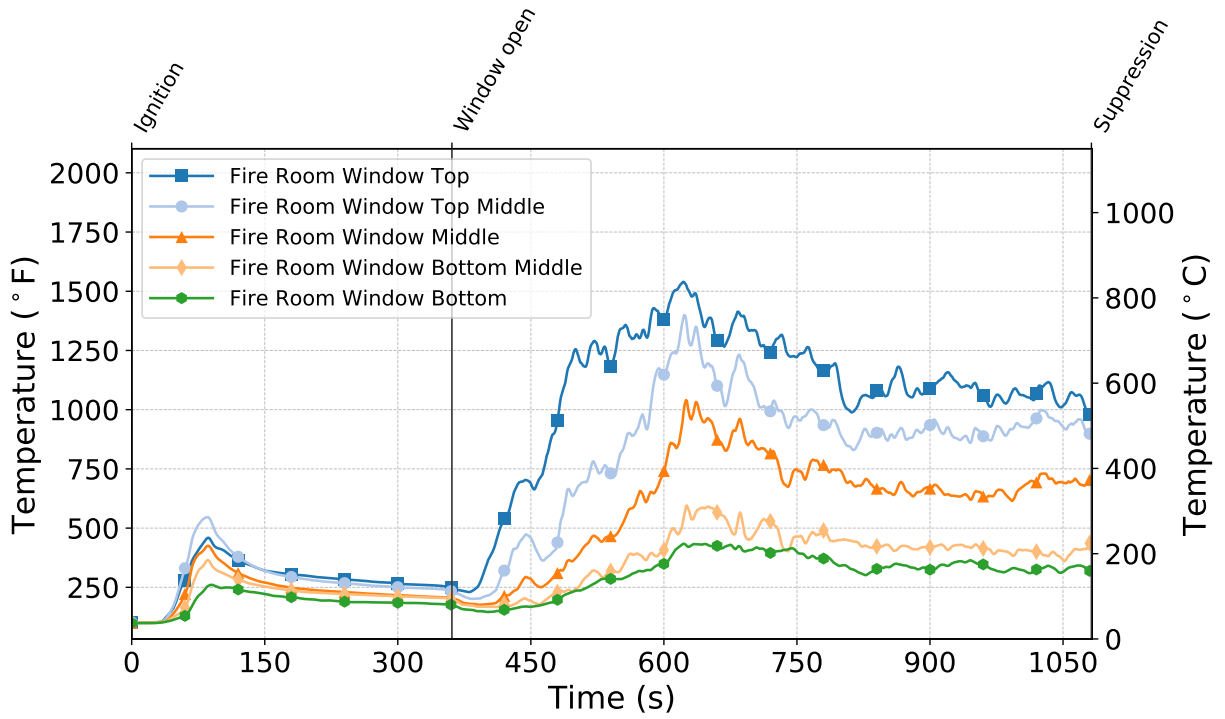


Figure C.266: Temperatures measured by the fire room window thermocouples during Test 25.

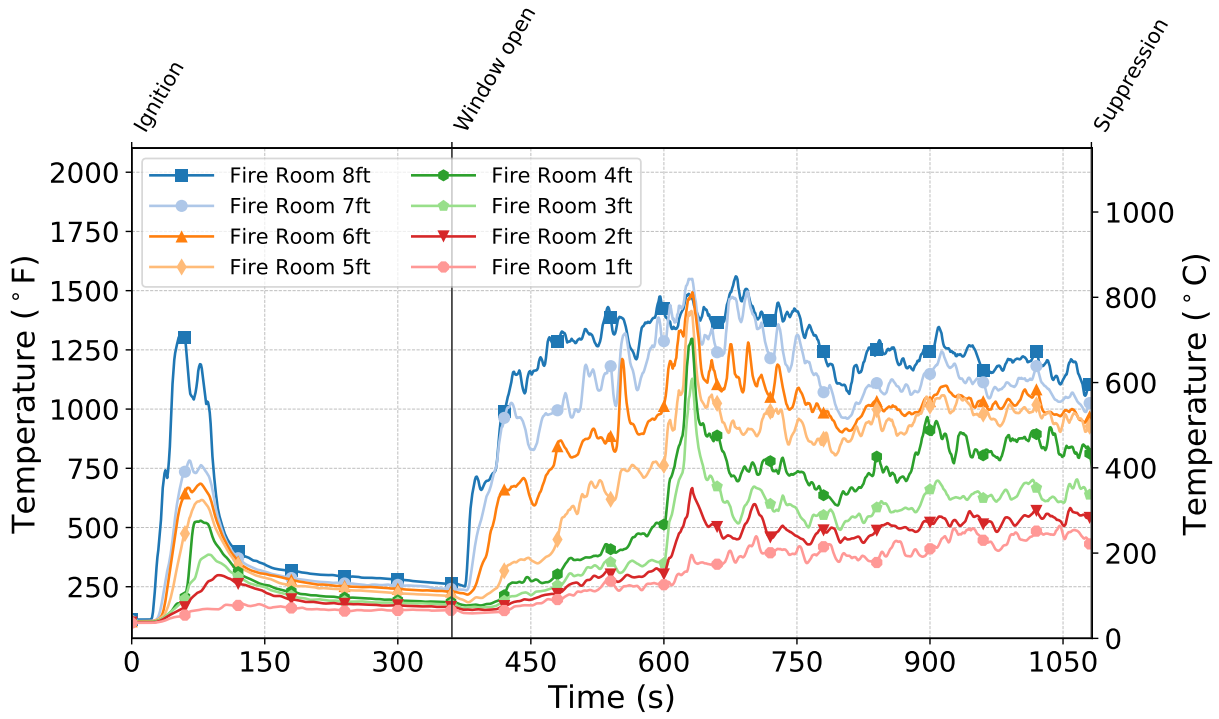


Figure C.267: Temperatures measured by the fire room thermocouples during Test 25.

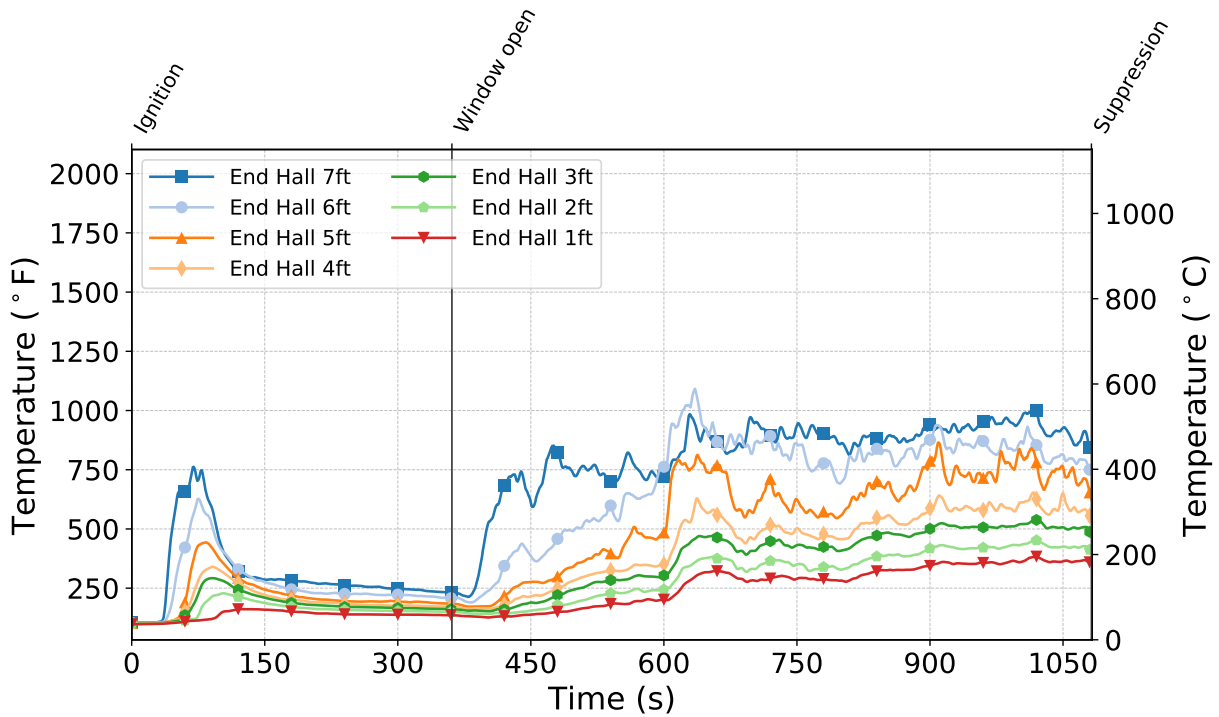


Figure C.268: Temperatures measured by the end hall thermocouples during Test 25.

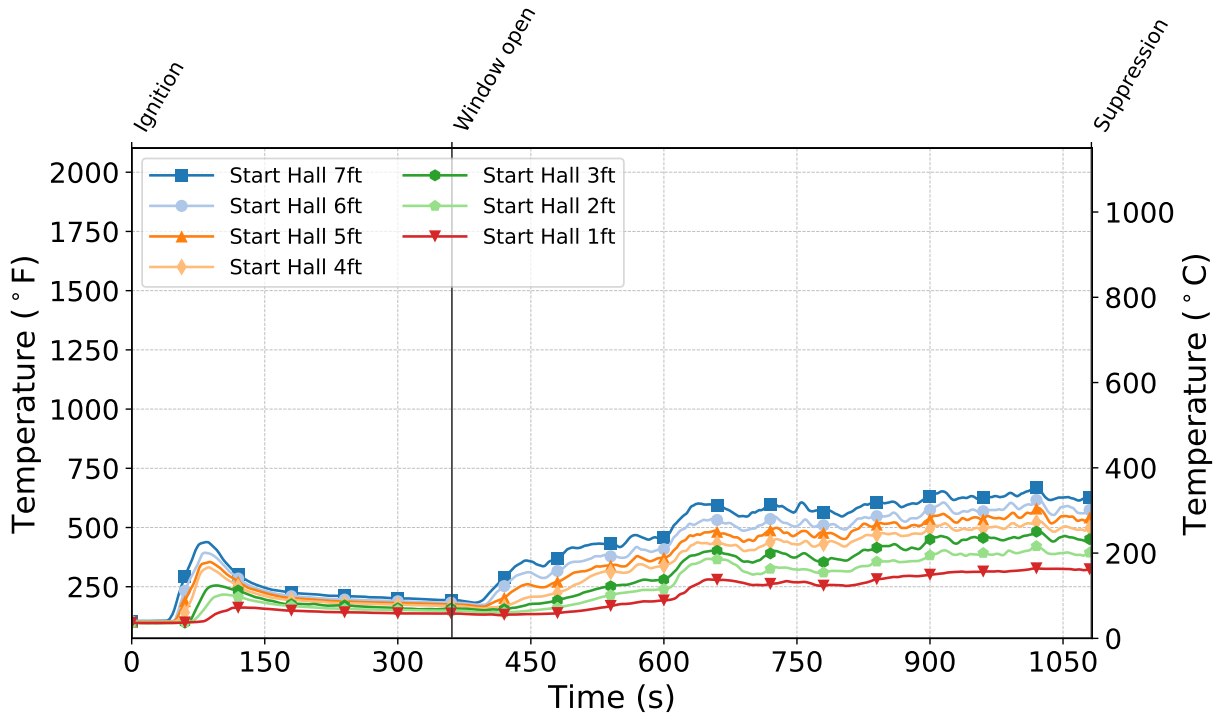


Figure C.269: Temperatures measured by the start hall thermocouples during Test 25.

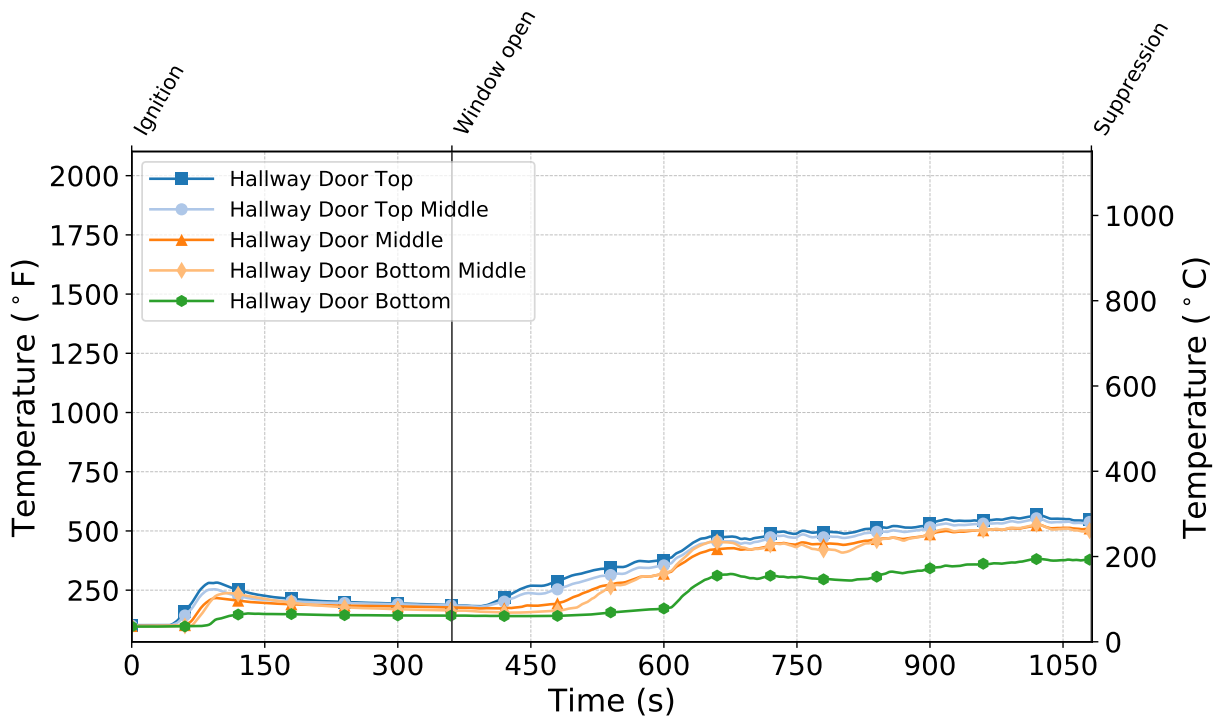


Figure C.270: Temperatures measured by the hallway door thermocouples during Test 25.

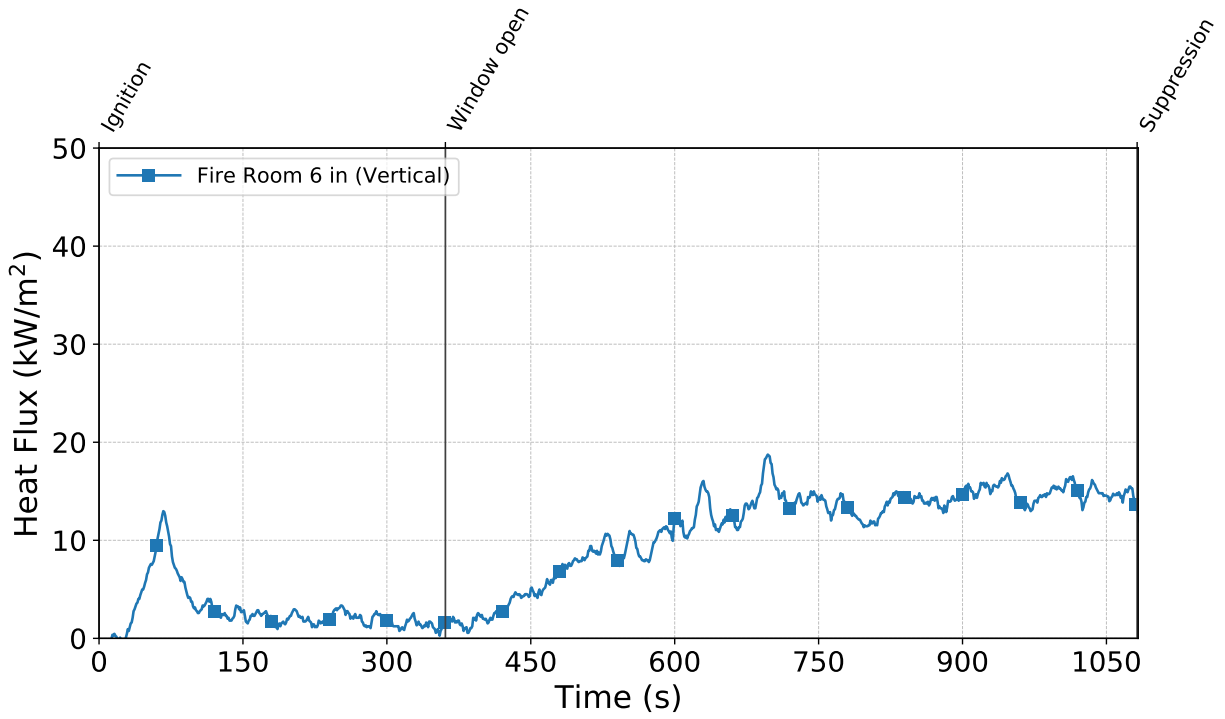


Figure C.271: Heat flux measured by the fire room gauge during Test 25.

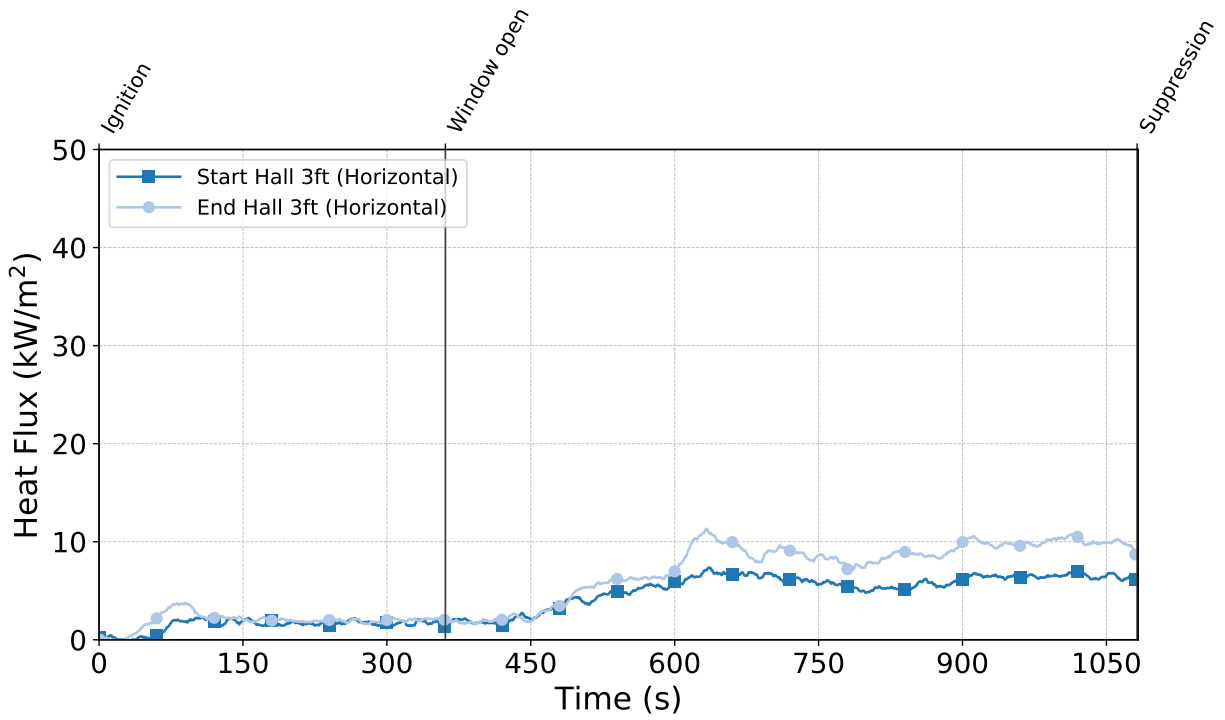


Figure C.272: Heat flux measured by the hallway gauges during Test 25.

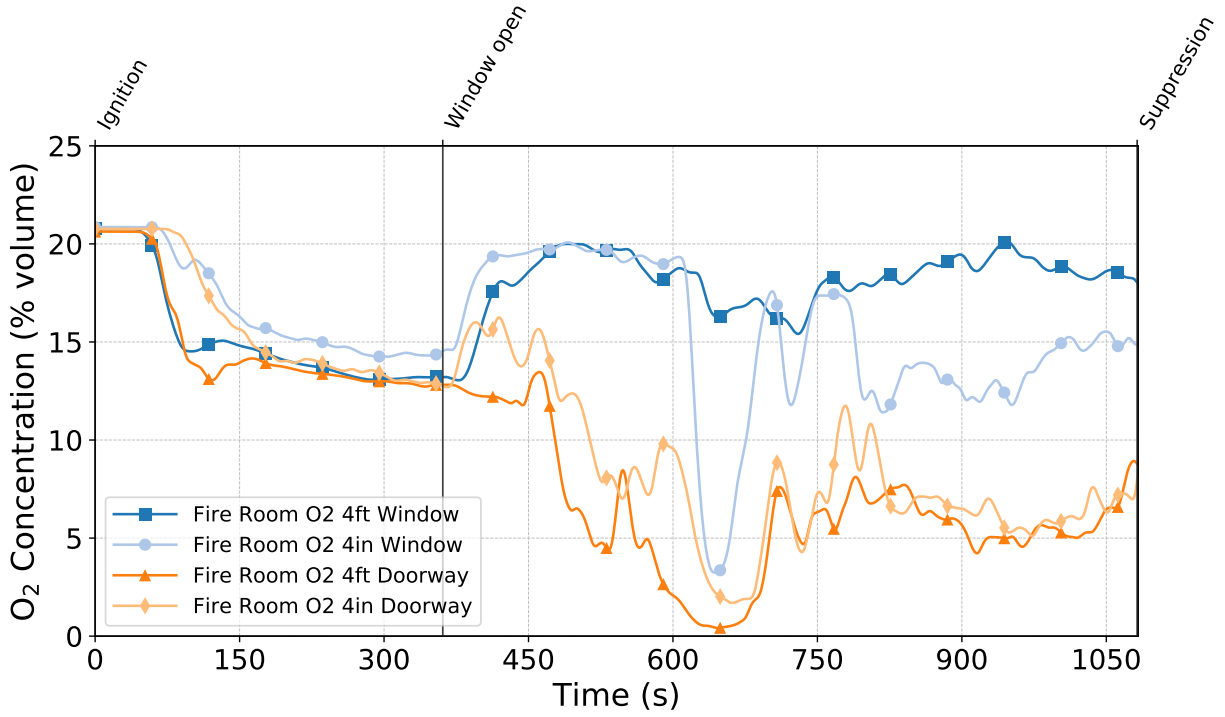


Figure C.273: Oxygen concentrations measured by the fire room gas sampling probes during Test 25.

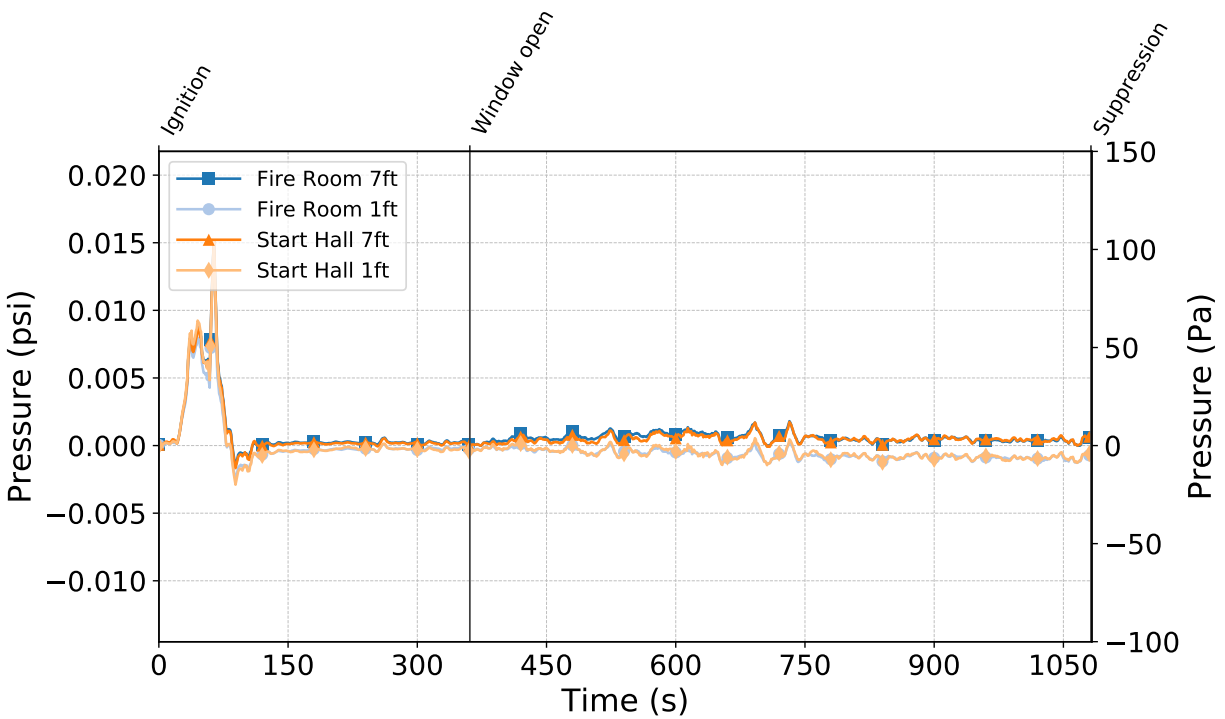


Figure C.274: Pressures measured by the fire room and hallway probes during Test 25.

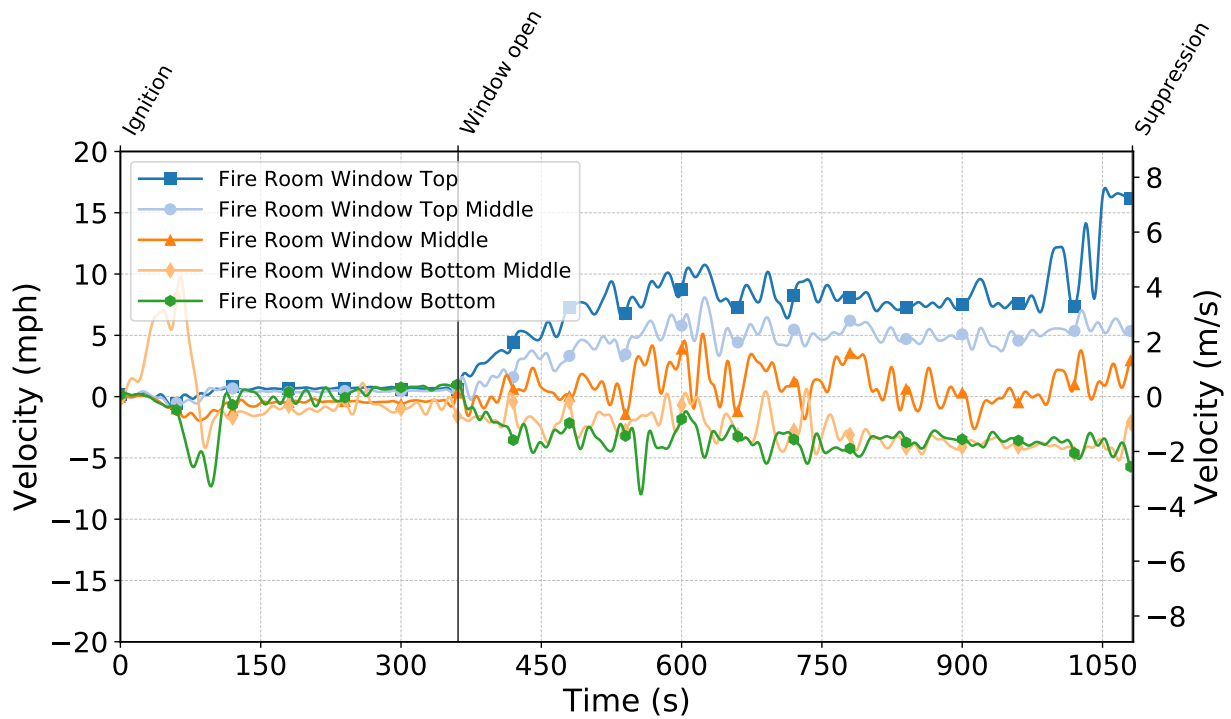


Figure C.275: Gas velocities measured by the fire room window bdps during Test 25.

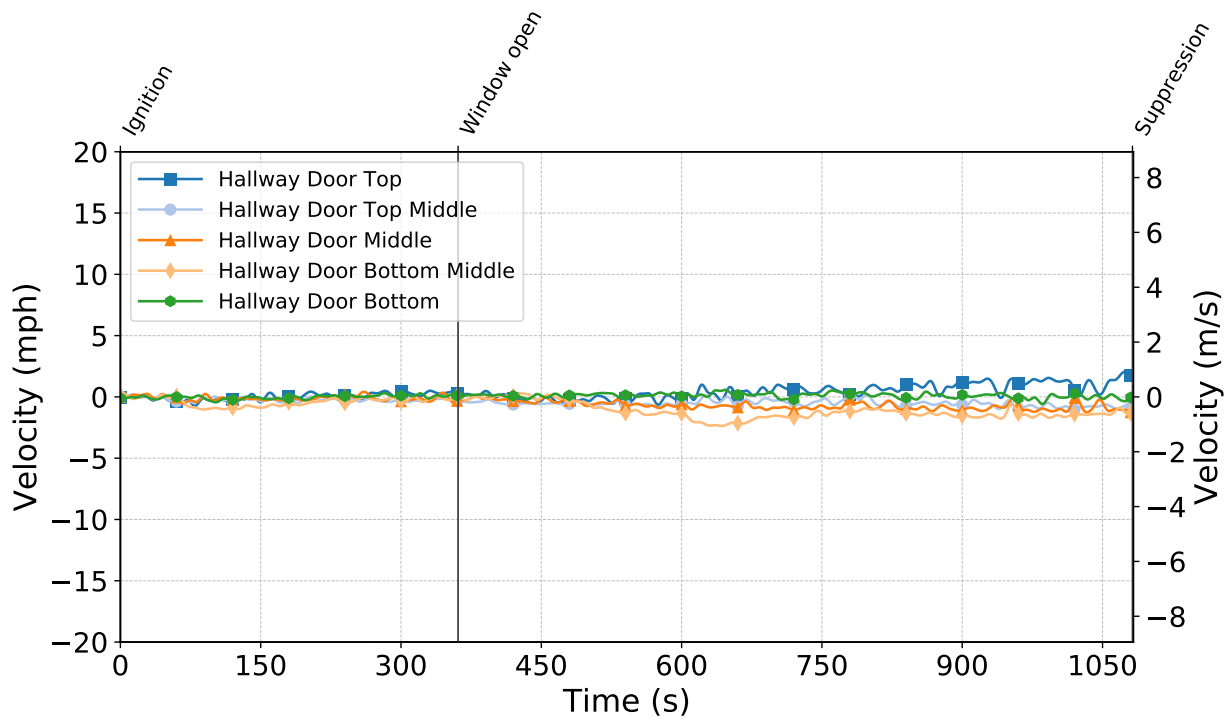


Figure C.276: Gas velocities measured by the hallway door bdps during Test 25.

Test 26

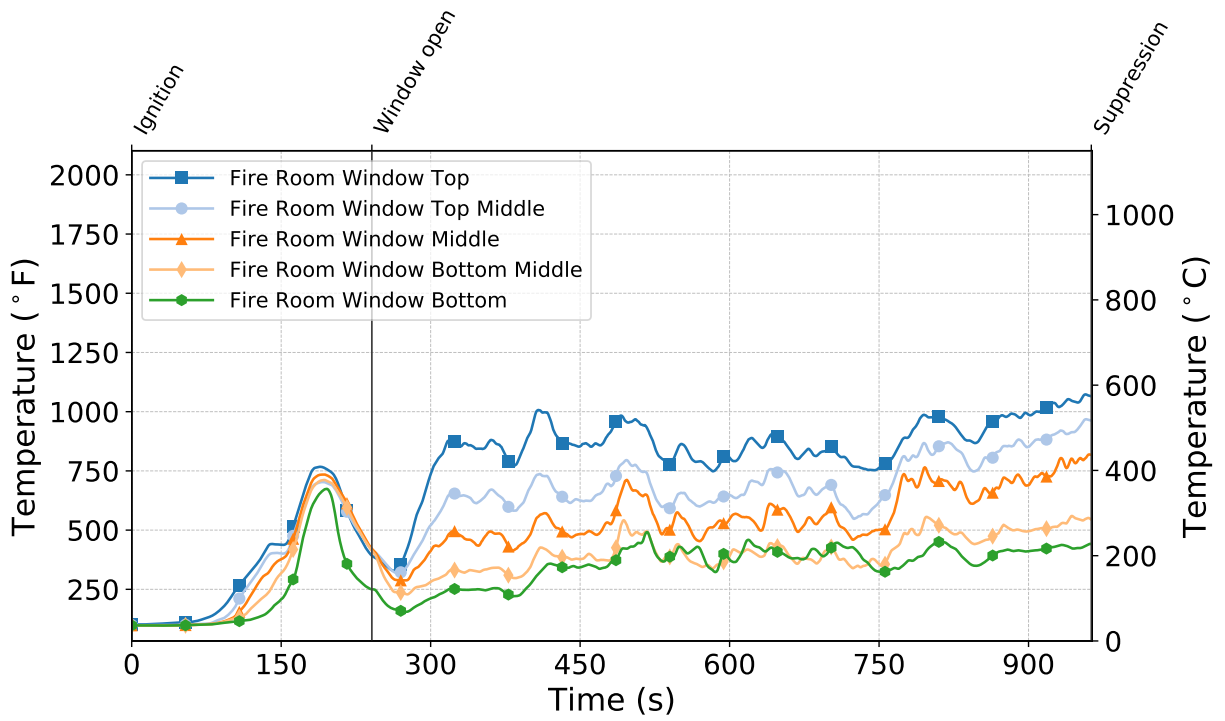


Figure C.277: Temperatures measured by the fire room window thermocouples during Test 26.

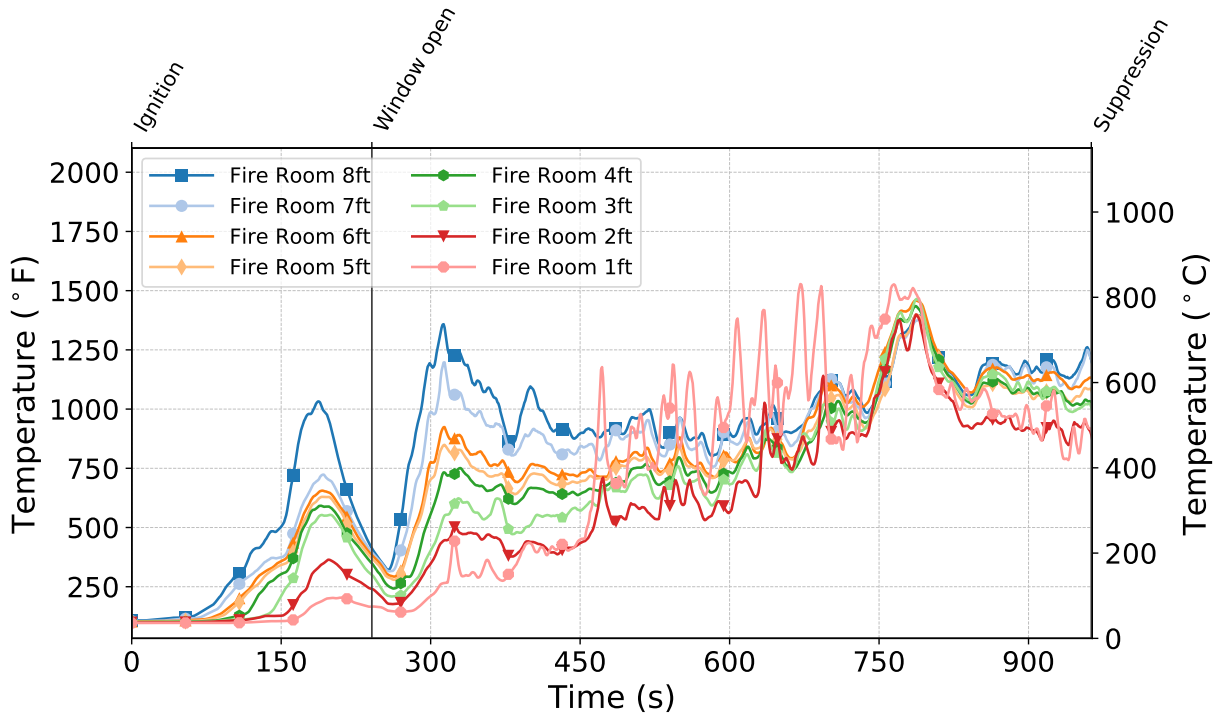


Figure C.278: Temperatures measured by the fire room thermocouples during Test 26.

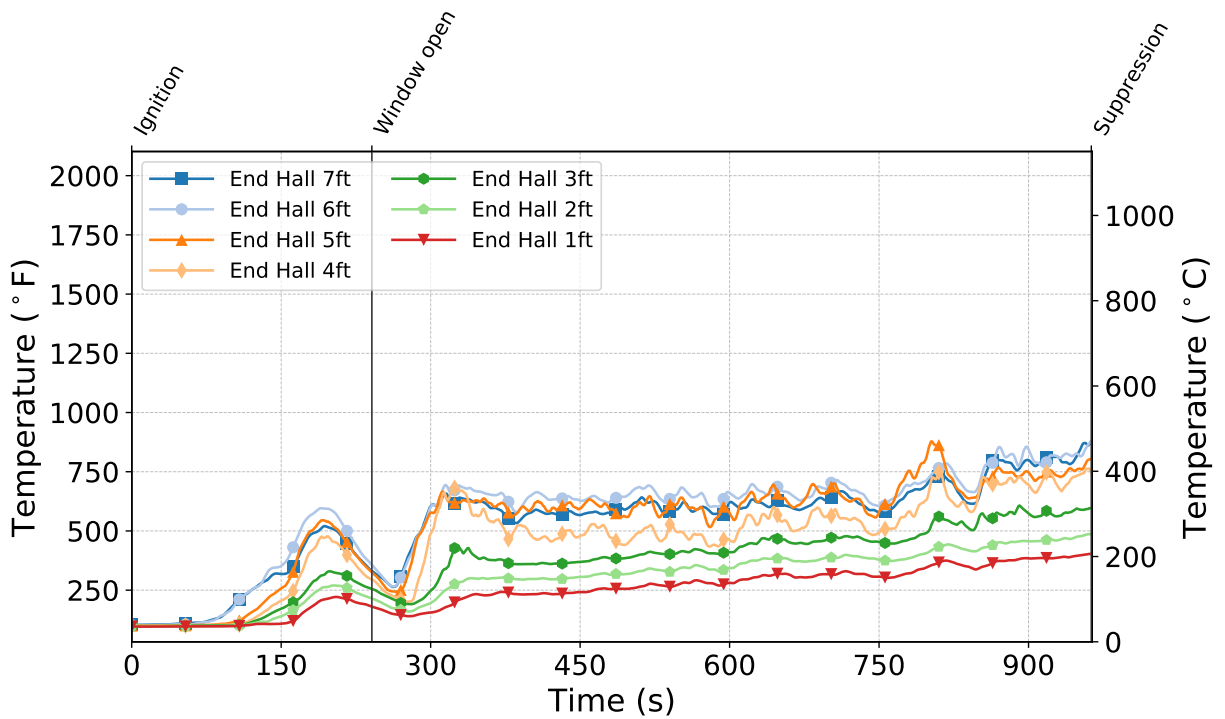


Figure C.279: Temperatures measured by the end hall thermocouples during Test 26.

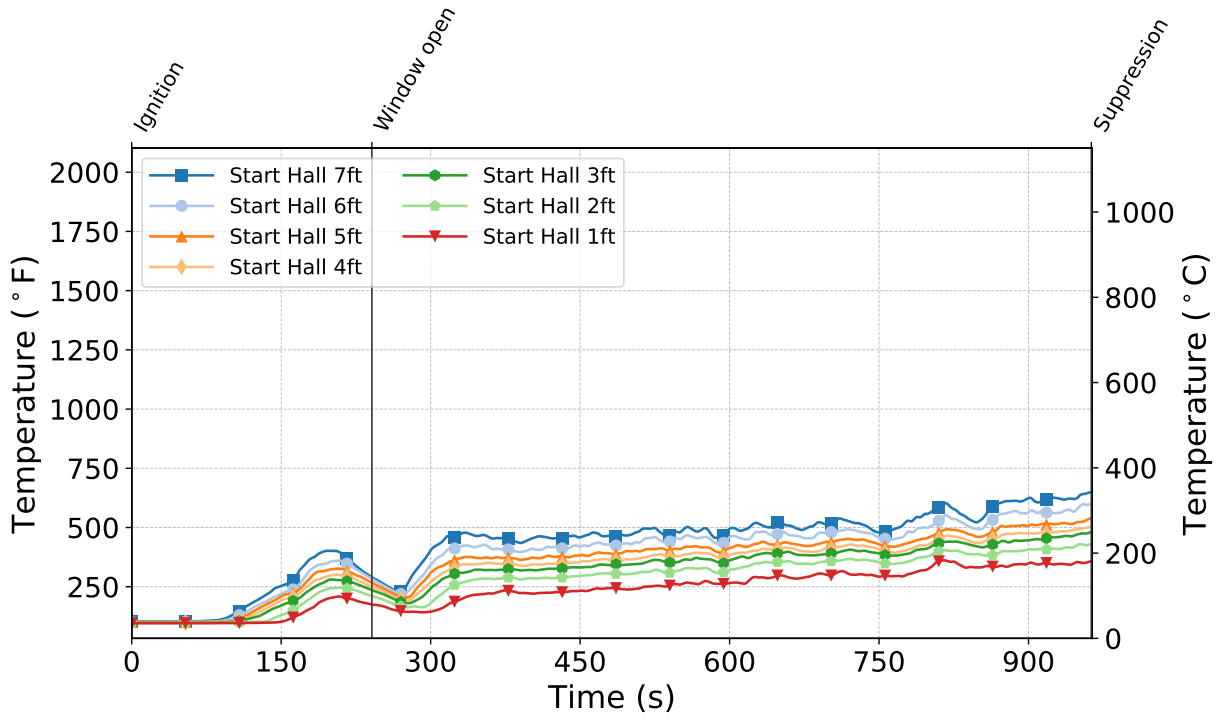


Figure C.280: Temperatures measured by the start hall thermocouples during Test 26.

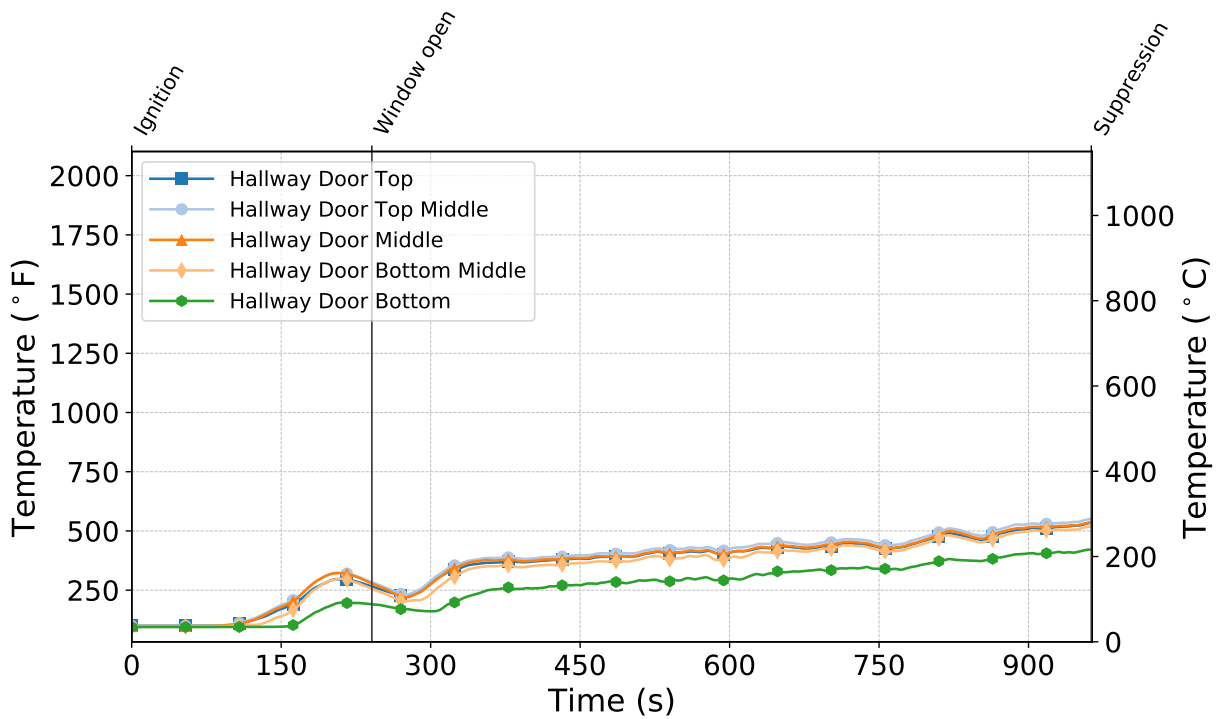


Figure C.281: Temperatures measured by the hallway door thermocouples during Test 26.

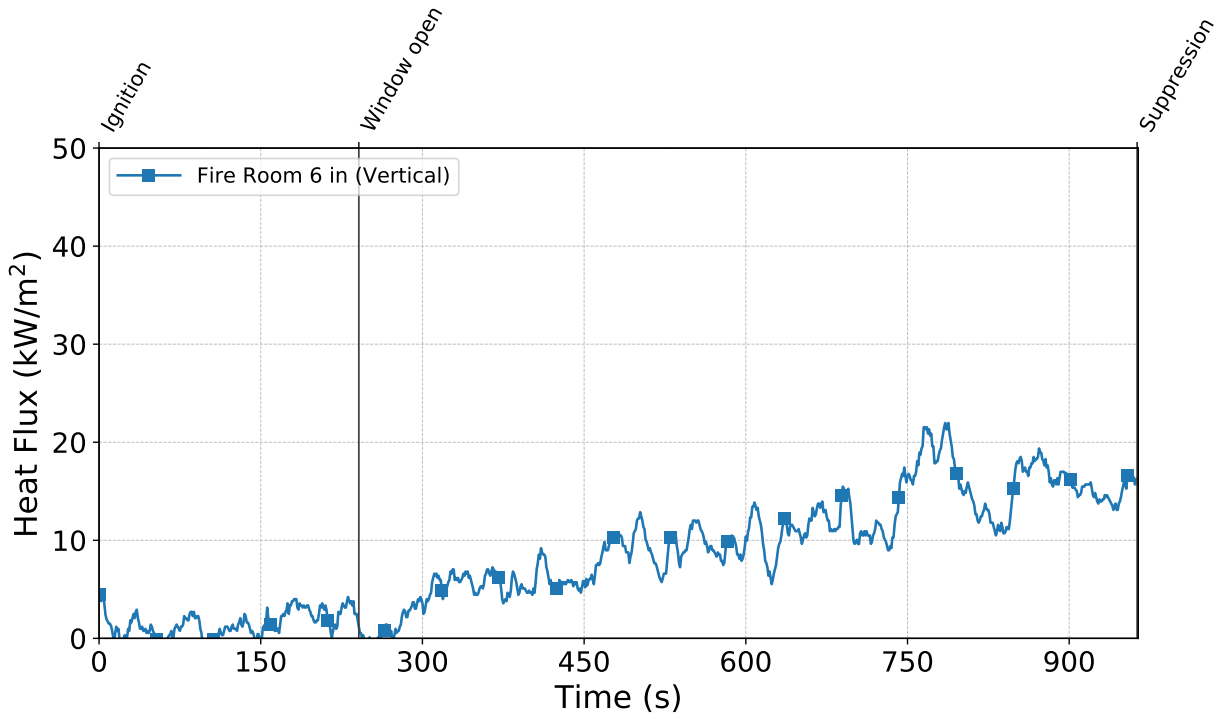


Figure C.282: Heat flux measured by the fire room gauge during Test 26.

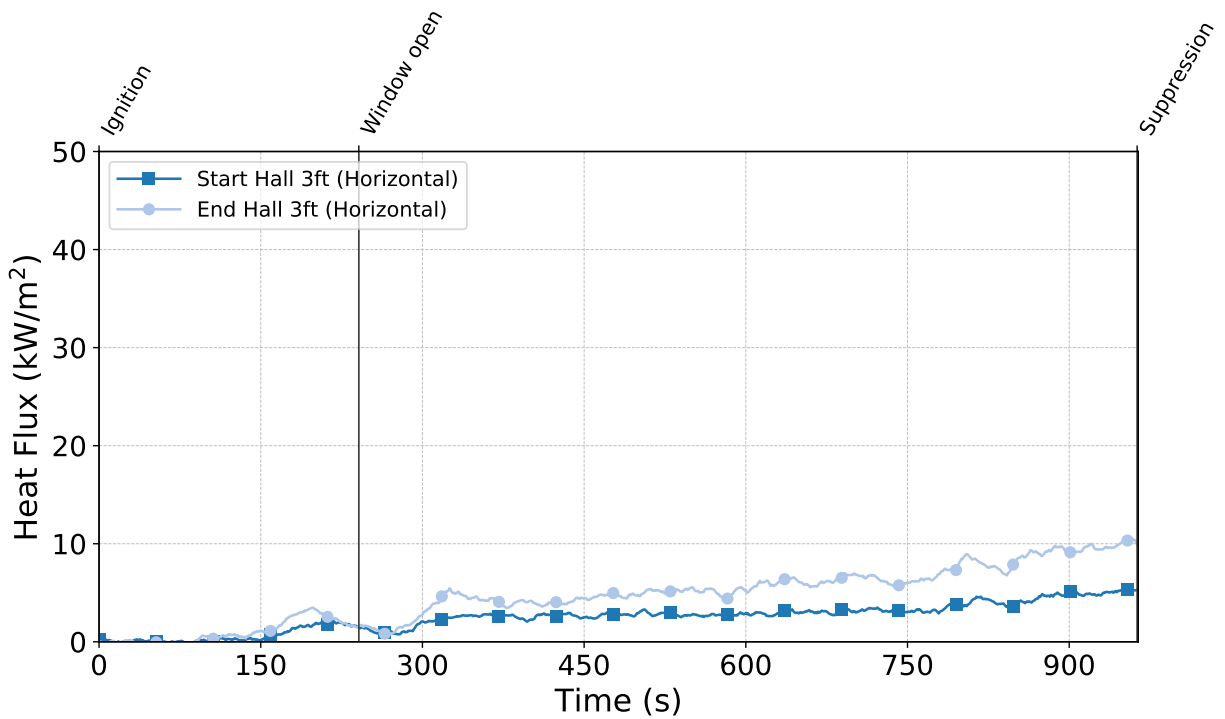


Figure C.283: Heat flux measured by the hallway gauges during Test 26.

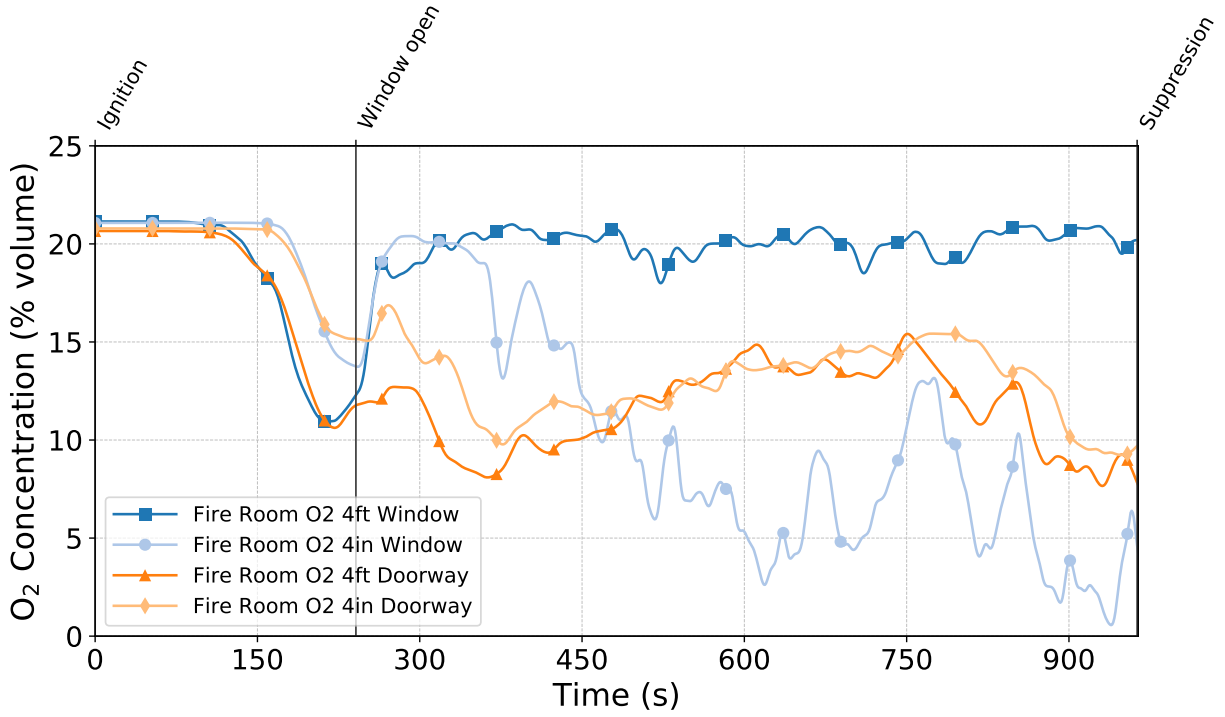


Figure C.284: Oxygen concentrations measured by the fire room gas sampling probes during Test 26.

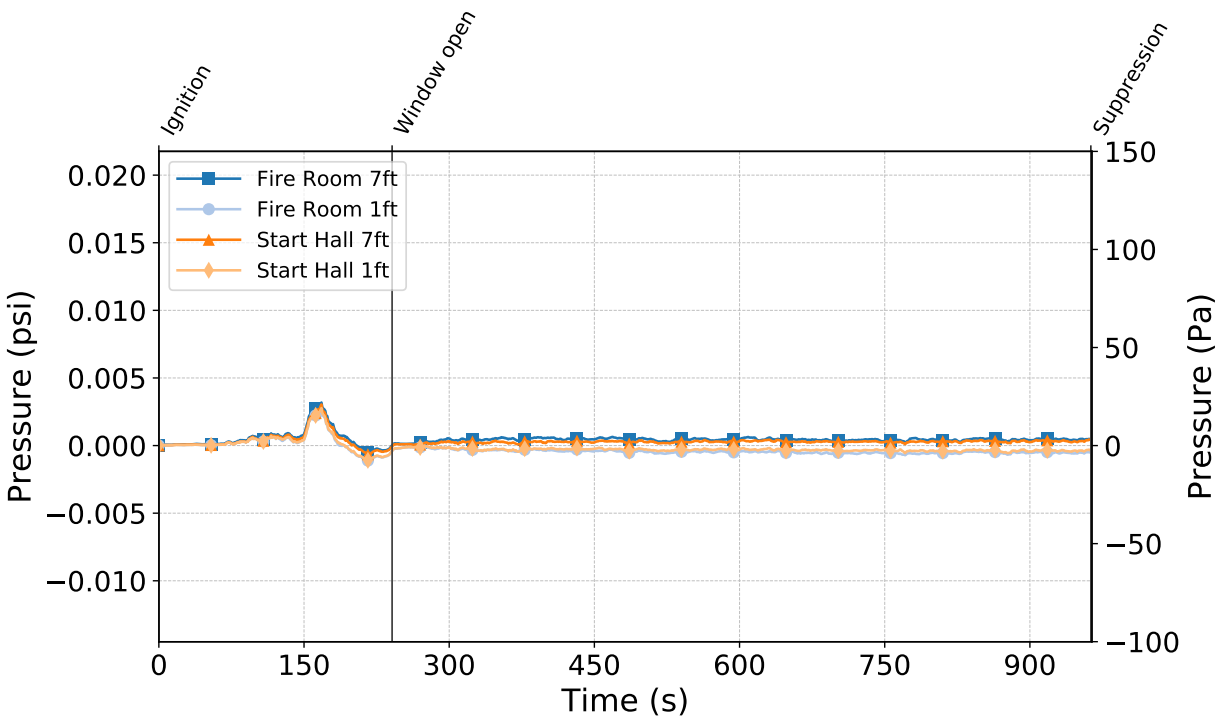


Figure C.285: Pressures measured by the fire room and hallway probes during Test 26.

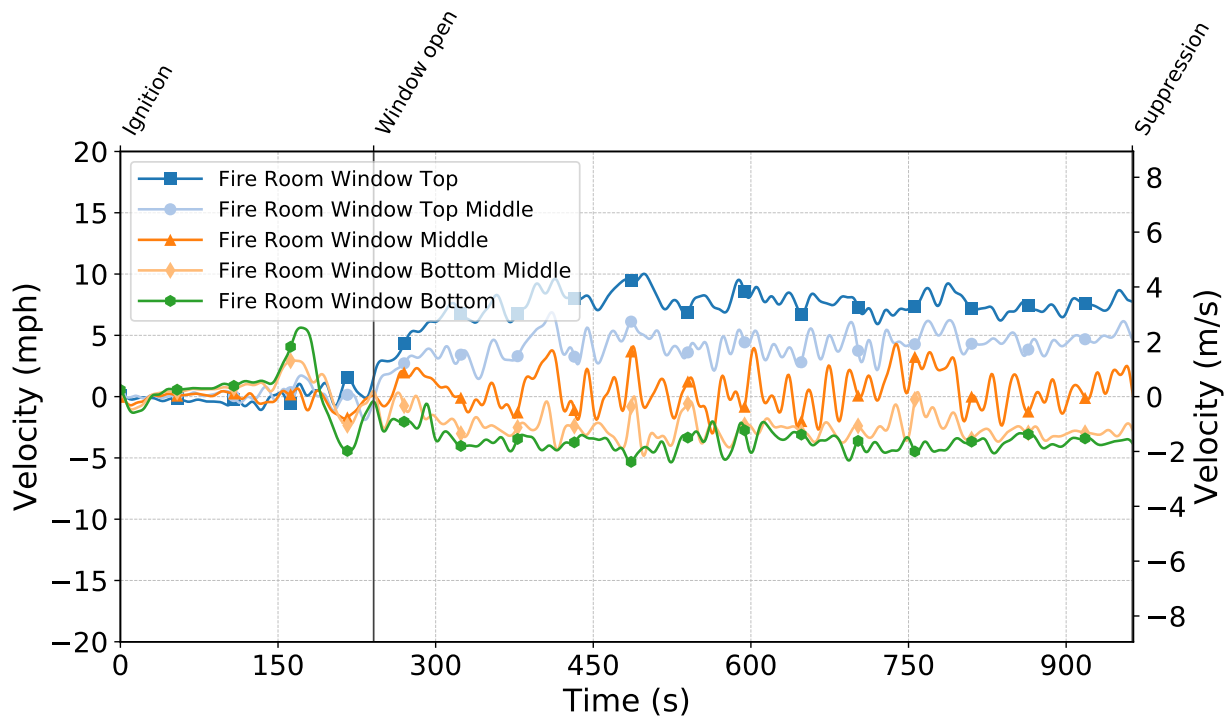


Figure C.286: Gas velocities measured by the fire room window bdps during Test 26.

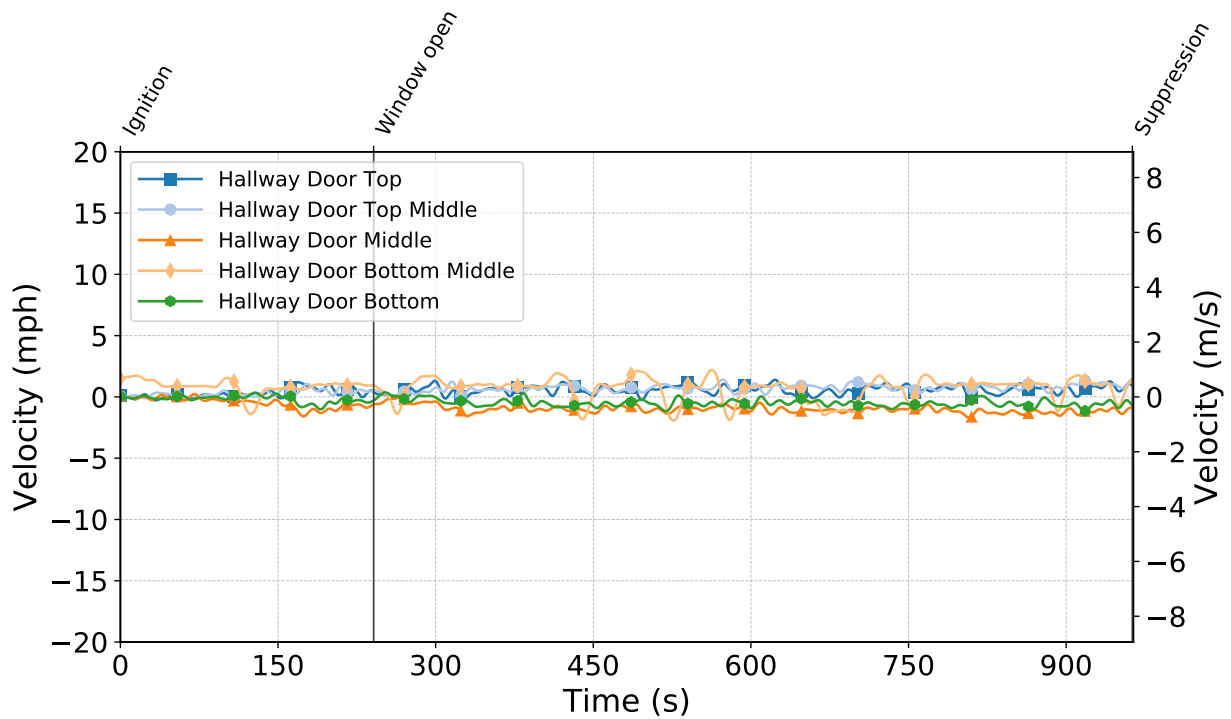


Figure C.287: Gas velocities measured by the hallway door bdps during Test 26.

Test 27

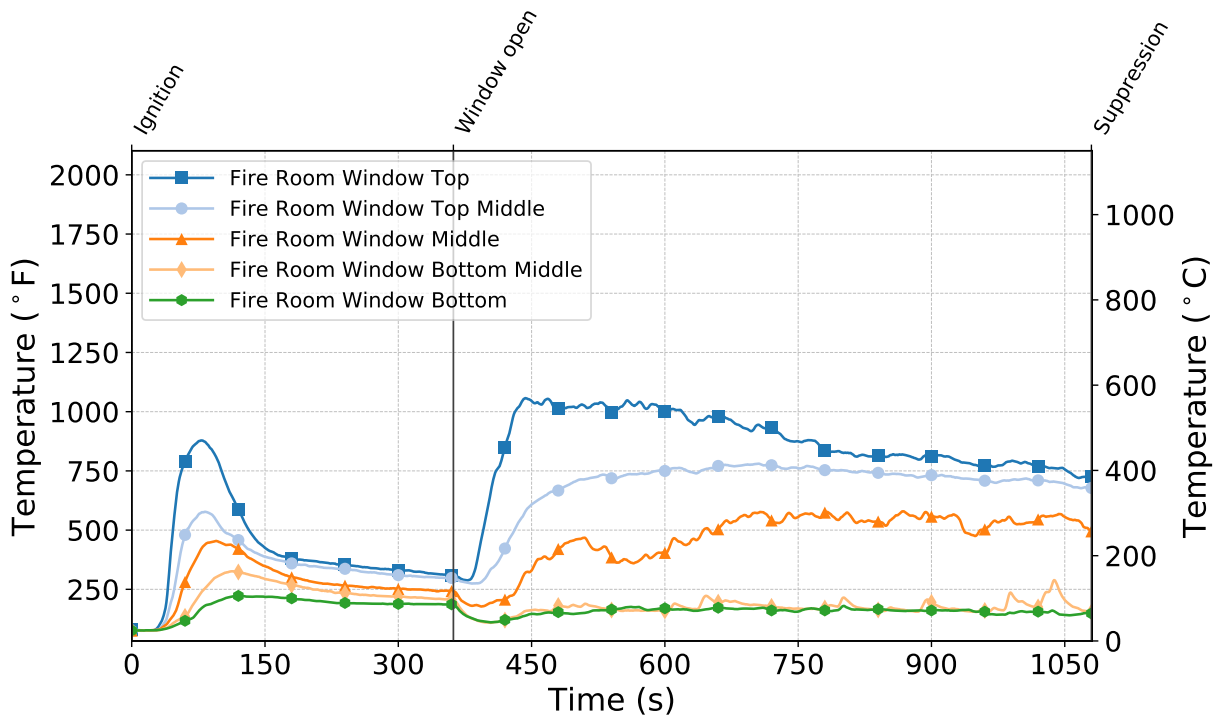


Figure C.288: Temperatures measured by the fire room window thermocouples during Test 27.

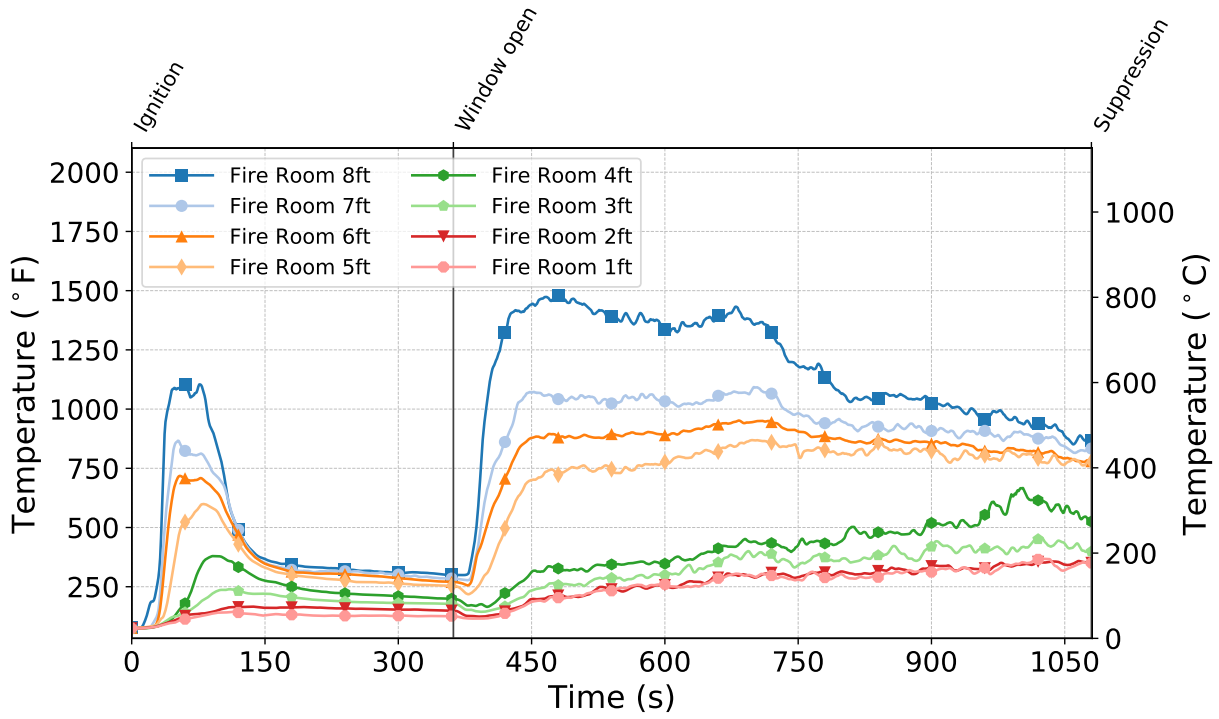


Figure C.289: Temperatures measured by the fire room thermocouples during Test 27.

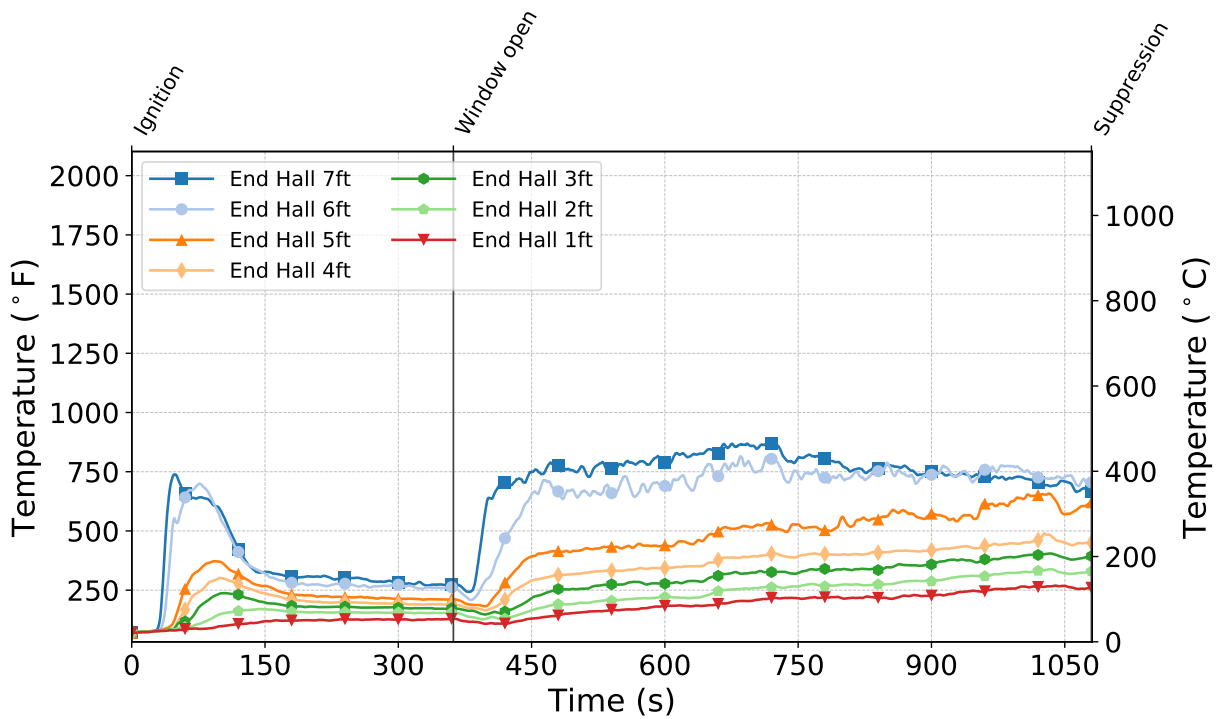


Figure C.290: Temperatures measured by the end hall thermocouples during Test 27.

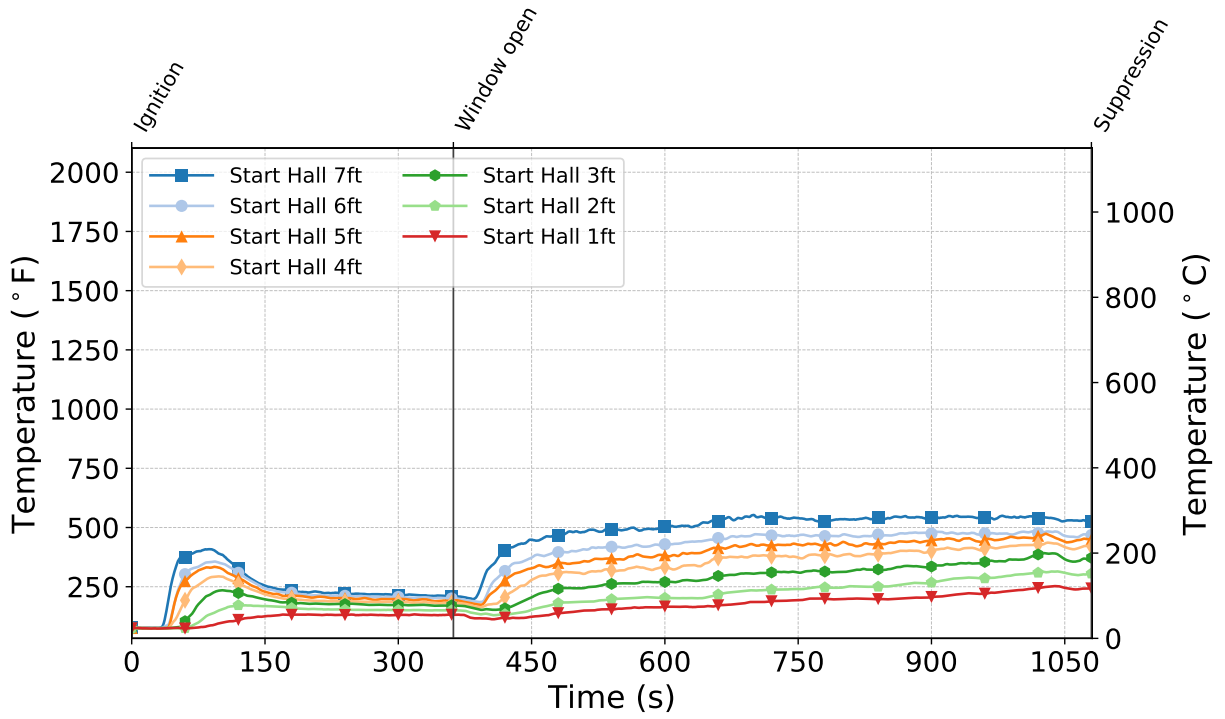


Figure C.291: Temperatures measured by the start hall thermocouples during Test 27.

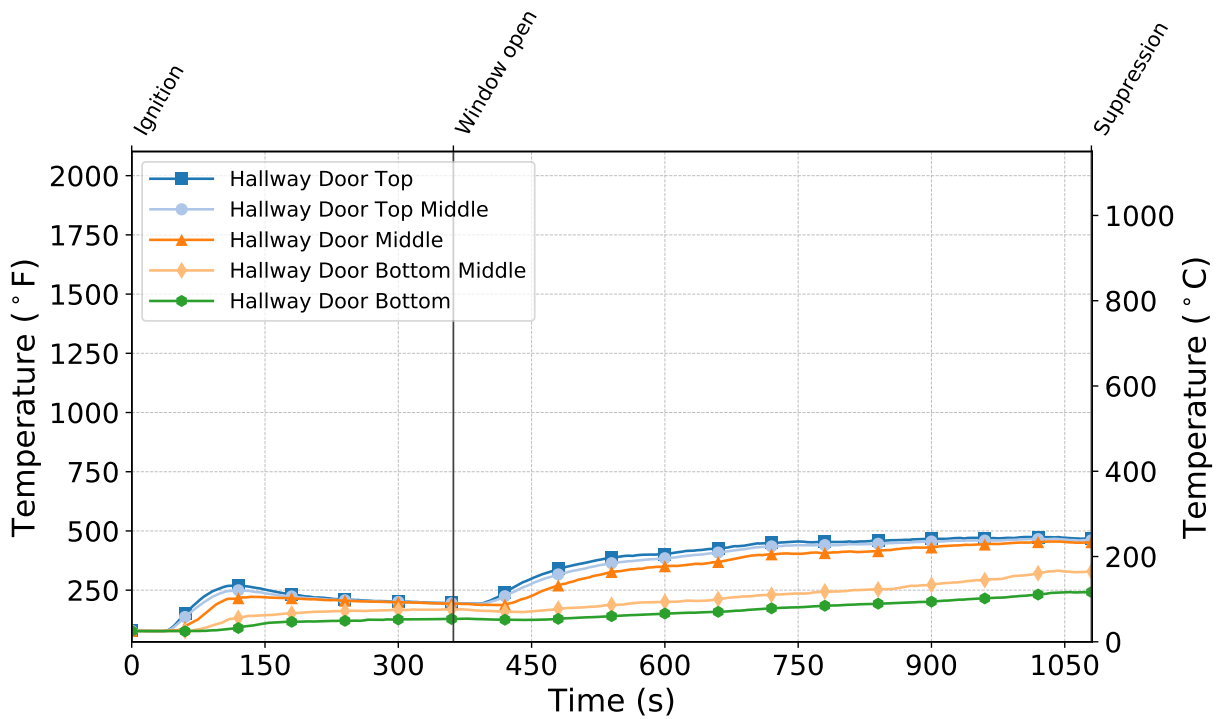


Figure C.292: Temperatures measured by the hallway door thermocouples during Test 27.

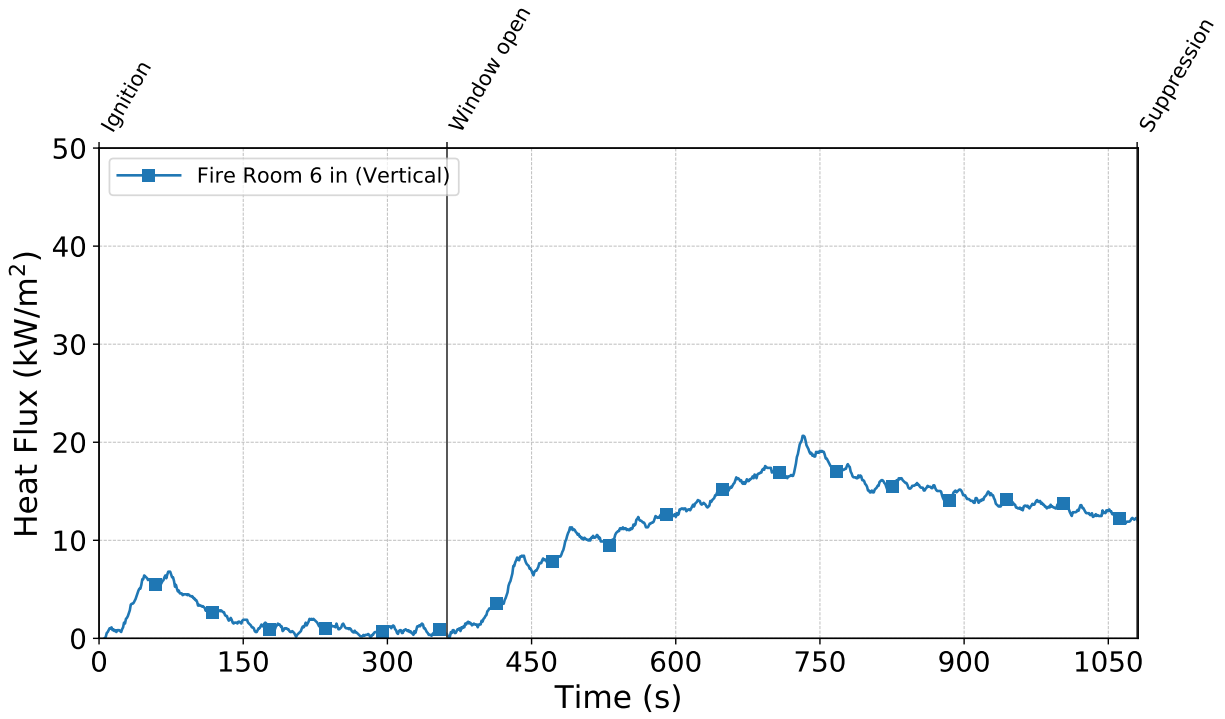


Figure C.293: Heat flux measured by the fire room gauge during Test 27.

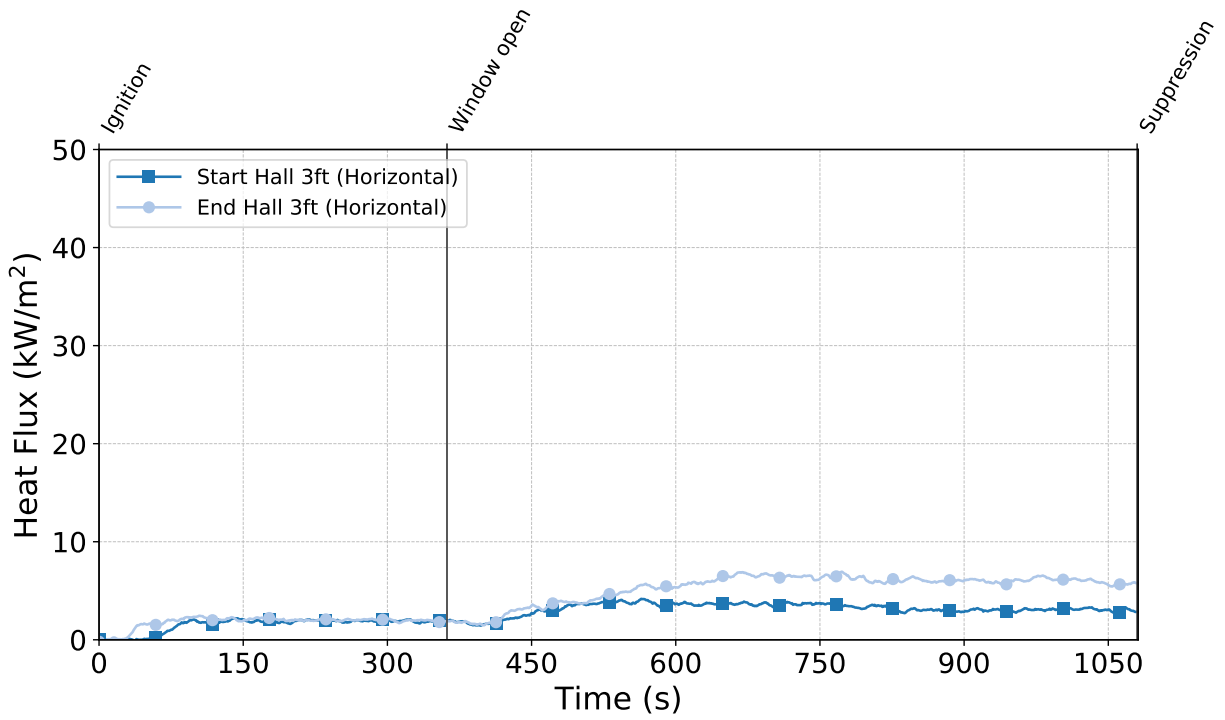


Figure C.294: Heat flux measured by the hallway gauges during Test 27.

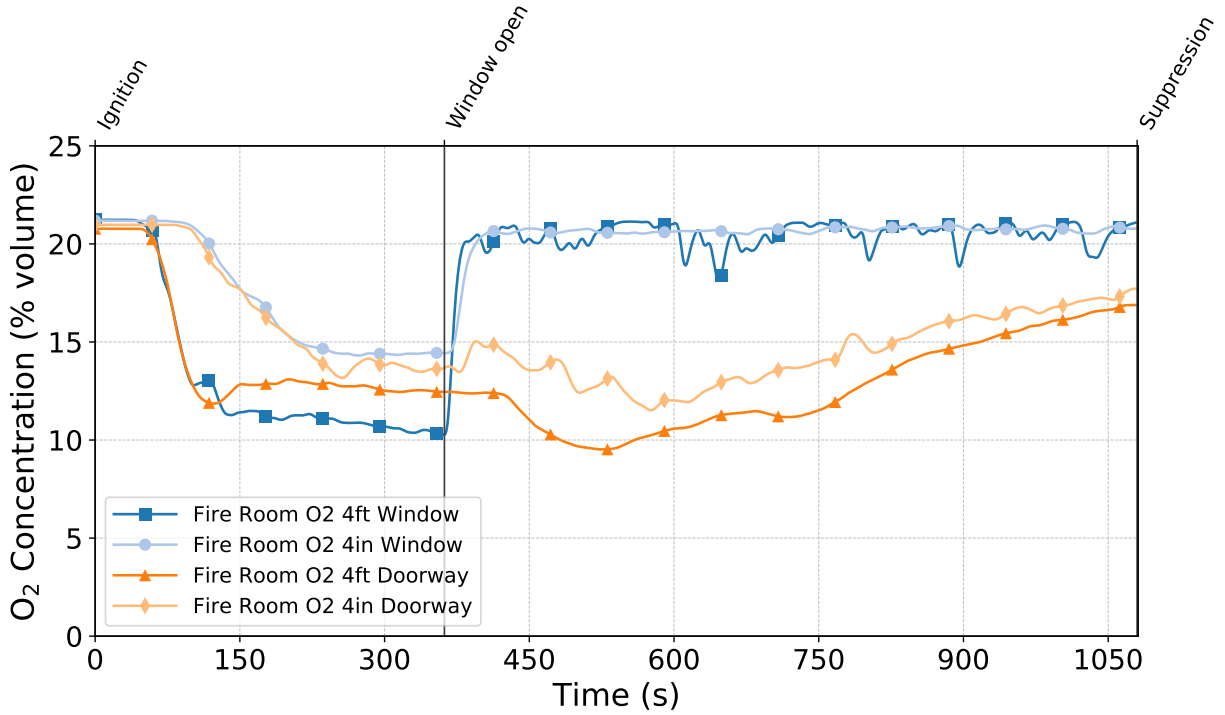


Figure C.295: Oxygen concentrations measured by the fire room gas sampling probes during Test 27.

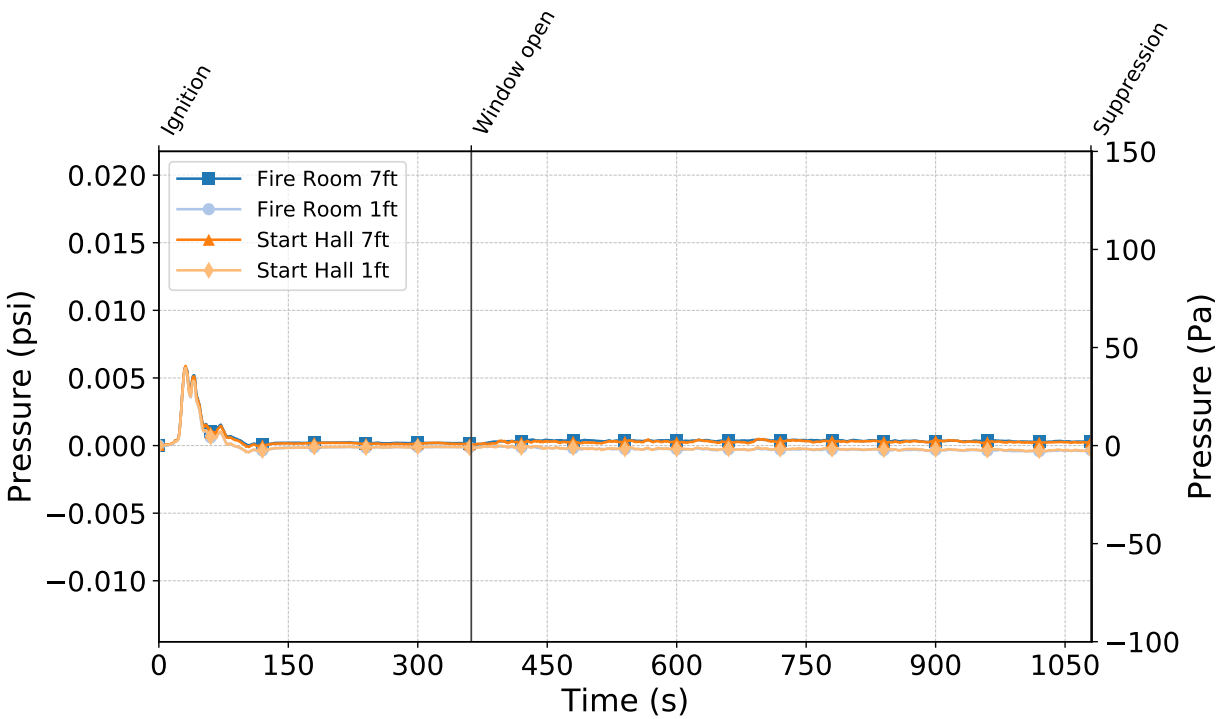


Figure C.296: Pressures measured by the fire room and hallway probes during Test 27.

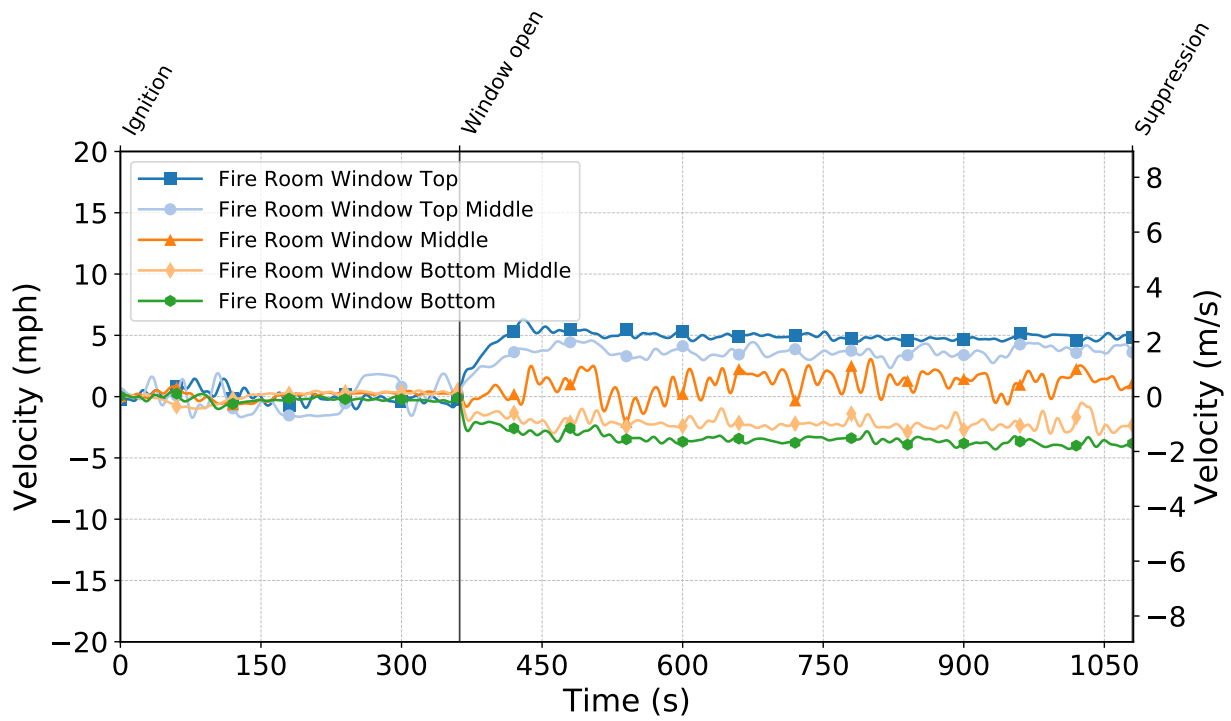


Figure C.297: Gas velocities measured by the fire room window bdps during Test 27.

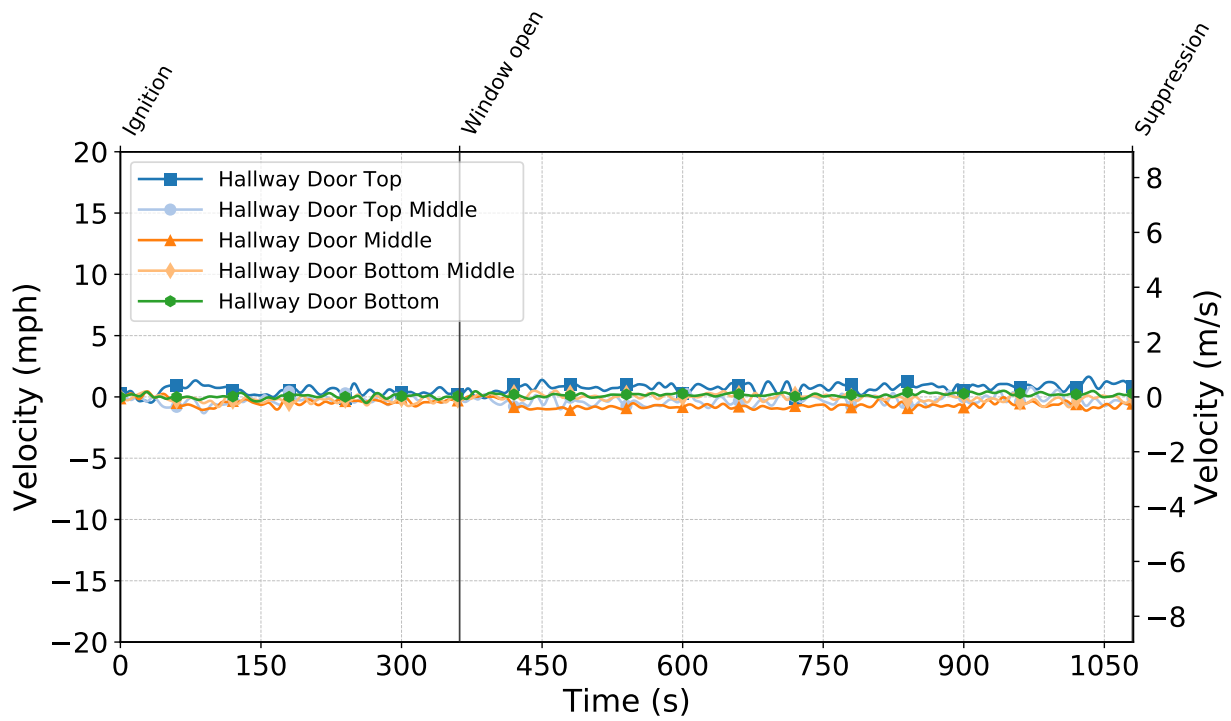


Figure C.298: Gas velocities measured by the hallway door bdps during Test 27.

Test 28

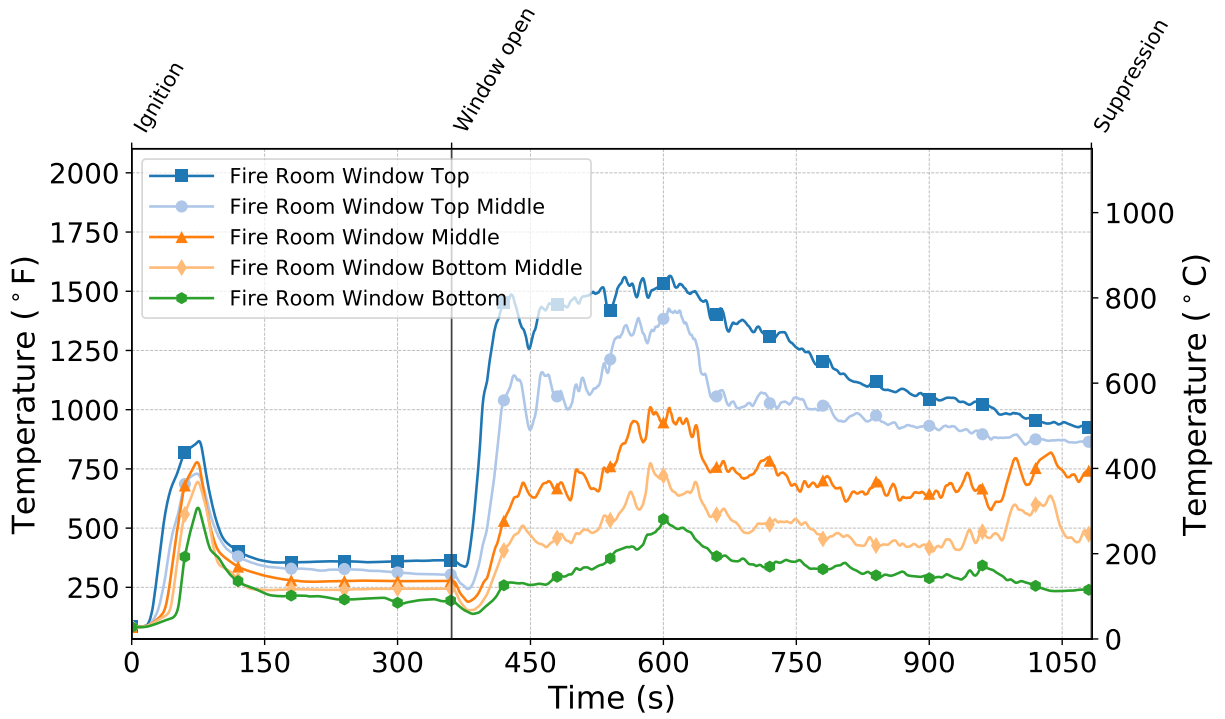


Figure C.299: Temperatures measured by the fire room window thermocouples during Test 28.

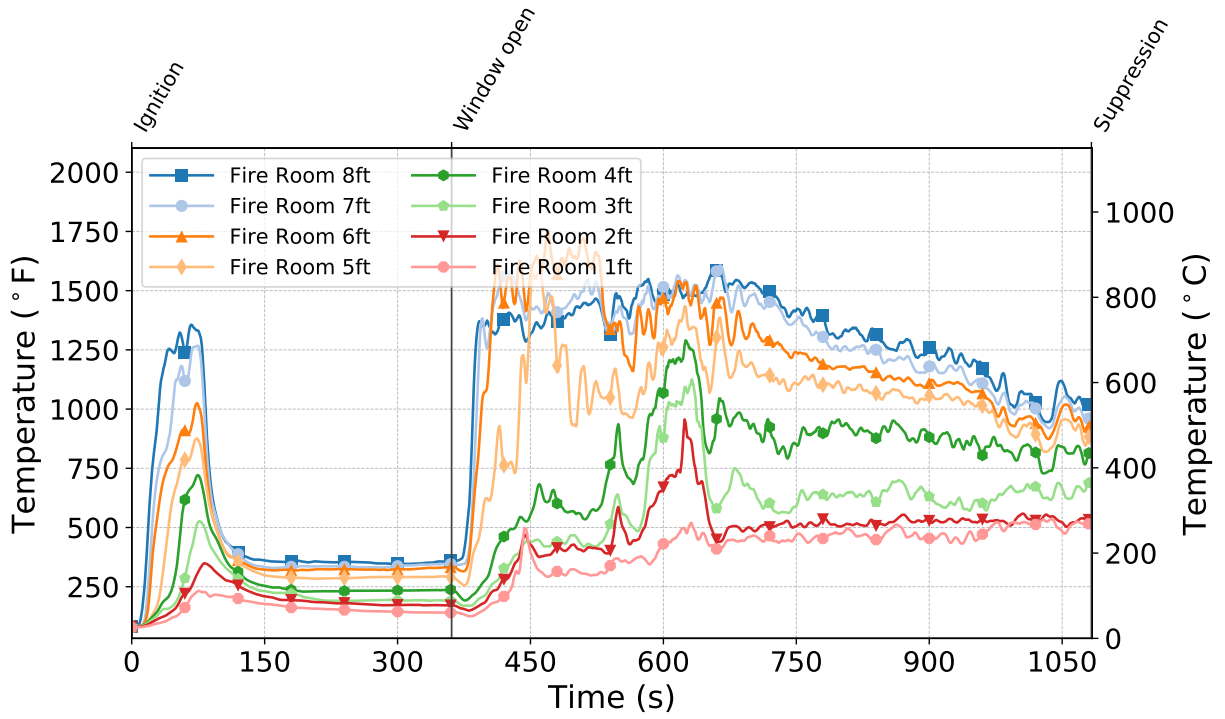


Figure C.300: Temperatures measured by the fire room thermocouples during Test 28.

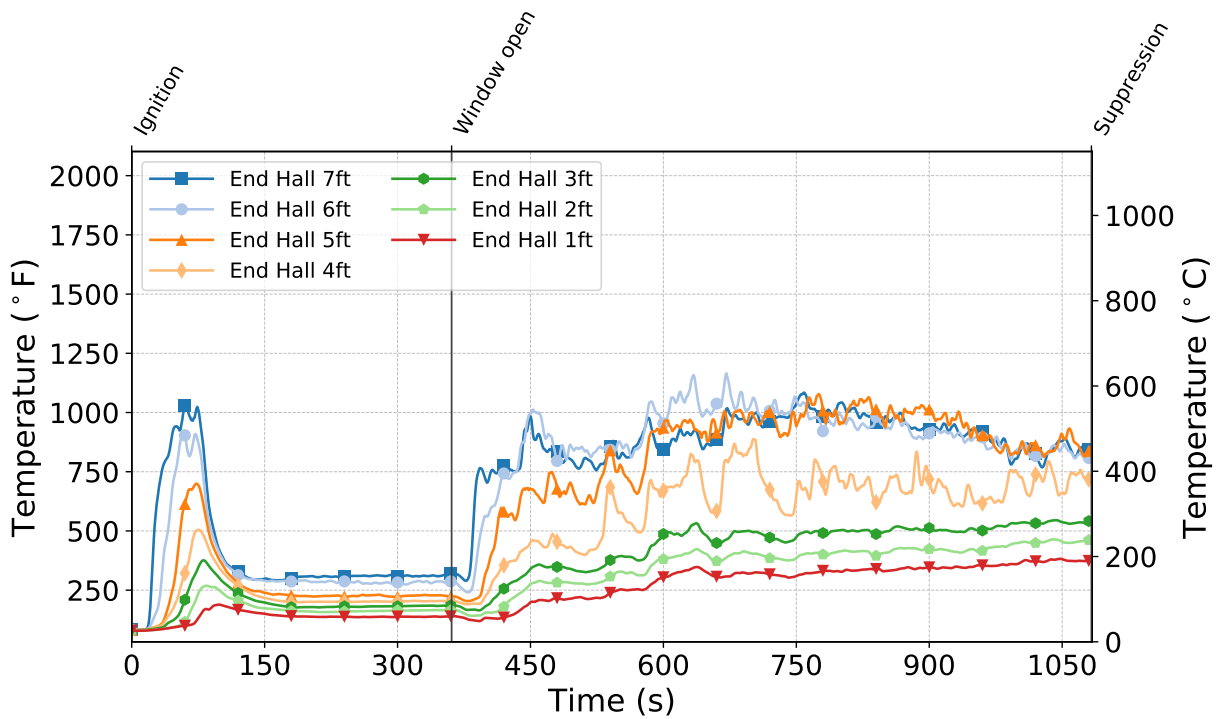


Figure C.301: Temperatures measured by the end hall thermocouples during Test 28.

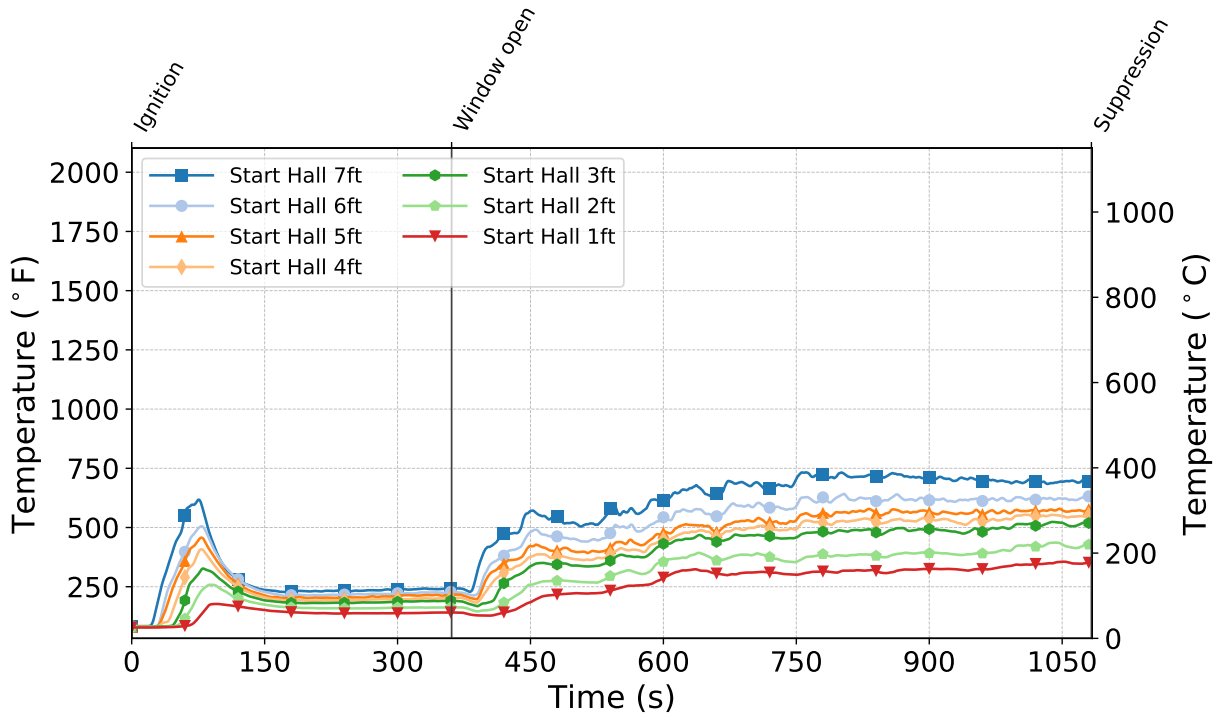


Figure C.302: Temperatures measured by the start hall thermocouples during Test 28.

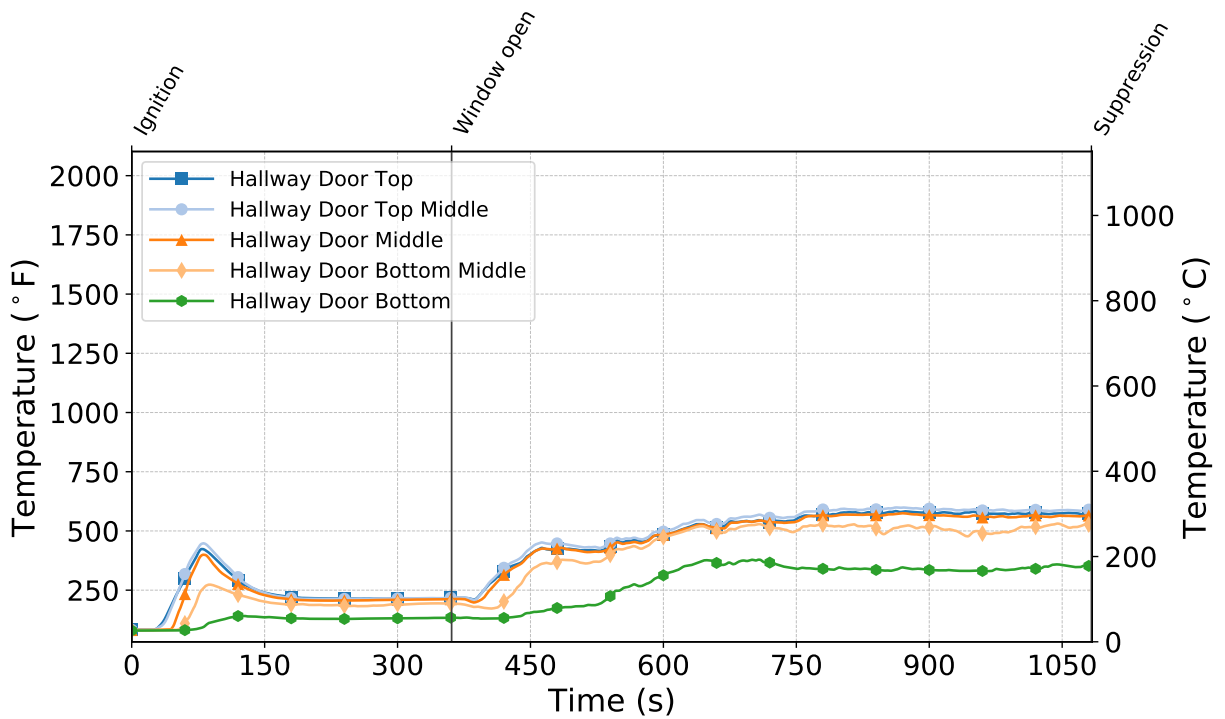


Figure C.303: Temperatures measured by the hallway door thermocouples during Test 28.

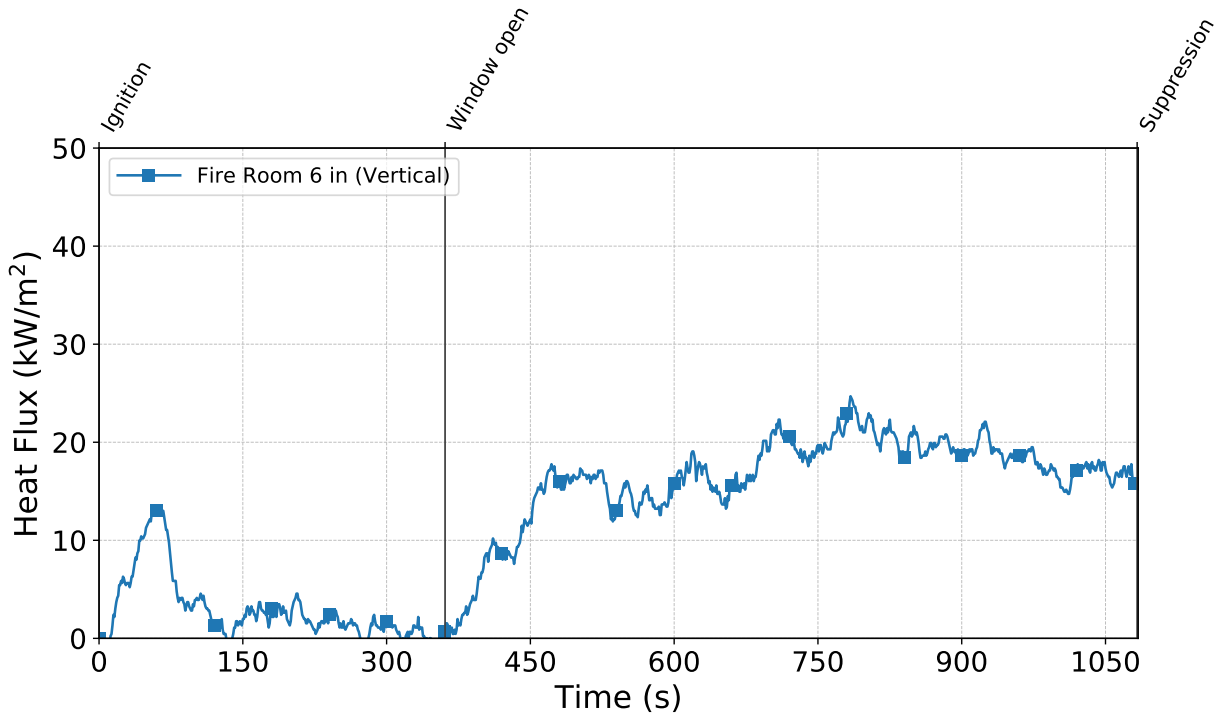


Figure C.304: Heat flux measured by the fire room gauge during Test 28.

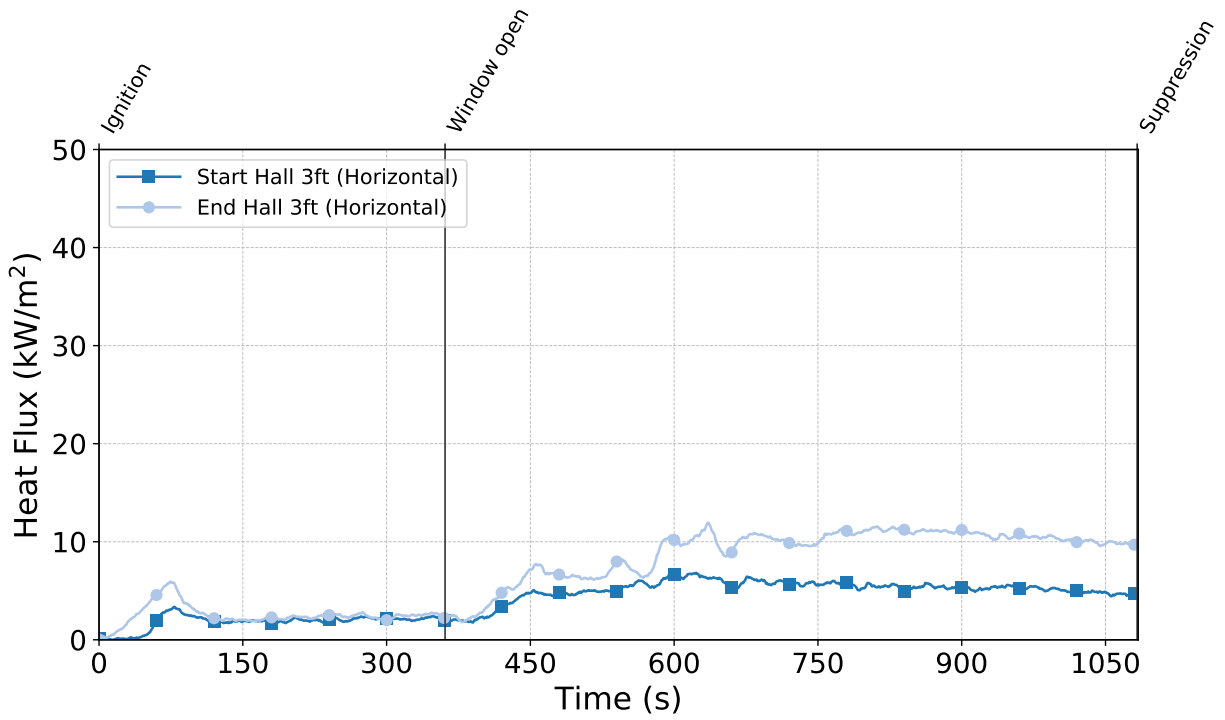


Figure C.305: Heat flux measured by the hallway gauges during Test 28.

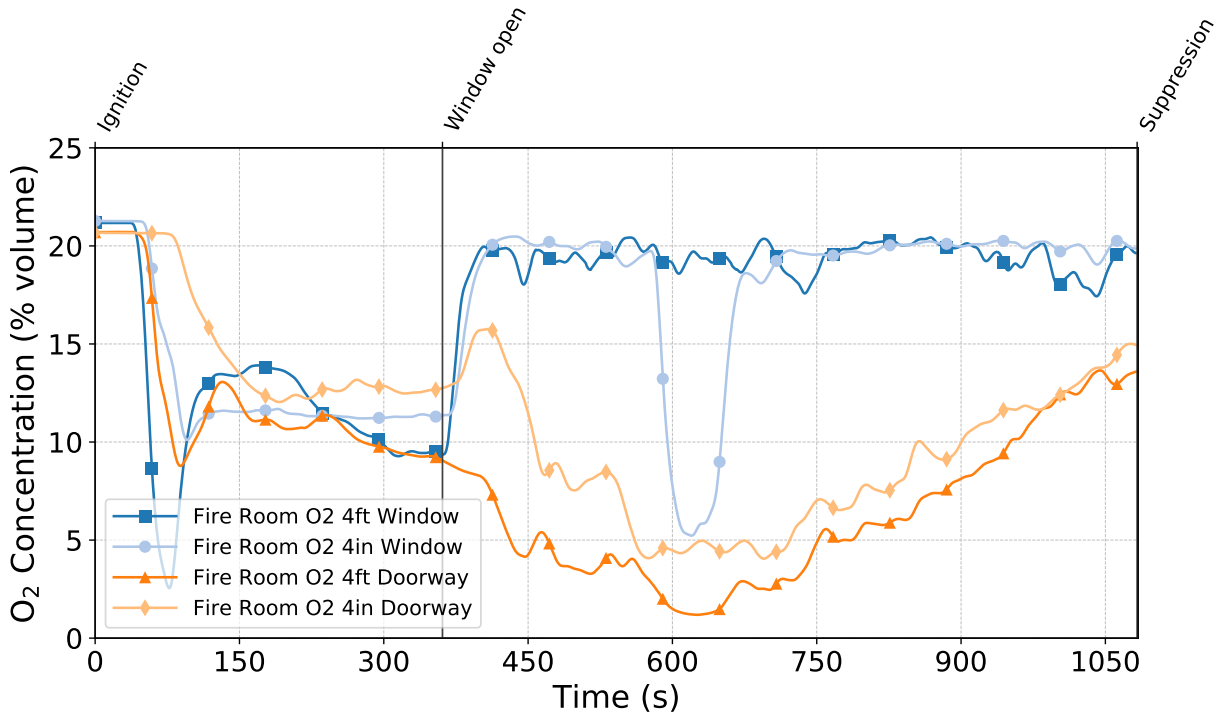


Figure C.306: Oxygen concentrations measured by the fire room gas sampling probes during Test 28.

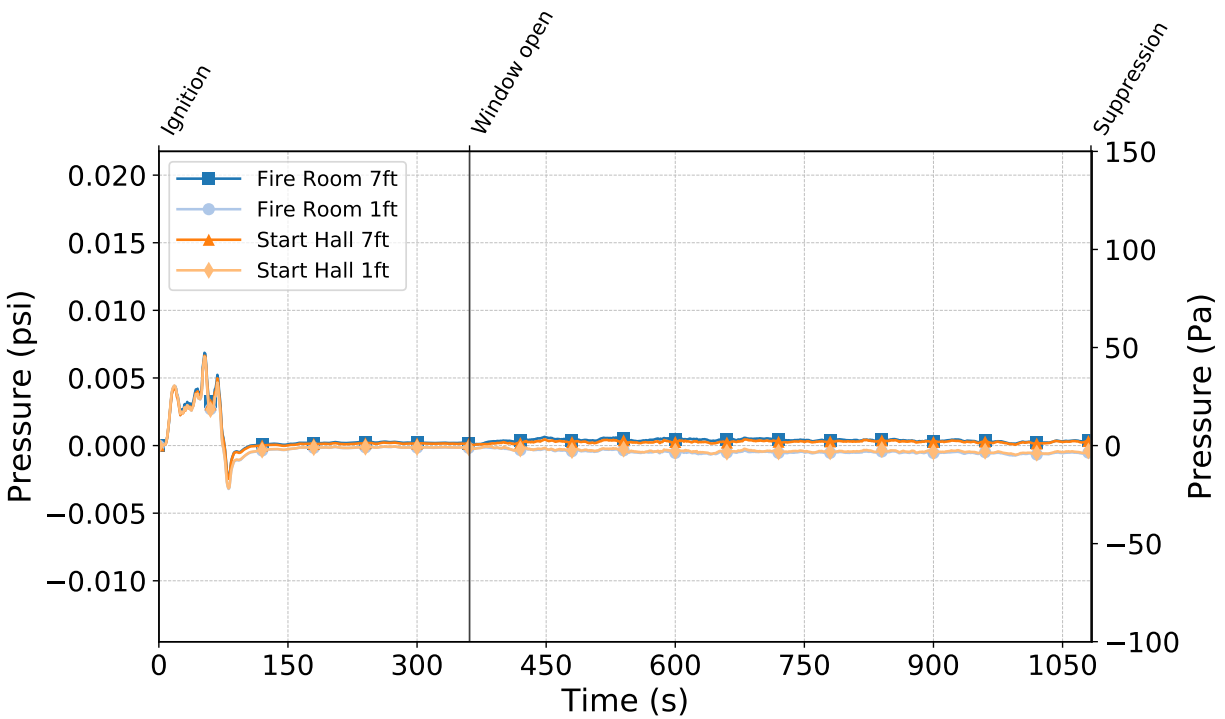


Figure C.307: Pressures measured by the fire room and hallway probes during Test 28.

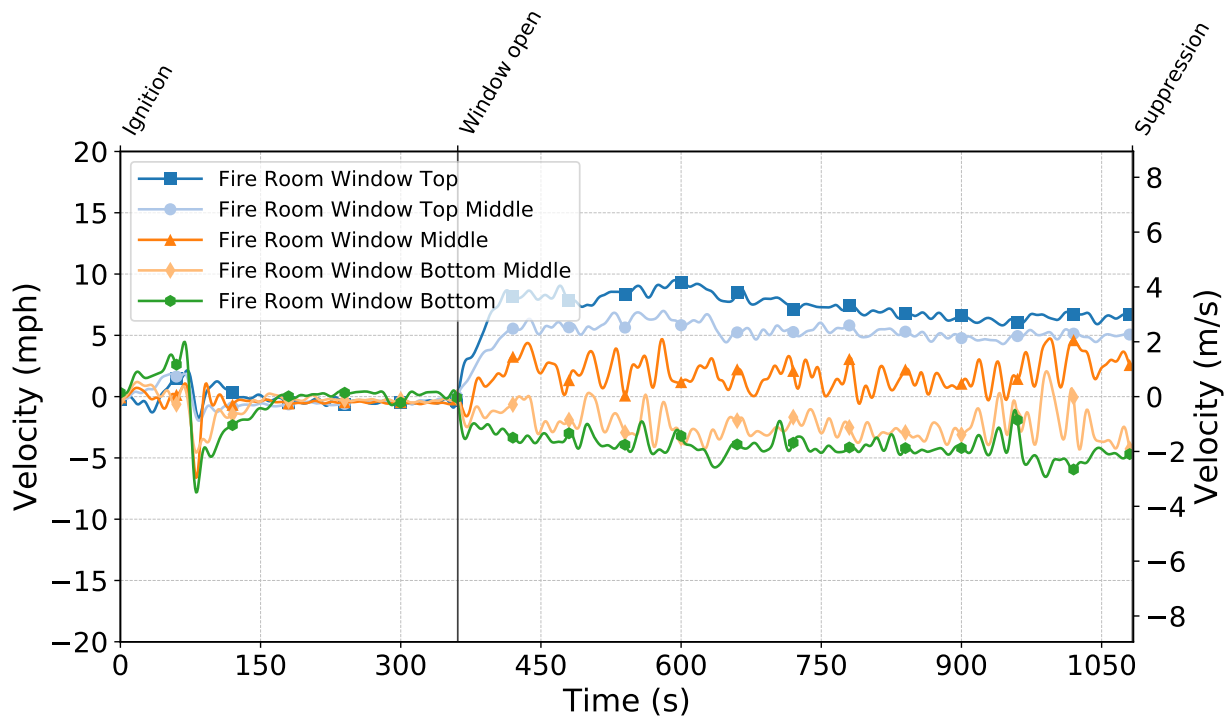


Figure C.308: Gas velocities measured by the fire room window bdps during Test 28.

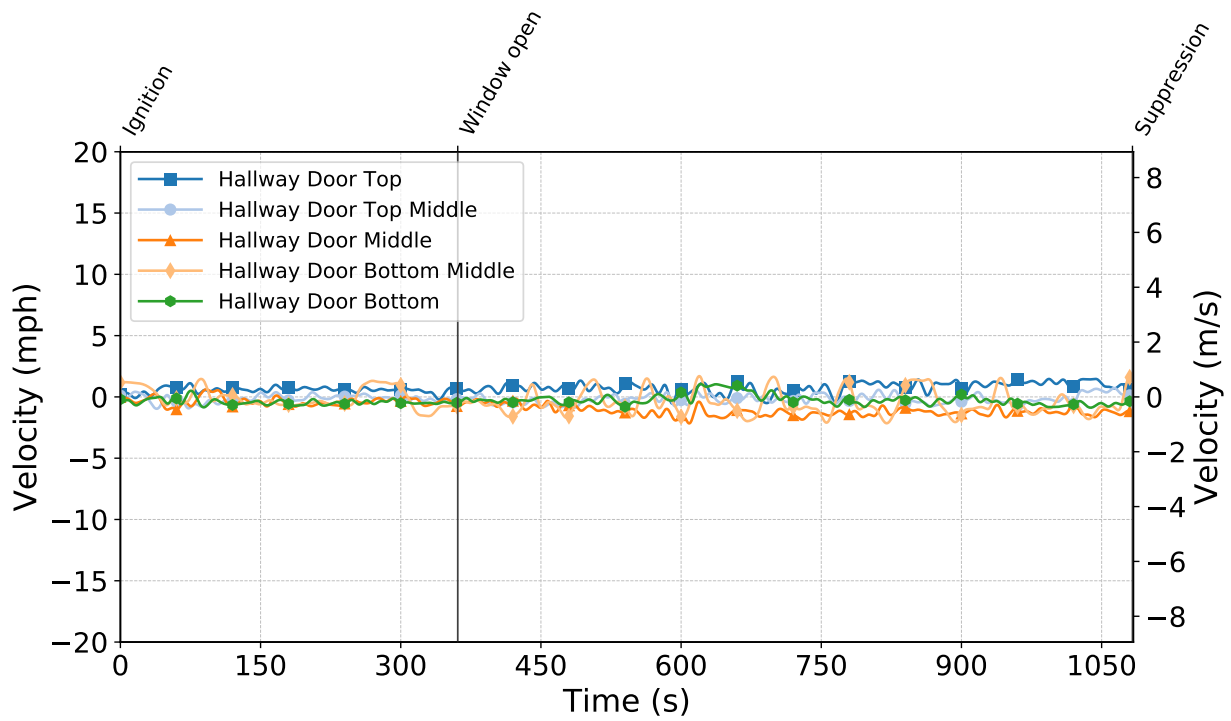


Figure C.309: Gas velocities measured by the hallway door bdps during Test 28.

Test 29

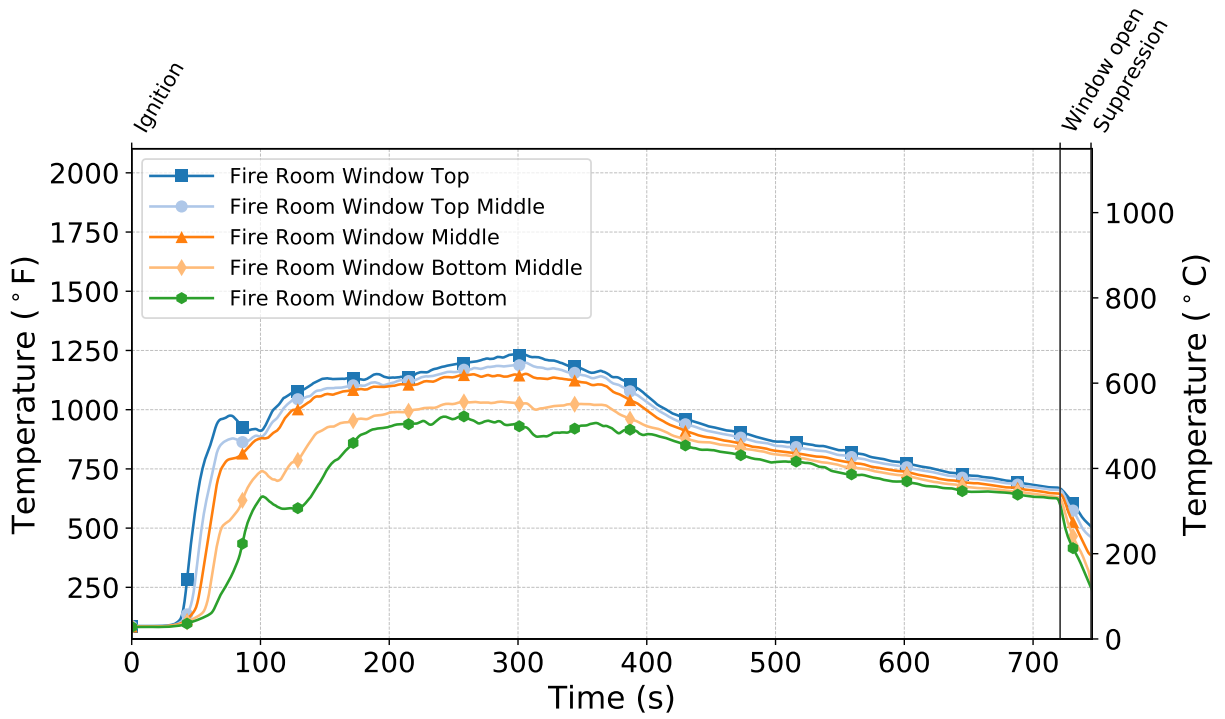


Figure C.310: Temperatures measured by the fire room window thermocouples during Test 29.

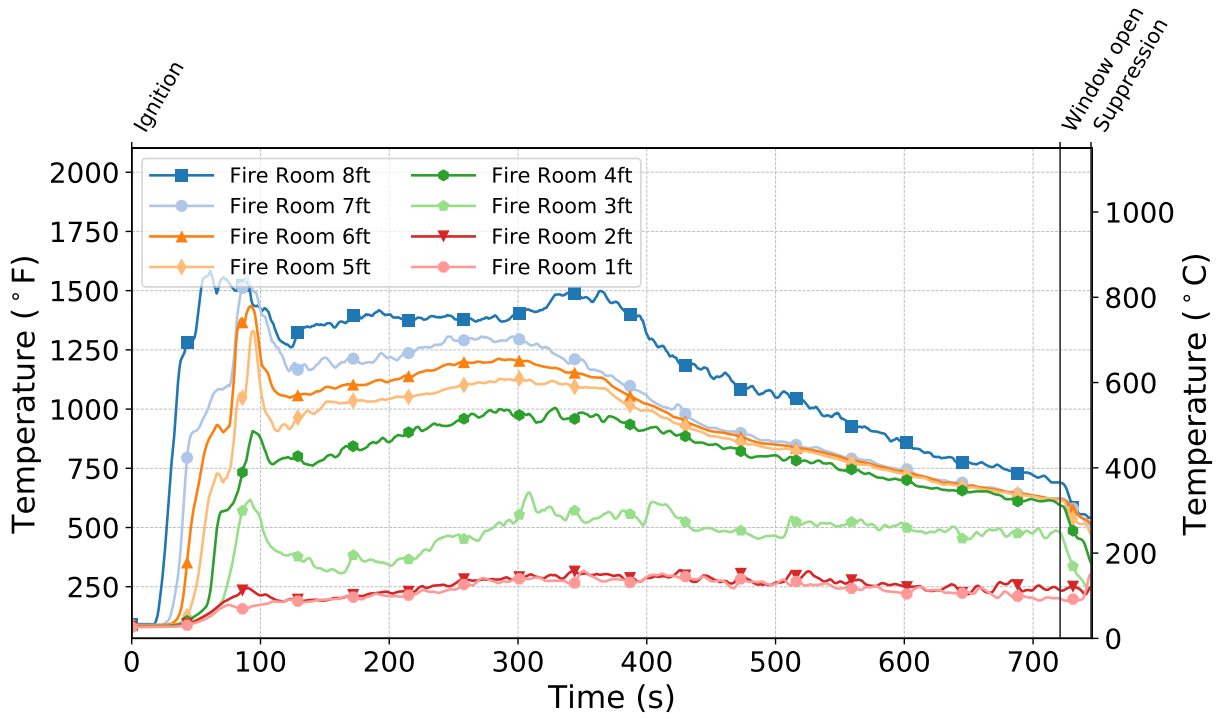


Figure C.311: Temperatures measured by the fire room thermocouples during Test 29.

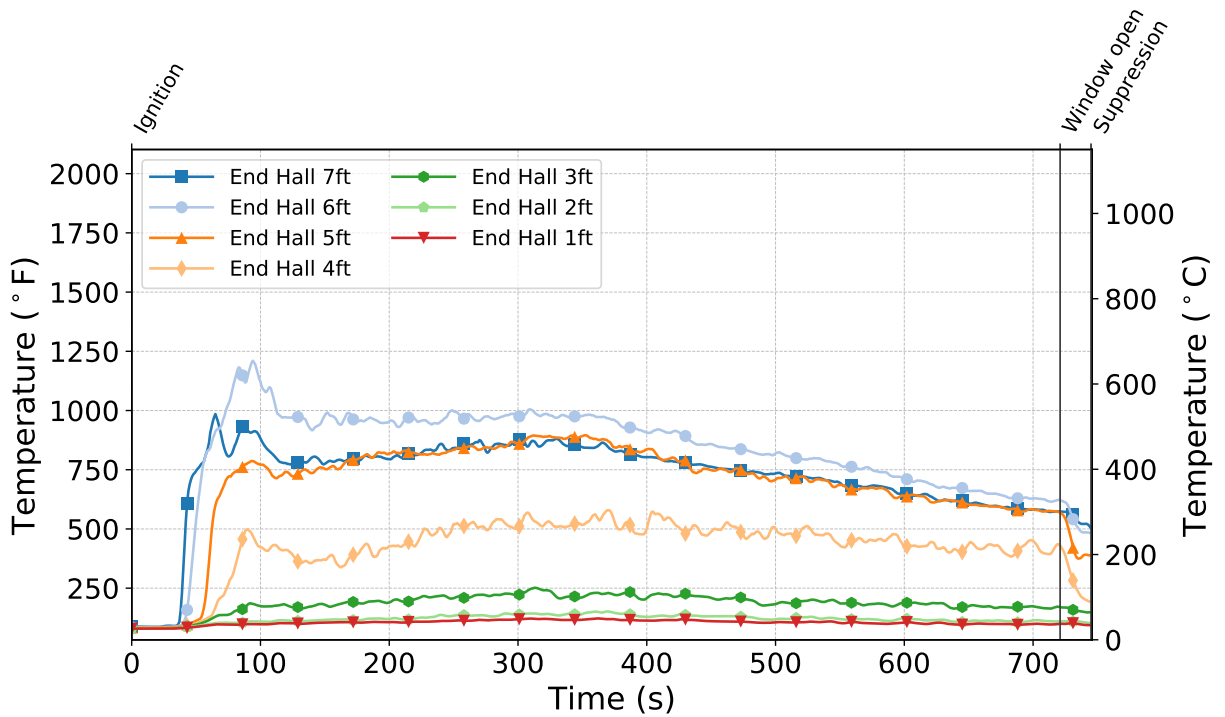


Figure C.312: Temperatures measured by the end hall thermocouples during Test 29.

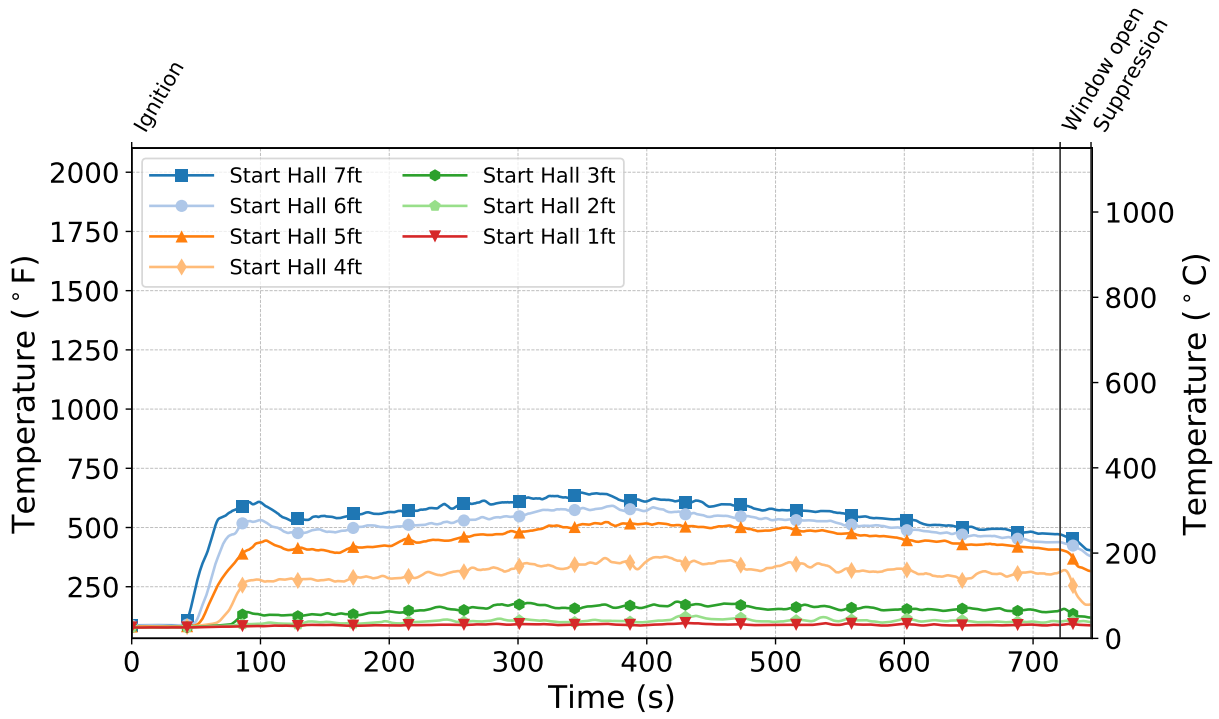


Figure C.313: Temperatures measured by the start hall thermocouples during Test 29.

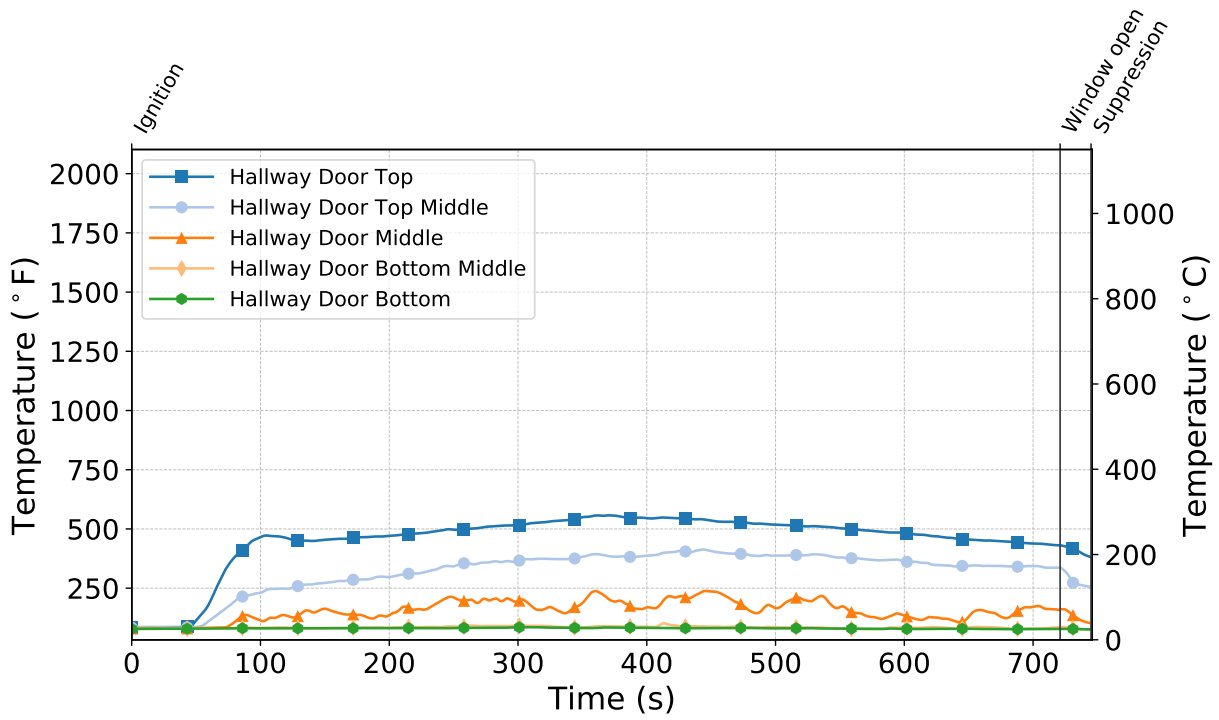


Figure C.314: Temperatures measured by the hallway door thermocouples during Test 29.

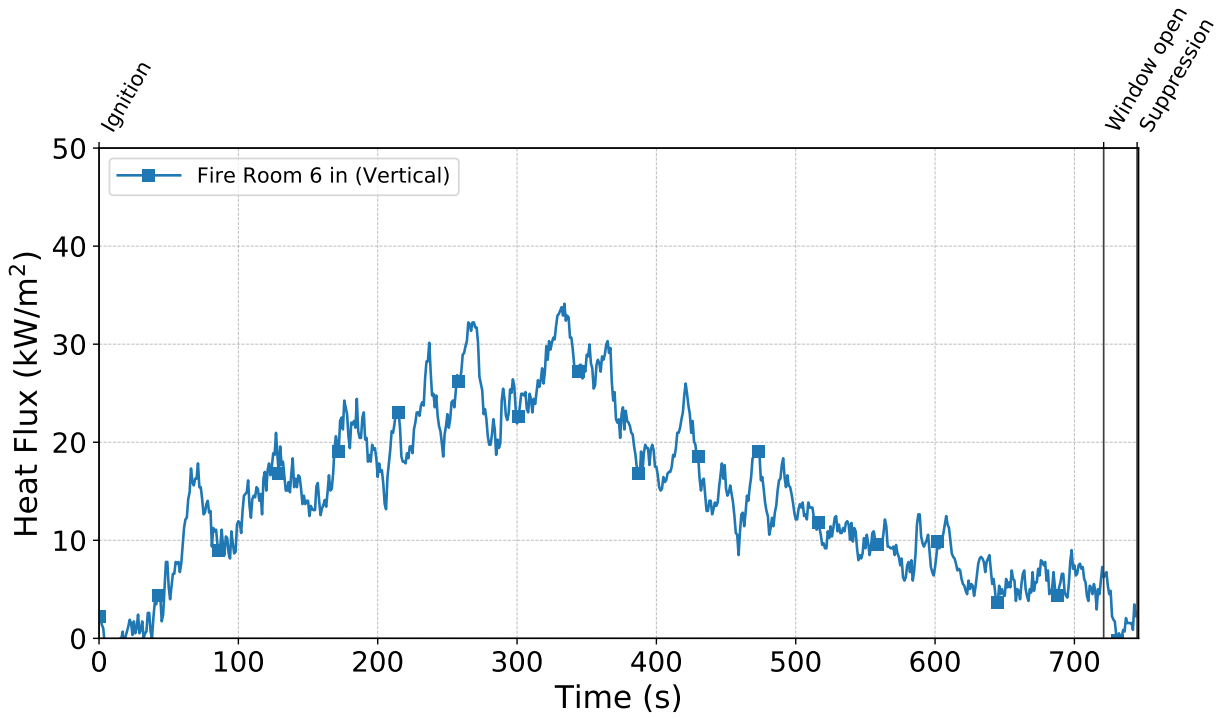


Figure C.315: Heat flux measured by the fire room gauge during Test 29.

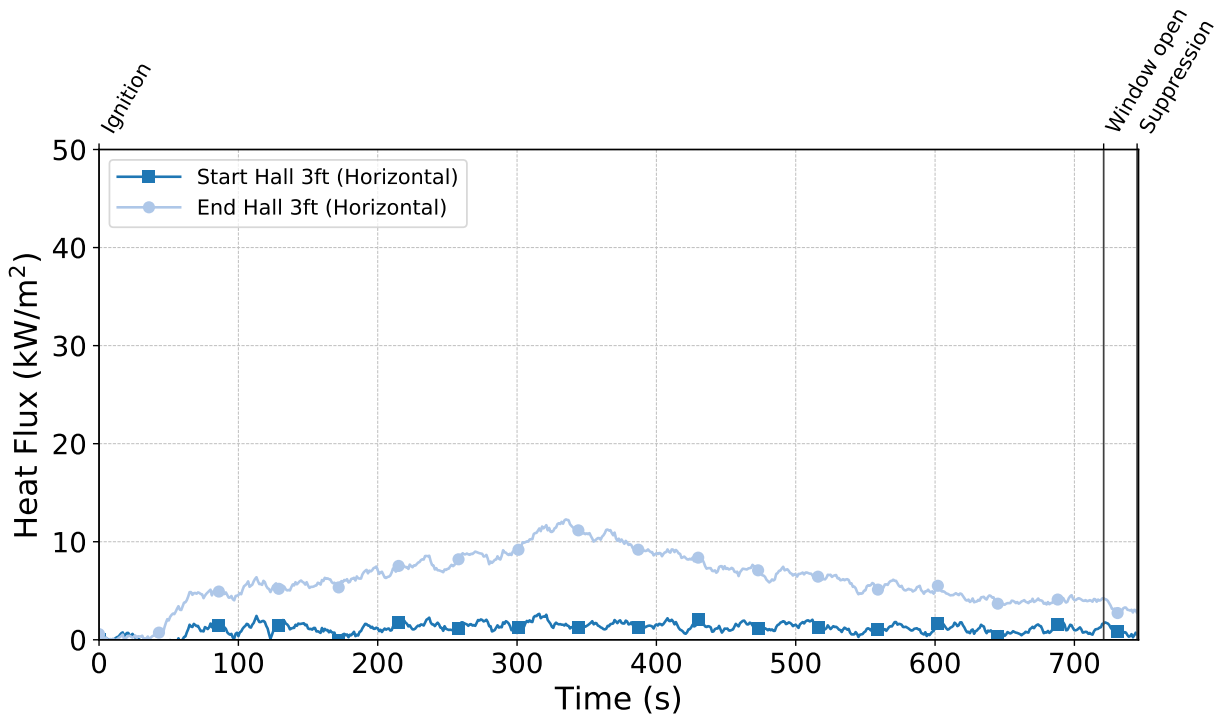


Figure C.316: Heat flux measured by the hallway gauges during Test 29.

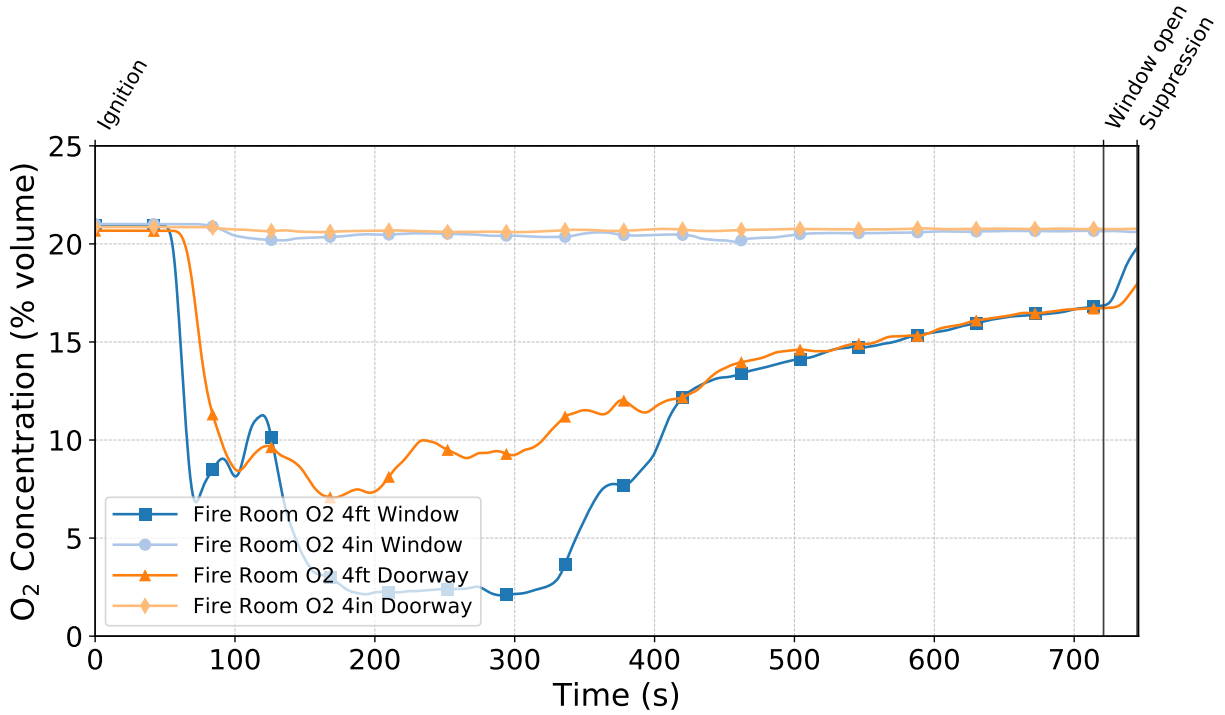


Figure C.317: Oxygen concentrations measured by the fire room gas sampling probes during Test 29.

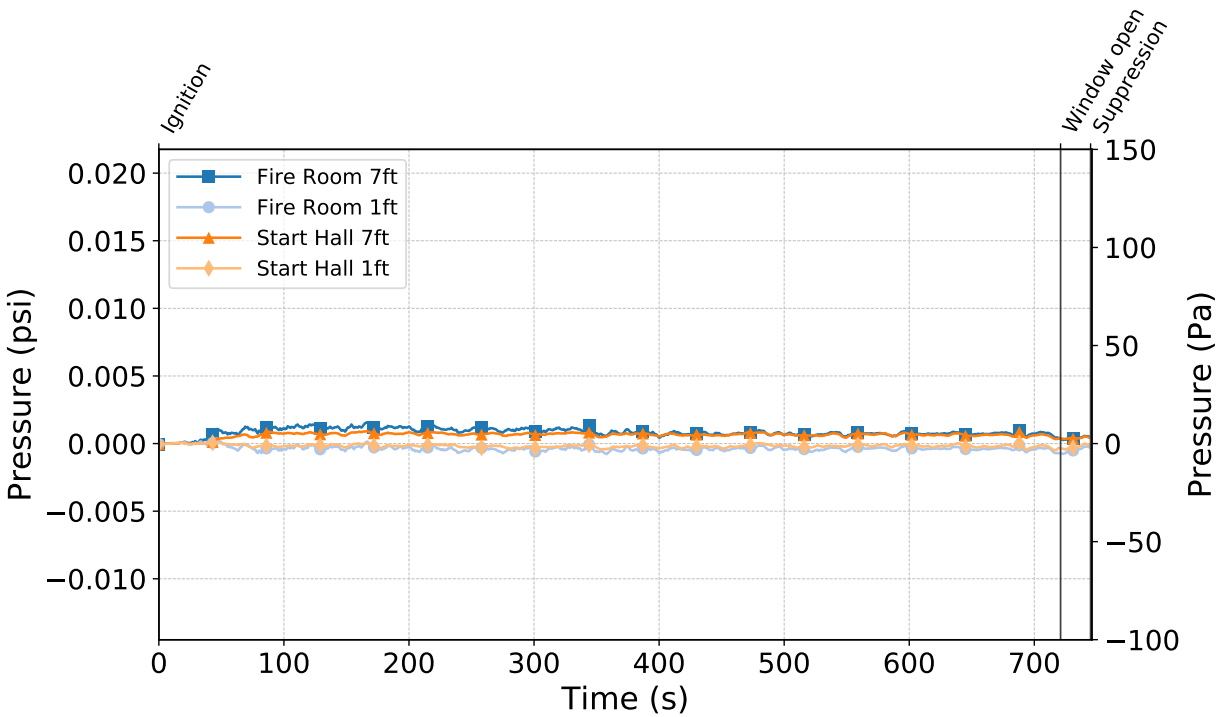


Figure C.318: Pressures measured by the fire room and hallway probes during Test 29.

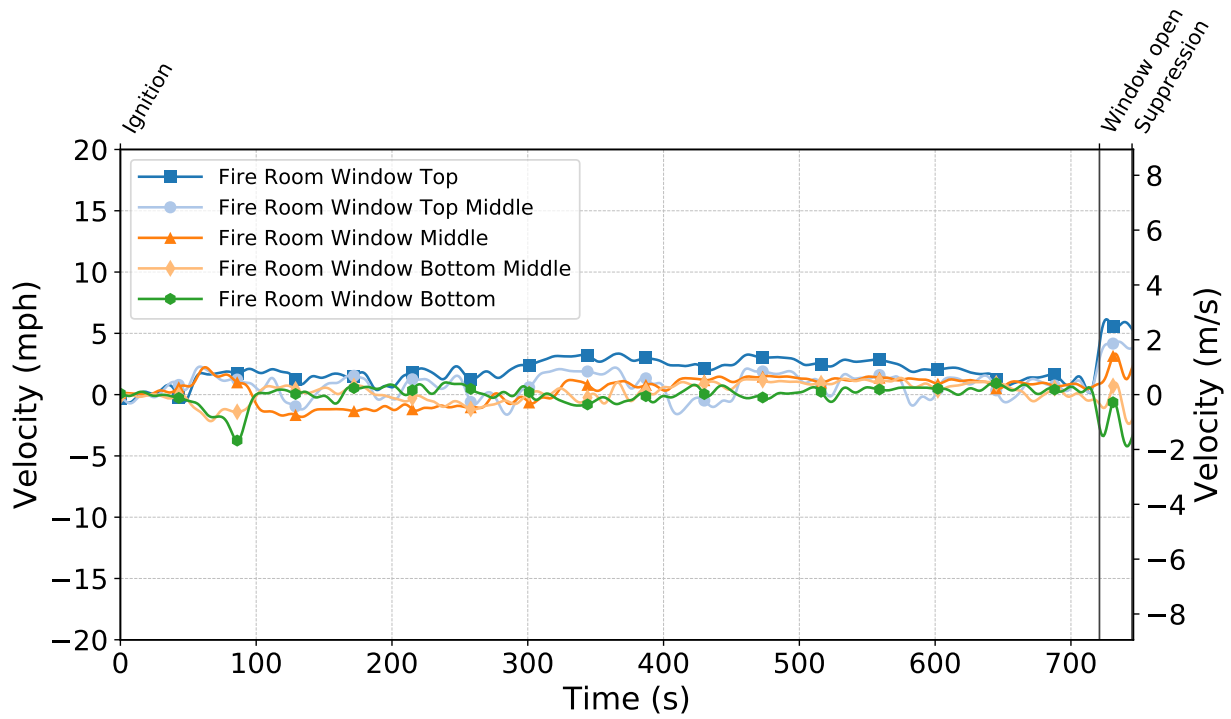


Figure C.319: Gas velocities measured by the fire room window bdps during Test 29.

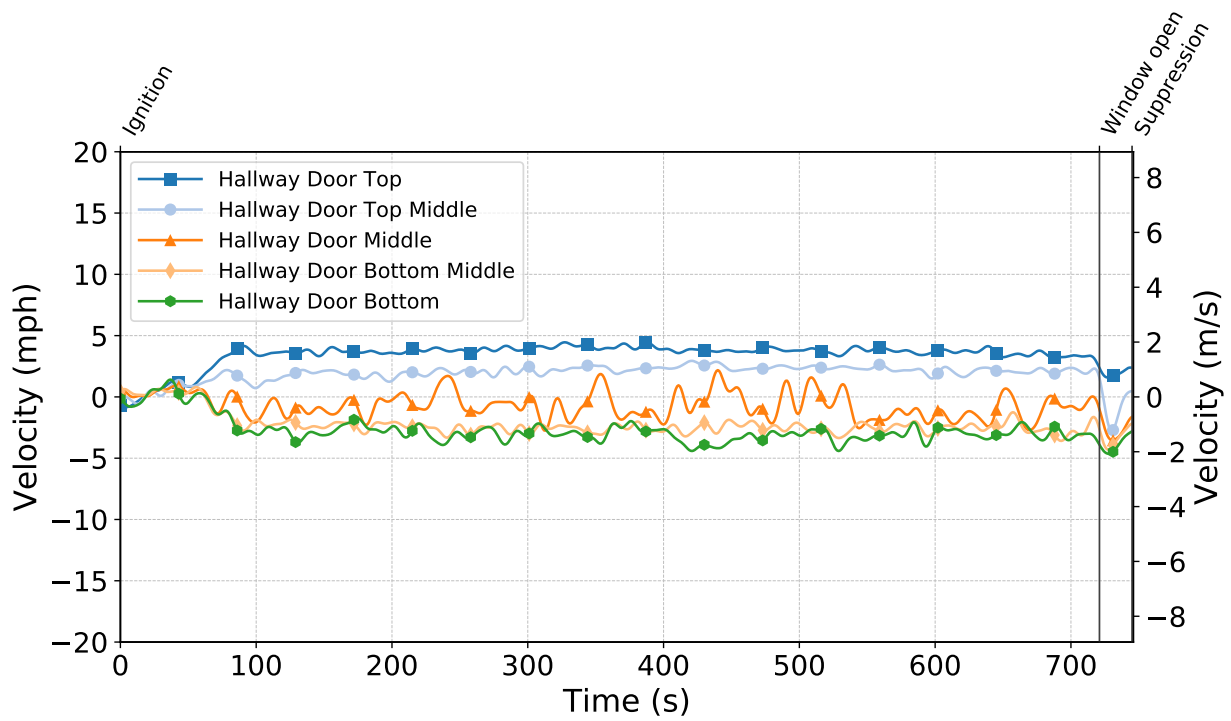


Figure C.320: Gas velocities measured by the hallway door bdps during Test 29.

Test 30

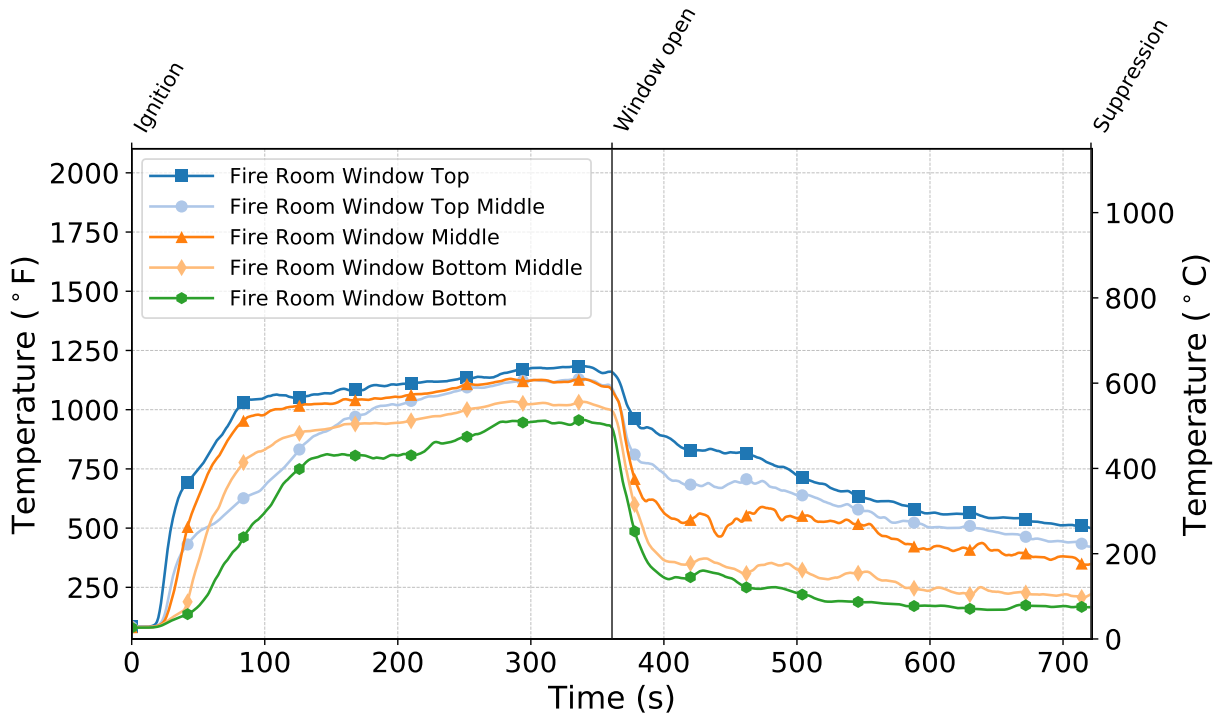


Figure C.321: Temperatures measured by the fire room window thermocouples during Test 30.

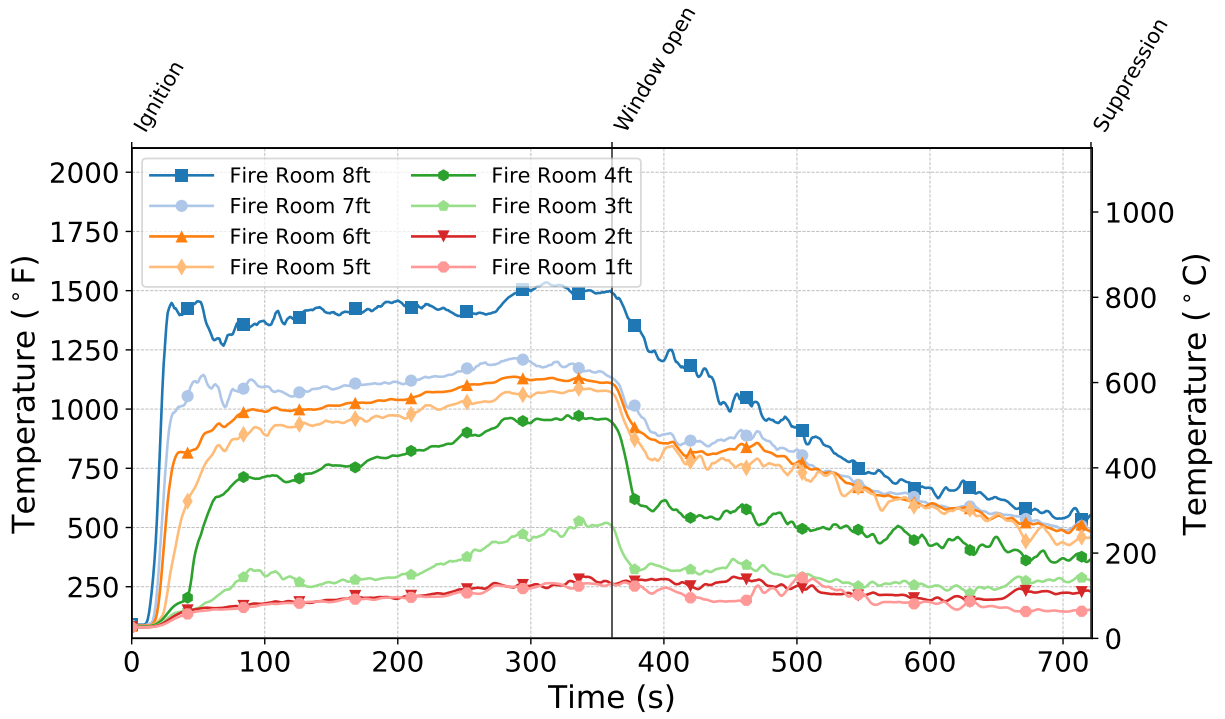


Figure C.322: Temperatures measured by the fire room thermocouples during Test 30.

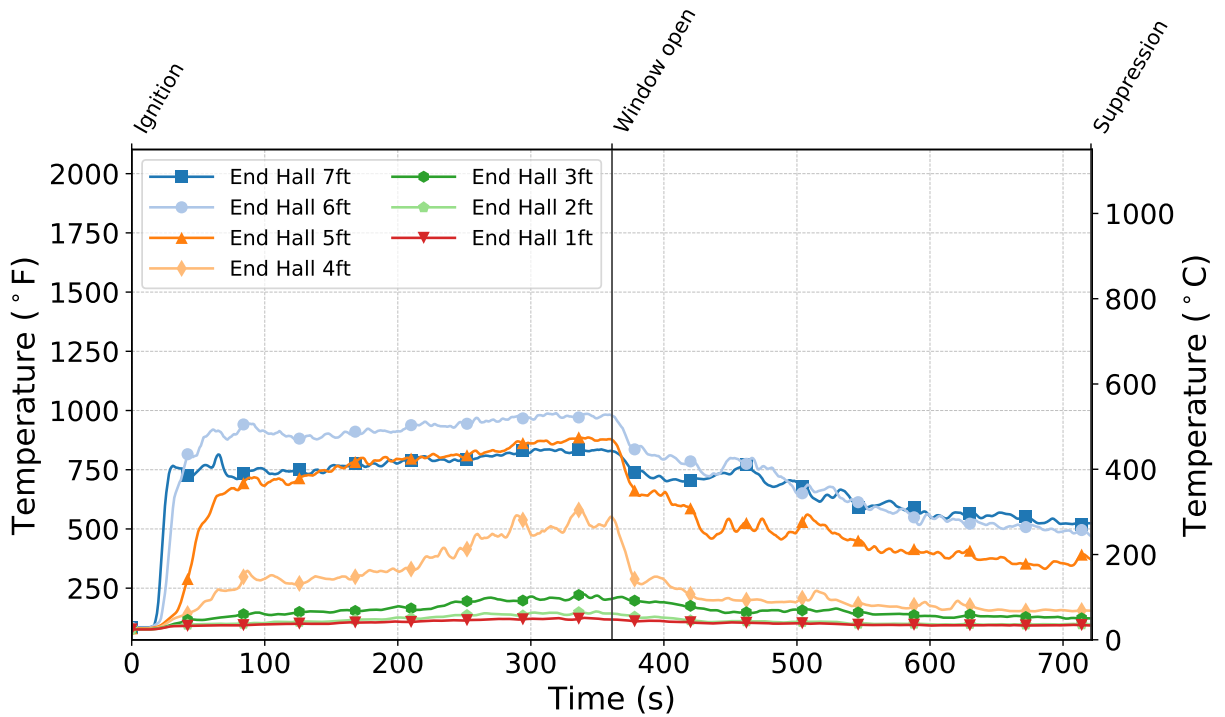


Figure C.323: Temperatures measured by the end hall thermocouples during Test 30.

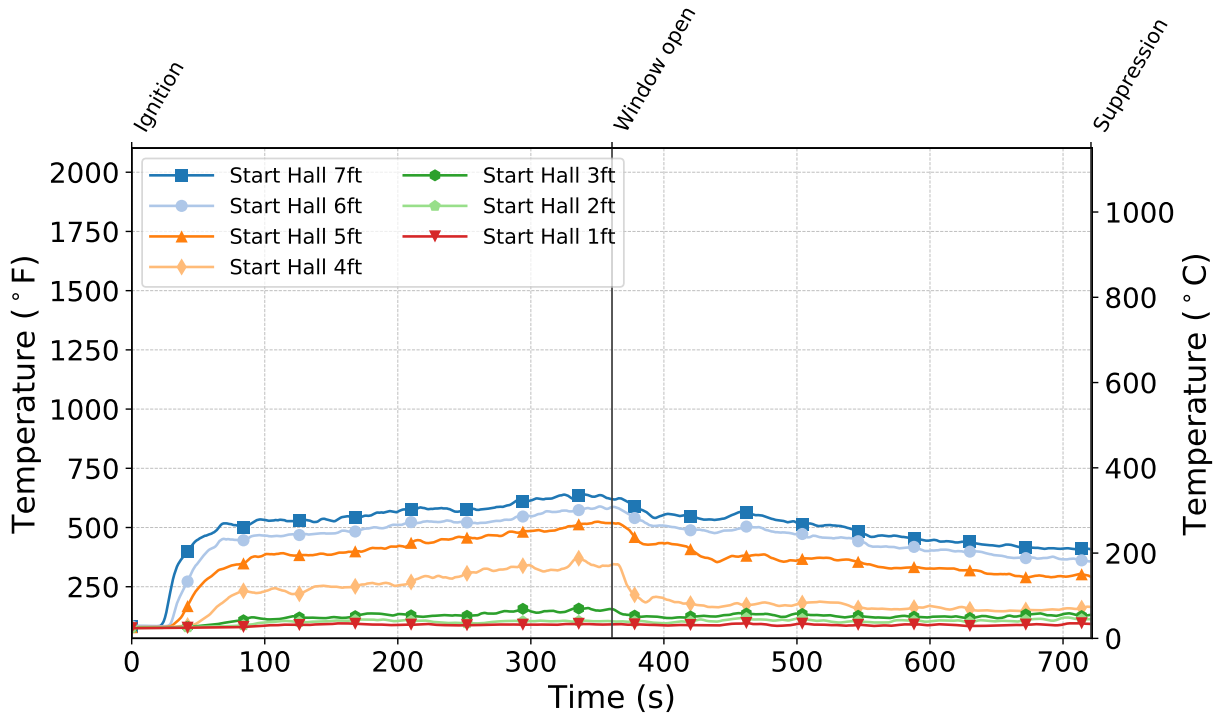


Figure C.324: Temperatures measured by the start hall thermocouples during Test 30.

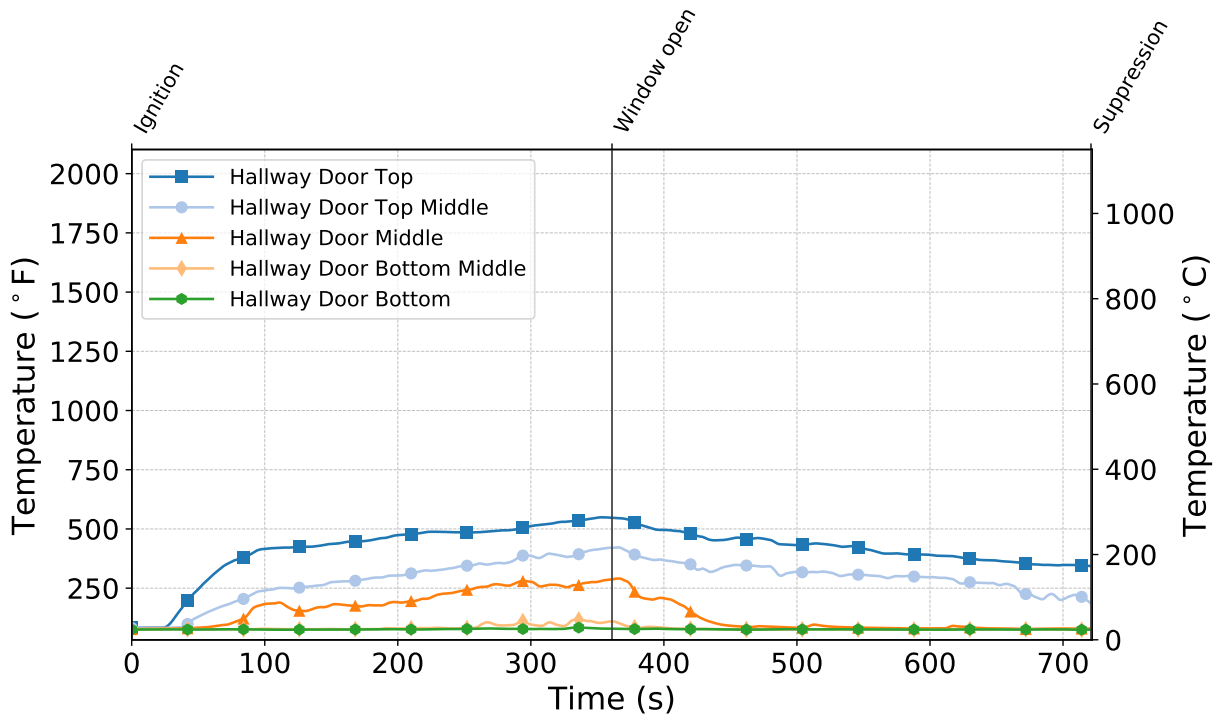


Figure C.325: Temperatures measured by the hallway door thermocouples during Test 30.

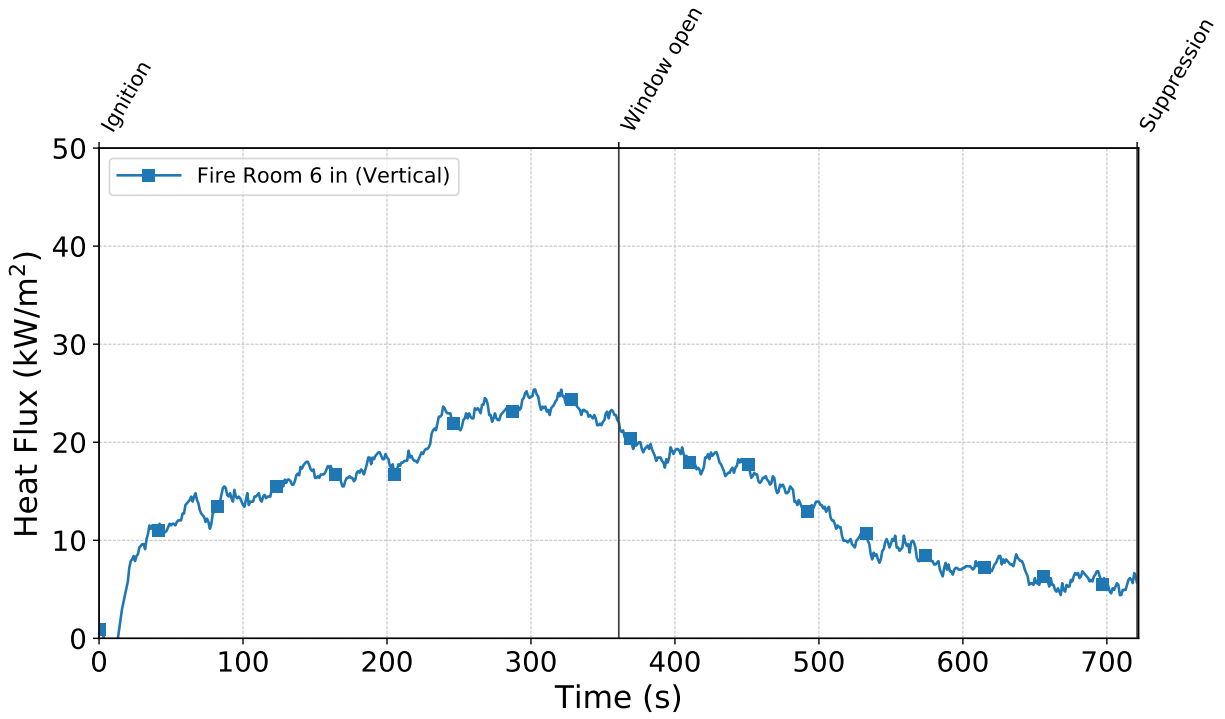


Figure C.326: Heat flux measured by the fire room gauge during Test 30.

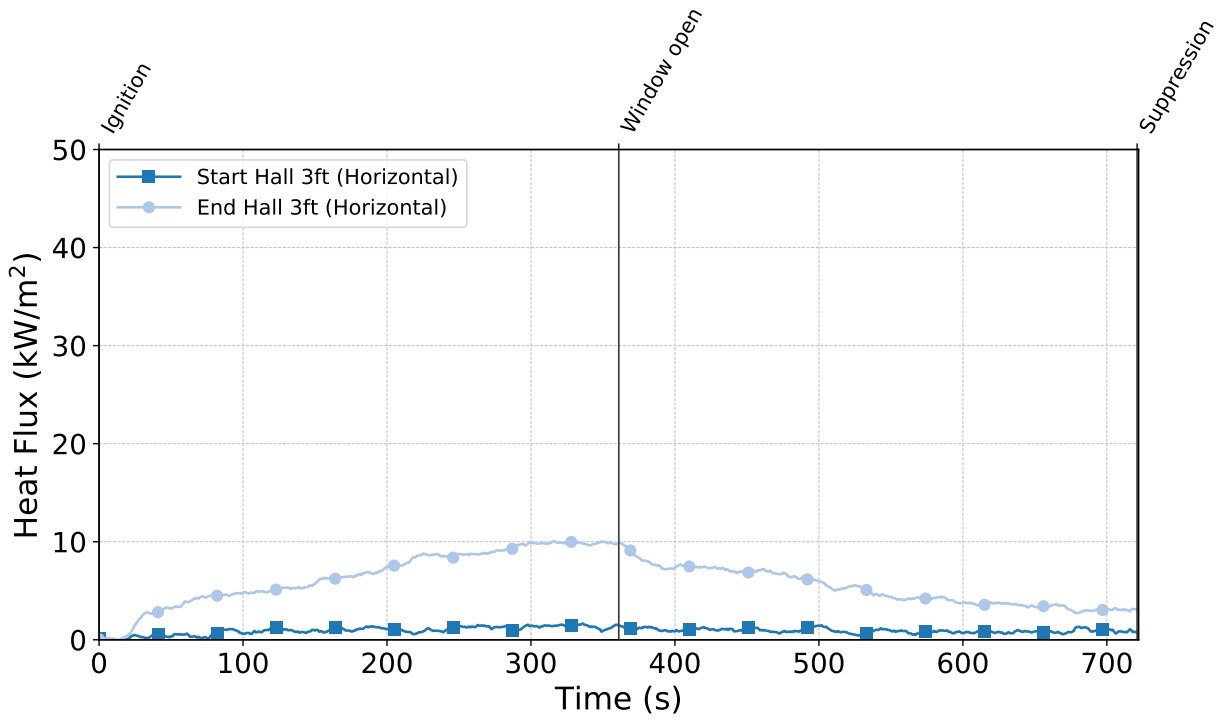


Figure C.327: Heat flux measured by the hallway gauges during Test 30.

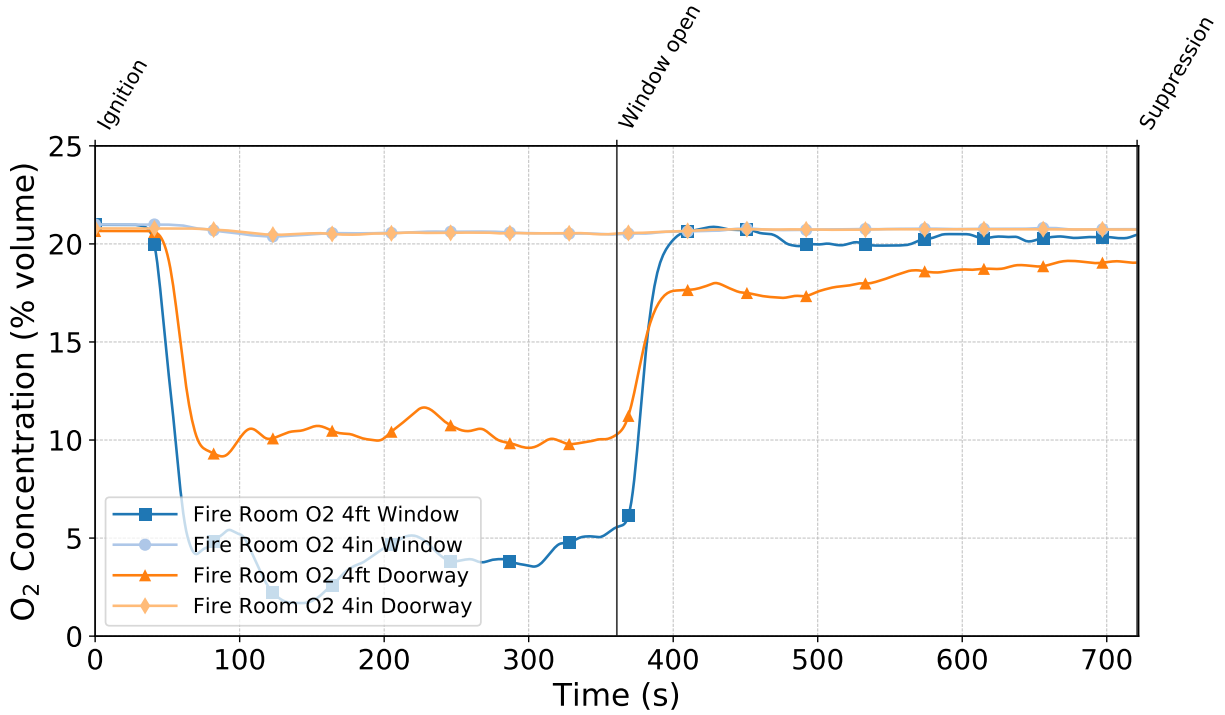


Figure C.328: Oxygen concentrations measured by the fire room gas sampling probes during Test 30.

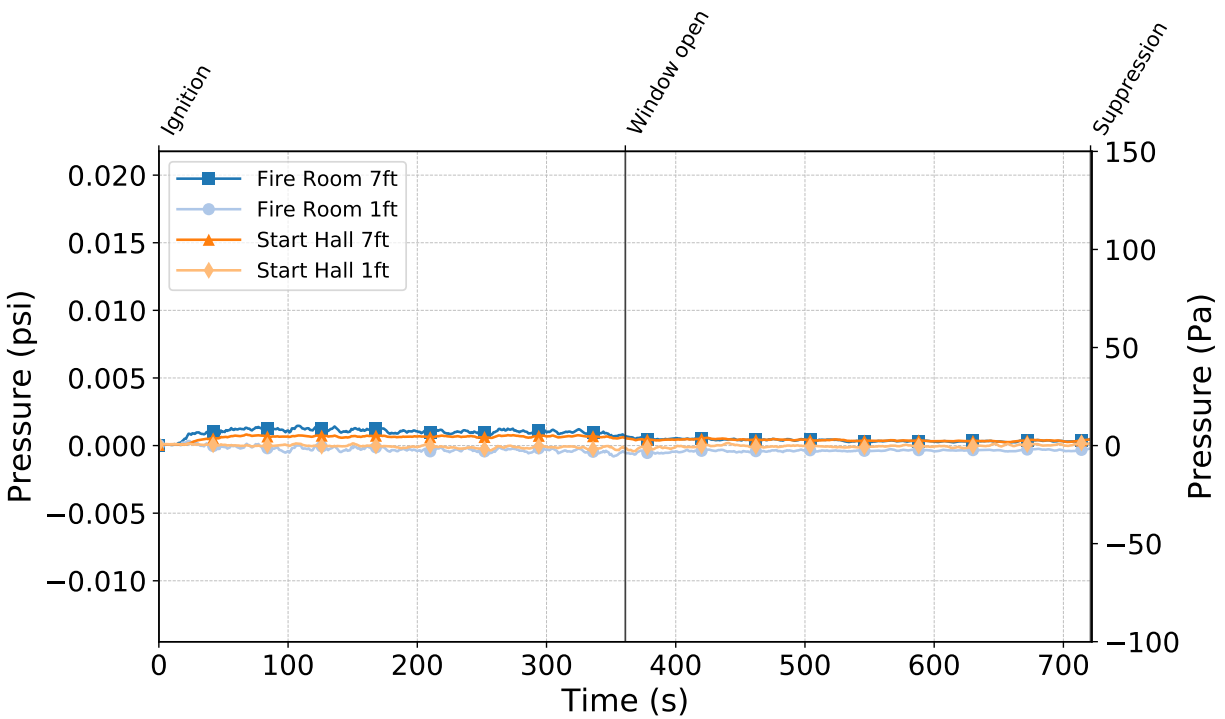


Figure C.329: Pressures measured by the fire room and hallway probes during Test 30.

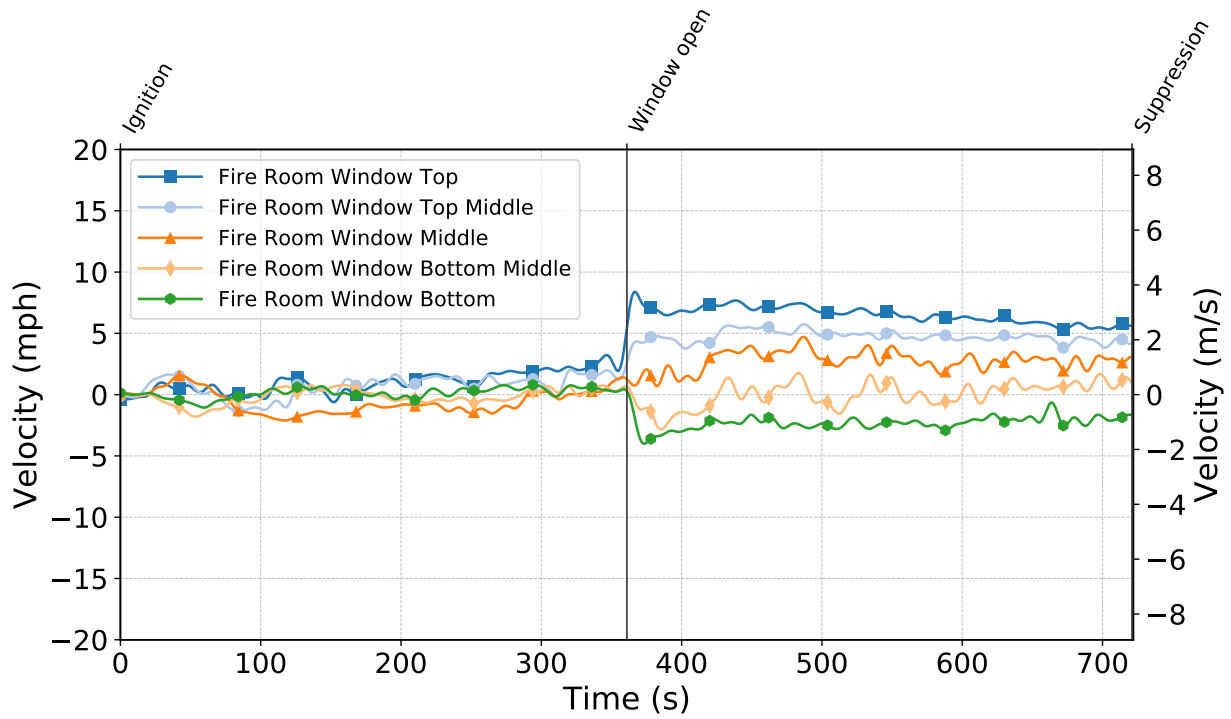


Figure C.330: Gas velocities measured by the fire room window bdp's during Test 30.

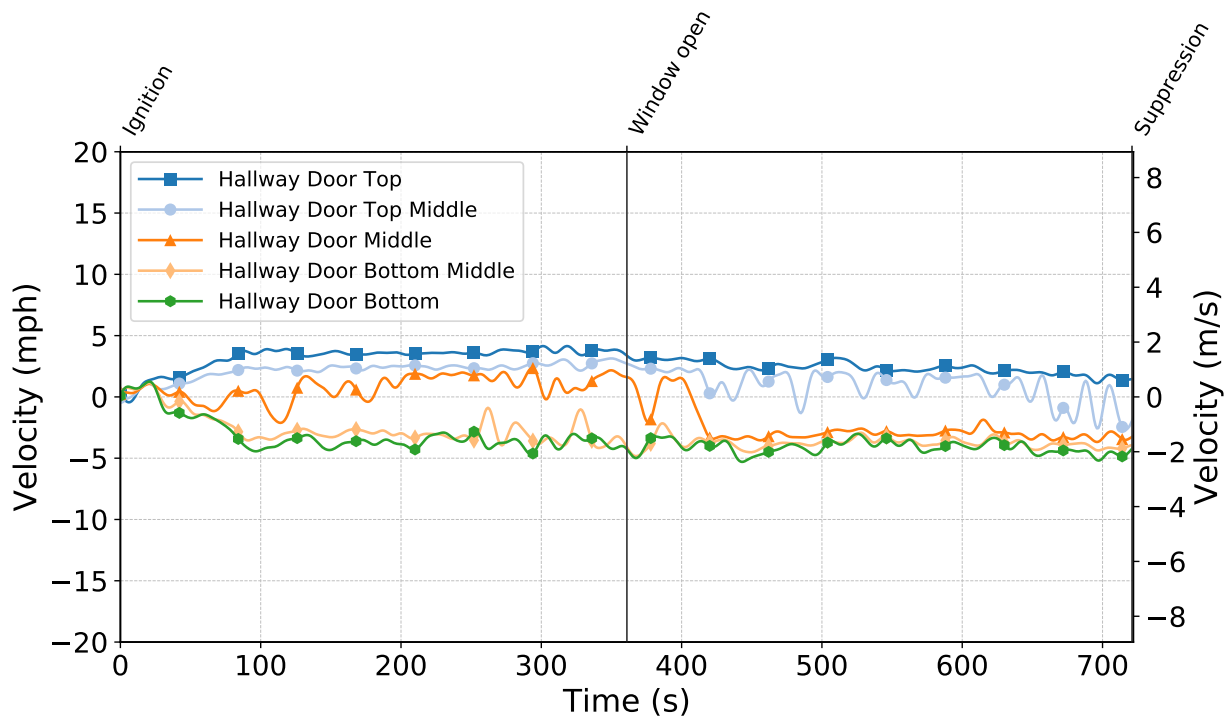


Figure C.331: Gas velocities measured by the hallway door bdp's during Test 30.

Test 31

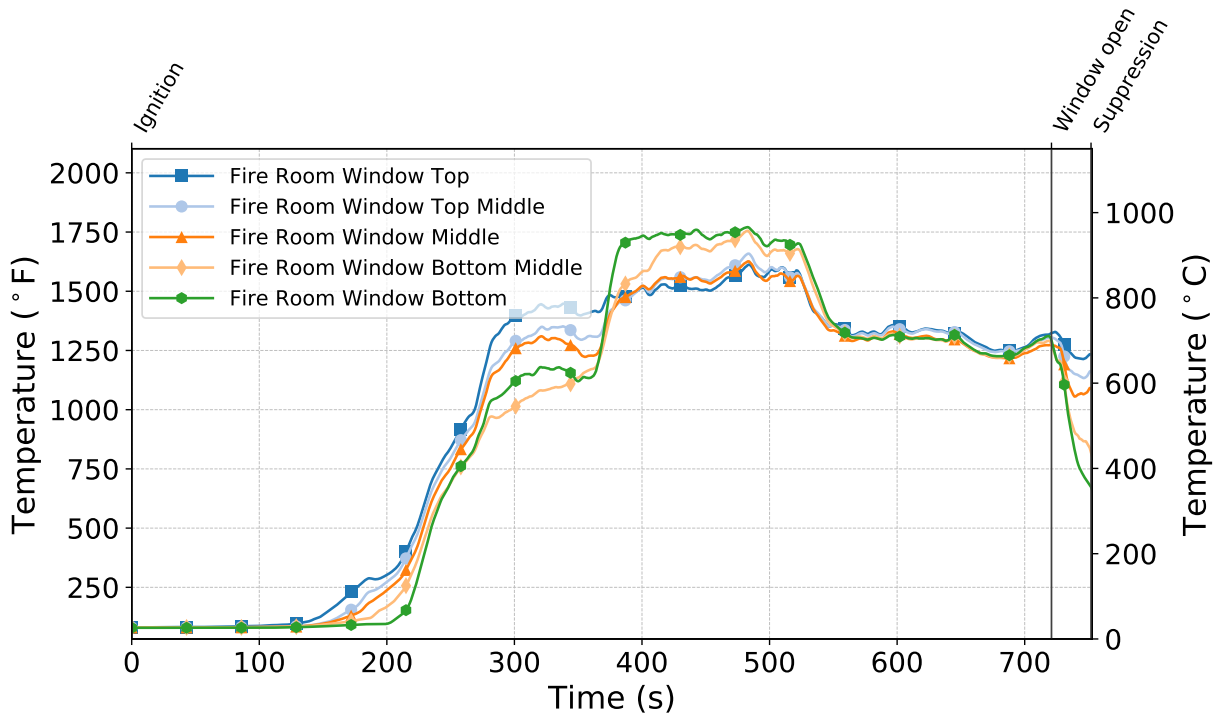


Figure C.332: Temperatures measured by the fire room window thermocouples during Test 31.

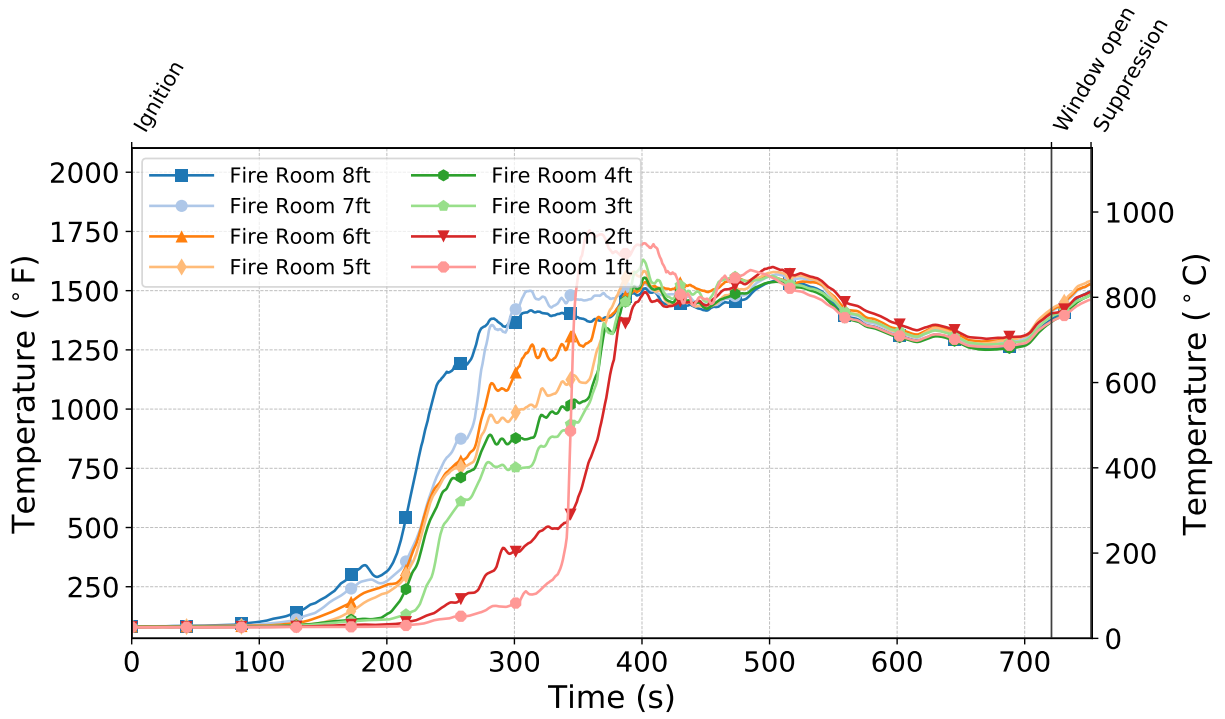


Figure C.333: Temperatures measured by the fire room thermocouples during Test 31.

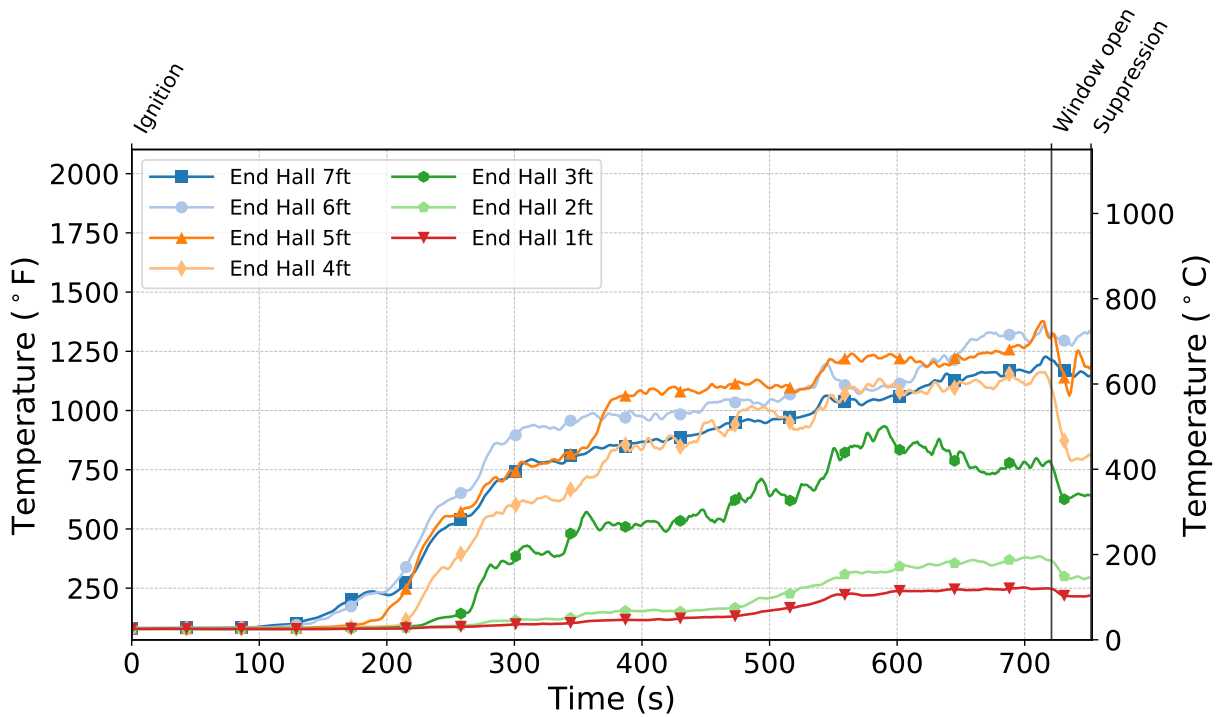


Figure C.334: Temperatures measured by the end hall thermocouples during Test 31.

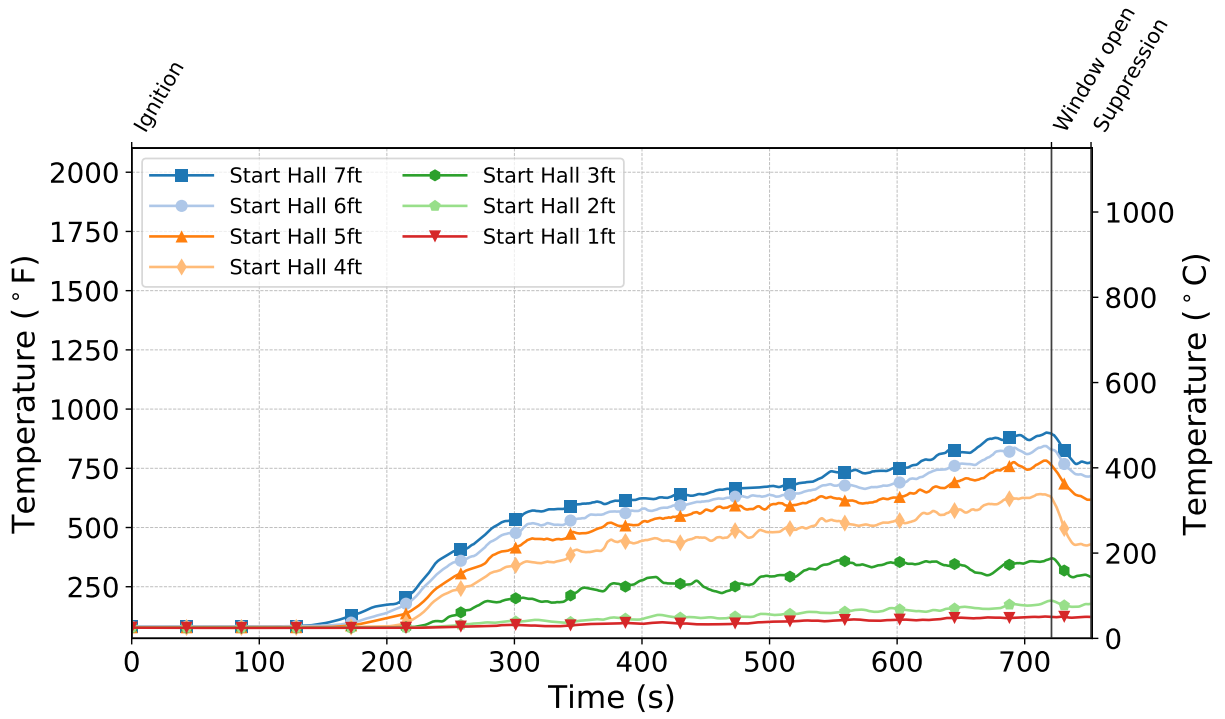


Figure C.335: Temperatures measured by the start hall thermocouples during Test 31.

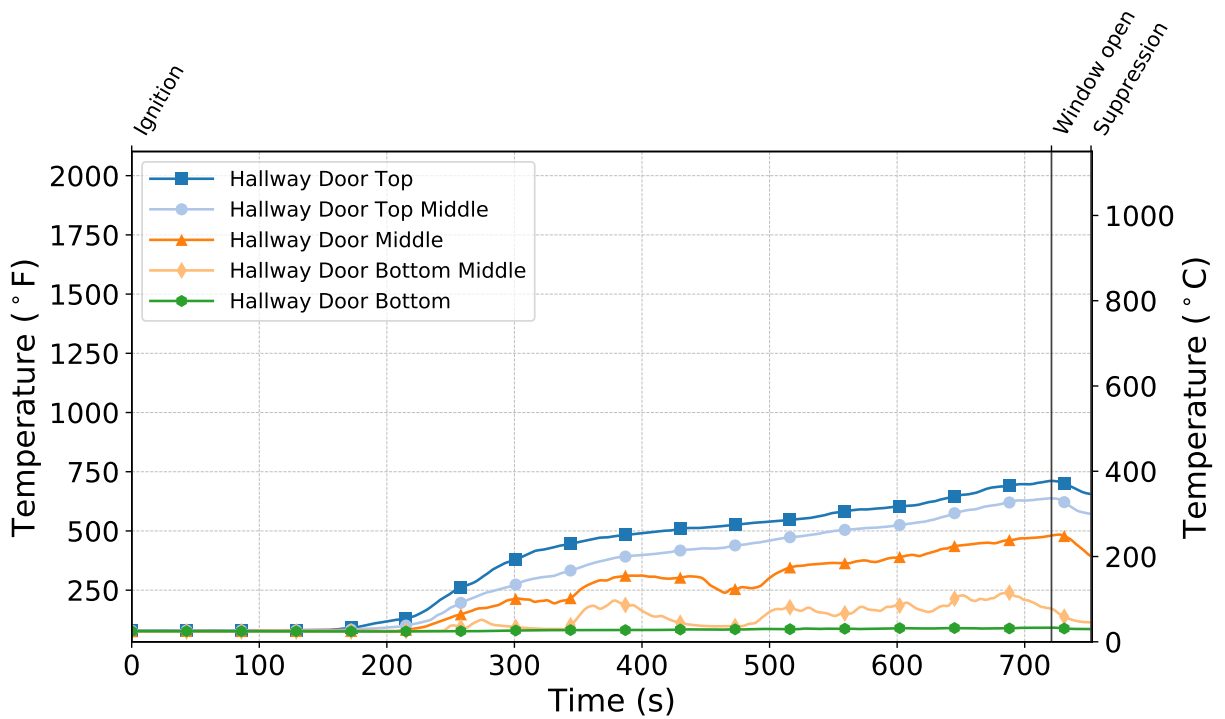


Figure C.336: Temperatures measured by the hallway door thermocouples during Test 31.

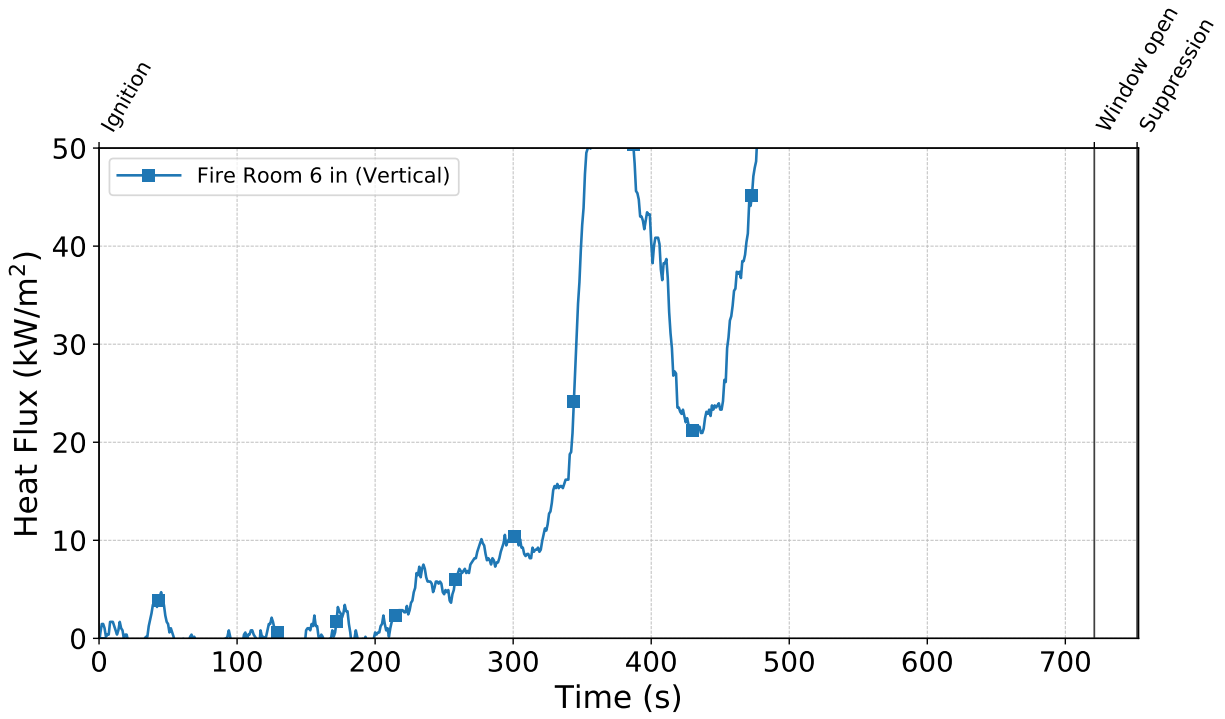


Figure C.337: Heat flux measured by the fire room gauge during Test 31.

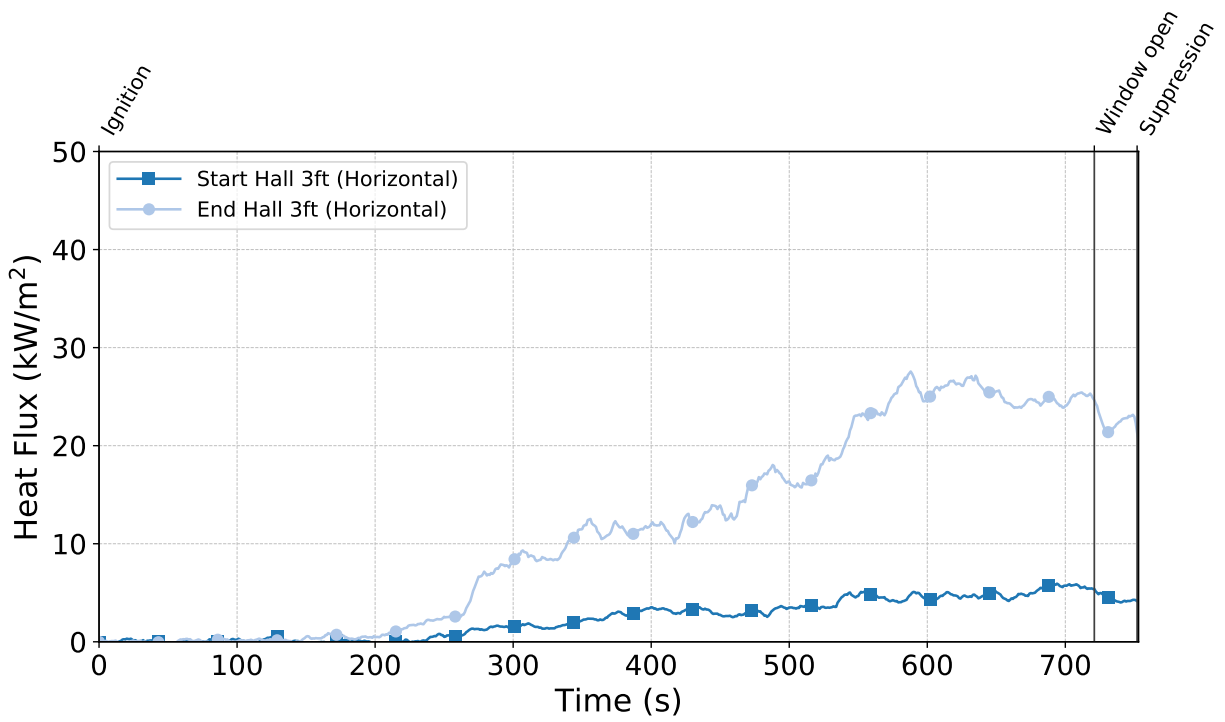


Figure C.338: Heat flux measured by the hallway gauges during Test 31.

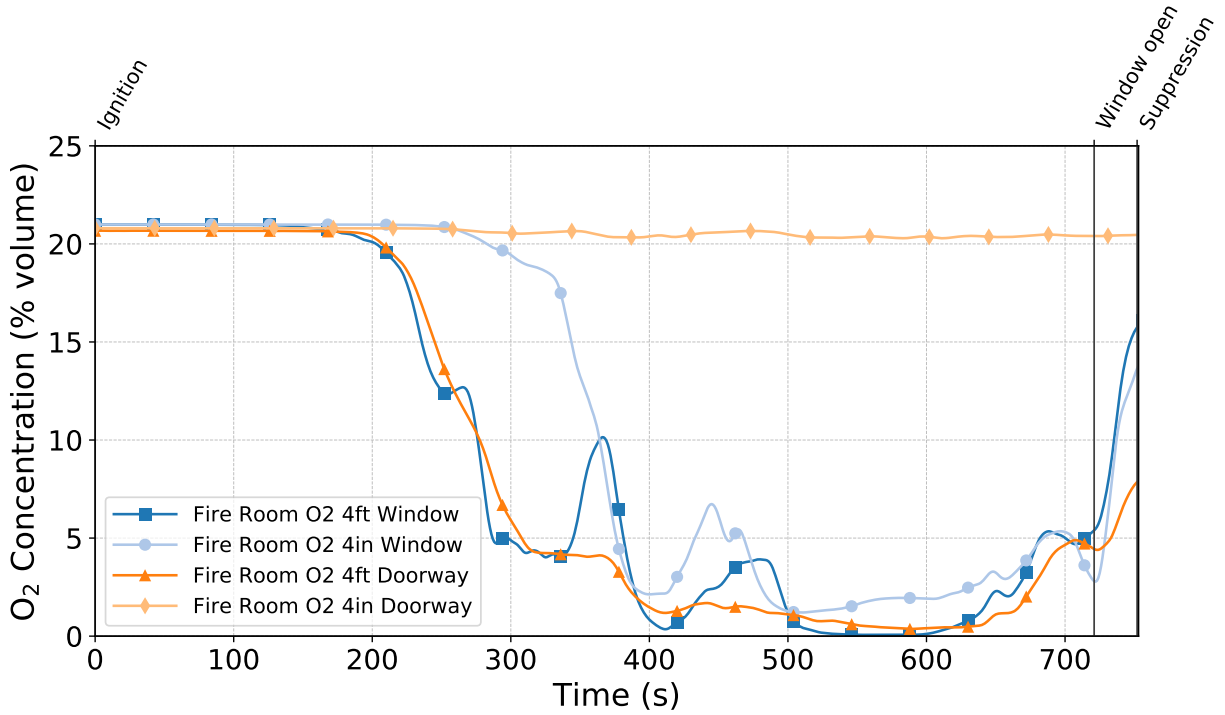


Figure C.339: Oxygen concentrations measured by the fire room gas sampling probes during Test 31.

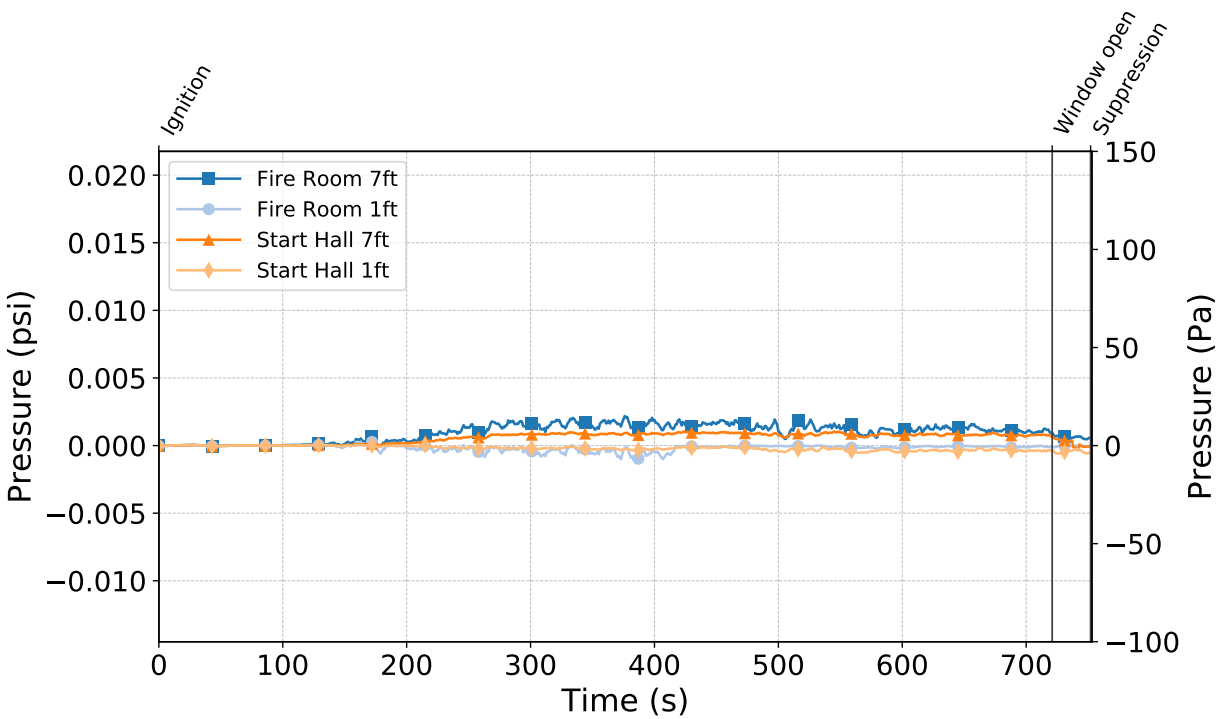


Figure C.340: Pressures measured by the fire room and hallway probes during Test 31.

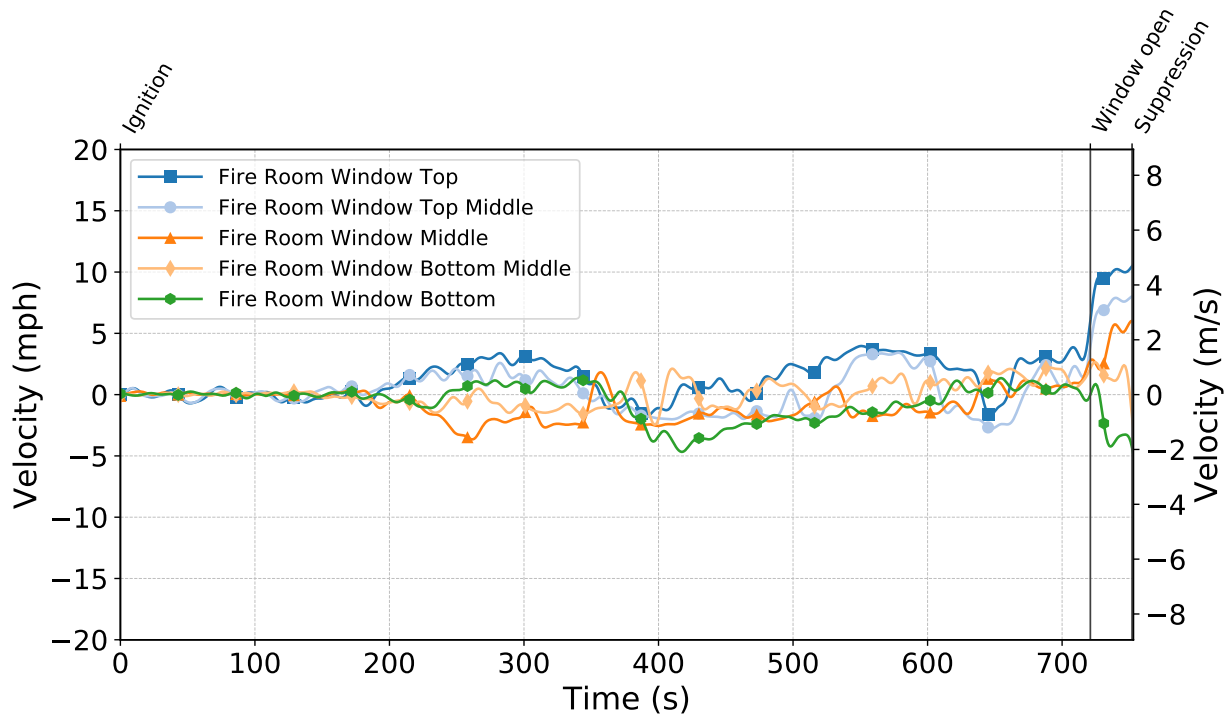


Figure C.341: Gas velocities measured by the fire room window bdps during Test 31.

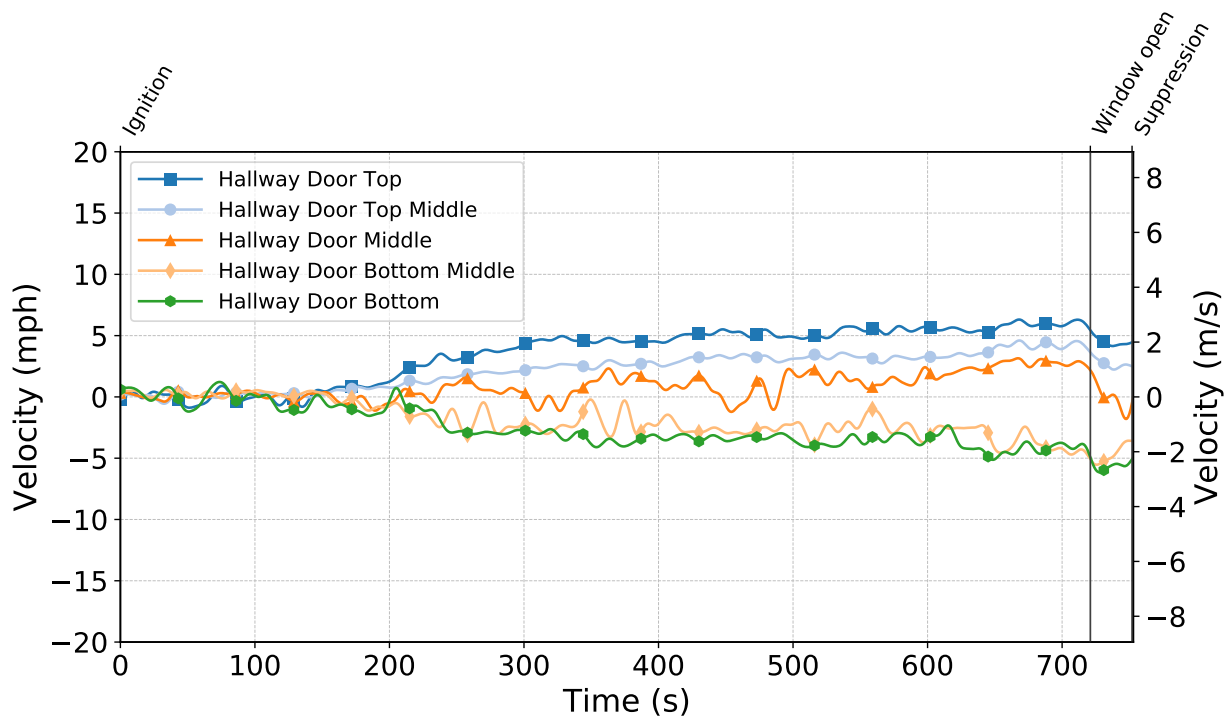


Figure C.342: Gas velocities measured by the hallway door bdps during Test 31.

Test 32

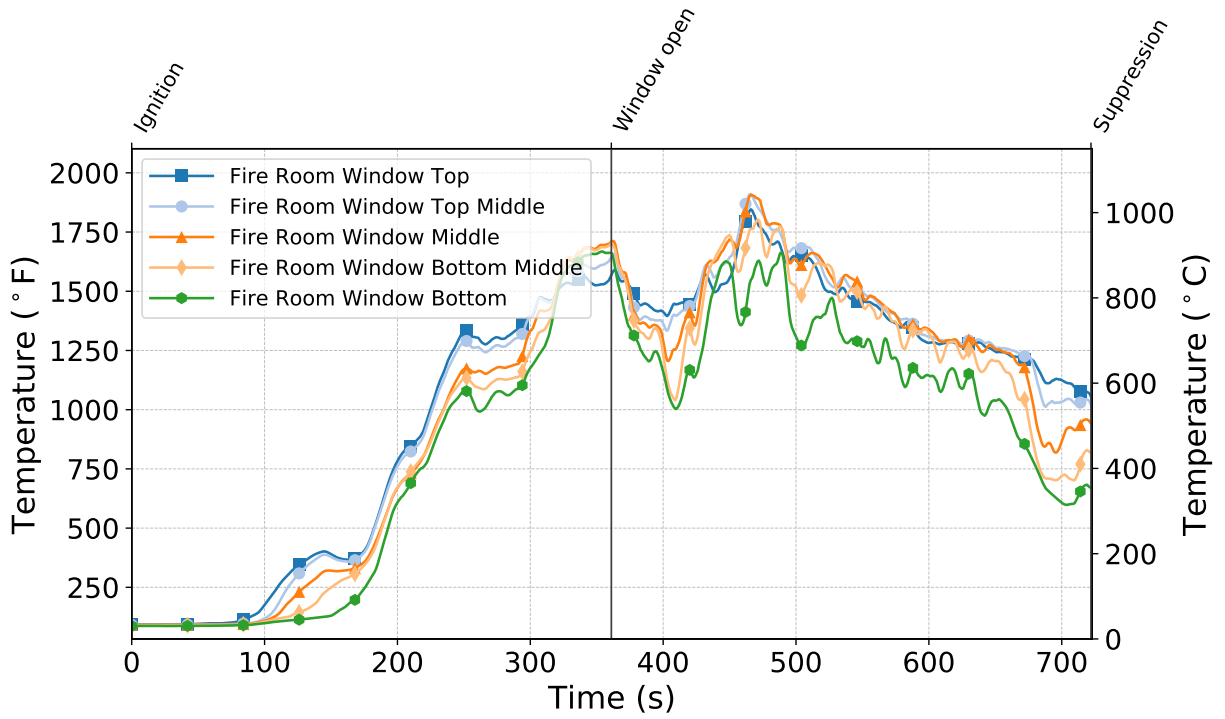


Figure C.343: Temperatures measured by the fire room window thermocouples during Test 32.

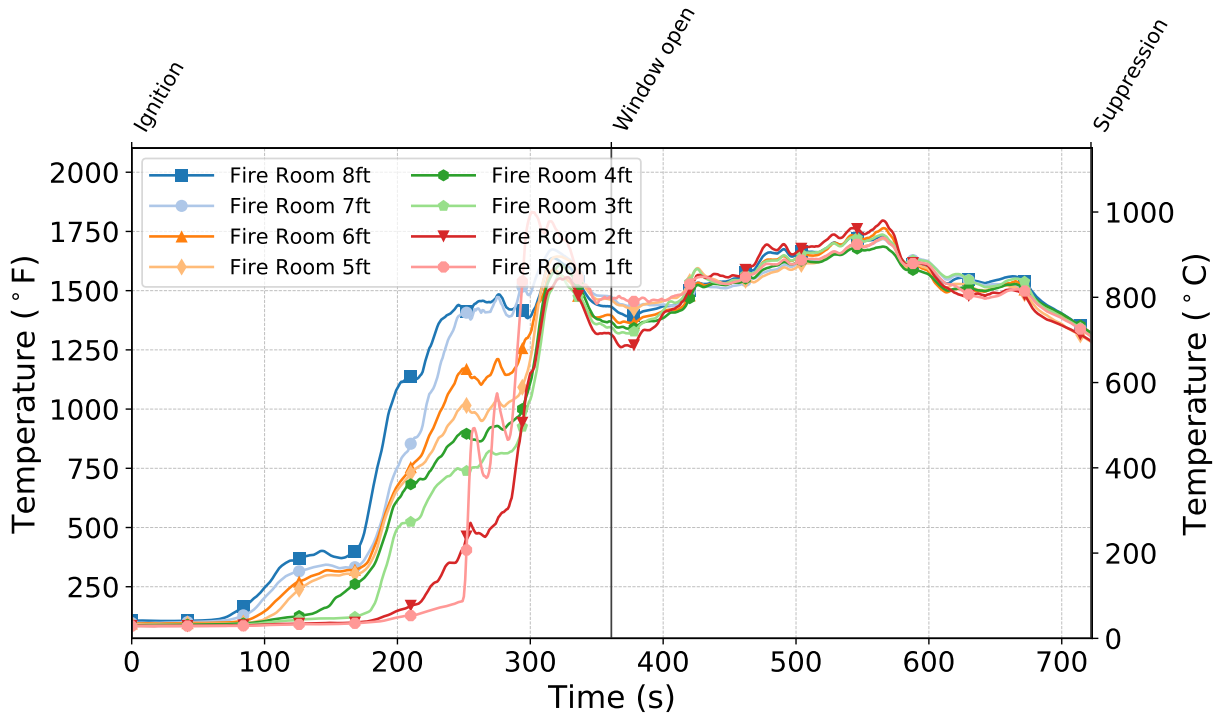


Figure C.344: Temperatures measured by the fire room thermocouples during Test 32.

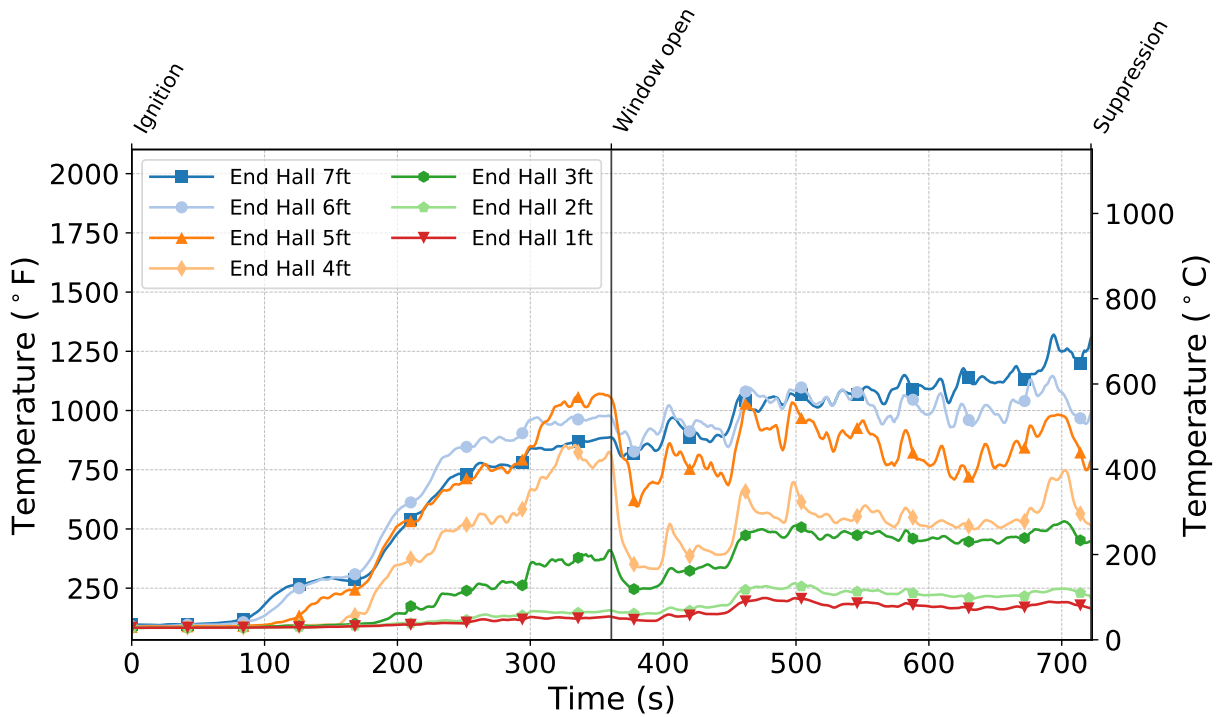


Figure C.345: Temperatures measured by the end hall thermocouples during Test 32.

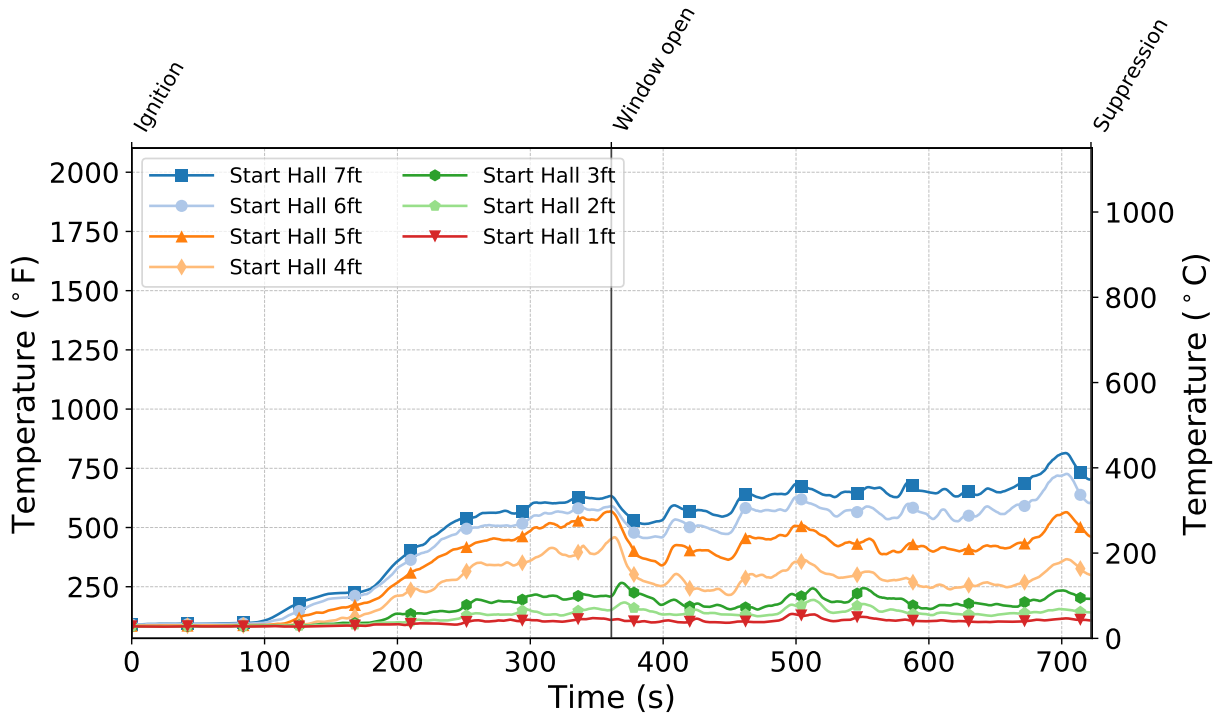


Figure C.346: Temperatures measured by the start hall thermocouples during Test 32.

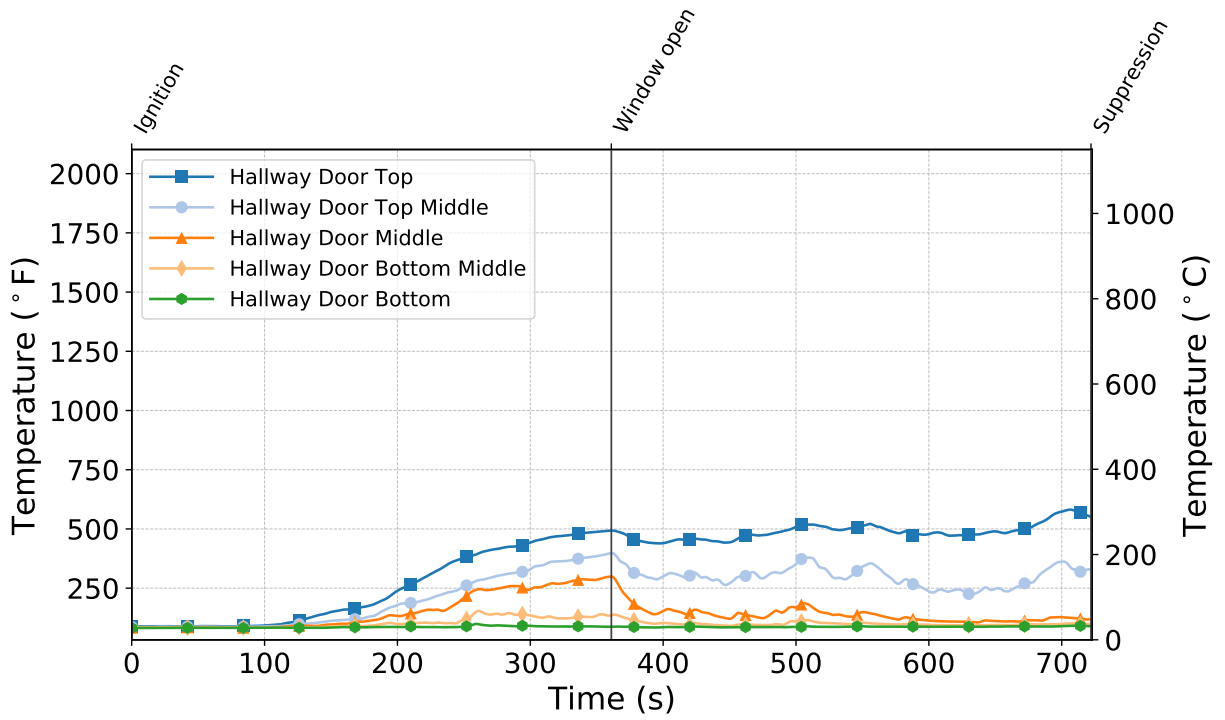


Figure C.347: Temperatures measured by the hallway door thermocouples during Test 32.

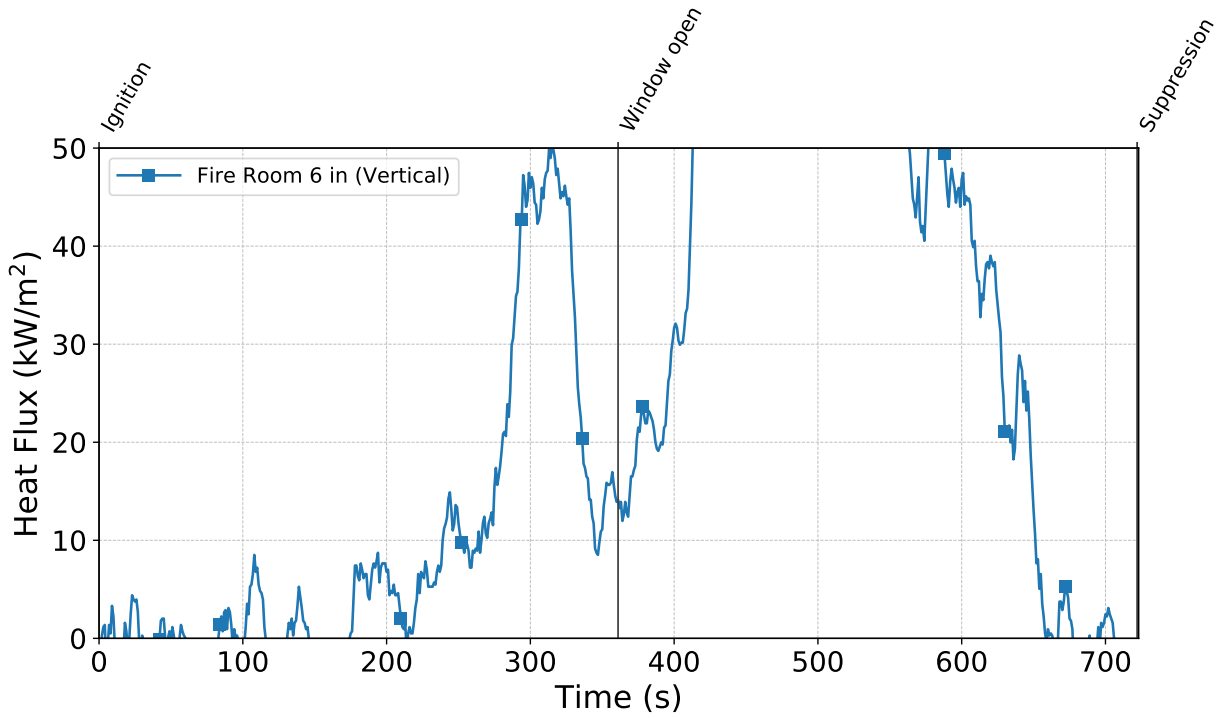


Figure C.348: Heat flux measured by the fire room gauge during Test 32.

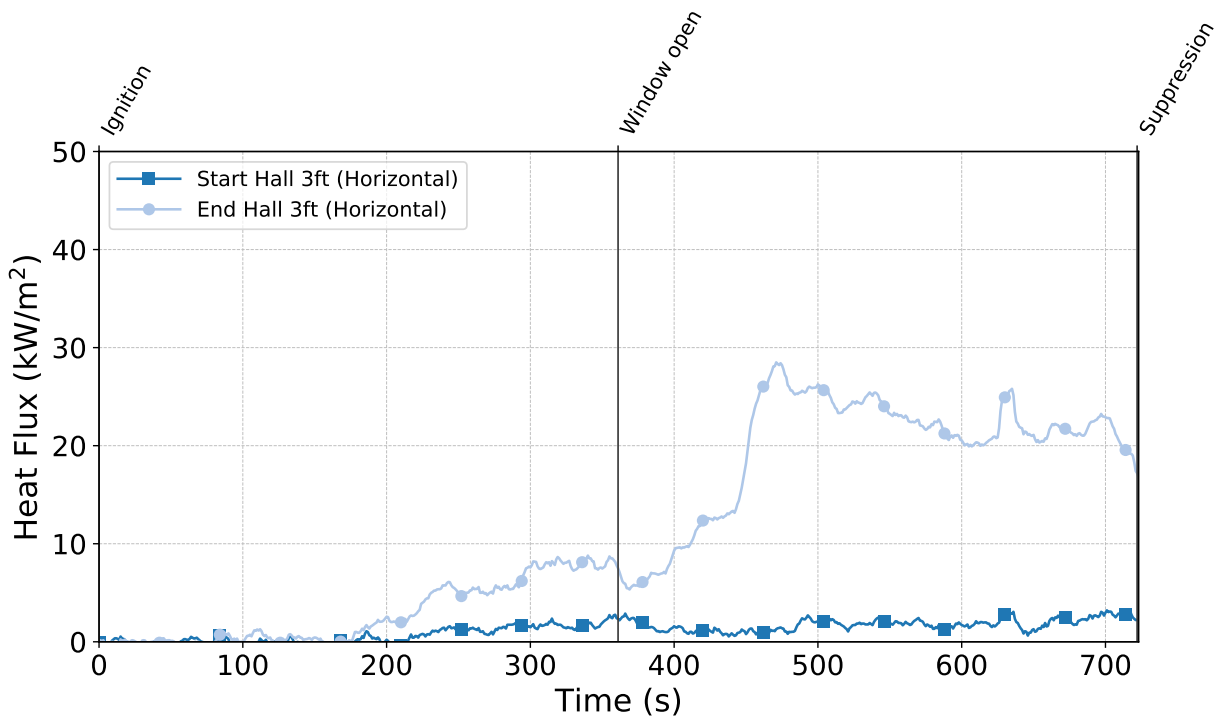


Figure C.349: Heat flux measured by the hallway gauges during Test 32.

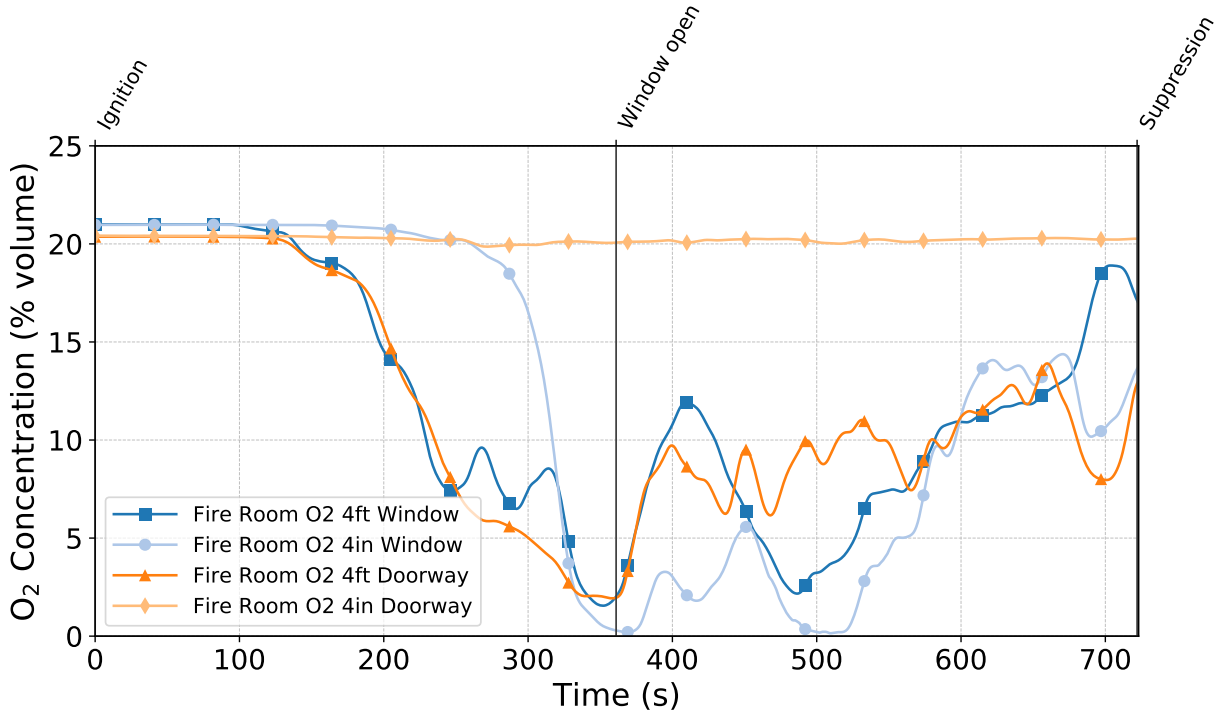


Figure C.350: Oxygen concentrations measured by the fire room gas sampling probes during Test 32.

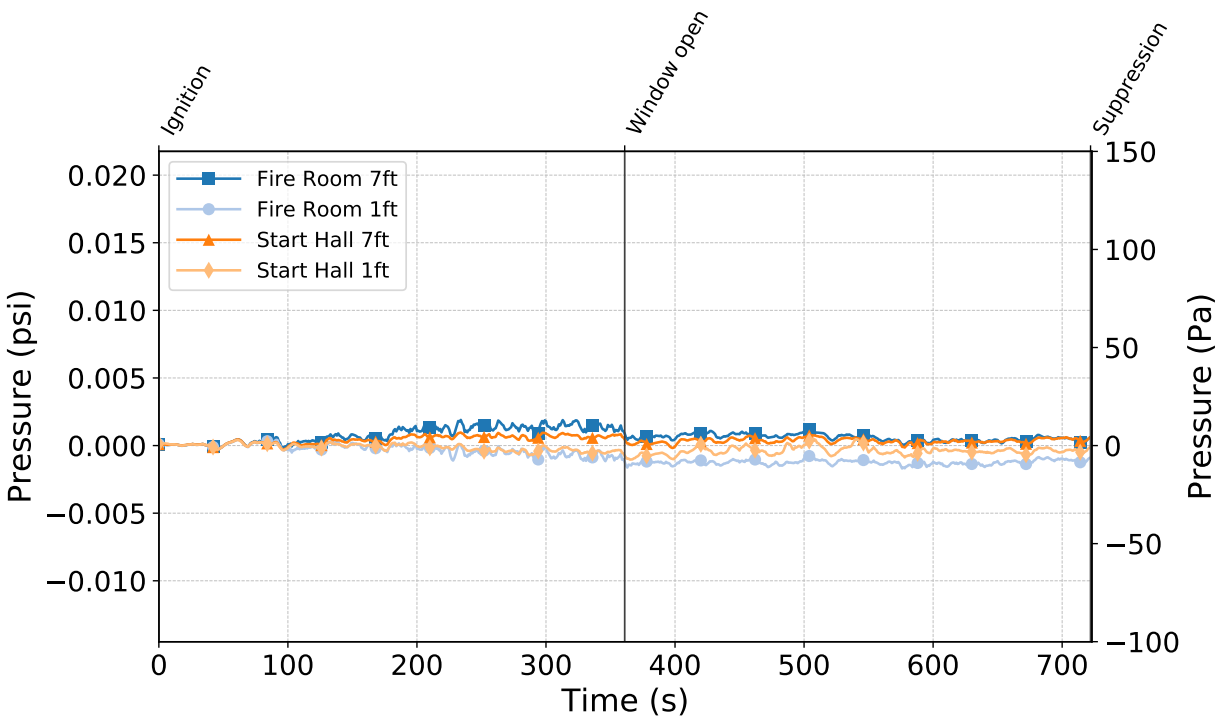


Figure C.351: Pressures measured by the fire room and hallway probes during Test 32.

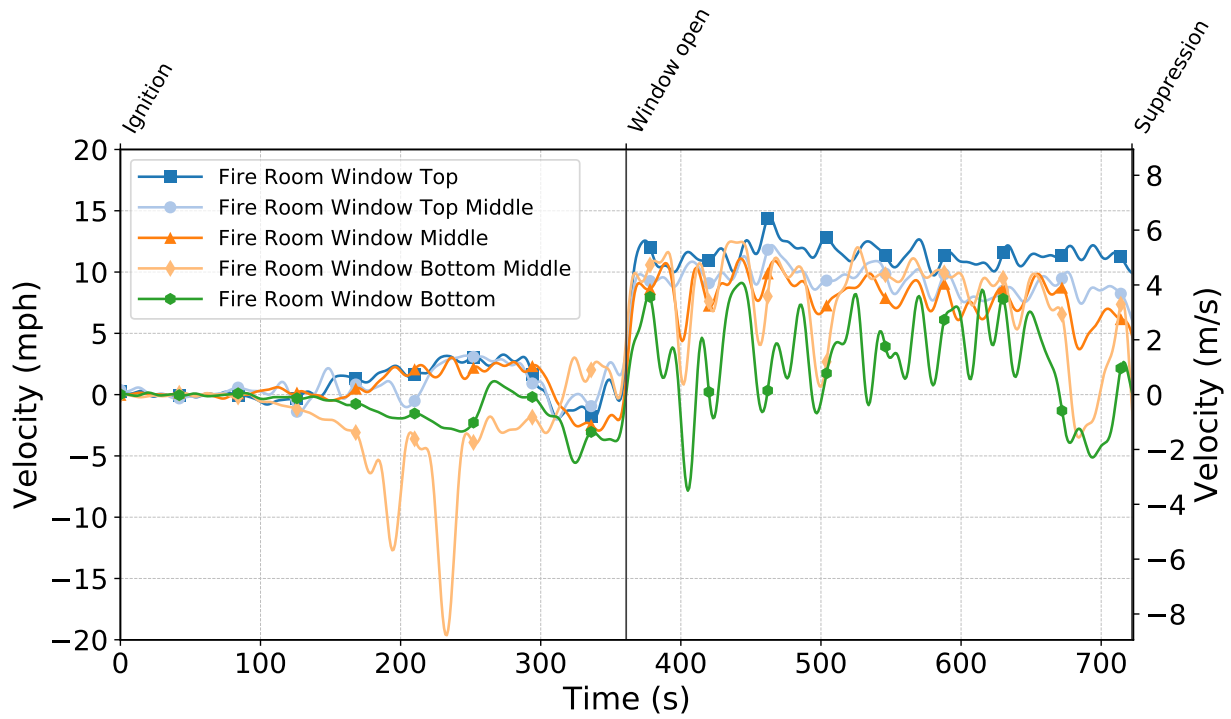


Figure C.352: Gas velocities measured by the fire room window bdps during Test 32.

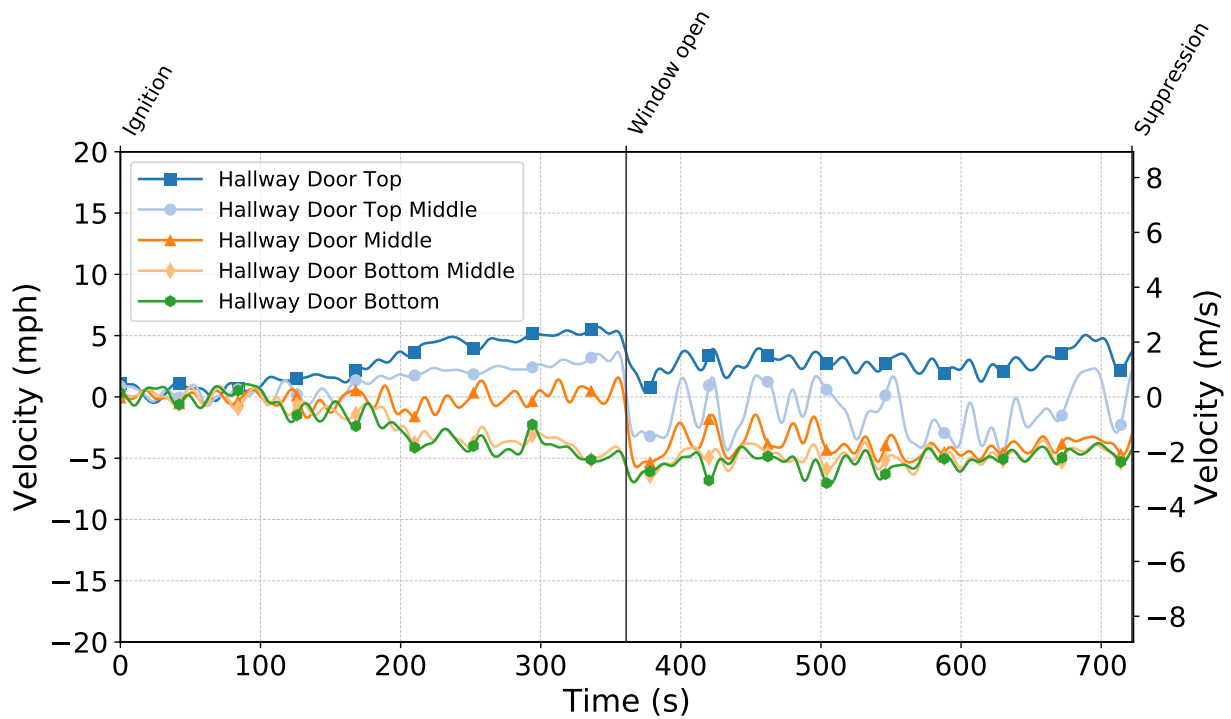


Figure C.353: Gas velocities measured by the hallway door bdps during Test 32.

Test 33

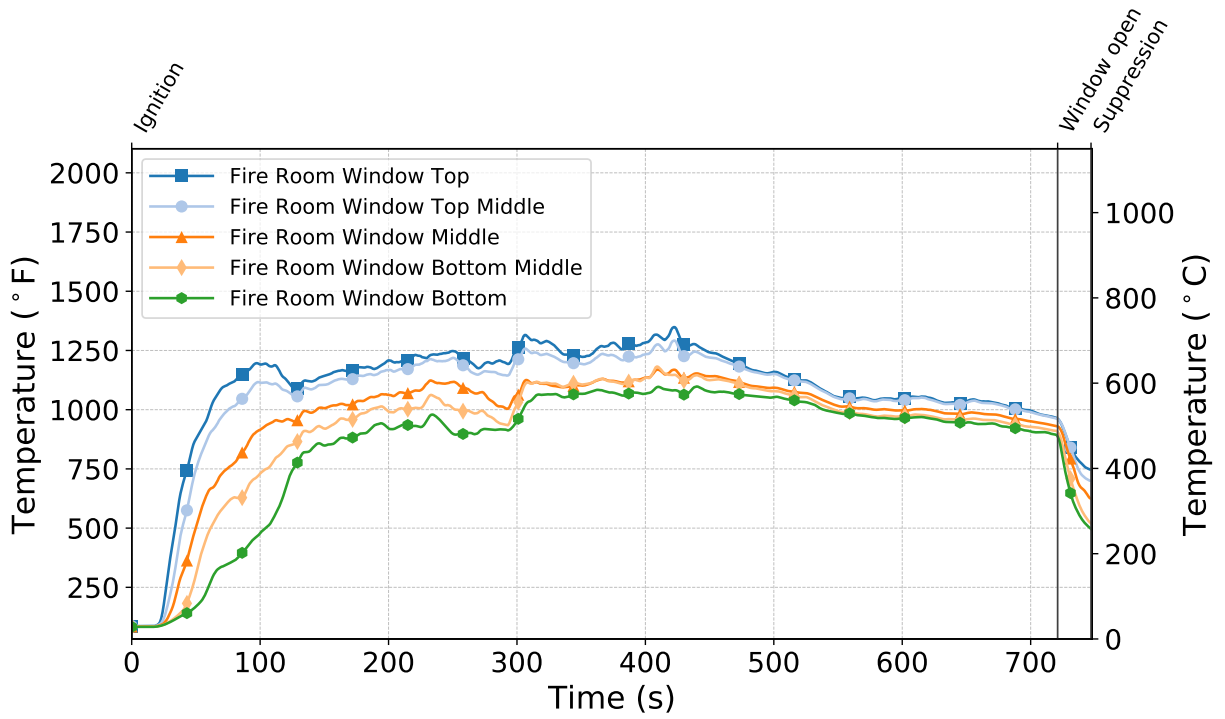


Figure C.354: Temperatures measured by the fire room window thermocouples during Test 33.

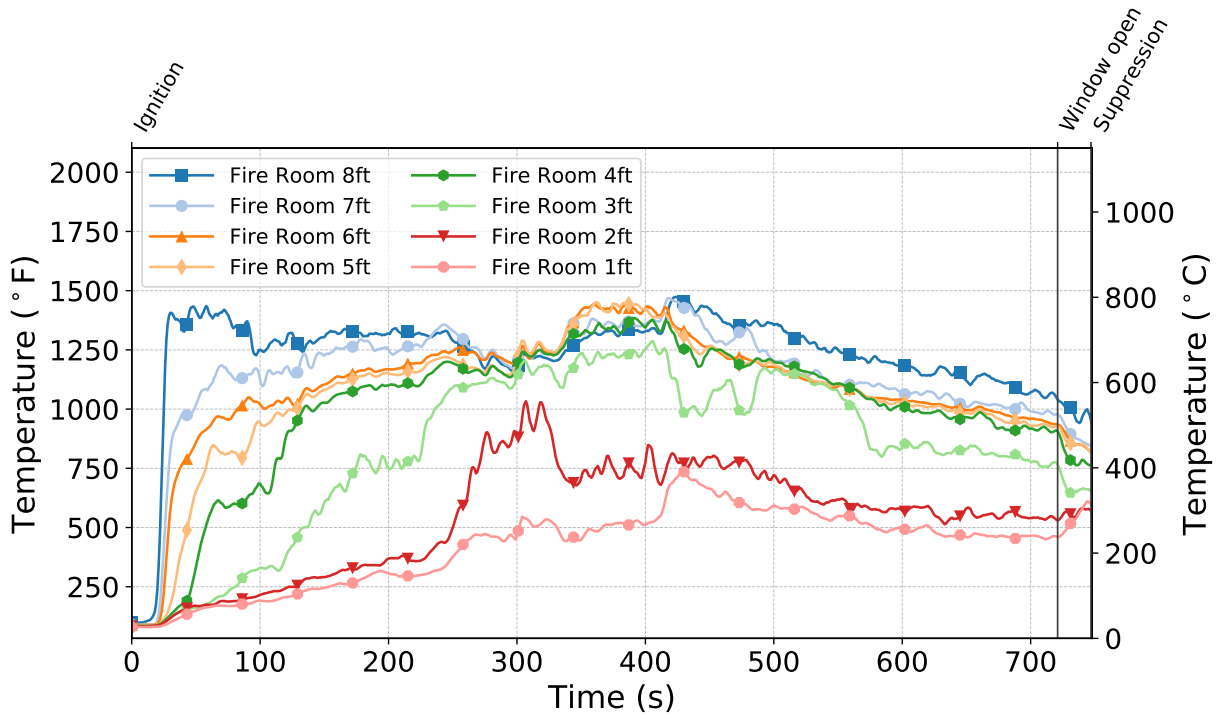


Figure C.355: Temperatures measured by the fire room thermocouples during Test 33.

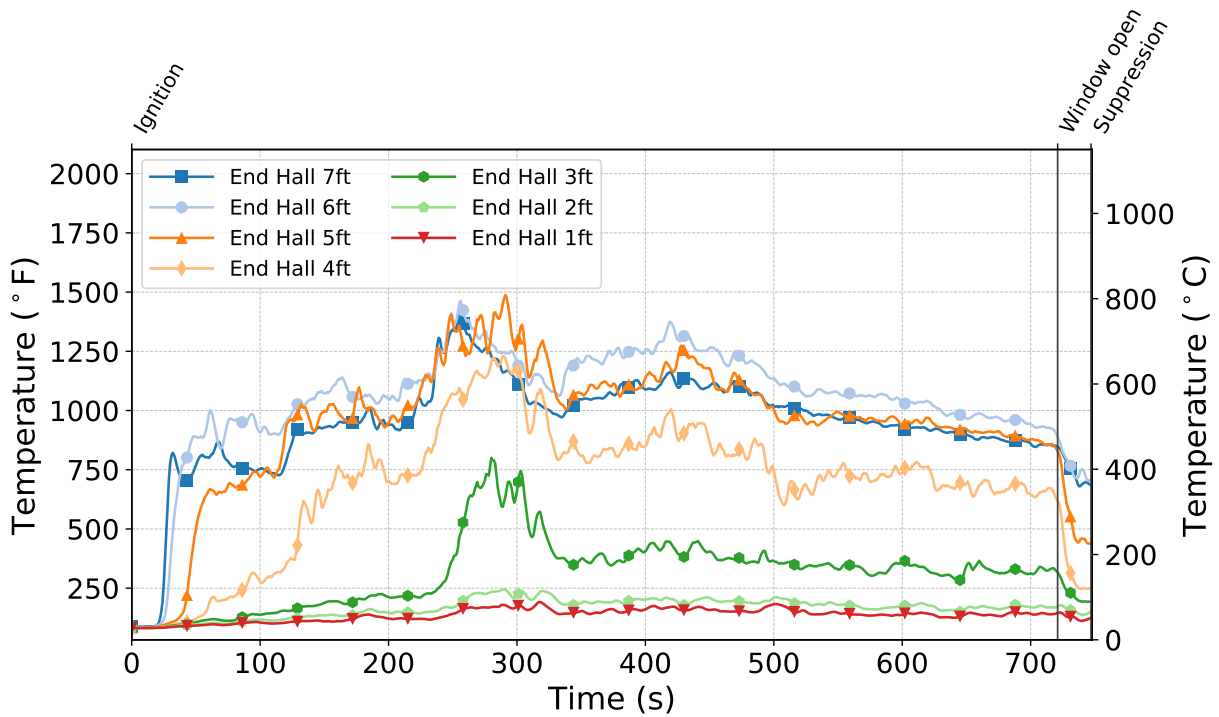


Figure C.356: Temperatures measured by the end hall thermocouples during Test 33.

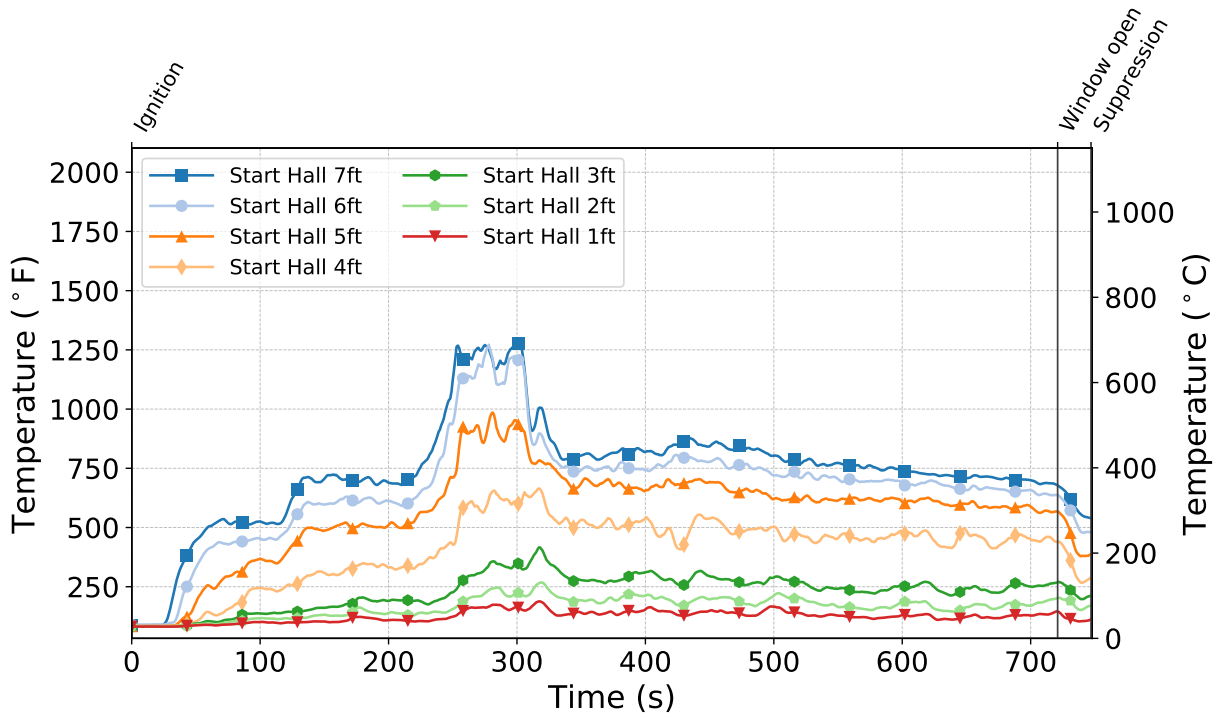


Figure C.357: Temperatures measured by the start hall thermocouples during Test 33.

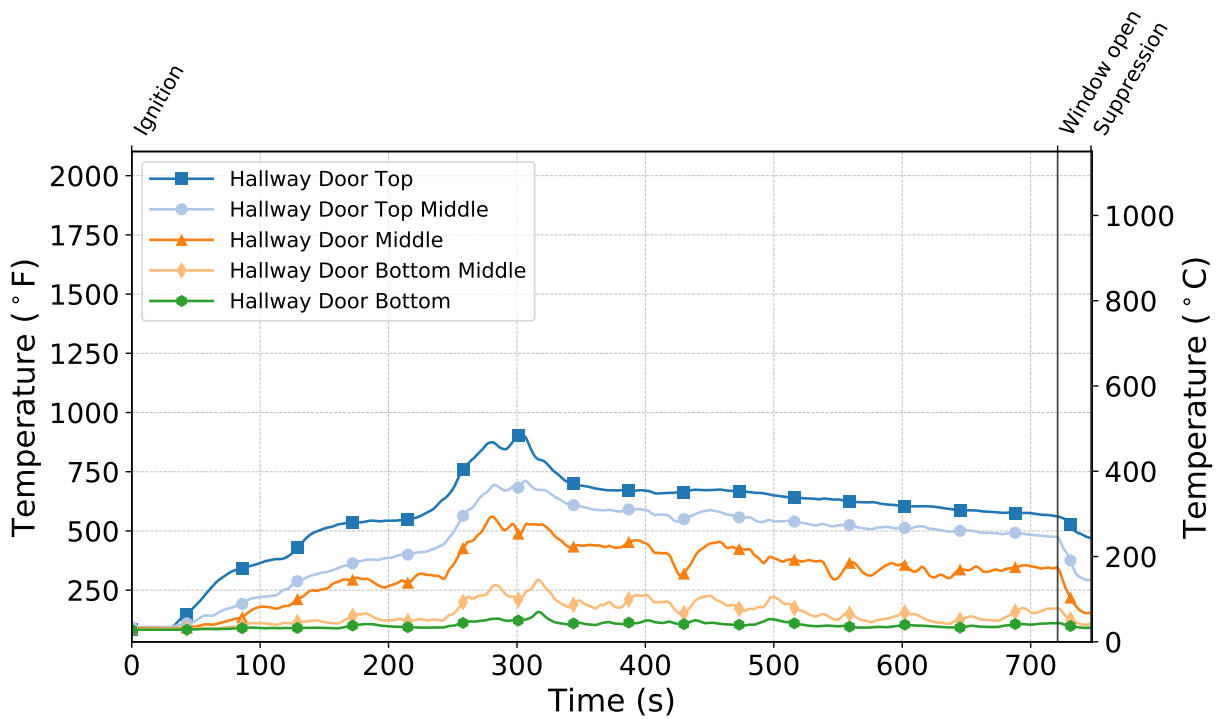


Figure C.358: Temperatures measured by the hallway door thermocouples during Test 33.

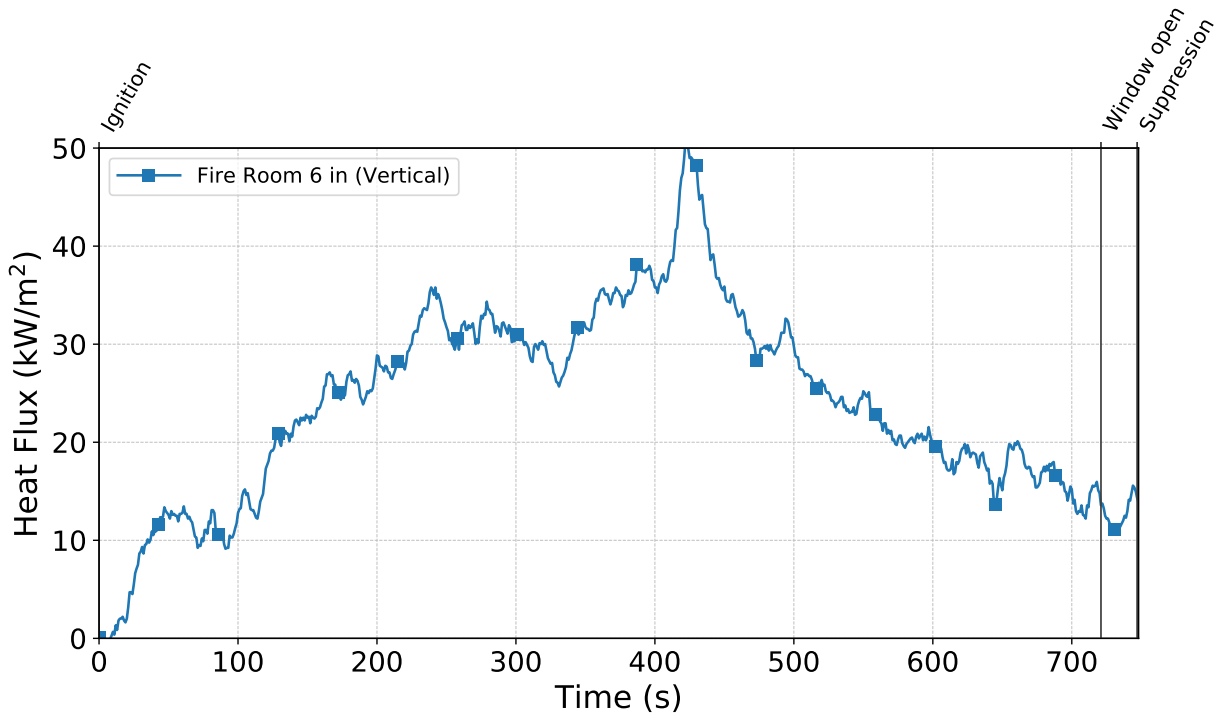


Figure C.359: Heat flux measured by the fire room gauge during Test 33.

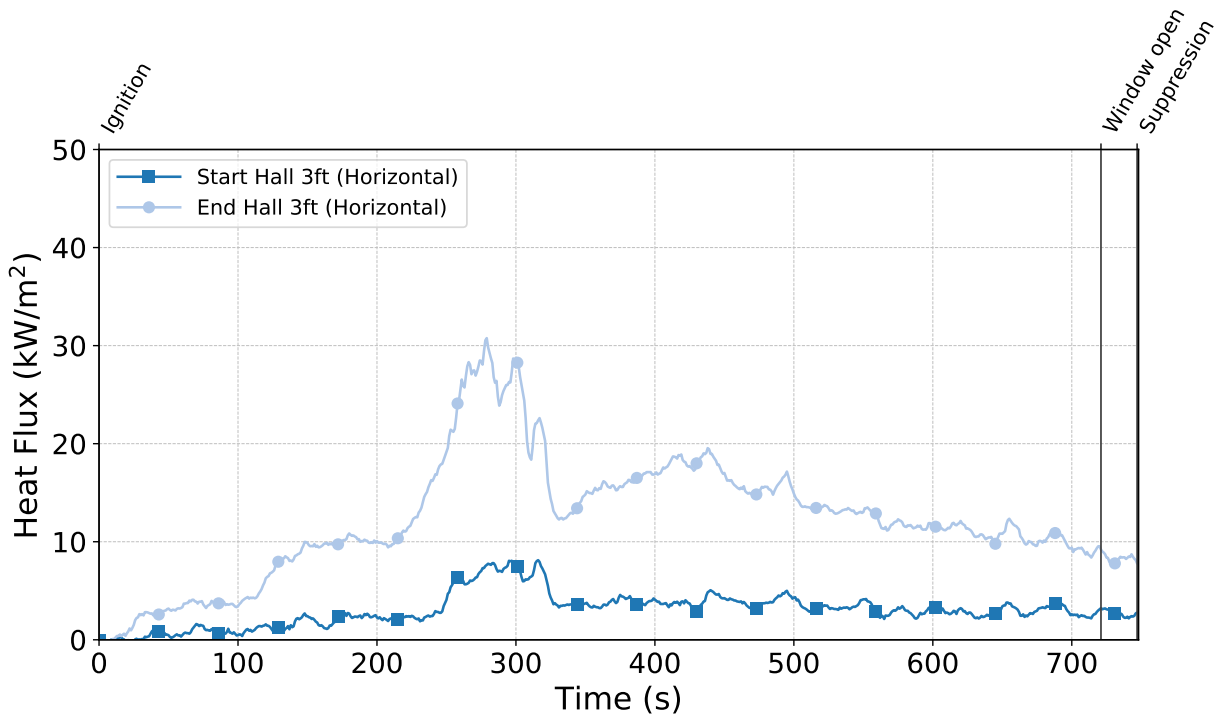


Figure C.360: Heat flux measured by the hallway gauges during Test 33.

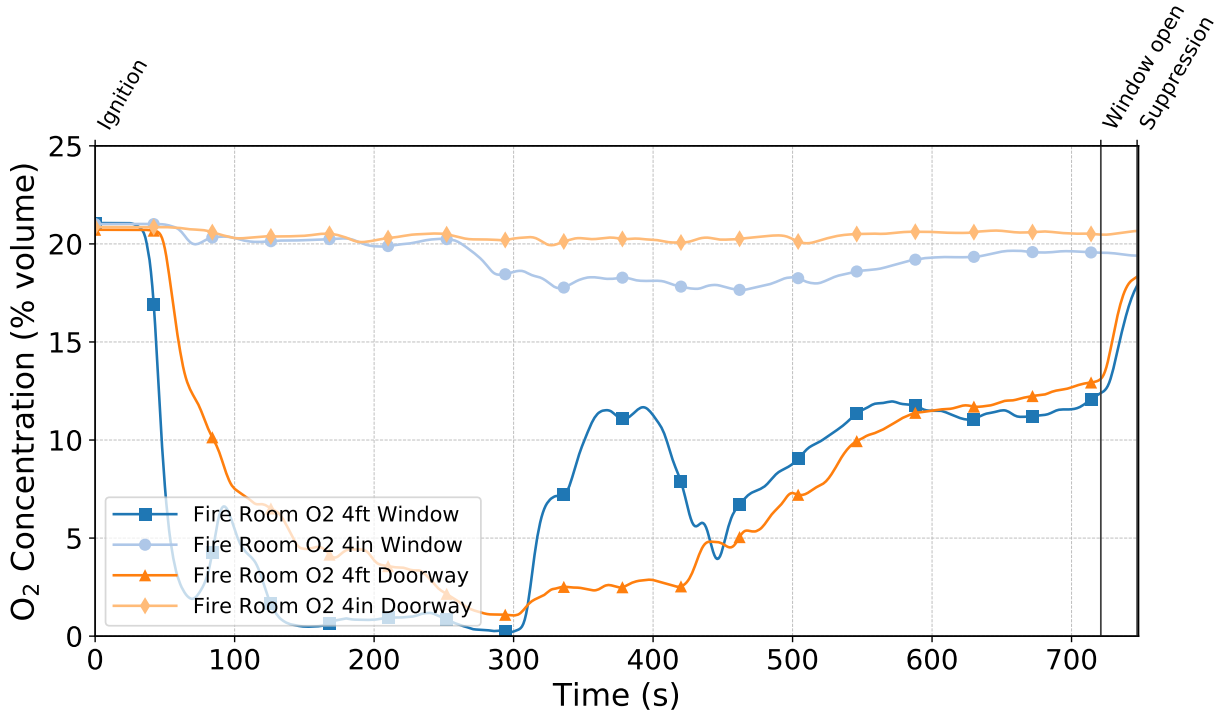


Figure C.361: Oxygen concentrations measured by the fire room gas sampling probes during Test 33.

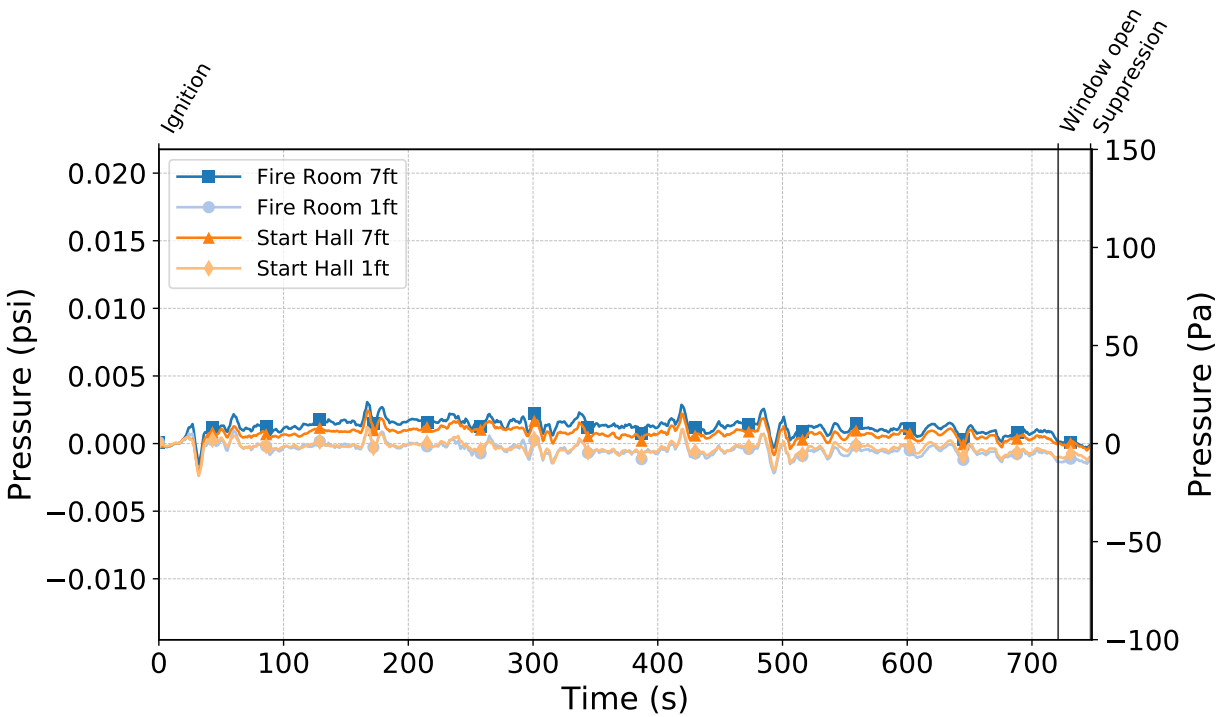


Figure C.362: Pressures measured by the fire room and hallway probes during Test 33.

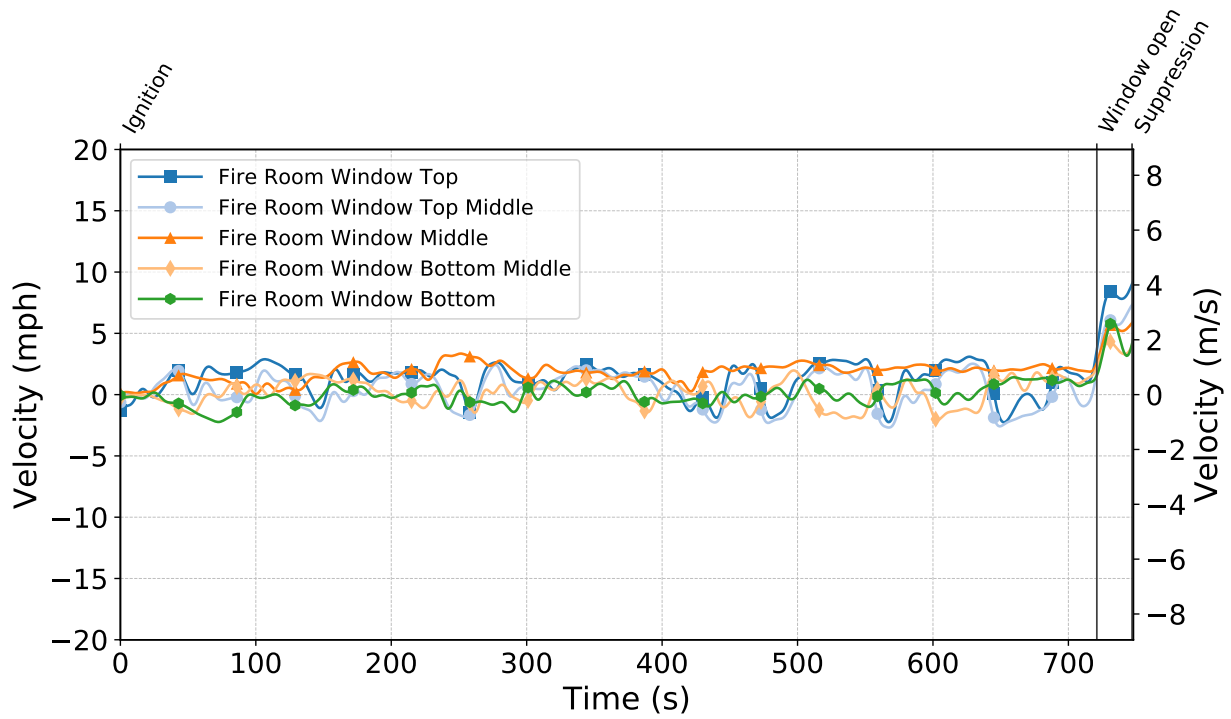


Figure C.363: Gas velocities measured by the fire room window bdps during Test 33.

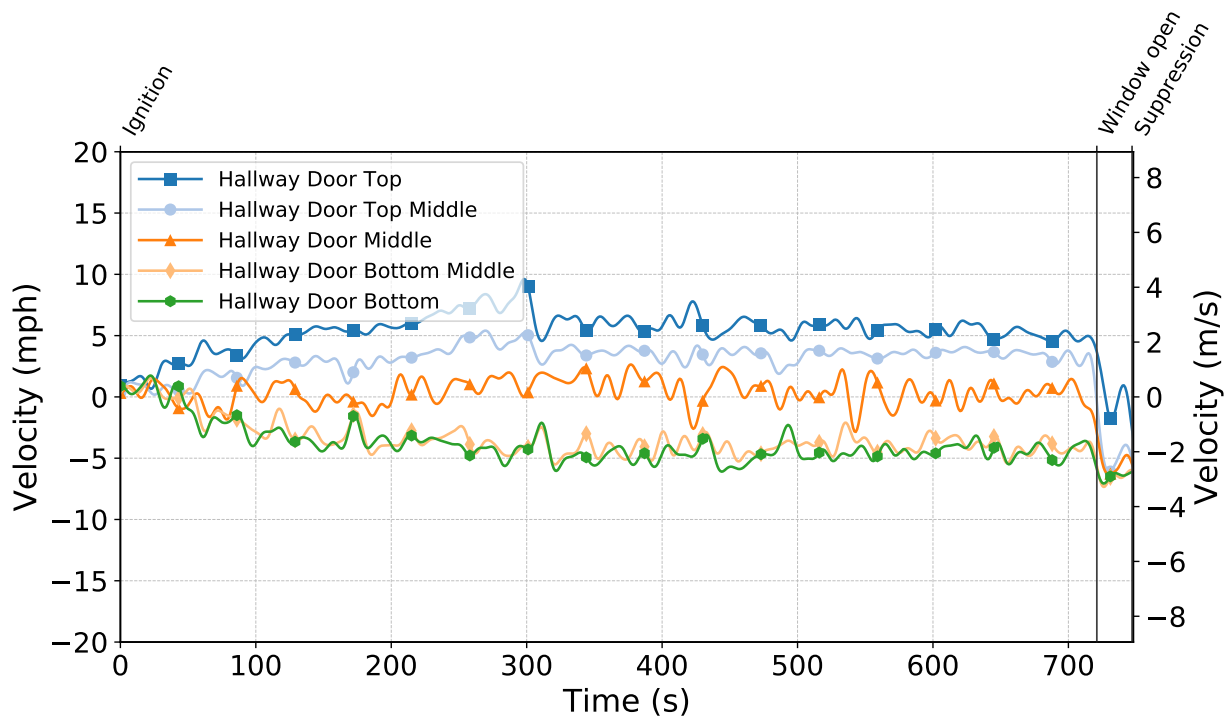


Figure C.364: Gas velocities measured by the hallway door bdps during Test 33.

Test 34

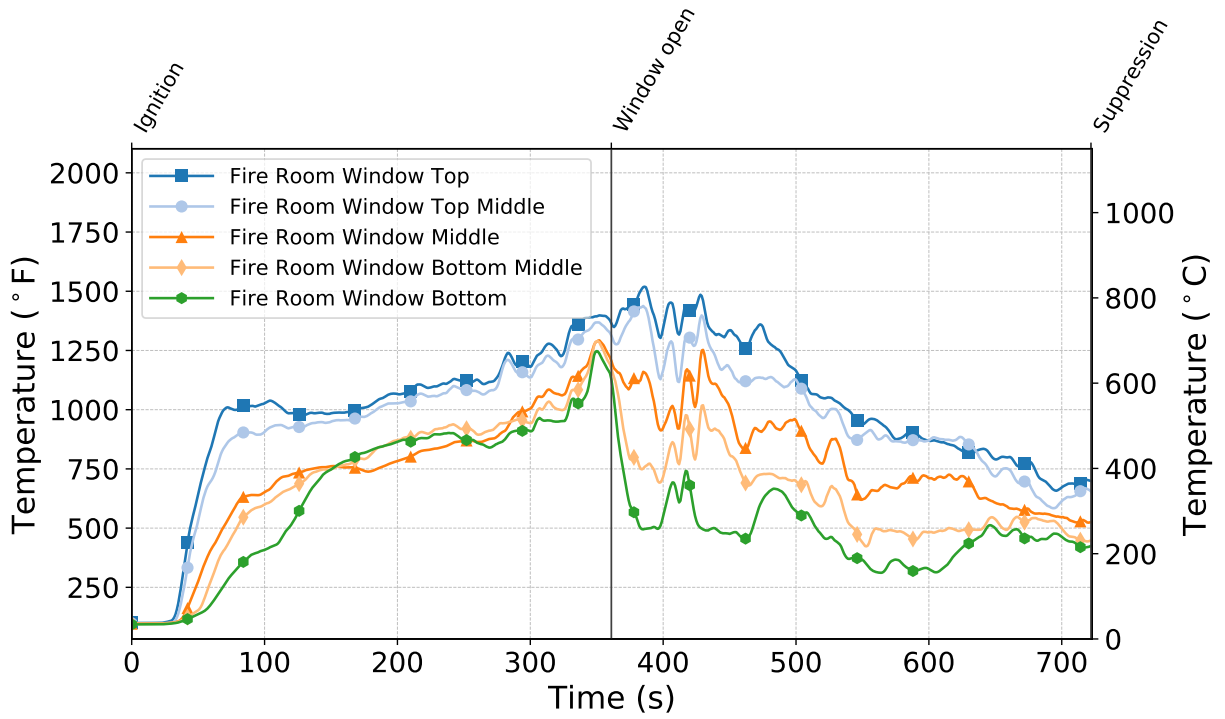


Figure C.365: Temperatures measured by the fire room window thermocouples during Test 34.

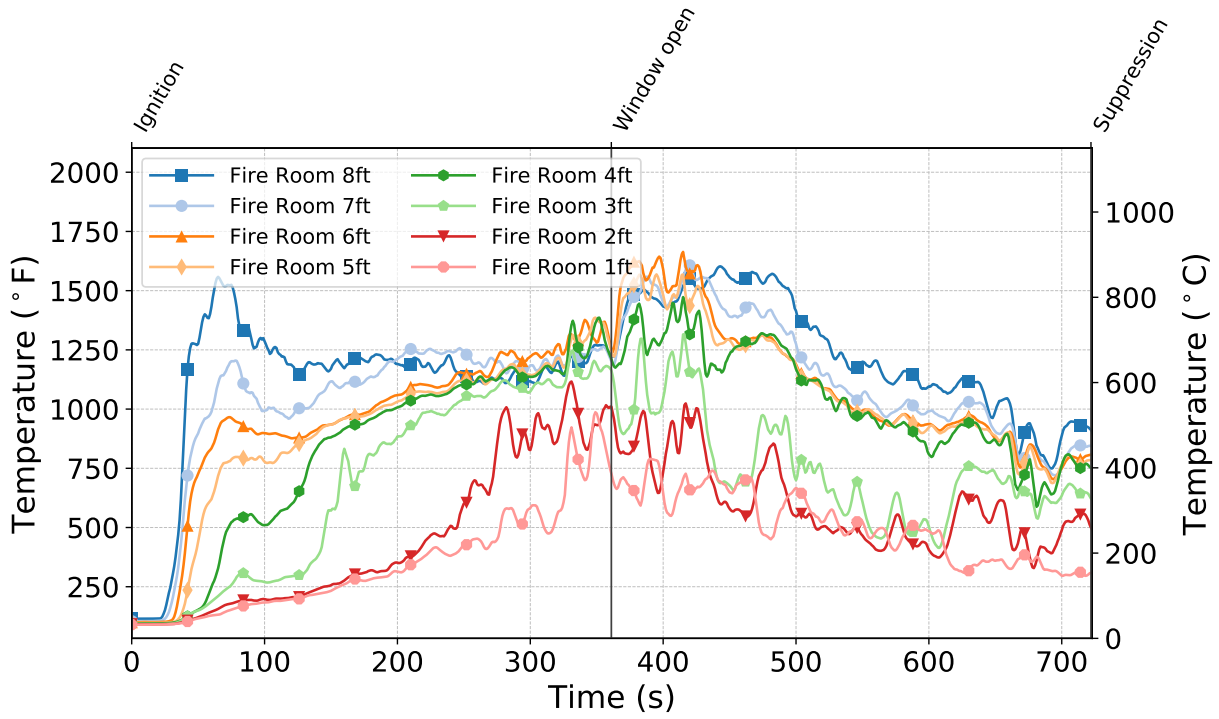


Figure C.366: Temperatures measured by the fire room thermocouples during Test 34.

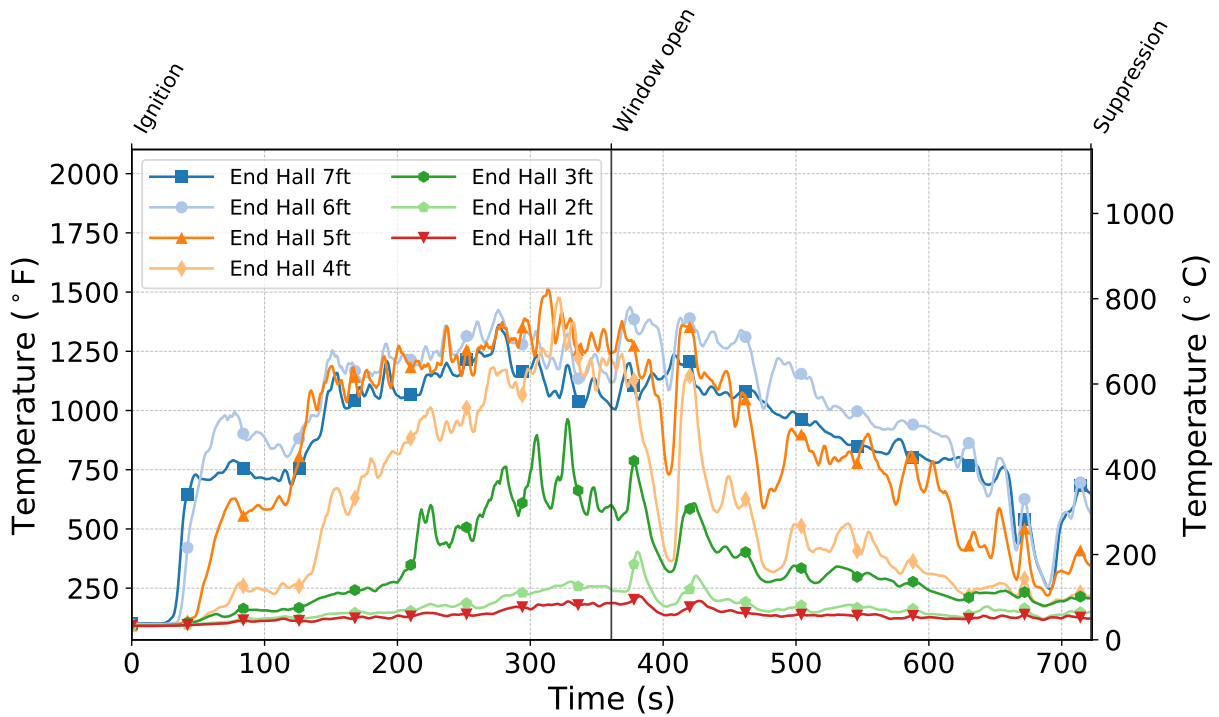


Figure C.367: Temperatures measured by the end hall thermocouples during Test 34.

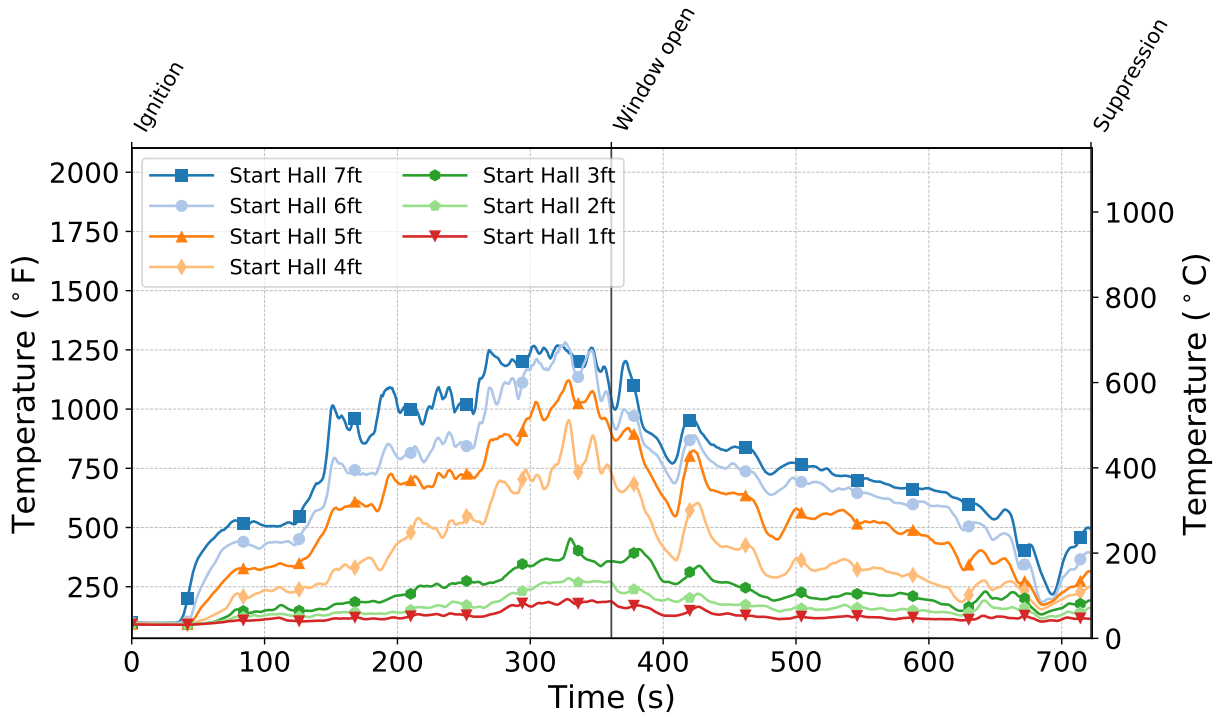


Figure C.368: Temperatures measured by the start hall thermocouples during Test 34.

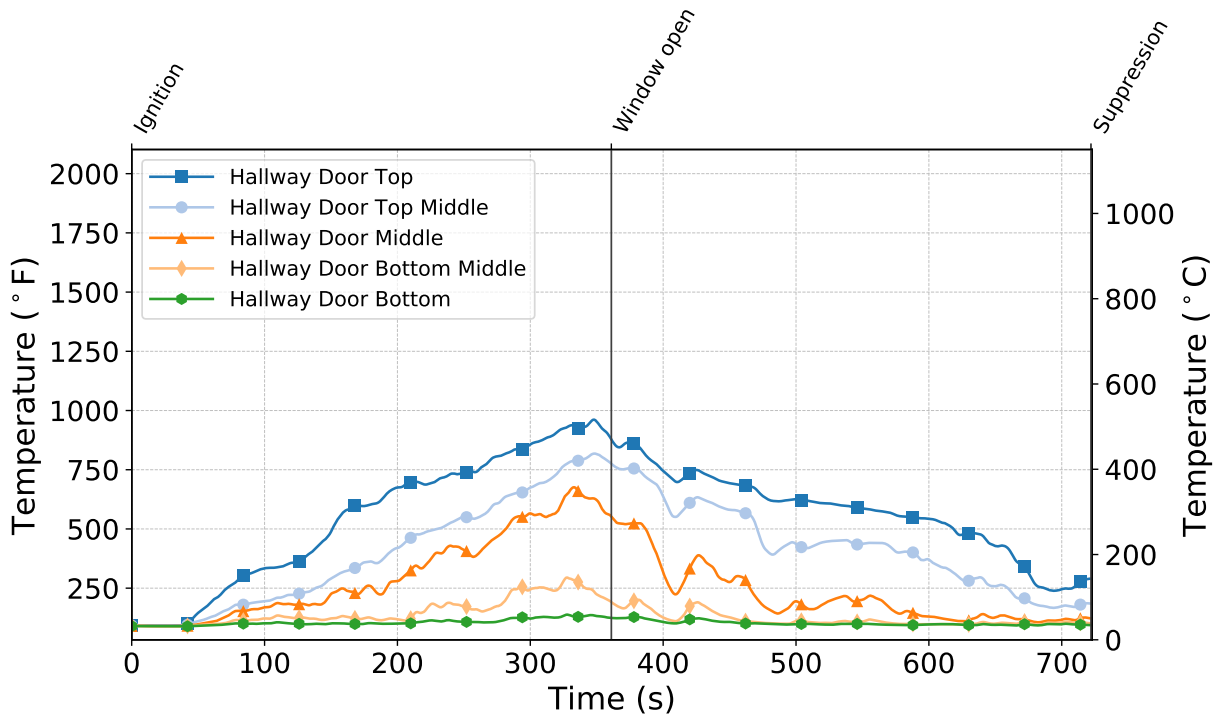


Figure C.369: Temperatures measured by the hallway door thermocouples during Test 34.

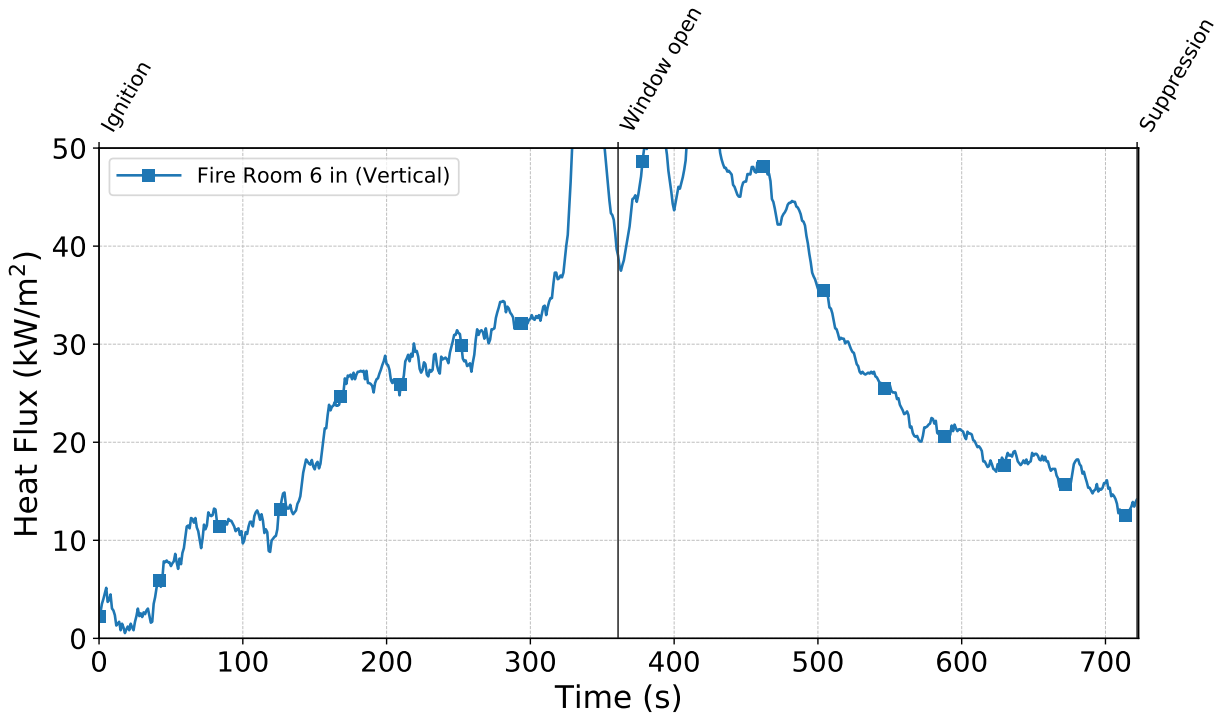


Figure C.370: Heat flux measured by the fire room gauge during Test 34.

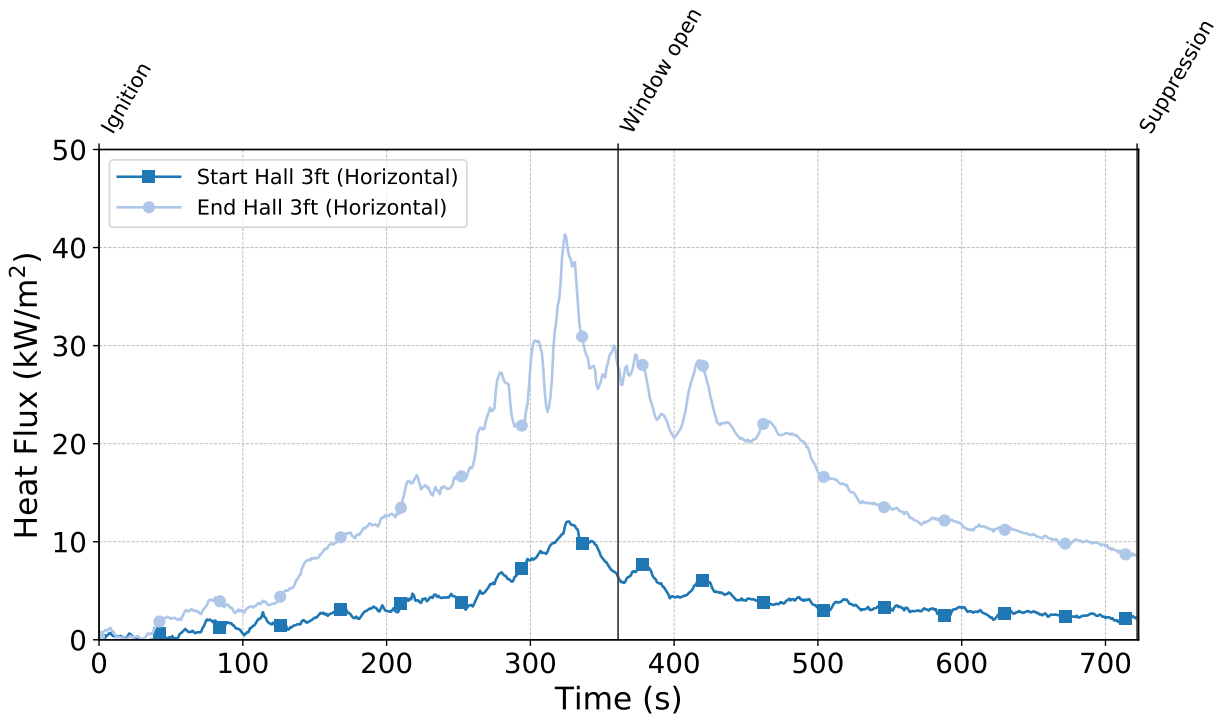


Figure C.371: Heat flux measured by the hallway gauges during Test 34.

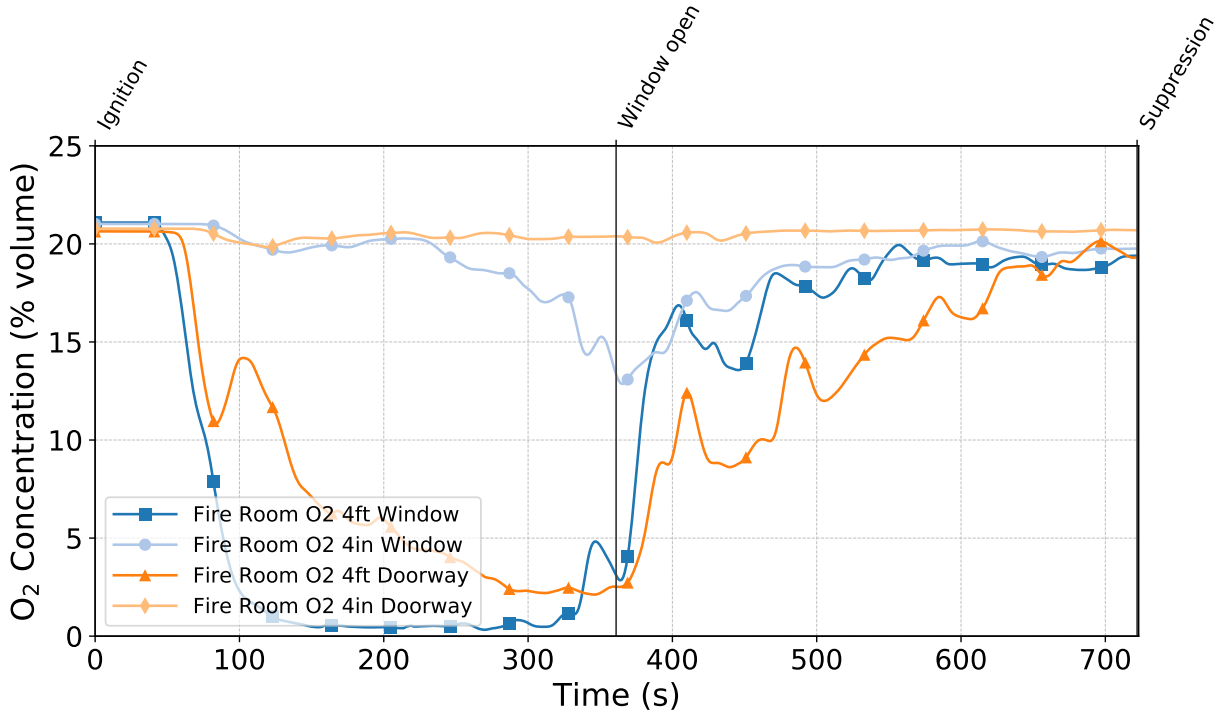


Figure C.372: Oxygen concentrations measured by the fire room gas sampling probes during Test 34.

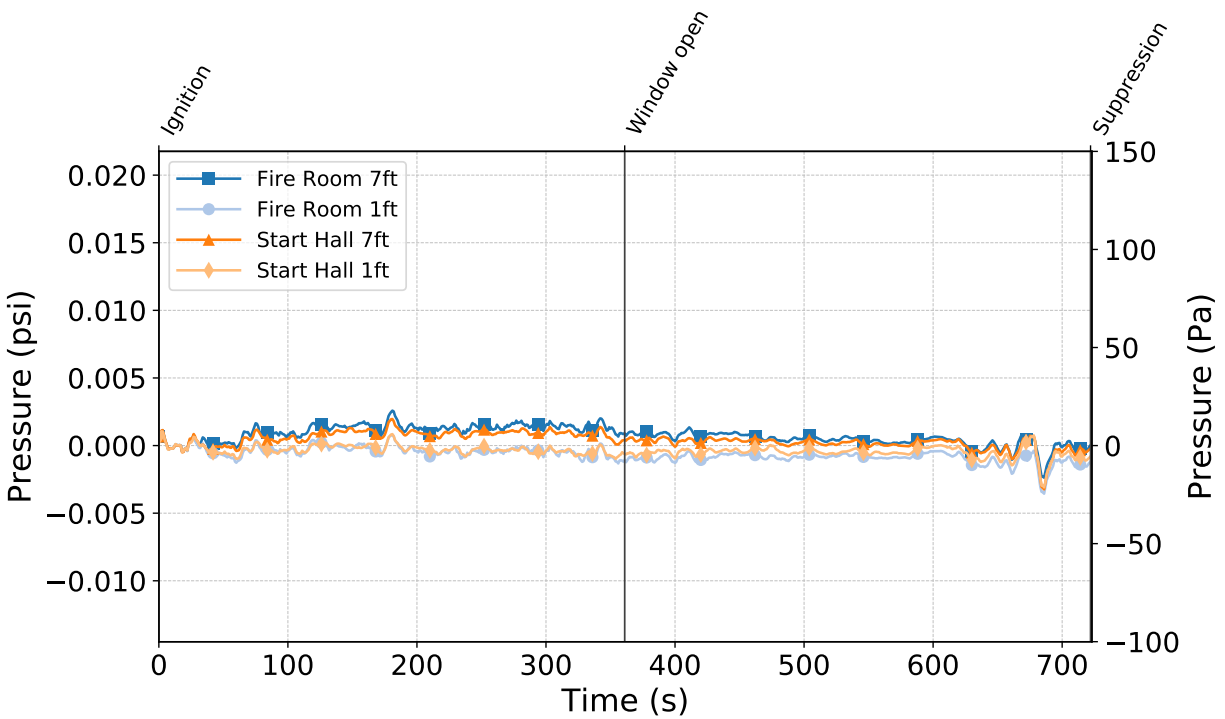


Figure C.373: Pressures measured by the fire room and hallway probes during Test 34.

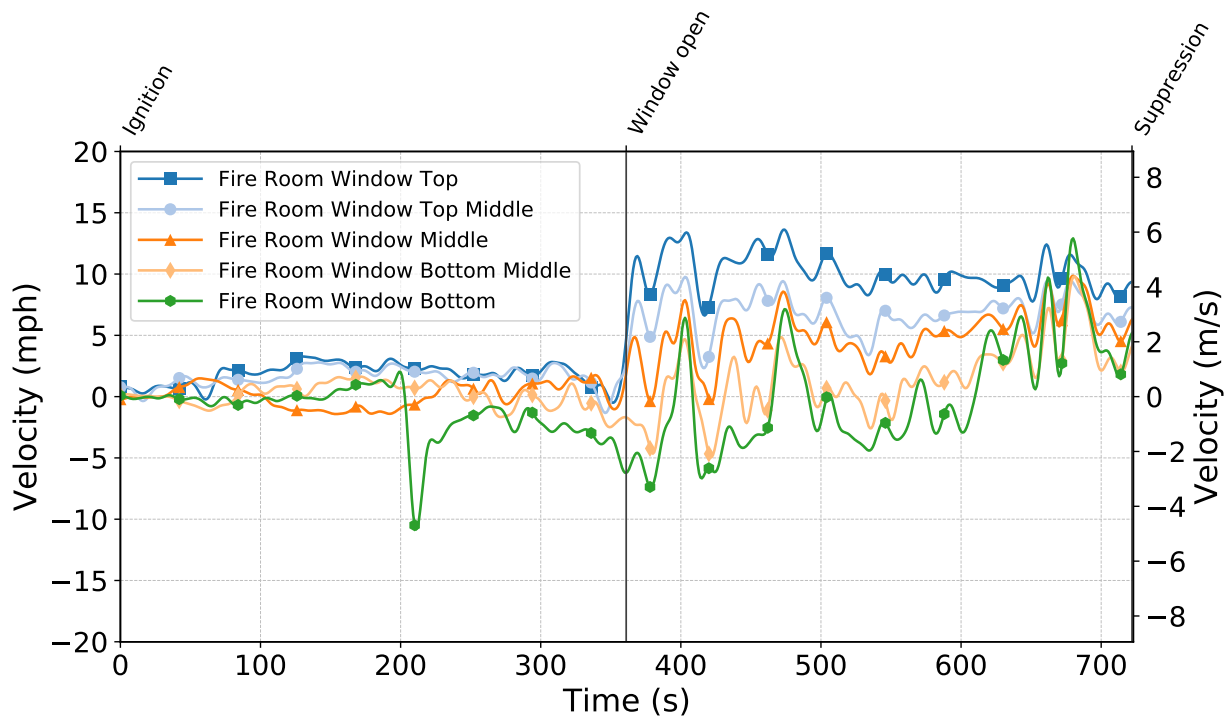


Figure C.374: Gas velocities measured by the fire room window bdp's during Test 34.

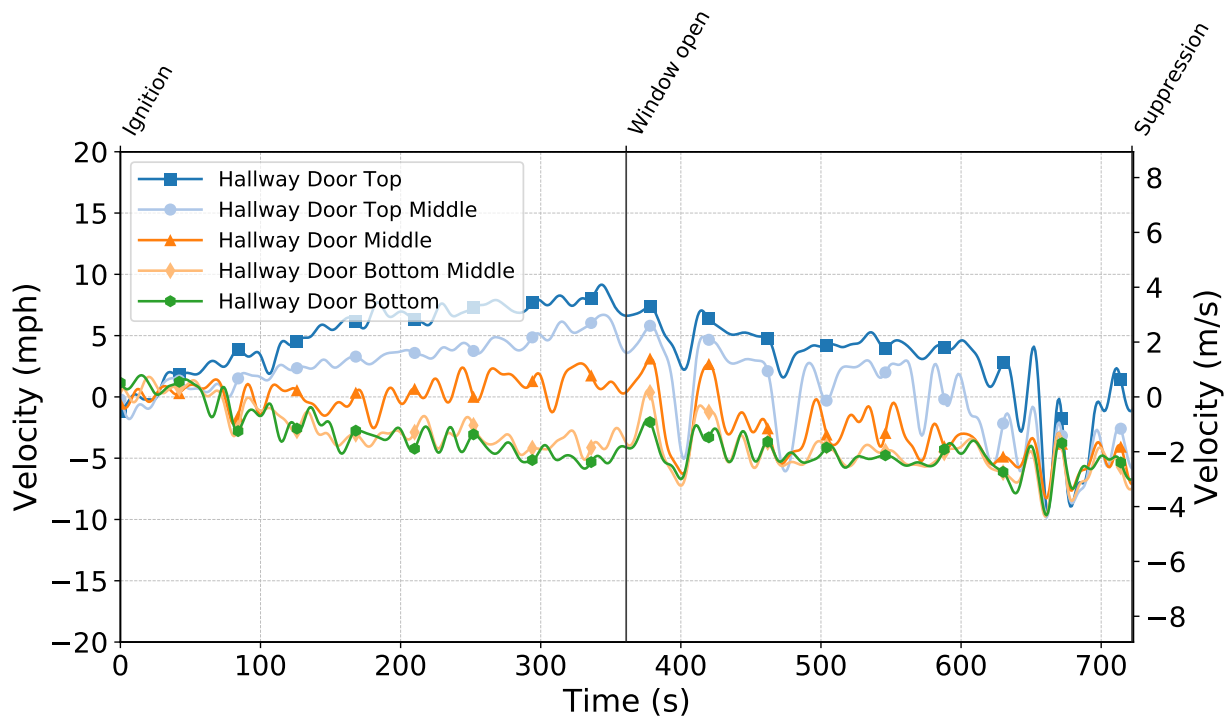


Figure C.375: Gas velocities measured by the hallway door bdp's during Test 34.

C.4 Suppression Effects Experiments

Test 35

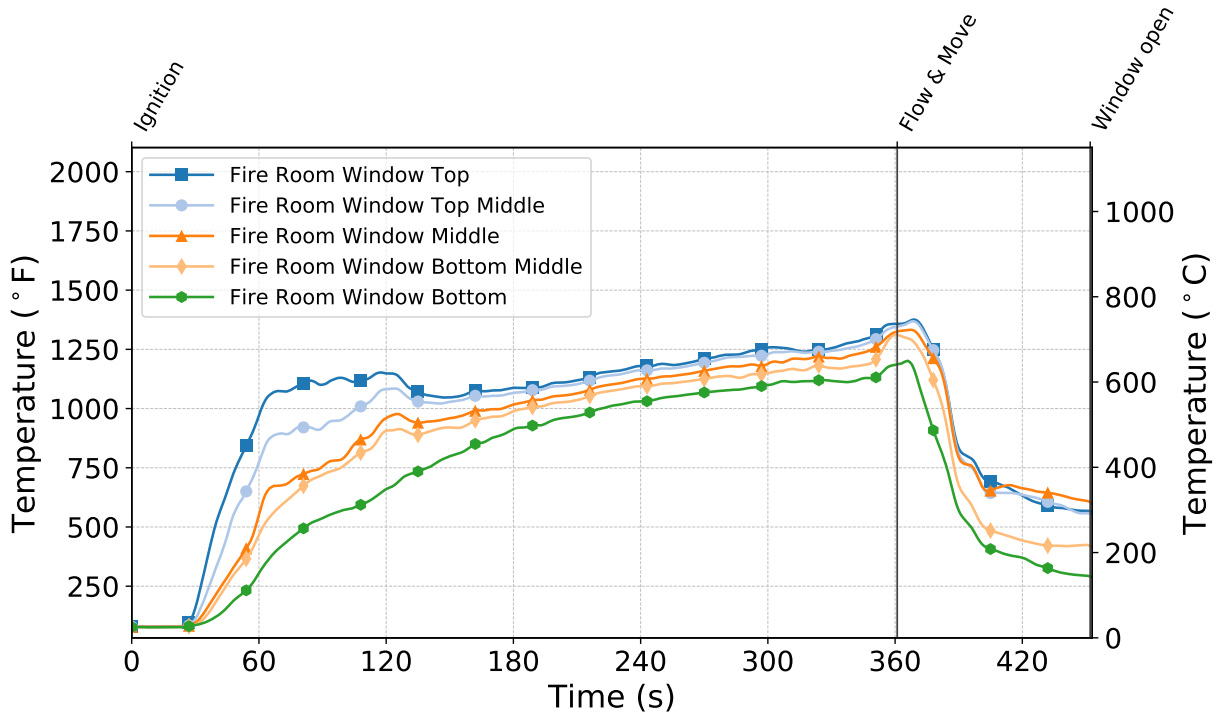


Figure C.376: Temperatures measured by the fire room window thermocouples during Test 35.

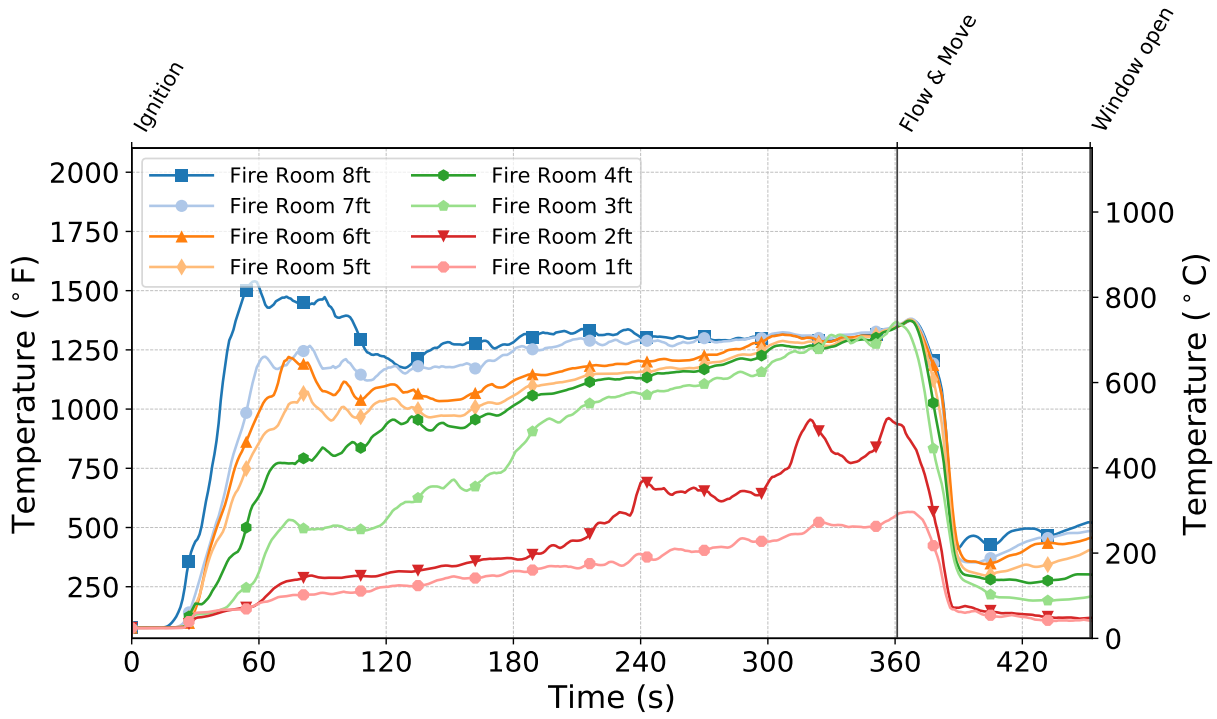


Figure C.377: Temperatures measured by the fire room thermocouples during Test 35.

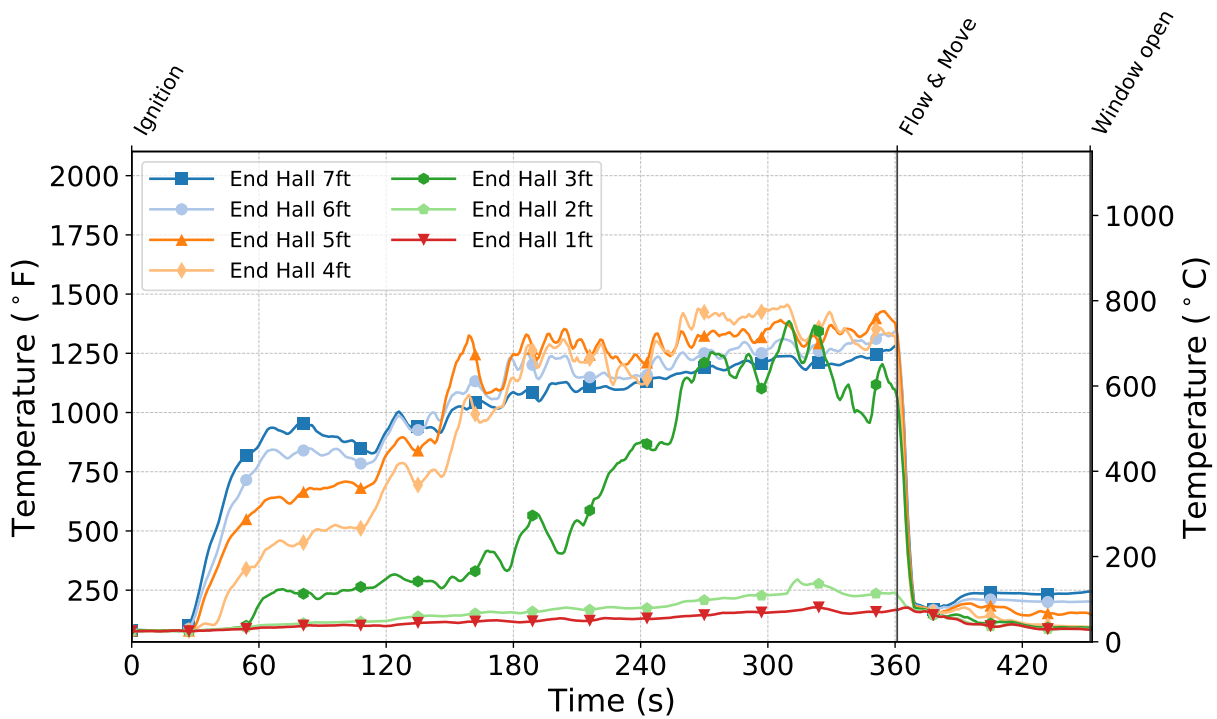


Figure C.378: Temperatures measured by the end hall thermocouples during Test 35.

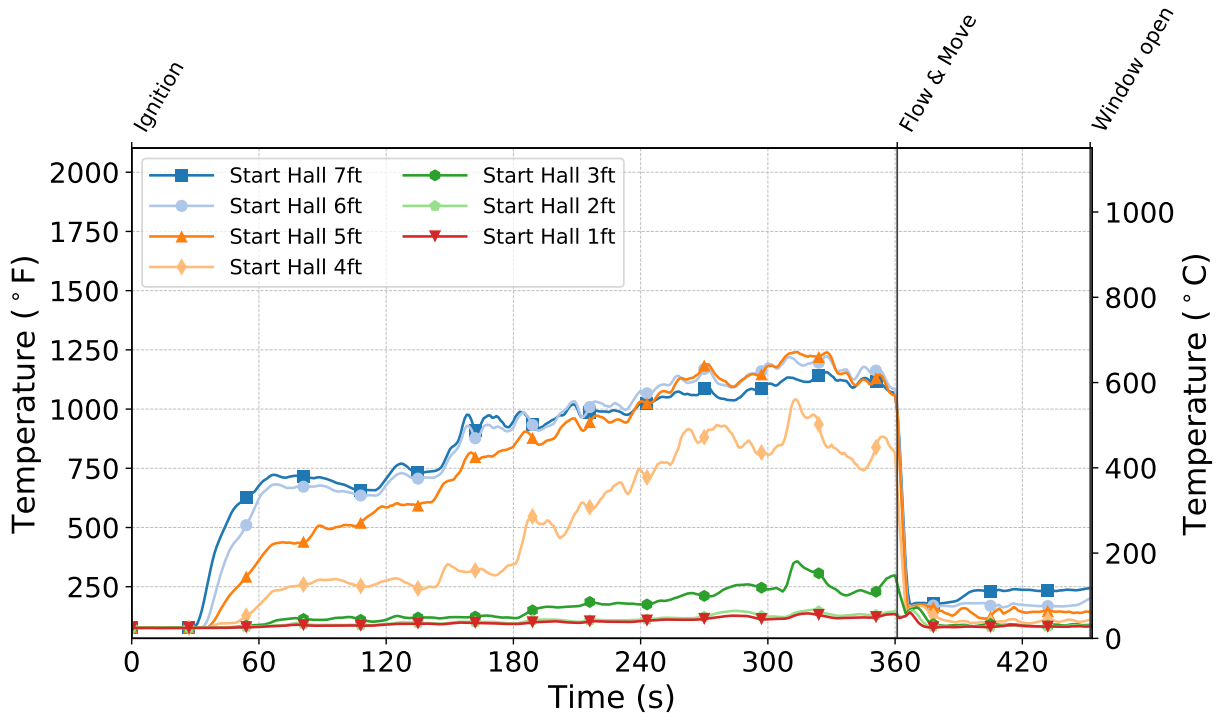


Figure C.379: Temperatures measured by the start hall thermocouples during Test 35.

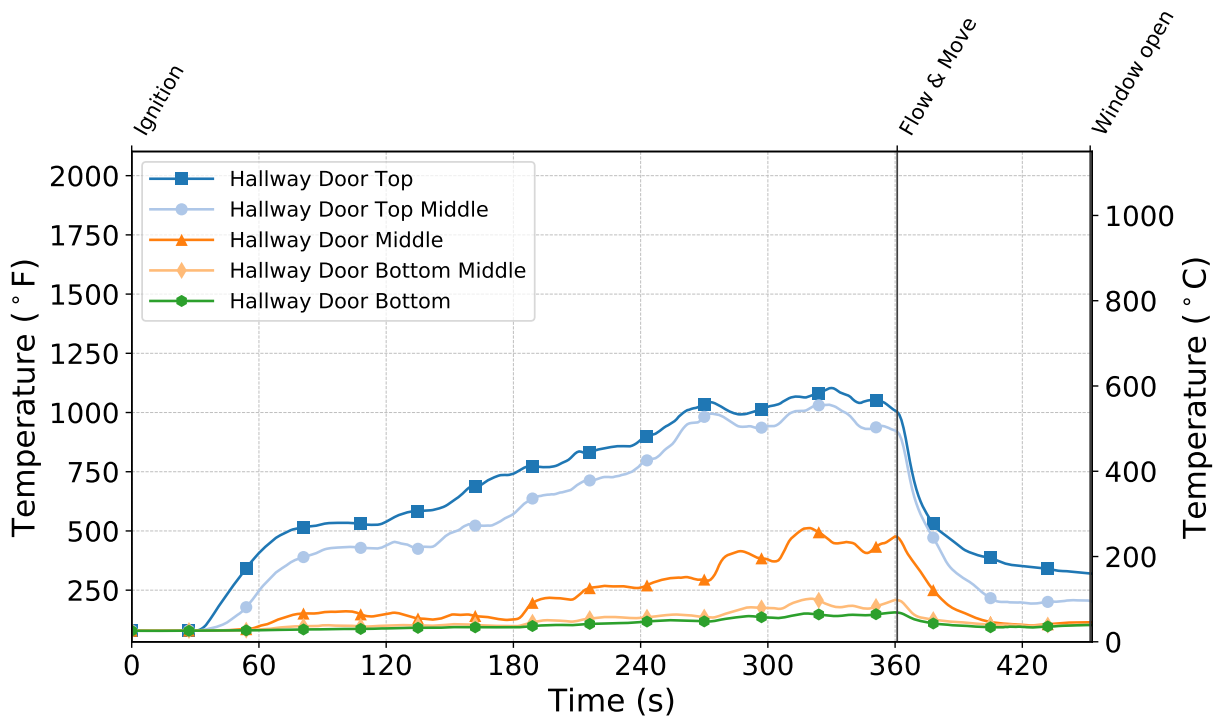


Figure C.380: Temperatures measured by the hallway door thermocouples during Test 35.

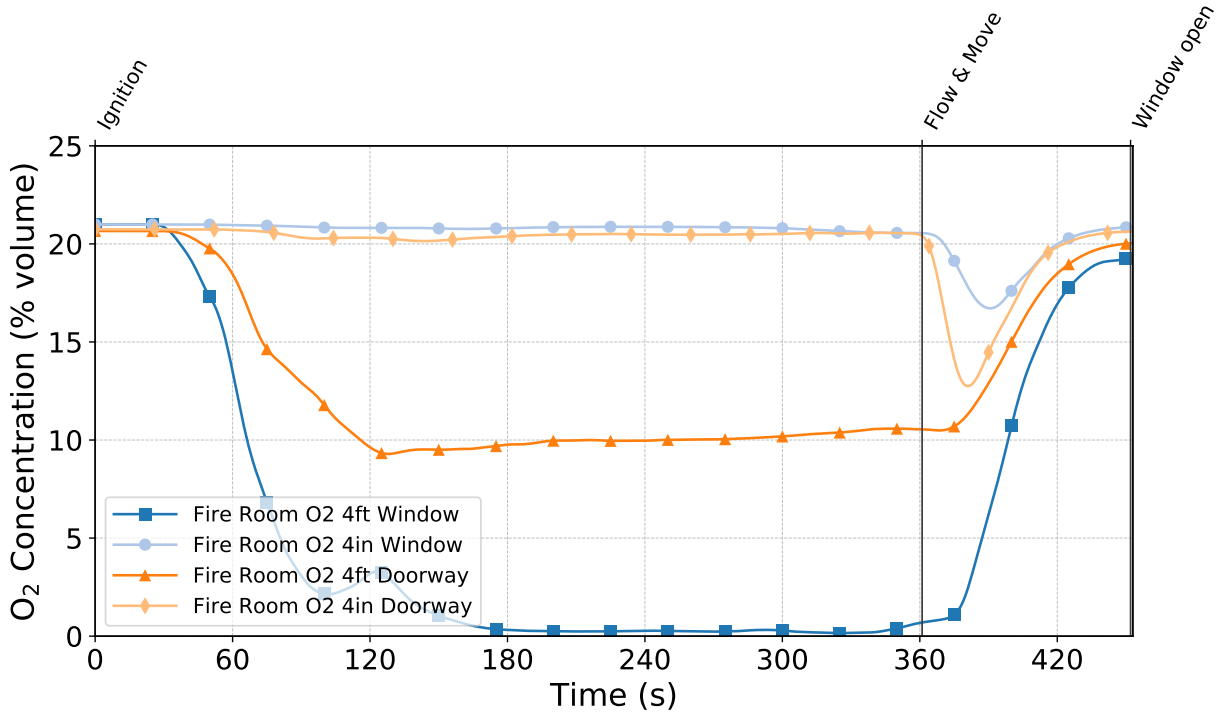


Figure C.381: Oxygen concentrations measured by the fire room gas sampling probes during Test 35.

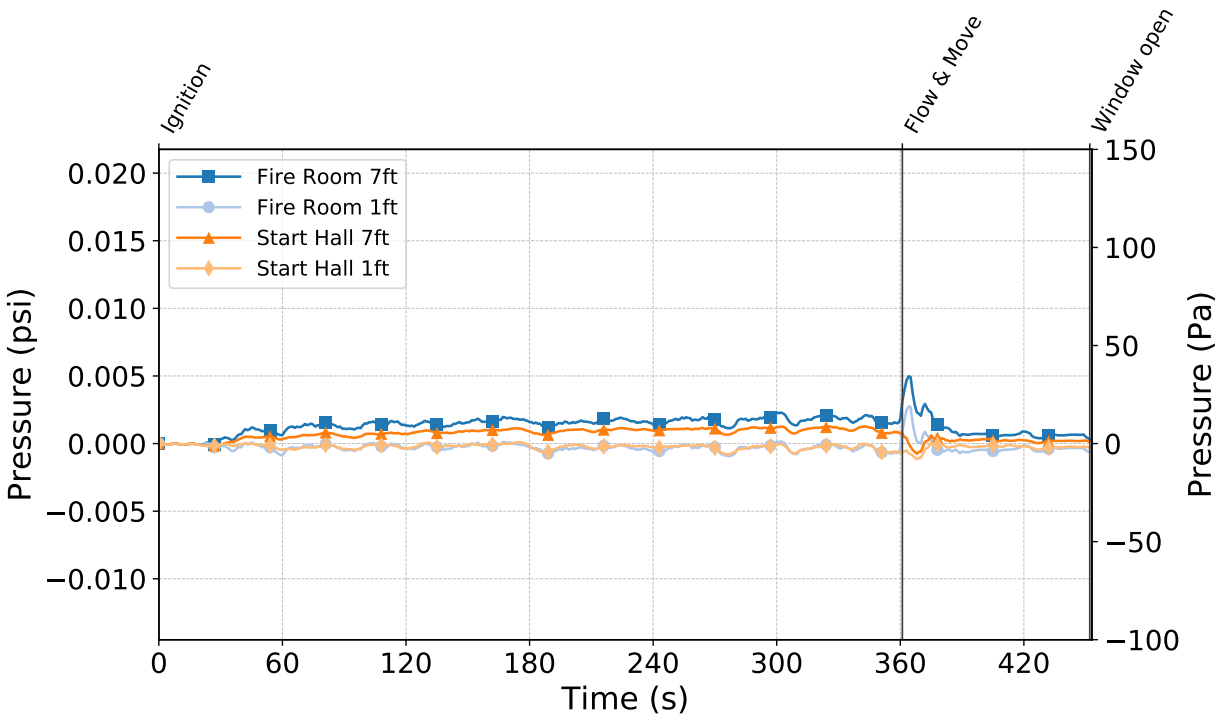


Figure C.382: Pressures measured by the fire room and hallway probes during Test 35.

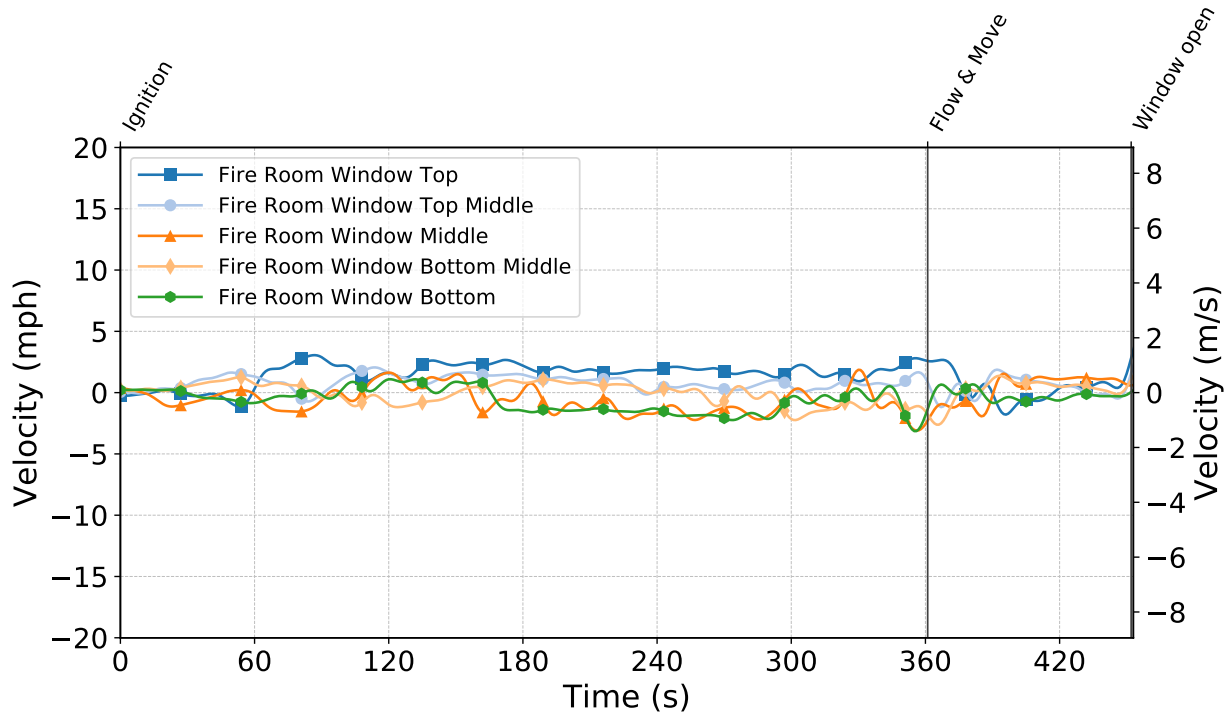


Figure C.383: Gas velocities measured by the fire room window bdps during Test 35.

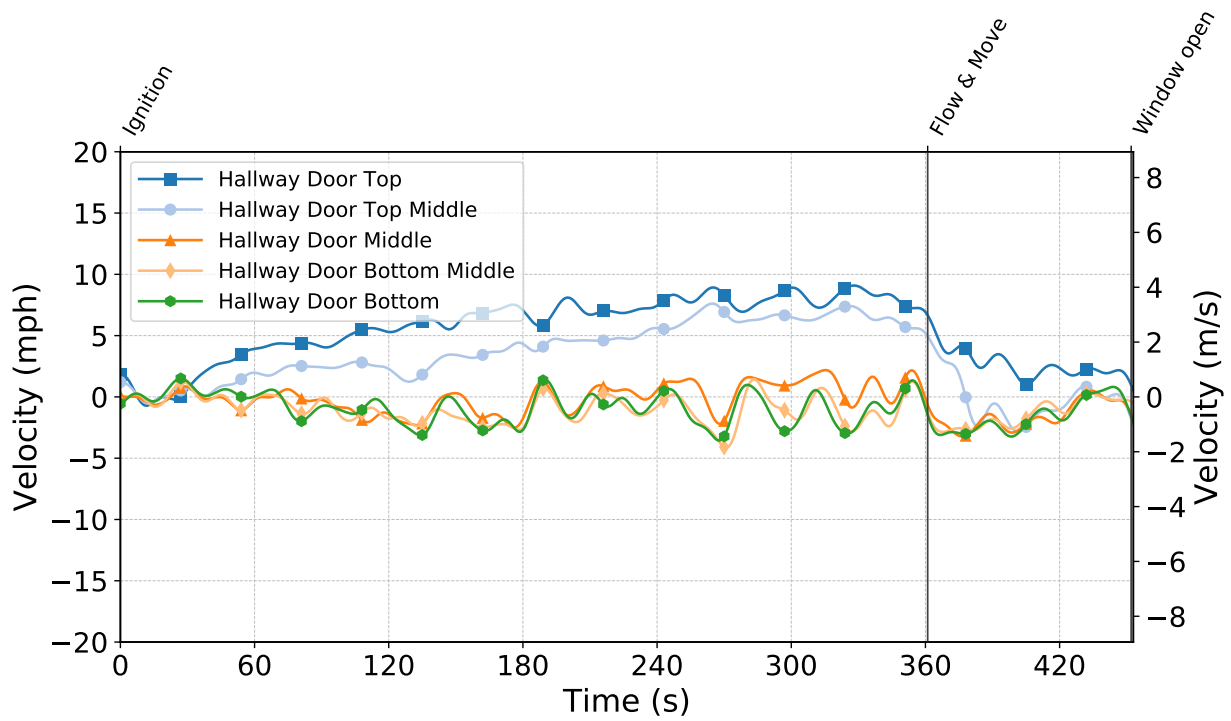


Figure C.384: Gas velocities measured by the hallway door bdps during Test 35.

Test 36

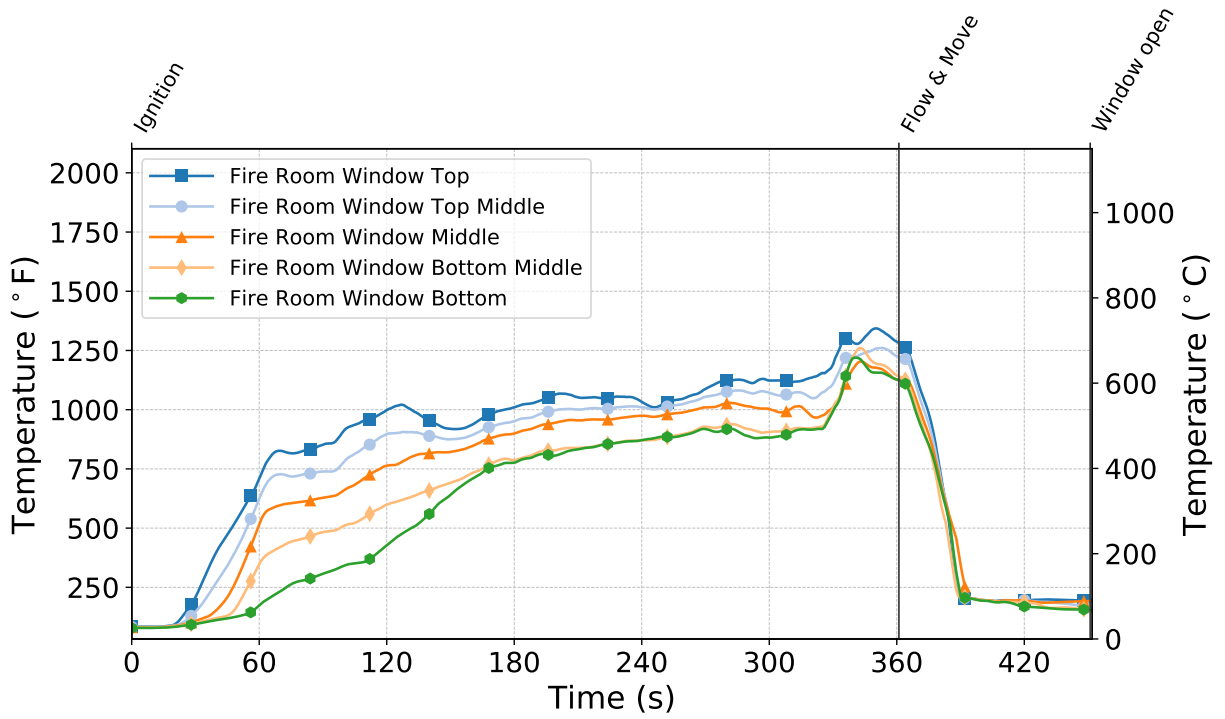


Figure C.385: Temperatures measured by the fire room window thermocouples during Test 36.

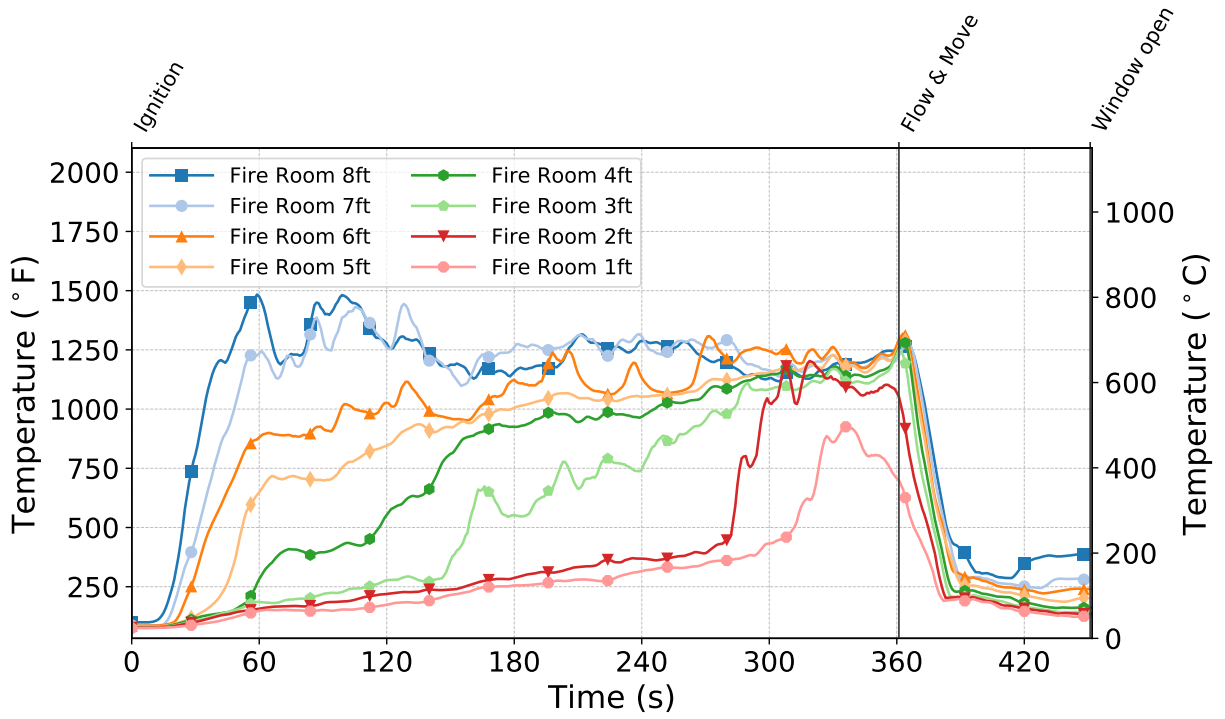


Figure C.386: Temperatures measured by the fire room thermocouples during Test 36.

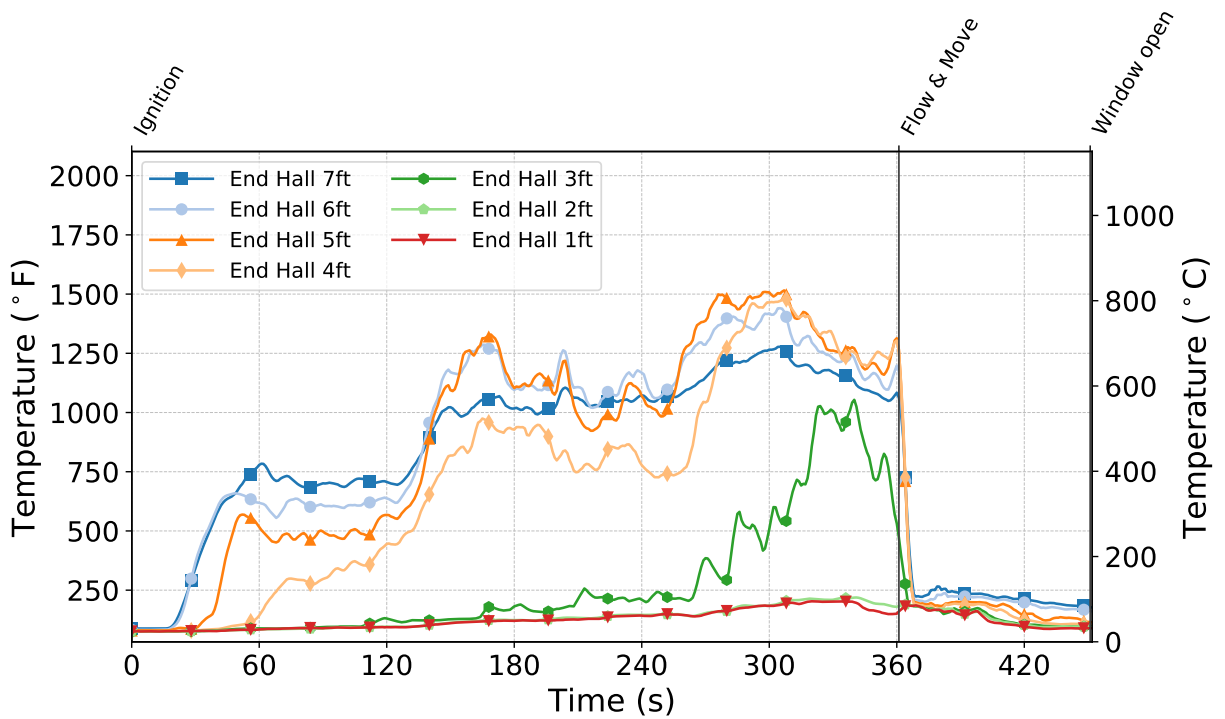


Figure C.387: Temperatures measured by the end hall thermocouples during Test 36.

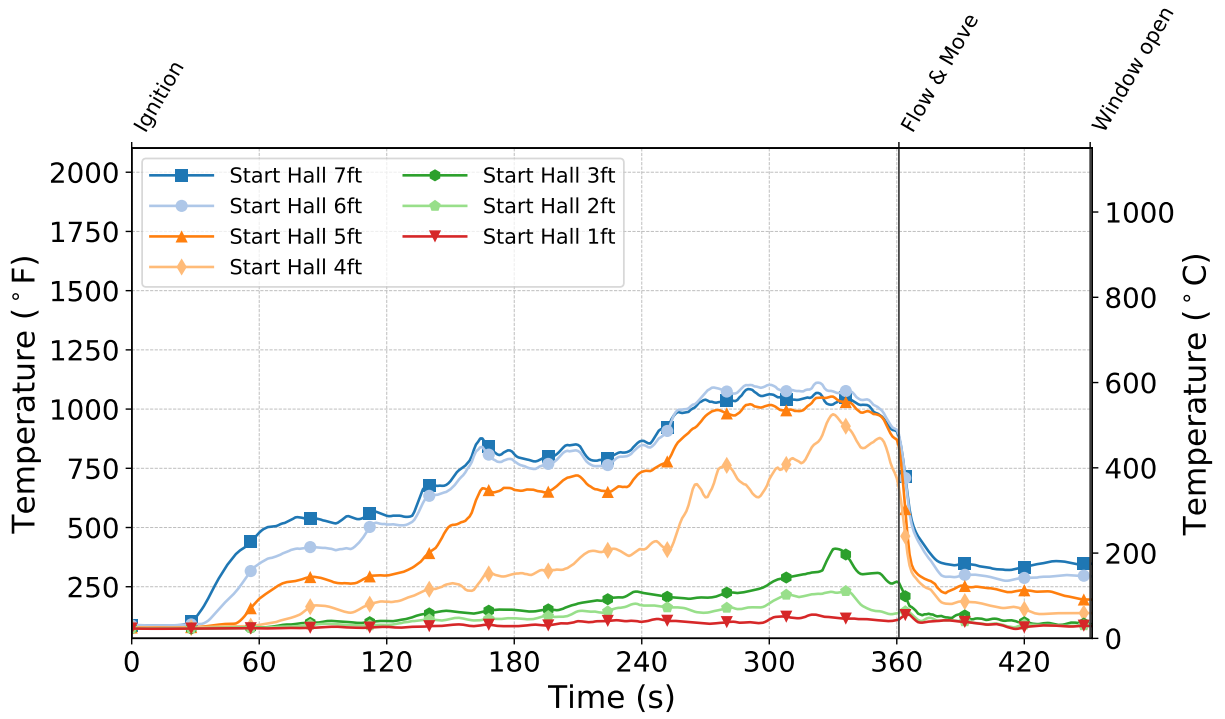


Figure C.388: Temperatures measured by the start hall thermocouples during Test 36.

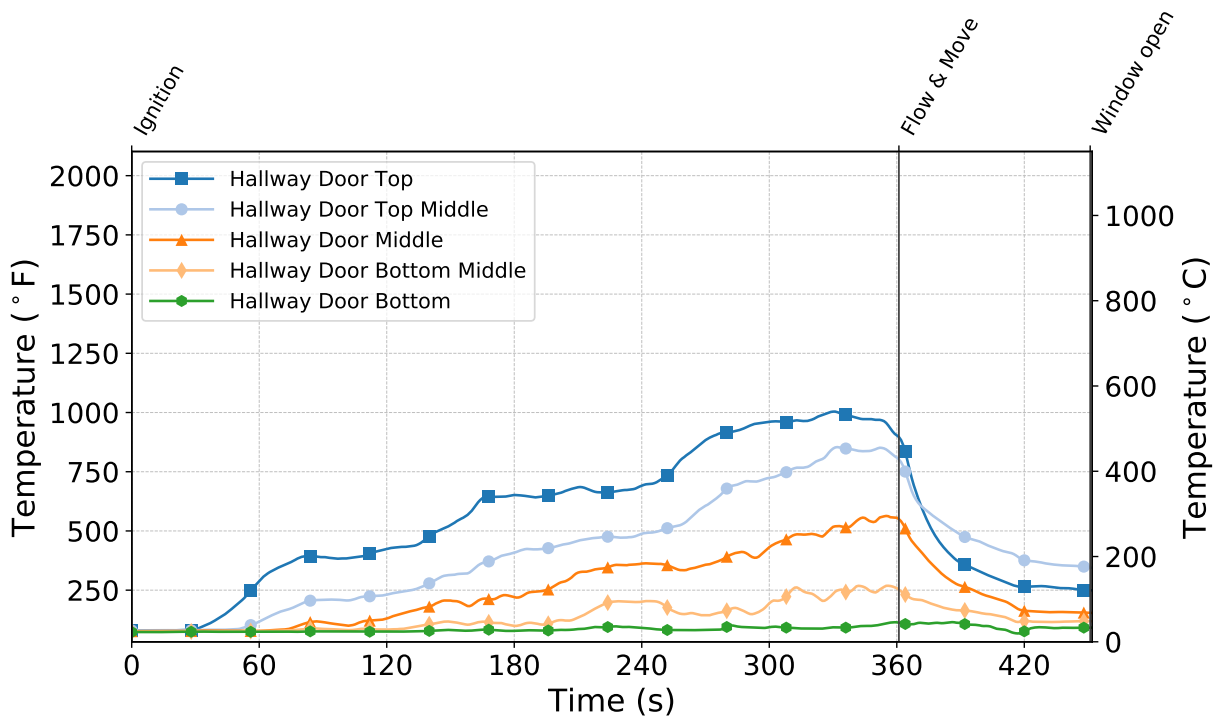


Figure C.389: Temperatures measured by the hallway door thermocouples during Test 36.

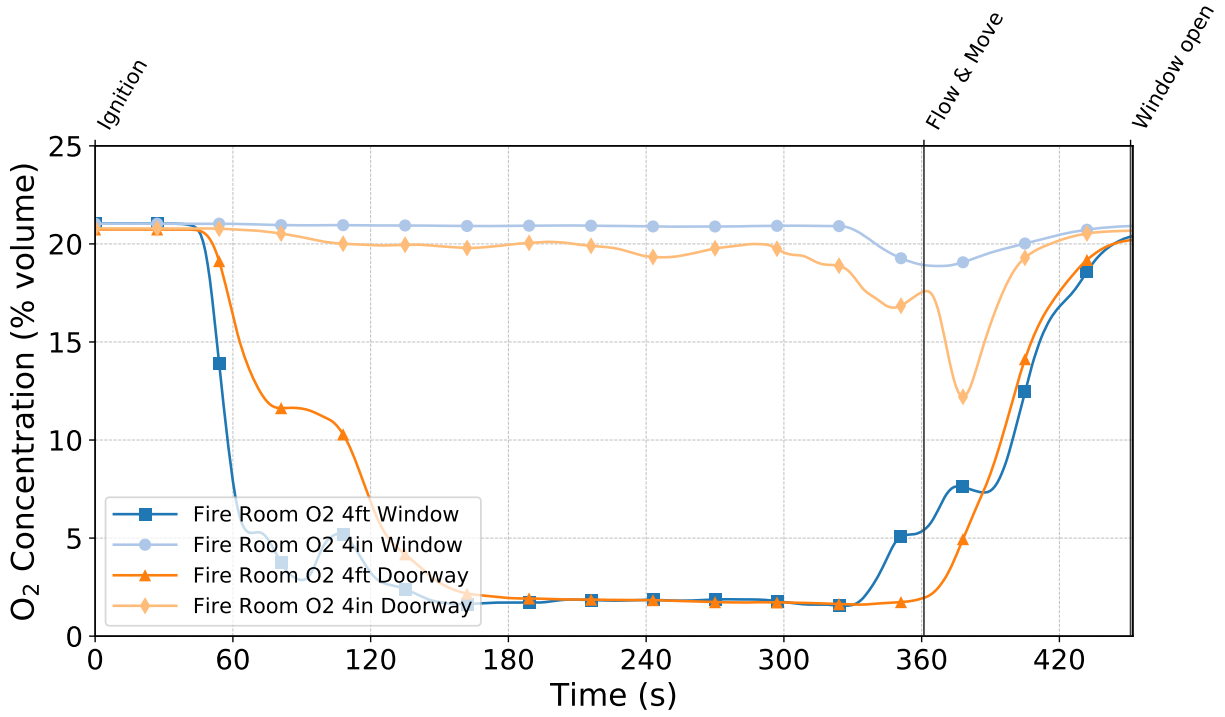


Figure C.390: Oxygen concentrations measured by the fire room gas sampling probes during Test 36.

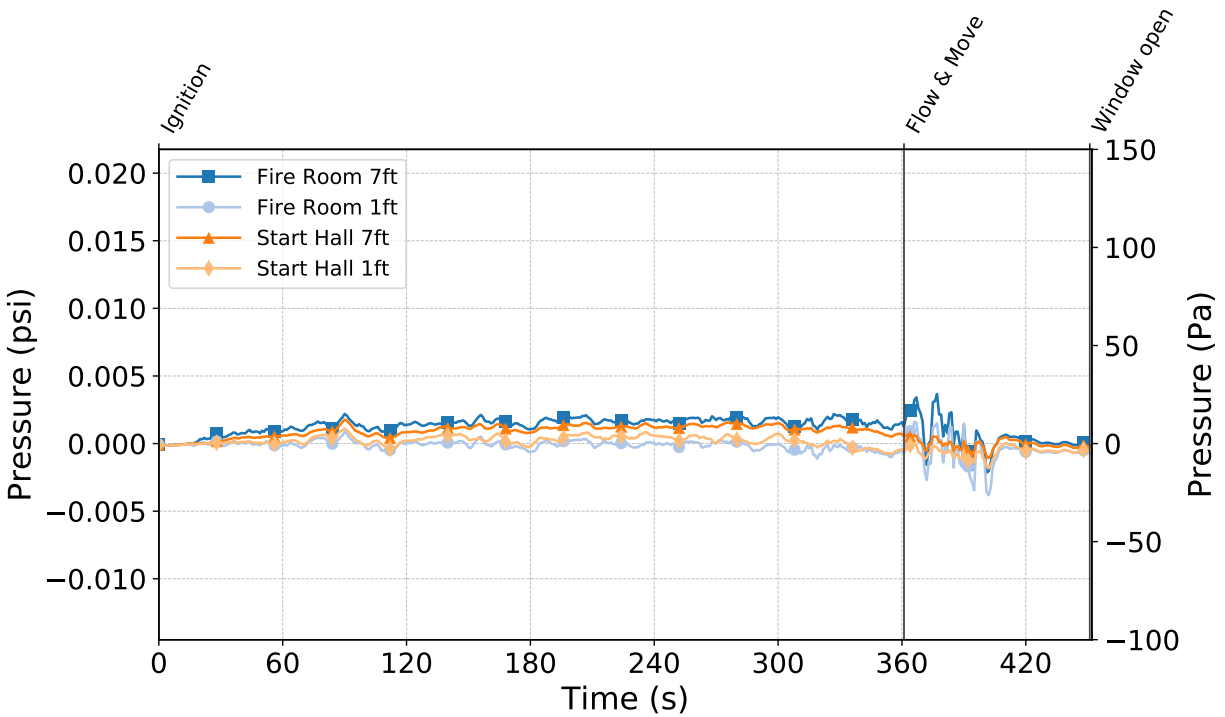


Figure C.391: Pressures measured by the fire room and hallway probes during Test 36.

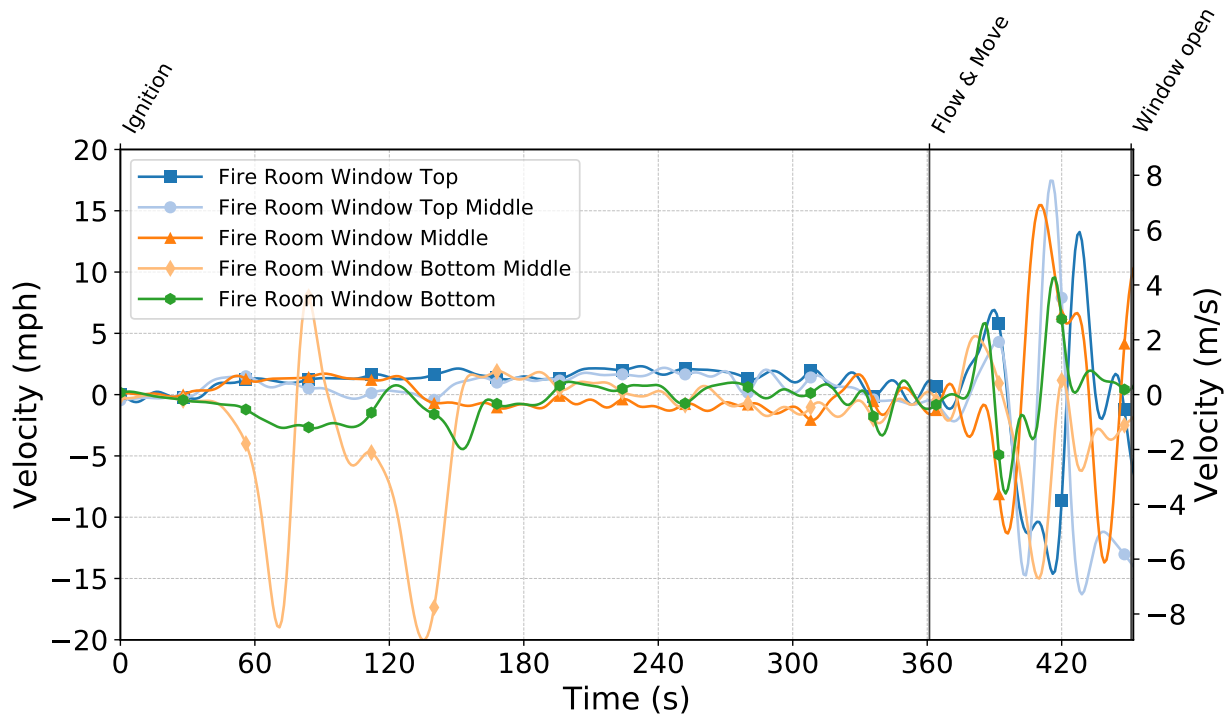


Figure C.392: Gas velocities measured by the fire room window bdps during Test 36.

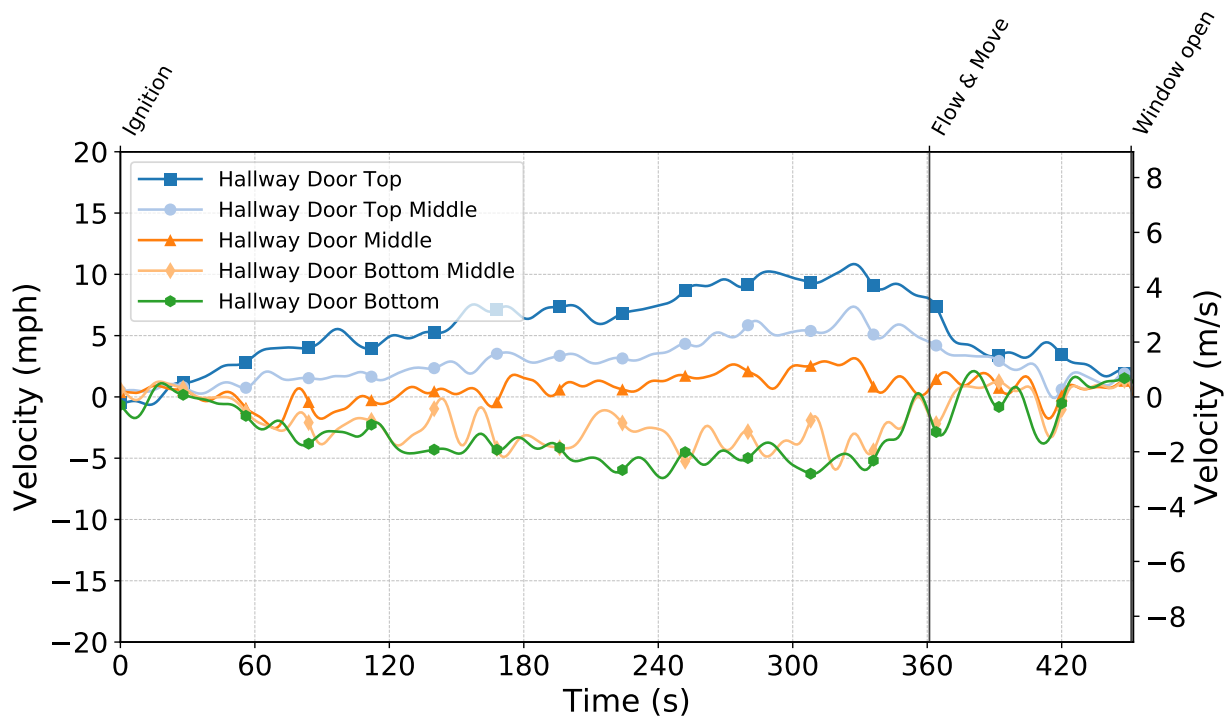


Figure C.393: Gas velocities measured by the hallway door bdps during Test 36.

Test 37

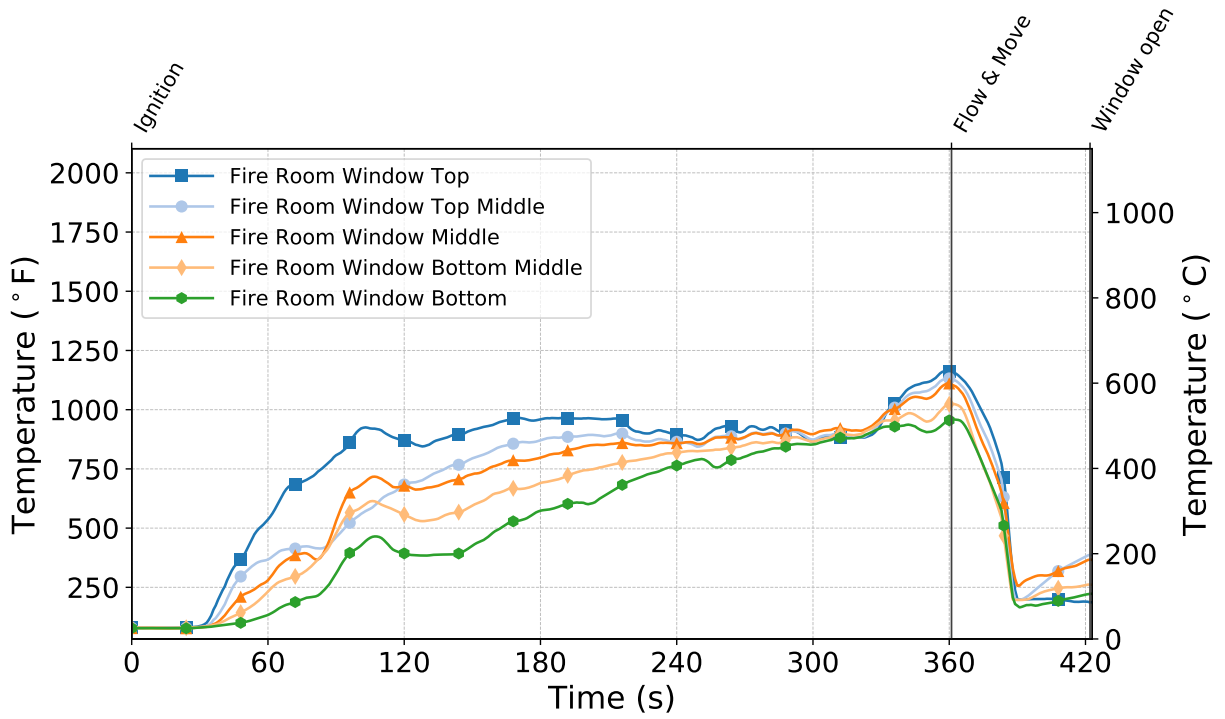


Figure C.394: Temperatures measured by the fire room window thermocouples during Test 37.

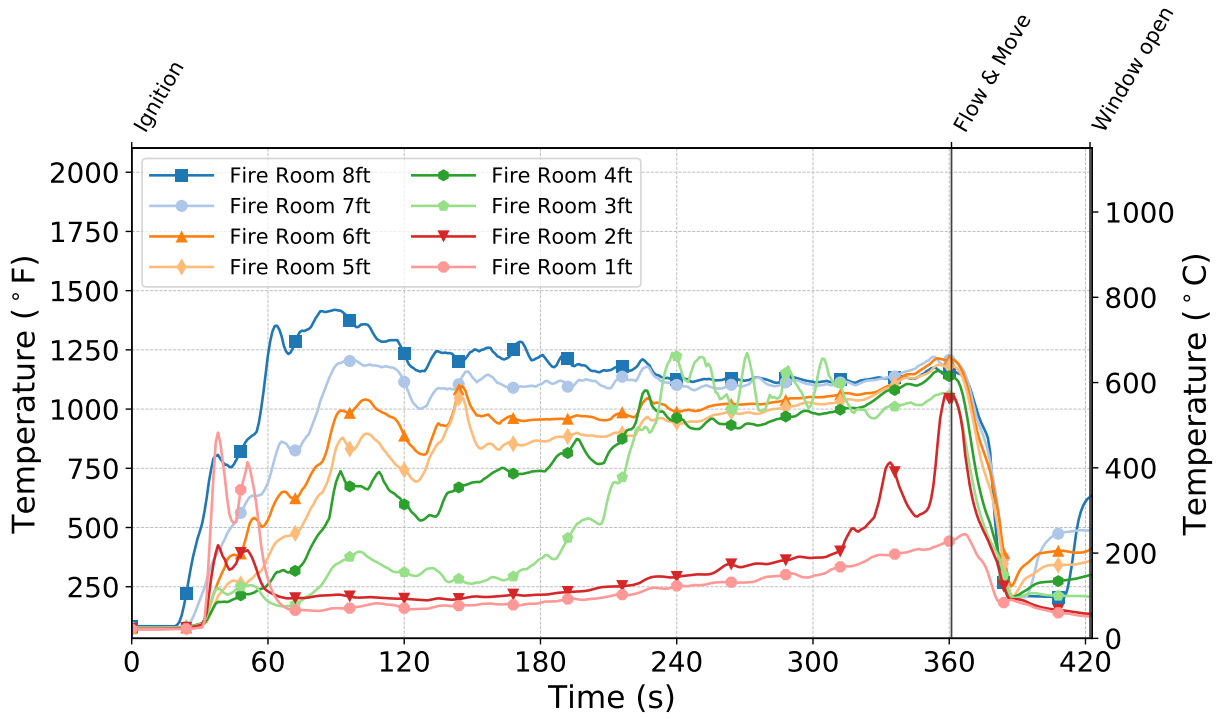


Figure C.395: Temperatures measured by the fire room thermocouples during Test 37.

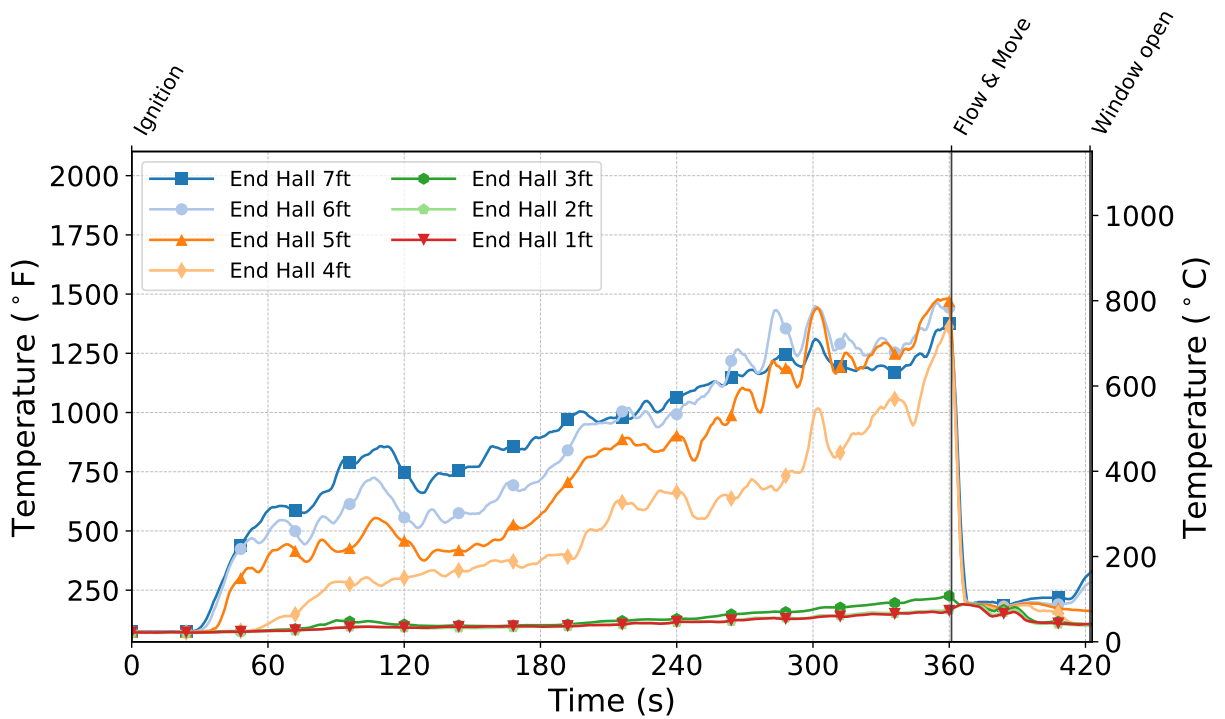


Figure C.396: Temperatures measured by the end hall thermocouples during Test 37.

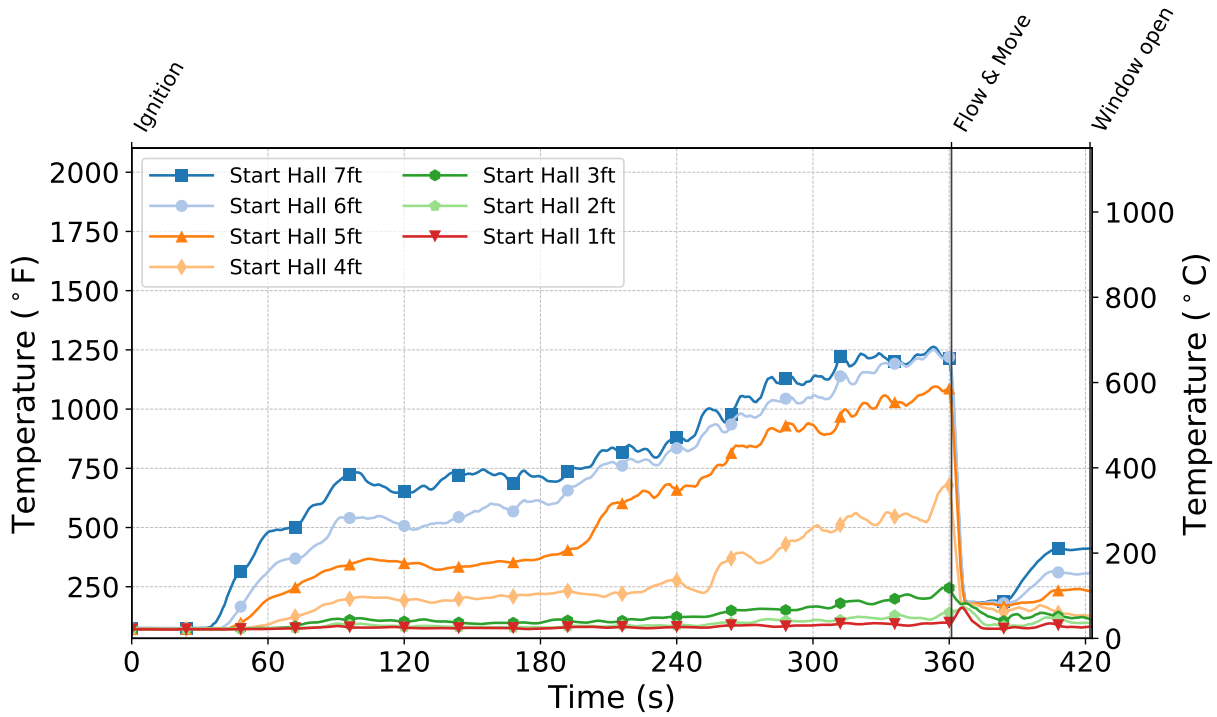


Figure C.397: Temperatures measured by the start hall thermocouples during Test 37.

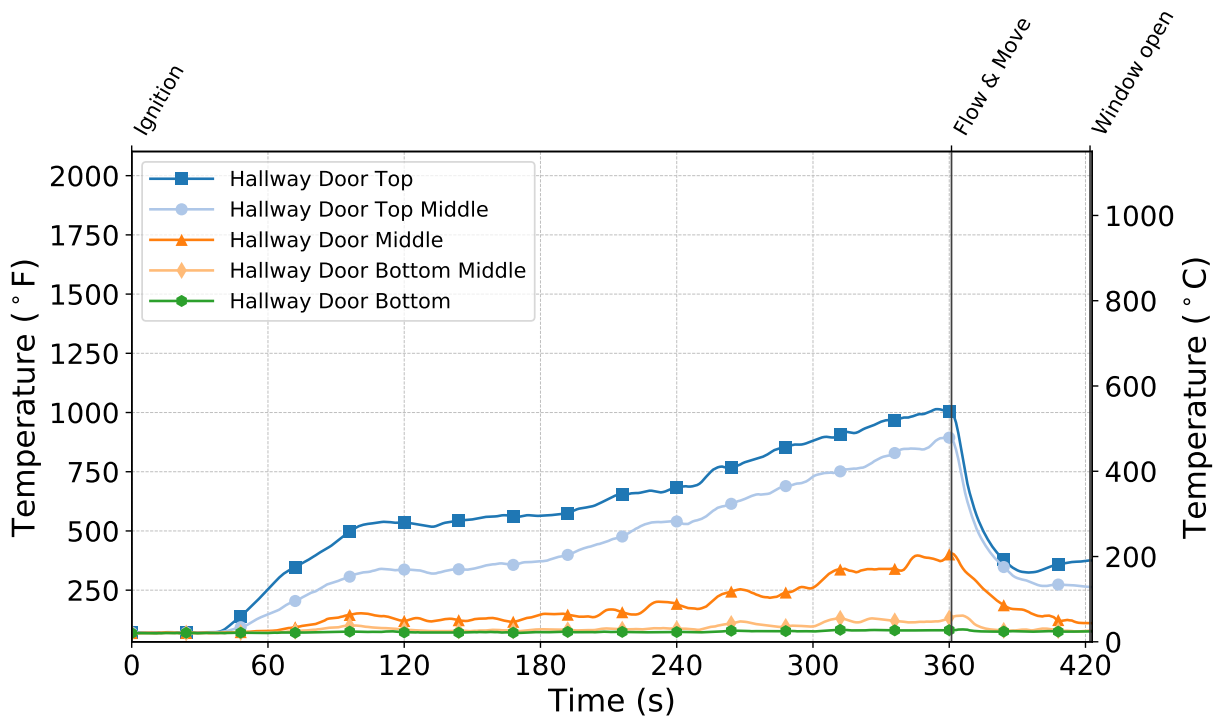


Figure C.398: Temperatures measured by the hallway door thermocouples during Test 37.

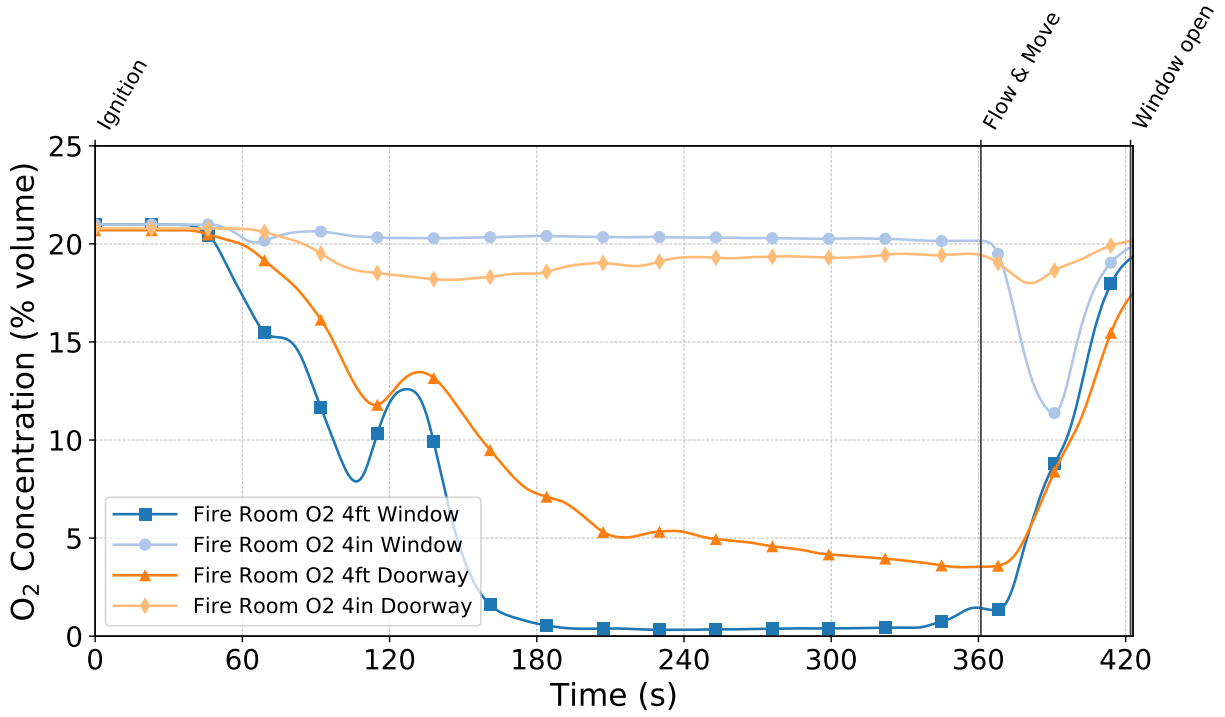


Figure C.399: Oxygen concentrations measured by the fire room gas sampling probes during Test 37.

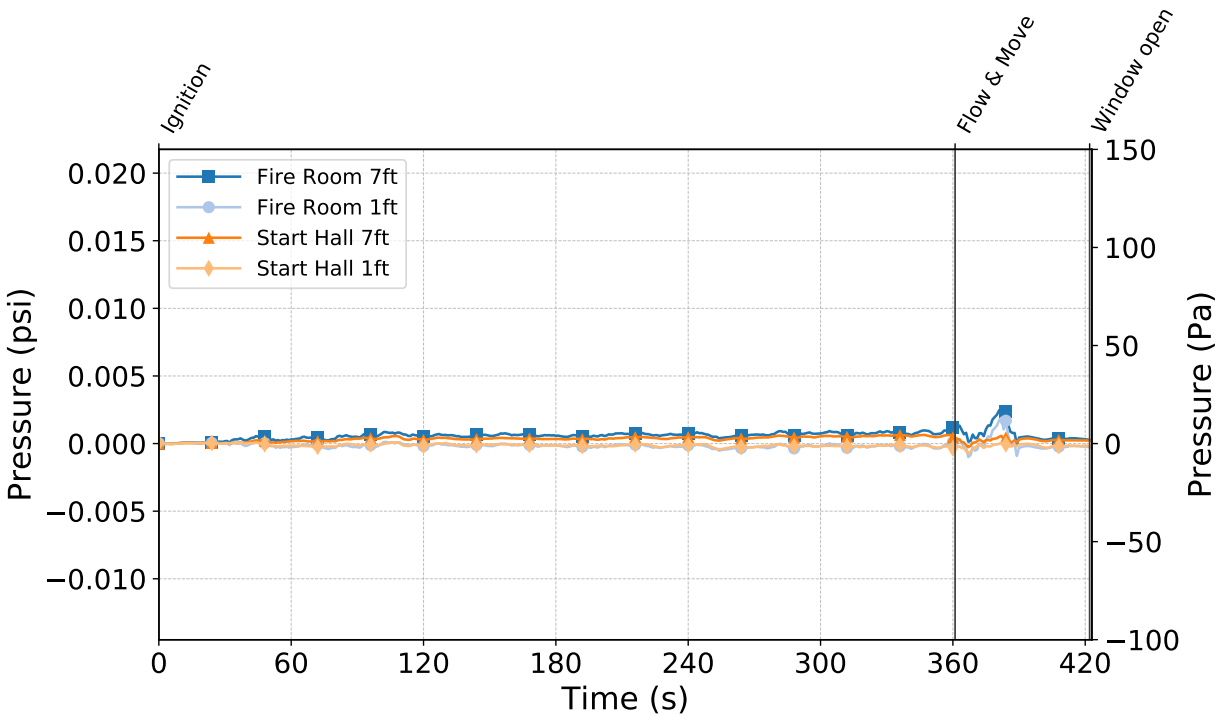


Figure C.400: Pressures measured by the fire room and hallway probes during Test 37.

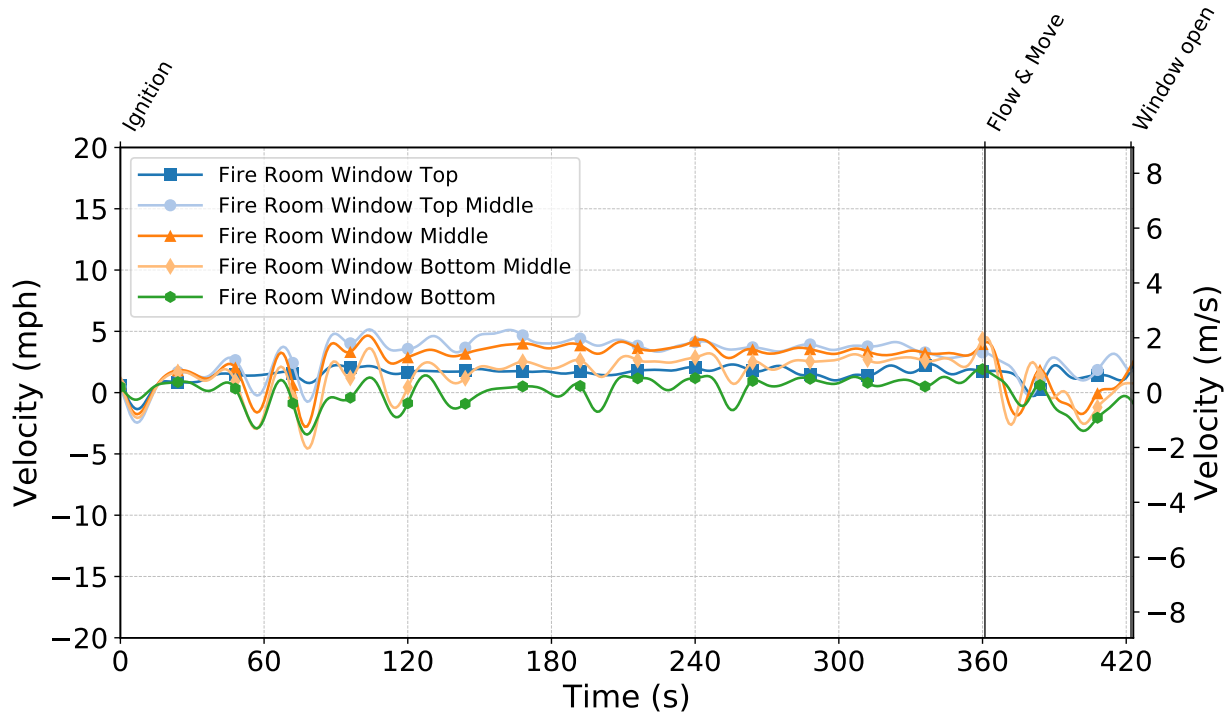


Figure C.401: Gas velocities measured by the fire room window bdp during Test 37.

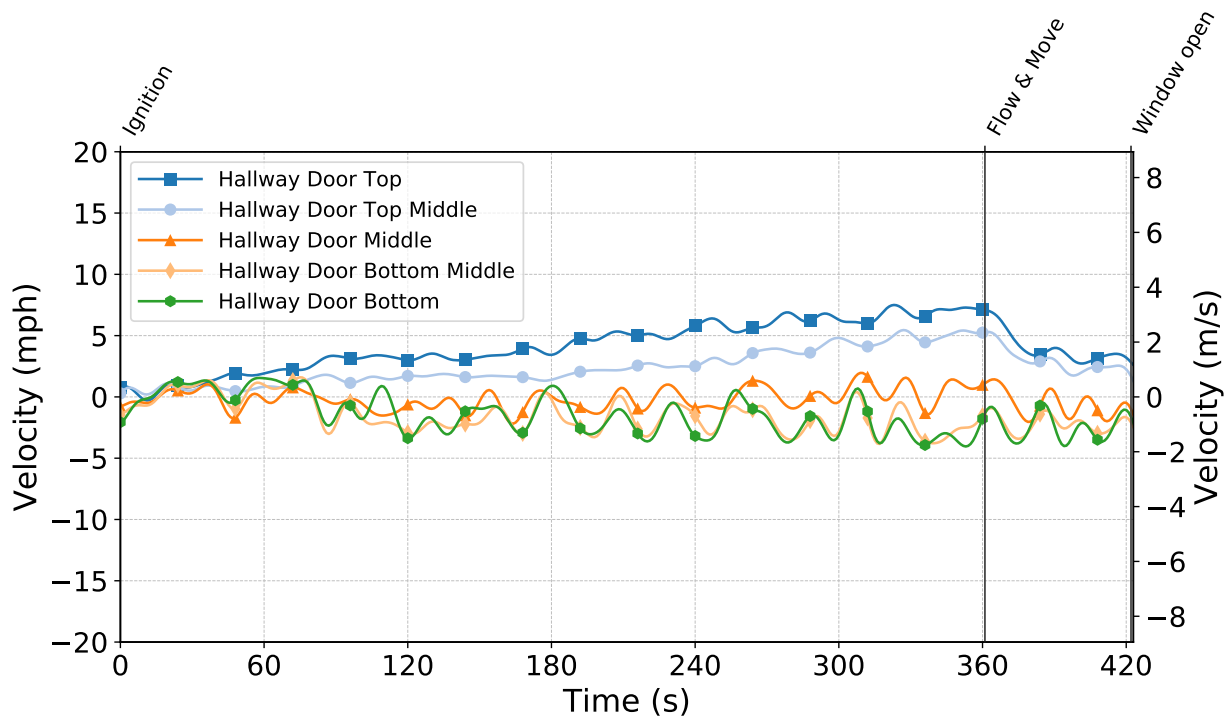


Figure C.402: Gas velocities measured by the hallway door bdp during Test 37.